Faculté des Sciences
Aix*Marseille Université

LISM
Laboratoire d'Ingénierie des Systèmes Macromoléculaires

Thesis

Submitted to the Aix-Marseille Université for the degree of

Doctor of Philosophy

Biology specialty Microbiology

Presented and publicly defended by:

Laureen Logger

Friday 8th December 2017

The Type VI secretion membrane complex: the central role of TssM for assembly and for baseplate recruitment

---

Jury

Dr. Nathalie Dautin	Reviewer
Dr. Pierre Genevaux	Reviewer
Dr. Benoît Chassaing	Examiner
Dr. Jean-Michel Jault	Examiner
Pr. Sophie Bleves	Examiner
Dr. Eric Cascales	Thesis advisor

Faculté des Sciences
Aix*Marseille Université

LISM
Laboratoire d'Ingénierie des Systèmes Macromoléculaires

Thesis

Submitted to the Aix-Marseille Université for the degree of

Doctor of Philosophy

Biology specialty Microbiology

Presented and publicly defended by:

Laureen Logger

Friday 8th December 2017

The Type VI secretion membrane complex: the central role of TssM for assembly and for baseplate recruitment

---

Jury

Dr. Nathalie Dautin	Reviewer
Dr. Pierre Genevaux	Reviewer
Dr. Benoît Chassaing	Examiner
Dr. Jean-Michel Jault	Examiner
Pr. Sophie Bleves	Examiner
Dr. Eric Cascales	Thesis advisor

"L'essentiel est invisible pour les yeux"
(Antoine de Saint-Exupéry)

Contents

Scientific Achievements

Funding

10/2013 - 09/2016	Ph.D fellowship from the French Ministry of Research
10/2016 - 09/2017	End-of-Ph.D fellowship from the Fondation pour la Recherche Médicale (contract FRM-FDT20160435498)

Publication list

Zhang, X.Y., Brunet, Y.R., **Logger, L.**, Douzi, B., Cambillau, C., Journet, L., Cascales, E., 2013. *Dissection of the TssB-TssC interface during type VI secretion sheath complex formation.* PloS One 8: e81074.

Zoued, A.*, Brunet, Y.R.*, Durand, E., Aschtgen, M.-S., **Logger, L.**, Douzi, B., Journet, L., Cambillau, C., Cascales, E., 2014. *Architecture and assembly of the Type VI secretion system.* Biochim. Biophys. Acta 1843: 1664–1673.

Nguyen, V.S.*, **Logger, L.***, Spinelli, S., Desmyter, A., Le, T.T.H., Kellenberger, C., Douzi, B., Durand, E., Roussel, A., Cascales, E., Cambillau, C., 2015. *Inhibition of Type VI secretion by an anti-TssM llama nanobody.* PloS One 10: e0122187.

Brunet, Y.R., Khodr, A., **Logger, L.**, Aussel, L., Mignot, T., Rimsky, S., Cascales, E., 2015. *H-NS silencing of the SPI-6-encoded Type VI secretion system limits Salmonella enterica serovar Typhimurium interbacterial killing.* Infect. Immun. 83: 2738-2750.

Durand, E.*, Nguyen, N.S.*, Zoued, A.*, **Logger, L.**, Péhau-Arnaudet, G., Aschtgen, M.S., Spinelli, S., Desmyter, A., Bardiaux, B., Dujeancourt, A., Roussel, A., Cambillau, C., Cascales, E., Fronzes, R., 2015. *Biogenesis and structure of a type VI secretion membrane core complex.* Nature. 523:555-60.

Logger, L., Aschtgen, M.S., Guérin M., Cascales, E., Durand E. 2016. *Molecular dissection of the interface between the Type VI secretion TssM cytoplasmic domain and the TssG baseplate component.* J Mol Biol. 428:4424-37.

Nguyen, N.S., **Logger, L.**, Spinelli, S., Legrand P., Huyen Pham TT., Nhung TT., Cherrak Y., Zoued A., Desmyter, A., Durand E., A., Roussel, A., Kellenberger C., Cascales, E., Cambillau, C. 2017. *Type VI secretion TssK baseplate protein exhibits structural similarity with phage receptor-binding proteins and evolved to bind the membrane complex.* Nat Microbiol. 2:17103.

Logger, L., Zoued, A., Cascales, E. 2017. *Fusion reporter approaches to monitoring transmembrane helix interactions in bacterial membranes.* Methods Mol Biol. 1615:100-210.

*co-first authors

Talks and poster presentations

JSM3 Junior Scientists Microbiology Meeting of Marseille, Marseille, France, 2016 May 19-20. *Poster: Mapping the tube-sheath interface within the Type VI secretion system tail.*

The New Bacteriology, London, UK, 2016 January 28-29. *Poster: Molecular dissection of the connexion between Type VI secretion membrane and baseplate complexes through TssMc.*

Molecular Genetics of Bacteria and Phages Meeting, Madison, USA, 2015 August 4-8. *Talk: Characterization of the TssM protein of the Type VI secretion system.*

Annual meeting of the doctoral school in biological and health sciences, Marseille, France 2015 June 4-5. *Talk and Poster: Characterization of the TssM protein of the Type VI secretion system.* 1st Prize 2015 : Best oral communication.

JSM3 Junior Scientists Microbiology Meeting of Marseille, Marseille, France, 2015 May 28-29. *Talk: The Type VI secretion missing link : the TssM cytoplasmic domain connects membrane and baseplate complexes.*

Institut Pasteur Minisymposium Bacterial Membranes, Paris, France, 2015 April 3

Ecole thématique de microbiologie moléculaire (7th Edition), Carry-Le-Rouet, France, 2014 October 6-10

3rd Molecular Microbiology Meeting, Wurzburg, Germany, 2014 May 7-9. *Poster: Interaction network during assembly of the type VI secretion system tail sheath/tube.*

Preamble

Humanity is a mystery. Since the very beginning, we have tried to understand why we are here and where we come from. On one hand soft sciences are dedicated to this purpose; on the other hand I think hard sciences do so. Maybe we have to look deeper around us and we will finally understand that "the essential is invisible to the eye". When I started to open my eyes, I was stunned and fascinated by the microbial world. Microbes are everywhere, all around, within and essential for us. We need them. They do not live alone and are able to build sophisticated interaction networks. Bacteria are social one-cell organisms and communicate to survive with each other. They can also be virulent and cause infections and diseases. These are why I chose microbiology. I wanted to understand the unrevealed world that is microbiology and more specifically molecular microbiology.

My PhD work focused on the Type VI secretion system (T6SS). The T6SS is a multiprotein apparatus that delivers toxin effectors directly into both prokaryotic and eukaryotic cells in a contact-dependent manner. At the molecular level, it is composed of three sub-complexes: a "contractile tail" assembled on a platform called "baseplate", which is anchored to the cell envelope by a "membrane complex". By delivering toxins into competitor cells, the T6SS participates in reshaping microbial communities.

In the introduction, I will first define what are bacterial communities, and the different types of interactions that bacteria have developed with each other. I will then emphasize on competitive behaviors, and will describe the T6SS: its role in bacterial antagonism, its architecture and its biogenesis. Finally, I will describe my work on the TssM protein as well as studies in which I have participated in the *Results and Discussion* part. The last part, *General conclusion and Perspectives*, will recapitulate the results and will discuss them in a more broad vision of the T6SS.

Part I

Introduction

Chapter 1

Microbial communities

A bacterium is a unicellular organism and exhibits all properties of life. However, bacteria are a social microorganisms and are rarely found as isolated cells. At one point, the bacterium divides, and its growth yields to the formation of a colony. A colony is a group of bacteria growing on the same medium from a single ancestor. Although each cell within a colony is issued from a common ancestor, the heterogeneity in gene expression is likely to give a colony assembled from distinct individuals. We can then define a bacterial colony as the first level of organization or the simplest microbial community. More widely, a microbial community is a group of microorganisms that shares a common living space. Microbial communities bear different names: consortium, biofilm, microbiome, etc. Why are there so many words to describe a group of microorganisms? In fact, depending on specific criteria such as the level of association and the link between cells, each type of community has a precise purpose and a proper functioning.

For example, a microbial consortium corresponds to two or more microbial groups living symbiotically; a biofilm is a multicellular community that adheres to a surface and in which bacteria stick together, embedded into an extracellular matrix. It can be more or less complex and is usually symbiotic. These two types of microbial associations are different from the microbiome, now a byword for microbiota, which is an ecological community of symbiotic, commensal and pathogenic microorganisms found on or within a multicellular organism, called the host (plants or animals). The symbiosis is the common factor between almost all microbial communities. However, the microbial population that forms the community can interact in different ways (*cf Chapter 1.2*). The following paragraphs will describe the main bacterial associations. I will define each association and will describe its principal characteristics and well-known examples.

1.1 Happy Together

1.1.1 Consortia

A consortium is a term introduced by Johannes Reinke in 1872 to denote the mutual relation between the organisms, which turns them into a unity. The concept of consortium has a slightly more specific contemporary usage in microbiology, where it marks the groups of functionally related species. A more recent definition, given by Radu Popa is *"a consortium is an association of*

microorganisms from different species living in metabolic interdependence" (Popa, 2004). A consortium could be then considered as a group of microorganisms that works together to fulfill certain biochemical transformation of the substrate (Caron, 2000)(Brenner et al., 2007). According to another description, a consortium is a *"spatial grouping of bacterial cells within a biofilm in which different species are physiologically coordinated with each other, often to produce phenomenally efficient chemical transformations"* (Elvers and Lappin-Scott, 2004). These occurrences can be seen as special cases of the same concept. A consortium can therefore be defined as a group of organisms in physical contact and participating to a common biological or biochemical process (Kull, 2010).

Microbial consortia might be involved in very distinct biological processes ranging from sewage treatment to marine nitrogen cycling. Fascinating examples are phototrophic consortia, which have been discovered by Robert Lauterborn at the beginning of the last century (Lauterborn, 1906). These associations between a colorless central rod-shaped bacterium and several cells of green-or brown-coloured epibionts have been reported in numerous stratified lakes worldwide (Glaeser and Overmann, 2003)(Overmann et al., 1998). An epibiont is an organism that lives on the surface of another living organism. Phototrophic consortia are unique in the microbial world as they are highly ordered structures. Overall, seven different morphotypes of motile phototrophic consortia have been repeatedly observed, and are distinguished according to the colour and shape of the epibionts and the presence of intracellular gas vesicles (Overmann and Van Gemerden, 2000). The best-characterized phototrophic consortium is the one named *Chlorochromatium aggregatum* (Overmann and Van Gemerden, 2000): the coloureless bacterium is surrounded by up to 69 green-coloured rod-shaped bacteria (Figure 1.1). The central rod was shown to be a β-proteobacterium (Fröstl and Overmann, 2000) that is monopolarly flagellated (Overmann et al., 1998). The consortium exhibits phototaxis: when it enters darkness, the green-coloured bacteria sense the light and the central cell reverses direction back into the light (Fröstl and Overmann, 1998). Although the mechanistic bases for this process are not yet described, a rapid communication must therefore occur between the nonmotile light-sensing epibiont and the motile colourless central bacterium.

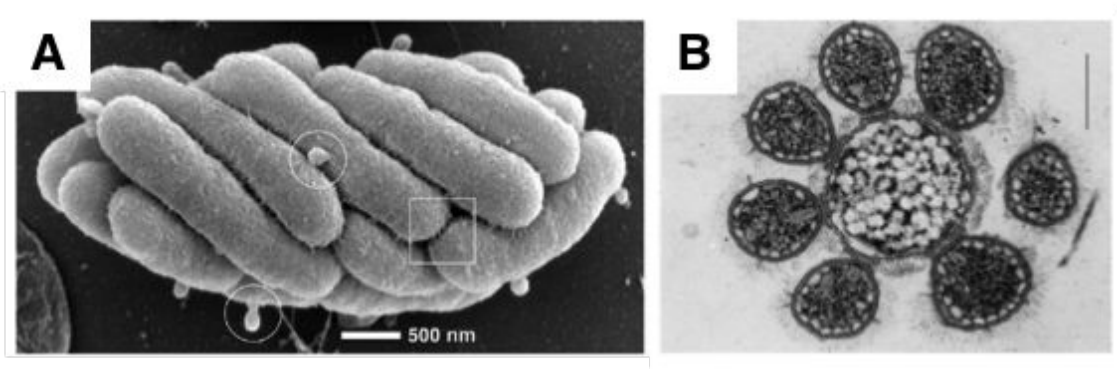

Figure 1.1: **The *Chlorochromatium aggregatum* consortium. (A)** Scanning electron microscopy imaging of *Chlorochromatium aggregatum* showing the epibionts tightly packed; the cell surface appears rough and exhibits numerous thin filaments interconnecting neighboring cells (frame). Epibionts exhibits numerous bulb-shaped protrusions (circles) (Wanner et al., 2008). **(B)** Negative-stain electron microscopy transversal section of *Chlorochromatium*. The central cell is an anaerobic heterotroph, and the seven peripheral cells are green sulfur bacteria showing their photosynthetic vesicles in the cell periphery. Scale bar, 0.5 μm (Fenchel, 2002).

How the different cells communicate has been suggested by the characterization of the ultrastructure (Wanner et al., 2008). Long, hair-like filaments connect epibionts and periplasmic tubules extend from the outer membrane of the central bacterium toward the cell surface of the epibionts. It has been thus hypothesized that the two bacteria share a common periplasmic space.

Direct exchange has not been yet characterized in this case, but it has been visualized for an artificial consortium. Indeed, bacterial consortia could be now engineered, based on known properties of microorganisms (Figure 1.2). A recent publication from one of the teams of our institute showed that two anaerobic bacteria, *Desulfovibrio vulgaris* and *Clostridium acetobutylicum* are able to grow in co-culture (Benomar et al., 2015). These two strains make physical contacts to exchange cytoplasmic molecules when starved: fluorescence microscopy experiments showed that calcein, GFP and mCherry are bidirectionally exchanged. Another group has reported a similar direct communication between bacteria. Pande et al. synthetically engineered cross-feeding interactions within and between two bacterial species, *Acinetobacter baylyi* and *Escherichia coli*. They showed that membrane-derived nanotubes allow to bidirectionally exchange amino-acids (Figure 1.2) (Pande et al., 2015).

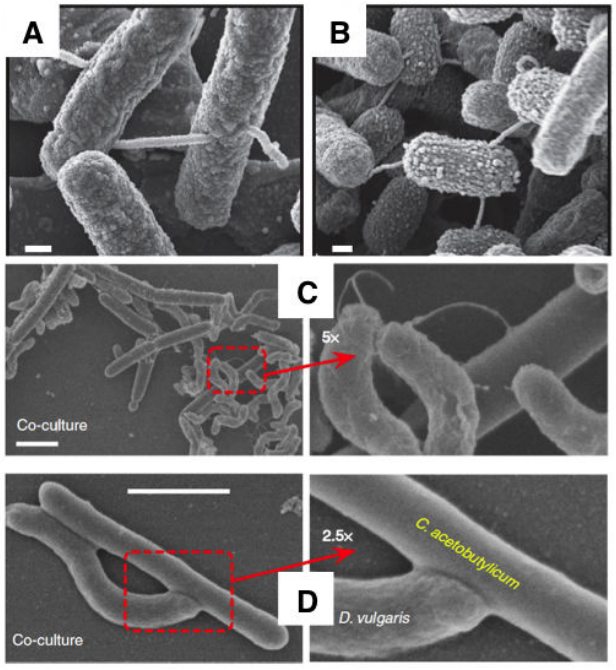

Figure 1.2: **Artificial consortia that exchange cytoplasmic contents. (A-B)** Scanning electron microscopy images showing nanotubular structures that connect two cross-feeding genotypes of *E.coli* cells **(A)** and between *A. baylyi* and *E. coli* **(B)**. Scale bar, 0.2 μm (Pande et al., 2015). **(C-D)** Scanning electron microscopy images of *D. vulgaris* cells in close contact with *C. acetobutylicum* cells. Scale bar, 1 μm (Benomar et al., 2015).

The study of simple microbial communities is undeniably essential to decipher higher or more complicated communities. We are still learning how bacteria can exist in adverse environments and how they help each other.

1.1.2 Biofilms

Microbial communities can reach a higher level of structuration with a temporal and spatial organization, termed biofilms (de Vos, 2015). Biofilms are populations of microorganisms that aggregate at an interface (usually solid-liquid) and that are typically embedded within a matrix comprising exopolysaccharides (EPS) and DNA (Hall-Stoodley et al., 2004). Biofilms are found ubiquitously in natural environments and can be responsible for chronic infectious diseases.

In natural environments, biofilms have many different aspects but usually form similar structures (Figure 1.3). In quiescent saline and hydrothermal waters, cyanobacteria assemble typical biofilms called stromatolites, a mushroom-like structure formed by layers of cyanobacteria and entrapped sediments (Dupraz and Visscher, 2005). In flowing waters, filamentous biofilm microcolonies form streamers. They are attached to the surface by one side while the other can oscillate in the current (Stewart, 2012). Another example is periphyton, an assemblage of organisms (algae, cyanobacteria, bacteria and fungi) attached to and living on submerged solid surfaces in natural environments such as rivers (Wu et al., 2014).

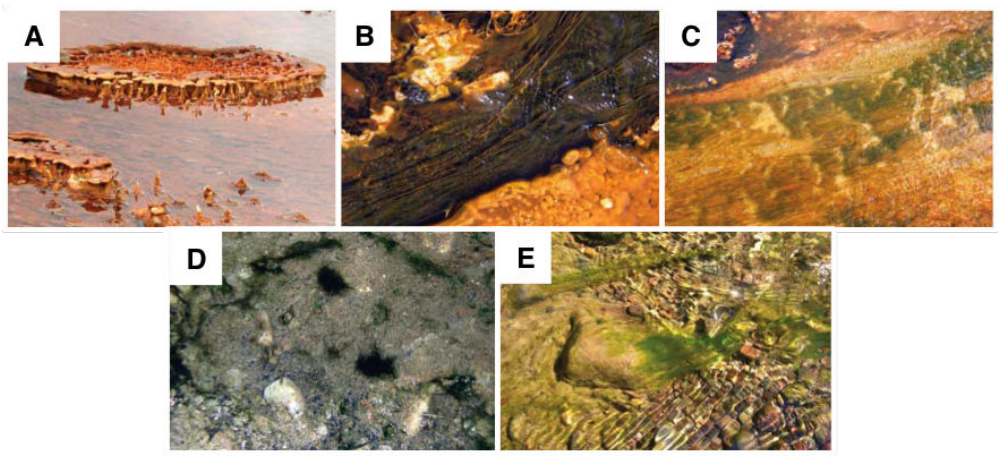

Figure 1.3: **Biofilms from natural environment growing in hydrothermal hot springs (A-C) and freshwater rivers (D-E).** In quiescent environment, biofilms tend to form circular structures such as mushrooms **(A)(D)** whereas in faster flows they form streamers **(B)(E)** and ripple structures **(C)**. Biofilms are from The Biscuit Basin thermal area (Yellowstone National Park, USA) **(A-C)**, Gardener River (Yellowstone National Park, USA) **(D)**, and Hyalite Creek (Bozeman, Montana, USA) **(E)** (Hall-Stoodley et al., 2004).

The best characterized example of biofilm is the one forms by the aggregation of bacteria on surfaces. Biofilm development follows five successive stages (Stoodley et al., 2002)(Beloin et al., 2008) (Figure 1.4). Stage 1 is referred as the "initial attachment" of cells to the surface. The motility is important for adhesion to surfaces as it helps bacteria to find the adequate surface. Then, flagella or surface adhesins such as curli (in the case of non-motile bacteria) play a role in addition to the physicochemical and electrostatic interactions that occurs between bacteria and surfaces. Stage 2 corresponds to the beginning of exopolysaccharides EPS production that results in "irreversible" attachment to the surface. The contribution of adhesive organelles of the fimbrial family such as type 1 fimbriae (or pili), curli and conjugative pili at this stage is well established. Stage 3 represents

the early development of biofilm architecture. Autotransporter adhesins (a subfamily of Type V secretion systems) participate in the establishment of the matrix. The biofilm matrix contains mainly water, but also EPS, proteins, nucleic acids, lipids, nutrients and metabolites. Stage 4 is the maturation of biofilm architecture. The matrix is totally formed and has its structural and protective role, channels and pores are generated within the biofilm to allow exchange of information and molecules. After an extended incubation, biofilm development reaches stage 5 or dispersion. Single cells detach from the biofilm reverting to the planktonic mode, which will form a new biofilm, somewhere else (Figure 1.4).

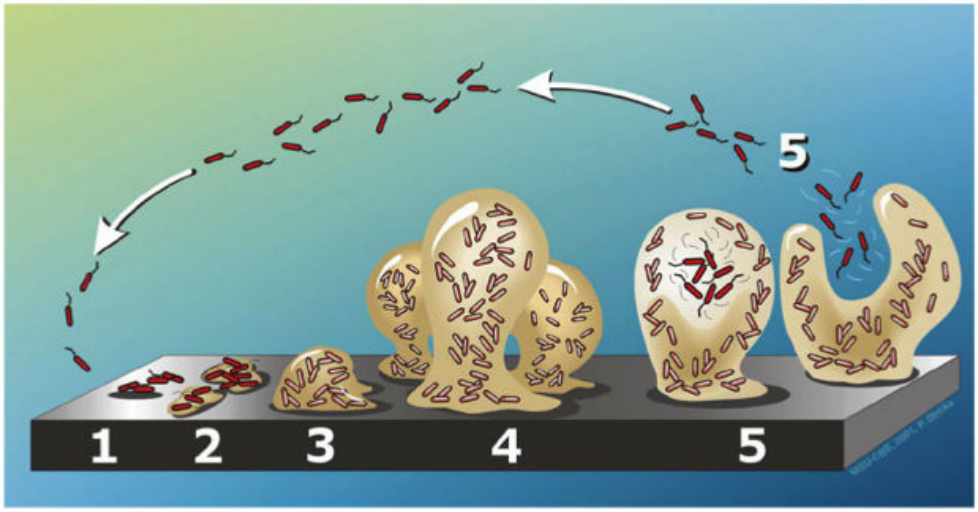

Figure 1.4: **Biofilm development is a five-stage process.** Stage 1: initial attachment of cells to the surface. Stage 2: production of EPS resulting in more firmly adhered "irreversible" attachment. Stage 3: early development of biofilm architecture. Stage 4: maturation of biofilm architecture. Stage 5: dispersion of single cells from the biofilm (Stoodley et al., 2002).

Biofilm formation is a tightly regulated process. The transcriptional landscape and physiological changes occur in order to allow the transition between each stage (Sauer et al., 2002). Several regulatory systems are implicated in sensing the environment, and controlling the expression of different sets of genes. As examples, we can briefly cite the two-component CpxRA system that senses envelope stresses via the CpxA sensor membrane protein and the CpxR cytoplasmic regulator, or the OmpR/EnvZ system that senses osmolarity in the milieu. Small molecules such as the second messager cyclic-di-GMP or the alarmone ppGpp are also part of this regulation with other global regulators such as H-NS or RpoS. More importantly, bacteria communicate between each other in other to synchronize. Quorum sensing is a mechanism that allows bacteria to function as multicellular organisms and to reap benefits that they could never obtain if they always acted as loners (Bassler and Losick, 2006).

While these biofilms might form in the environment, several bacteria are able to assemble biofilms within the host and hence cause chronic diseases. The best characterized examples include *Pseudomonas aeruginosa* that infect the respiratory system of cystic fibrosis patients and even reach lungs, or *Porphyromonas gingivalis* and members of the red complex that are involved in periodontal diseases (Hall-Stoodley et al., 2004). Because the extracellular matrix creates a

protection against the environment, biofilms are usually difficult to eradicate due to their higher ability to resist antibiotic treatments. In addition, biofilms, notably *Staphylococci*, *Streptococci* or *P. aeruginosa* biofilms, can grow in medical devices such as catheters or implants, and hence represent an important cause of infection (Xu et al., 2017)(Gominet et al., 2017).

The biofilm lifestyle is predominant compared to planktonic cells. In the aggregate, bacteria encounter different microenvironments, resulting to heterogeneous populations particularly regarding production of surface proteins and virulence factors, resistance to antibiotics, nutrient assimilation, etc. Because these characters are regulated by the microenvironments, biofilms could be considered as communities of differentiated cells (Stoodley et al., 2002). They can be regarded as a very efficient form of bacterial life because they allow bacteria to synergistically reach structural and functional properties that cannot be possible in a free-living bacterial cell (Flemming et al., 2016) (Sutherland, 2001).

Other biofilm-like structures exist, such as the pellicle, a structure that forms at the liquid/air interface. Pellicule formation has been extensively studied in the Gram-positive model *Bacillus subtilis* but several Gram-positive bacteria are also able to build a floating biofilm such as *E. coli*, *Pseudomonas*, *Salmonella* and *Vibrio* species (Armitano et al., 2014). Based on the genetic understanding of well-known organisms combined with their abilities to naturally degrade hydrocarbon, films of bacteria at interfaces might also be exploited in bioremediation in the future (Vaccari et al., 2017)

1.1.3 Microbiomes

A microbiota is a microbial community that shares a common and specific ecosystem. The term "microbiome" is now a byword for microbiota but was initially defined as the genetic material encoded by all members of the microbiota. I will describe in this paragraph two examples of microbiota that are well characterized.

The human body hosts a myriad of microorganisms named "human microbiome". At the beginning of the 21st century, the human microbiome was "*as much an unexplored frontier as the collection of life found at deep-sea thermal vents if not more*" (Relman, 2001). At that time, we had no idea of the composition and the variability of this myriad of microorganisms. A review even called the gut flora as the "forgotten organ" (O'Hara and Shanahan, 2006). A scientific "Consortium" was created in order to fill this gap, and the idea of a "Human Microbiome Project" emerged. In 2012, a study laid on the characterization of samples from different body habitats: gastrointestinal, urogenital, nasal, oral and skin. This work was unique as samples were taken from a large variety of individuals (The Human Microbiome Project Consortium, 2012). The analyses revealed that the diversity of the human microbiome is unique to each individual and that it is strongly determined by microbial habitat. They also defined the metabolic pathways of the microbial population and concluded that they remain stable within a healthy population while microbial taxa vary.

Recent estimations have shown that the human body is composed of $3x10^{13}$ eukaryotic cells and $4x10^{13}$ bacteria (Sender et al., 2016). The colonization of the human body starts very early

(*in utero*) and expands rapidly after birth. The composition of the microbiota is derived from the opportunistic colonization by the first bacteria to which the baby is exposed in its environment. It is highly variable during the first year of life (Palmer et al., 2007) but reaches a stable composition after 3 years of age (Yatsunenko et al., 2012). The instability during this period makes the bacterial community more sensitive to variations in the environment. Recently, it has been suggested that this period represents a "window of opportunity" for immune education (Gensollen et al., 2016) that will leave a durable imprint. Nevertheless, it is admitted that the microbiota influences host physiology and immunity. Indeed, the alteration of the composition of the gut microbiota, known as dysbiosis, occurs in many diseases including cardiovascular diseases, colitis, malignancy, type 2 diabetes mellitus, obesity, psychiatric disorders, asthma, numerous immune disorders and in elevated blood pressure diseases (Marques et al., 2017). The composition is closely influenced by lifestyle factors such as diet, which suggests that the gut microbiota and its metabolites might be as important for determining or preventing human diseases (Figure 1.5)(Marques et al., 2017).

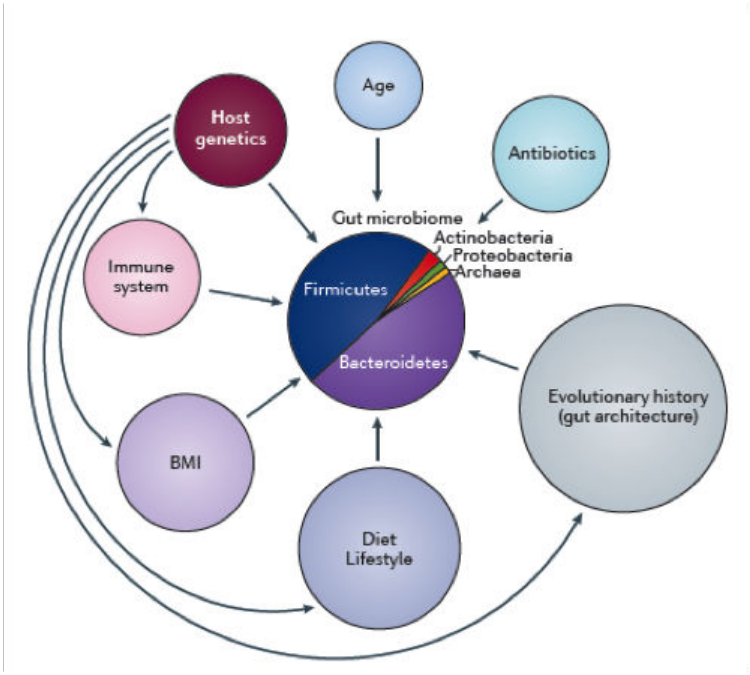

Figure 1.5: **Major factors influencing the composition of the gut microbiome.** Gut architecture is genetically defined, and phylogenetically related species tend to have more similar gut microbiomes than distantly related species. Diet and lifestyle are likely the largest causes of inter-individual variation in the composition of the gut microbiome in humans. Host genetic variants contribute to aspects such as gut architecture, diet, body mass index (BMI) and immune system activity. Antibiotic usage can also have marked effects on the composition of the gut microbiome. Age also has specific effects on the diversity and richness of the gut microbiome (Hall et al., 2017).

Across host species, a handful of bacteria and archae have emerged as heritable, and have been shown to associate with host genes related to immunity and diet (Goodrich et al., 2016). Indeed, classic twin studies have been used for decade to estimate the importance of genetic versus environmental influences on complex trait variations. Based on the comparison of resemblance in monozygotic twins (who share 100% of the genes across their genome) and dizygotic twins (who share on average 50%), it has been suggested that certain host genetic variants predispose an

individual toward microbiome dysbiosis (Hall et al., 2017).

In addition to environment and genetic influences, the biogeography can affect the development and maintenance of the microbiota (Figure 1.6). Bacterial communities form in microhabitats and are stratified within the gut on different scales and axes. These microhabitats such as crypts, the inner mucus layer, and the appendix are reservoirs of bacterial diversity. They facilitate immune homeostasis, protect commensal species from competitors and re-seed the gut microbiota after the bacterial community structure is altered or certain species are depleted from the lumen. The understanding of the biogeography within the gut ecosystem and their spatial relationships among microorganisms and between microorganisms and the host is crucial (Donaldson et al., 2015). Undeniably, great advances have been recently made on the human microbiome. But the *modus operanti* of our microbiota is in its infancy.

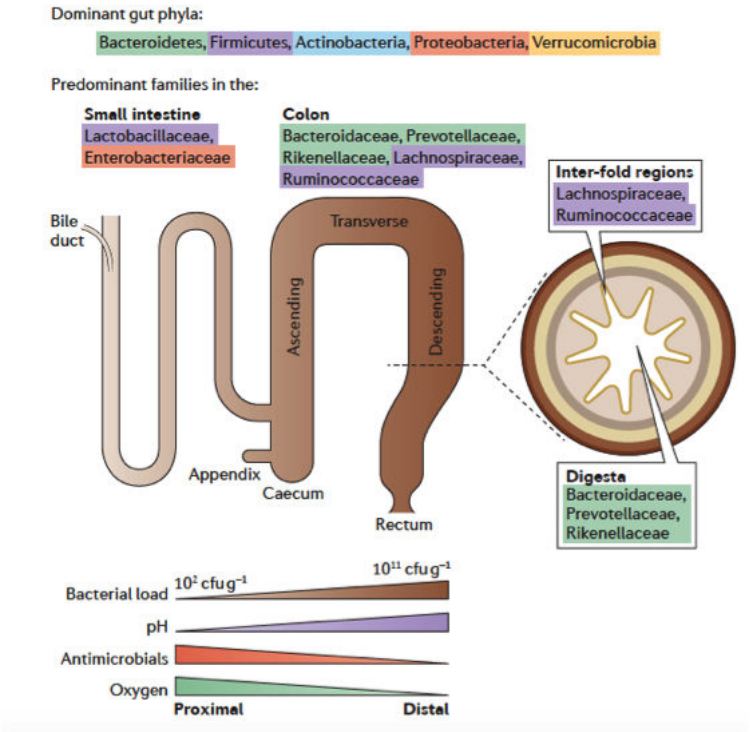

Figure 1.6: **Microbial habitats in the human lower gastrointestinal tract.** The dominant bacterial families of the small intestine and colon reflect physiological differences along the length of the gut. The gradient of oxygen, antimicrobial peptides and pH limits the bacterial density in the small intestinal community, whereas the colon carries high bacterial loads. cfu, colony-forming units (Donaldson et al., 2015).

Another interesting and well-studied example of microbiota is the one associated with the coral. A typical coral comprises three structures: the mucus layer, the coral tissue and the calcium carbonate skeleton (Figure 1.7). The coral hosts an endosymbiotic algae. In addition, each structure of the coral is associated with a distinct bacterial population that provides specific functions: photosynthesis, production of molecular oxygen for efficient respiration, nitrogen fixation, chitin degradation, etc... (Rosenberg et al., 2007). Coral can be attacked by bacterial pathogens that cause coral bleaching. In the case of the *Oculina patagonica* coral, the causative agent of bleaching is *Vibrio shiloi*. At high temperature, *V. shiloi* produces cell surface adhesins to attach to the

coral, and a toxin, Toxin P, that inhibits photosynthesis by the endosymbiotic algae Zooxanthelae (Banin et al., 2001).

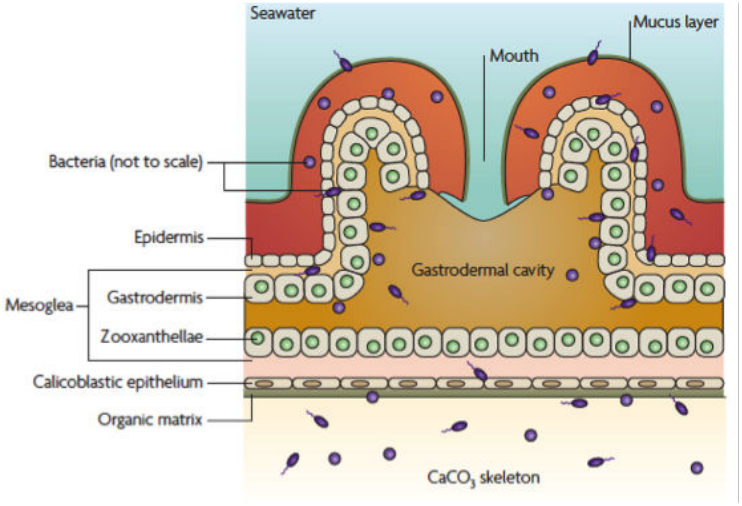

Figure 1.7: **The structure of the coral tissue.** Corals are composed of three structures that provide habitats for bacteria: the surface mucus layer, coral tissue (including the gastrodermal cavity) and the calcium carbonate ($CaCO_3$) skeleton. Zooxanthellae are present in the gastrodermis, shown in green in the figure. (Rosenberg et al., 2007).

Interestingly, although corals lack adaptive immunity system and do not produce antibodies, they develop resistance to the pathogen. It was shown that *V. shiloi* adheres and penetrates the coral but then lyses. This inhibitory property is attributed to bacteria of the *Roseobacter* and the *Pseudoalteromonas* genus (Nissimov et al., 2009). These two genus are known to produce antibiotics (Brinkhoff et al., 2004)(Bowman, 2007); so a cocktail of bacteria with different antibiotic properties could together prevent infection by the pathogen.

This phenomenon has led to the "coral probiotic" hypothesis that proposes the existence of dynamic relationship between corals and symbiotic microorganisms. First formulated by Lynn Margulis in 1991, Zilber-Rosenberg and Rosenberg (Zilber-Rosenberg and Rosenberg, 2008) generalized this hypothesis and retrieved it into the "*hologenome theory of evolution*". The hologenome is defined as the sum of the genetic information of the host and its microbiota. According to the theory, the holobiont should be considered as "a unit of selection in evolution". This idea converges to the "*superorganism theory*" proposed by Wilson and Sober in 1989 (Wilson and Sober, 1989). Indeed, they point out that communities (similarly to individuals) can possess similar properties of functional organization, and therefore be regarded as "superorganisms".

The hologenome theory of evolution is now also associated to humans and its microbiota. Indeed, some scientists raised the hypothesis that we are evolving as a complex system with our microbiome and that any perturbation can cause emerging diseases (Salvucci, 2014).

Then, we can represent our microbiome as double-edged: it is beneficial for us but it can cause severe effects. On one hand, thorough knowledge on the human microbiome will help to understand the links between the human microbiome with our health and disease. One the other

hand, the hologenome theory may help to better understand fitness potential of the holobiont and a deep understanding will aid therapeutic potential of microbiota in human health from the clinical perspective (Singh et al., 2013).

1.2 Interactions between bacteria

To assemble communities, bacteria should communicate, exchange and transfer information. Within the community, bacteria may have neutral, beneficial or antagonistic behaviors. These behaviors are grouped within the term "bacterial interactions" (Faust and Raes, 2012). The possible interactions between two species can be visualized and classified on a wheel (Figure 1.8).

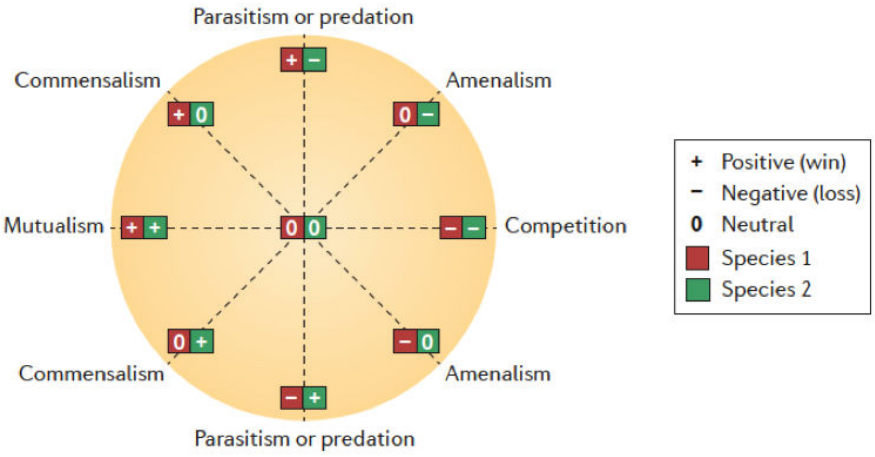

Figure 1.8: **Summary of ecological interactions between members of different species.** The wheel display introduced by Lidicker has been adapted to summarize all possible pairwise interactions. For each interaction partner, there are three possible outcomes: positive (+), negative (-) and neutral (0). For instance, in parasitism, the parasite benefits from the relationship (+), whereas the host is harmed (-); this relationship is thus represented by the symbol pair +/- (Faust and Raes, 2012)

1.2.1 Commensalism and amensalism

The term *commensalism* describes when one partner benefits without helping or harming the other. We can observe commensalism in biodegradation in which commensals cross-feed on compounds produced by other community members (such as in cellulose degradation) (Leschine, 1995).

By contrast, *amensalism* is an interaction in which one partner is harmed without providing any advantage to the other; for example when metabolic by-products of a microbial species alter the environment to the detriment of other microorganisms. *Pseudomonas taetrolens* is a producer of lactobionic acid from carbohydrates contained in dairy products whereas *Lactobacillus casei* classically produces lactic acid. When both strains are present in the same milieu, lactic acid and lactobionic acid are co-produced, hence inhibiting only the lactic metabolic pathways of *P. taetrolens* and its growth (García et al., 2017).

These asymmetric interactions affect unilaterally one species, and one may suspect that they will affect the dynamics of the bacterial community. Mougi used a theoretical approach and showed that commensalism and amensalism greatly increase the stability of the community compared to a symmetrical interaction (such as symbiosis) but less than asymmetric antagonistic interactions (such as competition or predation) (Mougi, 2016).

1.2.2 Parasitism and predation

Parasitism and *predation* are two distinct loss-win interactions. The term predator should be used for organisms that actively hunt to kill their prey and consume their macromolecules as nutrients, while the term parasite should be reserved for organisms that form close associations with their hosts without killing it.

Parasites do not kill their host as they exploit them for the resources necessary for their survival. As an example of parasitism, we can name the well-known relationship between bacteria and temperate bacteriophages. Temperate phages are bacteriophages that display lysogenic life cycles. They penetrate the bacterial cell and integrate their genome into the bacterial DNA to become prophages. Then, the bacterial replication machinery is used to duplicate the phage genome at each cell cycle.

Bacterial predation is well documented thanks to extensive studies carried out on the *Myxococcus* and *Bdellovibrio* genera. But many predatory strains with diverse hunting strategies have been identified, although the mechanistic details of the processes are not known (Pérez et al., 2016). Three different hunting strategies could be distinguished: epibiotic, endobiotic and group attack. In the epibiotic strategy, the predator does not invade the prey, but it remains attached to the outer surface of the cell where it degrades and assimilates the prey molecules. In the endobiotic strategy, the predator invades the prey cell by penetrating either into the periplasm or the cytoplasm. Finally, in the group attack strategy, bacteria move as a pack and melt on the prey to destroy them and grow on the leftovers.

Bdellovibrios include all *bdellovribrio*-like predatory bacteria with the same properties as *B. bacteriovorus*. *Bdellovibrio* is a short rod, motile δ-proteobacterium that is a predatory invader of Gram-negative bacteria (Sockett, 2009). Interestingly, *Bdellovibrio* have been shown to successfully prey upon hosts growing within biofilms (Kadouri and O'Toole, 2005) and also on prey that are encapsulated (Koval and Bayer, 1997). It has been shown that flagellar motility is important to hunt prey but not required to enter prey cells (Lambert et al., 2006a) and that the type IV pili plays a critical role (Evans et al., 2007). Once inside, predatory strains replicate within the periplasm (Figure 1.9) in a structure known as the bdelloplast, a sealed environment that protects against competition by other bacteria. It is worth to note that *Bdellovibrio* cannot replicate except inside the prey cell. The bacterium proceeds through a coencytic development process, septating to yield several progeny. During growth inside the bdelloplast, *B. bacteriovorus* uses prey molecules for its own biosynthesis and reproduction (Lambert et al., 2006b). Genome sequencing has revealed genes encoding the enzymatic players in the hydrolytic process. As an example, the breakdown of the prey's nucleic acids conducts to their assimilation into the newly-synthesized *Bdellovibrio* nucleic

acids (Matin and Rittenberg, 1972)(Rosson and Rittenberg, 1979). The fascinating molecular details of *Bdellovibrio* development in the bdelloplast is just starting to be delineated and many questions remain unanswered such as how attachment to the prey is mediated or how the bacteria cross the prey outer membrane to enter the periplasm.

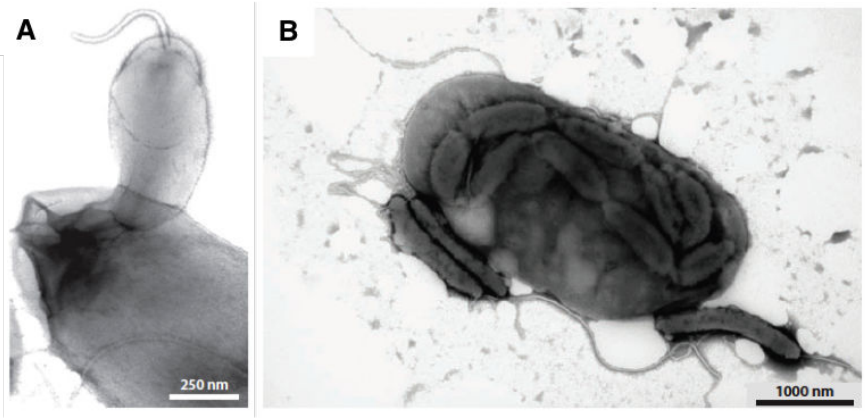

Figure 1.9: ***Bdellovibrio* invasion.** Electron micrographs showing **(A)** Narrow entry point of *Bdellovibrio* into the *E. coli* prey periplasm (Evans et al., 2007). **(B)** Replication of *Bdellovibrio* within the prey (Sockett, 2009).

Myxococcus xanthus is a well-studied predatory bacterium. *M. xanthus* has a complex life cycle and is considered as a model system for bacterial social behavior (Zhang et al., 2012b)(Keane and Berleman, 2016). This bacterium has the ability to move in order to colonize new territory thanks to two motility systems: the "social" (S-) motility and the "adventurous" (A-) motility. S-motility, or twitching motility, is characterized by the swarming movement of large cell groups and it is stimulated by cell-cell proximity (Shi and Zusman, 1993). It allows movement on soft and wet surfaces and it is known to be crucial for cooperative predation. Fibrils, the lipopolysaccharide and the retractile type IV pili are the extracellular components associated with this motility (Muñoz-Dorado et al., 2016). The A-motility system is a distinct process. A-motility or gliding motility drives the movement of single cells at the swarm edges. The A-motility cells glide slowly to explore new environments, change direction though reversal events, and leave behind extracellular matrix slime trails that may be followed by other cells (Ducret et al., 2012) (Muñoz-Dorado et al., 2016). Cells can then individually move on hard agar (Wolgemuth et al., 2002). *M. xanthus* penetrates prey colonies and lyses prey cells (Figure 1.10) using various secreted compounds (Dworkin, 1996). By contrast to *Bdellovibrio*, *M. xanthus* does not penetrate within the prey cell. However, it is able to kill both Gram-positive and Gram-negative bacteria. The roles in predation of the two motility systems are imprecise, but it seems that both A- and S- motility mechanisms are required for efficient predation (Pham et al., 2005) (Berleman and Kirby, 2009). The detailed mechanisms of prey sensing, prey attack and prey lysis are not yet defined.

1.2.3 Mutualism and competition

Bacteria may cooperate. These win-win relationships that are grouped under the term *mutualism*, which could be also called *cooperation* or *symbiosis*. However, symbiosis is also used in a broader

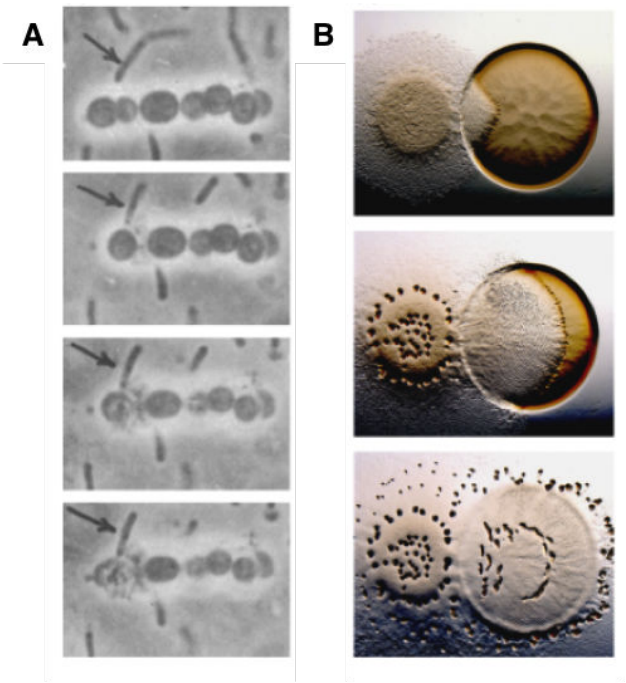

Figure 1.10: ***Myxococcus xanthus* predation.** Time course of **(A)** solitary predation by *M. xanthus* on cyanobacteria cells. The cyanobacterial species can be observed as a chain of large, spherical cells (Shilo, 1970). **(B)** *M. xanthus* invading and lysing a colony of *Escherichia coli* prey (Berleman and Kirby, 2009)

.

sense to include all ecological relationships whereas cooperation designates mutualism between single organisms rather than populations. The best examples of mutualism are the ability of bacteria to build a biofilm, which confers resistance to antibiotics, phages, and toxic compounds, and the exchange of metabolic products between two species to the benefits of both. I have already described two examples of mutualism in the previous paragraphs: biofilm formation, as well as the *Chlorochromatium aggregatum* consortium.

In the opposite, competition is a loss-loss interaction. The law of competitive exclusion indicates that two species with similar niches exclude each other. When two strains compete, there is formation of area of exclusion. The exclusion area between two colonies is called Dienes line (Senior, 1977). This phenomenon has been well-studied by the Karine Gibbs lab using *Proteus mirabilis* as it differentiates between self and non-self and shows a territorial behaviour. Indeed, *Proteus mirabilis* is capable of movement on solid surface using a swarming motility. It has also the ability to distinguish between self and non-self isolates. When it recognizes the other as foreign, it does not merge and forms Dienes lines (Gibbs et al., 2008). This social recognition is dependent on the *ids* and *idr* clusters (Gibbs et al., 2011). It has been shown that the Ids and Idr proteins are linked to the T6SS (Wenren et al., 2013)(Figure 1.11). Microscopy experiments have shown that Dienes lines results from T6S-mediated activities leading to lysis of non-self bacteria (Alteri et al., 2013). It is proposed that the entire population indiscriminately uses the T6SS to deliver effectors during its growth in order to maximize the cooperation, to acquire new resources or to get away from predators.

Indeed, the main purpose of interbacterial killing is to eradicate competitors in their own niche. A recent paper showed by mathematical modeling and experiments that *V. cholerae* favours evolu-

tion of public goods cooperation. Competition has a twin role: causing death to local competitors while creating good conditions for kin (McNally et al., 2017).

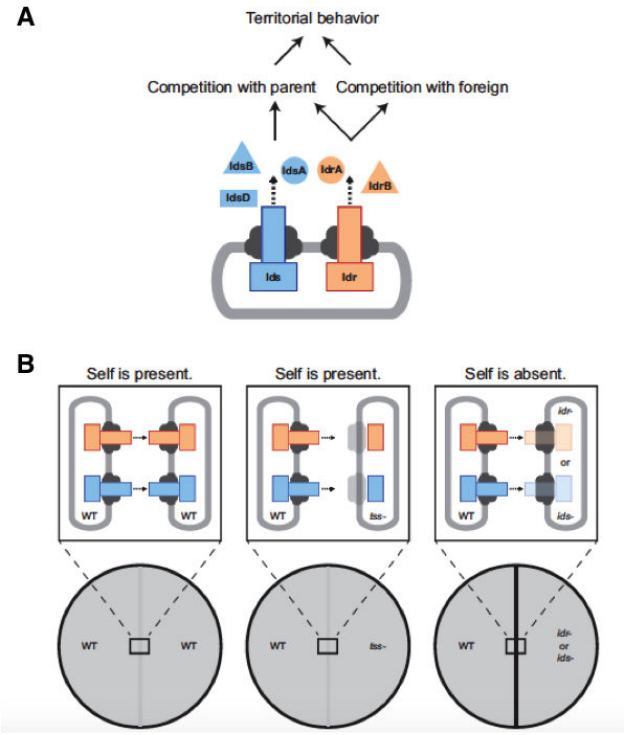

Figure 1.11: **Model for Ids and Idr functional roles in self-recognition. (A)** Functional flow chart for the roles of the Ids, Idr, and T6S proteins in self-recognition and territorial behaviors. A subset of Ids and Idr proteins are primarily exported via a shared T6S system (tss) and are necessary for competition on surfaces with the parent strain. Idr proteins are also needed for competition against foreign strains. **(B)** Model for self-recognition predicts that the combined actions of interactions between cognate Ids and Idr proteins between two neighbouring cells result in the determination that self is present, ultimately resulting in the merging of two swarms. Expression of the self-recognition components within the cells is sufficient, though in wild-type strains, some of these components are exported from the cell by a T6S system. In contrast, absence of one or more of the Ids and Idr self-recognition systems leads to the determination that self is absence of one or more of the Ids and Idr self-recognition systems leads to the determination that self is absent and ultimately to boundary formation (Wenren et al., 2013).

The next chapter will specifically describe the mechanisms and the actors of interbacterial competition.

Chapter 2

Interbacterial competition

In the environment, bacteria live in complex multispecies communities. In these communities, bacteria communicate and compete with one another for colonization and survival. They have developed several strategies as diverse as the competitors they encounter.

Competitive interactions are achieved indirectly by utilizing the nutrient resources to increase the grow rate at the detriment of the other species (Hibbing et al., 2010). Competition can also be achieved directly by (i) the production of diffusible antibacterial molecules such as antibiotics, lantibiotics and bacteriocins, secreted enzymes, metabolites and outer membrane vesicles (OMV) (Kommineni et al., 2015)(Riley and Wertz, 2002) or (ii) contact-mediated mechanisms such as exchange of outer membrane material, or specialized machines such as contact-dependent inhibition (CDI) or Type VI secretion system (T6SS)(Stubbendieck and Straight, 2016) (Figure 2.1). Beside these mechanisms developed by bacteria, bacteria are used as hosts by phages, which also indirectly participate to inter-bacterial competition.

I will describe in the next chapters the main actors of bacterial competition in Gram-negative Proteobacteria: colicins, phages, CDI and T6SS; emphasizing their mechanism of action, their structure and assembly as well as their role in microbial communities.

2.1 Generalities

Competition for a limiting resource can been categorized into two broad mechanisms: *scramble* and *contest* (Nicholson, 1954).

- Scramble competition, also called *exploitation competition*, involves the rapid use of the limiting resource without direct interaction between competitors. This competition is passive in the sense that one strain deprives the others of a resource (such as a nutrient or habitable space). In this case, the other strains will be outcompeted by the rapid growth of the cheater.
- Contest competition, also called *interference competition*, involves direct, antagonist interactions between competitors. After destroying the other strains, winners appropriate the available resources for its own growth. In this competition, one competitor actively harms the other, such as by delivering toxins (Hibbing et al., 2010).

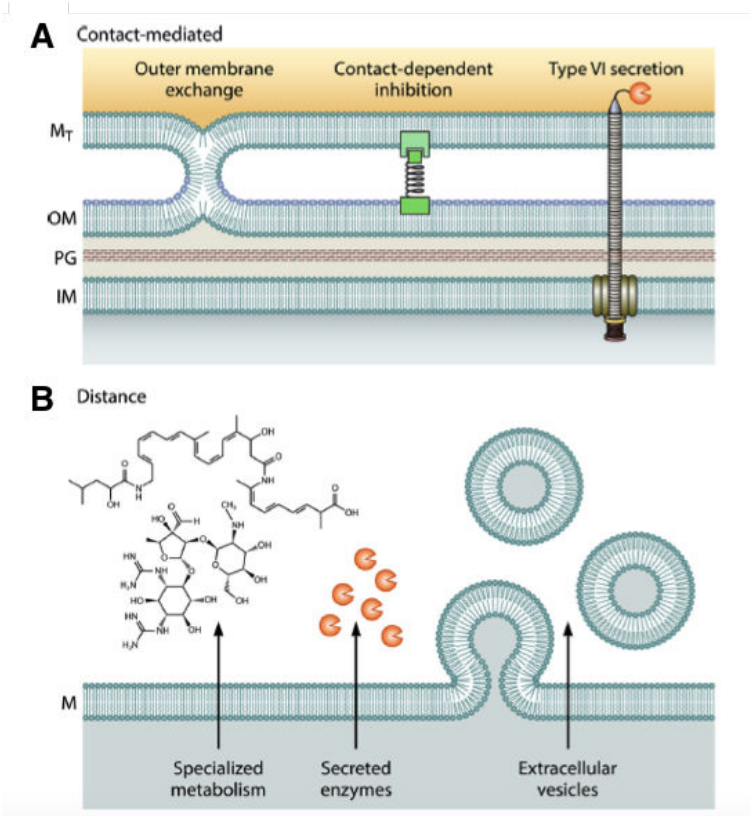

Figure 2.1: **Summary of mechanisms used in bacterial competition. (A)** Contact-mediated mechanisms involve either direct contact between cell envelopes (OME) or are facilitated by protein complexes (CDI and T6SS). In the case of CDI and T6SS, toxic effectors (square or wedged circle) are delivered into the target cell. **(B)** Bacteria compete at a distance using SMs (examples shown are bacillaene and streptomycin), secreted enzymes such as bacteriocins, and extracellular vesicles. CDI, contact-dependent inhibition; EVs, extracellular vesicles; M, membrane; MT, target cell membrane; IM, inner membrane; OM, outer membrane; PG, peptidoglycan; T6SS, type VI secretion system (Stubbendieck and Straight, 2016).

2.2 Specialized metabolites and secreted enzymes

The most intensively studied mechanism of bacterial competition is the production of small antimicrobial compounds (a subset of secondary metabolites). Specialized metabolites (SMs) previously called "secondary" metabolites are molecules produced by bacteria that are not involved in primary metabolism but are involved in other biological processes (Davies, 2013). In the context of competitive interactions, SMs are those affecting the growth and development of competing bacteria. Although some recent literature calls into question the role of antibiotics as bacterial growth inhibitors in the environment (Yim et al., 2007), extensive studies on a number of antibiotics have verified their importance in mediating competition (Chao and Levin, 1981). For instance, antibiotics provide some of the clearest mechanistic insights into chemical interactions between competing bacterial species. The biological functions of the SMs are numerous and largely unknown.

As mentioned above, exploitation competition can rise from direct consumption of nutrients, buildup of toxic waste products, or the activity of SMs. Siderophore production is an example of SMs implicated in exploitation competition (Figure 2.2). Siderophores are iron-scavenging molecules. They are produced and released in the environment to chelate external iron that is then imported as a complex into the producer cells (Wandersman and Delepelaire, 2004). Iron is

essential for bacterial respiration and metabolism as it is required for the biogenesis and the activity of cytochromes and iron-sulfur proteins. Many bacterial species are able to use heterologous siderophores, and hence sequester iron away from the siderophore producer. Siderophore-mediated competition relies also on differences in the iron-binding affinities. For example, when co-cultured with *Pseudomonas aeruginosa*, *Burkholderia cenocepacia* produces ornibactin siderophores. They sequester so much iron that *P. aeruginosa* expresses genes that are up-regulated in iron starvation and then will grab the ornibactin siderophores from the milieu (Weaver and Kolter, 2004). The smarter mechanism is developed by some species, called social cheaters, that have lost the ability to produce siderophores but have maintained the capacity to take them up (West and Buckling, 2003).

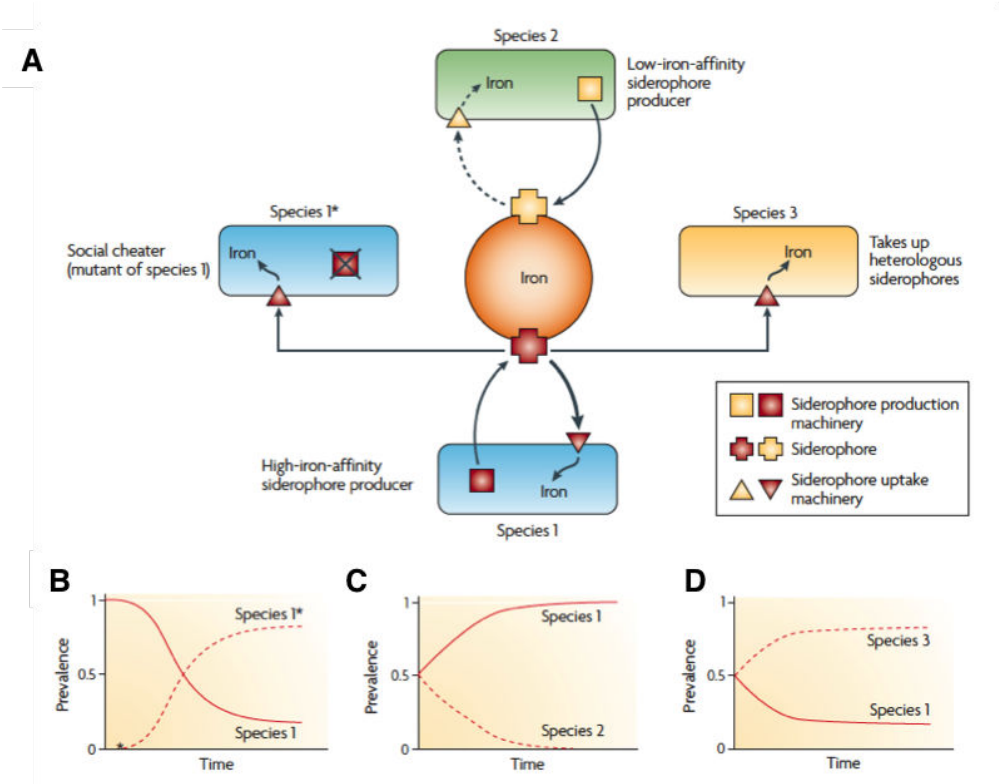

Figure 2.2: **Simplified models of siderophore-mediated bacterial competition. (A)** Three competitive scenarios in iron-limiting conditions in which the use of a siderophore is necessary for iron acquisition. Species 1* represents a cheater of species 1 that has lost the ability to produce siderophores but that maintains the ability to use siderophores that are produced by cooperating individuals. Species 1 produces a higher-affinity siderophore than species 2, which allows species 1 to monopolize the available iron. Competition between species 1 and 3 is analogous to that between species 1* and 1, but species 3 has evolved the ability to use the heterologously produced siderophore from species 1, having never had the ability to produce this siderophore itself. **(B-D)** The predicted outcome of competition between the indicated species (Hibbing et al., 2010).

Another involving iron is exemplified by the *P. aeruginosa*/*Staphylococcus aureus* pair. *P. aeruginosa* has the ability to lyse *Staphylococcus aureus*, liberating free iron. But *S. aureus* also competes with *P. aeruginosa* for free iron. It has been shown that in presence of *S. aureus*, and in iron-limited conditions, *P. aeruginosa* increases siderophore production and cheat selection, whereas siderophore production is downregulated and cheats evolve less readily in the absence of

S. aureus or in free iron culture (Harrison et al., 2008).

Bacteria produce many SMs, representing a huge chemical diversity with unknown function (Davies and Ryan, 2012). The effects of SMs on the development of a bacterial species have been reported in several studies, but the mechanistic bases for the competition or inhibition are usually not known. As an example, 2,4-diacetylphloroglucinol that is produced by *Pseudomonas protegens* inhibits the cellular differentiation of *Bacillus subtilis* (Powers et al., 2015).

One additional strategy is the interference of SMs with quorum sensing and thus the disruption of subsequent downstream processes linked to on communication between competitor cells (Teasdale et al., 2009)(Kwan et al., 2011).

In addition to the production of specialized metabolites, bacteria also secrete enzymes that are involved in competition. They confer antibiotics resistance or interfere with the development of competing species. Secreted enzymes have many active roles but how bacteria use them to kill or inhibit their competitors is not known. Some degradative enzymes have been shown to cleave acyl homoserine lactones that are used as signal molecules in quorum sensing (Wang and Leadbetter, 2005). In some cases, the degradation products can be used carbon or nitrogen sources for the cheater (Leadbetter and Greenberg, 2000).

2.3 Outer membrane vesicles (OMV)

Outer membrane vesicles (OMVs) are naturally produced from Gram-negative bacteria during growth. OMVs protrude from the outer membrane and are then released into the environment (Roier et al., 2016)(Figure 2.3). These OMVs contain outer membrane and periplasmic components such as lipopolysaccharide (LPS), phospholipids and proteins (Henry et al., 2004) but have been proposed to specifically encapsulate virulence factors (Allan et al., 2003)(Bielaszewska et al., 2017) or DNA (Renelli et al., 2004)(Bitto et al., 2017). Once released, vesicles can encounter another Gram-negative cell and fuse with its outer membrane (Kadurugamuwa and Beveridge, 1999). The cargo components are then delivered into the recipient periplasm. Gram-positive bacteria are also able to produce membrane vesicles but the mechanism is different as they lack an outer membrane (Brown et al., 2015).

OMVs are especially capable of vectoring proteins, lipids, nucleic acids, and small molecules implicated in competition and signaling processes (Berleman and Auer, 2013). These robust proteoliposomes have evolved naturally to be resistant to degradation and provide a supportive environment to extend the activity of encapsulated cargo (Alves et al., 2016). They also facilitate the transfer of hydrophobic molecules across aqueous environments (Mashburn and Whiteley, 2005) such as antibiotics or enzymes. As an example, *Streptomyces lividans* produces OMVs containing an antibacterial compound called prodigiosin (Schrempf and Merling, 2015) whereas *P. aeruginosa* produces peptidoglycan-degrading hydrolases (Kadurugamuwa and Beveridge, 1996).

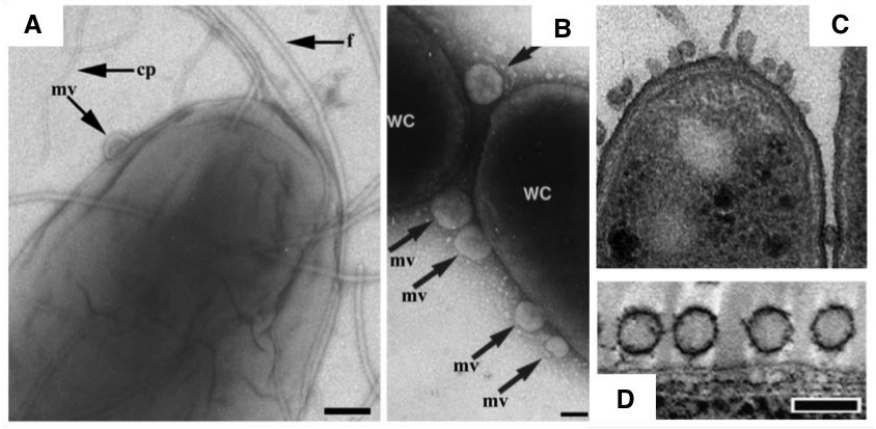

Figure 2.3: **Outer membrane vesicles (OMVs).** Negatively stained whole cells showing vesicles of **(A)** *Burkolderia cepacia* and **(B)** *Serratia marscens*. Mv membrane-vesicle WC;, whole cell; cp; cable pilus; f, flagella. (Allan et al., 2003). **(C)** Vesicles and membrane-blebbing in *M. xanthus* with TEM (Images from Remis and Auer). **(D)** Arrangement of vesicles along the cell membrane in *M. xanthus* cryo-tomography (Palsdottir et al., 2009). Bars= 100 nm.

2.4 Bacteriocins

2.4.1 Generalities

Bacteria produce a broad repertoire of *peptide antibiotics*. These antibiotics could be categorized in three main families based on the length of the peptide chain and on the producer, ranging from lantibiotics to bacteriocins. *Lantibiotics* and *microcins* are short peptides (15-40 residues) whereas *bacteriocins* are composed of a single, large, polypeptide, or of a high-molecular weight complex.

Bacteriocins are one of the most abundant and diverse classes of anti-microbial molecules. They are produced by almost every bacterial species from the Eubacteria and Archaebacteria kingdoms (Chak et al., 1991)(Riley and Gordon, 1992). Bacteriocins are usually produced under stressful conditions and most bacteriocins target strains of the same — or closely related — species, but few have a broader spectrum of targets. Bacteriocins kill rapidly neighboring cells (within minutes) that are non immune (Pugsley, 1984) and appear to mediate population dynamics (Chao and Levin, 1981).

Based on theoretical and experimental studies, a model emerged to explain the biological role of bacteriocins: the rock-paper-scissors model (Kerr et al., 2002). This non-transitive competition network comprises three actors: the producing strain dominates the sensitive strain, which outcompetes the resistant strain (because it does not incur the cost of resistance), which in turn outcompetes the producing strain as it is resistant to bacteriocins and does not incur the cost of production (Figure 2.4) (Hibbing et al., 2010). It is worth to note that the three types of strain persist only when the environment that they inhabit is structured, creating individual niches and suggest that the benefit of bacteriocin production in nutrient depletion environment will offset the cost of production. A study, based on a multispecies system comprising an antibiotic-producing *P. aeruginosa* strain P1, a resistant *Raoultella ornithinolytica* strain R1 and a sensitive *Brevibacillys borstelensis* strain S1, demonstrated the ability of the three species to establish a non-transitive competitive network (Narisawa et al., 2008).

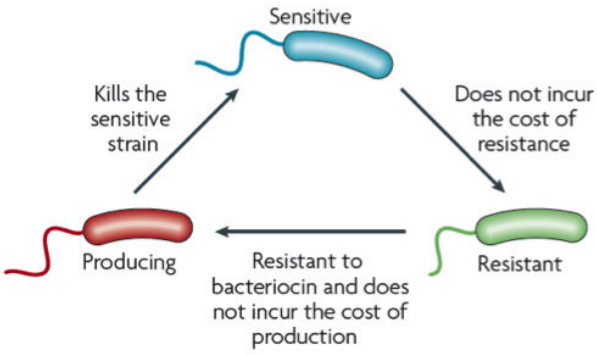

Figure 2.4: **Non-transitive competition network.** A model *Escherichia coli* non-transitive competition network. A strain producing a colicin toxin outcompetes a sensitive strain, which outcompetes a resistant strain, which in turn outcompetes the producing strain (Hibbing et al., 2010).

I will focus on two types of bacteriocins: colicins, which are single-protein anti-bacterial toxins produced by *Escherichia coli* species; and R-pyocins, high-molecular weight assemblies produced by *P. aeruginosa* that use a contractile mechanism to kill competitors.

2.4.2 Colicins

Colicins are anti-bacterial toxins that are released by *E. coli* strains. Colicin genes are present within a operon which also contains the gene encoding the lysis protein (to release the colicin in the milieu) and a gene encoding the immunity protein (which confers self-protection). Once in the environment, colicins bind to a receptor at the cell surface of the target sensitive cell, penetrate the cell envelope using the Tol (group A) or TonB (group B) complexes and then kill the cell by interfering with peptidoglycan synthesis, collapsing the proton-motive force or degrading nucleic acids.

2.4.2.1 Production of colicins

Colicins are produced by strains of *E. coli* that harbor colicinogenic plasmids (pCol). pCol plasmids are classified as type I and type II (Hardy et al., 1973). Type I pCol plasmids are small plasmids of 6-10 kb present in about 20 copies by cell and encode mainly colicins of group A such as colicins A, E1-E9, K, N, 5, and 10. Type II pCol plasmids are 40-kb large monocopy plasmids that usually encode colicins of group B such as colicins B, Ia, Ib, and M.

In agreement with colicin production during stress conditions, colicin operon promoters contain SOS boxes and are therefore under the control of the LexA repressor (Little and Mount, 1982)(Lloubes et al., 1986). The operon is usually constituted of (i) the structural gene for colicin, called *cxa* for colicin X activity, (ii) the gene encoding the immunity protein, designed *cxi* for colicin X immunity, and (iii) the gene encoding the colicin lysis protein, named *cxl* for colicin X lysis (Figure 2.5) (Cascales et al., 2007).

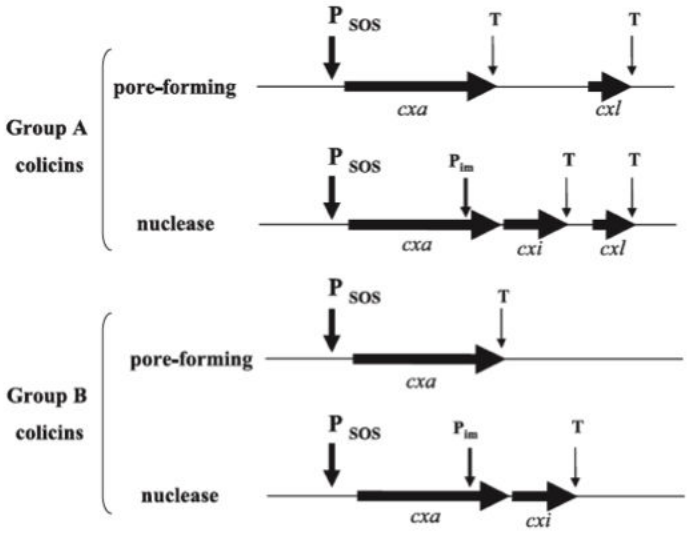

Figure 2.5: **Organization of colicin operons.** The genes are represented by arrowheads. SOS promoters (P_{SOS}), the immunity promoter (P_{im}), and transcription terminators (T) are indicated by arrows. Names of the colicin gene (*cxa*, in which x is specific to the colicin) and its immunity gene (*cxi*) and lysis protein gene (*cxl*) follow the nomenclature (Cascales et al., 2007).

2.4.2.2 Mechanism of action

The release of colicins into the medium is accompanied by the lysis of the producing cell, due to the colicin lysis protein. Colicin lysis proteins are small lipoproteins of 27-35 amino acids. By inserting into the outer membrane, colicin lysis proteins induce the formation of large pores in the outer membrane by the activation of the outer membrane phospholipase A (OmpLA) (Cavard et al., 1987)(Cascales et al., 2007). However, only a subpopulation of the colicin-producing strain will accumulate and release the colicin. Hence, it is considered that cells that release colicins sacrifice for the other cells of the progeny.

Colicins are 600-residue proteins in average, with a maximum of 697 residues for colicin D and a minimum of 271 residues for colicin M (Braun et al., 1994). Colicins are organized into three domains, each corresponding to one step of the colicin mode of action (de Graaf et al., 1978). The central domain binds to the outer membrane receptor of the target cell; the N-terminal domain is involved in the translocation through the outer membrane, while the C-terminal domain specifies the activity (Figure 2.6).

Reception: colicins bind to specific receptors at the surface of the sensitive strains (Fredericq, 1946). Mutations of the gene encoding the receptor lead to the loss of sensitivity to the corresponding colicin. Receptors are usually outer membrane proteins involved in the entry of specific nutrients such as nucleosides, siderophores and vitamins (Chai and Foulds, 1977)(Chai and Foulds, 1979)(Di Masi et al., 1973). The binding of colicins to receptors has been well characterized by genetic, biochemical, biophysical and structural approaches (Figure 2.7) (Housden et al., 2013) (Braun et al., 2002)(Cao and Klebba, 2002)(Lazdunski et al., 1998)(Kurisu et al., 2003)(Buchanan et al., 2007).

Colicin	Receptor	Import	Cytotoxicity
Group A			
A	BtuB	OmpF, TolABQR	Pore
E1	BtuB	TolC, TolAQ	Pore
E2-E7-E8-E9	BtuB	OmpF, TolABQR	DNase
E3-E4-E6	BtuB	OmpF, TolABQR	16S RNase
E5	BtuB	OmpF, TolABQR	tRNA-(Y-H-N-D)-specific RNase
K	Tsx	OmpF, OmpA, TolABQR	Pore
N	OmpF	OmpF, TolAQR	Pore
U	OmpA	OmpF, TolABQR	Pore
Cloacin DF13	IutA	OmpF, TolAQR	16S RNase
Group B			
B	FepA	TonB-ExbBD	Pore
D	FepA	TonB-ExbBD	tRNA-(R)-specific RNase
Ia-Ib	Cir	TonB-ExbBD	Pore
M	FhuA	TonB-ExbBD	Degradation of the C55 phosphate-linked peptidoglycan precursors
5–10	Tsx	TolC, TonB-ExbBD	Pore

Figure 2.6: **Outer membrane receptors and cytotoxicitic activities of group A and group B colicins.** Tol- and Ton-dependent import pathways: cell envelope proteins required for colicin reception and translocation (Cascales et al., 2007).

Translocation: colicins parasitize two machineries to enter the target cell (Davies and Reeves, 1975)(Day et al., 2002). Group A colicins use the Tol system while group B colicins use the Ton system. TonB and Tol system are two energized machineries that use the proton-motive force for regulating processes at the outer membrane (Figure 2.6) and (Figure 2.7) . The Ton system is constituted of three inner membrane proteins, TonB, ExbB and ExbD. The TonB complex is involved, with cognate TonB-dependent receptors, in the uptake of siderophores and vitamin B12 (Postle and Kadner, 2003). The Tol system comprises proteins that share the same topology and localization: TolA, TolQ and TolR, plus the periplasmic protein TolB. It also includes Pal, an outer membrane-anchored lipoprotein, which is not required for colicin import (Lazzaroni et al., 2002). The physiological role of the Tol system is not clear but it is required for stability of the cell envelope and for the late stages of cell division (Bernadac et al., 1998)(Gerding et al., 2007).

Activity: colicins have different modes of action. With few exceptions, the C-terminal domains of colicins bear pore-forming or nuclease activity (Bullock et al., 1983)(Martinez et al., 1983). Pore-forming colicins form large pores in the inner membrane, hence depolarizing the chemical gradient. A 2-helix hairpin inserts first, leading to an umbrella-like structure, before the insertion of the other 8 trans-membrane helices. The immunity of pore-forming colicins is located in the inner membrane (Weaver et al., 1981) and by interaction with the hairpin, prevents channel formation (Duché et al., 2006). Enzymatic colicins target phosphodiester bonds within genomic DNA (DNAses), 16S rRNA (rRNases), or tRNAs (tRNAses) (Cascales et al., 2007), eliciting cell death. The immunity of nuclease colicins forms complex with the cognate colicin, neutralizing its catalytic activity.

It is worth to note that colicin-like proteins are produced by various Gram-negative bacteria: S-pyocins, carocins, vibriocins are respectively produced by *Pseudomonas*, *Pectobacterium*, and *Vibrio* species. All these proteins share a similar organization and a similar mechanism of action. However, other bacteriocins are very distinct for both their architecture and their uptake. An important group of bacteriocins, such as R-pyocins, are particles comprising several polypeptide that use a contractile mechanism for injection of the toxin activity.

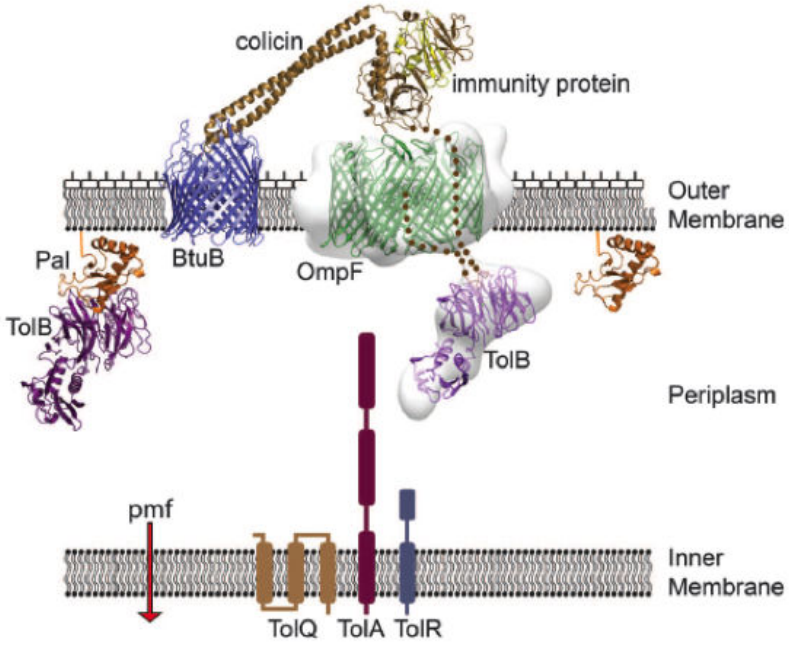

Figure 2.7: **ColE9 binds BtuB and uses OmpF to capture TolB on the other side of the membrane in a defined orientation.** Structural representation of the ColE9 translocon (the structure for the related ColE3-Im3 bound to BtuB is shown (PDB accession code 1UJW)) and its protein-protein interaction network across the Gram-negative cell envelope (Housden et al., 2013).

2.4.3 R-type pyocins

2.4.3.1 Generalities

First identified by Jacob in 1954, R-pyocins are high-molecular weight proteins or protein complexes produced and released in the extracellular medium by *Pseudomonas aeruginosa* (Jacob, 1954). Pyocins target bacterial cell from the same species. Their anti-bacterial activity appears to create a channel in bacterial membranes that dissipates the cell's proton potential. 90% of *Pseudomonas aeruginosa* strains produce pyocins upon DNA damage (Michel-Briand and Baysse, 2002). Three general types of bacteriocins can be differentiated: S-type (soluble), which are colicin-like proteins, R-type (retractile), which are non-flexible and contractile, and F-type (flexible), flexible but non-contractile structures. It is worth to note that the R-type pyocins are related to the tails of bacteriophages from the *Myoviridae* family whereas the F-type pyocins are related to *Siphoviridae* phage tails. Based on their targets, R-type pyocins can be classified into five groups (R1 to R5). They harbour the same general morphology, structure and mechanism of action.

2.4.3.2 Structure

The R-type pyocins gene cluster is located on the chromosome and comprises twelve genes that are essential for R-pyocin assembly (from ORF 11 to ORF 23). By comparison with the structure of the *Myoviridae* P2 or T4 bacteriophage, it is possible to assign functions to these ORFs (Michel-Briand and Baysse, 2002). The ORFs numbered 17 and 18 encode tail sheath and tail tube proteins and are homologous to gp18 and gp19 respectively. ORF 13 and ORF 15 encode baseplate and tail fiber protein (Nakayama et al., 2000).

The R-pyocins have been observed by negative-stain electron microscopy since the 60's (Ishii et al., 1965)(Takeda and Kageyama, 1975) but it is only recently that the atomic structures of the pyocin R2 sheath and tube was solved (Ge et al., 2015). By cryo-electron tomography, the authors solved the 3.4-Å resolution structure of pyocin R2 in its pre-contraction and post-contraction forms (Figure 2.8). The overall structure is composed of three major parts (Figure 2.9): (i) a baseplate resembling a ring-like structure with a diameter of 240 Å. The outer side of the baseplate is extended by six tail fibers whereas the inner side of the baseplate ring is connected to the central spike protein; (ii) a trunk formed by a sheath and a tube with a helical structure. The length of the trunk in the extended conformation is 1000 Å for a diameter of 180 Å; and (iii) a collar with a diameter of 65 Å. The tail structure has a 6-fold symmetry and is made of discs that contain six tube subunits and six sheath subunits.

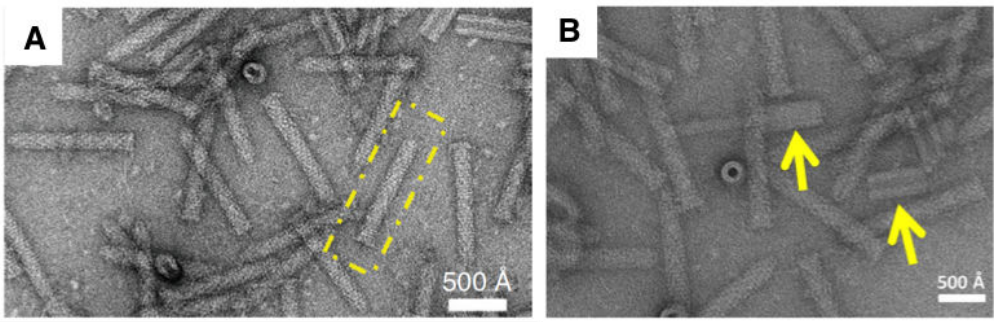

Figure 2.8: **R-type pyocin particles.** Electron microscopy images of the pyocin R2 embedded in uranyl acetate stain in a pre-contraction **(A)** and a post-contraction state **(B)** (Ge et al., 2015).

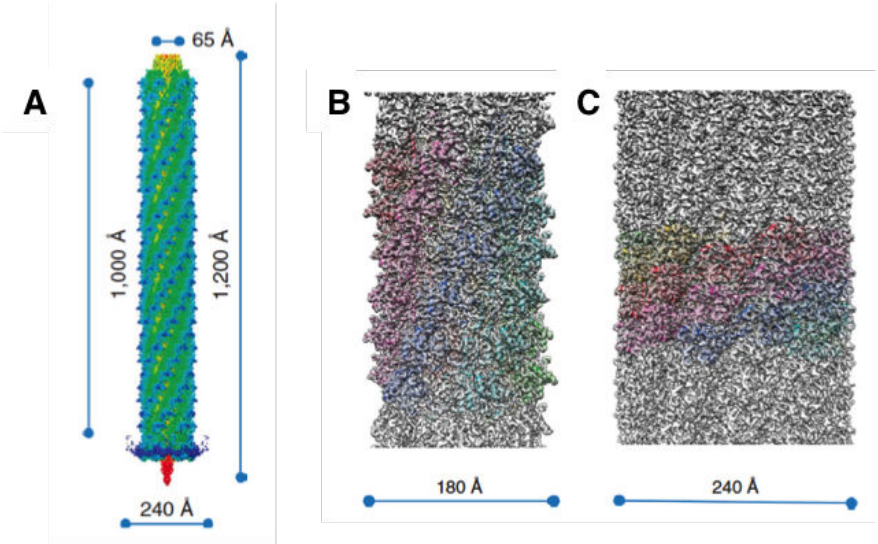

Figure 2.9: **Structure of R-type pyocin.** **(A)** Surface view of a 3D reconstruction of the entire pre-contraction R-pyocin. **(B-C)** Comparison of R-pyocin contraction between the pre-contraction and post-contraction sheath . The cryo-EM density map in **(B)** and in **(C)** is filtered to a comparable 3.9 Å-resolution (Ge et al., 2015).

2.4.3.3 Mechanism of action

The mechanism of action of the R-type pyocins is similar to the *Myoviridae* phages.

Release from the producing cell. Producing cell lysis is induced by five proteins: two holin proteins (ORF9) disrupt the inner membrane by forming large holes. The cell wall is then degraded by the R protein (ORF24) (Campbell and Delcampillo-Campbell, 1963). Finally, disruption of the outer membrane is caused by the "spanning complex" which comprises the Rz inner and Rz1 outer membrane proteins (ORF25 and ORF26) (Berry et al., 2012).

After their release in the environment, R-type pyocins bind the target cell surface via their tail fibers that recognize the lipopolysaccharide (Govan, 1974). The tail fibers confer specificity against target cells. By replacing the tail fibers of one R-pyocin by the tail fibers from the R-pyocin from another strain, the initial R-type pyocins could be retargeted to the species specific for the second one (Williams et al., 2008). Upon binding, R-pyocins contract their sheath leading to penetration of the tube through the bacterial cell, which creates a channel in the envelope. The pore leads to the dissipation of the cell's proton potential and then causes cell lysis.

2.4.4 Role of bacteriocins in microbial communities

Although bacteriocins mediate microbial dynamics in laboratory conditions, the real impact that bacteriocin production plays in microbial communities is unclear. Three potential roles have been proposed (Riley and Wertz, 2002)(Dobson et al., 2012): (i) They may serve as competitors or colonizing peptides facilitating the invasion of an occupied niche; (ii) They may play a defensive role as antimicrobial peptides by prohibiting invasion of microbial communities by other strains or pathogens; (iii) They can serve as signaling peptides for a 'quorum sensing'-like mechanism (Miller and Bassler, 2001).

Experimental studies were inconclusive and contradictory (Riley et al., 2003). At first, the narrow killing range of bacteriocins was the hallmark (Riley et al., 2003). However, bacteriocins from natural isolates of several species of enteric bacteria were shown to have effects against a large set of nonproducers isolated from the same sources (Riley et al., 2004). Some bacteriocin species are most effective at killing their own species whereas others kill more broadly or specifically kill isolates of different species. Thus, bacteriocins play equally roles in mediating both population level and community level interactions.

Several studies have been conducted on colicins, microcins and R-pyocins.

R-pyocins. Very few studies have provided information on the role of R-pyocins on microbial communities. However, it has been shown that two R-pyocins produced by the *Pseudomonas chlororaphis* 30-84 strain are involved in bacterial competition against plant-associated *Pseudomonas* species, both in mixed surfaced-attached biofilms and in wheat rhizophere communities (Dorosky et al., 2014).

Colicins. In 2011, Majeed et al. published a study using two colicigenic *E. coli* strains. Using *in vivo* and *in vitro* approaches, they confirmed *in silico* simulations demonstrating that, due to

the expression of colicin genes in stressful conditions, bacteriocin production by one strain induce the production of colicins by the other, leading to mutual exclusion in a structured environment. Therefore, cross-induction and co-existence maintain the diversity inside the community (Majeed et al., 2011). *In vivo* experimental models demonstrated that colicins promote microbial diversity in an animal host (Kirkup and Riley, 2004). However, although bacteriocin producers represent a important part of microbial communities, a specific environment comprises a mixture of bacteriocin producer, sensitive and resistant (*i.e.*, mutated in gene(s) of the reception and/or import pathway) species. This leads to the "Rock-Paper-Scissors" model, in which the bacteriocin producer (Rock) has a competitive advantage against sensitive strains (Scissors) but not against resistant species (Paper). The sensitive strain (Scissors) is disadvantaged against the producer (Rock) but has a better fitness that the resistant strain (Paper). Finally, resistant strains (Paper) are not impacted by the producer (Rock) but are overgrown by sensitive strains (Scissors). This model implies that equilibrium should be reached, the final outcome equilibrium depending on the difference of fitness between the sensitive and resistant strains.

Later, an *in vivo* study was performed to test whether bacteriocin production is a critical factor in determining the establishment of enteric bacteria into the gastro-intestinal (GI) tract of mice (Gillor et al., 2009). The authors showed that over a long time period, the colicigenic *E. coli* strain outcompetes non-producer strains. Thus, colicins appear to be beneficial by increasing persistence in the mouse GI tract.

Microcins. Very recently, an *E. coli* microcin producer strain was tested against enterobacterial competitors species such as *S. enterica* and Adherent-Invasive *E. coli* (AEIC) in a murine gut (Sassone-Corsi et al., 2016). Under homeostatic conditions, microcin production has no effect but when iron is limited such as during intestinal inflammation, microcins confer a great advantage to the producer strain.

Based on the *in vitro* and *in vivo* data on the role of bacteriocins on microbial communities, the use of bacteriocins as an alternative to antibiotics rises. They are attractive as therapeutic purpose against multidrug resistant bacteria and chronic infections (Behrens et al., 2017). However, more *in vivo* and preclinical experiments need to be carried out to fully confirm a potential bacteriocin therapy (Kirkup, 2006).

2.5 Bacteriophages

2.5.1 Generalities

Bacteriophages are bacterial viruses. They are ubiquitous as they are found in all natural environments. It is admitted that bacteriophages represent the most abundant and divers entities in the biosphere. The number of bacteriophages is estimated to 10^{31} (Wommack and Colwell, 2000). The extensive examination under the electron microscope of 5,500 particles allowed the definition of at least 14 families (Ackermann, 2009). Bacteriophages contain DNA or RNA in single or double-stranded forms. Based on their symmetry, they are divided in binary, cubic, filamentous and pleomorphic. Tailed bacteriophages of the *Caudovirales* order are categorized into three

large families: (i) *Podoviridae*; (ii) *Siphoviridae*; and (iii) *Myoviridae* (Figure 2.10). *Podoviridae* bacteriophages are defined by short tails. Bacteriophages from the *Siphoviridae* family, such as phage λ, are long, non-contractile tailed particles. The *Myoviridae* family comprises contractile bacteriophages, such as bacteriophages T4 or Mu.

Shape	Nucleic acid	Family	Genera	Particulars	Example	Members
Tailed	dsDNA (L)	*Myoviridae*	6	Tail contractile	T4	1,320
		Siphoviridae	7	Tail long, noncontractile	λ	3,229
		Podoviridae	4	Tail short	T7	771
Polyhedral	ssDNA (C)	*Microviridae*	4	Conspicuous capsomers	ϕX174	40
	dsDNA (C, S)	*Corticoviridae*	1	Complex capsid, lipids	PM2	3?
	dsDNA (L)	*Tectiviridae*	1	Double capsid, lipids, pseudo-tail	PRD1	19
	ssRNA (L)	*Leviviridae*	2	Poliovirus-like	MS2	39
	dsRNA (L, M)	*Cystoviridae*	1	Envelope, lipids	ϕ6	3
Filamentous	ssDNA (C)	*Inoviridae*	2	Long filaments, short rods	M13	67
	dsDNA (L)	*Lipothrixviridae*	4	Envelope, lipids	TTV1	7
	dsDNA (L)	*Rudiviridae*	1	Stiff rods, TMV-like	SIRV-1	3
Pleomorphic	dsDNA (C, S)	*Plasmaviridae*	1	Envelope, no capsid, lipids	L2	5
	dsDNA (C, S)	*Fuselloviridae*	1	Lemon-shaped, envelope, lipids?	SSV1	11

Figure 2.10: **Overview of bacteriophages.** Bacteriophages are highly diversified and can be classified based on theirs different characteristics. The *Caudovirales* order represent the most diversified groups and is categorized into three large families (*Myoviridae*, *Siphoviridae*, *Podoviridae*). L, linear; C, circular; S, supercoiled; M , multipartite. (Ackermann, 2001).

2.5.2 Mechanism of action of lytic bacteriophages

Based on their lifestyle, we can differentiate lytic and lysogenic (or temperate) bacteriophages. Lysogenic bacteriophages integrate their genome into the chromosome of the host cell. This piece of DNA, called "prophage", then replicates with the host genome and remains quiescent as far as the conditions are favorable. Upon stressful conditions, the prophage is excised and enters into a lytic cycle. Lytic bacteriophages inject their nucleic acid into the host cell and use the bacterial resources to assemble progeny virions. Once assembled into the host cell, they escape by inducing lysis of the host (Wang et al., 2000). Lysis of the Gram-negative host is accomplished through a three steps process: (1) permeabilization of the inner membrane by a holing protein; (2) degradation of the peptidoglycan using a muralytic enzyme (or endolysin); and (3) disruption of the outer membrane via a spanin complex. Four lysis genes are found clustered in cassettes and produce five proteins. The λ holin forms lethal holes or S-holes in the inner membrane, which allow the endolysin R to reach the peptidoglycan. To regulate the formation of the pore, an antiholin is produced with the holin protein. The last genes encode for Rz, which is an integral membrane protein or i-spanin,

and for Rz1 or o-spanin, an outer membrane protein. Together they form the complex that spans the entire periplasm connecting the IM and the OM (Young, 2013).

2.5.3 Structure and assembly of bacteriophages

The subject of my thesis being the T6SS, which uses a mechanism structurally and functionally similar to contractile bacteriophages, I will detail the structure and the assembly of the most studied and the most evolved phage of the *Myoviridae* family, bacteriophage T4. It is worth to note that it exists simpler phages from the *Myoviridae*, the Mu and P2 phages (Büttner et al., 2016)(Haggard-Ljungquist et al., 1995), which are probably more closely related to the T6SS, but also less characterized. The bacteriophage T4 comprises a capsid containing a double-strande DNA genome, a collar region that carries short whiskers, a contractile tail with a complex baseplate that harbors short tail fibers (STFs), and a set of long tail fibers (LTFs) (Figure 2.11)(Hu et al., 2015). The mechanism of action of *Myoviridae* is well understood. The LTFs recognize receptors at the cell surface of the host, and transmit the information to the baseplate. A conformational change of the baseplate induces sheath contraction, which provides the channel connecting the capsid interior to the host cell cytoplasm, through which the DNA moves.

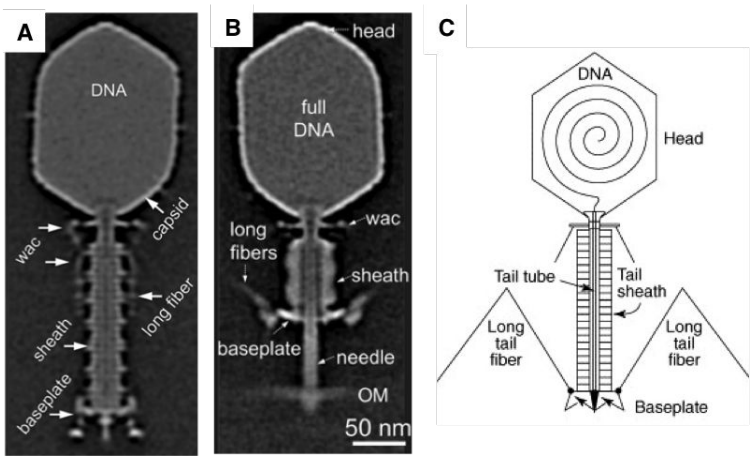

Figure 2.11: **3D structure of the bacteriophage T4 by cryo-EM.** The structures of the bacteriophage T4 during infection before **(A)** and after **(B)** sheath contraction (with full DNA in the capsid) are shown. **(C)** Schematic representation of the T4 bacteriophage showing the major elements (Hu et al., 2015)(Leiman and Shneider, 2012).

2.5.3.1 The capsid

The capsid. The capsid - or head - packages and protects a 170-kb dsDNA. The head is first assembled as an empty capsid. An ATP-dependent packaging machine is in charge to insert the DNA into the head. After completion of DNA packaging, the gp13-gp14 complex creates a site for attachment to the tail.

2.5.3.2 The bacteriophage T4 Tail.

The tail comprises an inner rigid tube surrounded by an outer contractile sheath. During the contraction of the sheath, the tube slides inside the sheath to be expelled.

The tail tube. The tube is formed by stacked gp19 hexamers. It is 924-Å long with an external diameter of 90 Å and an internal diameter of 40 Å (Leiman et al., 2004)(Kostyuchenko et al., 2003). A 4.1-Å resolution map was generated for the first two rings of the tube using the overall baseplate for alignment (Taylor et al., 2016). More recently, a 3.4-Å resolution structure of the T4 tail tube was solved by cryo-EM (Zheng et al., 2017).

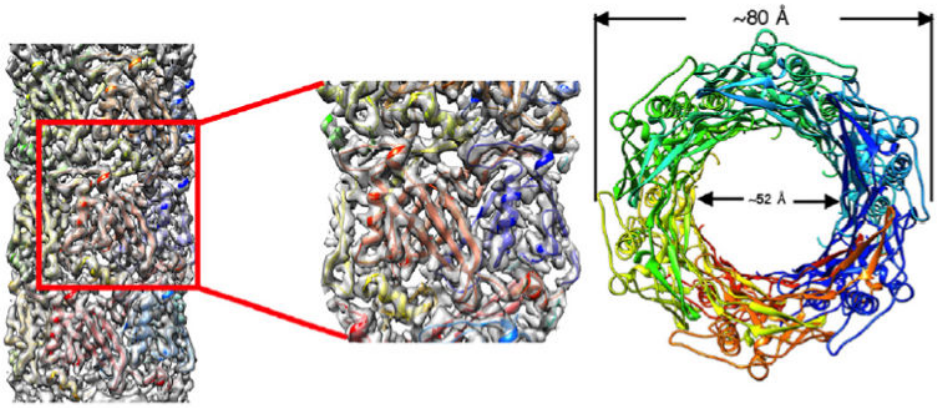

Figure 2.12: **Structure of the T4 tail tube.** A 3.4 Å resolution cryo-EM dose-weighted reconstruction of the T4 tube and the atomic model of a hexameric ring of gp 18 are shown (Zheng et al., 2017).

The tail sheath. The sheath is composed of 23 hexameric rings made of six gp18 proteins. In a pre-contraction state, it is 925-Å long and 240-Å wide to reach the length of 420 Å and a diameter of 330 Å in a post-contraction state (Kostyuchenko et al., 2005). The extended ring of the sheath is 40.6-Å high and rotates by 17.2° whereas the contracted ring is 16.4-Å high with a twist angle of 32.9°. The crystal structure of the sheath was solved and could be fitted into both conformations demonstrating that the overall structure is not altered during contraction (Aksyuk et al., 2011), but rather that the monomers slide on each other.

The tail initiator and terminator. The tail tube is a continuation of the spike complex from the baseplate. Additionally, two proteins, gp48 and gp54, form the first two rings ("tube initiator") and have the same helical symmetry than the tube. In addition, gp54 interacts with the first layer of the sheath, and has been proposed to initiate sheath polymerization.

On the other side compared to the baseplate, the gp3 and gp15 proteins cap the tail and form the tail terminator. The tail terminator prevents depolymerization of the tail tube/sheath before its attachment to the head (Yap and Rossmann, 2014). They form hexameric rings that bind both gp18 and gp19. The structure of gp15 revealed that gp15 interacts with gp18 and gp3 at the top and bottom, respectively (Fokine et al., 2013). It was shown that gp15 assembles before the baseplate to prime and control polymerization of the tail (Ferguson and Coombs, 2000).

2.5.3.3 The T4 bacteriophage baseplate.

Very recently, the atomic structure of the T4 baseplate-tail tube complex was published in its pre- and post-attachment states (Taylor et al., 2016). The baseplate attached to the extended sheath forms a high-energy hexagonal dome-shaped structure, which is 270-Å high and 520-Å in diameter. After contraction, the baseplate has a low-energy star-shaped structure which is 120 -high and 610 Å in diameter.

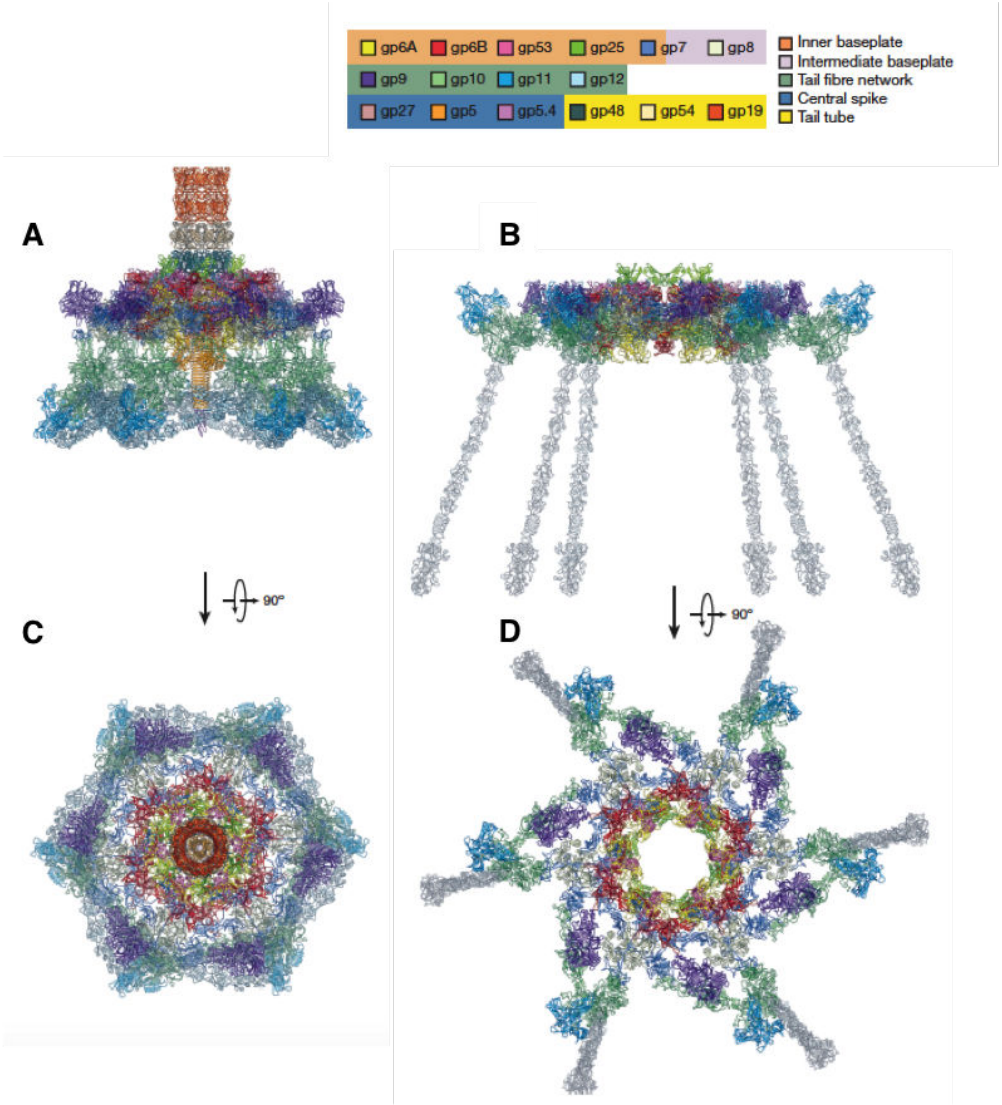

Figure 2.13: **Atomic models of T4 baseplate in pre- and post-atachment states.** The two states are with component proteins shown as ribbon diagrams. In **(C)** and **D**, the STFs (gp12 trimers) are displayed semi-transparently to indicate that they are not present in the refined model of the post-attachment baseplate. (Taylor et al., 2016).

The baseplate can be divided into distinct parts (Figure 2.13): (1) the proximal region of the gp19 tail tube is in closed contact with the gp48-gp54 tube initiator complex; (2) the gp29 tape measure protein locates inside the tube; (3) the central spike complex, that is an extension of the tube, is composed of the gp5.4, gp5 and gp27 proteins; (4) the inner baseplate comprising the gp6, gp25 and gp53 proteins, and part of gp7; (5) the intermediate baseplate essentially made of gp8

and part of gp7; and (6) the peripheral baseplate comprising the tail fiber network composed of gp9-12. The inner, intermediate and peripheral baseplates can be also called "wedges". Briefly, the wedges surround the central hub and form a structure on which the short and long tail fibers attach.

The central hub. The central hub is part of the cell-puncturing device or spike (Figure 2.14). The spike is composed of the gp5 and gp27 subunits, which are organized as a double trimer. The distal part of the spike interacts with gp5.4 that sharpens the spike. The base of the spike, comprising gp27, contacts the inner tube and forms the "hub", *i.e.*, the structure on which the wedges connect. The crystal structure of the gp5-gp27 complex has been solved. The Gp5 trimer forms the needle and is composed of three domains connected by long linkers. The C-terminal domain is a rigid β-helix, the central part is the lysozyme domain that is attached via flexible linkers, the N-terminal OB-fold domain connects the donut-like structure of the gp27 trimer. On the other side, gp27 contacts the tail tube. Gp27 is an adaptor as it connects the trimeric spike to the hexameric tail tube. It is worth to note that the gp5 lysozyme domain, that degrades the target cell peptidoglycan after penetration, is cleaved during infection of the host cell (Kanamaru et al., 2005).

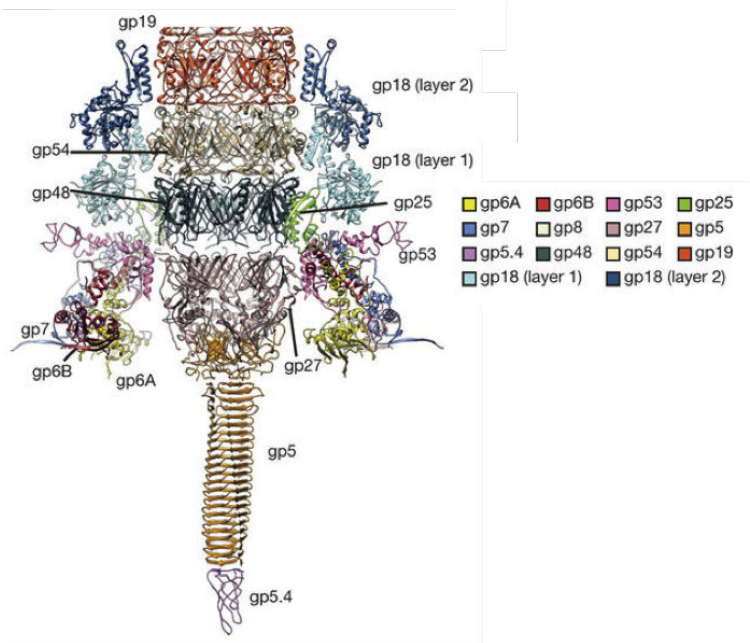

Figure 2.14: **Structure of the conserved inner baseplate .** The minimal composition of a contractile injection system is derived from the T4 tail structure: the central spike complex (gp5, gp5.4, gp27), the conserved part of the wedge (gp6, gp7, gp25, gp53), the tail tube (gp19, gp48, gp54) and the conserved part of the sheath (gp18), some of which is modeled using the pyocin sheath (Taylor et al., 2016).

The wedges. Six wedges are assembled around the central hub. One wedge is composed of seven proteins and thirteen subunits: gp11(3)-gp10(3)-gp7- gp8(2)- gp6(2)-gp53- gp25 (Yap et al., 2010).

Gp8 interacts with gp10, gp7 and gp6. A dimer of gp8 and twelve gp6 proteins (one dimer per wedge) form a ring constituting the backbone of the baseplate. The gp6-gp8 complex is at the center. The gp6 ring maintains the integrity of the baseplate during conformational changes (Yap

and Rossmann, 2014). The N- and C-terminal domains of each gp6 monomer interact with two different neighboring gp6 molecules depending on whether these are inter or intra-wedges dimers (Aksyuk et al., 2009). The gp6 subunit is in close contact with six copies of gp25 and gp53 proteins (one per wedge). The gp6-gp53-gp25 complex contacts the sheath and form the upper part of the baseplate that surrounds the hub as a ring-like complex. The gp6-gp53-gp25 complex adopts a six-fold symmetry with gp25 in the center. Gp25 has a fold similar to the domain IV of the gp18 tail sheath subunit, and it has been proposed that it initiates sheath polymerization from the baseplate by giving an arm to the first row of the gp18 monomers (Leiman and Shneider, 2012). The structure of gp6 is slightly modified between the two baseplate conformations, and hence it is considered that gp6 transmits the signal from the periphery to the center of the baseplate and triggers sheath contraction (Aksyuk et al., 2009).

Attachment proteins and tail fibers. Tails fibers serve both as host cell recognition determinants, and sensors. They have a crucial role during infection as they allow attachment to the host cell and they transduce the signal to the baseplate. The gp9-11 proteins, which locate at the periphery of the baseplate, are adaptors to connect the LTFs to the baseplate (Figure 2.15). The C-terminal domain of gp9 interacts with a trimeric LTFs whereas its N-terminal domain associates with the gp7 baseplate component. Gp9 allows the LFT to be articulated (Kostyuchenko et al., 1999) which is crucial when the LTFs bind to the host and when the baseplate undergoes large conformational changes .

Gp12 trimers form a 340-Å long structure called short tail fibers (STFs). They are located at the periphery of the baseplate's underside. During contraction, the STFs unfold and extend the C-terminal receptor-binding domain near to the host cell surface (Kostyuchenko et al., 2003).

Six 1450-Å long LTF are attached to the periphery of the hexagonal baseplate. They consist of four different proteins (gp34-37). The proximal half of the fiber is formed by gp34, which interacts with the adaptor protein gp9. Gp35 forms the knee or the hinge and the distal part of the LTF is formed by gp36 and gp37 (Yap and Rossmann, 2014).

2.5.3.4 Assembly of the T4 bacteriophage

The assembly pathway of the T4 bacteriophage is a highly ordered process in which independent intermediates are assembled. It is worth to note that the tail genes are expressed simultaneously, and hence the precise order is dictated by protein-protein interactions between each subunit. At each intermediate stage, changes in the conformation of the components create new binding sites for the following partner. Wedges are first assembled by the sequential recruitment of the various subunits (Ferguson and Coombs, 2000)(Bartual et al., 2010)(Yap et al., 2010)(Plishker et al., 1988): a trimer of gp11 associates with a trimer of gp10, and the gp10-gp11 hetero-hexamer recruits gp7. Then, a dimer of gp8, a dimer of gp6, gp53 and gp25 are recruited to form the wedge complex gp11(3)-gp10(3)-gp7-gp8(2)-gp6(2)-gp53-gp25 (Yap et al., 2010). Six wedges assemble around the hub, whereas STFs and gp9 are then added to the baseplate. Finally, gp48 and gp54 form a doughnut-like ring as the junction between the baseplate and the tail. The tube and the sheath both polymerize in an extended conformation (King, 1968)(King, 1971)(Meezan and Wood, 1971). To complete the assembly, a mature head is attached to the tail.

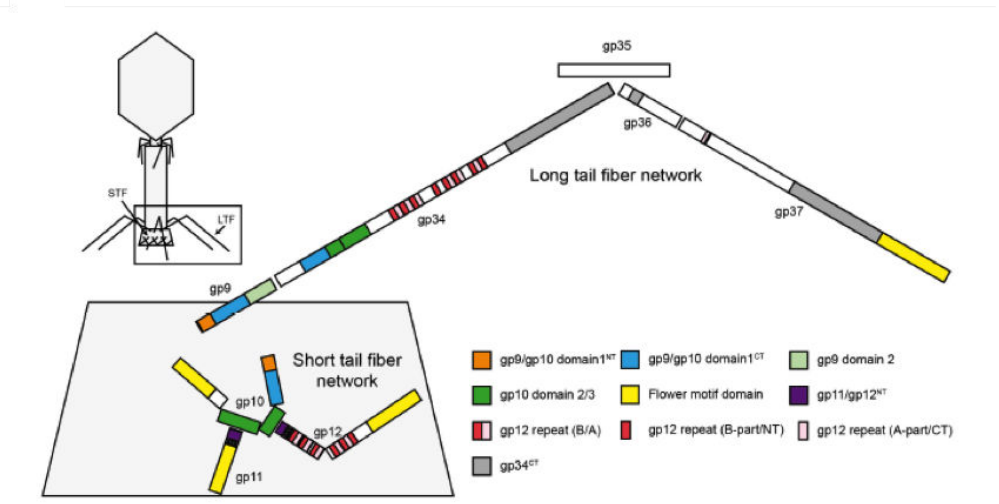

Figure 2.15: **Domain organization of T4 fibers.** Evolutionary relationships between different 14 proteins comprising baseplate's periphery and fibers. The size of each bar is proportional to the amino acid sequence length (Taylor et al., 2016).

.

2.5.4 Differences between *Myoviridae* and *Siphoviridae*

As mentioned above, tailed phages of the *Caudovirales* are categorized into three families (*Podoviridae*, *Siphoviridae* and *Myoviridae*). The phage-related complex of the Type VI secretion is structurally and functionally homologous to contractile bacteriophages of the *Myoviridae* family. However, the T6SS is a very mosaic structure, and we recently found that the baseplate-associated TssK protein is structurally and functionally homologous to receptor-binding proteins (RBP) of *Siphoviridae* phages (Figure 2.16).

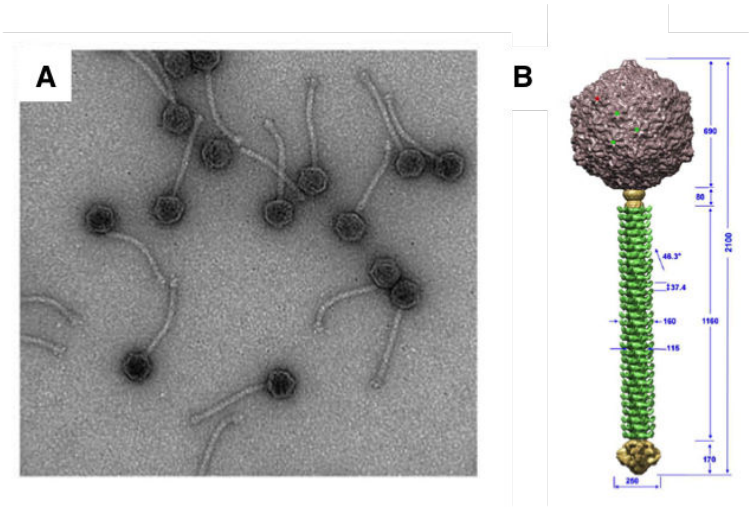

Figure 2.16: **The siphophage p2. (A)** Electron microscopy images of phage p2. **(B)** Structure of phage p2 was generated by assembling the reconstructions of the capsid (top), connector and tail (middle), and the tail-tip (bottom) on low-resolution maps of the full phage. Dimensions are given in angstrom and the angle of rotation between hexamers is given in degrees. (Spinelli et al., 2014)

.

Phages of the *Siphoviridae* are the most abundant of the tailed phages as they represent 61 % of the tailed phages (by comparison, *Myoviridae*, which are the most highly evolved phages, represent 25 %) (Ackermann, 2009). *Siphoviridae* phages have simple, noncontractile, flexible or rigid tails. By contrast to *Myoviridae*, they do not use tail fibers to bind the target cell, but the first step of the infection process rather involves interactions between the RBP and carbohydrate receptors at the cell wall.

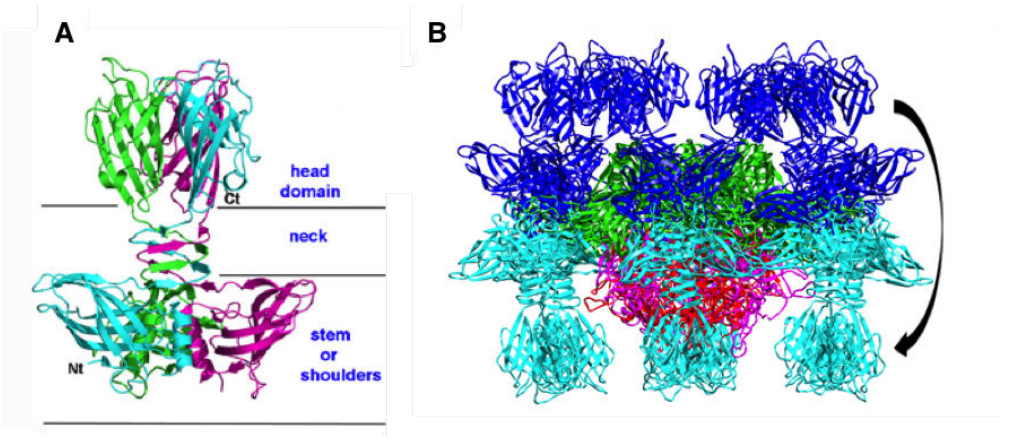

Figure 2.17: **Structure of the receptor binding proteins (RBPs) of phage p2. (A)** Ribbon view of the p2 RBP trimer (Spinelli et al., 2014). **(B)** The crystal structure of the "heads-down" conformations of p2 baseplate. The central ring is formed by ORF15 hexamers (green) and ORF16 trimers (pink). RBP (ORF18) trimers (blue) have under a 200° rotation downwards (Sciara et al., 2010).

The RBP is the last component of the baseplate to be assembled and is located at the tip of its tail (Vegge et al., 2005). Only few RBPs have been identified. Crystal structures of the RBPs from phages TP901-1, 1358 and P2 have been reported (Spinelli et al., 2006a)(Spinelli et al., 2006b)(Farenc et al., 2014). RBPs are homotrimers that are organized into three domains: a shoulder, a neck and a head (Figure 2.17 A). The shoulder domain is inserted into the baseplate whereas the head domain is receptor-specific. The comparison of the RBP structures reveals that RBPs exhibit a modular assembly, with the head domain being very diverse (Simpson et al., 2016). It appears that each phage evolves along with its host cell to ensure efficient entry. Then, the receptor head domain differs highly in agreement with their distinct host range.

A model for the baseplate activation during attachment, and more specifically on the conformational changes that occur has been proposed based on the structure of the p2 baseplate (Figure 2.17 B) (Sciara et al., 2010). The host recognition is a two-step process. The head domains of RBPs bind the receptor in a "head'up" conformation that is destabilized upon contact with the host cell. This reversible binding induces a baseplate conformational change into a "head's down" conformation.

2.6 Contact-dependent growth inhibition

Contact-dependent growth inhibition (CDI) was first described in an *E. coli* isolate, EC93. Aoki et al. found that *E. coli* EC93 inhibits the growth of *E. coli* K-12 strains (Aoki et al., 2005) and that the growth inhibitory activity was not due to soluble, diffusible antibacterial toxins.

2.6.1 General mechanism of action

Contact-dependent growth inhibition is mediated by the *cdiBAI* gene cluster (Figure 2.18). CDI is considered as a subfamily of Type V secretion systems, and more specifically of the Two-Partner Secretion (TPS) pathway (Leo et al., 2012)(Jacob-Dubuisson et al., 2013). TPS systems comprise the TpsB β-barrel transporter and the secreted TpsA virulence factor. TpsA proteins include a number of important adhesins that are used by bacterial pathogens to adhere to eukaryotic host cells (Cotter et al., 1998)(Relman et al., 1990)(Noel et al., 1994). In CDI, two proteins, CdiA and CdiB share functional homologies with the TpsA and TpsB proteins respectively, whereas an additional protein CdiI is the immunity that confers self-protection.

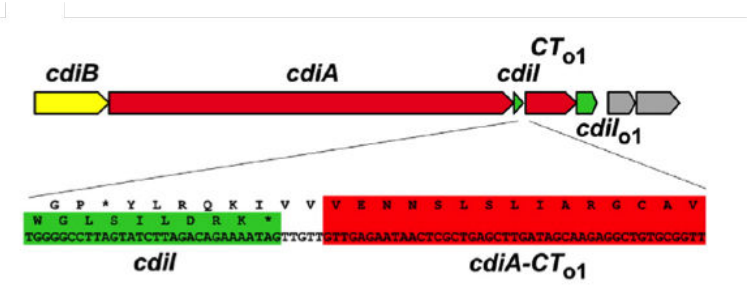

Figure 2.18: **Genomic organization and genetic rearrangements.** The *cdi* gene cluster from *E. coli* EC93 is depicted with the *cdiA-CT/cdiIo1* orphan gene pair. The genes colored in gray encode a predicted IS3 family transposase. The cdiA-CTo1 toxin coding sequence is outlined in red and lacks an initiating methionine codon (Ruhe et al., 2013a).

CdiA is a very large, usually >300-kDa, hemagglutinin-repeat protein that carries the growth inhibition activity within the carboxy-terminal region (CdiA-CT). All CdiA proteins bear N-terminal signal sequence for Sec-dependent export, with an unusual extended signal peptide region (Desvaux et al., 2006). The N-terminal region of the mature protein contains the TPS transport domain, which is required for secretion across the outer membrane.

CdiB is a predicted outer-membrane β-barrel protein. It recognizes the TPS transport domain, and supposedly translocates CdiA through the central pore of its β-barrel domain to the cell surface (Delattre et al., 2011).

Due to its size and the known structural information on β-prism hemagglutinins, CdiA are predicted to extend several tens of nanometers from the surface, hence allowing binding receptors at the cell surface of target bacteria. Different CdiA receptors have been identified, such as the outer membrane barrel assembly protein BamA (Aoki et al., 2008). Upon contact with the target cell,

CdiA are cleaved to release CdiA-CT that then translocates into target cells, where CdiA-CT will fulfill its activity. Similarly to colicins, CdiA-CT can bear various activities including nucleases and pore-formation. In producing cells, the CdiI immunity protein neutralizes CdiA-CT and protects the cell from autoinhibition (Figure 2.19).

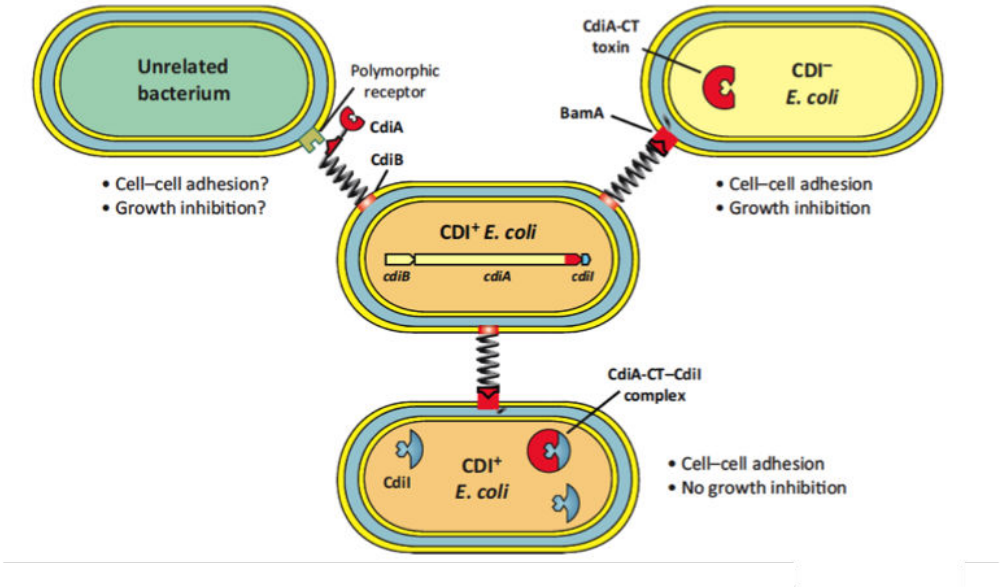

Figure 2.19: **Contact-dependent growth inhibition (CDI) in *Escherichia coli*.** CDI$^+$ *E. coli* cells express *cdiBAI* gene clusters and present CdiB/CdiA on the cell surface. CdiA binds receptors on neighboring *E. coli* cells and delivers its C-terminal activity domain (CdiA-CT) into the target cell. CdiA-CT toxins inhibit the growth of CDI$^-$ cells, but isogenic CDI$^+$ inhibitors produce CdiI immunity proteins that protect them from toxin activity. The extracellular residues of most outer membrane proteins are highly variable between species, suggesting that the CDI only targets closely related bacteria (Ruhe et al., 2013a)

.

2.6.2 Architecture of CdiA effector and CDI systems are modular

CDI are widespread among Gram-negative bacteria. *cdi* gene clusters are found in several α-, β- and γ-proteobacteria (Aoki et al., 2010) and are commonly found in human, plant and arthropod pathogens. Over the years, it has become clear that *Burkholderia pseudomallei* serves as a good model to decipher CDI action. More than a hundred of *B. pseudomallei* isolates have been sequenced and their *cdi* loci have been categorized into 10 distinct *cdi* locus types, each characterized by unique CdiA-CT-CdiI pairs (Nikolakakis et al., 2012)(Anderson et al., 2012).

CdiA-CT polymorphism is a hallmark of CDI (Aoki et al., 2011)(Poole et al., 2011). Comparative analyses of CdiA proteins typically show that the CdiA proteins share large regions of sequence identity but a significant variability over the C-terminal region after a conserved motif (VENN in *E. coli*, (E/Q)LYN in *Burkholderia*) that likely represents the processing motif (Aoki et al., 2011)(Nikolakakis et al., 2012), suggesting that CDI$^+$ strains deploy many different toxins. These observations suggest that CdiA proteins are modular and that *cdiA* genes evolve rapidly by horizontal gene and recombination. Indeed, functional CdiA chimera were generated with the N-terminal of CdiA from uropathogenic *E. coli* 536 fused downstream the VENN sequence to the

C-terminal domains of the CdiA from *Yersina pestis* CO92, *E. coli* EC93 or *Dickeya dadantii* 3937 (Aoki et al., 2010). In agreement with the variability of the CdiA-CT between families, CdiI are also variable between families. CdiI are very specific for their cognate CdiA-CT, and hence CdiA-CT/CdiI pairs represent polymorphic toxin-immunity modules.

2.6.3 Orphan toxin immunity modules

In addition to the *cdiBAI* operon, many CDI systems encode additional CdiA-CT-CdiI pairs in tandem array downstream of the main *cdiBAI* genes. The toxin open reading frame (ORF) lacks an initiation codon but codes for conserved VENN motif followed by an activity domain (Figure 2.18). These toxin-immunity protein pairs have been termed "orphans" because they appear to be DNA fragments displaced from full-length *cdiA* genes (Poole et al., 2011). Orphan regions usually contain predicted transposase and integrase genes, as well as insertion sequence elements, suggesting that the regions are subject to horizontal gene transfer and are issued from DNA acquisition (Figure 2.18).

It has been proposed that orphan CdiA-CT-CdiI modules represent a reservoir of toxin diversity. This reservoir may confer a growth advantage to bacteria that produce them after homologous recombinaison leading to the fusion of the CdiA-CT orphan domain to the main CdiA TPS domain (Figure 2.20) (Ruhe et al., 2013a). Interestingly, evolution experiments in mice showed that this fusion event by recombination occurs in a clonally derived population of *Salmonella enterica* Typhimurium (Koskiniemi et al., 2014).

2.6.4 Cell target recognition and CdiA-Ct activities

Cell target recognition. Genetic selections for *E. coli* K-12 mutants that are resistant to the EC93 CDI identified the outer membrane protein BamA as the receptor for $CdiA^{EC93}$ (Aoki et al., 2008). BamA is highly conserved, essential, protein that is required for the insertion of β-barrel proteins into the outer membrane (Bos et al., 2007b)(Ricci and Silhavy, 2012). A multiple sequence alignment of BamA proteins from γ-proteobacteria shows a high degree of sequence identity, with the exception of the extracellular loops 4, 6 and 7 that are highly variable in sequence and length (Noinaj et al., 2013). Indeed, binding of $CdiA^{EC93}$ to *E. coli* K-12 BamA was shown to require both loops 6 and 7 (Ruhe et al., 2013b). These loop sequences vary considerably between different species, restricting the CDI^{EC93} target cell range to *E. coli*. Interestingly, the BamA proteins from *Burkholderia* species lack extracellular loops, suggesting that the CdiA parasitizes a different surface receptor. There is evidence that the lipopolysaccharide (LPS) serves as a receptor for the *B. pseudomallei* 1026b CdiA (Nikolakakis et al., 2012)(Anderson et al., 2012). Hence, it seems likely that CdiA effectors recognize different cell surface receptors to identify susceptible target cells. Indeed, studies have demonstrated that the CdiA-CTs exploit a broad repertoire of cell entry pathways. For example, the CdiA from other *E. coli* strains uses the F-pilus, the OmpC porin or the Tsx nucleoside transporter as receptor (Beck et al., 2014)(Beck et al., 2016)(Ruhe et al., 2017).

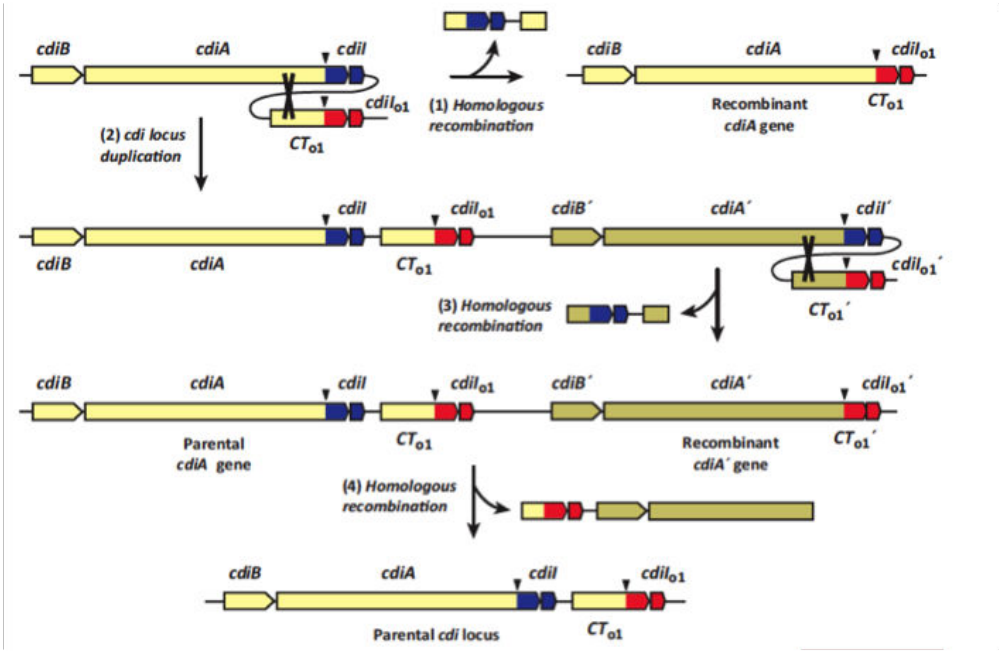

Figure 2.20: **Models of orphan toxin-immunity protein gene rearrangements.** Orphan *cdiA-CT* genes that contain conserved sequences upstream of the VENN-encoding region (downward arrow) can undergo homologous recombination with the full-length *cdiA* gene (indicated by crossover step 1). Recombination would delete the parental toxin-immunity protein coding sequences and fuse the orphan module (red) to *cdiA*. Alternatively, the *cdi* locus could undergo spontaneous duplication (step 2) followed by homologous recombination (step 3) to generate a recombinant *cdiA* gene. Further recombination between the orphan *cdiA-CT* and the recombined *cdiA'* could regenerate the original parental genotype (step 4) (Ruhe et al., 2013a).

.

CdiA-CT activities. All the CDI toxins characterized so far disrupt target cell membrane integrity or degrade cellular nucleic acids. However, a comprehensive analysis predicts that other CDI toxins may have adenosine deaminase, ADP-ribosyl cyclase and metallopeptidase activities (Zhang et al., 2011)(Zhang et al., 2012a).

As many CDI toxins are nucleases, they must translocate into the target cell cytoplasm. Recent work shows that CDI toxin translocation requires the proton gradient across the inner membrane of the target bacteria (Ruhe et al., 2014). In addition, a number of mutations within genes encoding inner membrane or cytoplasmic proteins, such as the FtsH protease or elongation factors, have been isolated in a screen for CDI resistance (Willett et al., 2015)(Jones et al., 2017). It has been proposed that these proteins may serve as inner membrane receptors and/or translocators.

2.6.5 Regulation

The expression of most CDI genes is tightly regulated with the notable exception of the *E. coli* EC93 *cdiBAI* operon, which is constitutively expressed under laboratory conditions. Plant pathogens appear to express their *cdi* genes only when colonizing specific hosts. As examples, the *D. dadantii* EC16 *cdi* genes are regulated by VirA, a plant-responsive regulator (Rojas et al., 2004), whereas the *D. dadantii* 3937 *cdi* gene cluster is expressed when the bacterium grows on chicory leaves (Aoki et al., 2010). In addition to its role in bacterial competition, CDI systems also contribute

to virulence towards hosts and to cooperative behaviour. *D. dadantii* EC16 *cdi* mutants present defects in adherence to plant cells and fail to autoaggregate. Similar findings have been reported for *Neisseria meningitidis* (Neil and Apicella, 2009)(Talà et al., 2008), *Xylella fastidiosa* (Guilhabert and Kirkpatrick, 2005)(Voegel et al., 2010) and *Xanthomonas axonopodis* (Gottig et al., 2009) suggesting that intercellular adhesion contributes to host colonization and infection. Regarding the role of CDI in cooperative behaviours, *cdiA* mutants in *B. thailandensis* E264 and in *E. coli* EC93 abolish biofilm formation, suggesting that these CDI participate to establishing and maintaining monospecies communities in mixed microbial populations (Anderson et al., 2012)(Ruhe et al., 2015). Thus, they promote collective behaviours by collaborating to form biofilms and by excluding non-identical bacteria (Anderson et al., 2014).

2.6.6 Role of CDI in microbial communities

Very few studies have addressed the role of CDI systems *in vivo*. Surprisingly, in *Burkholderia thailandensis*, BcpA-CT has been shown to mediate biofilm formation (Garcia et al., 2013). A later work revealed that the delivery of the BcpA-CT toxin into an immune cell results in a change in gene expression and promotes biofilm formation. This phenomenon has been called contact-dependent signaling (CDS; (García et al., 2017). Then, during biofilm formation, CDI proteins segregate the biofilm structure. In a pre-establish biofilm community, a set of bacteria producing a specific CDI system inhibit growth of another set producing a different CDI system, which exclude this population from the community (Anderson et al., 2014). CDI systems allow bacteria to distinguish self from non-self and to discriminate kin cells amongst neighboring bacteria. This suggests that CDI systems have evolved as a mechanism to allow microbes to discern those in the population that do not contribute to the persistence of their own genetic material variability in microbial communities (Danka et al., 2017).

Chapter 3

The Type VI secretion system

The type VI secretion system (T6SS) is a multiprotein apparatus that resembles a nano-crossbow. It uses a spring-like mechanism to deliver a needle loaded with toxins directly into target cells. The needle (also called the cell-puncturing device) is built on an assembly platform - the baseplate - that is anchored to a membrane-associated complex. A contractile structure polymerizes on the baseplate: a tail tube surrounded by a contractile sheath Figure 3.1. More details are in the section *Structure and Assembly* below.

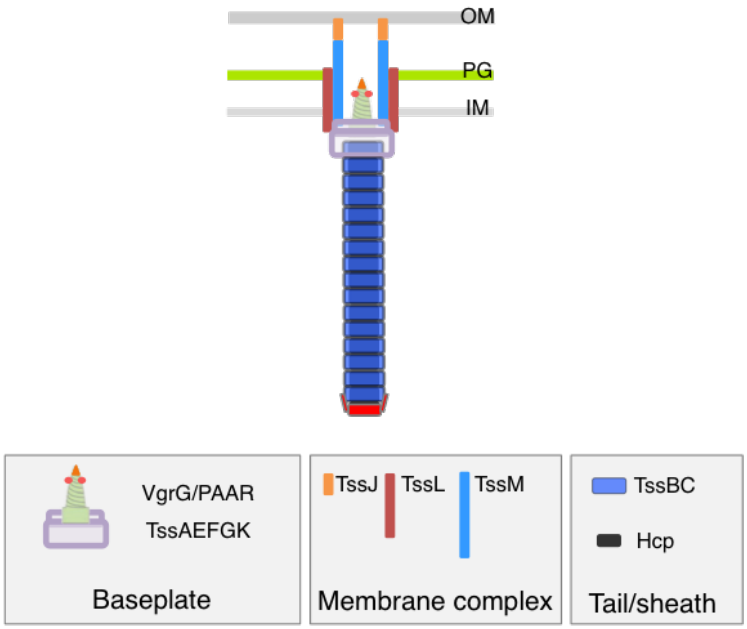

Figure 3.1: **T6SS overview.** The T6SS is composed of an assembly platform - the baseplate - that is anchored to a membrane-associated complex. A contractile structure polymerizes on the baseplate: a tail tube surrounded by a contractile sheath.

How it works? The overall mechanism is comparable to contractile bacteriophages. Basically, once in contact with a target cell, the sheath will contract to propel the inner tube toward the target. The membrane complex serves: (i) to orient the tail toward the exterior, and (ii) as channel for passage of the tube. By delivering effectors into prokaryotic and eukaryotic cells, the T6SS participates to bacterial competition and virulence.

3.1 What does the T6SS in bacterial competition?

3.1.1 The antibacterial T6SS

Since the discovery of the T6SS as a secretory apparatus (Mougous, 2006)(Pukatzki et al., 2006), its role as an antibacterial weapon has been extensively studied: effectors have been identified and we have now a general overview on how these effectors are loaded and transported to the target cell. Nevertheless, the real impact of this apparatus in *in vivo* competition is not yet well documented. Compared to colicins and CDI that are restricted to a few bacterial geniuses, the T6SS is distributed within the genomes of about 25 % of Gram-negative bacteria, with an over-representation in γ-Proteobacteria. Most T6SS are involved in bacterial competition but several studies have pointed its role in pathogenesis. In agreement with a main role in competition, T6SS genes clusters are widely distributed in both pathogenic and non-pathogenic bacteria (Das and Chaudhuri, 2003)(Bingle et al., 2008)(Boyer et al., 2009).

The first reports on the implication of the T6SS in interbacterial competition were published in 2010. Hood *et al.* analyzed the secretome of *P. aeruginosa* and identified three substrates: Tse1-3 and showed that Tse2 is a toxin that targets prokaryotic cells (Hood et al., 2010). A few months later, MacIntyre *et al.* releaved that *V. cholerae* T6SS provides interbacterial activity against other Gram-negative bacteria. The authors hypothesized that this interspecies competition may have a role in enhancing survival in the environment (MacIntyre et al., 2010) but also might be of clinical significance (Russell et al., 2012).

Many studies then demonstrated that the T6SS encoded in the genomes of other bacteria have antibacterial activity: *Serratia marcescens* (Murdoch et al., 2011), *Citrobacter rodentium* (Gueguen and Cascales, 2013), enteroaggragative *E.coli* (Brunet et al., 2013)(Flaugnatti et al., 2016), *Acinetobacter baumanii* (Carruthers et al., 2013), *V. parahaemolyticus* (Salomon et al., 2013), *Agrobacterium tumefaciens* (Ma et al., 2014), *Salmonella enterica* Typhimurium (Brunet et al., 2015a), *P. putida* (Bernal et al., 2017), *Erwinia amylovora* (Tian et al., 2017).

This unique machinery is able to secrete a bunch of effectors and can target specific compartments of the bacterial cell. In the following chapter, I will summarize all antibacterial effectors known.

3.1.2 Effectors targeting prokaryotic cells

In order to efficiently kill competitors, T6SS$^+$ bacteria need to produce and deliver harmful effectors into vital compartments of the target. The T6SS utilizes different pathways to deliver enzymatic activities into the prey cell: the direct injection of toxins that are bound to the injection device (the Hcp-VgrG-PAAR needle) or to inject a component of the machinery (VgrG or Hcp) that carries an extension with a deleterious activity (cf *Chapter 3.3*). So far, a number of anti-bacterial effectors have been identified and characterized.

Based on the macromolecule that is targeted, the effectors categorize in distinct families: cell wall-degrading effectors, membrane-targeting effectors and nucleases (Durand et al., 2014)(Russell

et al., 2014)(Alcoforado Diniz et al., 2015) (Figure 3.2). It is worth noticing that anti-bacterial effectors are co-produced with a cognate immunity protein that is usually encoded directly downstream the effector gene in T6SS clusters or effector islands.

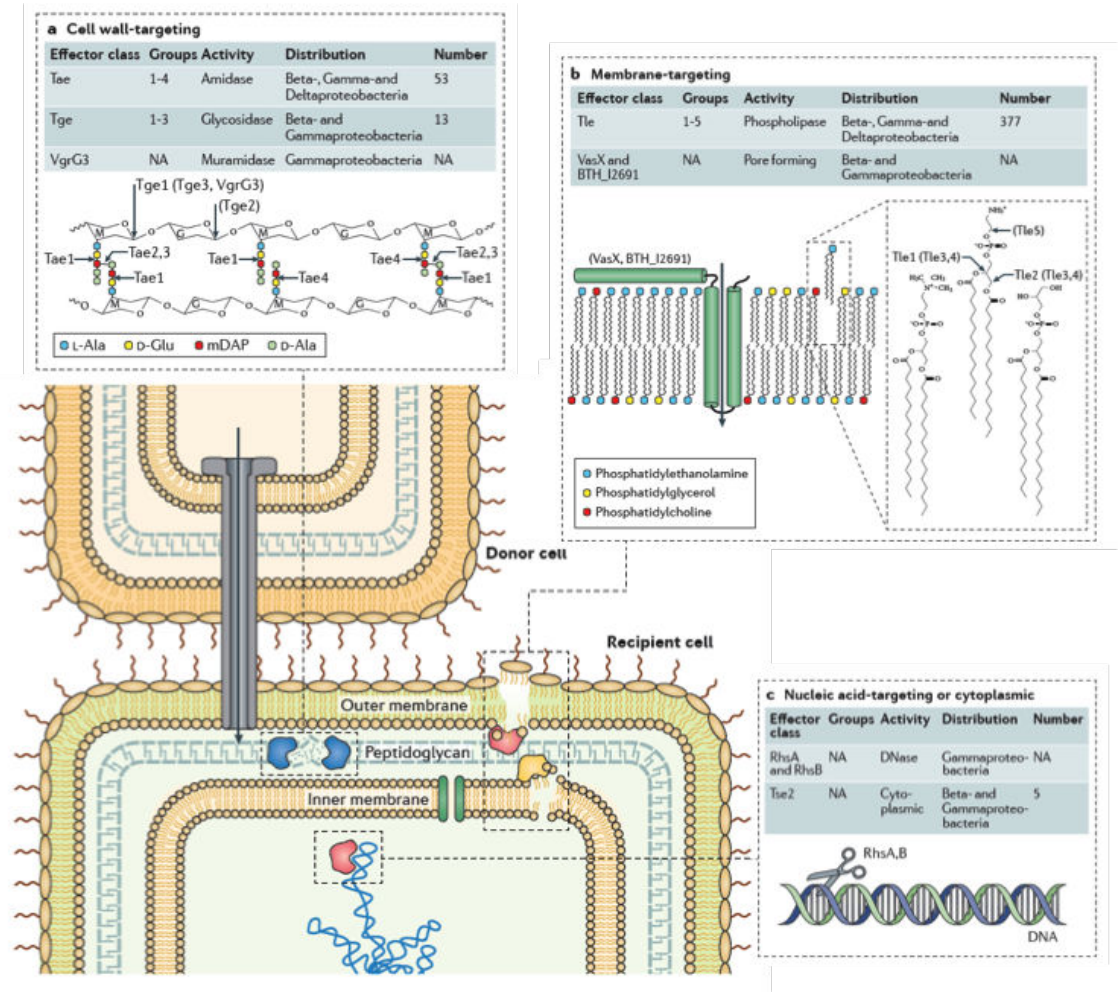

Figure 3.2: **T6SS effectors target varying aspects of bacterial physiology.** Localization and activity of interbacterial T6S effectors delivered by an attacking donor cell to a recipient cell via the T6S apparatus. Effector targets include the cell wall peptidoglycan **(part a)**, the inner and outer membrane **(part b)** and nucleic acids or other unknown cytoplasmic targets **(part c)**. Precise enzymatic specificity is indicated, where known; parentheses indicate enzymatic activities predicted from structure-function and/or nonspecific enzymatic analyses that have yet to be biochemically confirmed. In the tables, group refers to the number of evolutionarily distinct families of effector proteins within an enzymatic class, and number to the unique instances of homologues in those groups. The numbers presented are limited to those reported in the literature; groups and numbers are provided only when a systematic effort has been made to characterize a class of effectors. G, N-acetylglucosamine; M, N-acetylmuramic acid; mDAP, meda-diaminopimelic acid; NA, not applicable (Russell et al., 2014).

3.1.2.1 Cell wall-targeting effectors: amidases and glycosidases

In this category, there are two super-families: the type VI secretion glycoside hydrolase effectors (Tge) and the type VI secretion amidase effectors (Tae). Glycoside hydrolase effectors hydrolyse the glycan strands backbone whereas amidase effectors cleave the peptidoglycan peptide units and

their cross-bridges (Figure 3.2 - part a). These two super-families are themselves divided into three sub-families for the Tge named Tge1-3 (Whitney et al., 2013) and four sub-families for the Tae named Tae1-4 (Russell et al., 2014). Tae1 and Tae4 are DL-endopeptidases as they hydrolase the D-Glu/meso-diaminopimelic acid (mDAP) bond. Tae2 and Tae3 are DD-endopeptidases as they cleave the cross-bridge between the mDAP and D-Ala (Durand et al., 2014)(Russell et al., 2011).

Two Tge super-family effectors have been characterized: Tge1^{PA} from *P. aeruginosa* (Li et al., 2013) and Tge2^{PP} from *P. protegens* (Whitney et al., 2013). No member of the Tge3 sub-family has been structurally characterized yet.

Regarding the Tae super-family effectors, we have access to more information. Tae1^{PA} from *P. aeruginosa* is an amidase with a high activity compared to housekeeping enzymes (Chou et al., 2012). Briefly, we can name some structure solved such as the Tae2^{BT} from *B. thailandensis*, the Tae3^{RP} from *Ralstonia pickettii* (Dong et al., 2013) or the Tae4-1^{SM} and Tae4-2^{SM} from *S. marcescens* (English et al., 2012)(Srikannathasan et al., 2013).

Based on the crystal structures of Tae and Tge toxins that have been reported, alone or in complex with their cognate immunity proteins, we can conclude that they usually have classic folds of housekeeping peptidoglycan remodelling enzymes, and in general, the inhibition of their activity by the immunity protein is caused by the insertion of a loop from the immunity into the catalytic site of the enzyme (Durand et al., 2014).

3.1.2.2 Membrane-targeting proteins: phospholipases and pore-forming

The bacterial membrane is the target of a number of Type VI effectors including the characterized lipolytic enzymes (Tle for Type VI secretion lipase effector) (Russell et al., 2013) and likely the uncharacterized pore-forming colicin-like effectors (Figure 3.2 - part b). Tle effectors are classified into five families. Enzymes of the Tle1-4 families have activities associated with esterases, lipases or phospholipases whereas Tle5 has a phospholipase D activity.

With the exception of families 3 and 4, Tle effectors have been characterized. The *B. thailandensis* Tle1 effector, Tle1^{BT}, acts as a phospholipase A2 (Russell et al., 2013) whereas the same enzyme from enteroaggregative *E. coli*, Tle1^{EAEC}, has strong phospholipase A1 and weak phospholipase A2 activities (Flaugnatti et al., 2016). The *V.cholerae* Tle2 effector, Tle2^{VC}, acts as a phospholipase A1 (Brooks et al., 2013)(Jiang et al., 2014). The *P. aeruginosa* Tle5 effector, Tle5^{PA}, exhibits phospholipase D activity (Russell et al., 2013) whereas its *Klebsiella pneumonia* homologue, Tle5^{KP}, targets cardiolipins (Lery et al., 2014), which indicate a potential role in targeting eukaryotic cells.

A pore-forming protein can also disrupt the membrane. An antibacterial T6SS effector from *V. cholerae*, VasX, and two other effectors from *B. thailandensis* (BTH.I2691) and *P. aeruginosa* (PA14.69520) are predicted to share structural conservation with pore-forming colicins (Durand et al., 2014)(Russell et al., 2014).

3.1.2.3 Nucleases

An effector with DNase activity, named Tde (for Type VI DNase effector), has been identified in *Agrobacterium tumefaciens* where it confers a competitive advantage in plant co-infection assays (Ma et al., 2014). Additional Tde toxins are encoded in T6SS clusters: the VP1415 and VPA1263 effectors of *Vibrio parahaemolyticus* carry nuclease domains of the AHH and colicin DNase families (Salomon et al., 2014), whereas the *P. aeruginosa* H1-T6SS PA0099 potential toxin has characteristics of the superfamily nuclease 2 toxin members (Hachani et al., 2014). In addition to PA0099, it also has a Tse2 effector with a bacteriostatic role, but its activity and the macromolecule it targets are unknown. However, Tse2 is toxic when produced into the cytosol of both prokaryotic and eukaryotic cells suggesting its target is conserved across kingdoms (Li et al., 2012)(Hood et al., 2010).

Nuclease domains can also be fused to T6SS-associated proteins with repetitive sequences, named RHS (rearrangement hot-spot) and YD (tyrosine-aspartate (YD)-repeat-containing protein) (Busby et al., 2013). Koskiniemi *et al.* reported two Rhs proteins from *Dickeya dadantii*, RhsA and RhsB, carry nuclease domains that degrade target cell DNA (Koskiniemi et al., 2013) (Figure 3.2 - part c).

3.1.2.4 What else?

Other activities have been reported. The Tse6 from *P. aeruginosa* is capable of degrading the dinucleotides $NAD(P)^+$ and hence induces cell stasis when injected (Whitney et al., 2015). Three recent studies by the group of Shen showed that one of the *B. thailandensis* and *Y. pseudotuberculosis* T6SS secretes $Mn2^+$-binding and $Zn2^+$-binding effectors (TseM, TseZ and YezP) that sequester manganese and zinc respectively. TseM then binds MnoT, a $Mn2^+$-dependent outer membrane transporter, whereas TseZ binds HmuR, an outer membrane heme transporter, allowing $Mn2^+$ and $Zn2^+$ acquisition in *B. thailandensis* (Si et al., 2017a)(Si et al., 2017b).

These recent examples open new horizons for discovering effectors with diverse, and unexpected functions. We can hypothesize that by secreting regulators or enzymes, the T6SS can be involved in other process such as signaling (Russell et al., 2014).

3.1.3 Role of the T6SS in bacterial communities

In the last years, a number of studies have tested the impact of T6SS in different models. Basically, it has been shown that the T6SS confers a competitive advantage: in certain cases, it allows symbiotic strains to protect the host against pathogenic strains, whereas in others it permits pathogenic strains to better colonize the host.

The first clue that the T6SS might have a significant role in microbial communities came with the work of Fu et al. Using high-throughput Tn-seq in a rabbit ileal loop model of infection, they showed that mutant *V. cholerae* cells missing an immunity protein against an anti-bacterial T6SS effector was outcompeted (Fu et al., 2013). This result suggested that T6SS-deficient cells are rapidly eliminated from the population.

The human gut is mainly composed of bacterial cells of the *Bacteroidetes* clade (The Human Microbiome Project Consortium, 2012). Interestingly, the vast majority of *Bacteroidetes* strains harbours an active T6SS-like secretion system that is implicated in antagonistic interactions (Russell et al., 2014). It was shown that a *B. fragilis* strain uses its T6SS - and more specifically the T6SS Bte2 effector - to have a competitive advantage in the mammalian gut (Chatzidaki-Livanis et al., 2016)(Hecht et al., 2016). The T6SS of this non-toxigenic symbiotic strain targets certain *Bacteroidetes* species such as *B. thetaiotaomicron* and toxigenic *B. fragilis* in this polymicrobial environment and hence protects the host against inflammatory diseases (Wexler et al., 2016).

On the opposite, T6SS$^+$ pathogenic bacteria also use the T6SS to colonize new niches. A recent study showed that the T6SS confers a competitive advantage to *S. enterica* Typhimurium in a mouse model of infection. The observation that establishment of *S.* Typhimurium during infection of the mouse gut requires the anti-bacterial Tae4 peptidoglycan-degrading effector suggested that the T6SS is used for efficient colonization. Indeed, the *S.* Typhimurium T6SS targets enterobacterial species of the normal mouse gut flora such as *Klebsiella oxytoca* (Sana et al., 2016). A similar study demonstrated that *Shigella sonnei*, a pathovar of *E. coli*, eliminate *E. coli* and the T6SS$^-$ related *S. flexneri* strain in the mice gut. The authors proposed that this ability to destroy related strains explains the prevalence of *S. sonnei* compared to *S. flexneri* (Anderson et al., 2017).

However, T6SS$^-$ cells may develop immunity-independent mechanism of protection. Computer simulation experiments, confirmed by *in vivo* studies, suggest that sensitive T6SS$^-$ cells can dominate T6SS$^+$ competitors by defending their established niche against invasion by forming microcolonies (Borenstein et al., 2015).

The exact ecological role of the T6SS in microbial communities is still in its infancy but these recent studies shed light on the evolution of a highly complex behaviour developed by microorganisms.

3.2 What does the T6SS in virulence?

The current literature on T6SS emphasizes its role in bacterial competition. Although eliminating competitors may have an impact on colonization and hence an indirect effect on virulence, several T6SS effectors are directly involved in impeding cell host functions and promoting immune invasion (Figure 3.3) (Hachani et al., 2016).

For examples, the T6SS of *V. cholerae* and *A. hydrophila* and the H1-T6SS of *P. aeruginosa* confer resistance to phagocytosis or promote internalization in non-phagocytic cells by altering the dynamics of cytoskeleton components. The effectors responsible for these activities have been identified and characterized.

The *V. cholerae* VgrG1 protein possesses a C-terminal extension with an actin cross-linking domain (ACD) that is active *in vitro* (Durand et al., 2012a) and *in vivo* (Pukatzki et al., 2007)(Ma and Mekalanos, 2010)(Durand et al., 2012a). By cross-linking G-actin in an ATP-dependent manner, VgrG1 prevents phagocytosis of *V. cholerae* cells (Ma et al., 2009a).

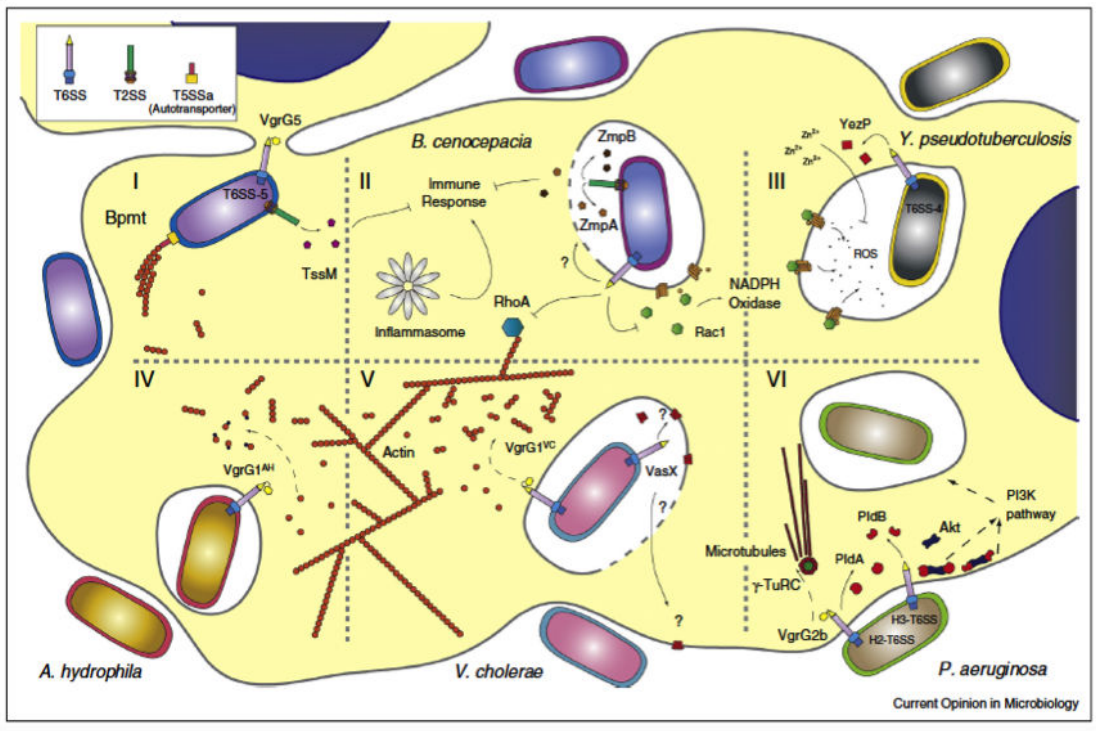

Figure 3.3: **T6SS-dependent mechanisms of host cell subversion I.** *Burkholderia mallei*, *Burkholderia pseudomallei* and *Burkholderia thailandensis* (grouped as Bpmt) encode a T6SS-5 which is essential for full virulence during infection. VgrG5 is responsible for the fusion of host cell membranes. The T6SS-5 cluster also encodes TssM, a T2SS-dependent effector. **II.** *Burkholderia cenocepacia* causes the deregulation of cytoskeleton-associated Rho-GTPases inluded RhoA and Rac1. T2SS substrates ZmpA and ZmpB are released from the vacuole. **III.** *Yersinia pseudotuberculosis* T6SS-4 secretes a zinc-binding effector, YezP, which protects the bacterium from the generated reactive oxygen species (ROS). **IV.** VgrG1 is secreted by *Aeromonas hydrophila*, and its evolved catalytic domain possesses ADP-ribosyltransferase activity, inhibiting actin polymerization. **V.** *Vibrio cholerae* secretes VgrG1, harboring a C-terminal actin cross-linking domain into the cytosol of macrophages and predatory amoebae. VasX is thought to form pores in lipid bilayers. **VII.** *Pseudomonas aeruginosa* secretes VgrG2b that modulates microtubule-mediated bacterial internalization. PldA and PldB bind Akt to facilitate bacterial internalization using the PI3K pathway (Hachani et al., 2016).

The *A. hydrophila* T6SS injects VgrG1 which displays a vegetative insecticidal protein-2 (VIP-2) domain with ADP-ribosyltransferase activity. By modifying actin, it also prevents phagocytosis (Suarez et al., 2010).

P. aeruginosa promotes its entry into non-phagocytic cells using VgrG2b. The C-terminus of VgrG2b interacts *in vivo* with the γ-tubulin ring complex and promotes internalization of *P. aeruginosa* (Sana et al., 2012)(Sana et al., 2015).

The *B. thailandensis* T6SS-5 promotes entry and replication in phagocytic and non-phagocytic eukaryotic cells (Schwarz et al., 2010)(Whiteley et al., 2017). Although the mechanistic bases are not yet defined, the VgrG-5 effector has been proposed to induce host cell fusion and to facilitate intercellular spreading (Schwarz et al., 2014)(Toesca et al., 2014).

The $Mn2^+$ and $Zn2^+$ scavanging effectors delivered by the *B. thailandensis* and *Y. pseudotuberculosis* T6SS, as well as the enterohemorrhagic *E. coli* KatN catalase T6SS effector, may also protects the bacterium from host reactive oxygen species and may therefore participate in host colonization (Wang et al., 2015)(Si et al., 2017a)(Si et al., 2017b)(Wan et al., 2017).

In addition to effectors that target eukaryotic cells, several trans-kingdom T6SS effectors have been reported.

P. aeruginosa secretes two phospolipases: PldA (Tle5a) and PldB (Tle5b) via the H2- and H3-T6SS (Russell et al., 2013)(Jiang et al., 2014). Both toxins target the phospholipid bilayers of competing bacteria and are also translocated into epithelial cells to promote intracellular invasion of non-phagocytic cells (Jiang et al., 2014). PldB induces PI3K/Akt pathway and facilitates intracellular invasion.

Very recently, an additional trans-kingdom phospholipase effector of *P. aeruginosa* has been identified: when it reaches the host endoplasmic reticulum, TplE (or Tle4) induces autophagy in epithelial cells but is also capable to kill competitor bacteria (Jiang et al., 2016)(Bleves, 2016).

Finally, *V. cholerae* secretes VasX, a T6SS effector required to resist amoeba predation. VasX binds to phosphatidic acid and phosphatidylinositol phosphates that are components of the inner leaflet of eukaryotic cell membranes (Miyata et al., 2011).

3.3 Mechanism of secretion

How effectors are recruited to the T6SS and delivered is not totally understood yet. Nevertheless, recent findings highlighted that varied effectors can be simultaneously delivered into a target cell. The current model suggests that an effector can either be fused to one of the components of the Hcp-VgrG-PAAR needle as an additional domain called "specialized effector" or can non-covalently interact with one of the components of this structure ("cargo effector") (Figure 3.4). Effectors are then linked to and depend on a particular component (Hcp, VgrG or PAAR) for delivery. In addition, adaptor proteins have been identified to facilitate the secretion (Durand et al., 2014)(Cianfanelli et al., 2016).

Specialized effectors. Several VgrG or C-terminal domains of PAAR-containing Rhs proteins are fused to an effector domain. Many VgrG with a C-terminal domain have been characterized (Schwarz et al., 2014)(Sana et al., 2015)(Brooks et al., 2013). As an example, VgrG-1 of *V. cholera* displays a C-terminal domain that is capable of cross-linking actin and inducing cell rounding (Pukatzki et al., 2007)(Durand et al., 2012a). Rhs proteins are polymorphic toxins composed of an N-terminal PAAR motif-containing domain, a central Rhs repeat domain and a variable C-terminal toxin domain (Hachani et al., 2014)(Whitney et al., 2014)(Alcoforado Diniz et al., 2015).

Cargo effectors. Effectors are secreted via a direct interaction with Hcp, VgrG or PAAR. The Hcp tail tube forms a 40-Å wide conduit , a diameter sufficient to accommodate small or unfolded proteins (Ballister et al., 2008)(Brunet et al., 2014). The effector EvpP from *Edwarsiella tard* interacts with Hcp (Zheng and Leung, 2007). Tse2 from *Pseudomonas aeruginosa* was shown to bind the inner face of Hcp and occupied the lumen of the Hcp ring (Silverman et al., 2013). Larger effectors can interact with VgrG (Liang et al., 2015)(Flaugnatti et al., 2016) or PAAR proteins (Shneider et al., 2013).

Accessory proteins. Adaptor proteins play the intermediate between effectors and one of the components. The interaction is indirect, via adaptors of PAAR or EagR proteins families (Alco-

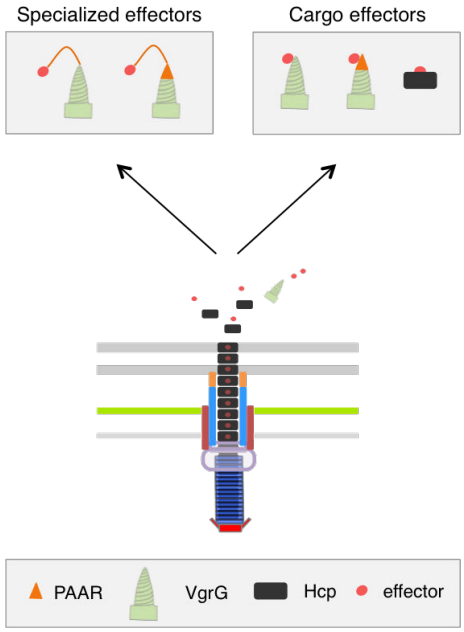

Figure 3.4: **Model of the mechanism of secretion** After sheath contraction, effectors are delivered into the target cell. The current model suggests that an effector can either be fused to a homologue of one of the components of the Hcp-VgrG-PAAR needle ("specialized effector") or can non-covalently interact with one of the components of the needle ("cargo effector").

forado Diniz et al., 2015)(Unterweger et al., 2015). Tse6 from *P. aeruginosa* possesses transmembrane segments that will insert into the inner membrane of the recipient cell. An accessory EagR protein has been shown to help its transport (Whitney et al., 2015).

Isolated or non-identified effectors. Using great advances in the field, potential strategies have been proposed by Lien and Lay in order to identify new effectors in the future (Lien and Lai, 2017).

3.4 Regulation of the T6SS gene clusters

As emphasized in the previous paragraphs, the T6SS is involved in various functions such as interbacterial competitions or virulence. These functions occur in diverse niches and hence it exists as many regulatory mechanisms as T6SS functions and niches. It is worthy to note that most species carry several T6SS gene clusters, which are usually independently regulated and may act on different target, in different conditions. T6SS gene expression responds to different cues, including temperature, pH, and iron, phosphate, magnesium, or zinc concentration. Almost all regulatory mechanisms identified so far in bacteria, are used to control the expression of T6SS gene clusters: quorum-sensing, two-component systems, transcriptional activators and repressors, alternative sigma factors, histone-like proteins, small RNAs, etc (Bernard et al., 2010)(Miyata et al., 2013)(Alteri and Mobley, 2016).

During my thesis, I have participated to a study that demonstrated that the *Salmonella enterica* serovar Typhumium T6SS gene cluster is repressed by H-NS, a histone-like protein that usually silences horizontally-acquired DNA fragments (Brunet et al., 2015a)(*Annexe 1*). I will not describe

all these mechanism but will concentrate on the regulation of the *sci-1* and *sci-2* T6SS clusters in EAEC, which is the model bacterium studied in our laboratory.

The EAEC 17-2 strain genome encodes two complete sets of T6SS genes called *sci-1* and *sci-2* (Dudley et al., 2006)(Journet and Cascales, 2016). The *sci-1* cluster is under the control of the Fur (Ferric uptake regulator) repressor (Figure 3.5) (Brunet et al., 2011). In presence of iron, Fur binds to a specific sequence motif called Fur box and represses target genes. Two Fur boxes are present within the promoter region of the *sci-1* cluster, overlapping with the transcriptional -10 and -35 elements and preventing RNA polymerase recruitment. This simple mechanism is complexified by an epigenetic circuit depending on the action of the DNA adenine methyltransferase (Dam), which couples T6SS expression to the replication state. The Fur-10 box contains a GATC motif that is recognized and methylated by Dam.

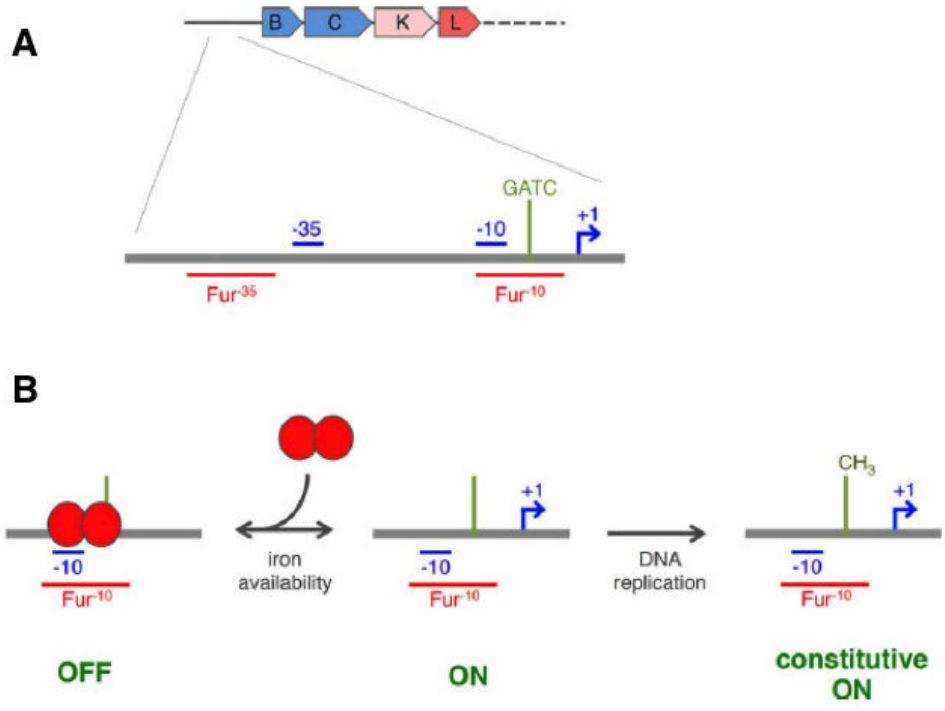

Figure 3.5: **Regulation of the EAEC *sci-1* gene cluster (A)** Schematic representation of the promoter organization of the EAEC *sci-1* gene cluster. The localisation of the -10 and -35 transcriptional elements (blue), of the Fur-binding sequences (red) and of one of the GATC sites (green) are shown. **(B)** Regulatory mechanism of the EAEC *sci-1* gene cluster. In iron-replete conditions, a Fur dimer (red balls) represses the expression of the *sci-1* gene cluster by binding to the Fur-10 box, which overlaps with the -10 element (OFF). When iron is limiting, the -10 element is available for the RNA polymerase allowing expression of the *sci-1* genes (ON). Upon replication, the GATC site is methylated (CH3) and by preventing Fur binding allows Fur-independent, constitutive expression of the *sci-1* gene cluster (Journet and Cascales, 2016).

Interestingly, Fur and Dam compete on the same site. Under high iron concentrations, Fur binds to the promoter and represses expression of the *sci-1* genes. By preventing access to Dam, the GATC site is not methylated (OFF expression). However, under low iron conditions, Fur is relieved from the Fur box allowing expression of the *sci-1* cluster (ON condition). If cells replicate, the Fur-10 box is methylated after the first replication. Methylation of the GATC site prevents

binding of Fur, and therefore turns *sci-1* expression under a constitutive ON state. Fur therefore controls the passage between the OFF and ON states whereas Dam is a sensor of replication and controls the passage between the reversible and constitutive ON states.

In agreement, with these data, the EAEC *sci-1* gene cluster is activated in minimal media supplemented with glucose (to be limiting in iron without being limited in carbon source) or in iron depletion conditions (addition of the iron chelator 2,2'-dipyridyl). However, this mechanism is unlikely to be conserved because no Fur box could be readily identified in the promoter regions of the *sci-1* clusters encoded in the other pathogenic *E. coli* genomes (Journet and Cascales, 2016).

By contrast, the regulation of the *sci-2* cluster depends on a AraC-like transcriptional regulator called AggR (Dudley et al., 2006). This transcriptional activator is a global virulence regulator as it regulates other EAEC virulence factors such as the Aaf fimbriae, the dispersin and the dispersin transporter (Morin et al., 2013). Although the signal inducing AggR activation is unknown, the cascade is activated in synthetic media mimicking the macrophage environment such as Eagle's medium (Dudley et al., 2006)(Brunet et al., 2013).

3.5 Sensing and response

M. Basler observed a phenomenon called "T6SS duelling" for the first time in 2012 (Basler and Mekalanos, 2012). He observed that *P. aeruginosa* cells respond to a T6SS attack occurring in a neighbouring sister cell by a T6SS counterattack. This "Tit-for-Tat" mechanism stimulates the T6SS activity and increases its own dynamics (Basler et al., 2013). Leroux et al. also analysed this double-edged sword quantitatively by fluorescence microscopy (LeRoux et al., 2012). This activity was not observed in *Vibrio cholerae* which fires at high levels without any obvious regulation whereas it could be visualized in *Salmonella enterica* cells when de-repressed by *hns* (Brunet et al., 2015a). The two different behaviours of T6SS activities lead to differentiate the "offensive T6SS" such as *V. cholerae* or *E. coli*, and the "defensive T6SS" such as *P. aeruginosa*.

The specificity of the *P. aeruginosa* H1-T6SS is that it is regulated at a posttranslationnal level by a signal transduction cascade (Figure 3.6) (Mougous et al., 2007). The TagQRST system senses membrane perturbation and controls the phosphorylation and dephosphorylation of the forkhead-associated protein Fha1 by the Threonine kinase/phosphatase pair PpkA and PppA (Casabona et al., 2013). This system called "threonine phosphorylation pathway" (TPP) reflects the requirement to respond rapidly and reversibly by triggering the assembly of the machinery. It has been noticed that this response occurs at the precise attack (Basler et al., 2013). However, the molecular mechanism on how Fha1 phosphorylation status is transmitted to the T6SS machinerie is not known. In *A. tumefaciens*, Fha1 transfers the phosphate to TssL, a component of the T6SS membrane complex (Lin et al., 2014)

Recently, LeRoux et al. identified another distinct pathway to sense an attack. The authors call it the "*P.aeruginosa* response to antagonism" (PARA) (Le Roux et al., 2015). *P. aeruginosa* cells actually detect the signal indirectly. Lysed cells serve as a signal for a Gac/Rsm-mediated

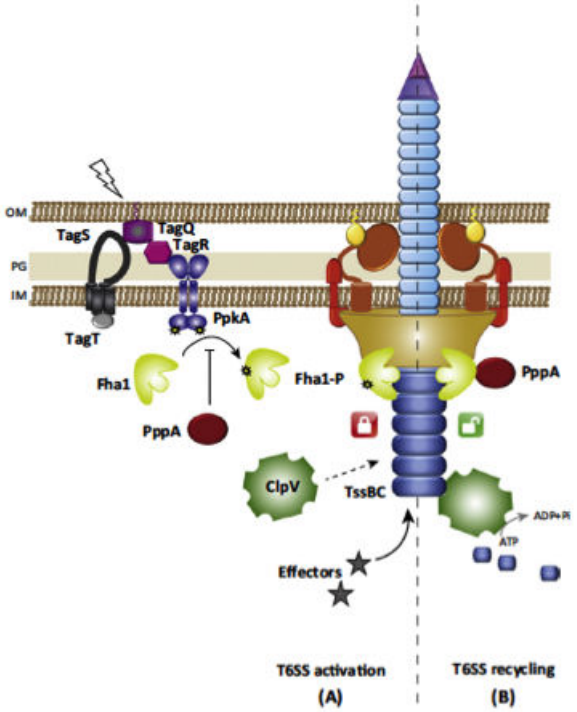

Figure 3.6: **Post-translational regulation of the H1-T6SS of *Pseudomonas aeruginosa* by the Threonine Phosphorylation Pathway (TPP). (A)** Membrane perturbation caused by an attacker cell is sensed by a complex of TagQ, TagR, TagS, and TagT. This causes autophosphorylation of PpkA which in turn phosphorylates Fha1. Phosphorylated Fha1 (Fha1-P) then somehow interacts with the T6SS machinery, promoting an active state, firing and effector secretion. **(B)** Once effectors are released, ClpV is recruited to the contracted sheath, in order to recycle TssBC subunits. PppA can dephosphorylate Fha1, perhaps unlocking the machinery to allow it to dissassemble and reassemble at a new location (Cianfanelli et al., 2016).

stimulation. The surviving cells then turn on a pathway that activates the type VI secretion system. This mechanism is not yet well understood.

3.6 Structure and assembly

3.6.1 Generalities

Most bacterial species have one or two copies of T6SS clusters, but a few species, including *Burkholderia* and *Yersinia* species, may have up to six clusters. T6SS gene clusters therefore exist as multiple copies in many microorganisms, although, whether these clusters arise from duplication or distinct genetic transfer is not clear (Bingle et al., 2008). T6SS gene clusters are usually encoded within pathogenicity islands (Cascales, 2008). A minimal set of 14 genes is required to assemble a functional T6SS. These 14 genes encode for components called "core components" (Figure 3.7) (Boyer et al., 2009)(Zheng and Leung, 2007). Aside from these core components, T6SS clusters may encode accessory components, which might be structural components required for the proper assembly of the apparatus, transcriptional or post-translational regulators that control the expression or the activity of the T6SS, or effector-immunity pairs (Silverman et al., 2012). Core and accessory components are differentiated by a universal nomenclature: core components are

named Tss (for Type six secretion) whereas accessory subunits are refereed as Tag (for Type six associated gene) (Shalom et al., 2007).

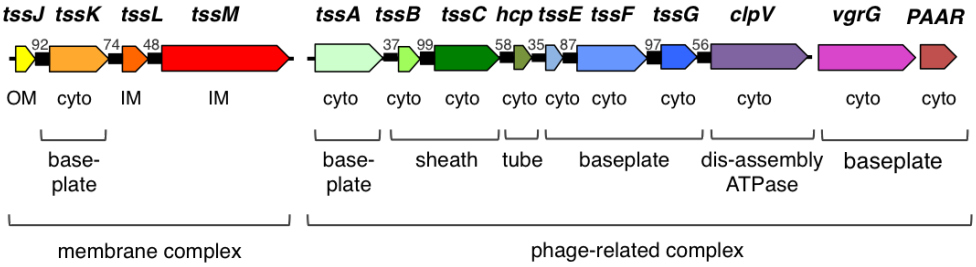

Figure 3.7: **Type VI secretion gene organization** The minimal set of T6SS genes required for assembly of a functional T6SS is shown. Genes are partitioned as genes involved in the assembly of the membrane complex (*tssJ,tssK, tssL, tssM*) or of the tail complexe (*tssA, tssB, tssC, hcp, tssE, tssF, tssG, clpV, vgrG* and *paar*). Genes with conserved transcriptional orientation are connected, the percentage value indicating the conservation frequency. The localization of the products of these genes is indicated (cyto, cytoplasm; IM, inner membrane; OM, outer membrane). For T6SS subunits implicated in the assembly of the tail complex, the localization in the tail structure is also indicated (using phage nomenclature: tube, sheath and baseplate). The *clpV* gene, although not related to any phage protein, is classified in the tail complex based on its interaction with the TssBC proteins and its role in the dissassembly of the contracted TssBC sheath (Zoued et al., 2014).

The core components assemble two distinct subcomplexes: a structure related to the tail of contractile bacteriophages that is anchored to the cell envelope by a membrane-associated complex. Based on its structural homologies with tailed bacteriophages, the T6SS could be represented as an upside-down bacteriophage that secretes toxins directly into target cells. This representation has been supported by the first visualization of the T6SS by electron cryo-tomography in *V. cholerae* cells (Basler et al., 2012). These cryo-tomograms revealed that the T6SS assembles long tubular structures in the cytoplasm that exist in either extended or contracted conformation, and connected to the membrane by two sub-complexes (Figure 3.8). This long tubular structure corresponds to the tail: a tail tube wrapped by the sheath. In the same study, time-lapse fluorescence microscopy using a fusion between one sheath protein with GFP (TssB) demonstrated that this tail is contractile: it assembles at a constant speed of approximately 20-30 seconds per micrometre. The contraction occurs in few milliseconds and is followed by disassembly of the sheath (Basler and Mekalanos, 2012).

Based on these results, the mode of action of the T6SS is divided into three steps (Figure 3.9): (1) *Assembly*: the membrane complex composed of TssJ, TssL and TssM is assembled first into the cell envelope. TssA is recruited and positions the baseplate components. The baseplate is constituted by TssA, VgrG/PAAR – the cell-puncturing device –TssE, TssF, TssG and TssK. Finally, T6SS assembly is completed by the polymerization of the tail tube (Hcp) and tail sheath (TssB and TssC). (2) *Contraction of the sheath*: the inner tube tipped by VgrG/PAAR is propelled by the sheath contraction through the membrane complex into the target cells. The current models for T6SS-mediated protein secretion propose that toxins are associated with VgrG/PAAR or Hcp or additional adaptor proteins (Durand, 2014). Penetration of the Hcp-VgrG/PAAR syringe in the

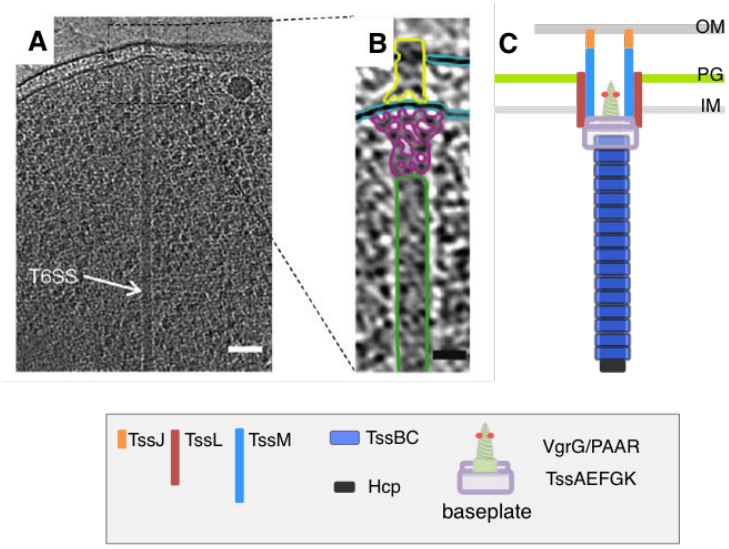

Figure 3.8: **Overview of the T6SS. (A)** Electron cryo-tomography of *Vibrio cholerae* cells producing the T6SS. The arrow points the long cytoplasmic tubular structure corresponding to the T6SS sheath. A magnification of the upper part of the tomograph is shown in panel **(B)**, emphasizing the presence of distinct complexes (green, tail sheath; purple, putative baseplate; yellow, putative membrane complex). **(C)** Schematic representation of the T6SS based on the electron cryo-tomographs and on genetic, biochemical, microscopy and structural data (IM, inner membrane; PG, peptidoglycan layer; OM, outer membrane). Scale bar is 50 nm (Zoued et al., 2014).

target cell delivers toxins. (3) *Disassembly*: ClpV, the AAA+ ATPase, recognizes the contracted sheath and recycles sheath components (Basler and Mekalanos, 2012)(Kapitein et al., 2013).

Based on its structure and mechanism of action, the T6SS is categorized in the contractile phage-like structure family, which comprises bacteriophages, R-type pyocins, anti-feeding prophage (Afp) (Hurst et al., 2007)(Heymann et al., 2013)(Rybakova et al., 2015), *Photorhabdus* virulence cassettes (PVC) (Yang et al., 2006)(Gillespie et al., 1997), and metamorphosis-associated contractile structures (MAC) (Huang et al., 2012)(Shikuma et al., 2014)(Sarris et al., 2014)(Ge et al., 2015)(Böck et al., 2017). All these structures act as a molecular syringe and adopt common features (Cascales, 2017). They harbour an internal tube capped by a needle and surrounded by a contractile sheath. This tubular structure is built on an assembly platform.

However, beside these common features, these structures have notable differences (Cascales, 2017). First, the T6SS injects toxins from the inside the predator cell into the prey cell periplasm or cytoplasm, and thus needs to cross three or four membranes. To do so, the length of the tail is much longer than in the other machineries (app. 670-nm long for T6SS compared to 92 nm for bacteriophages). Another difference is that bacteriophage tail structures are associated with a capsid that contains the nucleic acid to be delivered, whereas the T6SS tail is connected to a membrane-associated complex. The membrane complex has then a distinct evolutionarily history and hence phage-like T6SS components must have evolved to structurally and functionally fit with membrane components.

In the next sub-headings, I will describe the T6SS sub-complexes and will detail the structures, interactions and functions of the different components.

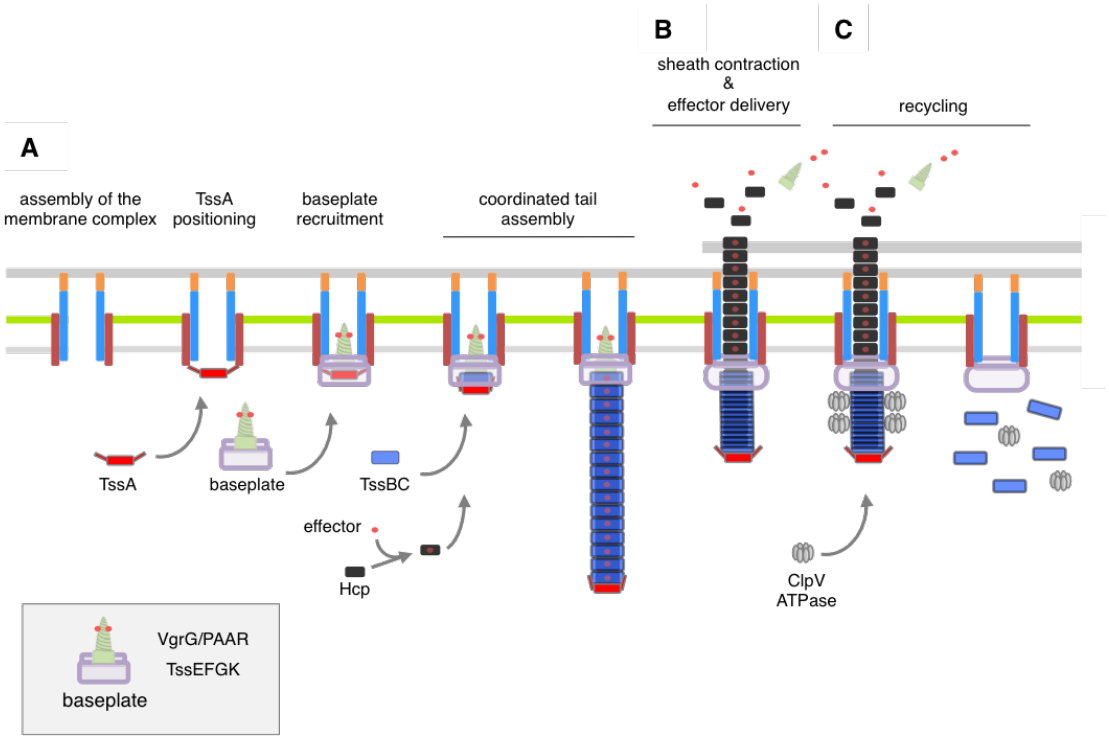

Figure 3.9: **Schematic representation of the different stages of the assembly and mechanism of action of the T6SS.** **(A)** The biogenesis of the macromolecular complex starts with the assembly of the membrane complex at the site of secretion and recruitment of TssA and the baseplate, which initiates polymerization of the tail by the incorporation of Hcp hexamers and TssBC building blocks. During elongation of the tail structure, effectors can be loaded inside the inner tube lumen or attached to the VgrG spike. **(B)** Once in contact with a prey cell, the T6SS sheath contracts hence propulsing the internal tube towards the target prey cell to deliver effector proteins. **(C)** The contracted sheath recruits the ClpV ATPase that dis-assembles and recycles the TssBC sheath proteins (Journet and Cascales, 2016).

3.6.2 Tail complex

As described above, the T6SS tail complex shares a common evolutionary origin with contractile systems. Similarly to contractile tail-like structures, it comprises an inner tube, a contractile sheath and a baseplate.

3.6.2.1 The tail tube Hcp

Structure. The tail tube is formed by the superimposition of hexamers of the Hcp (haemolysin co-regulated protein) protein (Figure 3.10). Hcp is structurally homologous to the tail tube proteins GpV and Gp19 from bacteriophages λ and T4 (Pell et al., 2009)(Leiman et al., 2009). Hcp hexamers form 100-Å wide donut-shaped rings with an internal diameter of 40 Å (Mougous, 2006)(Jobichen et al., 2010)(Douzi et al., 2014).

Assembly. Using cysteine cross-linking, it has been shown that nanotubes formed by the superimposition of Hcp hexamers can be assembled *in vitro* (Ballister et al., 2008). A similar approach revealed that *in vivo* Hcp hexamers stack onto each other in a head-to-tail manner (Brunet et al., 2014). *In vivo*, the proper head-to-tail assembly of the tube is controlled by baseplate components,

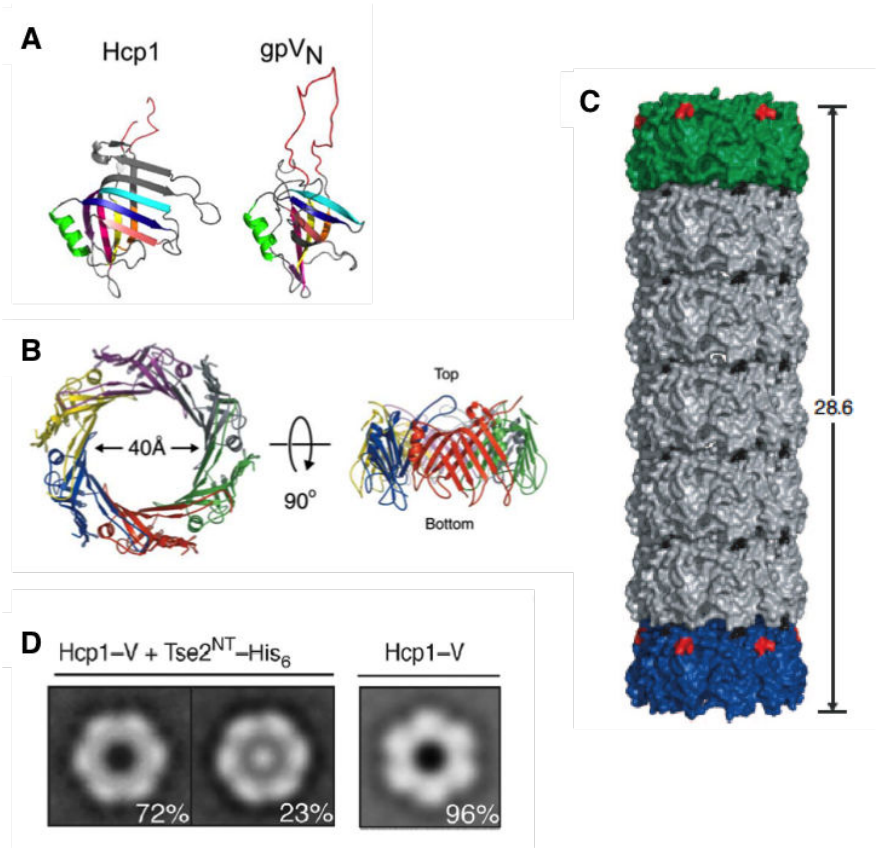

Figure 3.10: **Stucture of the Hcp hexameric ring.** **(A)** Structural similarities between gpV$_N$ and Hcp1. Each secondary structure element in Hcp1 is colored-coded based on its alignment with gpV$_N$. Loops and secondary structure differences are colored in grey, with the exception of the β2-3 loop that is colored red (Pell et al., 2009). **(B)** Top view and edge-on views of a ribbon representation of the crystallographic Hcp1. The individual subunits are colored differently to highlight their organization (Mougous, 2006). **(C)** Model of an Hcp engineered *in vitro* by disulphide bounds chemical cross-linking. The sites of each cysteine substitution are indicated in black (Ballister et al., 2008). **(D)** Class averages from analysis of transmission electron micrographs of $Tse2^{(NT)}$-His_6 – Hcp1-V and a Hcp1-V-only control. The percentage of particles represented by each class average is indicated in the corresponding frame (Silverman et al., 2013).

a result consistent with bacteriophage tail biogenesis (Brunet et al., 2014)(Brunet et al., 2015b). Biophysical studies determined that Hcp hexamers interacts with a 7 μM affinity (Douzi et al., 2014). This low affinity indicates that these nanotubes are instable. *In vivo*, the tail tube should be stabilized by the polymerization of the sheath. The stability of the T6SS tube is a striking difference compared to phage tail tubes, which are very stable and could be readily purified without cross-linking agents (Kostyuchenko et al., 2005). However, it is noteworthy that phage tubes should be maintained stable for a relatively long period to allow the passage of the entire nucleic acid to the target. By contrast, the T6SS tube should be rapidly dissociated once in the target cell to liberate effectors present within the lumen. Recently, Vettiger et al. proposed that Hcp proteins are exchanged among sister cells for new T6SS assemblies suggesting that Hcp hexamers reach the cytoplasm of the target cells (Vettiger and Basler, 2016). Because Hcp tubes are propelled during T6SS firing, the presence of Hcp in the culture supernatant is a reporter of T6SS activity (Mougous, 2006)(Cascales, 2008).

3.6.2.2 The tail sheath

In most contractile structures, such as bacteriophages, the sheath is assembled by the polymerization of a single subunit. In the T6SS, two proteins are necessary to assemble the sheath: TssB and TssC. These two proteins interact and stabilize each other (Bönemann et al., 2009)(Broms et al., 2009)(Lossi et al., 2013)(Zhang et al., 2013). TssB and TssC form heterodimers that polymerize using the Hcp tube as template (Brunet et al., 2014) in an extended conformation that is metastable, energetically unfavourable.

Sheath dynamics. In 2012, Basler et al reported the first *in vivo* observation of the sheath (Figure 3.11) (Basler et al., 2012). They conclusively showed that T6SS sheath exists in two conformations: a short wider contracted (370 nm) and long thinner extended (670 nm) form (Basler and Mekalanos, 2012). In the contracted state, the tubular structure is hollow whereas in the extended state an extra-density is observed inside suggesting that it could accommodate the inner tube Hcp (Basler et al., 2012). A complete cycle of assembly/contraction could be observed by fluorescence microscopy using functional TssB-GFP or TssB-mCherry fusions (Basler and Mekalanos, 2012)(Brunet et al., 2013)(Brunet et al., 2014). In *V. cholerae*, the assembly duration is about 20-60 sec, whereas the sheath contracts in less than 2 msec and is dissassembled within few minutes (Basler and Mekalanos, 2012)(Kapitein et al., 2013)(Brunet et al., 2013)(Vettiger et al., 2017).

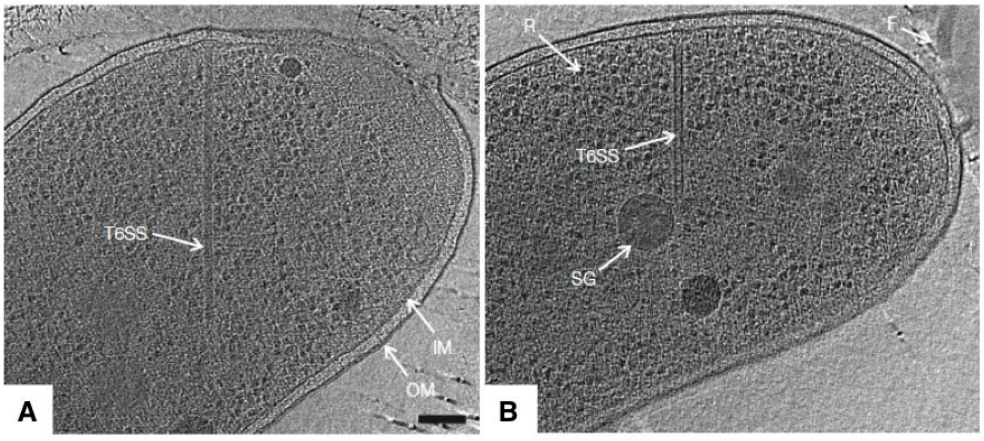

Figure 3.11: **Electron cryotomographic imagining of T6SS structures inside intact cells.** Shown are different tomographic slices (19 nm) of an extended **(A)** and a contracted **(B)** structures imaged in two different wild-type cells (IM, inner membrane; OM, outer membrane; F, flagellum; R, putative ribosome; SG, polyphosphate storage granule). Scale bars, 100 nm (Basler et al., 2012).

Assembly. Recently, it has been elegantly showed that the polymerization of the sheath starts at the baseplate and proceeds with the addition of new subunits at the distal end (Vettiger et al., 2017). Brunet *et al.* showed that the assembly of the sheath is coordinated with that of the inner tube: sheath can not polymerize in absence of Hcp, and only two Hcp hexamers can superimpose in absence of sheath (Brunet et al., 2014). Hence, the addition of a Hcp hexamer immediately precedes that of a tube. In EAEC, the coordinated assembly of the tail tube/sheath is mediated by the TssA chaperone (Zoued et al., 2016b). TssA assembles dodecameric complexes that harbour a starfish-like

conformation (Figure 3.12): the N-terminal domain constitutes the long arm around the central C-terminal domain. Protein-protein interaction and fluorescence microscopy experiments showed that TssA binds the baseplate and then primes and leads polymerization of the tail tube/sheath (Zoued et al., 2016b)(Zoued et al., 2017). An independent study shows divergent results. The *P. aeruginosa* TssA1 protein presents sequence and structural similarities with the gp6 C-terminus and forms ring-shaped structures. TssA1 has been shown to interact with baseplate components (Planamente et al., 2016). However, TssA1 is not essential for T6SS assembly and activity (Planamente et al., 2016), and has a very distinct architecture compared to the EAEC TssA protein, and therefore the two proteins should not be confused (Zoued et al., 2017). In EAEC and *V. cholerae*, a third protein of the TssA family, named TagA, is encoded within the T6SS gene cluster but its function is unknown (Zoued et al., 2017). By contrast to the situation in contractile phages and R-pyocin, the length of the sheath is not controlled by a tape measure protein. Modification of the bacterial size yields sheaths with lengths that adapt to the new dimensions (Vettiger et al., 2017).

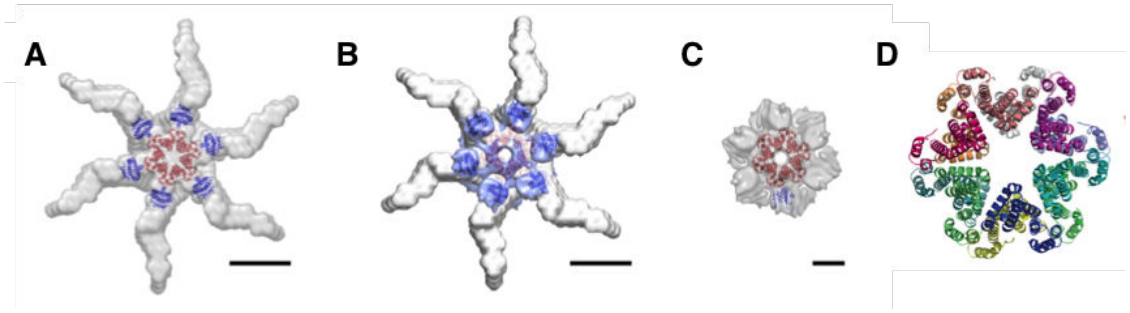

Figure 3.12: **Structures of TssA. (A)** SAXS/X-ray comparison: fitting of TssANt2 (blue ribbon) and TssACt (red ribbon) X-ray structures into the TssA SAXS envelope (transparent grey surface). **(B)** SAXS (grey surface) / EM (transparent light-blue surface) / X-ray comparison. **(C)** EM/X-ray comparison: fitting of TssANt2 (blue ribbon) and TssACt (red ribbon) X-ray structures into the TssA SAXS envelope (transparent grey surface). **(D)** X-ray structure of the C-terminal domain of TssA (PDB: 4YO5). Top view of the dodecamer structure, shown in ribbon representation with each monomer differently coloured. Scale bars are 10 nm (Zoued et al., 2016b).

Structure. Contracted sheaths can be easily purified: they consist to tubular structures that exhibit cogwheel-like cross sections with external and internal diameters of 300 Å and 110 Å respectively. The structure of *V. cholerae* and *Francisella novicida* contracted sheaths was solved by cryo-electron microscopy at low (Kube et al., 2014) and high resolution (Kudryashev et al., 2015)(Clemens et al., 2015)(Figure 3.13). The atomic-resolution structure revealed that TssB and TssC assemble into a six-start helix with interlaced β-sheets that stabilize the heterodimer. In addition, domain swapping occurs between neighbouring TssBC heterodimers and between consecutive rows. By contrast, the extended form is not stable enough to be purified in its native form. However, by substituting residues at the sheath row interface, a recent study has provided a high resolution of the extended T6SS sheath (Wang et al., 2017)

Disassembly. After the contraction of the sheath, the N-terminal helix of TssC, hidden in the extended conformation, is recognized by the ClpV AAA$^+$ ATPase (Pietrosiuk et al., 2011)(Douzi et al., 2016). ClpV disassembles TssBC tubules *in vitro* in an ATP dependent manner (Bönemann

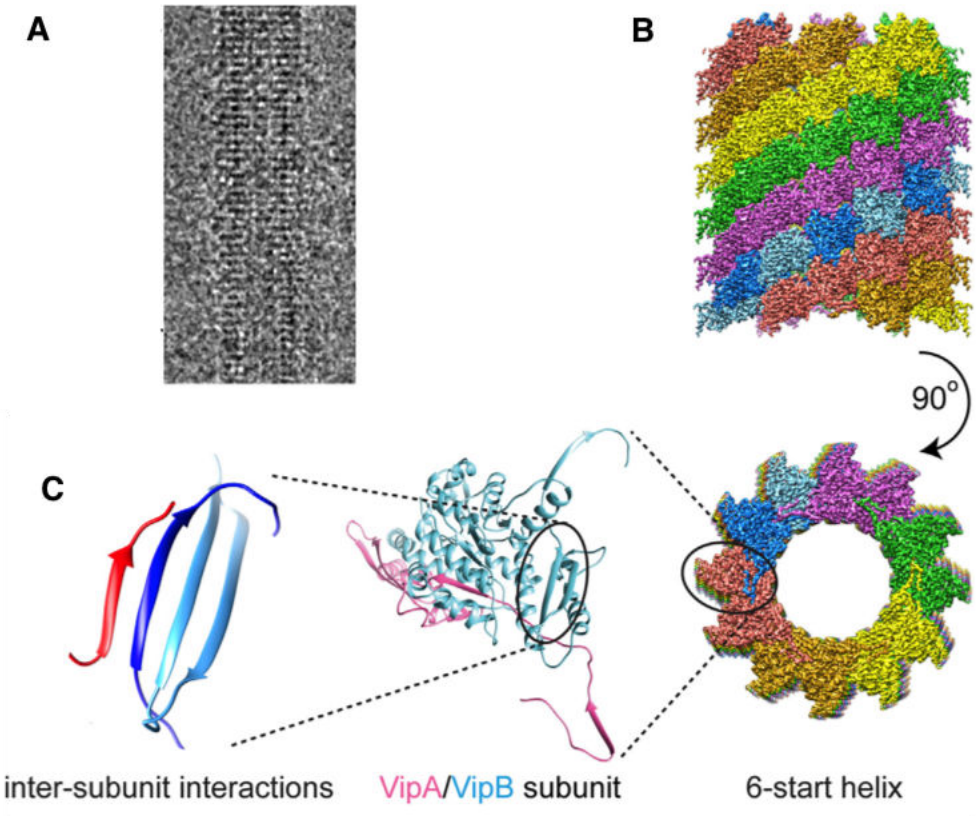

Figure 3.13: **Structure of the T6SS contractile sheath (A)** Cryo-electron microscopy image of a contracted TssBC sheath. **(B)** Atomic structure of the *V. cholerae* TssBC sheath revealing promoter assembly into a 6-start helix, side and top view. **(C)** Representation of TssB/TssC subunit interactions. The "handshake domain" is composed of two antiparallel β-strands from one TssC molecule (light blue), one parallel β-strand from a second TssC on the same helical strand (dark blue) and one parallel β-strand of TssB from a neighbouring helical strand (red) (Kudryashev et al., 2015).

et al., 2009) and also prevents formation of aberrant, aggregated TssBC tubules in the cytoplasm (Kapitein et al., 2013). ClpV is essential for the dynamics of TssBC tubules (Basler and Mekalanos, 2012). Yet, we do not know whether the disassembled TssB and TssC subunits are recycled (*i.e.*, incorporated in a newly polymerized sheath) or whether they are degraded.

3.6.2.3 The baseplate

The tail tube/sheath is built on an assembly platform named "baseplate". This structure likely corresponds to the bell-like density that connects the tubular structure and membrane complex in *V. cholerae* cryo-tomograms (Basler et al., 2012). Baseplate-like structures are also conserved features of all contractile injection systems. Using the *in vivo* cysteine cross-linking approach, Brunet, Zoued *et al.* revealed that 6 T6SS subunits are required for proper assembly of the tail: TssA, TssE, TssF, TssG, TssK and VgrG (Brunet et al., 2015b). In agreement with the proposal that the baseplate connects the membrane complex to the tail tube/sheath, many interactions of baseplate subunits with the cytoplasmic domains of the TssL and TssM inner membrane proteins and with tail tube/sheath have been reported (Zoued et al., 2016b)(Brunet et al., 2015b)(Zoued et al., 2013)(Logger et al., 2016) (see page 64). My Ph.D work identified new contacts between the

TssM cytoplasmic domain and TssG, as well as between TssL and TssM with TssK. These results will be described in the Results part.

TssE. TssE proteins share a high degree of similarity with gp25, a component of the baseplate wedges of bacteriophage T4 (Bingle et al., 2008)(Leiman et al., 2009)(Lossi et al., 2011). During phage tail biogenesis, gp25 initiates the polymerization of the sheath by an arm-exchange mechanism with the first row of gp18 sheath subunits.

TssF and TssG. Bioinformatic analyses show that TssF and TssG share limited homologies to two proteins associated with phage baseplate: phage P2 gpI and gpJ, and phage Mu Mup47 and Mup48 (Brunet et al., 2015b)(Büttner et al., 2016). Like gp25, these proteins are components of the wedges. gpI and Mup47 share homologies with phage T4 gp6. gp6 is a structural component of the baseplate, and has a second function as a connector between the baseplate and the fibers (Taylor et al., 2016). It is thus involved in the signalling cascade leading to baseplate conformational change and sheath contraction after sensing the host cell (Taylor et al., 2016). In the T6SS, TssF and TssG interact and stabilize each other.

TssK. TssK is a cytoplasmic protein that oligomerizes to form a three-armed structure with an overall pyramidal shape (Figure 3.14) (Zoued et al., 2013). The recent structure of TssK showed that it is composed of three domains: a β-stranded N-terminal domain, an α-helical central domain and a mixed α/β C-terminal globular domain. Interestingly, the N-terminal domain of TssK is structurally homologous to the shoulder domain of phage receptor-binding proteins (Nguyen et al., 2017). *In vivo* interaction studies with TssK partners support the idea that TssK acts as a connector between two T6SS complexes that are evolutionarily unrelated: the phage-like baseplate and the membrane complex (Zoued et al., 2013)(English et al., 2014)(Nguyen et al., 2017). The description of TssK domains and contacts will be detailed in the *Results* part.

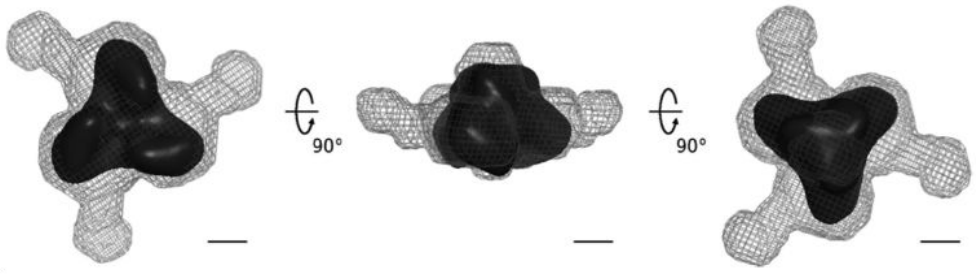

Figure 3.14: **Small-angle X-ray scattering data and low-resolution structure of TssK.** SAXS envelope (light gray mesh) of the "best representative" model of TssK. The EM model is fitted in the SAXS envelope. Each view is rotated by 90 degree around the Y-axis. The scale bar is 3 nm (Zoued et al., 2013).

The VgrG-PAAR spike complex. VgrG is a trimeric protein that shares structural homology with the cell-puncturing devices of bacteriophages, which is composed of a trimer of $(gp27)_3$-$(gp5)_3$ complex in phage T4 (Pukatzki et al., 2007)(Leiman et al., 2009)(Spínola-Amilibia et al., 2016). The crystal structure of the VgrG trimer was solved: the N-terminal domain structure is similar to gp27 and superimposes well with the Hcp hexamer, whereas the central and C-terminal domains

resemble the OB fold and β-prism domains of gp5 (Figure 3.15) (Leiman et al., 2009)(Spínola-Amilibia et al., 2016)(Uchida et al., 2014). The base of VgrG is presumably recognized by the first hexamer of Hcp during biogenesis. A number of VgrG proteins called "specialized VgrG" carry C-terminal extensions located downstream the β-prism, which bear enzymatic activities or adaptor domains. VgrG trimers might be capped by PAAR proteins (Figure 3.16). By forming a conical cap at the extremity of the VgrG spike, PAAR sharpens the tip of the needle (Shneider et al., 2013)(Bondage et al., 2016). In addition to sharpen the needle, several roles have been attributed to PAAR proteins: (i) they can act as adaptor proteins between VgrG and effectors or even can be directly fused to effector domains and (ii) they helps VgrG folding (Shneider et al., 2013)(Cianfanelli et al., 2016)(Ma et al., 2017).

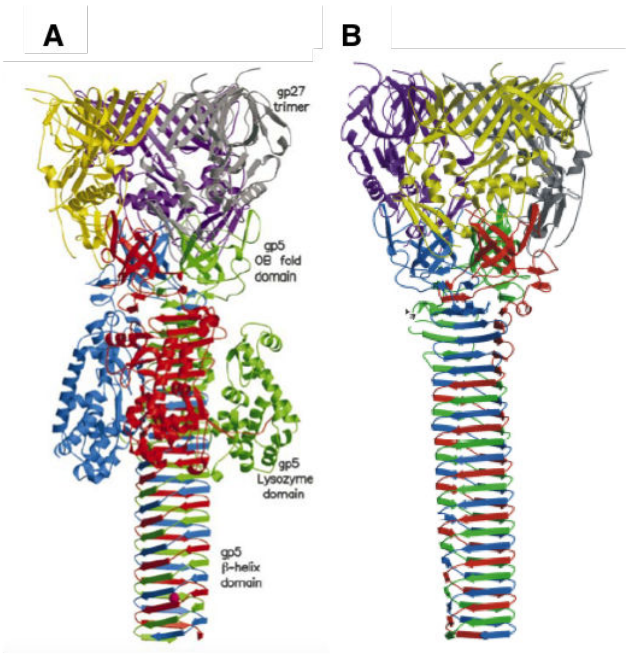

Figure 3.15: **The cell-puncturing device VgrG shares structural features with the phage tail spike of bacteriophage T4.** VgrG is a fusion of the phage tail proteins gp27 and gp5 omitting the OB-fold and lysozyme domains of the phage gp5 protein. **(A)** Structure of the $(gp27)_3$-$(gp5)_3$ complex **(B)** Structure of the *E. coli* CFT073 VgrG protein (Kanamaru et al., 2002)(Leiman et al., 2009)

TssA. The TssA chaperone coordinates the assembly of the tail tube/sheath. However, it is transiently associated with the baseplate by interacting with TssE and VgrG. Because TssA interacts first with the TssJLM membrane complex, prior to baseplate docking, it has been proposed that TssA recruits the baseplate or participate to its recruitment, and stabilizes the TssEFGK-VgrG complex (Zoued et al., 2016b).

In addition to its role in controlling the assembly of the tail, the baseplate serves as connector between the tail and the membrane complex. Numerous interactions between baseplate subunits and tail and membrane complex proteins have been reported (Figure 3.17).

Interactions between baseplate subunits. In EAEC, Brunet et al. showed that TssG interacts with TssF and TssE and that VgrG and TssK interact with the TssFG complex (Brunet et al.,

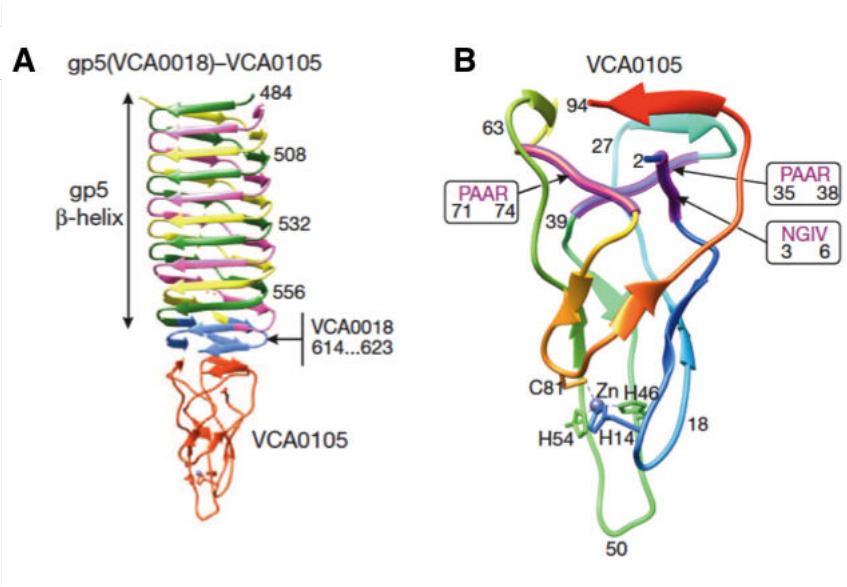

Figure 3.16: **Crystal structure of the T6SS PAAR protein bound to gp5. (A)** Ribbon diagram of the gp5 domain-PAAR complex. **(B)** The polypeptide chain of the VCA0105 PAAR protein is coloured in rainbow colours with the N terminus in blue and C terminus in red. Residues responsible for Zn binding are labelled. PAAR motifs are highlighted with thick purple coils. The sequence and residue members of the starting and ending position for each of the three PAAR motifs are boxed. (Shneider et al., 2013).

2015b). In *S. marcescens*, a complex containing (TssK)4-(TssF)2-(TssG)1 was purified (English et al., 2014) whereas in uropathogenic *E. coli* a complex comprising TssK, -F, -G and -E was purified. However, a different stoichiometry was proposed with (TssK)3- (TssF)2-(TssG)1-(TssE)1 (Taylor et al., 2016). Recently, the EAEC TssK protein was also co-purified with TssFG forming a complex of (TssK)4-(TssF)2-(TssG)1 stoichiometry (Nguyen et al., 2017). However, no structural information has been reported for the TssKFG or TssKFGE complexes. Finally, although it is not a component of the baseplate *per se*, the TssA protein was shown to interact with TssK (Zoued et al., 2013) TssE and VgrG (Zoued et al., 2016a). In *P. aeruginosa*, the H1 gene cluster encodes a TssA-like protein, TssA1, which is required for T6SS activity but that has been proposed to associate with the baseplate (Planamente et al., 2016). As described in the bacteriophage section, the minimal bacteriophage baseplate comprises gp25, gp6, gp53 and the gp27 hub. The T6SS counterparts are TssE, TssF, TssG and VgrG respectively. Therefore, the T6SS baseplate comprises an additional subunit, TssK.

Interactions between the baseplate and the tail tube/sheath. Many interactions have been shown between the tail and the baseplate. TssK, TssF, and TssG interact with the inner tube component Hcp (Zoued et al., 2013)(Brunet et al., 2015b). TssK and TssG interact with TssC (Zoued et al., 2013)(Brunet et al., 2015b). It is also proposed that TssE is initiating the polymerization of the sheath and should interact with TssB and/or TssC (Leiman and Shneider, 2012)(Taylor et al., 2016). Indeed, unpublished data from our laboratory have shown that TssE interacts with TssC.

Interactions between the baseplate and the membrane complex. Baseplate components also interact with the cytoplasmic portion of the membrane complex. The cytoplasmic loop of TssM interacts with TssG and TssK (Logger et al., 2016)(Brunet et al., 2015b)(Zoued et al., 2013) whereas the

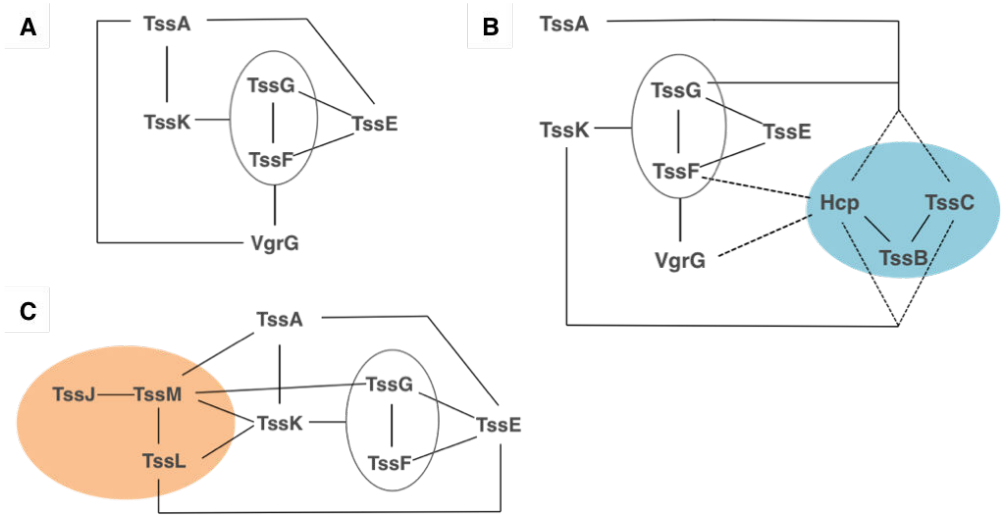

Figure 3.17: **Interactions within T6SS subunits** Schematic representation of the interactions between baseplate subunits **(A)**, between the baseplate and the tail tube/sheath **(B)** and between the baseplate and the membrane complex **(C)**.

TssL cytoplasmic domain interacts with TssE and TssK (Zoued et al., 2016a)(Zoued et al., 2013). By interacting with both TssL and TssM, and because of the strong co-occurrence of the *tssK* and *tssL* genes in bacterial genomes, the TssK protein appears clearly as a key player for connecting the baseplate and the membrane complex.

3.6.3 Membrane complex

The T6SS membrane-anchoring complex is composed of three proteins: TssJ, TssM and TssL (Cascales, 2008). The localization, the topology and the structure of most soluble domains of these subunits are known (Figure 3.18). In several bacteria, an additional component called TagL associates with the three proteins (Aschtgen et al., 2010b)(Aschtgen et al., 2010a). Recently, the EAEC TssJ-L-M proteins were co-purified and the structure of the 1.7-MDa TssJLM complex was solved at 11.6 Å resolution by negative-stain electron microscopy (Figure 3.22) (Durand et al., 2015).

3.6.3.1 The outer membrane TssJ lipoprotein

TssJ is a lipoprotein. The unprocessed form of TssJ bears a classical lipobox at its N-terminus including a cysteine residue that is processed by acylation. The glycine residue at the position +2 is responsible for the targeting of TssJ at the outer membrane (Aschtgen et al., 2008). The crystal structures of TssJ from EAEC (Figure 3.19), *S. marcescens* and *P. aeruginosa* were solved (Felisberto-Rodrigues et al., 2011)(Rao et al., 2011)(Robb et al., 2013). They present the same overall structure: TssJ is a β-sandwich with a transthyretin-fold with an additional L1-2 loop and a helical domain. The two loops L1-L2 and L5-L6 may have a functional importance as they adopt similar sizes and conformations. Indeed, the L1-2 loop of TssJ is involved in the interaction with TssM. This loop varies in sequence when comparing other TssJ orthologs, which could indicate a specificity determinant between cognate TssJ and TssM subunits (Felisberto-Rodrigues et al.,

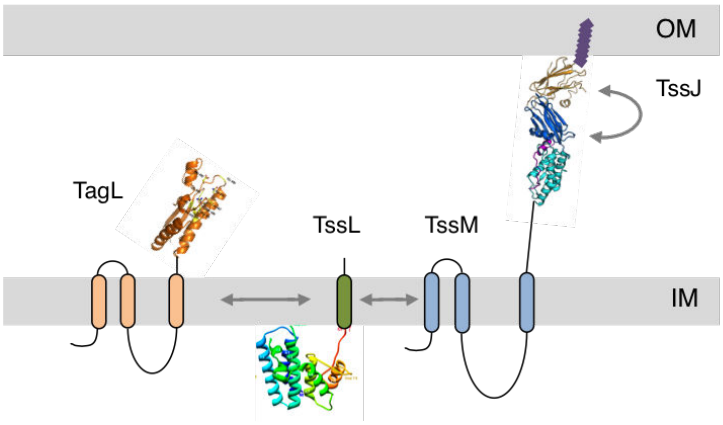

Figure 3.18: **The T6SS membrane-anchoring complex.** Schematic representation of the membrane complex with localization, topology and structure of its subunits. Are represented the outer membrane lipoprotein TssJ and the inner membrane components TssL, TssM and TagL. The interaction network is indicated with arrows. IM, inner membrane; OM, outer membrane.

2011).

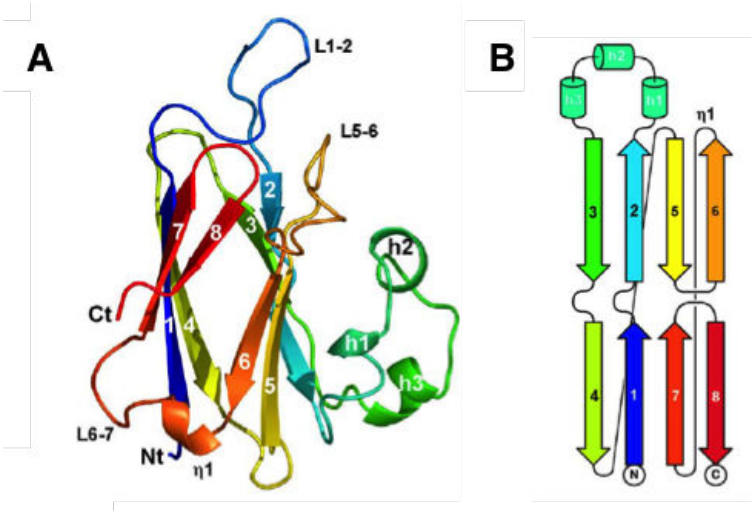

Figure 3.19: **Structure of the EAEC outer membrane TssJ lipoprotein. (A)** Ribbon diagram of the soluble part (residues 25-178) of the TssJ protein represented in rainbow color running from the N- (blue) to C-terminal (red). **(B)** Topology cartoon of TssJ using the same color scheme as in the (A). (Felisberto-Rodrigues et al., 2011).

3.6.3.2 The inner membrane TssM polytopic protein

With the exception of the *P. aeruginosa* H1-T6SS protein that is predicted to have a single transmembrane segment, TssM are inner membrane proteins inserted by three transmembrane helices (Ma et al., 2009b)(Logger et al., 2016). The second and third transmembrane segments delimitate a 35-kDa cytoplasmic loop.

The large C-terminal domain of approximately 800 amino-acids resides in the periplasm. The periplasmic portion is composed of a large α-helical region followed by a C-terminal β-domain.

This β-domain is responsible for contacting the TssJ lipoprotein. TssJ and TssM form a complex with a 1:1 stoichiometry and interact with a K_D of 2-4 μM (Felisberto-Rodrigues et al., 2011). The crystal structure of a 26-kDa fragment of the periplasmic domain of TssM comprising the last four α-helices of the helical domain, the β-domain and the C-terminal helix has been solved alone and in complex with TssJ (Durand et al., 2015).

The second and third transmembrane helices delimit a cytoplasmic loop of 300 amino-acids. This loop harbours a classical NTPase fold but NTP-binding and hydrolysis motifs (Walker A, Walker B and NTP specific motifs) are missing in EAEC (Logger et al., 2016). The relevance of these motifs is not clear, as they do not have the same impact on T6SS function. In *Edwardsiella tarda*, the TssM Walker A motif is not necessary (Zheng and Leung, 2007) whereas it is essential in *A. tumefaciens* (Ma et al., 2009b). The *A. tumefaciens* TssM protein binds and hydrolyses ATP, which modulates the structural conformation of TssM and the recruitment of Hcp to the TssM-TssL complex (Ma et al., 2012).

During my Ph.D work, I have defined the topology of the EAEC TssM protein and the interaction network of its cytoplasmic loop with the other T6SS components. I have participated to additional studies on the TssJLM complex and on the *in vivo* characterization of llama nanobodies that target the TssM periplasmic domain and disrupt the TssJ-TssM interaction. These data will be described in *Articles 1, 2 and 3*.

It is worth to note that TssM is a homologue of IcmF, an accessory protein of the *Legionella pneumophila* and *Coxiella burnetii* Type IVb secretion system (T4bSS). TssM and IcmF share similar topology and architecture. In addition, IcmF interacts with IcmH, a homologue of TssL, to form a complex required for the stability of the T4bSS complex (Sexton et al., 2004)(Zusman et al., 2004).

3.6.3.3 The inner membrane TssL bitopic protein

TssL is an inner membrane protein with a unique transmembrane segment located at the C-terminus leaving the vast majority of the protein in the cytoplasm (Aschtgen et al., 2012). This unusual topology categorizes TssL as a C-tail anchored protein. Its insertion in the membrane is mediated by the YidC insertase and the DnaK chaperone (Aschtgen et al., 2012)(Pross et al., 2016). TssL dimerizes and the dimerization is required for the proper function of the T6SS. The crystal structures of the TssL cytoplasmic domain from EAEC, *F. novicida* and *V. cholerae* were solved (Durand et al., 2012b)(Robb et al., 2013)(Chang and Kim, 2015). TssL is constituted of two three-helix bundles resembling of a hook. In addition to the negatively-charged cavity at the intersection of the two bundles, TssL harbours interesting features such as highly charged loop. A structure-function analysis of the different conserved motifs of TssL determined the contribution of each of these motifs in the interaction with the different TssL partners (Zoued et al., 2016a).

Several TssL carry an additional periplasmic C-terminal domain that shares similarities with the OmpA/Pal/MotB or SPOR peptidoglycan-binding motifs (Aschtgen et al., 2010b). In the absence of such domain, such as for the EAEC *sci-1* cluster, T6SS clusters encode for an accessory protein capable of binding the peptidoglycan (Aschtgen et al., 2010a).

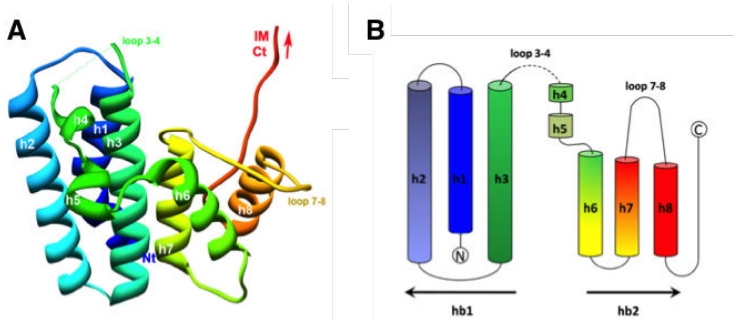

Figure 3.20: **Structure of the EAEC TssL cytoplasmic domain.** **(A)** Ribbon diagram of the soluble part of the TssL protein represented in rainbow color running from the N- (blue) to C-terminal (red). **(B)** Topology cartoon of TssL using the same color scheme as in the A. The three-helix bundles (hb1 and hb2) are indicated (Durand et al., 2012b).

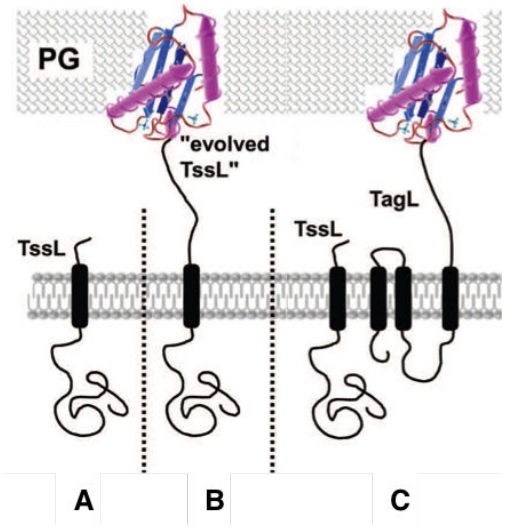

Figure 3.21: **Schematic representation and topology of the TssL proteins. Case A:** no PG-binding domain on TssL. **Case B:** TssL proteins carrying a PG-binding domain of the OmpA/MotB/Pal. **Case C:** TssL interacts with TagL carrying the PG-binding domain (Aschtgen et al., 2010b)

In EAEC, TagL is an inner membrane protein containing three transmembrane domains and a large C-terminal domain of 32 kDa in the periplasm. This C-terminal domain contains the OmpA/Pal/MotB peptidoglycan-binding motif. TagL anchors the TssJLM complex to the cell wall and is required for the function of the T6SS (Aschtgen et al., 2010a).

3.6.3.4 The TssJLM complex

Structure. The TssJLM membrane complex from enteroaggregative *E. coli* was purified and visualized by negative-stain electron microscopy (EM) (Durand et al., 2015). The overall structure of this 1.7-MDa complex was solved at 11.6 Å resolution with a clear five-fold symmetry (Figure 3.22). The T6SS membrane core complex is 300 Å in height and 205 Å in diameter. In the centre of the structure a small hole of 15 Å in diameter is observed. The membrane complex is composed of a base and a tip complex linked by arches. We can distinguish five internal pillars and five

external pillars in concentric rings that are the TssM proteins in 10 copies and a large domain in the cytoplasmic side, probably the cytoplasmic domains of TssL ans TssM.

Stepwise assembly. A simple but elegant experiment revealed in which order the three membrane proteins are assembled. The reasoning is if an early protein is missing, the recruitment of a later protein will be affected (Durand et al., 2015). Fusion proteins from their native chromosomal loci were produced in the wild-type strain or in deletion backgrounds. The proper localization of each protein with or without partners was analysed. The recruitment of TssM is affected by the absence of TssJ, whereas TssL requires both TssJ and TssM for its recruitment. Thus, TssJ is the first protein to be recruited and is followed by the sequential additions of TssM and TssL

Peptidoglycan local degradation. The TssJLM complex is inserted in both inner and outer membrane. More specifically, TssM extends into the periplasm and interacts with TssL and TssJ. The TssJLM thus crosses the peptidoglycan layer. Two independent studies revealed that a lytic transglycosylase -MltE- and a peptidoglycan hydrolase –TagX- locally degrade the cell wall to allow proper insertion of the T6SS membrane complex. in EAEC and *Acinetobacter* respectively (Santin and Cascales, 2016)(Weber et al., 2016).

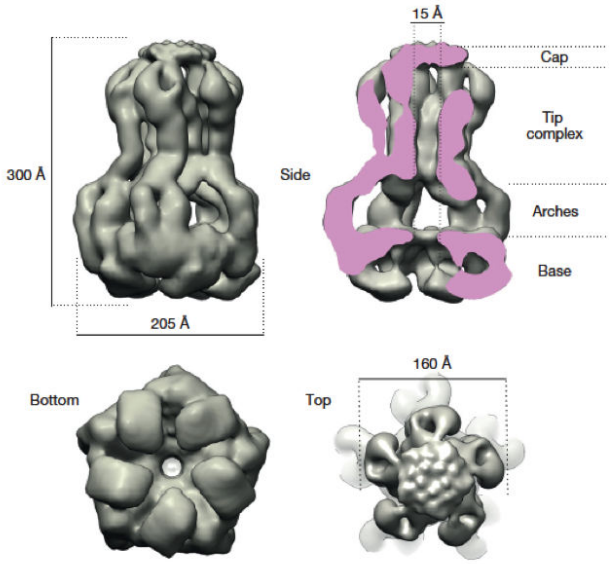

Figure 3.22: **TssJLM complex structure.** Structure of the TssJLM complex. Side, cut-away, bottom and top views are shown from top left to bottom right respectively. The different regions of the complex are indicated on the cut-away view (Durand et al., 2015).

Part II

Results and Discussion

Introduction

The bacterial model used in the laboratory is enteroaggregative *Escherichia coli*, a pathotype of the *E. coli* group. The *E. coli* species regroups commensal and pathogenic bacteria of the gastro-intestinal tract. The commensal species are inoffensive inhabitants and are part of the healthy flora. By contrast, adapted clones that have acquired virulence factors cause diseases (Kaper et al., 2004). A number of mobile genetic elements bearing secretion systems or toxin genes have contributed to the evolution of the harmless *E. coli* strains into pathogenic strains (Kaper et al., 2004). Based on the acquired virulence factors, and hence on the mode of infection to cause diseases, a number of *E. coli* pathotypes could be distinguished: extraintestinal pathogenic *E. coli* (ExPEC) and intestinal *E. coli* pathogens. The ExPEC sub-group includes strains that cause cystitis and polynephritis, such as uropathogenic *E. coli* (UPEC), and strains that are responsible for meningitidis-like syndroms and cause neurological lesions (MNEC). Intestinal *E. coli* strains are responsible for diarrheal diseases, and depending on the mode of colonization and infection, are categorized in six pathotypes (Figure 1.23): enterotoxigenic (ETEC), enteropathogenic (EPEC) enterohemorrhagic (EHEC), enteroinvasive (EIEC), diffusely adherent (DAEC) and enteroaggregative (EAEC) *E. coli*. Each of them has unique features in their interaction with eukaryotic cells (Kaper et al., 2004)(Harrington et al., 2006). However, horizontal transfers occur between these strains, and hence new clones combining adaptive traits from several of these pathotypes regularly emerge.

The model that is used in the laboratory is the EAEC 17-2 strain. The EAEC pathotype could be distinguished by its ability to form packed biofilm-like structures that adhere to Hep-2 cells (Nataro et al., 1987). Several EAEC strains have been isolated, including the prototypical 042 and 17-2 strains. 042 was isolated from a child with diarrhea in Peru whereas 17-2 was isolated from a child with diarrhea in Chile (Nataro et al., 1995). Using experiments on volunteers, it has been shown that these strains exhibit heterogeneity in virulence levels (Nataro et al., 1995). Only 1 of 19 volunteers fed with the 17.2 strain experienced diarrhea whereas the 042 strain caused diarrhea in 3 of 5 volunteers (Nataro et al., 1995).

The microbiological and pathogenic characterization of EAEC isolates revealed that a 60-MDa plasmid, pAA, is the major genetic element responsible for the EAEC-specific mode of colonization (Vial et al., 1988). pAA encodes important virulence factors such as the heat-stable enterotoxin (EAST) and the AAF/I adherence factor, a bundle-forming fimbria responsible for the hemagglutination of human erythrocytes (Nataro et al., 1992). The AAF/I genes are positively regulated by AggR, an AraC family transcriptional activator (Nataro et al., 1994). Interestingly, AggR also

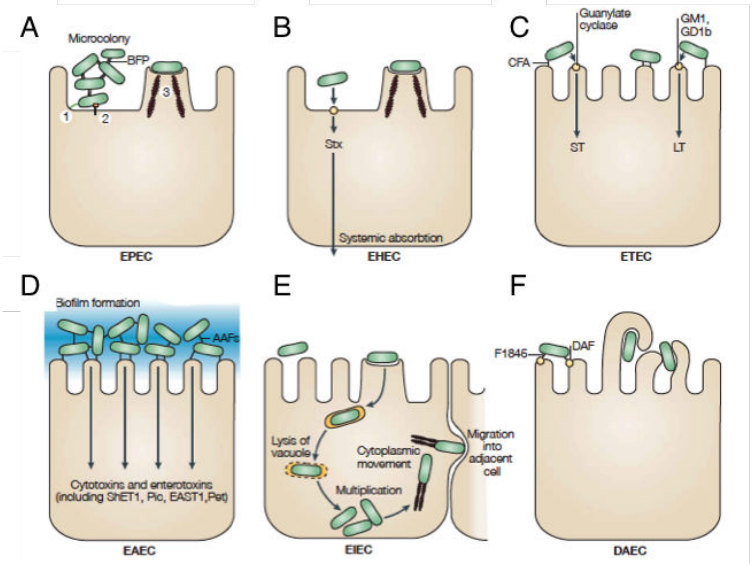

Figure 1.23: **Schematic representation of diarrhoeagenic *E. coli*.** The six recognized categories of diarrhoeagenic *E. coli* have unique features in their interaction with eukaryotic cells. **(A)** EPEC adhere to enterocytes (1. Initial adhesion, 2. Protein translocation by T3SS, 3. Pedestal formation. **(B)** EHEC induce lesions in the colon by the elaboration of the Shiga toxin (Stx). **(C)** ETEC adhere to enterocytes and induce diarrhoea by the secretion of heat-labile (LT) and/or heat-stable (ST) enterotoxins. **(D)** EAEC adheres to bowel epithelia in a thick biofilm and elaborates secretory enterotoxins and cytotoxins. **(E)** EIEC invades the colonic epithelial cell, lyses the cell and migrate into adjacent cell. **(F)** DAEC elicits a characteristic signal transduction effect in small bowel enterocytes (Kaper et al., 2004).

activates the expression of one chromosomal cluster encoding a T6SS. This cluster, named *sci-2*, is localized within a pathogenicity island (PAI) inserted at the *pheU* tRNA locus. The fact that AggR is a global regulator of EAEC virulence determinants suggests that the Sci-2 T6SS may also contribute to EAEC pathogenesis (Dudley et al., 2006). The EAEC *pheU* PAI encodes a second T6SS gene cluster: the *sci-1* locus, which is the main model used in the laboratory. The expression of this gene cluster is under the control of the ferric uptake repressor (Fur) and modulated by Dam-dependent methylation (Brunet et al., 2011). Finally, the complete genome sequence of the archetypal EAEC 042 strain revealed the existence of a third T6SS cluster localized at the *aspV* tRNA locus.

According to the gene organization and to homologies/similarities, the *E. coli* T6SS gene clusters categorize in three distinct phylogenetic groups: T6SS-1 to T6SS-3 (Figure 1.24) (Journet and Cascales, 2016). The T6SS-1 (*sci1-like*) and T6SS-2 gene clusters are the most commonly found in *E. coli* chromosomes. Concerning the T6SS-2 gene cluster, it is overrepresented in pathogenic strains with high virulence traits. For example, in EAEC, the 042 strain which is a T6SS-2$^+$ strain causes diarrhea whereas the attenuated 17-2 strain that is T6SS-2- fails to elicit diarrhea in human volunteers. However, the T6SS-1 and T6SS-2 ((*sci2-like*) gene cluster are also found in non-pathogenic strains of *E. coli* such as *E. coli* W indicating that they are probably not directly involved in pathogenesis (Journet and Cascales, 2016). Indeed, the Sci-1 (T6SS-1) and Sci-2 (T6SS-3) T6SSs are involved in bacterial competition (Brunet et al., 2013)(Flaugnatti et al., 2016).

Because of its weak virulence, its sensitivity to most of the common antibiotics and its ease

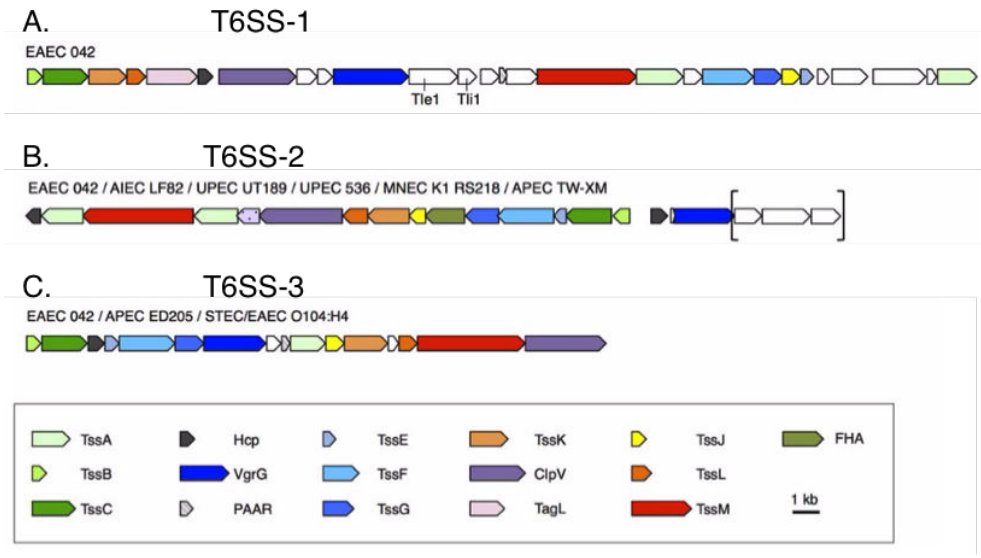

Figure 1.24: **Organization of T6SS-1 to -3 gene clusters of EAEC 042.** Homologous genes are colored similarly (see box below). Open reading frames with unknown function are shown in white. Genes into brackets are not present or not identical in all strains listed. Genes were identified using the SecReT6 database. (Journet and Cascales, 2016).

for genetic manipulations, we use the 17-2 strain as model in the laboratory. The study of the EAEC T6SS has been a major research topic in the team since 2008. The goal of the team is to contribute to the understanding of the T6SS mode of action, by determining how it is regulated, by structurally and functionally characterizing the different subunits that compose the T6SS, by understanding its biogenesis pathway and by defining the toxin delivered by the T6SS and how they are transferred into target cells. Before my arrival in the laboratory, three PhD students had already worked on the T6SS and have contributed new information.

Marie-Stéphanie Aschtgen (thesis defended in 2011) characterized the four T6SS membrane proteins - TssJ, TssL, TssM and TagL - in terms of localization, topology and function. She found that TagL binds the peptidoglycan layer and anchors the T6SS to the cell wall (Aschtgen et al., 2010b)(Aschtgen et al., 2010a). TagL binds to the TssL C-tail protein (Aschtgen et al., 2012)(Durand et al., 2012b). She also reported that TssJ is an outer membrane lipoprotein (Aschtgen et al., 2008) that interacts with the periplasmic domain of TssM (Felisberto-Rodrigues et al., 2011).

Yannick Brunet (Thesis defended in 2013) was interested in 2 main topics: the T6SS phage-related complex - more specifically the assembly of the sheath and the inner tube - and the regulation of T6SS clusters. He first identified the regulation mechanisms of the EAEC *sci-1* and the *Salmonella* T6SS gene clusters (Brunet et al., 2011)(Brunet et al., 2015a). He then found that the Sci-2 T6SS is responsible for antibacterial competition and demonstrated that contraction of the T6SS sheath coincides with the lysis of the target prey cell (Brunet et al., 2013). By working on the T6SS tail, he demonstrated that the inner tube is made by the stacking of Hcp hexamers in a head-to-tail manner, and that the inner tube serves as template for the assembly of the sheath (Brunet et al., 2014). Finally, by using the Hcp assembly assay, he showed that a number of T6SS subunits, that likely assemble the baseplate, are necessary for proper polymerization of the inner tube (Brunet et al., 2015b).

Abdelrahim Zoued (Thesis defended in 2015) characterized the assembly pathway of the T6SS membrane complex (Durand, Zoued, 2015), participated to the characterization of the baseplate (Brunet et al., 2015b) and more specifically on the TssK subunit and its interaction with the TssL membrane protein (Zoued et al., 2013)(Zoued et al., 2016a). He also identified TssA, the subunit that coordinates the polymerization of the inner tube with that of the sheath (Zoued et al., 2016b)(Zoued et al., 2017).

Based on these previous studies, the projects that I developed during my PhD work were focused on the TssM membrane protein: its topology and the link between the TssM C-terminal extension and the outer membrane. I then provided details on the docking of the baseplate to the membrane complex by characterizing the cytoplasmic domain of TssM and the TssK baseplate component. The description of the *Results* will be divided in two chapters. In the first chapter, I will concentrate on the "periplasmic" portion of TssM, including the characterization of specific camelid antibodies targeting TssM (*Article 1*) and the extracellular localization of the TssM C-terminal extension (*Article 2*). I will provide in this chapter unpublished results regarding a mutagenesis and functional study of this C-terminal extension, and the construction and characterization of EAEC mini-cells aimed at providing *in vivo* structural information on the T6SS membrane complex by electron cryo-tomography. In the second chapter, I will present the topology of TssM and the characterization of its cytoplasmic domain (*Article 3*) and notably, its interactions with baseplate components. *Article 4* describes the structure of TssK, and the contribution of its C-terminal head domain to docking to the membrane complex. During my thesis I have also participated to other studies, including the characterization of the TssB-TssC interaction and a structure-function analysis of the TssB C-terminal domain. These articles, as well as review and protocol chapters on which I have participated are listed in the *Annexes*.

Article 1: Inhibition of type VI secretion by an anti-TssM llama nanobody

Article 1: Inhibition of type VI secretion by an anti-TssM llama nanobody

As mentioned in the *Introduction*, the T6SS is a contact-dependent mechanism and hence is likely activated by a close contact with a target bacterium. Sensing the presence of a target is thus of primary importance. "Defensive" T6SS utilize a post-translational activation pathway to sense an attack or a perturbation of the cell envelope, and the genetic determinants of this pathway are known and characterized. By contrast, nothing is known for "offensive" T6SS for which the genes encoding the post-translational pathway are not present. The simplest hypothesis is that the outermost part of the T6SS is likely to sense the target cell. Hence, the characterization of the outer shell components is crucial.

The membrane complex of the T6SS comprises three proteins: TssJ, TssL and TssM. TssJ is an outer membrane lipoprotein (Aschtgen et al., 2008) with a β-sandwich transthyretin fold (Felisberto-Rodrigues et al., 2011). The extended L1-L2 loop mediates interaction with the periplasmic domain of TssM (TssMp, residues 386-1129), and more specifically with the C-terminal β-stranded domain of TssM (Felisberto-Rodrigues et al., 2011). Interestingly, in other trans-envelope apparati, outer membrane lipoproteins are involved in the proper insertion of β-stranded secretins in the outer membrane. One exciting hypothesis is that TssJ mediates insertion of the C-terminal TssM domain into the outer membrane. To test this hypothesis, we sough to gain structural and functional information of the periplasmic portion of TssM. When I started this project, no information was available for the periplasmic domain of TssM, and crystallization trials have been unsuccessful. To by-pass crystallization problems, our collaborators proposed to raise camelid nanobodies. Camelid antibodies are devoid of light chains and are composed of a heavy-chain homodimer terminated by monomeric variable antigen-binding V_HH domains called nanobodies. These single-domain V_HH antibodies are the smallest antibodies and can be easily produced in the *E. coli* periplasm. They improve protein solubility and co-crystallization with the protein of interest. In this work, two nanobodies - nb25 and nb02 - that bind TssMp with nanomolar affinities were selected and their structures were described. The nb25 nanobody competes with TssJ binding on TssMp and can even disrupt the TssM-TssJ complex *in vitro*. I then tested the impact of the production of the nanobodies in the periplasm of EAEC. The data showed that the nanobodies also compete for formation of the TssJ-TssM complex *in vivo* and that they disrupt T6SS function: Hcp is not released and no antibacterial activity could be observed in presence of the nanobody in

the periplasm. These data showed that these nanobodies are indeed very good TssM binders and that they compete for TssJ binding, resulting in T6SS dysfunction.

PLOS | ONE

RESEARCH ARTICLE

Inhibition of Type VI Secretion by an Anti-TssM Llama Nanobody

Van Son Nguyen[1,2☯], Laureen Logger[3☯], Silvia Spinelli[1,2], Aline Desmyter[1,2], Thi Thu Hang Le[1,2], Christine Kellenberger[1,2], Badreddine Douzi[1,2¤a], Eric Durand[1,2¤b], Alain Roussel[1,2], Eric Cascales[3]*, Christian Cambillau[1,2]*

1 Architecture et Fonction des Macromolécules Biologiques, Centre National de la Recherche Scientifique (CNRS)—UMR 7257, Marseille, France, **2** Architecture et Fonction des Macromolécules Biologiques, Aix-Marseille Université, Campus de Luminy, Case 932, Marseille, France, **3** Laboratoire d'Ingénierie des Systèmes Macromoléculaires, Institut de Microbiologie de la Méditerranée, Aix-Marseille Université, CNRS—UMR 7255, 31 chemin Joseph Aiguier, Marseille, France

☯ These authors contributed equally to this work.
¤a Current address: Department of Biochemistry and Molecular Biology, Faculty of Medicine, 2350 Health Sciences Mall, Vancouver BC, Canada
¤b Current address: G5 Biologie Structurale de la Sécrétion Bactérienne, CNRS UMR 3528, Institut Pasteur, Paris, France
* ccambillau@gmail.com (CC); cascales@imm.cnrs.fr (EC)

OPEN ACCESS

Citation: Nguyen VS, Logger L, Spinelli S, Desmyter A, Le TTH, Kellenberger C, et al. (2015) Inhibition of Type VI Secretion by an Anti-TssM Llama Nanobody. PLoS ONE 10(3): e0122187. doi:10.1371/journal.pone.0122187

Academic Editor: Erh-Min Lai, Academia Sinica, TAIWAN

Received: December 21, 2014

Accepted: February 12, 2015

Published: March 26, 2015

Data Availability Statement: All relevant data are within the paper.

Funding: This work was supported by grants from the Agence Nationale de la Recherche to EC (ANR-10-JCJC-1303-03) and from the Fondation pour la Recherche Médicale (FRM) to CC (DEQ2011-0421282). VSN is supported by a PhD grant from the French Embassy in Vietnam, and TTHL is supported by a PhD grant from the University of Sciences and Techniques of 1 Hanoi (USTH). LL is supported by a doctoral fellowship from the French Ministry of Research. ED was supported by a FRM post-doctoral fellowship (FRM-SPF20101221116). The funders had

Abstract

The type VI secretion system (T6SS) is a secretion pathway widespread in Gram-negative bacteria that targets toxins in both prokaryotic and eukaryotic cells. Although most T6SSs identified so far are involved in inter-bacterial competition, a few are directly required for full virulence of pathogens. The T6SS comprises 13 core proteins that assemble a large complex structurally and functionally similar to a phage contractile tail structure anchored to the cell envelope by a trans-membrane spanning stator. The central part of this stator, TssM, is a 1129-amino-acid protein anchored in the inner membrane that binds to the TssJ outer membrane lipoprotein. In this study, we have raised camelid antibodies against the purified TssM periplasmic domain. We report the crystal structure of two specific nanobodies that bind to TssM in the nanomolar range. Interestingly, the most potent nanobody, nb25, competes with the TssJ lipoprotein for TssM binding *in vitro* suggesting that TssJ and the nb25 CDR3 loop share the same TssM binding site or causes a steric hindrance preventing TssM-TssJ complex formation. Indeed, periplasmic production of the nanobodies displacing the TssM-TssJ interaction inhibits the T6SS function *in vivo*. This study illustrates the power of nanobodies to specifically target and inhibit bacterial secretion systems.

Introduction

The type VI secretion system (T6SS) is a machinery widespread in Gram-negative bacteria and dedicated to the delivery of toxins in bacterial and eukaryotic host cells. By its anti-bacterial antagonistic action, the T6SS is one of the main players in the bacterial warfare for the access to nutrients and for colonization of the ecological niche [1, 2]. The T6SS assembles from 13

no role in study design, data collection and analysis, decision to publish, or preparation of the manuscript.

Competing Interests: The authors have declared that no competing interests exist.

conserved components. Architecturally, the T6SS can be seen as a micrometer-long syringe anchored to the cell membrane by a trans-envelope complex [3–6]. The phage tail-related syringe-like tubular structure is composed of an internal tube tipped by a spike-like complex, wrapped by a contractile sheath and tethered to the membrane through contacts with components of a trans-envelope multiprotein complex [6, 7]. This membrane-associated complex is composed of the TssL and TssM inner membrane proteins and of the TssJ outer membrane lipoprotein [8–13]. The TssM and TssL proteins interact and stabilize each other and share homologies with the Type IVb secretion system IcmF and DotU subunits respectively [12, 14, 15]. In enteroaggregative *Escherichia coli* (EAEC), TssM (accession number: EC042_4539; gene ID: 387609960) is a 1129-amino-acid protein anchored to the inner membrane by three transmembrane helices and bearing a large ~ 750 amino-acid periplasmic domain (amino-acids 386–1129). The C-terminal extremity of the TssM periplasmic domain interacts with the L1-2 loop of the TssJ lipoprotein with a K_D of 2–4 μM [11]. By combining interactions with inner membrane and outer membrane-associated components, the TssM protein crosses the cell envelope and is therefore central to the T6SS membrane complex.

Although the EAEC TssM periplasmic domain purified readily, we did not succeed to gain structural information [11]. One of the most efficient approaches to improve the crystallization process is to use co-crystallization of the protein of interest with cognate camelid nanobodies. Camelid (llamas, dromaderies and alpacas) antibodies differ from classical antibodies as they only associate two heavy-chains, lacking the CH1 domain and terminated by monomeric variable antigen-binding V_HH domains called nanobodies [16, 17, 18]. By contrast to the conventional immunoglobulin domains, these single-domain V_HH antibodies are highly convenient: in addition to be the smallest antibodies, they are easy to produce in the *E. coli* periplasm [19]. Therefore, they have remarkable potential in the biotechnology and bio-pharmaceutical fields [18, 20, 21]. More important for structural biologists, they also demonstrated their efficiency to improve protein solubility and facilitating crystallization when complexed with the protein of interest [19], in particular for membrane-associated or flexible proteins [22, 23, 24, 25, 26]. Finally, due to their high affinity and selectivity and their small size, nanobodies are excellent enzymes and receptors inhibitors and can be used for functional studies.

To gain further information on the EAEC TssM protein, the purified TssM periplasmic domain was used for llama immunization. Here we report the selection and the structural analysis of two specific nanobodies. These antibodies bind to the TssM periplasmic domain with a K_D in the nanomolar range. One of these nanobodies disrupts the TssM-TssJ interaction *in vitro* and prevents the proper function of the T6SS apparatus.

Results and Discussion

Selection and crystal structures of TssM-specific nanobodies

Nanobodies were raised by immunization of llamas with the purified periplasmic domain of the EAEC TssM protein (TssMp). Three strong TssMp binders were identified from the immune library by three rounds of panning using phage display coupled to ELISA. Two nanobodies, called nb02 and nb25, were selected for further studies based on their high affinity for TssM and on their amino-acid differences in the variable regions, suggesting they bind distinct regions of TssMp (Fig. 1A). The third nanobody, nb42, is very similar to nb25, and was not retained for the structural studies. The two selected nanobodies, nb02 and nb25, sharing 77% sequence identity, were produced in the periplasm of *E. coli*, purified to homogeneity and concentrated to 10 mg/ml. Both nb02 and nb25 behaved as monomers in size-exclusion chromatography and both crystallized readily, allowing to solve their three-dimensional structures by molecular replacement (Fig. 1B and 1C). Crystal structures were refined to 1.7 Å and 1. 38

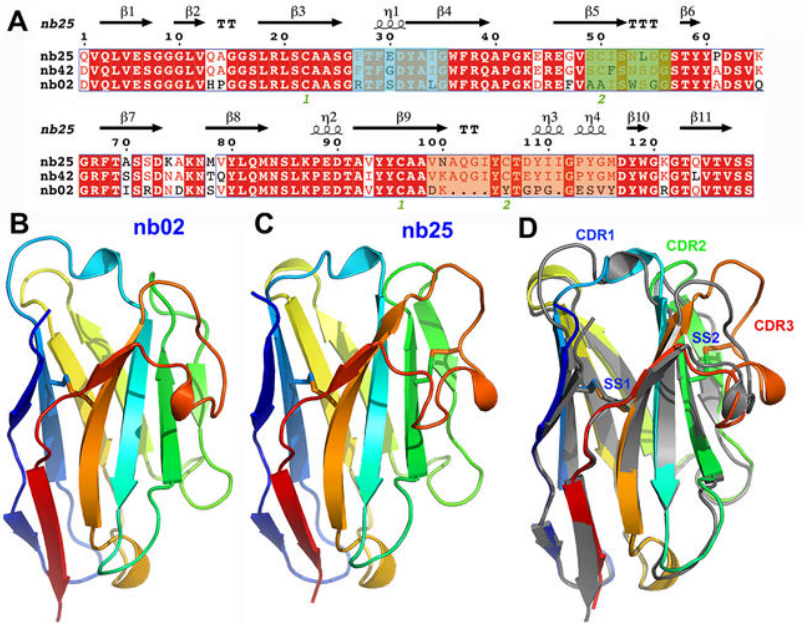

Fig 1. Structure of the anti-TssM nanobodies. (**A**) Sequence alignment of nanobodies nb02, nb25 and nb42. Identical amino-acids are in white and underlined in red, similar amino-acids are colored in red, different amino-acids are in black. The CDR1, CDR2 and CDR3 are highlighted in blue, green and yellow, respectively. The green numbers (1 or 2) below the sequence indicate cysteine residues involved in disulphide bridges SS1 (1, Cys22 and Cys96) and SS2 (2, Cys50 and Cys106) disulphide bridges formation. Crystal structure of nanobodies nb02 (**B**) and nb25 (**C**), represented as ribbons and colored in rainbow mode. (**D**) Superimposition of the structures of nb02 (grey) and nb25 (rainbow color). The locations of the CDR1, CDR2 and CDR3 variable regions are indicated as well as the positions of disulphide bridges (SS1 and SS2).

doi:10.1371/journal.pone.0122187.g001

Å resolution with R/Rf values of 25.1/20.5% and 19.1/19.8%, respectively (Table 1). Overall, the two structures (nb02, PDB 4QLR; nb25, PDB 4QGY) are very similar. The superimposed structures of nb02 and nb25 differ by a rmsd of 1.13 Å on 118 aligned residues (Fig. 1D). However, despite identical lengths, the conformations of the nb02 and nb25 CDR1 and CDR2 regions differ significantly (Fig. 1D). More importantly, large differences can be observed on the CDR3 regions, notably in terms of size (14-residue long for nb02, 19-residue long for nb25). Noteworthy, the nb25 CDR3 region is stabilized by a disulfide bridge between Cys-106 and CDR2 Cys-50 and extends out of the nanobody core, providing a large putative binding area for the antigen (Fig. 1C).

Nanobodies bind TssM with nanomolar affinities

To gain further information on the nanobodies, the strengths of their interactions with TssMp were measured by surface plasmon resonance (SPR). Nb02, nb25 and the nb25 variant nb42 were covalently coupled to the CHIP and sensorgrams were recorded after injection of the purified TssMp fragment in the microfluidic channel (Fig. 2). Analysis of the SPR curves indicate that nb02, nb25 and nb42 bind to TssMp with K_D values of 66.8±2 nM, 1.61± 0.1 nM and 1.76± 0.1 nM, respectively (Table 2).

Nb25 interferes with TssJ binding to TssM

We previously reported that TssJ binds to TssMp with a K_D value of 2–4 μM. This interaction is mediated by the L1-2 loop of TssJ and is essential for the proper function of the T6SS [11].

Table 1. Data collection and refinement statistics for the nb02 and nb25 anti-TssM nanobodies.

DATA COLLECTION	nb02 (PDB:4QLR)	nb25 (PDB:4QGY)
Diffraction source	ESRF	Soleil PX1
Detector	Pilatus 6M	Pilatus 6M
Space group	P 2_1	$C222_1$
Cell dimensions (Å,°)	a = 50.0, b = 48.6, c = 52.9 Å^3 β = 118.8°	a = 52.0, b = 70.9, c = 145.7 Å^3
Resolution range[a] (Å)	50–1.70 (1.76–1.70)	50–1.38 (1.42–1.38)
R-merge[a] (%)	7.0 (52)	3.1 (70)
CC(1/2)[a] (%)	99.7 (73.1)	100 (85)
Mean((I)/sd(I))[a]	9.6 (1.7)	29 (2.6)
Total number of reflections[a]	62041 (5333)	395611 (25318)
Number of unique reflections[a]	23496 (2222)	55440 (3886)
Completeness[a] (%)	94.3 (90.3)	99.6 (95)
Multiplicity[a]	2.64 (2.4)	7.1 (6.5)
REFINEMENT		
Resolution[a] (Å)	44.1–1.7 (1.78–1.7)	20–1.38 (1.42–1.38)
Nr of reflections[a]	23498 (2742)	55416 (3814)
Nr protein / water	1931 / 211	1918 / 309
Nr test set reflections	1201	2813
R_{work}/R_{free}[a] (%)	20.5/25.1 (24.0/25.4)	19.1/19.8 (32.2/36.7)
r.m.s.d.bonds (Å) / angles (°)	0.01 / 1.02	0.01 / 1.09
B-wilson / B-average	21.0 / 23.6	20.3 / 24.8

[a] numbers in brackets refer to the highest resolution bin.

doi:10.1371/journal.pone.0122187.t001

Based on these results, we hypothesized that the TssJ L1-2 loop will contact a crevice within TssM [11]. Because nanobodies are known to target enzymatic sites or crevices [27], we sought to determine whether the nanobodies and TssJ share the same TssM-binding site. We therefore performed Bilayer interferometry (BLI) competition experiments between the nanobodies and TssJ on TssMp. The TssJ protein (devoid of its N-terminal Cys acylation residue) was biotinylated and coupled to the streptavidine BLI chip. The chip was immersed on solution containing TssMp-nanobody complexes. Due to the 50- to 1000-fold magnitude differences between the K_Ds of TssJ and that of the nanobodies to TssMp, we expected that the occupation of the TssJ binding site by the nanobody would prevent TssMp binding to TssJ. Fig. 3 shows that the TssMp-nb02 complex can readily interact with TssJ. The formation of the nb02-TssMp-TssJ ternary complex demonstrates that TssJ and nb02 bind TssM differently. By contrast, the TssMp-nb25 complex does not bind TssJ demonstrating that nb25 interferes with TssJ binding on TssMp. This result suggests that nb25 and TssJ share the same TssM binding site or that nb25 binding on TssMp causes steric hindrance preventing TssJ binding.

Nb25 disrupts the TssMp-TssJ interaction *in vitro*

We hypothesized that if nb25 and TssJ share the same TssM binding site, nb25 should disrupt the TssM-TssJ complex. We therefore analyzed the effect of nb25 on the stability of the TssM-TssJ complex. Competition experiments were performed by incubating the purified TssMp-TssJ complex with an excess of nb25, prior to analysis by gel filtration. Three peaks were observed on the chromatogram (Fig. 4). Analysis of the peaks by SDS-PAGE (Fig. 4, inset) showed that peak 1 (~ 90 kDa) contained TssMp and nb25 (theoretical weight of the TssMp-nb25 complex = 98 kDa), while peak 2 (~ 18 kDa) contained TssJ (theoretical

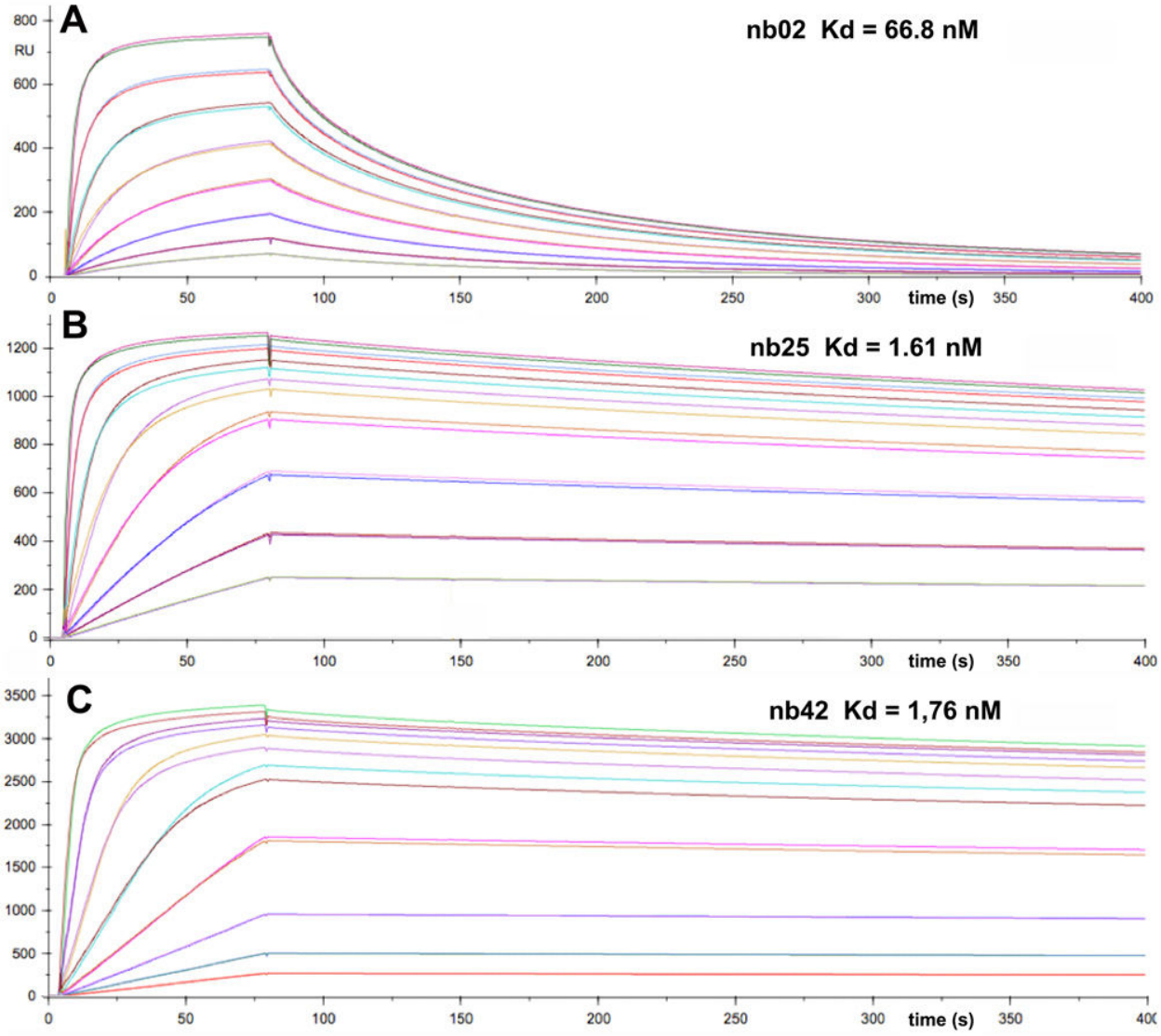

Fig 2. Nanobodies nb02 and nb25 bind TssMp with nanomolar affinity. Surface Plasmon Resonance recordings representing binding and release of the purified periplasmic domain of TssM (from bottom to top: 1.95, 3.9, 7.8, 15.6, 31.25, 62.5, 125 and 250 nM) to nanobody nb02 (**A**), nb25 (**B**) or nb42 (**C**) immobilized on the Chip. The variation of the Surface Plasmon Resonance (shown as the experimental and fitting curves) is reported on the *y* axis (in arbitrary unit, RU) plotted versus the reaction time on the *x* axis (in sec.). The apparent K_Ds are indicated on the top of each graph. The kinetic and thermodynamic parameters are indicated in Table 2.

doi:10.1371/journal.pone.0122187.g002

Table 2. Kinetic and thermodynamic parameters of the interactions between anti-TssM nanobodies with TssMp.

	k_{on} ($M^{-1}.s^{-1}$)	k_{off} (s^{-1})	K_D (nM)	R_{max}
nb02	6.02 10^5	402 10^{-4}	66.8 ± 2.5	734
nb25	3.5 10^5	5.6 10^{-4}	1.61 ± 0.05	1165
nb42	2.04 10^5	3.6 10^{-4}	1.76 ± 0.08	3155

doi:10.1371/journal.pone.0122187.t002

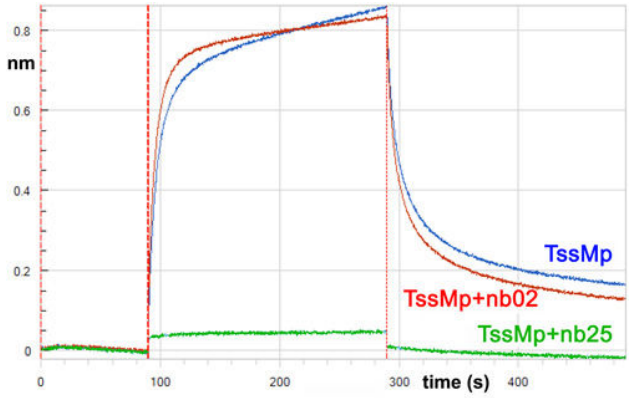

Fig 3. Binding of TssMp:nanobody complexes to TssJ. Bilayer interferometry recordings representing binding of TssMp alone (blue) or the TssMp:nb02 (red) or TssMp:nb25 (green) complexes to chip coupled to TssJ. The response (in nm) is plotted versus the time (in sec.). The absence of response in the green sensorgram indicates that nb25 prevents attachment of TssMp to TssJ.

doi:10.1371/journal.pone.0122187.g003

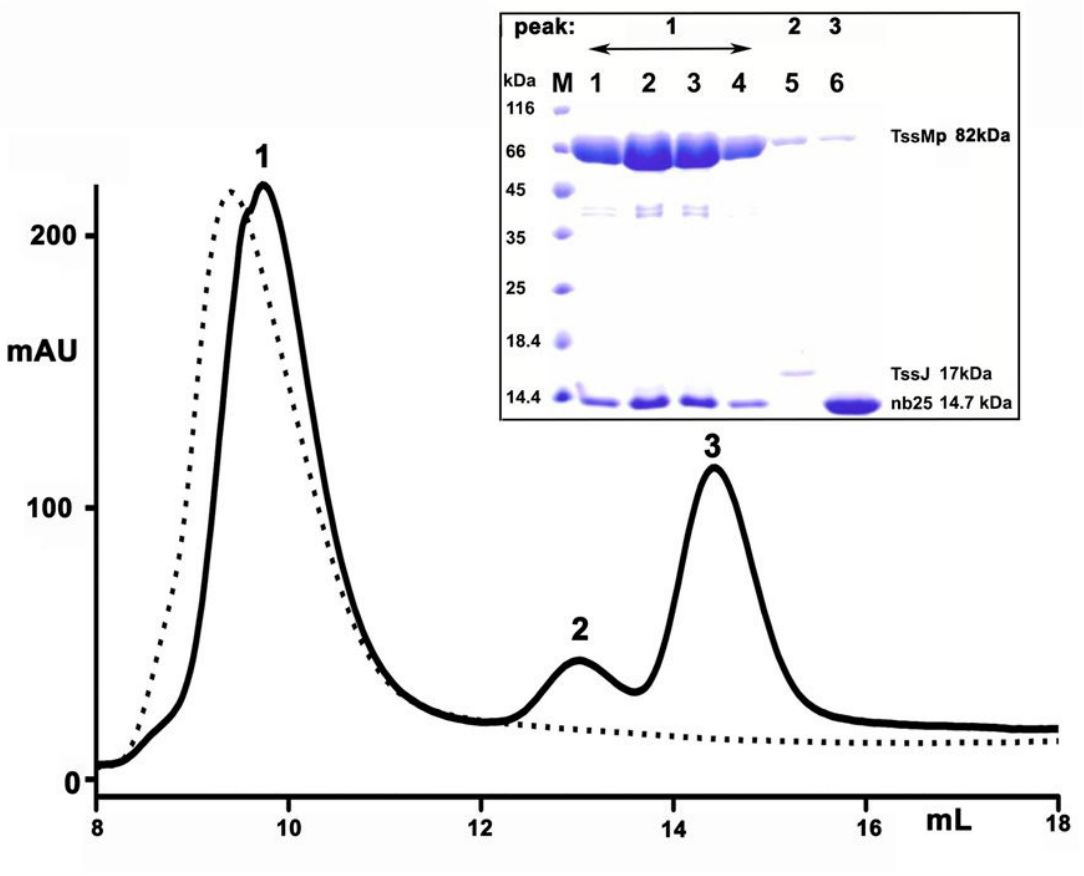

Fig 4. Nanobody nb25 disrupts the TssMp:TssJ complex. The pre-formed TssM-TssJ complex was analyzed by size exclusion chromatography before (dash line) and after incubation with an excess of nb25 (plain line). The composition of the different complexes, eluting at different volumes, was analysed by SDS-PAGE and Coomassie blue staining (inset). The fractions corresponding to peak 1–3 are indicated on the top. The molecular masses of the protein markers (in kDa) are indicated on the left. According to the calibration of the column, the apparent molecular weights for peak 1 (9.72 ml), peak 2 (13.02 ml) and peak 3 (14.43 ml) are about 90, 18 and 14 kDa, respectively. The faint band at the position of TssMp in peaks 2 and 3 of the SDS gel arise from contamination by the large main TssMp peak 1.

doi:10.1371/journal.pone.0122187.g004

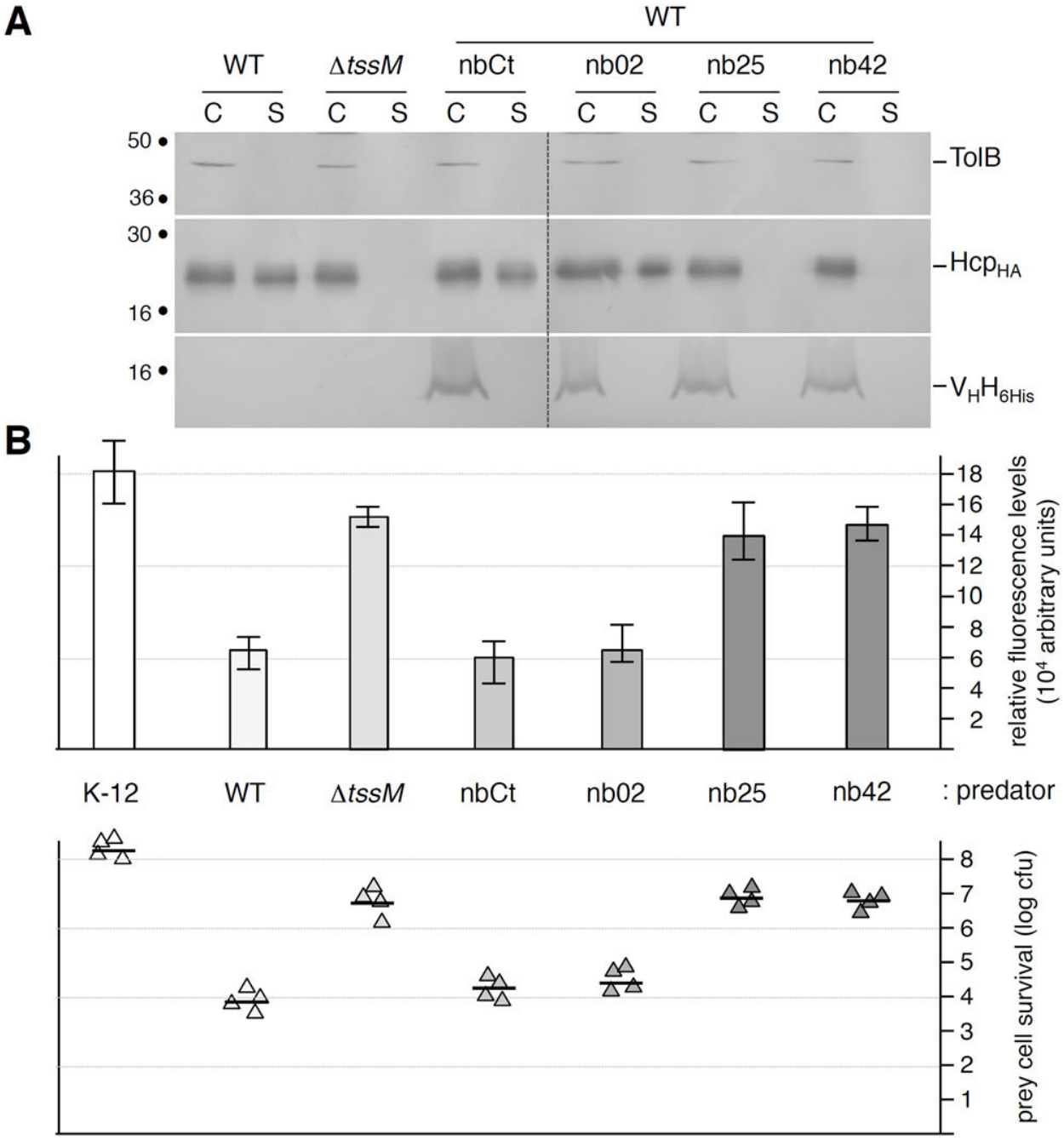

Fig 5. TssM-specific nanobodies nb25 and nb42 specifically affect T6SS function. (A) Hcp release assay. HA-epitope-tagged Hcp (Hcp$_{HA}$) release was assessed by separating whole cells (C) and supernatant (S) fractions from wild-type (WT), Δ*tssM* cells or WT cells producing 6His-tagged nanobodies as indicated. 2×10^8 cells and the TCA-precipitated material of the supernatant from 5×10^8 cells were loaded on a 12.5%-acrylamide SDS-PAGE and the nanobodies (lower panel), Hcp (middle panel) and periplasmic TolB (cell integrity control, upper panel) proteins were immunodetected using anti-5His, anti-HA and anti-TolB antibodies respectively. **(B)** Anti-bacterial assay. The Sci-1 T6SS-dependent anti-bacterial activity was assessed by mixing prey cells (W3110 *gfp*$^+$, kan^R) with the indicated attacker cell (K-12, W3110; WT, EAEC 17–2; Δ*tssM*, 17–2Δ*tssM* or WT cells producing the indicated nanobody) for 16 hours at 37°C in *sci-1*-inducing medium (SIM). The recovered fluorescent level (in arbitrary units) is shown in the upper graph (mean of fluorescence levels per OD_{600nm} obtained from four independent experiments). The number of recovered viable prey cells, expressed in colony forming unit (cfu) is shown in the lower graph (the triangles indicate values from four independent assays, and the average is indicated by the bar).

doi:10.1371/journal.pone.0122187.g005

weight = 17 kDa) and peak 3 (~ 14 kDa), the excess of nb25 (theoretical weight = 14 kDa). These data confirm that nb25 binds to TssMp and chases TssJ from the pre-assembled TssMp-TssJ complex.

Nb25 prevents formation of a functional T6SS

The TssM-TssJ interaction was previously shown to be indispensable for the proper function of the Type VI secretion apparatus in enteroaggregative *E. coli* [11]. As nb25 (and nb42) compete with TssJ for TssM binding *in vitro*, we wondered whether these nanobodies would disrupt the TssM-TssJ interaction *in vivo*. The vectors allowing the periplasmic production of the nb02, nb25 and nb42 nanobodies, as well as a control nanobody (a nanobody targeting the *Lactococcus lactis* phage 1358 receptor binding protein) were introduced into the wild-type EAEC strain 17–2. The function of the T6SS was assessed by the Hcp1 release assay and by the Sci1--dependent antibacterial activity. As shown in Fig. 5, the control nanobody and nb02 had no—or little—effect on the function of the T6SS as 17–2 cells producing nb02 released the Hcp1 protein and retained anti-bacterial activities at levels comparable to that of wild-type 17–2 cells. By contrast, the periplasmic production of nb25 and nb42 inhibited the function of the T6SS as (i) no Hcp1 was found in the culture supernatant of 17–2 cells producing these V_HHs and (ii) these cells did not have any growth advantage when co-cultured with *E. coli* K-12 cells. Taken together, these results suggest that disruption of the TssM-TssJ interaction prevents the formation of a functional Type VI secretion apparatus in EAEC.

Concluding Remarks

In this study, we raised and selected two camelid variable fragments of heavy-chain antibodies specific to the EAEC T6SS TssM periplasmic domain. Although this strategy was originally initiated to help the crystallization of the TssM protein, we used here these nanobodies to gain functional information on the assembly of the T6SS apparatus. We showed that the two selected nanobodies bind TssMp with nanomolar affinities. These values are in agreement with the affinities of nanobodies, including that targeting the *Salmonella* Typhimurium actin ADP-ribosylating toxin or the *Pseudomonas aeruginosa* flagellin [28, 29]. BLI and gel filtration experiments showed that nb25 is a competitor of TssJ *in vitro*, suggesting that nb25 binds at—or close to—the TssJ binding site on TssMp or at least causes a steric hindrance or a TssM conformational change preventing TssM-TssJ complex formation. Due to the variability of the CDR3 protruding loop and the observation that nanobodies are often targeting crevices [27], we hypothesize that the nb25 CDR3 loop mediates the interaction with a crevice in TssM, such as the TssJ L1-2 loop does [11]. Significant sequence differences occur in the CDR1 and CDR2 of nb25 and nb42, while the CDR3 are identical. This observation is in line with our hypothesis of CDR3 binding to the TssJ binding site of TssM. Sequence alignment between the TssJ LI-2 loop and the CDR1, CDR2 and CDR3 of nb25 shows that, except an A-X-G-I motif, very limited similarities exist between TssJ and CDR3. However, the TssJ L1-2 loop being elongated whereas the CDR3 having a compact fold, no structural conservation is observed between these loops suggesting that TssJ L1-2 and nb25/nb42 CDR3 do not bind identically to TssM, although we cannot exclude loop rearrangements upon binding. In view of these results, the co-crystallization between TssMp and nb25 is therefore essential, not only to gain structural information on TssM but also to identify the nb25-binding site and to test whether this region is also responsible for making contacts with the TssJ L1-2 loop. Interestingly, the use of nanobodies for co-crystallization was successful in this specific case as we recently obtained co-crystals between a fragment of the periplasmic domain of TssM and nb25 and performed a preliminary X-ray diffraction analysis [30].

By contrast, although nb02 has strong affinity for TssM, we showed that nb02 does not compete with TssJ for TssM binding *in vitro*. Because of the formation of an nb02-TssMp-TssJ ternary complex, nb02 is an interesting tool to assist the crystallization of the TssMp-TssJ complex. Hcp release and growth competition assays showed that nb02 has no inhibitory effect *in vivo*. Therefore, defining the site of binding of nb02 on TssM is also interesting as this nanobody targets a region that is not critical for the assembly of the T6SS membrane complex.

Nanobodies targeting bacterial multi-protein complexes or toxins have already been reported. For examples, specific nanobodies to the *Vibrio* Type II secretion (T2SS) GspD secretin and EspI/J pseudopilin complex have been selected and used for structural studies but their effect on the assembly of the T2SS *in vivo* has not been addressed [31]. By contrast, nanobodies interacting with the *P. aeruginosa* or *Campylobacter jejuni* flagellin decrease the swimming rate and biofilm formation of these strains [29, 32]. Similarly, nanobodies that bind to and interfere with the catalytic site of the *S.* Typhimurium ADP-ribosylation toxin diminish the cytotoxicity *in vivo* [28]. Our study not only paves the way to the structural characterization of the TssM periplasmic domain and of the TssMp-TssJ complex, but also demonstrates that nanobodies can be used to inhibit the assembly of the T6SS or of secretion systems in general with the goal to diminish or abolish the fitness or the virulence of bacterial pathogens in their ecological niche.

Materials and Methods

Bacterial strains, growth conditions and chemicals

The entero-aggregative *E. coli* EAEC strain 17–2 and its Δ*tssM* isogenic derivative [10] were used for this study. The *E. coli* K-12 WK6 strain was used for nanobody production. The *E. coli* K-12 W3110 strain carrying the pUA66-*rrnB* plasmid (*gfp* under the control of the constitutive *rrnB* ribosomal promoter, specifying strong and constitutive fluorescence, and kanamycin resistance [33]) was used as prey in antibacterial competition experiments. Strains were routinely grown in lysogeny broth (LB) or Terrific broth at 37°C, with aeration. For antibacterial competition assays, cells were grown in *sci-1*-inducing medium (SIM: M9 minimal medium, glycerol 0.2%, vitamin B1 1 μg/ml, casaminoacids 100 μg/ml, LB 10%, supplemented or not with bactoagar 1.5%). Plasmids were maintained by the addition of ampicillin (200 μg/mL) or kanamycin (50 μg/mL). The expression of the nanobody constructs cloned into pHEN6 vector derivatives was induced by the addition of isopropyl-β-thio-galactoside (IPTG).

Generation of llama nanobodies against TssM

The periplasmic domain of TssM (amino-acids 386–1129; TssMp) was produced and purified as described previously [11]. Four injections of 1 mg of recombinant TssMp (in Tris-HCl 20 mM (pH 8.0), NaCl 150 mM) were performed subcutaneously with two weeks intervals followed by a fifth injection one month later in two llamas (*Lama glama*) (Capralogics Inc., Hardwick, MA 01037 USA). Lymphocytes were isolated from blood sample obtained 1 week after the last immunization. cDNA was synthesized from purified total RNA by reverse transcription. The cDNA was used as template for PCR amplification to amplify sequences corresponding to the variables domains of the heavy-chain antibodies. PCR fragments were cloned into the phagemid vector pHEN4 [34] to create a nanobody phage display library. Selection and screening of nanobodies were performed as previously published [35]. Three rounds of panning resulted in the isolation of TssMp-specific binders. Nanobodies nb02, nb25 and its variant nb42 were selected, sequenced and cloned into the pHEN6 expression vector downstream the *pelB* signal peptide and fused to a C-terminal 6×His tag [36].

Purification of nanobodies

E. coli WK6 cells carrying the pHEN6 derivatives were grown at 37°C in Terrific Broth medium containing 0.1% glucose and ampicillin to an optical density (OD_{600nm}) ~ 0.8. The expression of the nanobody was induced by the addition of 1 mM IPTG and incubation for 16 hours at 28°C. The periplasmic fraction containing the nanobodies was prepared by osmotic shock. The His-tail-containing fusion proteins were purified by immobilized metal affinity chromatography on a 5-mL Ni-NTA column equilibrated in 50 mM Na/K phosphate (pH 8.0), 300 mM NaCl, 10% glycerol. Nanobodies were eluted in 250mM imidazole and concentrated (Amicon-Ultra 10-kDa cut-off) prior to be loaded on a HiLoad 16/60 Superdex 75 gel filtration column equilibrated in 20 mM Tris–HCl (pH 8.0), 150 mM NaCl.

Nanobodies structure determination

Crystallization screening experiments were performed with several commercial kits. The nanodrop crystallization experiments were performed in Greiner plates. The reservoirs of the Greiner plates were filled up using a TECAN pipetting robot, while the nano-L drops were dispensed by a Mosquito robot using nano-crystallization protocols [37]. All crystallization experiments were performed at 293K. Nanobody nb02 crystallized at 15 mg/mL in 100 mM sodium cacodylate (pH 6.5), 25% w/v PEG 8000, 200 mM $(NH_4)_2SO_4$. Nanobody nb25 crystallized at 15 mg/mL in 100 mM CHES (pH 10), 1 M K/Na tartrate, 200 mM Li_2SO_4. Crystals were mounted in loops and soaked in their crystallization solution supplemented by 4M TMAO before cryocooling.

Data collection of nb02 and nb25 were performed at synchrotrons ESRF (Grenoble, France) beamline ID29 and Soleil PX1 (saint-Aubin, France), respectively (Table 1). Data were integrated with XDSME and scaled with XSCALE. The nb02 crystals belong to space-group $P2_1$, with cell dimensions a = 50.0, b = 48.6, c = 52.9 $Å^3$, β = 118.8°. Two molecules in the symmetric unit yield a Vm value of 2.0 $Å^3$/Da and 38% solvent. The nb25 crystals belong to space-group $C222_1$, with cell dimensions a = 52.0, b = 70. 9, c = 145.7 $Å^3$. Two molecules in the asymmetric unit yielded a Vm value of 2.20 $Å^3$/Da and 45% solvent. These crystals diffracted to 1.70 Å and 1.38 Å resolution, respectively (Table 1). Molecular replacement was performed using MOLREP [38] and nanobody structures with high sequence similarity to nb25 (PDB: 4KRP) and nb02 (PDB: 4HEP) as starting models. Refinement was performed using autoBUSTER [39] alternated with rebuilding with COOT [40].

Accession numbers

Atomic coordinates have been deposited in the Protein Data Bank as identifiers 4QLR (nb02) and 4QGY (nb25).

Surface Plasmon Resonance (SPR) measurements

The interaction between TssMp and nanobodies was tested by SPR using a Biacore X100 (GE healthcare). Nb02, nb25 and nb42 were covalently linked to a CM5 chip and different concentrations of TssMp were injected in the microfluidic channel. Regeneration was achieved by the injection of glycine-HCl (pH 2.5) buffer. The K_D values were calculated by the multi-cycle kinetics method (Biacore, GE-healthcare).

Biolayer interferometry (BLI)

TssJ was first biotinylated using the EZ-Link NHS-PEG4-Biotin kit (Perbio Science, France). The reaction was stopped by removing the excess of the biotin using a Zeba Spin Desalting

column (Perbio Science, France). BLI studies were performed in black 96-well plates (Greiner) at 25°C using an OctetRed96 (ForteBio, USA). Streptavidin biosensor tips (ForteBio, USA) were first hydrated with 0.2 ml Kinetic buffer (KB, ForteBio, USA) for 20 min and then loaded with biotinylated TssJ (10 μg/ml in KB). The association of TssJ with TssM (300 nM) was monitored for 200 sec, as well as the dissociation in KB. For TssM/nanobody competition experiments, nb02 or nb05 nanobodies were used at a TssJ:nanobody ratio of 3:1.

Size Exclusion Chromatography (SEC)

Size exclusion chromatography was performed on an Alliance 2695 HPLC system (Waters) using a pre-calibrated Superdex 75 10/300 GL gel filtration column run in 20 mM Tris-HCl (pH 8.0), 100 mM NaCl at 0.5 mL/min.

Hcp release assay

The expression of the nanobody constructs cloned into pHEN6 vector derivatives was induced by the addition of 0.5 mM isopropyl-β-thio-galactoside (IPTG) for 45 min. Supernatant and cell fractions were separated as previously described [12, 13] with the addition of the iron chelator 2,2'-dipyridyl (125 μM final concentration) to the culture medium 30 min before harvesting the cells to induce the expression of the *sci-1* T6SS [41]. Briefly, 2×10^9 cells producing HA epitope-tagged Hcp (from plasmid pOK-HcpHA; [10]) and the 6×His-tagged nanobody constructs were harvested and collected by centrifugation at 2,000 × *g* for 5 min. The supernatant fraction was then subjected to a second low-speed centrifugation and then at 16,000 × *g* for 15 min. The supernatant was filtered on sterile polyester membranes with a pore size of 0.2 μm (membrex 25 PET, membraPure GmbH) before overnight precipitation with trichloroacetic acid (TCA) 15% on ice. Cells and precipitated supernatants were resuspended in loading buffer and analyzed by Sodium Dodecyl Sulfate-Polyacrylamide Gel Electrophoresis (SDS-PAGE) and immunoblotting with the anti-HA antibody. As control for cell lysis, Western blots were probed with antibodies raised against the periplasmic TolB protein. The production of the nanobodies was verified by immunoblotting with the anti-5His antibody.

Sci-1-dependent antibacterial assay

The antibacterial competition growth assay was performed as described for the studies on the *Citrobacter rodentium* and EAEC Sci-2 T6SSs [42, 43] with modifications. The wild-type *E. coli* strain W3110 bearing the pUA66-*rrnB* plasmid Kan^R [33] was used as prey in the competition assay. The pUA66-*rrnB* plasmid provides a strong constitutive green fluorescent (GFP^+) phenotype. Attacker and prey cells were grown for 16 hours in LB medium, then diluted 100-fold in SIM. Once the culture reached an OD_{600nm} = 0.8, the cells were harvested and resuspended to an OD_{600nm} of 0.5 into SIM. For the attacker cells, the expression of the V_HH-encoding genes was induced for 45min. with 0.5 mM IPTG prior to cell harvest. Attacker and prey cells were mixed to a 4:1 ratio and 25-μl drops of the mixture were spotted in triplicate onto a pre-warmed dry SIM agar plate supplemented with 0.5 mM IPTG. After overnight incubation at 30°C, the bacterial spots were cut off, and cells were resuspended in LB to an OD_{600nm} of 0.5. Triplicates of 150 μl were transferred into wells of a black 96-well plate (Greiner), and the absorbance at 600 nm and fluorescence (excitation, 485 nm; emission, 530 nm) were measured with a Tecan Infinite M200 microplate reader. The relative fluorescence was expressed as the intensity of fluorescence divided by the absorbance at 600 nm, after subtracting the values of a blank sample. For enumeration of viable prey cells, bacterial suspensions recovered from the spots were serially diluted and spotted onto selective LB agar plates supplemented with kanamycin (for the *E. coli* prey cells).

Miscellaneous

SDS-Polyacrylamide gel electrophoresis was performed using standard protocols. For immunostaining, proteins were transferred onto nitrocellulose membranes, and immunoblots were probed with primary antibodies, and goat secondary antibodies coupled to alkaline phosphatase, and developed in alkaline buffer in presence of 5-bromo-4-chloro-3-indolylphosphate and nitroblue tetrazolium. The anti-TolB polyclonal antibodies are from our laboratory collection, while the anti-HA (3F10 clone, Roche), the anti-5His (Qiagen) monoclonal antibodies and alkaline phosphatase-conjugated goat anti-rabbit, mouse, or rat secondary antibodies (Millipore) have been purchased as indicated.

Ethics statement

Please note that Eric Cascales is a PLOS ONE Academic Editor. This does not alter the authors' adherence to all the PLOS ONE policies on sharing data and material.

Acknowledgments

We thank the ERSF and Soleil Synchrotron radiation facilities for beamline allocation, Nicolas Flaugnatti and Laure Journet for the development of the Sci-1-dependent antibacterial competition assay, the members of the Cascales and Cambillau research groups for helpful discussions, Olivier Uderso, Isabelle Bringer and Annick Brun for technical assistance, and Amar Dissoir for encouragements.

Author Contributions

Conceived and designed the experiments: AR EC CC. Performed the experiments: VSN LL SS AD TTHL CK BD ED AR EC CC. Analyzed the data: VSN LL SS AD TTHL CK BD ED AR EC CC. Wrote the paper: VSN AD CK AR EC CC.

References

1. Russell AB, Peterson SB, Mougous JD. Type VI secretion system effectors: poisons with a purpose. Nat Rev Microbiol 2014; 12: 137–148. doi: 10.1038/nrmicro3185 PMID: 24384601
2. Durand E, Cambillau C, Cascales E, Journet L. VgrG, Tae, Tle, and beyond: the versatile arsenal of Type VI secretion effectors. Trends Microbiol 2014; 22: 498–507. doi: 10.1016/j.tim.2014.06.004 PMID: 25042941
3. Cascales E, Cambillau C. Structural biology of type VI secretion systems. Philos Trans R Soc Lond B Biol Sci 2012; 367: 1102–1111. doi: 10.1098/rstb.2011.0209 PMID: 22411981
4. Coulthurst SJ. The Type VI secretion system—a widespread and versatile cell targeting system. Res Microbiol 2013; 164: 640–654. doi: 10.1016/j.resmic.2013.03.017 PMID: 23542428
5. Ho BT, Dong TG, Mekalanos JJ. A View to a Kill: The Bacterial Type VI Secretion System. Cell Host Microbe 2014; 15: 9–21. doi: 10.1016/j.chom.2013.11.008 PMID: 24332978
6. Zoued A, Brunet YR, Durand E, Aschtgen MS, Logger L, Douzi B, et al. Architecture and assembly of the Type VI secretion system. Biochim Biophys Acta 2014; 1843: 1664–1673. doi: 10.1016/j.bbamcr.2014.03.018 PMID: 24681160
7. Zoued A, Durand E, Bebeacua C, Brunet YR, Douzi B, Cambillau C, et al. TssK is a trimeric cytoplasmic protein interacting with components of both phage-like and membrane anchoring complexes of the Type VI secretion system. J Biol Chem 2014; 288: 27031–27041. doi: 10.1074/jbc.M113.499772 PMID: 23921384
8. Aschtgen MS, Bernard CS, De Bentzmann S, Lloubes R, Cascales E. SciN is an outer membrane lipoprotein required for type VI secretion in enteroaggregative Escherichia coli. J Bacteriol 2008; 190: 7523–7531. doi: 10.1128/JB.00945-08 PMID: 18805985
9. Ma LS, Lin JS, Lai EM. An IcmF family protein, ImpLM, is an integral inner membrane protein interacting with ImpKL, and its walker a motif is required for type VI secretion system-mediated Hcp secretion in

Agrobacterium tumefaciens. J Bacteriol 2009; 191: 4316–4329. doi: 10.1128/JB.00029-09 PMID: 19395482

10. Aschtgen MS, Gavioli M, Dessen A, Lloubes R, Cascales E. The SciZ protein anchors the enteroaggregative Escherichia coli Type VI secretion system to the cell wall. Mol Microbiol. 2010; 75: 886–899. doi: 10.1111/j.1365-2958.2009.07028.x PMID: 20487285
11. Felisberto-Rodrigues C, Durand E, Aschtgen MS, Blangy S, Ortiz-Lombardia M, Douzi B, et al. Towards a structural comprehension of bacterial type VI secretion systems: characterization of the TssJ-TssM complex of an Escherichia coli pathovar. PLoS Pathog 2011; 7: e1002386. doi: 10.1371/journal.ppat.1002386 PMID: 22102820
12. Durand E, Zoued A, Spinelli S, Watson PJ, Aschtgen MS, Journet L, et al. Structural characterization and oligomerization of the TssL protein, a component shared by bacterial type VI and type IVb secretion systems. J Biol Chem 2012; 287: 14157–14168. doi: 10.1074/jbc.M111.338731 PMID: 22371492
13. Aschtgen MS, Zoued A, Lloubes R, Journet L, Cascales E. The C-tail anchored TssL subunit, an essential protein of the enteroaggregative Escherichia coli Sci-1 Type VI secretion system, is inserted by YidC. Microbiologyopen 2012; 1: 71–82. doi: 10.1002/mbo3.9 PMID: 22950014
14. Bingle LE, Bailey CM, Pallen MJ. Type VI secretion: a beginner's guide. Curr Opin Microbiol 2008; 11: 3–8. doi: 10.1016/j.mib.2008.01.006 PMID: 18289922
15. Cascales E. The type VI secretion toolkit. EMBO Rep 2008; 9: 735–741. doi: 10.1038/embor.2008.131 PMID: 18617888
16. Hamers-Casterman C, Atarhouch T, Muyldermans S, Robinson G, Hamers C, Songa EB, et al. Naturally occurring antibodies devoid of light chains. Nature 1993; 363: 446–448. PMID: 8502296
17. Muyldermans S, Cambillau C, Wyns L. Recognition of antigens by single-domain antibody fragments: the superfluous luxury of paired domains. Trends Biochem Sci 2001; 26: 230–235. PMID: 11295555
18. Muyldermans S. Nanobodies: Natural Single-Domain Antibodies. Ann Rev Bioch, 2013; 82: 775–797. doi: 10.1146/annurev-biochem-063011-092449 PMID: 23495938
19. Pardon E, Laeremans T, Triest S, Rasmussen SG, Wohlkonig A, et al. A general protocol for the generation of Nanobodies for structural biology. Nat Protoc 2014; 9: 674–693. doi: 10.1038/nprot.2014.039 PMID: 24577359
20. Muyldermans S, Baral TN, Retarnozzo VC, De Baetselier P, De Genst E, Kinne J, et al. Camelid immunoglobulins and nanobody technology. Vet Immunol Immunopath 2009; 128: 178–183. doi: 10.1016/j.vetimm.2008.10.299 PMID: 19026455
21. Steyaert J. Structural investigation of GPCR transmembrane signaling by use of nanobodies. Eur Biophys J. 2011; 40: 223–223.
22. Rasmussen SGF, Choi HJ, Fung JJ, Pardon E, Casarosa P, Chae PS, et al. Structure of a nanobody-stabilized active state of the beta(2) adrenoceptor. Nature 2011; 469: 175–180. doi: 10.1038/nature09648 PMID: 21228869
23. Ring AM, Manglik A, Kruse AC, Enos MD, Weis WI, Garcia KC, et al. Adrenaline-activated structure of b2-adrenoceptor stabilized by an engineered nanobody. Nature 2013; 502:575–579. doi: 10.1038/nature12572 PMID: 24056936
24. Hassaine G, Deluz C, Grasso L, Wyss R, Tol MB, Hovius R, et al. X-ray structure of the mouse serotonin 5-HT3 receptor. Nature 2014; 512: 276–281. doi: 10.1038/nature13552 PMID: 25119048
25. Lam AY, Pardon E, Korotkov KV, Hol WGJ, Steyaert J. Nanobody-aided structure determination of the EpsI:EpsJ pseudopilin heterodimer from Vibrio vulnificus. J Struct Biol 2009; 166: 8–15. doi: 10.1016/j.jsb.2008.11.008 PMID: 19118632
26. Desmyter A, Spinelli S, Roussel A, Cambillau C. Camelid nanobodies: killing two birds with one stone. Curr Opin Struct Biol 2015; 32C: 1–8. doi: 10.1016/j.sbi.2015.01.001 PMID: 25614146
27. Desmyter A, Transue TR, Ghahroudi MA, Thi MHD, Poortmans F, Hamers R, et al. Crystal structure of a camel single-domain V-H antibody fragment in complex with lysozyme. Nat Struct Biol 1996; 3: 803–811. PMID: 8784355
28. Alzogaray V, Danquah W, Aguirre A, Urrutia M, Berguer P, Garcia Vescovi E, et al. Single-domain llama antibodies as specific intracellular inhibitors of SpvB, the actin ADP-ribosylating toxin of Salmonella typhimurium. Faseb J. 2011; 25: 526–534. doi: 10.1096/fj.10-162958 PMID: 20940265
29. Adams H, Horrevoets WM, Adema SM, Carr HEV, van Woerden RE, Koster M, et al. Inhibition of biofilm formation by Camelid single-domain antibodies against the flagellum of Pseudomonas aeruginosa. J Biotech 2014; 186: 66–73. doi: 10.1016/j.jbiotec.2014.06.029 PMID: 24997356
30. Nguyen VS, Spinelli S, Desmyter A, Le TTH, Kellenberger C, Cascales E, et al. Production, crystallization and X-ray diffraction analysis of a complex between a fragment of the TssM T6SS protein and a camelid nanobody. Acta Crystallogr F. 2015; 71:in press

31. Korotkov KV, Pardon E, Steyaert J, Hol WGJ. Crystal Structure of the N-Terminal Domain of the Secretin GspD from ETEC Determined with the Assistance of a Nanobody. Structure 2009; 17: 255–265. doi: 10.1016/j.str.2008.11.011 PMID: 19217396

32. Hussack G, Riazi A, Ryan S, van Faassen H, MacKenzie R, Tanha J, et al. Protease-resistant single-domain antibodies inhibit Campylobacter jejuni motility. Protein Eng Des Select 2014; 27: 191–198. doi: 10.1093/protein/gzu011 PMID: 24742504

33. Zaslaver A, Bren A, Ronen M, Itzkovitz S, Kikoin I, Shavit S, et al. A comprehensive library of fluorescent transcriptional reporters for Escherichia coli. Nat Methods 2006; 3: 623–628. PMID: 16862137

34. Ghahroudi MA, Desmyter A, Wyns L, Hamers R, Muyldermans S. Selection and identification of single domain antibody fragments from camel heavy-chain antibodies. Febs Letters 1997; 414: 521–526. PMID: 9323027

35. Desmyter A, Farenc C, Mahony J, Spinelli S, Bebeacua C, Blangy S, et al. Viral infection modulation and neutralization by camelid nanobodies. Proc Natl Acad Sci U S A 2013; 110: 1371–1379.

36. Conrath K, Pereira AS, Martins CE, Timoteo CG, Tavares P, Spinelli S, et al. Camelid nanobodies raised against an integral membrane enzyme, nitric oxide reductase. Prot Sci 2009; 18: 619–628.

37. Sulzenbacher G, Gruez A, Roig-Zamboni V, Spinelli S, Valencia C, Pagot F, et al. A medium-throughput crystallization approach. Acta Crystallogr D Biol Crystallogr 2002; 58: 2109–2115. PMID: 12454472

38. Vagin A, Teplyakov A. Molecular replacement with MOLREP. Acta Crystallogr D Biol Crystallogr 2010; 66: 22–25. doi: 10.1107/S0907444909042589 PMID: 20057045

39. Blanc E, Roversi P, Vonrhein C, Flensburg C, Lea SM, Bricogne G. Refinement of severely incomplete structures with maximum likelihood in BUSTER-TNT. Acta Crystallogr D Biol Crystallogr 2004; 60: 2210–2221. PMID: 15572774

40. Emsley P, Cowtan K. Coot: model-building tools for molecular graphics. Acta Crystallogr D Biol Crystallogr 2004; 60: 2126–2132. PMID: 15572765

41. Brunet YR, Bernard CS, Gavioli M, Lloubes R, Cascales E. An epigenetic switch involving overlapping fur and DNA methylation optimizes expression of a type VI secretion gene cluster. PLoS Genet 2011; 7: e1002205. doi: 10.1371/journal.pgen.1002205 PMID: 21829382

42. Gueguen E, Cascales E. Promoter swapping unveils the role of the Citrobacter rodentium CTS1 type VI secretion system in interbacterial competition. Appl Environ Microbiol 2013; 79: 32–38. doi: 10.1128/AEM.02504-12 PMID: 23064344

43. Brunet YR, Espinosa L, Harchouni S, Mignot T, Cascales E. Imaging type VI secretion-mediated bacterial killing. Cell Rep 2013; 3: 36–41. doi: 10.1016/j.celrep.2012.11.027 PMID: 23291094

Article 2: Biogenesis and structure of a type VI secretion membrane core complex

Article 2: Biogenesis and structure of a type VI secretion membrane core complex

As shown in *Article 1*, three nanobodies raised against the periplasmic domain of TssM were good binders. Two of them, nb25 and nb42, compete with TssJ and hence are proposed to bind to - or close to - the TssJ binding site(s). The third anti-TssM nanobody, nb02, binds TssMp with high affinity but did not displace the TssJ-TssMp complex. These nanobodies were used to help crystallization of TssMp or of the TssJ-TssMp complex. The use of nanobodies was combined with limited proteolysis to obtain stable fragments. The high-resolution X-ray structures of the C-terminal 26-kDa and 32-kDa subdomains of TssMp, alone or in association were TssJ were then obtained. These structures were incorporated into a manuscript that reports information on the assembly and structure of the TssJLM complex. This multidisciplinary study combined electron microscopy, fluorescence microscopy, X-ray crystallography and functional assays.

Eric Durand succeeds to purify, image and solve the overall structure of the purified TssJLM membrane complex. After the co-production of the three proteins, the membrane proteins were solubilized with detergents, and the TssJLM complex was purified to homogeneity by two consecutive affinity chromatographies (His-tag and Strep-tag) and gel filtration. Analyses of the purified sample demonstrated that TssJ, TssL and TssM assemble a 1.7-MDa membrane complex with a 1:1:1 stoichiometry. The TssJLM complex was visualized by negative-stain electron microscopy (EM) and processing based on 2D-class average obtained with 50,000 particles yielded a reconstruction at a resolution of 11.6 Å. The membrane complex has a 5-fold symmetry and is composed of 10 copies of each protein. This pentamer of dimers of heterotrimeric complexes has the overall structure of a rocket, with a large base linked to the tip by arches and pillars. The base comprises the cytoplasmic domains of TssL and TssM, the arches likely correspond to the transmembrane segments whereas the pilars are composed of the periplasmic domain of TssM and the TssJ lipoprotein. Although the two arches of each dimer start at the periphery of the base, the corresponding pillars separate to distinguish internal and external pillars. The internal pillars converge to the center of the complex and hence close the central lumen at the outer membrane.

Using functional chromosomal fluorescent fusions to TssM and TssL in wild-type cells, Abdelrahim Zoued defined that up to 8 static membrane complexes can assemble per cell and that, as expected from the biogenesis model, that the TssJLM complex forms first and serves as a docking

station for the tail. He also demonstrated that membrane complexes could be reused for several firing events. By engineering the same constructs in different mutant backgrounds, he unveiled that assembly of the TssJLM complex proceeds inward: it starts with the positioning of the TssJ. lipoprotein and continues with the recruitment of TssM and then TssL.

Son Nguyen obtained the high-resolution structure of TssMp subdomains, alone or in complex with TssJ. The C-terminal portion of TssM comprises two domains: a helical domain composed of a bundle of four α-helices followed by nine β-strands, a long α-helix and an approx. 30-residue non-folded tail.

Because in the involvement of lipoproteins in the insertion of β-barrel channels in the outer membrane, the interaction of TssJ with the TssM C-terminal β-domain, and the absence of an outer membrane protein in the T6SS, we wondered whether the β-domain of TssM may assemble the outer membrane pore. To test this hypothesis, I substituted residues located in between each β-strand (positions 989, 972, 1005, 1019, 1035, 1062, 1075, 1092 and 1109) by cysteine residues. Each of these variants of TssM were functional. I then tested the accessibility of each cysteine to maleimide-activated Bovine Serum Albumine. BSA is a large protein that is unable to cross the outer membrane, while the maleimide moiety reacts with the thiol group of free cysteines to form a covalent bond. Hence, only extracellularly exposed cysteine side-chains will be labelled with maleimide-BSA, thus causing an increase of the molecular weight of the protein that could be observed by SDS-PAGE. Using this approach, I showed that 5 variants were labelled *in vivo*. Interestingly, these substitutions include position 1109, located in the C-terminal tail (*i.e.*, after the long α-helix), and four positions that are located on the upper part of the β-domain. These results suggest that either the β-domain is inserted in the outer membrane, with its upper part exposed to the extracellular milieu, or that its upper part is accessible from the exterior (by a large, unknown, pore). When the same experiment was repeated in $\Delta tssBC$ cells, only position 1109 was labelled, suggesting that the TssM C-terminal tail is exposed at the cell surface, whereas the upper part of the β-domain is accessible only when the sheath assembles or contracts. Finally, none of the positions was labelled in $\Delta tssJ$ cells. Based on these results, we propose that TssJ facilitates the insertion of the long α-helix of TssM in the outer membrane, a situation that is reminiscent to the insertion of the T4SS VirB10 antennae (Bayliss et al., 2007). Then, the β-strands of the TssM β-domain insert into the membrane during sheath assembly or contraction, allowing formation of the outer pore necessary for the passage of the needle.

ARTICLE

doi:10.1038/nature14667

Biogenesis and structure of a type VI secretion membrane core complex

Eric Durand[1,2,3,4,5]*, Van Son Nguyen[2,5]*, Abdelrahim Zoued[1]*, Laureen Logger[1], Gérard Péhau-Arnaudet[4], Marie-Stéphanie Aschtgen[1], Silvia Spinelli[2,5], Aline Desmyter[2,5], Benjamin Bardiaux[4,6], Annick Dujeancourt[3,4], Alain Roussel[2,5], Christian Cambillau[2,5], Eric Cascales[1] & Rémi Fronzes[3,4]

Bacteria share their ecological niches with other microbes. The bacterial type VI secretion system is one of the key players in microbial competition, as well as being an important virulence determinant during bacterial infections. It assembles a nano-crossbow-like structure in the cytoplasm of the attacker cell that propels an arrow made of a haemolysin co-regulated protein (Hcp) tube and a valine-glycine repeat protein G (VgrG) spike and punctures the prey's cell wall. The nano-crossbow is stably anchored to the cell envelope of the attacker by a membrane core complex. Here we show that this complex is assembled by the sequential addition of three type VI subunits (Tss)—TssJ, TssM and TssL—and present a structure of the fully assembled complex at 11.6 Å resolution, determined by negative-stain electron microscopy. With overall C_5 symmetry, this 1.7-megadalton complex comprises a large base in the cytoplasm. It extends in the periplasm via ten arches to form a double-ring structure containing the carboxy-terminal domain of TssM ($TssM_{ct}$) and TssJ that is anchored in the outer membrane. The crystal structure of the $TssM_{ct}$–TssJ complex coupled to whole-cell accessibility studies suggest that large conformational changes induce transient pore formation in the outer membrane, allowing passage of the attacking Hcp tube/VgrG spike.

In the environment, bacteria have evolved collaborative or aggressive mechanisms to communicate, exchange information and chemicals, or compete for space and resources[1–3]. One of the main weapons of bacterial conflicts is a multi-protein device called the type VI secretion system (T6SS) that is assembled in the attacker bacterium[4]. The T6SS is a versatile nanomachine that can deliver toxin proteins directly not only into prey prokaryotes but also into eukaryotic cells during bacterial infections[3,5–9]. Anti-host activities have been shown to inhibit phagocytosis and therefore to disable macrophages, while the anti-bacterial activities allow the bacterium to destroy competitors and to have a privileged access to the niche, to nutrients or to new DNA[3,9,10]. The T6SS is composed of 13 different proteins, encoded by genes that are usually clustered[11]. It assembles a tubular puncturing device that is evolutionarily, structurally and functionally similar to the tail of contractile bacteriophages. Its sheath is a tubular structure, hundreds of nanometres long, that extends in the cytoplasm and is built by the polymerization of TssBC building blocks[12–14]. It is assembled on an assembly platform, the baseplate[13,15–17], and maintained in an extended, metastable conformation[16–18]. The attacking arrow, wrapped by the sheath, comprises an inner tube that is built by stacked Hcp hexameric rings[19] and tipped by a puncturing spike composed of VgrG[20]. Upon contact with the prey, structural rearrangements of the sheath subunits induce its contraction and propulsion of the Hcp tube/VgrG spike towards the target cell, allowing toxin delivery[16,17,21]. The phage-like T6SS tail is anchored to the attacker cell membrane by a trans-envelope complex[22]. This membrane complex not only serves as a docking station but has been proposed as a channel for the passage of the inner tube after sheath contraction, thereby preventing membrane damage in the attacker[16,17]. The membrane core complex of the T6SS (that is, the minimal module required to function and conserved in all T6SS) is composed of the TssL and TssM inner-membrane proteins and the TssJ outer membrane lipoprotein[15–17,22–26]. These proteins are connected through a network of interactions between TssM and TssL, and TssM and TssJ[22,24,25]. Although the localization and topology of these subunits, their interactions and the crystal structures of the soluble domains of TssJ and TssL have been described[17,22–29], we still lack crucial information on the biogenesis and overall architecture of this complex and how it is used as a channel during T6SS action.

Localization, dynamics and biogenesis of the T6SS membrane core complex

We first sought to determine the assembly pathway of the enteroaggregative *Escherichia coli* (EAEC) T6SS membrane core complex. Strains producing fluorescently labelled T6SS membrane subunits were engineered. The sequence encoding the super-folder green fluorescent protein (sfGFP) was inserted upstream of the stop codon of the *tssJ* gene or downstream of the start codon of the *tssL* and *tssM* genes. In these constructs, the fusion proteins were produced from their native chromosomal loci. Hcp release and anti-bacterial assays demonstrated that the sfGFP–TssL and sfGFP–TssM fusion proteins were functional (Extended Data Fig. 1a). By contrast, strains producing TssJ–sfGFP or TssJ–mCherry had a non-functional T6SS (Extended Data Fig. 1b). Fluorescence microscopy analyses showed that sfGFP–TssL and sfGFP–TssM cluster at discrete positions at the cell periphery, in agreement with their membrane localization (Fig. 1a and Extended Data Fig. 1c). These foci are stable and static (Fig. 1a and Extended Data Fig. 1d). Statistical analyses further showed that one or two foci are observable in cells expressing the T6SS (Fig. 1b) and that these clusters are randomly distributed around the cell (Fig. 1c). Co-localization experiments with strains producing

[1]Laboratoire d'Ingénierie des Systèmes Macromoléculaires, Aix-Marseille Université - CNRS, UMR 7255, 31 Chemin Joseph Aiguier, 13402 Marseille Cedex 20, France. [2]Architecture et Fonction des Macromolécules Biologiques, CNRS, UMR 7257, Campus de Luminy, Case 932, 13288 Marseille Cedex 09, France. [3]G5 Biologie structurale de la sécrétion bactérienne, Institut Pasteur, 25–28 rue du Docteur Roux, 75015 Paris, France. [4]UMR 3528, CNRS, Institut Pasteur, 25–28 rue du Docteur Roux, 75015 Paris, France. [5]AFMB, Aix-Marseille Université, IHU Méditerranée Infection, Campus de Luminy, Case 932, 13288 Marseille Cedex 09, France. [6]Unité de Bioinformatique Structurale, Institut Pasteur, 25–28 rue du Docteur Roux, 75015 Paris, France.
*These authors contributed equally to this work.

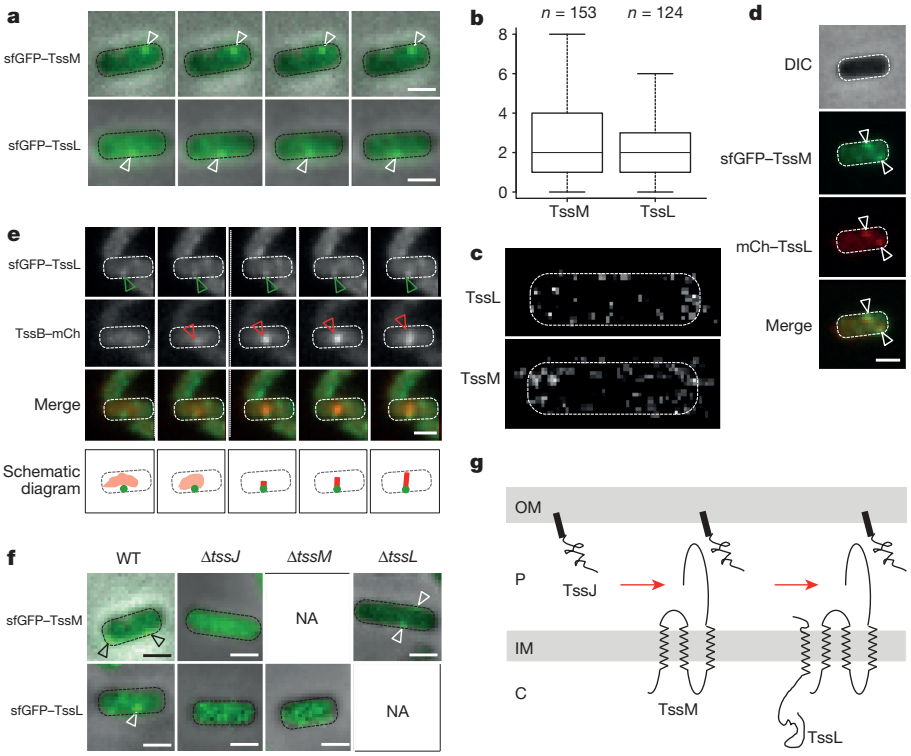

Figure 1 | Biogenesis of the T6SS membrane-associated core complex. **a**, Time-lapse fluorescence microscopy recordings showing localization and dynamics of the sfGFP–TssM and sfGFP–TssL fusion proteins. Individual images were taken every 30 s. The positions of the foci are indicated by arrowheads. Scale bars, 1 μm. Larger fields are presented in Extended Data Fig. 1c. **b**, Statistical analysis of sfGFP–TssM and sfGFP–TssL localization. Shown are box-and-whisker plots of the measured number of sfGFP–TssM and sfGFP–TssL foci per cell for each strain with the lower and upper boundaries of the boxes corresponding to the 25% and 75% percentiles respectively. The black horizontal bar represents the median values for each strain and the whiskers represent the 10% and 90% percentiles. The number of cells studied per strain is indicated above the bars. **c**, Spatial repartition of the sfGFP–TssM and sfGFP–TssL foci. Shown is a superposition of the different foci analysed in a single cell. **d**, sfGFP–TssM and mCh–TssL proteins co-localize. Fluorescence microscopy recordings showing co-localization between sfGFP–TssM and mCh–TssL fusion proteins. The positions of the foci are indicated by the arrowheads. Scale bar, 1 μm. **e**, The membrane complex serves as a docking site for tail sheath polymerization. Time-lapse fluorescence microscopy recordings showing co-localization between sfGFP–TssL and TssB–mCh fusion proteins. Individual images were taken every 30 s. Assembly/contraction of the sheath and TssL localization events is schematized in the bottom row of panels. Scale bars, 1 μm. **f**, Assembly pathway of the T6SS TssJLM membrane complex. Fluorescence microscopy recordings showing sfGFP–TssM and sfGFP–TssL localization in the absence of the TssJ or TssL and TssJ or TssM proteins respectively. The positions of the foci are indicated by the arrowheads. Scale bars, 1 μm. The quantification of the sfGFP–TssM and sfGFP–TssL clusters per cell is presented in Extended Data Fig. 1g. **g**, Schematic representation of the sequential biogenesis of the T6SS membrane complex. The names of the proteins, their localizations and topologies are shown.

sfGFP–TssM and mCherry-tagged TssL showed that the two subunits are present in the foci, demonstrating that each focus corresponds to the position of an assembled membrane complex (Fig. 1d). To test whether these foci are used to anchor the phage-like tail tubular structure, mCherry was fused to the *tssB* sheath gene, at its original chromosomal locus in the strain producing sfGFP–TssL. Time-lapse recordings showed that T6SS sheathes polymerize and extend from the membrane complex (Fig. 1e). On the basis of these results, we conclude that membrane complexes comprising TssL and TssM (and probably TssJ) assemble at discrete positions in the cell and are then used to recruit the tail-complex subunits. Statistical analyses showed that the number of sfGFP–TssL or sfGFP–TssM foci per cell is higher than the number of sheathes (Extended Data Fig. 1e), suggesting that the membrane complexes exist in a pre-assembled form. Interestingly, long-term time-lapse recordings showed that these membrane complexes can be re-used for new tail polymerization events (Extended Data Fig. 1f). To gain further information on the biogenesis of this initial step, *tssJ* or *tssM* were deleted in the sfGFP–TssL-producing strain, and *tssJ* or *tssL* were deleted in the sfGFP–TssM-producing strain. The rationale behind these experiments is that if a protein assembled early is missing, the recruitment of late proteins will be affected, yielding a diffuse fluorescent signal. Figure 1f shows that the recruitment of sfGFP–TssM and sfGFP–TssL is affected in the absence of TssJ, and that of sfGFP–TssL is affected in the absence of TssM. Conversely, the absence of TssL had no effect on TssM recruitment (Fig. 1f and Extended Data Fig. 1g). On the basis of these results, we conclude that TssJ is used as a nucleation factor and that the biogenesis of the T6SS membrane core complex is pursued by the inward sequential addition of TssM and TssL (Fig. 1g).

Architecture of the T6SS membrane core complex

To gain further insights on the architecture of the T6SS membrane core complex, the *tssJ*, *tssL* and *tssM* genes were co-expressed in *E. coli* BL21(DE3). Constructs were designed to add StrepII, Flag and 6×His tags at the carboxy (C) terminus of TssJ, amino (N) terminus of TssL and N terminus of TssM, respectively (Extended Data Fig. 2). Total membranes were isolated and solubilized using detergents. Two-step affinity chromatography followed by gel filtration resulted in the purification of a complex containing TssJ, TssL and TssM (Fig. 2a and Extended Data Fig. 2f–h). In this complex, we determined the TssM–TssL stoichiometry as 1 to 1 (Extended Data Fig. 2h). Purified complexes were visualized by negative-stain electron microscopy (EM) (Fig. 2b and Extended Data Fig. 3a). A data set was collected, and reference-free classification and averaging revealed characteristic views of the complex (class averages) (Fig. 2b). We observed rocket-shaped and ring-shaped views corresponding to side

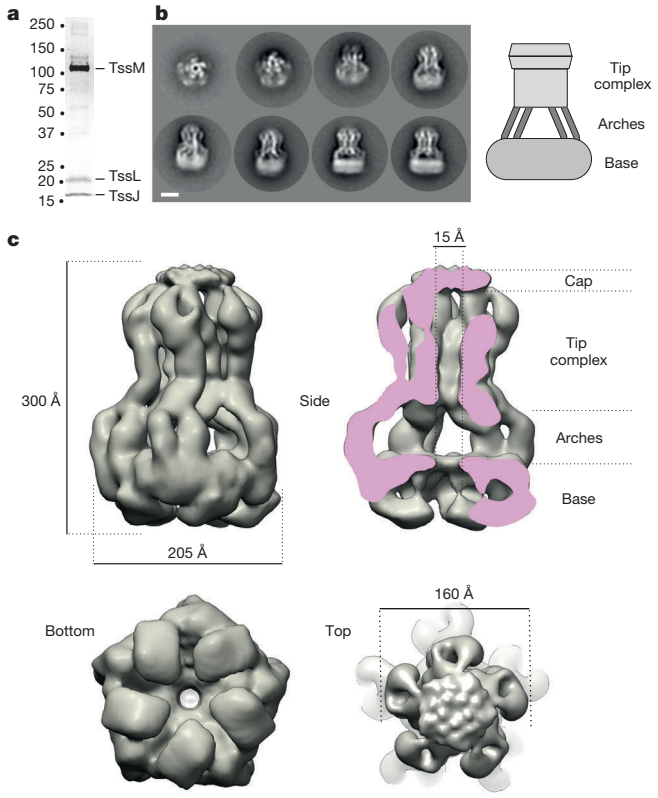

Figure 2 | TssJLM complex purification and structure. **a**, SDS–polyacrylamide gel electrophoresis (SDS–PAGE) analysis of the purified EAEC TssJLM complex. The bands corresponding to TssM (130 kDa), TssL (24 kDa) and TssJ (18 kDa) after SDS–PAGE and Coomassie blue staining are indicated. **b**, Representative views (class averages) of purified TssJLM complexes. End to side views are shown from top left to bottom right. Scale bar, 10 nm. **c**, Structure of the TssJLM complex. Side, cut-away, bottom and top views are shown from top left to bottom right respectively. The different regions of the complex are indicated on the cut-away view.

and end views of the T6SS membrane core complex respectively (Fig. 2b). Rotational symmetry analysis of end-view class-averages revealed a clear five-fold symmetry in the whole TssJLM population (Extended Data Fig. 3b). The complex is composed of a base and a tip complex linked by arches (Fig. 2b). The negative-stain data set was used to reconstruct a 11.6-Å resolution three-dimensional (3D) volume of the complex with five-fold symmetry applied (Fig. 2c and Extended Data Fig. 3c, d). Local resolution calculations using ResMap[30] indicated that the local resolution was significantly lower in the base (Extended Data Fig. 3e, f). This impaired a correct interpretation of this part of the TssJLM map. Since this could be due to flexibility between the base and the rest of the complex, we performed a local 3D refinement on the base region only, which yielded a 3D reconstruction of the base at 16.6-Å resolution. A composite map where this new reconstruction of the base replaces the equivalent densities in the reconstruction of the whole complex is shown in Fig. 2c. The T6SS membrane core complex is 300 Å in height and 205 Å in diameter (Fig. 2c). It is made of a base that is decorated at its bottom by five hooks and is pierced at its centre by a small hole of 15 Å in diameter (Fig. 2c). Ten arches connect this base to a tip complex of 160 Å in diameter covered by a small cap. Remarkably, five arches gather at the centre of the tip complex to define a 15- to 20-Å diameter channel. The five other arches form a scaffold at the periphery of this complex (Extended Data Fig. 4a). Overall, the tip complex is made of internal and external pillars arranged in concentric rings (Extended Data Fig. 4a).

To define how the core complex is inserted in the cell envelope, we first performed differential solubilization of the inner and outer membranes. The total membrane fraction was solubilized with *N*-lauryl sarkosyl, a detergent that preferentially solubilizes inner-membrane proteins. This differential solubilization resulted in the fractionation of the core complex in both inner and outer membrane fractions (Extended Data Fig. 4b), indicating that this complex resides in both membranes. To determine its orientation in the cell envelope, the purified core complex was incubated with anti-StrepII antibodies or Ni-NTA-coated gold particles targeting the TssJ C-terminal StrepII and TssM N-terminal 6×His tags respectively (Extended Data Fig. 4c), before EM analyses. Anti-StrepII antibodies labelled the tip complex/cap while the base was labelled by the Ni-NTA gold particles (Extended Data Fig. 4c). We concluded that the TssJ C terminus is located in the tip complex while the TssM N terminus is located in the base (Extended Data Fig. 4c). When the N-terminal cysteine residue of the TssJ lipoprotein was substituted by Ser (C1S) to prevent its acylation, an intact $TssJ^{C1S}$–L–M core complex was formed (Extended Data Fig. 4b), but differential solubilization proved the complex mis-localized to the inner membrane fraction only (Extended Data Fig. 4b). Hence, TssJ acylation tethers the apex of the complex to the outer membrane whereas the base of the complex is located in the cytoplasm.

We next analysed the EM reconstruction to assign the different regions of the core complex to its components. The volume corresponding to one arch and the corresponding pillar within the tip complex (Extended Data Fig. 4a) is comparable in size and shape to that of the isolated TssM periplasmic domain (amino acids 386–1129; TssMp) in complex with TssJ obtained by small-angle X-ray scattering (SAXS) (Extended Data Fig. 4d, e). Segmentation of this volume yielded five different sub-volumes (Fig. 3a). We propose that the sub-volume closest to the cap corresponds to TssJ, in agreement with its location close to the outer membrane. The other four sub-volumes would correspond to sub-domains of TssMp. Sub-volume 4 is in close contact with TssJ, suggesting that it corresponds to the C-terminal domain of TssM domain, which was previously shown to mediate contact with TssJ[25]. With sub-volume 3, it forms the tip complex while sub-volumes 1 and 2 correspond to the arches (Fig. 3a). Interestingly, the last TssM transmembrane segment crossing the inner membrane is located just upstream of TssMp. This would place the inner membrane at the bottom of the arches or at the top of the base. The volume of the base (1,450 $Å^3$) is much bigger than the estimated volume occupied by ten copies of the cytoplasmic domains of TssM and TssL (825 $Å^3$). The crystal structure of the TssL cytoplasmic domain dimer[28,29] could be fitted in the hooks with 88% correlation (Extended Data Fig. 4f). This indicates that the remainder of the base could correspond to the cytoplasmic domain of TssM and the 40 transmembrane segments bound to detergent (Extended Data Fig. 4f).

To gain more insight into the structure of the TssMp–TssJ complex, TssMp was produced and purified as described previously[25]. To help crystallization, TssMp complex was subjected to controlled proteolytic digestion[31]. A protease-resistant fragment of an apparent size of ~32 kDa (called hereafter $TssM_{32Ct}$; residues 836–1129; Extended Data Fig. 5a) was further purified and co-crystallized with nb25, a specific camelid single-chain nanobody[31,32]. The structure of the $TssM_{32Ct}$–nb25 complex was solved by molecular replacement using the X-ray structure of nb25 reported previously[32] (Extended Data Fig. 5b and Extended Data Table 1). In the complex, the $TssM_{32Ct}$ amino-acid chains are defined in the electron density map between residues 868 and 1107. We therefore purified a new TssMp fragment ($TssM_{26Ct}$) encompassing the crystallographic visible chain. This shorter fragment crystallized readily alone as well as in complex with the unacylated TssJ protein (Extended Data Table 1). The structure of $TssM_{26Ct}$ is composed of two domains. The N-terminal domain (residues 870–974) is a bundle of four α-helices, covered on one side by a β-hairpin (Fig. 3b) and on the other by the C-terminal elongated stretch of the protein. The C-terminal domain (residues 975–1085) is a nine-stranded β-sandwich

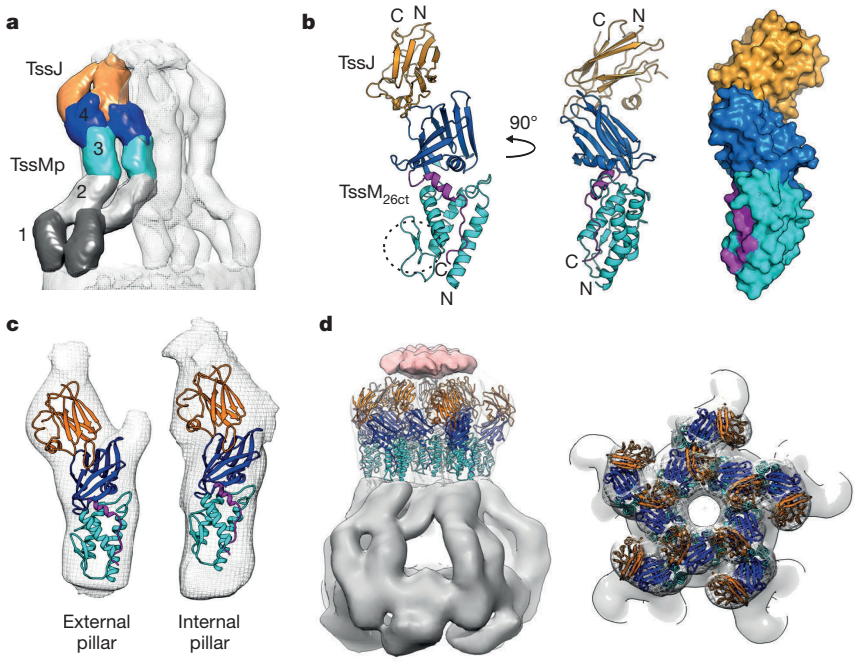

Figure 3 | Structure of the TssJLM tip complex. **a**, Segmentation of the TssJLM complex reconstruction. Each volume encompassing one arch and the corresponding pillar within the tip complex is segmented in five different domains (shown in different colours). **b**, Crystal structure of the $TssM_{26Ct}$–$TssJ_{sol}$ complex represented as ribbons. $TssJ_{sol}$ is coloured orange, while $TssM_{26Ct}$ is coloured cyan (α-domain) and blue (β-domain). The C-terminal α5-helix and the extended stretch are coloured magenta. The β-hairpin (β1–β2) is highlighted in the dashed circle. Two orthogonal views of the crystal structure and its surface representation are shown from left to right (coloured as in **a**). **c**, $TssM_{26Ct}$–TssJ crystal structure docked into the EM volume corresponding to TssJ and the TssM periplasmic domains 3 and 4 extracted from both internal and external pillars of the tip complex. **d**, Energy-minimized atomic model of the tip complex structure (left panel, side view; right panel, top view).

that contacts nb25 or TssJ (Fig. 3b and Extended Table 2a, b). This C-terminal domain is followed by a stretch of residues (1086–1107) comprising helix α5 (Fig. 3b). TssJ binds to the apex of the C-terminal domain, and the 590-$Å^2$ interaction area involves contacts between TssJ loops L1–2, L3–4 and L5–6 with $TssM_{26Ct}$ loops L3–4 and L5–6 (Extended Data Fig. 5c and Extended Data Table 2b), in agreement with a previous study demonstrating the importance of TssJ loop L1–2 for TssM–TssJ complex formation[25]. Superimposition of the structures of $TssM_{32Ct}$–nb25 and $TssM_{26Ct}$–TssJ shows that nb25 and TssJ cannot bind simultaneously to TssM (Extended Data Fig. 5d), explaining the nb25 *in vivo* inhibitory effect on T6SS function[32]. The comparison between $TssM_{26Ct}$–TssJ crystal structure and the volume proposed to correspond to TssJ and domains 3 and 4 of TssMp determined by EM resulted in 95% correlation between the two structures (Fig. 3c). This confirms the location of $TssM_{26Ct}$–TssJ in the tip complex (Fig. 3d).

Cell surface accessibility and transient pore formation

The orientation of the TssJ N terminus places the outer membrane above TssJ, where the cap is located (Figs 2c and 4a and Extended Data Fig. 5e). Accordingly, close inspection of the proposed oligomeric structure of the $TssM_{26Ct}$–TssJ complex could not reveal any obvious transmembrane region (Extended Data Fig. 5f). To test this, we engineered functional cysteine derivatives between the β-strands of the C-terminal domain of TssM (Extended Data Fig. 6a). The extracellular accessibility of these residues was assessed by incubating whole cells with an outer membrane-impermeant cysteine-reactive maleimide. We observed that positions 989, 1005, 1035, 1075 and 1109 were labelled whereas positions 972, 1019, 1062 and 1092 were not (Extended Data Fig. 6b and Extended Data Table 2c). With the exception of position 1092, all other positions were labelled when cell lysates were used instead of intact cells (Extended Data Table 2c). The labelled cysteine substitutions are on the tip of TssM facing the outer membrane (Fig. 4a). Interestingly, residues 989 and 1005 are buried at the interface with TssJ (Extended Data Fig. 6c). Therefore, for these residues to be labelled, the TssM–TssJ complex has to dissociate. This result also suggests that the tip of $TssM_{26Ct}$ is exposed to the cell exterior. To test whether TssM stably crosses the outer membrane or accesses the cell exterior temporarily, similar experiments were conducted in a *tssBC*-deleted background. In the absence of the TssB and TssC sheath components, the TssJLM membrane complex is properly assembled but the T6SS is inactive as no sheath assembly or contraction could occur. In *tssBC* cells, only position 1109 was labelled (Extended Data Fig. 6b and Fig. 4a). These results suggest that the TssM α5-helix crosses the outer membrane permanently, exposing the C-terminal extension to the extracellular medium whereas part of $TssM_{26Ct}$ domain is exposed transiently at the cell surface during the T6SS mechanism of action.

Closing remarks and outlook

The data presented here allow an unprecedented understanding of the biogenesis, architecture and role of the T6SS TssJLM membrane core complex. This complex anchors the phage tail-like structure to the cell envelope and is thought to serve as conduit to guide the Hcp tube/VgrG spike upon sheath contraction[15–17]. Using fluorescence microscopy, we demonstrate that the three subunits are recruited in a specific order, starting from the outer membrane TssJ lipoprotein and pursued by the sequential addition of TssM and TssL, a hierarchy in agreement with previously published localization and interaction studies[17,22–27]. Therefore, T6SS biogenesis is initiated by an outer membrane lipoprotein nucleation factor and progresses inwards, like the assembly mechanisms of other bacterial secretion systems[33–39]. Our fluorescence microscopy analyses also showed that the T6SS membrane core complex assembles randomly in the cell envelope, without specific localization. The complex is stable and can be used for several events of sheath assembly/contraction, increasing the amount of toxin effectors delivered to the target cell.

The TssJLM complex has a five-fold symmetry and is composed of ten copies of each component that assemble a 1.7-MDa structure crossing the inner membrane, the periplasm and anchored to the outer membrane via the TssJ N-terminal lipid moiety. Its architecture is unique compared with other trans-envelope bacterial secretion systems (Extended Data Fig. 7a). On the basis of our accessibility experiments, we propose that upon assembly of other T6SS subunits with the membrane core complex, the TssM C-terminal extension (C-terminal extended stretch following helix α5 in the crystal structure and the remaining 22 non-visible amino acids) will change its conformation and will cross the outer membrane. The base of the TssJLM complex defines a small cavity and hole that cannot accommodate the VgrG protein and potential effectors bound to it (Fig. 4b, stages 1 and 2)[9,20]. We propose that the base changes its conformation

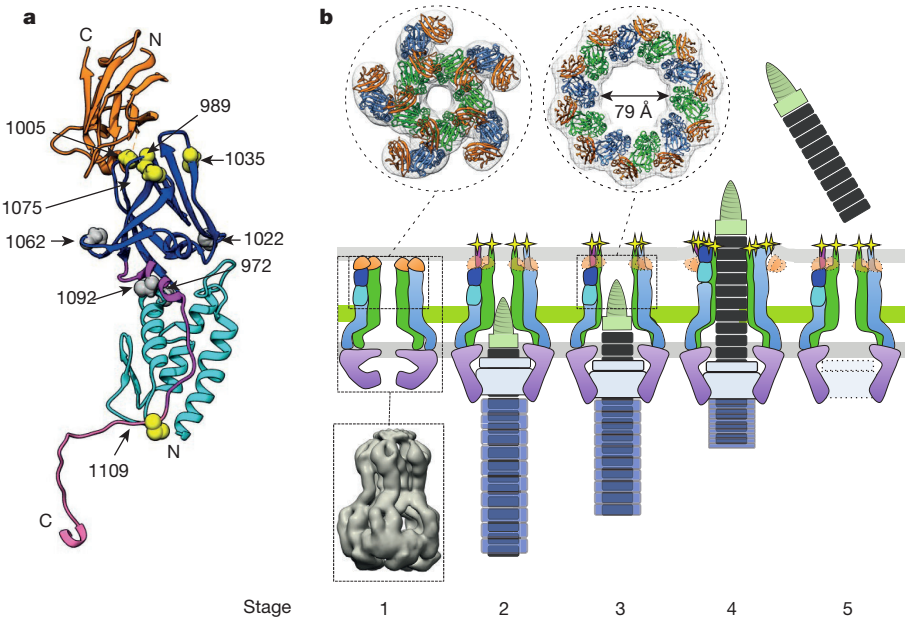

Figure 4 | Cell surface accessibility and mechanism of action of the T6SS membrane core complex during secretion. a, Cell surface accessibility studies. Crystal structure of the $TssM_{26Ct}$ represented as ribbons, coloured cyan (α-domain) and blue (β-domain). The C-terminal α5-helix and the extended stretch are coloured magenta. The C terminus (lacking in the crystallized fragment) is represented as a random structure beyond the last residue in the crystallographic model. The cysteine substitutions (in sphere representation) used for labelling experiments are positioned in the $TssM_{26Ct}$ crystal structure. Cysteines with extracellular accessibility when the T6SS is active are coloured yellow, while the unlabelled ones are coloured grey. **b**, Model of action. The proposed mechanism of action involves five sequential stages. Stage 1: the assembled TssJLM complex is not integrally inserted in the outer membrane, but anchored to it by the TssJ N-terminal lipid moiety. This stage corresponds to the EM reconstruction of the purified TssJLM complex (bottom inset) and the crystal structure of the $TssM_{26Ct}$–TssJ complex (top inset) presented in this study. Stage 2: upon assembly of T6SS baseplate and tail components, the C-terminal extremity of TssM inserts into the outer membrane and is therefore accessible at the cell surface (yellow star). This stage corresponds to the 'resting' state of the T6SS membrane complex. Stages 3 and 4: the membrane core complex opens to allow the passage of the Hcp tube/VgrG spike or the sheath contraction force induces conformational changes of the TssJLM complex. A molecular model of a C_{10} symmetrized TssJ/$TssM_{26Ct}$ ring is presented (top inset). The apical loops of TssM are exposed at the cell surface (yellow stars). Stage 5: after release of the Hcp tube/VgrG spike, the TssJLM membrane complex returns to the resting state, ready to perform another cycle of secretion.

to receive the baseplate components. This state would correspond to a 'resting' state of the T6SS machinery (Fig. 4b, stage 2). Ten arches cross the periplasm and are followed by ten pillars positioned in two concentric layers in the tip complex. The inner pillars define a channel of 15–20 Å in diameter that is not large enough to allow the passage of the ~110 Å Hcp tube[16–18] (Extended Data Fig. 7b). Interestingly, it was previously shown that TssM undergoes large conformational changes during secretion[26]. Therefore, we propose that the inner TssM pillars are pushed outwards to define a wider TssM ring with internal dimensions compatible with the passage of the Hcp tube/VgrG spike (Fig. 4b, stages 3 and 4, and Extended Data Fig. 7b, c). In other secretion systems, specific components are dedicated to assemble the outer membrane pore. No obvious transmembrane region could be found in the TssM C-terminal domain or in TssJ. It is unlikely that the C-terminal portion of TssM would form a pore of sufficient dimension by itself. Therefore, we propose that the stroke of the Hcp–VgrG arrow would mechanically push the C-terminal TssM domain towards the cell exterior, allowing the transient formation of a pore through the outer membrane (Fig. 4b, stage 4). To avoid deleterious effects for the bacterium, one may expect that the C-terminal domain of TssM returns to its initial 'resting' conformation at the periplasmic face of the outer membrane once the Hcp tube has been released, closing the outer membrane channel (Fig. 4b, stage 5). Overall, the membrane core complex appears to act like a docking station for the phage-like T6SS device. It nucleates the assembly of the rest of the secretion system and then guides the Hcp tube/VgrG spike through the bacterial cell envelope upon sheath contraction. Further studies will be necessary to fully understand the complete assembly process of the T6SS, the trigger that releases sheath contraction and how the Hcp tube/VgrG spike crosses both bacterial and host membranes.

Online Content Methods, along with any additional Extended Data display items and Source Data, are available in the online version of the paper; references unique to these sections appear only in the online paper.

Received 10 March; accepted 15 June 2015.
Published online 22 July 2015.

1. West, S. A., Griffin, A. S. & Gardner, A. Evolutionary explanations for cooperation. *Curr. Biol.* **17,** 661–672 (2007).
2. Blango, M. G. & Mulvey, M. A. Bacterial landlines: contact-dependent signaling in bacterial populations. *Curr. Opin. Microbiol.* **12,** 177–181 (2009).
3. Russell, A. B., Peterson, S. B. & Mougous, J. D. Type VI secretion system effectors: poisons with a purpose. *Nature Rev. Microbiol.* **12,** 137–148 (2014).
4. Silverman, J. M., Brunet, Y. R., Cascales, E. & Mougous, J. D. Structure and regulation of the type VI secretion system. *Annu. Rev. Microbiol.* **66,** 453–472 (2012).
5. Pukatzki, S., Ma, A. T., Revel, A. T., Sturtevant, D. & Mekalanos, J. J. Type VI secretion system translocates a phage tail spike-like protein into target cells where it cross-links actin. *Proc. Natl Acad. Sci. USA* **104,** 15508–15513 (2007).
6. Russell, A. B. *et al.* Type VI secretion delivers bacteriolytic effectors to target cells. *Nature* **475,** 343–347 (2011).
7. Russell, A. B. *et al.* Diverse type VI secretion phospholipases are functionally plastic antibacterial effectors. *Nature* **496,** 508–512 (2013).
8. Ma, L. S., Hachani, A., Lin, J. S., Filloux, A. & Lai, E. M. *Agrobacterium tumefaciens* deploys a superfamily of type VI secretion DNase effectors as weapons for interbacterial competition in planta. *Cell Host Microbe* **16,** 94–104 (2014).
9. Durand, E., Cambillau, C., Cascales, E., Journet, L. & Vgr, G. Tae, Tle, and beyond: the versatile arsenal of Type VI secretion effectors. *Trends Microbiol.* **22,** 498–507 (2014).
10. Borgeaud, S., Metzger, L. C., Scrignari, T. & Blokesch, M. Bacterial evolution. The type VI secretion system of *Vibrio cholerae* fosters horizontal gene transfer. *Science* **347,** 63–67 (2015).
11. Cascales, E. The type VI secretion toolkit. *EMBO Rep.* **9,** 735–741 (2008).
12. Bönemann, G., Pietrosiuk, A., Diemand, A., Zentgraf, H. & Mogk, A. Remodelling of VipA/VipB tubules by ClpV-mediated threading is crucial for type VI protein secretion. *EMBO J.* **28,** 315–325 (2009).
13. Basler, M., Pilhofer, M., Henderson, G. P., Jensen, G. J. & Mekalanos, J. J. Type VI secretion requires a dynamic contractile phage tail-like structure. *Nature* **483,** 182–186 (2012).

14. Kudryashev, M. *et al.* Structure of the type VI secretion system contractile sheath. *Cell* **160,** 952–962 (2015).
15. Coulthurst, S. J. The type VI secretion system – a widespread and versatile cell targeting system. *Res. Microbiol.* **164,** 640–654 (2013).
16. Ho, B. T., Dong, T. G. & Mekalanos, J. J. A view to a kill: the bacterial type VI secretion system. *Cell Host Microbe* **15,** 9–21 (2014).
17. Zoued, A. *et al.* Architecture and assembly of the type VI secretion system. *Biochim. Biophys. Acta* **1843,** 1664–1673 (2014).
18. Bönemann, G., Pietrosiuk, A. & Mogk, A. Tubules and donuts: a type VI secretion story. *Mol. Microbiol.* **76,** 815–821 (2010).
19. Brunet, Y. R., Hénin, J., Celia, H. & Cascales, E. Type VI secretion and bacteriophage tail tubes share a common assembly pathway. *EMBO Rep.* **15,** 315–321 (2014).
20. Shneider, M. M. *et al.* PAAR-repeat proteins sharpen and diversify the type VI secretion system spike. *Nature* **500,** 350–353 (2013).
21. Brunet, Y. R., Espinosa, L., Harchouni, S., Mignot, T. & Cascales, E. Imaging type VI secretion-mediated bacterial killing. *Cell Rep.* **3,** 36–41 (2013).
22. Aschtgen, M. S., Gavioli, M., Dessen, A., Lloubès, R. & Cascales, E. The SciZ protein anchors the enteroaggregative *Escherichia coli* type VI secretion system to the cell wall. *Mol. Microbiol.* **75,** 886–899 (2010).
23. Aschtgen, M. S., Bernard, C. S., de Bentzmann, S., Lloubès, R. & Cascales, E. SciN is an outer membrane lipoprotein required for type VI secretion in enteroaggregative *Escherichia coli*. *J. Bacteriol.* **190,** 7523–7531 (2008).
24. Ma, L. S., Lin, J. S. & Lai, E. M. An IcmF family protein, ImpLM, is an integral inner membrane protein interacting with ImpKL, and its walker a motif is required for type VI secretion system-mediated Hcp secretion in *Agrobacterium tumefaciens*. *J. Bacteriol.* **191,** 4316–4329 (2009).
25. Felisberto-Rodrigues, C. *et al.* Towards a structural comprehension of bacterial type VI secretion systems: characterization of the TssJ-TssM complex of an *Escherichia coli* pathovar. *PLoS Pathog.* **7,** e1002386 (2011).
26. Ma, L. S., Narberhaus, F. & Lai, E. M. IcmF family protein TssM exhibits ATPase activity and energizes type VI secretion. *J. Biol. Chem.* **287,** 15610–15621 (2012).
27. Aschtgen, M. S., Zoued, A., Lloubès, R., Journet, L. & Cascales, E. The C-tail anchored TssL subunit, an essential protein of the enteroaggregative *Escherichia coli* Sci-1 type VI secretion system, is inserted by YidC. *MicrobiologyOpen* **1,** 71–82 (2012).
28. Durand, E. *et al.* Structural characterization and oligomerization of the TssL protein, a component shared by bacterial type VI and type IVb secretion systems. *J. Biol. Chem.* **287,** 14157–14168 (2012).
29. Chang, J. H. & Kim, Y. G. Crystal structure of the bacterial type VI secretion system component TssL from *Vibrio cholerae*. *J. Microbiol.* **53,** 32–37 (2015).
30. Kucukelbir, A., Sigworth, F. J. & Tagare, H. D. Quantifying the local resolution of cryo-EM density maps. *Nature Methods* **11,** 63–65 (2014).
31. Nguyen, V. S. *et al.* Production, crystallization and X-ray diffraction analysis of a complex between a fragment of the TssM T6SS protein and a camelid antibody. *Acta Crystallogr F.* **71,** 266–271 (2015).
32. Nguyen, V. S. *et al.* Inhibition of type VI secretion by an anti-TssM llama nanobody. *PLoS ONE* **10,** e0122187 (2015).
33. Diepold, A. *et al.* Deciphering the assembly of the *Yersinia* type III secretion injectisome. *EMBO J.* **29,** 1928–1940 (2010).
34. Judd, P. K., Kumar, R. B. & Das, A. Spatial location and requirements for the assembly of the *Agrobacterium tumefaciens* type IV secretion apparatus. *Proc. Natl Acad. Sci. USA* **102,** 11498–11503 (2005).
35. Hardie, K. R., Lory, S. & Pugsley, A. P. Insertion of an outer membrane protein in *Escherichia coli* requires a chaperone-like protein. *EMBO J.* **15,** 978–988 (1996).
36. Drake, S. L., Sandstedt, S. A. & Koomey, M. PilP, a pilus biogenesis lipoprotein in *Neisseria gonorrhoeae*, affects expression of PilQ as a high-molecular-mass multimer. *Mol. Microbiol.* **23,** 657–668 (1997).
37. Burghout, P. *et al.* Role of the pilot protein YscW in the biogenesis of the YscC secretin in *Yersinia enterocolitica*. *J. Bacteriol.* **186,** 5366–5375 (2004).
38. Crago, A. M. & Koronakis, V. *Salmonella* InvG forms a ring-like multimer that requires the InvH lipoprotein for outer membrane localization. *Mol. Microbiol.* **30,** 47–56 (1998).
39. Daefler, S. & Russel, M. The *Salmonella typhimurium* InvH protein is an outer membrane lipoprotein required for the proper localization of InvG. *Mol. Microbiol.* **28,** 1367–1380 (1998).

Supplementary Information is available in the online version of the paper.

Acknowledgements This work was funded by Agence Nationale de la Recherche (ANR) grants ANR-10-JCJC-1303-03 to E.C., Bip:Bip to R.F., ANR-14-CE14-0006-02 to C.C. and E.C., and supported by the French Infrastructure for Integrated Structural Biology (FRISBI) ANR-10-INSB-05-01. E.D. was supported by a post-doctoral fellowship from the Fondation pour la Recherche Médicale (SPF20101221116) and ANR grants Bip:Bip and ANR-10-JCJC-1303-03. V.S.N. was supported by a PhD grant from the French Embassy in Vietnam (792803C). A.Z., L.L. and M.S.A. were recipients of doctoral fellowships from the French Ministère de la Recherche. A.Z. received a Fondation pour la Recherche Médicale fellowship (FDT20140931060). We thank O. Francetic for providing anti-DglA and anti-OmpF antibodies. We thank E. Marza, P. Violinova Krasteva and H. Remaut for comments on the manuscript, and T. Mignot, M. Guzzo and L. Espinosa for advice about the fluorescence microscopy experiments and the statistical analyses. We also thank the members of the R.F. and E.C. research groups for discussions and suggestions, and R. Lloubès, J. Sturgis and A. Galinier for encouragement. We thank the ERSF and Soleil Synchrotron radiation facilities for beamline allocation.

Author Contributions E.D., A.Z., C.C., E.C. and R.F. designed the experiments. A.Z. constructed the EAEC mutant and fluorescent strains and performed the fluorescence microscopy experiments and statistical analyses. L.L. and M.S.A. constructed the TssM cysteine derivatives and performed the accessibility experiments. E.D. assisted by An.D. purified the TssJLM complex and performed its biochemical characterization. E.D. and G.P.A. collected the EM data. E.D. and R.F. obtained the 3D reconstruction of the TssJLM complex. V.S.N., S.S., A.R. and C.C. purified, crystallized and solved the X-ray structures. Al.D. generated the nanobody. B.B. obtained the energy-minimized models of the closed and open states of the $TssM_{26Ct}$–TssJ complex.

Author Information The EM structure of the TssJLM complex has been deposited in the Electron Microscopy Data Bank (EMDB) under accession number emd-2927. The crystal structures of the $TssM_{32Ct}$–nb25 complex, and of the $TssM_{26Ct}$ fragment and $TssM_{26Ct}$–TssJ complexes, have been deposited in the Protein Data Bank under accession numbers 4Y7M, 4Y7L and 4Y7O, respectively. Reprints and permissions information is available at www.nature.com/reprints. The authors declare no competing financial interests. Readers are welcome to comment on the online version of the paper. Correspondence and requests for materials should be addressed to C.C. (cambillau@afmb.univ-mrs.fr), E.C. (cascales@imm.cnrs.fr) or R.F. (remi.fronzes@pasteur.fr).

METHODS

No statistical methods were used to predetermine sample size. The experiments were not randomized. The investigators were not blinded to allocation during experiments and outcome assessment.

Strains, media and chemicals. The strains, plasmids and oligonucleotides used in this study are listed in Supplementary Table 1. The *E. coli* K-12 DH5α strain was used for cloning steps whereas *E. coli* K-12 BL21(DE3) and T7-Iq pLys strains were used for protein purification. The enteroaggregative *E. coli* EAEC strain 17-2 was used to engineer gene knockouts and fusions with fluorescent labels. Strains were routinely grown in lysogeny broth (LB) rich medium (or Terrific broth medium for protein purification) or in Sci-1-inducing medium (SIM; M9 minimal medium, glycerol 0.2%, vitamin B1 1 μg ml^{-1}, casaminoacids 100 μg ml^{-1}, LB 10%, supplemented or not with bactoagar 1.5%)[40] with shaking at 37 °C. Plasmids were maintained by the addition of ampicillin (100 μg ml^{-1} for *E. coli* K-12, 200 μg ml^{-1} for EAEC) or kanamycin (50 μg ml^{-1}). Expression of genes from pETG20A and pRSF vectors was induced with 1 mM of isopropyl-β-D-thiogalactopyrannoside (IPTG, Eurobio) for 16 h.

Strain construction. Gene deletion into the enteroaggregative *E. coli* 17-2 strain was achieved by using a modified one-step inactivation procedure[41] as previously described[23] using plasmid pKOBEG[42]. Briefly, a kanamycin cassette was amplified from plasmid pKD4[41] using oligonucleotide pairs carrying 5′ 50-nucleotide extensions homologous to regions adjacent to the gene to be deleted. After electroporation of 600 ng of column-purified PCR product, kanamycin-resistant clones were selected and verified by colony-PCR. The kanamycin cassette was then excised using plasmid pCP20 (ref. 41). Gene deletions were confirmed by colony-PCR. The same procedure was used to introduce the *mCherry*- or *sfGFP*-coding sequences downstream from the start codon (vector pKD4-*sfGFP* or pKD4-*mCherry*) or the *mCherry*-coding sequence upstream from the stop codon (vector p*mCherry*-KD4). This procedure yields strains producing fusion proteins from their original chromosomal loci.

Plasmid construction. PCRs were performed using the Phusion DNA polymerase (Thermo Scientific). Restriction enzymes were purchased from New England Biolabs and used according to the manufacturer's instructions. Custom oligonucleotides were synthesized by Sigma Aldrich and are listed in Supplementary Table 1. Enteroaggregative *E. coli* 17-2 chromosomal DNA was used as a template for all PCRs. *E. coli* strain DH5α was used for cloning procedures. The pETG20A vector derivative encoding the periplasmic domain of the TssM periplasmic domain (TssMp, residues 386–1129) or the TssJ soluble domain have been previously described[25]. The fragment encoding TssM$_{26Ct}$ (residues 869–1107) was cloned into the pETG20A vector by restriction-free cloning[43]. The pRSF–TssJ^{S} intermediate plasmid was constructed by restriction cloning. Briefly, the sequence encoding the full-length *tssJ* gene (residues 1–178) was PCR-amplified using primers RSF-sJ-F and RSF-sJ-R. The PCR introduced a 5′ NdeI and a 3′ XhoI restriction site and a C-terminal streptavidin extension. The *tssJ* PCR product was sub-cloned into the pRSF-Duet (Novagen) MCS2 corresponding restriction sites. The pRSF–TssJ^{S}-^{F}L-^{H}M (encoding C-terminally StrepII-tagged TssJ, N-terminally Flag-tagged TssL and N-terminally 6×His-tagged TssM) was constructed by restriction-free cloning[43] as previously described[22]. Briefly, the sequence encoding the full-length *tssL* (residues 1–217) and full-length *tssM* (residues 1–1129) genes were PCR-amplified using the primer pairs RSF-fL-F/RSF-fL-R and RSF-hM-F/RSF-hM-R, respectively. The two PCR products (*tssL* and *tssM*) were synthesized with 30-base-pair overhangs, from both 5′ and 3′ ends, corresponding to the designed integration sites into the pRSF–TssJ^{S} plasmid. The double-stranded product of the first PCR was then used as oligonucleotides for a second PCR using the target vector as template. The introduction of the C1S mutation in TssJ was performed by QuikChange mutagenesis of the pRSF–TssJ^{S}-^{F}L-^{H}M plasmid using oligonucleotides Jcs-F and Jcs-R. Plasmid pIBA37-TssM was constructed by restriction-free cloning and cysteine derivatives were obtained by QuikChange mutagenesis using pIBA37-TssM-C757S mutant as template.

Hcp release assay. Cells producing Flag- or HA-tagged Hcp from plasmids pUCHcp$_{Flag}$ or pOKHcp$_{HA}$[22,23] were grown in SIM to an absorbance $A_{600\ nm} \sim 0.8$. Supernatant and cell fractions were separated as previously described[22]. Briefly, 2×10^9 cells were harvested and collected by centrifugation at 2,000*g* for 5 min. The supernatant fraction was then subjected to a second low-speed centrifugation and then at 16,000*g* for 15 min. The supernatant was filtered on sterile polyester membranes with a pore size of 0.2 μm (Membrex 25 PET, membraPure) before overnight precipitation with trichloroacetic acid 15% on ice. Cells and precipitated supernatants were resuspended in loading buffer and analysed by SDS–PAGE and immunoblotting with the anti-Flag or anti-HA antibody. As control for cell lysis, western blots were probed with antibodies raised against the periplasmic TolB protein. The assays were performed from three independent cultures, and a representative experiment is shown.

Interbacterial competition assay. The antibacterial growth competition assay was performed as described for the studies on the *Citrobacter rodentium* and EAEC Sci-2 T6SSs[21,44] with modifications. The wild-type *E. coli* strain W3110 bearing the Kan^{R} pUA66-*rrnB* plasmid[45] was used as prey in the competition assay. Attacker and prey cells were grown for 16 h in LB medium, then diluted in SIM to allow maximal expression of the *sci-1* gene cluster[40]. Once the culture reached $A_{600\ nm} \sim 0.8$, the cells were harvested and normalized to $A_{600\ nm} = 0.5$ in SIM. Attacker and prey cells were mixed to a 4:1 ratio and 20-μl drops of the mixture were spotted in triplicate onto a pre-warmed dry SIM agar plate supplemented or not with anhydrotetracyclin 0.02 μg ml^{-1}. After overnight incubation at 37 °C, the bacterial spots were then cut off, and cells were resuspended in SIM to $A_{600\ nm} = 0.5$. Two hundred microlitres of serial dilutions were plated on kanamycin LB plates and the number of colonies was scored after overnight incubation at 37 °C. The assays were performed from at least three independent cultures, with technical triplicates and a representative technical triplicate shown.

Fluorescence microscopy, image treatment and statistical analyses. Fluorescence microscopy experiments were performed essentially as described[21,46]. Briefly, cells were grown overnight in LB medium and diluted to $A_{600\ nm} \sim 0.04$ in SIM. Exponentially growing cells ($A_{600\ nm} \sim 0.8$–1) were harvested, washed in phosphate buffered saline buffer (PBS), resuspended in PBS to $A_{600\ nm} \sim 50$, spotted on a thin pad of 1.5% agarose in PBS, covered with a cover slip and incubated for 1 h at 37 °C before microscopy acquisition. For each experiment, ten independent fields were manually defined with a motorized stage (Prior Scientific) and stored (*x*, *y*, *z*, Perfect Focus System (PFS) offset) in our custom automation system designed for time-lapse experiments. Fluorescence and phase contrast micrographs were captured every 30 s using an automated and inverted epifluorescence microscope TE2000-E-PFS (Nikon) equipped with PFS. PFS automatically maintains focus so that the point of interest within a specimen is always kept in sharp focus at all times despite mechanical or thermal perturbations. Images were recorded with a CoolSNAP HQ 2 (Roper Scientific) and a ×100/1.4 DLL objective. The excitation light was emitted by a 120 W metal halide light. All fluorescence images were acquired with a minimal exposure time to reduce bleaching and phototoxicity effects. The sfGFP images were recorded by using the ET-GFP filter set (Chroma 49002) with an exposure time of 200–400 ms. The mCherry images were recorded by using the ET-mCherry filter set (Chroma 49008) using an exposure time of 100–200ms. Slight movements of the whole field during the time of the experiment were corrected by registering individual frames using StackReg and Image Stabilizer plugins for ImageJ. sfGFP and mCherry fluorescence channels were adjusted and merged using ImageJ (http://rsb.info.nih.gov/ij/). sfGFP fluorescence sets of data were treated to monitor foci detection. Noise and background were reduced using the 'Subtract Background' (20 pixels Rolling Ball) plugin from Fiji (Image J/National Institutes of Health). The sfGFP foci were automatically detected by simple image processing: (1) create a mask of cell surface and dilate, (2) detect the individual cells using the 'Analyse Particle' plugin of Fiji and (3) identify foci by the 'Find Maxima' process in Fiji. To avoid false positive results, each event was manually controlled in the original data. Microscopy analyses were performed at least six times, each in technical triplicate, and a representative experiment is shown. Box-and-whisker plots representing the number of detected foci for each strain were made with R software. To compare each population, *t*-tests were performed in R. Sub-pixel resolution tracking of fluorescent foci: Fluorescent foci were detected using a local and sub-pixel resolution maxima detection algorithm and tracked over time with a specifically developed plug-in for ImageJ. The *x* and *y* coordinates were obtained for each fluorescent focus on each frame. The mean square displacement was calculated as the distance of the foci from its location at t_0 at each time using R software and plotted over time. For each strain tested, the mean square displacement of at least ten individual focus trajectories was calculated.

Inner and outer membrane separation. Cells were broken using an Emulsiflex-C5 (Avestin) and the crude membrane fraction was isolated by ultracentrifugation at 100,000*g* for 45 min. Outer and inner membranes were separated by differential solubilization. Inner membranes were solubilized by 0.5% sodium *N*-lauroyl sarcosyl in 50 mM Tris-HCl pH 8.0 for 30 min at 20 °C. The insoluble material containing the outer membrane fraction was isolated by ultracentrifugation at 100,000*g* for 20 min. The outer membrane pellet was then solubilized in SDS-loading buffer. The assay was performed in triplicate, from three independent cultures and a representative experiment is shown.

TssJLM complex production and purification. The pRSF–TssJ^{S}-^{F}L-^{H}M plasmid was transformed into the *E. coli* BL21(DE3) expression strain (Invitrogen). Cells were grown at 37 °C in lysogeny broth (LB) to $A_{600\ nm} \sim 0.7$ and the expression of the *tssJLM* genes was induced with 1.0 mM IPTG for 16 h at 16 °C. Cell pellets were resuspended in ice-cold 50 mM Tris-HCl pH 8.0, 50 mM NaCl, 1 mM EDTA

and 1 mM TCEP, supplemented with 100 μg ml^{-1} of DNase I, 100 μg ml^{-1} of lysozyme and EDTA-free protease inhibitor (Roche). After sonication, $MgCl_2$ was added to the final concentration of 10 mM and the cell suspension was further broken using an Emulsiflex-C5 (Avestin). The broken cell suspension was clarified by centrifugation at 38,500*g* for 20 min. The membrane fraction was then collected by centrifugation at 98,000*g* for 45 min. Membranes were mechanically homogenized and solubilized in 50 mM Tris-HCl pH 8.0, 50 mM NaCl, 0.5% (w/v) *n*-dodecyl-β-D-maltopyranoside (DDM, Anatrace), 0.75% (w/v) decyl maltose neopentyl glycol (DM-NPG, Anatrace), 0.5% (w/v) digitonin (Sigma-Aldrich), 100 μM TCEP and 1 mM EDTA at 22 °C for 45 min. The suspension was clarified by centrifugation at 98,000*g* for 20 min. The supernatant was loaded onto a 5-ml StrepTrap HP (GE Healthcare) column and then washed with 50 mM Tris-HCl pH 8.0, 50 mM NaCl, 0.05% (w/v) DM-NPG (Affinity buffer) at 4 °C. The TssJLM core complex was eluted in the affinity buffer supplemented with 2.5 mM desthiobiotin (IBA) into a 5-ml HisTrap HP (GE Healthcare) column. The column was then washed in the affinity buffer supplemented with 20 mM imidazole and the TssJLM core complex was eluted in the same buffer supplemented with 500 mM imidazole. Peak fractions were pooled and loaded onto a Superose 6 10/300 column (GE Healthcare) equilibrated in 50 mM Tris-HCl pH 8.0, 50 mM NaCl, 0.025% (w/v) DM-NPG. The TssJLM core complex eluted as a single monodisperse peak close to the void volume of the column. The sample was used immediately for EM sample preparation.

Stoichiometry analyses. The purified TssJLM core membrane complex was diluted to a final concentration of 0.1 mg ml^{-1} and denaturated at 100 °C for 10 min after the addition of 1% sodium dodecyl sulfate. The denatured sample was incubated in presence of 40 μM of Alexa Fluor 532 C5-maleimide (Invitrogen) and 1 mM TCEP (Pierce) for 2 h at room temperature. The labelled proteins were separated by SDS–PAGE and protein-bound fluorescence was visualized and quantified using a Fujifilm FLA-3000 scanner. The assay was performed in triplicate, from three independent TssJLM complex preparations, and a representative experiment is shown. The quantification is expressed with the standard deviation from the three biological replicates.

EM and image processing. Determination of the TssJLM core membrane complex structure was achieved by negative-stain EM. Nine microlitres of suitably diluted (~0.01 mg ml^{-1}) TssJLM complex sample was spotted to glow-discharged carbon-coated copper grids (Agar Scientific). After 30 s of absorption, the sample was blotted, washed with three drops of water and then stained with 2% uranyl acetate. Images were recorded automatically using the EPU software on an FEG microscope operating at a voltage of 200 kV and a defocus range of 0.6–25 nm, using an FEI Falcon-II detector (Gatan) at a nominal magnification of 50,000, yielding a pixel size of 1.9 Å. A dose rate of 25 electrons per square ångström per second, and an exposure time of 1 s, were used. A total of 72,146 particles were automatically selected from 1,200 independent images and extracted within boxes of 280 pixels × 280 pixels using EMAN2/BOXER[47]. The defocus value was estimated and the contrast transfer function was corrected by phase flipping using EMAN2 (e2ctf). All 2D and 3D classifications and refinements were performed using RELION 1.3 (refs 48, 49). We used three rounds of reference-free 2D class averaging to clean up the automatically selected data set. Only highly populated classes displaying high-resolution features were conserved during this procedure and a final data set of 26,544 particles was assembled. An initial 3D model was generated in EMAN2 using 30 classes. Three-dimensional classification was then performed in Relion with five classes. The particles corresponding to the most populated class (~16,738) were used for refinement. Relion auto-refine procedure was used to obtain a final reconstruction at 11.56-Å resolution after masking and with C_5 symmetry imposed. Reported resolutions are based on the 'gold standard' Fourier shell correlation (FSC) 0.143 criterion, and FSC curves were corrected for the effects of a soft mask on them by using high-resolution noise substitution[50]. Before visualization, all density maps were corrected for the modulation transfer function of the detector and then sharpened by applying an ad hoc negative B-factor (−1,000). Local resolution variations were estimated using ResMap[51].

Three-dimensional maps display and analysis. Three-dimensional reconstructions were displayed and rendered in USCF Chimera segmented using the SEGGER module implemented in UCSF Chimera[52]. Segments corresponding to individual structural domains are represented in Fig. 3c–e. All other maps were left un-segmented. A volume/mass conversion of 0.81 Da Å^{-3} was used to estimate the volume occupied by TssM and TssL cytoplasmic domains.

Protein production and purification for SAXS and X-ray analyses. The periplasmic domain of the TssM protein, TssMp (residues 386–1129), was produced and purified as described previously[25]. The purified recombinant TssMp was digested with trypsin (at a 1,000:1 molecular ratio) at room temperature for 24 h. The reaction was quenched by the addition of 1 mM phenyl-methanesulfonyl fluoride (PMSF) and the insoluble TssMp fragments were discarded by centrifugation at 20,000*g* for 30 min. A proteolysis-resistant fragment of apparent size ~32 kDa (called hereafter $TssM_{32Ct}$) was further purified by consecutive ion-exchange (Mono Q 5/50 GL column, GE Healthcare) and size-exclusion (Superdex 75 16/600 HL column) chromatographies using an Äkta system (GE Healthcare). The purified fragment was subjected to N-terminal Edman sequencing. A PVDF membrane was rinsed three times with a water/ethanol mixture (10/90) and inserted in the A cartridge of a Procise 494A sequencer. After five cycles of Edman degradation, the sequence DYGSL was identified by mass spectrometry, indicating that cleavage after Arg834 generated a C-terminal fragment of theoretical mass 32,398 Da, in agreement with the 32-kDa band observed by SDS–PAGE analyses.

For production and purification of the $TssM_{26Ct}$ fragment (Thr869 to Glu1107), *E. coli* BL21(DE3) cells cultivated in the TB medium carrying plasmid pETG20A-$TssM_{26Ct}$ were grown to $A_{600\ nm}$ ~ 0.6 and the expression of $TssM_{26Ct}$ was induced by the addition of 0.5 mM IPTG for 16 h at 17 °C. Cells were collected by centrifugation at 10,000*g* at 4 °C for 15 min. The cell pellet was resuspended in lysis buffer and lysed by sonication. The lysate was clarified by centrifugation at 20,000*g* at 4 °C for 15 min, and the supernatant containing the Trx–His_6–tev–$TssM_{26ct}$ fusion protein was purified by consecutive Ni^{2+}-affinity and size-exclusion (Superdex 75 column) chromatographies on an Äkta purifier (GE Healthcare). The fractions containing the protein of interest were pooled and the 6×His-tagged TEV protease was added (5% w/w). The cleaved protein was purified using Ni^{2+} affinity, removing the Trx-His_6, followed by size-exclusion chromatography (Superdex 75 column) on an Äkta purifier (GE Healthcare). Over 100 mg of $TssM_{26ct}$ fragment were obtained per litre of culture. The purified protein was verified by mass spectrometry, before being concentrated up to 8.7 mg ml^{-1} in 20 mM Tris-HCl pH 8.0, NaCl 150 mM.

The production of nanobody nb25 and the formation of its complex with $TssM_{32Ct}$ have been described previously[31,32]. The production of unacylated TssJ was previously described[25]. The $TssM_{26Ct}$–TssJ complex was obtained by mixing $TssM_{26Ct}$ (8.7 mg ml^{-1}) with purified TssJ (30 mg ml^{-1}) in a 1:1.2 molecular ratio and the complex was then concentrated up to 15 mg ml^{-1} using centricon (cut-off of 10,000 Da) in 20 mM Tris-HCl pH 8.0, 150 mM NaCl.

SAXS and *ab initio* 3D shape reconstruction. SAXS analyses were performed at the ID29 beamline (European Synchrotron Radiation Facility, Grenoble, France) at a working energy of 12.5 keV ($\lambda = 0.931$ Å). Thirty microlitres of protein solution at 1.6 mg ml^{-1} in Tris-HCl 20 mM pH 8.0, NaCl 150 mM, were loaded by a robotic system into a 2-mm quartz capillary mounted in a vacuum. Ten independent 10-s exposures were collected on a Pilatus 6M-F detector placed at a distance of 2.85 m for each protein concentration. Individual frames were processed automatically and independently at the beamline by the data collection software (BsxCUBE), yielding radially averaged normalized intensities as a function of the momentum transfer q, with $q = 4\pi\sin(\theta)/\lambda$, where 2θ is the total scattering angle and λ is the X-ray wavelength. Data were collected in the range $q = 0.04$–$6\ nm^{-1}$. The ten frames were combined to give the average scattering curve for each measurement. Data points affected by aggregation, possibly induced by radiation damage, were excluded. Scattering from the buffer alone was also measured before and after each sample analysis and the average of these two buffer measures was used for background subtraction using the program PRIMUS[53] from the ATSAS package[54]. PRIMUS was also used to perform Guinier analysis[55] of the low q data, which provides an estimate of the radius of gyration (R_g). Regularized indirect transforms of the scattering data were performed with the program GNOM[56] to obtain $P(r)$ functions of interatomic distances. The $P(r)$ function has a maximum at the most probable intermolecular distance and goes to zero at D_{max}, the maximum intramolecular distance. The values of D_{max} were chosen to fit with the experimental data and to have a positive $P(r)$ function. Three-dimensional bead models that fitted with the scattering data were built with the program DAMMIF[57]. Twenty independent DAMMIF runs were performed using the scattering profile of the TRX–His–TssJp and TRX–His–TssMp complexes, with data extending up to 0.35 nm^{-1}, using slow mode settings, assuming no symmetry and allowing for a maximum 500 steps to grant convergence. The models resulting from independent runs were superimposed using the DAMAVER suite[58]. This yielded an initial alignment of structures based on their axes of inertia followed by minimization of the normalized spatial discrepancy[59]. The normalized spatial discrepancy was therefore computed between a set of 20 independent reconstructions, with a range of normalized spatial discrepancies from 0.678 to 0.815. The aligned structures were then averaged, giving an effective occupancy to each voxel in the model, and filtered at half-maximal occupancy to produce models of the appropriate volume that were used for all subsequent analyses. All the models were similar in terms of agreement with the experimental data, as measured by DAMMIF χ parameter and the quality of the fit to the experimental curve. The DAMFILT average volume was used as the final model of the TRX–His–TssJ and TRX–His–TssMp complexes.

Ni-TNA-Nanogold labelling. The TssJLM complex was spotted onto a glow-discharged carbon coated grid (CF-400, Electron Microscopy Sciences). After 1 min, excess liquid was blotted, and the grid was washed on a drop of cold purification buffer (50 mM Tris pH 8, 50 mM NaCl, 0.025% (w/v) DM-NPG) containing 50 mM imidazole, quickly blotted and deposited on a second drop of the same buffer in the presence of 5 nM Ni-TNA-Nanogold beads (Nanoprobes). After 2 min, the grid was rinsed sequentially for 20 s with one drop of purification buffer, one drop of the same buffer without detergent and three drops of 2% uranyl acetate. Images were collected on an FEI Tecnai F20 FEG microscope operating at a voltage of 200 kV, equipped with a direct electron detector (Falcon II). Particles were selected manually using EMAN2. The assay was performed at least in triplicate, from independent TssJLM complex preparations, and representative particles are shown.

Anti-Strep labelling. The TssJLM complex was mixed with monoclonal anti-Strep antibodies (Sigma) at a ratio of complex:antibody of 2:1. The mixture was incubated at 4 °C for 30 min and the labelled complex was isolated by gel filtration. The sample was analysed by negative-stain EM as described above for negative-stain EM of the unlabelled TssJLM complex. The assay was performed at least in triplicate, from independent TssJLM complex preparations, and representative particles are shown.

Crystallization and structure determination. The crystallization of the $TssM_{32Ct}$–nb25 complex has been described previously[31]. For $TssM_{26Ct}$ alone, several kits were used for crystallization screening, including STURA, WIZARD, MDL, INDEX and PEGs. A hit was observed in the PEGs kit, within a well containing 0.2 M zinc acetate and 20% (m/v) PEG3350. Crystal optimization was performed by varying PEG3350 amount in the 15–25% range in 0.1 M sodium acetate and 0.2 M $ZnCl_2$ at pH varying between 3.8 and 5.5. Crystals appeared after few days in 20% PEG3350, 0.1 M sodium acetate pH 4 and 0.2 M $ZnCl_2$. Crystals were tested at the European Synchrotron Radiation Facility (ESRF) ID23-1 beamline after cryo-cooling in the crystallization liquor supplemented with 12.5% propylene glycol.

The $TssM_{26Ct}$–TssJ complex was screened for crystallization using the PEGs and PACT1 kits. Hits were observed in PACT1. All contained Zn^{2+}: 0.01 M zinc chloride, 0.1 M sodium acetate pH 5, 20% (w/v) PEG 6000; or 0.01 M zinc chloride, 0.1 M MES pH 6, 20% (w/v) PEG 6000. Crystal optimization was performed by using PEG6000 in the 10–20% range in 0.1 M sodium acetate/MES pH 4.75–6, and $ZnCl_2$ at 0, 0.01, 0.05 and 0.2 M. No crystals were obtained in conditions without $ZnCl_2$ or containing 0.2 M $ZnCl_2$. By contrast, well-shaped crystals appeared in 50 mM $ZnCl_2$, 15% PEG6000 and 0.1 sodium acetate pH 4.75. Crystals were cryo-cooled with polypropylene glycol 12.5% but diffracted to only ~4.0 Å at the Soleil Proxima 2 beamline (Saint Aubin, France). Further crystals were obtained in LIMBRO plates. Large crystals were obtained by mixing 6 µl of protein and 2 µl of well solution in 50 mM $ZnCl_2$, 15% PEG6000, 94 mM sodium acetate pH 4.75 and 6 mM MES pH 6. Crystals were dipped in polypropylene glycol for ~20 s and exposed at the ESRF ID23-1 beamline.

Data collection was performed at 100 K at the Soleil Proxima 1 beamline (Saint Aubin, France) for $TssM_{32Ct}$–nb25 and at the ID23-1 beamline (ESRF synchrotron, Grenoble, France) for $TssM_{26Ct}$ alone and for the $TssM_{26Ct}$–TssJ complex. Data were processed by the XDS[60] package and scaled with XSCALE (Extended Data Table 1).

The structure of the $TssM_{32Ct}$–nb25 complex was determined by molecular replacement with Molrep[61] using the previously determined structure of nb25 (Protein Data Bank accession number 4QGY)[32]. After refining the positions of the two nb25 molecules in the asymmetric unit by rigid body refinement with AutoBuster[62], an electron density map was calculated at 1.92-Å resolution. Features such as α-helices were easily identified, making it possible to trace manually the model of $TssM_{32Ct}$ using COOT[63], alternated with cycles of refinement with AutoBuster[62], with non-crystallographic symmetry restraints, and translation, rotation and screw-rotation (TLS) group refinement[64], features used in all refinement procedures described below. The final structure at 1.92-Å resolution had R_{work}/R_{free} values of 18.4/21.0%, 96.3% of the residues in the preferred area of the Ramachandran plot and no outliers (Extended Data Table 1).

The structure of $TssM_{26Ct}$ alone was solved by molecular replacement with Molrep[61] using the refined model of $TssM_{32Ct}$ from the $TssM_{32Ct}$–nb25 complex. The initial structure model was improved through iterative refinement with AutoBuster[62] and manual refitting with COOT[63]. The final structure at 1.51-Å resolution had R_{work}/R_{free} values of 19.2/20.2%, 97.4% of the residues in the preferred area of the Ramachandran plot and no outliers (Extended Data Table 1).

The structure of the $TssM_{26Ct}$–TssJ complex was solved by molecular replacement with Molrep[61] using the refined structure of $TssM_{26ct}$ and the previously determined TssJ structure (Protein Data Bank 3RX9)[25] in which all the other conformations were removed. A first round of rigid body refinement and four cycles of Phenix[65] cartesian-simulated annealing were performed. The resulting model was improved through iterative refinement with AutoBuster[62] and manual refitting with COOT[63]. The final structure at 2.24-Å resolution had R_{work}/R_{free} values of 20.0/22.3%, 96.9% of the residues in the preferred area of the Ramachandran plot and four outlier residues in very poorly defined loops (Extended Data Table 1). The $TssM_{32Ct}$–nb25, $TssM_{26Ct}$ and $TssM_{26Ct}$–TssJ structures form similar homodimers in the asymmetric unit. However, as reported by PISA[66], and the known topologies of TssM and TssJ[23,24], these dimers are not biologically relevant. Molecular contacts were analysed by the PISA server[33] and figures were prepared with Chimera[52] and Pymol[67].

The crystal structures of the $TssM_{32Ct}$–nb25 complex, and of the $TssM_{26Ct}$ fragment and $TssM_{26Ct}$–TssJ complexes, have been deposited in the Protein Data Bank under accession numbers 4Y7M, 4Y7L and 4Y7O respectively.

Docking $TssM_{26ct}$–TssJ structure and $TssL_{cyto}$. The crystal structures of the $TssM_{26ct-TssJ}$ complex and of the TssL cytoplasmic domain (Protein Data Bank 3U66)[28] were docked automatically using Chimera[52] after map segmentation.

Refinement of docked $TssM_{26Ct}$-J pentamer in the EM density map. The atomic model of the docked $TssM_{26Ct}$-J structure was refined in the EM density with RSRef[68]. First, missing side-chain and polar hydrogen atoms were added with Modeller[69]. The structure was minimized using 2,000 steps of least-squares conjugate gradient refinement in the presence of distance restraints for hydrogen bonds and backbone dihedral angle restraints to maintain secondary structures. The minimization was performed with the real-space objective function calculated by RSRef in CNS[70]. The C_5 symmetry was enforced by strict non-crystallographic symmetry restraints. The total energy included internal parameters (bond length, bond angle, improper and dihedral angles) and non-bonded interactions with full Van der Waals and electrostatic potentials using a 7.5 Å cutoff. The final correlation coefficient between the EM reconstruction and the refined $TssM_{26Ct}$-J atomic model was 0.929 (as calculated by RSRef), whereas it was 0.706 before minimization.

Modelling of $TssM_{26Ct}$-J decamer. The atomic position of a $TssM_{26Ct}$-J protomer from the outer ring of the pentamer served as the starting structure to generate a $TssM_{26Ct}$-J decamer model with cyclic ten-fold symmetry using CNS[70]. The symmetry was enforced by strict non-crystallographic symmetry restraints (rotations of 36° around the symmetry axis). First, 5,000 steps of rigid body minimization were performed including only inter-protomer energetic contributions (full Van der Waals and electrostatic potentials). After a short all-atom minimization (300 steps), 1.5 ps of molecular dynamics simulation at 1,000 K was performed, followed by 300 steps of minimization and 10 ps of molecular dynamics simulation at 200 K. Minimizations and molecular dynamics simulations were realized with both intra-protomer and inter-protomer energetic contributions activated, and the backbone conformation of the protomer was restrained with harmonic constraints.

Substituted cysteine accessibility method. Cysteine accessibility experiments were performed on whole cells, mainly as described[71,72] with modifications. A 20-ml culture of wild-type or Δ*tssBC* strains producing a periplasmic cysteine-less TssM (Cys727-to-Ser) or derivatives bearing cysteine substitutions were induced for *tssM* gene expression with 0.05 µg ml^{-1} anhydrotetracyclin (AHT) for 1 h. Cells were harvested and resuspended in buffer A (100 mM Hepes (pH 7.5), 150 mM NaCl, 25 mM $MgCl_2$) to a final $A_{600\ nm}$ of 12 in 500 µl of buffer A. Bovine serum albumin (BSA)-coupled maleimide (Sigma-Aldrich) was added to a final concentration of 100 µM (from a 20 mM stock freshly dissolved in DMSO) and the cells were incubated for 30 min at 25 °C. β-Mercaptoethanol (20 mM final concentration) was added to quench the biotinylation reaction, then cells were washed twice in buffer A and resuspended in buffer A containing *N*-ethyl maleimide (final concentration 5 mM) to block all free sulfhydryl residues. After incubation for 20 min at 25 °C, cells were disrupted by sonication. Membranes recovered by ultracentrifugation at 100,000*g* for 40 min were resuspended in Laemmli buffer before SDS–PAGE analysis and immunodetection with anti-Flag antibodies (to detect the TssM proteins). Controls were performed by labelling total membranes from the same samples instead of whole cells. The assay was performed in triplicate, from three independent cultures, and a representative experiment is shown.

SDS–PAGE, protein transfer, immunostaining and antibodies. SDS–PAGE was performed on Bio-Rad Mini-PROTEAN systems using standard protocols. For immunostaining, proteins were transferred onto 0.2-µm nitrocellulose membranes (Amersham Protran). Immunoblots were probed with primary antibodies and goat secondary antibodies coupled to alkaline phosphatase, and developed in alkaline buffer in presence of 5-bromo-4-chloro-3-indolylphosphate and nitro-blue tetrazolium. The anti-TolB was from our laboratory collection, whereas the anti-HA (3F10 clone, Roche), anti-Flag (M2 clone, Sigma Aldrich), anti-StrepII (Sigma Aldrich), anti-5his (Sigma Aldrich) monoclonal antibodies and

alkaline-phosphatase-conjugated goat anti-rabbit or mouse secondary antibodies (Millipore) were purchased as indicated.

40. Brunet, Y. R., Bernard, C. S., Gavioli, M., Lloubès, R. & Cascales, E. An epigenetic switch involving overlapping fur and DNA methylation optimizes expression of a type VI secretion gene cluster. *PLoS Genet.* **7,** e1002205 (2011).
41. Datsenko, K. A. & Wanner, B. L. One-step inactivation of chromosomal genes in *Escherichia coli* K-12 using PCR products. *Proc. Natl Acad. Sci. USA* **97,** 6640–6645 (2000).
42. Chaveroche, M. K., Ghigo, J. M. & d'Enfert, C. A rapid method for efficient gene replacement in the filamentous fungus *Aspergillus nidulans*. *Nucleic Acids Res.* **28,** e97 (2000).
43. van den Ent, F. & Löwe, J. RF cloning: a restriction-free method for inserting target genes into plasmids. *J. Biochem. Biophys. Methods* **67,** 67–74 (2006).
44. Gueguen, E. & Cascales, E. Promoter swapping unveils the role of the *Citrobacter rodentium* CTS1 type VI secretion system in interbacterial competition. *Appl. Environ. Microbiol.* **79,** 32–38 (2013).
45. Zaslaver, A. *et al.* A comprehensive library of fluorescent transcriptional reporters for *Escherichia coli*. *Nature Methods* **3,** 623–628 (2006).
46. Zoued, A. *et al.* TssK is a trimeric cytoplasmic protein interacting with components of both phage-like and membrane anchoring complexes of the type VI secretion system. *J. Biol. Chem.* **288,** 27031–27041 (2013).
47. Tang, G. *et al.* EMAN2: an extensible image processing suite for electron microscopy. *J. Struct. Biol.* **157,** 38–46 (2007).
48. Scheres, S. H. RELION: implementation of a Bayesian approach to cryo-EM structure determination. *J. Struct. Biol.* **180,** 519–530 (2012).
49. Scheres, S. H. Semi-automated selection of cryo-EM particles in RELION-1.3. *J. Struct. Biol.* **189,** 114–122 (2015).
50. Chen, S. *et al.* High-resolution noise substitution to measure overfitting and validate resolution in 3D structure determination by single particle electron cryomicroscopy. *Ultramicroscopy* **135,** 24–35 (2013).
51. Kucukelbir, A., Sigworth, F. J. & Tagare, H. D. Quantifying the local resolution of cryo-EM density maps. *Nature Methods* **11,** 63–65 (2014).
52. Pettersen, E. F. *et al.* UCSF Chimera – a visualization system for exploratory research and analysis. *J. Comput. Chem.* **25,** 1605–1612 (2004).
53. Konarev, P. V., Volkov, V. V., Sokolova, A. V., Koch, M. H. & Svergun, D. I. PRIMUS: a Windows PC-based system for small-angle scattering data analysis. *J. Appl. Crystallogr.* **36,** 1277–1282 (2003).
54. Konarev, P. V., Petoukhov, M. V., Volkov, V. V. & Svergun, D. I. ATSAS 2.1, a program package for small-angle scattering data analysis. *J. Appl. Crystallogr.* **39,** 277–286 (2006).
55. Guinier, A. La diffraction des rayons X aux très petits angles; application à l'étude de phénomènes ultramicroscopiques. *Ann. Phys. (Paris)* **12,** 161–237 (1939).
56. Svergun, D. I. Determination of the regularization parameter in indirect-transform methods using perceptual criteria. *J. Appl. Crystallogr.* **25,** 495–503 (1992).
57. Franke, D. & Svergun, D. I. DAMMIF, a program for rapid *ab-initio* shape determination in small-angle scattering. *J. Appl. Crystallogr.* **42,** 342–346 (2009).
58. Volkov, V. V. & Svergun, D. I. Uniqueness of *ab initio* shape determination in small-angle scattering. *J. Appl. Crystallogr.* **36,** 860–864 (2003).
59. Kozin, M. B. & Svergun, D. I. Automated matching of high- and low-resolution structural models. *J. Appl. Crystallogr.* **34,** 33–41 (2001).
60. Kabsch, W. XDS. *Acta Crystallogr. D* **66,** 125–132 (2010).
61. Vagin, A. & Teplyakov, A. Molecular replacement with MOLREP. *Acta Crystallogr. D* **66,** 22–25 (2010).
62. Blanc, E. *et al.* Refinement of severely incomplete structures with maximum likelihood in BUSTER-TNT. *Acta Crystallogr. D* **60,** 2210–2221 (2004).
63. Emsley, P., Lohkamp, B., Scott, W. G. & Cowtan, K. Features and development of Coot. *Acta Crystallogr. D* **66,** 486–501 (2010).
64. Winn, M. D., Murshudov, G. N. & Papiz, M. Z. Macromolecular TLS refinement in REFMAC at moderate resolutions. *Methods Enzymol.* **374,** 300–321 (2003).
65. Adams, P. D. *et al.* PHENIX: a comprehensive Python-based system for macromolecular structure solution. *Acta Crystallogr. D* **66,** 213–221 (2010).
66. Krissinel, E. & Henrick, K. Inference of macromolecular assemblies from crystalline state. *J. Mol. Biol.* **372,** 774–797 (2007).
67. The PyMOL Molecular Graphics System. v.1.5.0.4 (Schrödinger, LLC, 2014).
68. Chapman, M. S., Trzynka, A. & Chapman, B. K. Atomic modeling of cryo-electron microscopy reconstructions – joint refinement of model and imaging parameters. *J. Struct. Biol.* **182,** 10–21 (2013).
69. Sali, A. & Blundell, T. L. Comparative protein modelling by satisfaction of spatial restraints. *J. Mol. Biol.* **234,** 779–815 (1993).
70. Brunger, A. T. Version 1.2 of the Crystallography and NMR system. *Nature Protocols* **2,** 2728–2733 (2007).
71. Bogdanov, M., Zhang, W., Xie, J. & Dowhan, W. Transmembrane protein topology mapping by the substituted cysteine accessibility method (SCAM™): application to lipid-specific membrane protein topogenesis. *Methods* **36,** 148–171 (2005).
72. Goemaere, E. L., Devert, A., Lloubès, R. & Cascales, E. Movements of the TolR C-terminal domain depend on TolQR ionizable key residues and regulate activity of the Tol complex. *J. Biol. Chem.* **282,** 17749–17757 (2007).
73. Du, D. *et al.* Structure of the AcrAB–TolC multidrug efflux pump. *Nature* **509,** 512–515 (2014).
74. Hodgkinson, J. L. *et al.* Three-dimensional reconstruction of the *Shigella* T3SS transmembrane regions reveals 12-fold symmetry and novel features throughout. *Nature Struct. Mol. Biol.* **16,** 477–485 (2009).
75. Low, H. H. *et al.* Structure of a type IV secretion system. *Nature* **508,** 550–553 (2014).

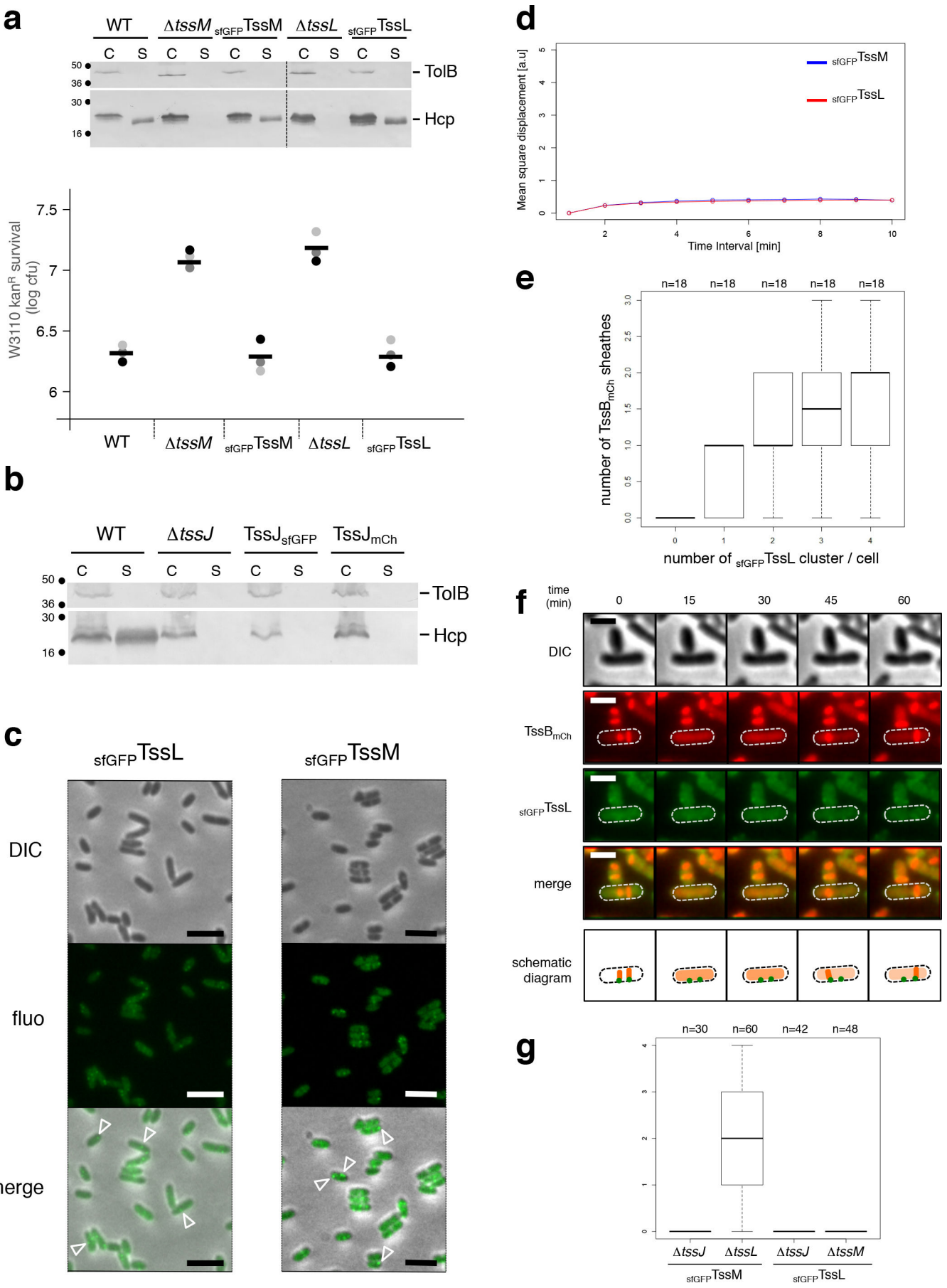

Extended Data Figure 1 | Functional and dynamic properties of fluorescently labelled Tss proteins. **a**, GFP–TssM and GFP–TssL fusion proteins are functional. Top: Hcp release assay. Hcp release was assessed by separating whole cells (C) and supernatant (S) fractions from the indicated strains. A total of 1×10^9 cells and the TCA-precipitated material from the supernatant of 2×10^9 cells were analysed by western blot using anti-Flag monoclonal antibody (lower panel) and anti-TolB polyclonal antibodies as a lysis control (upper panel). The molecular mass markers (in kilodaltons) are indicated on the left. Bottom: anti-bacterial assay. The anti-bacterial activity was assessed by mixing kanamycin-resistant prey *E. coli* K-12 cells with the indicated attacker cells for 16 h at 37 °C in SIM. The number of recovered *E. coli* prey cells is indicated in the graph (as log of colony-forming units (c.f.u.)). The circles indicate values from three independent assays, and the average is indicated by the bar. **b**, TssJ–sfGFP and TssJ–mCh fusion proteins are non-functional. Hcp release was assessed by separating whole cells (C) and supernatant (S) fractions from the indicated strains. A total of 1×10^9 cells and the TCA-precipitated material from the supernatant of 2×10^9 cells were analysed by western blot using anti-Flag monoclonal antibody (lower panel) and anti-TolB polyclonal antibodies as a lysis control (upper panel). The molecular mass markers (in kilodaltons) are indicated on the left. **c**, sfGFP–TssM and sfGFP–TssL cluster in foci. Large fields of fluorescence microscopy recordings showing localization of the sfGFP–TssL (left) and sfGFP–TssM (right) fusion proteins. The positions of selected foci are indicated by arrowheads. Scale bars, 5 μm. **d**, sfGFP–TssM and sfGFP–TssL foci are stable and static. Mean square displacement (in arbitrary units (a.u.)) of sfGFP–TssM (blue line) and sfGFP–TssL (red line) clusters were measured by sub-pixel tracking of fluorescent foci and plotted over time (in minutes). **e**, The TssBC sheath tubular structures assemble on TssJLM membrane complexes. Statistical analyses reporting the average number of sheath per cell compared with the number of membrane complexes per cell, highlighting the observation that the number of membrane complexes is at least equal to the number of sheathes. Lower and upper boundaries of the boxes correspond to the 25% and 75% percentiles respectively. Black bold horizontal bar, median values for each strain; whiskers, 10% and 90% percentiles; *n* indicates the number of cells studied per strain. **f**, Long-term fluorescence microscopy recordings. Time-lapse fluorescence microscopy recordings showing localization and dynamics of the sfGFP–TssL and TssB–mCherry fusion proteins. Individual images were taken every 15 min. Assembly/contraction of the sheath and TssL localization events are schematized in the lowest panel. Scale bars, 1 μm. **g**, Statistical analysis of sfGFP–TssM and sfGFP–TssL localization in various *tss* backgrounds. Shown are box-and-whisker plots of the measured number of sfGFP–TssM and sfGFP–TssL foci per cell for each indicated strain with the lower and upper boundaries of the boxes corresponding to the 25% and 75% percentiles respectively (horizontal bar, the median values for each strain; whiskers, the 10% and 90% percentiles); *n* indicates the number of cells studied per strain.

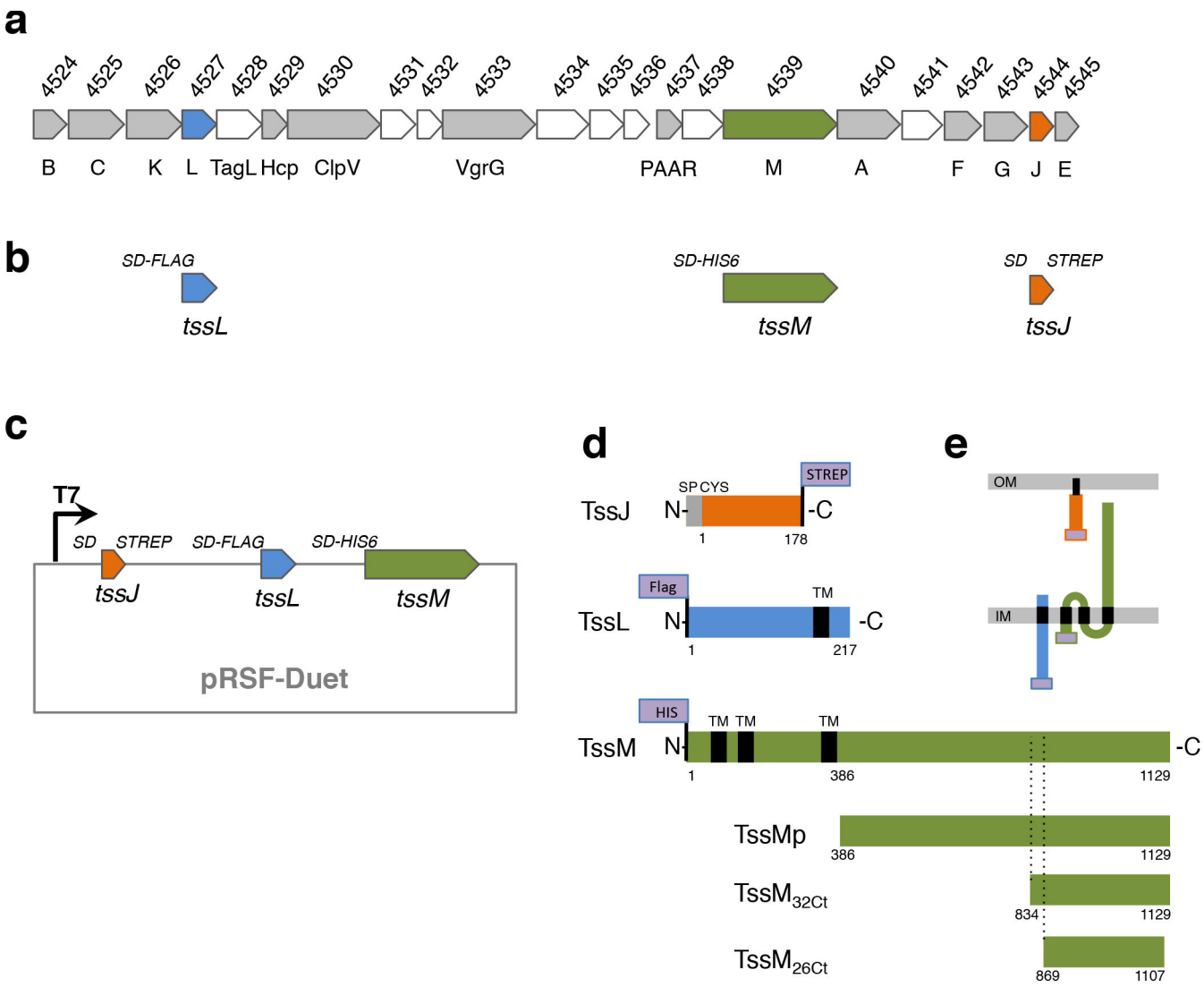

Extended Data Figure 2 | Expression and purification of the T6SS membrane core complex. **a**–**e**, T6SS operon genomic organization and constructs used for *in vitro* analyses. **a**, Schematic representation of the T6SS *sci-1* gene cluster from entero aggregative *E. coli*. The numbers on top refer to the gene locus tag (EC042_XXXX). Genes encoding core components (identified by their names on bottom, for example, 'B' refers to the *tssB* gene) are coloured grey. Genes of unknown function are coloured white. The three genes used to reconstitute the core membrane complex are coloured orange (*tssJ*), blue (*tssL*) and green (*tssM*). **b**, Schematic representation of the engineered constructs: the *tssJ*, *tssL* and *tssM* genes were amplified with an additional Shine Dalgarno (SD) sequence and 3′ StrepII, 5′ Flag and 5′ 6×His tags respectively. These three fragments were cloned into the pRSF-Duet vector (**c**). This construct allows the production of the C-terminally StrepII-tagged TssJ outer membrane (OM) lipoprotein and N-terminally Flag-tagged TssL and 6×His-tagged TssM inner-membrane (IM) proteins (**d**, **e**). The proteins are schematized and their boundaries and principal characteristics (TM, transmembrane segments; SP, signal peptide; CYS, acylated cysteine) are indicated (**d**) and their topologies are shown (**e**). The additional TssM constructs (TssMp, $TssM_{32Ct}$ and $TssM_{26Ct}$) used for SAXS or X-ray analyses are shown at the bottom. **f**–**h**, Purification and biochemical characterization of the T6SS membrane core complex. **f**, Analytical size-exclusion chromatography analysis of the purified TssJLM complex (continuous line) on a Superose 6 column, calibrated with 75-, 158-, 440- and 660-kDa molecular mass markers (dotted lines). The molecular mass of each marker (in kilodaltons) is indicated on the top of the corresponding peak. An arrow indicates the position of the peak fraction corresponding to the TssJLM complex. **g**, SDS–PAGE of the purified TssJLM complex analysed by Coomassie staining (CB) or immunoblotting using anti-His (α-His), -Flag (α-Flag) and -StrepII (α-STREP) antibodies. **h**, Left: cysteine labelling of the purified TssJLM complex in reducing and denaturing conditions as described in Methods. The total number of cysteine residues was nine for TssM, five for TssL and none for TssJ (the N-terminal cysteine is acylated). Right: the relative amount of TssL compared with TssM (densitometry relative to the number of free cysteine residues, fixed at 1 for TssM).

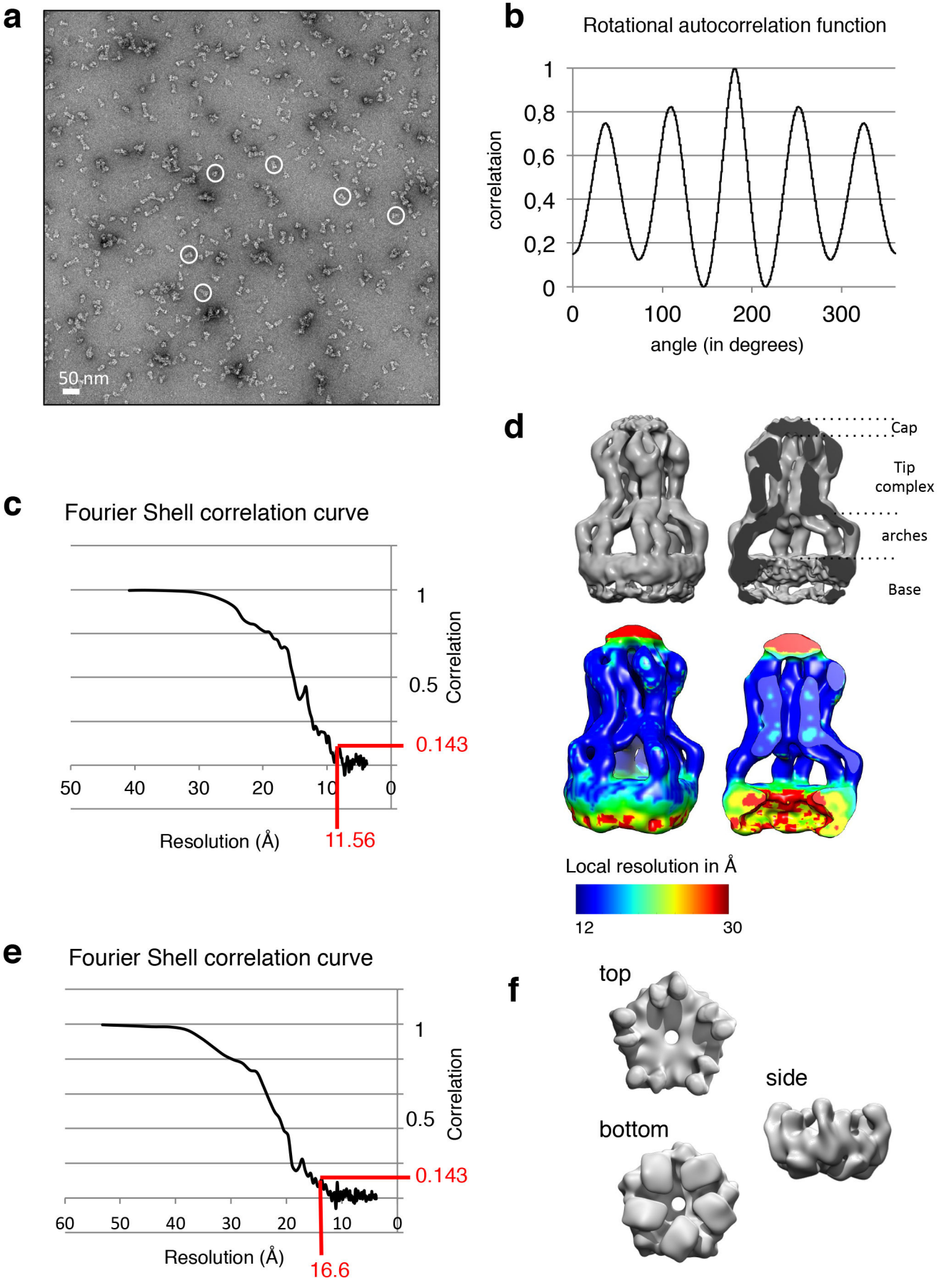

Extended Data Figure 3 | Architecture of the T6SS membrane core complex. **a**, Negative-stain EM of the EAEC TssJLM complex. Representative micrograph of the data set used for image processing. Isolated TssJLM complexes were clearly visible (white circles). **b**, Plot of the rotational autocorrelation function for a representative class average of an end-view. **c**, FSC curve of the TssJLM reconstruction. The 'gold standard' FSC curve was calculated in Relion using the masked reconstruction of the TssJLM complex. The resolution at 0.143 correlation was 11.56 Å. **d**, Top: side and corresponding cut-away views of the 3D reconstruction for the whole TssJLM complex. Bottom: local resolution as calculated by Resmap. The TssJLM volume (left reconstruction, side view; right reconstruction, cut-away view) is coloured according to the local resolution from high resolution (~12 Å) in blue to low resolution (>30 Å) in red. **e**, FSC curve of the TssJLM base. The 'gold standard' FSC curve was calculated in Relion using the unmasked reconstruction of the TssJLM base. The resolution at 0.143 correlation was 16.6 Å. **f**, Top, side and bottom views of the 3D reconstruction after specific refinement of the base.

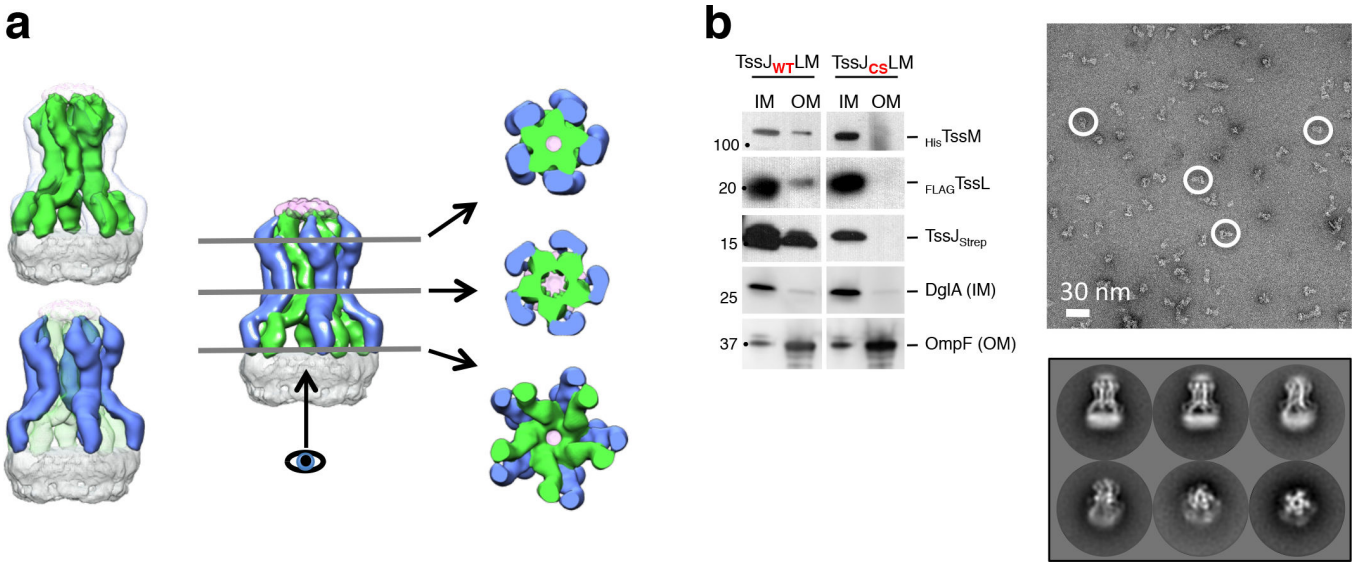

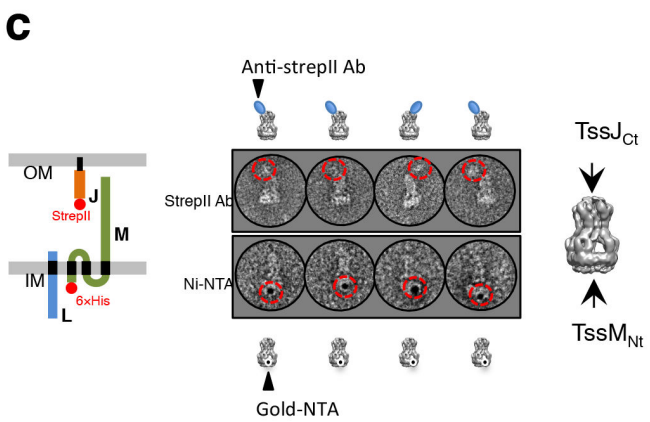

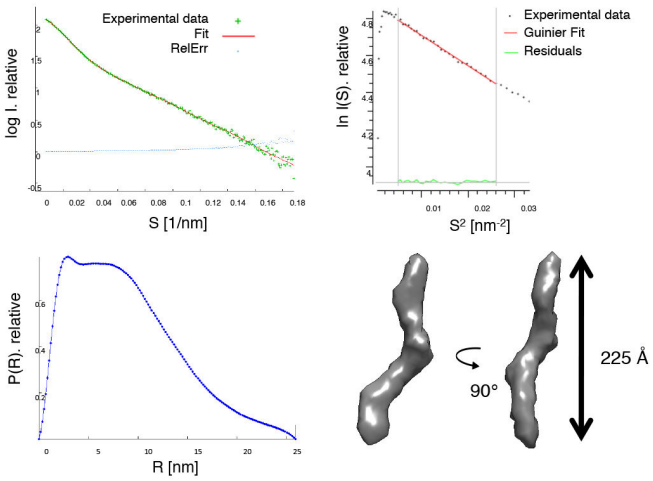

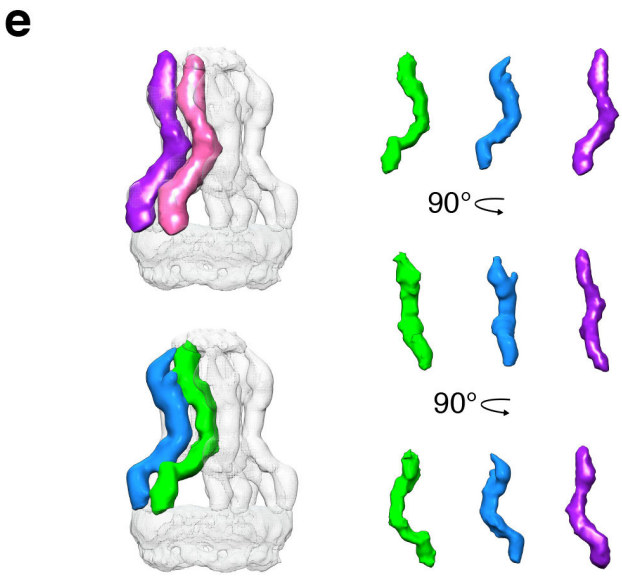

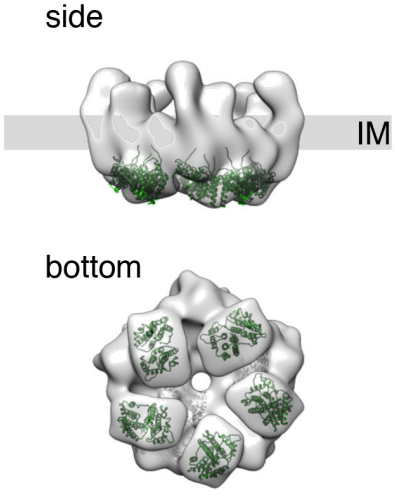

Extended Data Figure 4 | Structural analysis and segmentation. **a**, Segmentation of the TssJLM reconstruction. Left: above the base, ten equivalent densities could be defined by segmentation. They are arranged in two concentric rings. The internal ring is represented in green in the top panel and the external ring is represented in blue in the bottom panel. Right: cut-out views of the complex showing the arrangement of the two concentric rings at different levels (grey lines) along the periplasmic portion of the TssJLM complex. The cut-out views are seen from the bottom of the complex. **b**, Requirement of TssJ lipidation for complex assembly and insertion into the outer membrane. Left: membrane fractionation by differential solubilization followed by immunoblot analysis. Total membrane extracts from cells producing the wild-type TssJLM complex or the TssJLM complex with an unacylated variant of TssJ (Cys1-to-Ser substitution, CS) were solubilized by lauroyl sarcosine to separate inner membranes and outer membranes. $_{His}$TssM, $_{Flag}$TssL and TssJ$_{Strep}$ (indicated on the right) were revealed by anti-His, anti-Flag and anti-StrepII antibodies respectively. Controls included immuno-detection of the inner membrane DglA diacylglycrol lipase and the outer membrane OmpF porin. Wild-type TssJLM complex co-fractionates with both the inner and outer membrane fractions whereas the Cys1-to-Ser substitution mutated complex co-fractionates only with the inner-membrane fraction. Top right: negative-stain EM of the mutated TssJ$_{CS}$LM complex. Representative micrograph of the data set used for image processing. Isolated TssJ$_{CS}$LM complexes were clearly visible (white circles). Bottom right: gallery of representative class averages generated after reference-free 2D classification in Relion. End to side views are shown from top left to bottom right. **c**, Orientation of the TssJLM complex in the cell envelope. Left: schematic representation of the TssJ (J, orange), TssL (L, blue) and TssM (M, green) proteins. Their localization, main characteristics (lipidation or transmembrane segments shown in black) and the location of the 6×His and StrepII tags (red balls) are indicated. The strepII and 6×His tags were introduced at the C terminus and N terminus of TssJ and TssM respectively. Middle: immune and Nanogold labelling coupled to EM. Anti-StrepII or Nanogold-NTA were incubated with the TssJLM complex and visualized by negative-stain EM. A gallery of representative views is presented (top row, StrepII labelling; bottom row, Ni-NTA labelling). StrepII antibodies (a schematic diagram with StrepII antibodies depicted as blue circles is shown on top) and Nanogold-NTA are highlighted in red circles. Right: the positions of the StrepII antibody (targeting TssJ C terminus) and of the Ni-NTA gold particle (targeting TssM N terminus) are indicated on the TssJLM reconstruction. **d**, SAXS data and low-resolution structure of the TssM$_p$–TssJ complex. Top left: experimental scattering data (green crosses) and the fitting curve (continuous red line) calculated from an *ab initio* model of the TssM$_p$–TssJ complex. Top right: Guinier plot (dots) with the linear fit (continuous line). Bottom left: distance distribution function of the TssM$_p$–TssJ complex. Bottom right: SAXS envelope (grey surface) of the 'best representative' model of the TssM$_p$–TssJ complex. Each view is rotated by 90° around the *y*-axis. **e**, Location of the TssMp–TssJ complex SAXS envelope in the 3D reconstruction of TssJLM complex. Left: the volume of the TssM$_p$–TssJ complex determined by SAXS was docked into the EM 3D reconstruction of the TssJLM complex (top). Two optimal docking positions were found, both with 82% correlation with the EM map (coloured magenta and pink). The corresponding volumes in the EM map were extracted (bottom). They correspond to the same volume displayed in Extended Data Fig. 4a. Right: direct comparison of the SAXS (magenta) and EM (blue and green) volumes corresponding to the TssM$_p$–TssJ complex. The volumes are equivalent in size and shape. **f**, TssL cytoplasmic domain docking into the TssJLM complex base. Fitting of the TssL cytoplasmic domain (TssL$_{cyto}$)[28] dimer in green ribbons in the hooks found in the base. Top and bottom: side and bottom views, respectively.

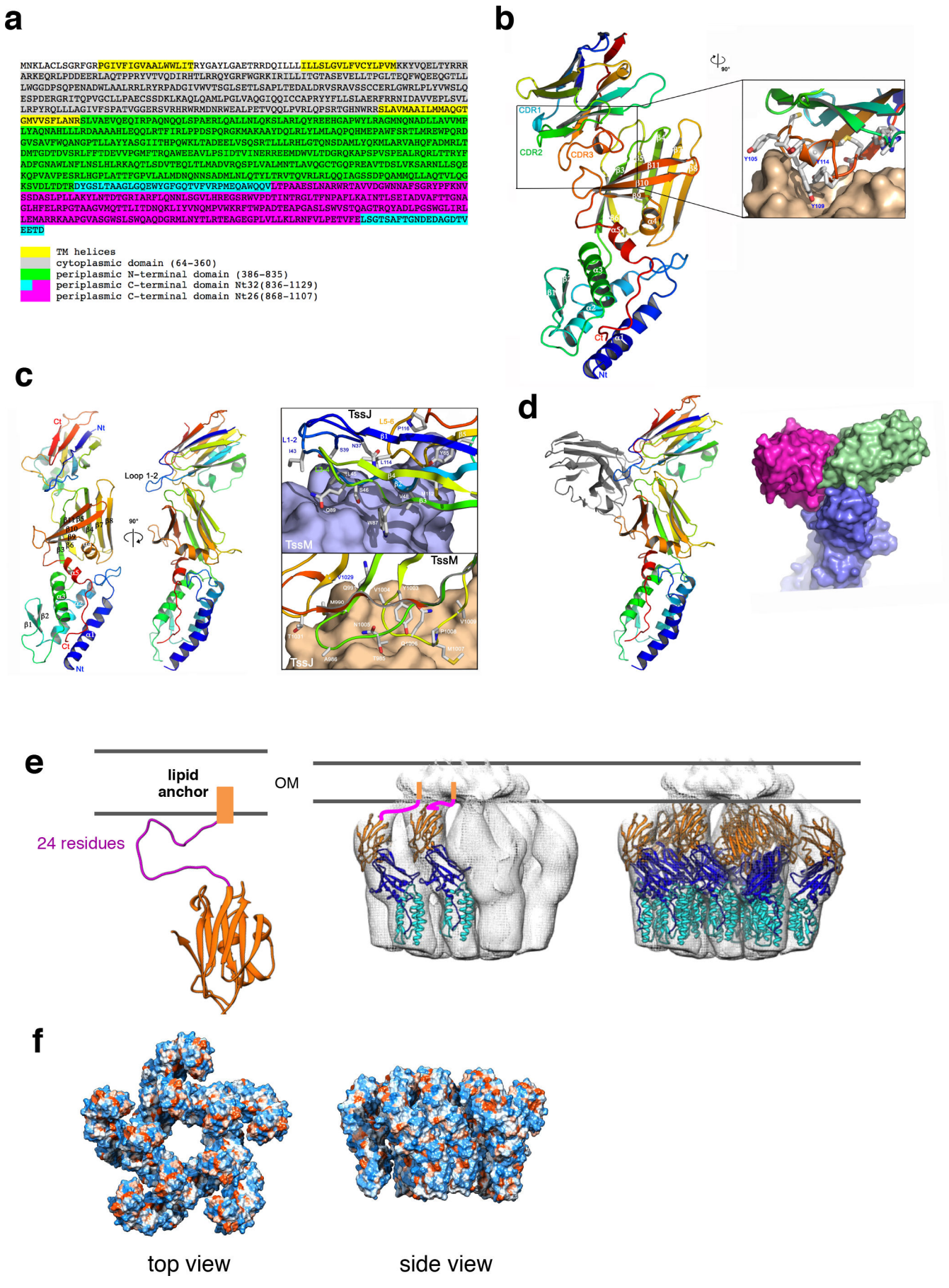

Extended Data Figure 5 | Crystal structure of the TssJ–TssM C-terminal domain complex. **a**, Amino-acid sequence of TssM. The different domains as well as the fragments used in this study are indicated (yellow, transmembrane helix; grey, cytoplasmic domain; green, blue and purple, periplasmic domain; blue and purple, C-terminal domain corresponding to the $TssM_{32Ct}$ fragment; purple, C-terminal domain corresponding to the $TssM_{26Ct}$ fragment). **b**, Crystal structure of the $TssM_{32Ct}$–nb25 complex. The two proteins are represented as rainbow-coloured ribbons. The complementary determining regions (CDRs 1–3, coloured blue, green and red, respectively) of nb25 are indicated. The inset highlights the $TssM_{32Ct}$–nb25 interface: the $TssM_{32Ct}$ surface is coloured beige whereas nb25 is represented as rainbow-coloured ribbons; the side chains of the amino acids in contact with $TssM_{32Ct}$ are indicated. The nb25 nanobody binds the TssM C-terminal domain, and covers a surface area of 580 $Å^2$ by inserting its protruding CDR3 between $TssM_{32Ct}$ loops L5–6 and L9–10. The contacts between the two proteins are listed in Extended Data Table 2a. **c**, Crystal structure of the $TssM_{26Ct}$–TssJ complex. Left: the two proteins are represented as ribbons and coloured in rainbow mode. Middle: same view rotated by 90°. The TssJ loop 1–2, previously shown to contact TssM[25], is indicated. Right: $TssM_{26Ct}$–TssJ interface. Top panel: the $TssM_{26Ct}$ surface is coloured violet, whereas TssJ is represented as rainbow-coloured ribbons. The TssJ side-chains of the amino acids in contact with TssM are indicated. The loops are numbered according to the flanking β-strands. Bottom panel: the TssJ surface is coloured beige whereas $TssM_{26Ct}$ is represented as rainbow-coloured ribbons. The TssM side-chains of the amino acids in contact with TssJ are indicated. The contacts between the two proteins are listed in Extended Data Table 2b. **d**, Comparison of the binding sites of nb25 and TssJ on TssM. Left: the structure of the $TssM_{26Ct}$–TssJ complex (rainbow coloured) has been superimposed to the structure of the $TssM_{32Ct}$–nb25 complex (only nb25 is shown in grey for clarity). Right: the same partners as in the left panel in surface representation. $TssM_{26Ct}$ (violet), TssJ (green) and nb25 (pink). **e**, Insertion of the TssJ lipid anchor in the outer membrane. Left: TssJ structure[25] with the N-terminal 24 residues (absent in the crystal structure). This N-terminal extension (in magenta), predicted to be disordered, was modelled in Chimera using Modeller. The first cysteine residue is acylated to allow anchorage to the inner leaflet of the outer membrane (orange rectangle). Right: docking of the $TssM_{26Ct}$–TssJ complex in the EM 3D reconstruction of the TssJLM complex (only the uppermost (tip) part of the TssJLM complex is shown). Left panel: two $TssM_{26Ct}$–TssJ were docked into the inner and outer pillars of the tip complex. Right panel: docking in each pillar of the TssJLM tip complex (C_5 symmetry). **f**, Hydrophobicity of the $TssM_{26Ct}$–TssJ complex. Surface representation of the $TssM_{26Ct}$–TssJ decamer (left, top view; right, side view). The hydrophobicity of the surface residues is displayed (blue to red scale from most hydrophilic to most hydrophobic). No obvious hydrophobic patch is visible at the surface of the complex.

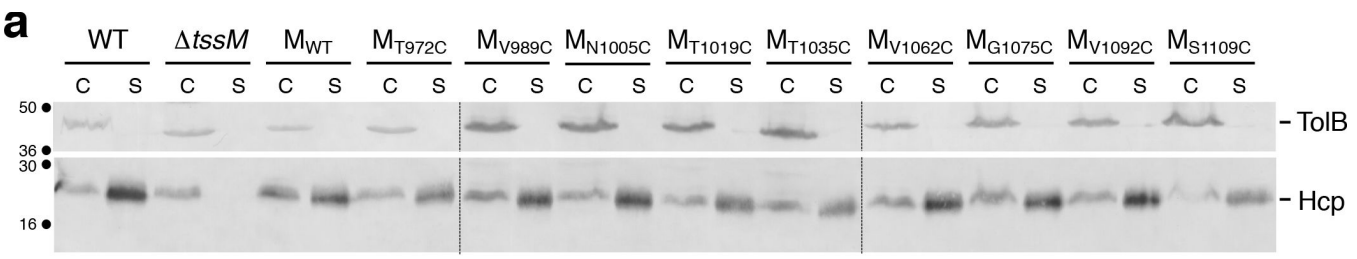

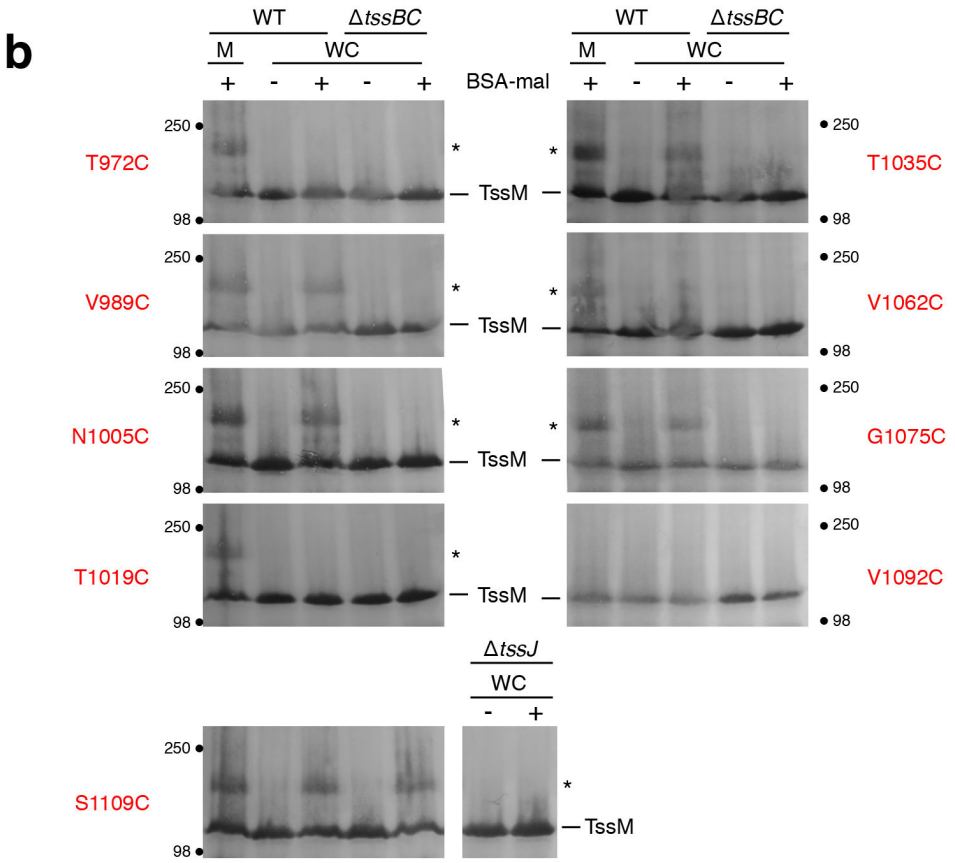

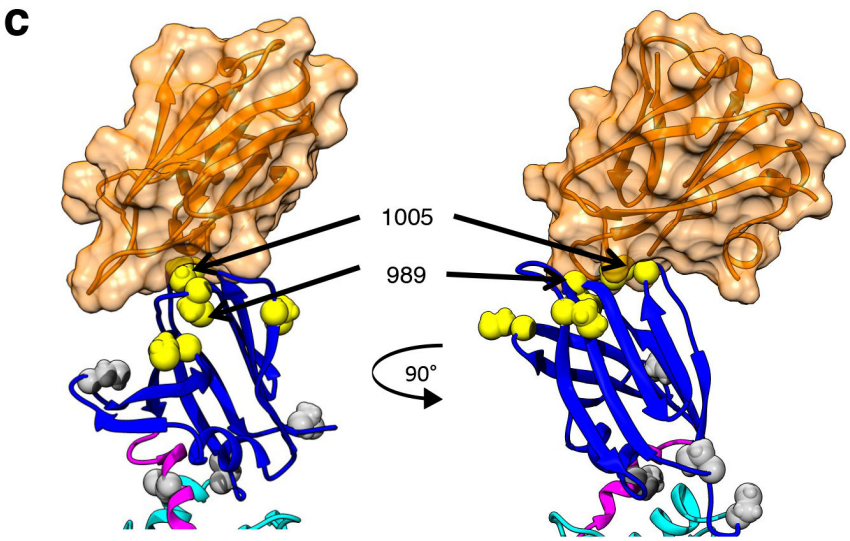

Extended Data Figure 6 | Cell surface accessibility of TssM C-terminal domain. **a**, Functionality of the TssM cysteine variants. Hcp release was assessed by separating whole cells (C) and supernatant (S) fractions from the wild-type (WT) 17-2 strain and its Δ*tssM* derivative producing a wild-type allele of TssM or TssM cysteine substitution derivatives (as indicated). A total of 1×10^9 cells and the TCA-precipitated material from the supernatant of 2×10^9 cells were analysed by western blot using anti-HA monoclonal antibody (lower panel) and anti-TolB polyclonal antibodies as a lysis control (upper panel). The molecular mass markers (in kilodaltons) are indicated on the left. **b**, Cysteine substitution labelling. Accessibility to cysteine residues positioned in TssM domain 4 loops was assessed by treating isolated membranes (M) or whole cells (WC) of the indicated strain (WT, wild-type 17-2; Δ*tssBC*; Δ*tssJ*) producing the indicated TssM cysteine derivative (in red letters) with the cysteine-reactive, membrane-impermeant BSA-maleimide (BSA-mal). Samples corresponding to a total of 5×10^9 cells were analysed by western blot using anti-Flag monoclonal antibody. The position of the TssM protein (~125 kDa) is indicated as well as that of a retarded band corresponding to BSA-maleimide-coupled TssM (~190 kDa; asterisk). The molecular mass markers (in kilodaltons) are indicated. **c**, Close-up of the $TssM_{26Ct}$–TssJ interface. $TssM_{26Ct}$ is represented in blue ribbons. TssJ is represented in orange ribbons and orange transparent surface. TssM residues accessible from the cell exterior when the T6SS is functional are indicated by yellow spheres whereas unaccessible residues are shown by grey spheres. The accessible residues 989 and 1005 are buried at the interface between TssM and TssJ, suggesting that this interface is probably disrupted during T6SS assembly and/or function. Left and right panels are orthogonal views of the same molecule.

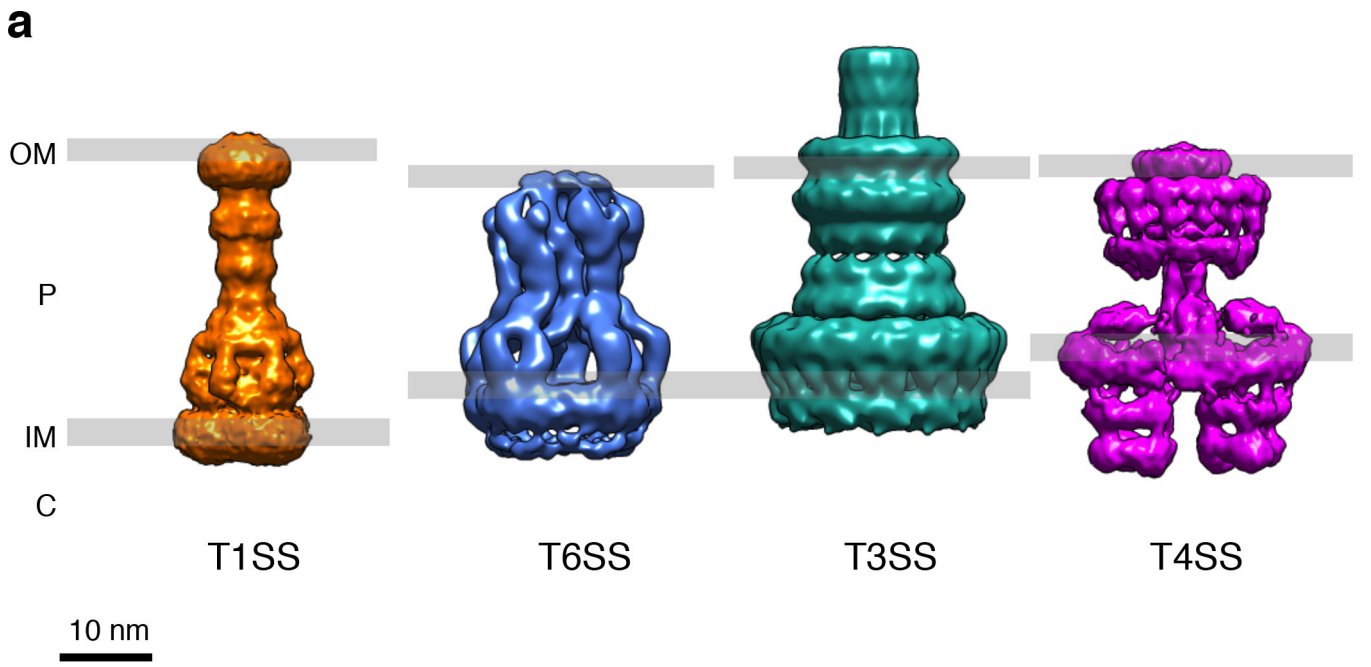

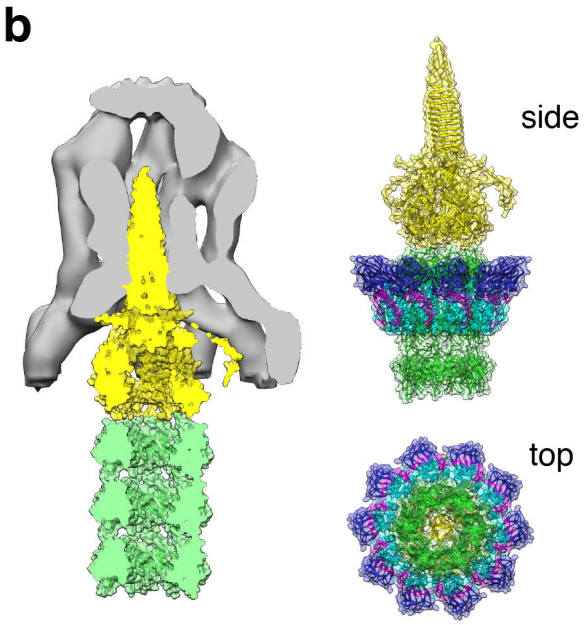

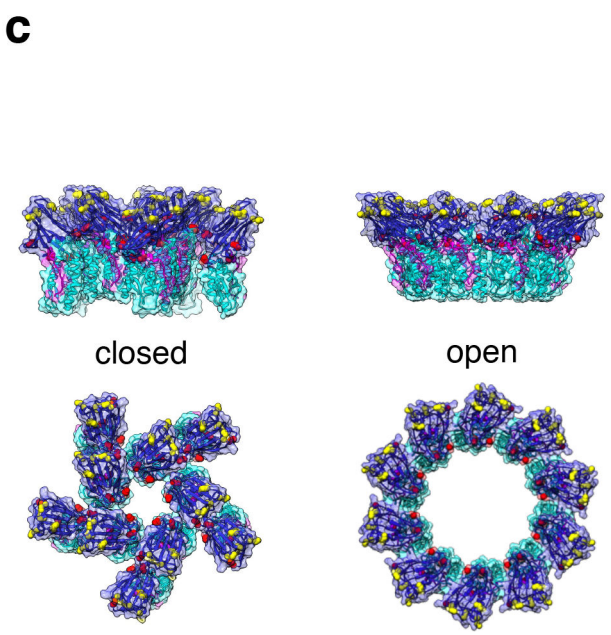

Extended Data Figure 7 | Comparison with other bacterial secretion systems and model for channel opening. **a**, Comparison between the T6SS TssJLM membrane core complex structure and other bacterial secretion systems. From left to right, the *E. coli* AcrAB-TolC multi-drug efflux pump (EMDB accession number emd-5915)[73], the EAEC T6SS membrane core complex (this study, EMDB accession number emd-2927), the *Shigella* T3SS transmembrane complex (EMDB accession number emd-1617)[74] and the *E. coli* R388 T4SS complex (EMDB accession number emd-2567)[75]. The positions on the inner membrane (IM) and outer membrane (OM) are indicated (C, cytoplasm; P, periplasm). Scale bar, 10 nm. **b**, Docking of the Hcp tube/VgrG spike into the TssJLM 3D reconstruction. Left: before sheath contraction. The Hcp tube/VgrG spike (VgrG in yellow and Hcp in green; surface representation) was manually docked in the 3D reconstruction of TssJLM complex (grey surface). The diameter of the channel defined by the closed tip complex is not large enough to allow the passage of the tube/spike, suggesting that large conformational changes probably occur. The cavity at the tip of VgrG could be filled by VgrG-bound PAAR modules or toxin effectors[20]. Right: during sheath contraction. The diameter of the C_{10}-symmetrized $TssM_{26Ct}$ model (represented as ribbons) is compatible with the passage of the Hcp tube/VgrG spike (same colours as in the left panel). **c**, Closed and open forms of the $TssM_{26Ct}$ oligomer. Crystal structure of $TssM_{26Ct}$ represented as ribbons and transparent surface. The $TssM_{26Ct}$ α- and β-domains are coloured cyan and blue, respectively. The C-terminal α5-helix and the extended stretch are coloured pink. Cysteines with extracellular accessibility when the T6SS is active are coloured yellow, while the unlabelled ones are coloured red. Left: docking of the $TssM_{26Ct}$–TssJ crystal structure in the EM 3D reconstruction of the TssJLM tip complex. Top and bottom panels, side and top views, respectively. Right: model of a C_{10}-symmetrized oligomer of the $TssM_{26Ct}$ domain. Top and bottom panels, side and top views, respectively.

Extended Data Table 1 | Data collection and refinement statistics

	$TssM_{32Ct}$-nb25	$TssM_{26Ct}$	$TssM_{26Ct}$-TssJ
Data collection§			
Space group	$P6_4$	$P\ 4_12_12$	$P\ 4_12_12$
Cell dimensions			
a, *b*, *c* (Å)	95.2, 95.2, 172.95	64.0, 64.0, 249.7	85.5, 85.5, 256.4
α, β, γ (°)	90.0, 90.0, 120.0	90.0, 90.0, 90	90.0, 90.0, 90
Resolution (Å)	50.0-1.92(1.97-1.92)*	30.0-1.51(1.6-1.51)*	50.0-2.24(2.38-2.24)*
R_{merge}	0.079 (1.08)	0.067 (0.59)	0.067 (0.73)
$I/\sigma I$	18.0 (2.0)	19.2 (3.0)	21.5 (3.1)
Completeness (%)	100.0 (100.0)	99.9 (89.3)	99.7 (98.4)
Redundancy	11.4 (11.3)	9.9 (9.9)	10 (10)
Refinement			
Resolution (Å)	47.6-1.92(1.97-1.92)*	22.1-1.51 (1.55-1.51)*	49.3-2.24(2.3-2.24)*
No. reflections	67543 (4721)	82127 (5359)	46047 (3015)
R_{work}/ R_{free}	0.184/0.21(0.234/0.25)	0.192/0.202(0.241/27.6)	0.208/0.228(0.224/0.25)
No. atoms			
Protein	5522	3784	5521
Ligand/ion	15	22	4
Water	805	536	379
B-factors			
Protein	42.3	27.4	51.7
Ligand/ion	98.8	55.0	81
Water	49.9	39.5	63.8
R.m.s deviations			
Bond lengths (Å)	0.009	0.010	0.010
Bond angles (°)	1.05	1.03	1.19

§Each data set has been collected on a unique crystal.
*Highest resolution shell is shown in parenthesis.

Extended Data Table 2 | Interactions and accessibility data

Extended Table 2a. Interactions between TssM and nb25

n25/CDR3			$TssM_{26Ct}$				
number	type	atom	number	type	atom	distance (Å)	bond
103	Gly	O	1063	Ala	N	2.89	H
104	Ile	CA	1061	Gly	O	3.08	
105	Tyr	N	1061	Gly	O	2.85	H
107	Thr	OG1	1060	Pro	O	2.67	H
107	Thr	CG2	1061	Gly	CA	3.56	
109	Tyr	CE1	1067	Ser	CB	3.50	
109	Tyr	OH	1080	Tyr	O	3.47	H
109	Tyr	OH	1081	Thr	OG1	2.64	H
110	Ile	CD1	1062	Val	CG2	3.73	
113	Pro	O	984	Gly	CA	3.12	
113	Pro	O	985	Thr	N	3.00	H
114	Tyr	CE1	982	Arg	CD	3.55	
114	Tyr	CZ	982	Arg	NE	3.63	
114	Tyr	OH	1010	Trp	NE1	2.99	H
114	Tyr	O	982	Arg	NE	2.88	H
115	Gly	O	982	Arg	NH2	2.76	H
116	Met	O	1008	Pro	CD	3.32	
117	Asp	OD1	982	Arg	NH2	2.80	H

Extended Table 2c. TssM cysteine accessibility.

Cysteine position	Labelled at rest	Labelled in action	Position	WAS #
972	-	-	helix α3	107 / 107
989	-	++	loop β3- β4	14 / 10
1005	-	++	loop β5- β6	76 / 0
1019	-	-	loop β6- β7	35 / 35
1035	-	+	loop β7- β8	113 / 113
1062	-	-	loop β11- α5	94 / 94
1075	-	++	loop β10- β11	51 / 51
1092	-	-	helix α5	0 / 0
1109	++	++	C-terminus	NA*

Extended Table 2b Interactions between TssM and TssJ.

TssJ

Loop L1,2

Loop L3,4

Loop L5,6

TssM

Loop L3,4

Loop L5,6

TssJ			TssM			dist ance(Å)
37	Asn	Nd2	1005	Asn	O	3.06 H
39	Ser	Cb	985	Thr	Og1	3.80
43	Ile	Cg2	987	Ala	Cb	3.79
45	Leu	Cd1	985	Thr	Cg2	3.63
		Cb	1005	Asn	Nd2	3.56
46	Ser	Og	990	Met	Ca	3.14
		O	1005	Asn	Nd2	3.27 H
		Og	1005	Asn	Nd2	3.19 H
48	Val	Cg2	1004	Val	Cb	3.82
65	Tyr	Ce1	1007	Met	Cg	3.51
		Oh	1007	Met	N	3.30 H
87	Trp	Ch2	990	Met	C	3.56
89	Gln	Oe1	1031	Thr	O	2.87 H
		Ne2	1031	Thr	Og1	2.79 H
112	Met	Ce	1006	Gln	Ne2	3.35
113	Phe	O	1007	Met	N	3.24 H
114	Leu	Cd1	1003	Tyr	OH	3.16
		N	1005	Asn	O	3.33 H
		Cd1	1006	Gln	O	3.40
		O	1007	Met	Cg	3.51
		Cd1	1008	Pro	Cd	3.73
116	Pro	Cd	1007	Met	Cg	3.74

The letter H in right-hand columns indicates that atoms establish a hydrogen bond.
WAS, water-accessible surface of the original amino acids (measured in the unbound TssM/in the TssM–TssJ complex).
*Not visible in the electron density map.

doi:10.1038/nature14667

Supplementary table 1. Strains, plasmids and oligonucleotides used in this study.

Strains

Strains	Description and genotype	Source
E. coli K-12		
DH5α	F-, Δ(*argF-lac*)U169, *phoA*, *supE44*, Δ(lacZ)M15, *relA*, *endA*, *thi*, *hsdR*	New England Biolabs
T7 Iq pLysS	MiniF *lysY lacI*^{q}(Cam^{R}) / *fhuA2 lacZ::T7 gene1 [lon] ompT gal sulA11 R(mcr-73::miniTn10--*Tet^{S}*)2 [dcm] R(zgb-210::Tn10--*Tet^{S}*) endA1 Δ(mcrC-mrr) 114::IS10*	New England Biolabs
BL21(DE3)	*fhuA2 [lon] ompT gal (λ DE3) [dcm] ΔhsdS λ DE3 = λ sBamHIo ΔEcoRI-B int::(lacI::PlacUV5::T7 gene1) i21 Δnin5*	New England Biolabs
Enteroaggregative *E. coli*		
17-2	WT enteroaggregative *Escherichia coli*	Arlette Darfeuille-Michaud
17-2Δ*tssL*	17-2 deleted of the *tssL* gene of the *sci1* T6SS gene cluster	Aschtgen *et al.*, 2010
17-2Δ*tssM*	17-2 deleted of the *tssM* gene of the *sci1* T6SS gene cluster	Aschtgen *et al.*, 2010
17-2 *gfp-tssL*	*gfp-mut2* inserted downstream the start codon of *tssL* in 17-2	This study
17-2 *gfp-tssM*	*gfp-mut2* inserted downstream the start codon of *tssM* in 17-2	This study
17-2 *tssJ-gfp*	*gfp-mut2* inserted upstream the stop codon of *tssJ* in 17-2	This study
17-2 *gfp-tssL tssB-mCherry*	*mCherry* inserted upstream the stop codon of *tssB* in 17-2 *gfp-tssL*	This study

17-2 *gfp-tssM mCherry-tssL*	*mCherry* inserted downstream the start codon of *tssL* in 17-2 *gfp-tssM*	This study
17-2 Δ*tssM gfp-tssL*	*gfp-mut2* inserted downstream the start codon of *tssL* in 17-2Δ*tssM*	This study
17-2 Δ*tssJ gfp-tssL*	*gfp-mut2* inserted downstream the start codon of *tssL* in 17-2Δ*tssJ*	This study
17-2 Δ*tssL gfp-tssM*	*gfp-mut2* inserted downstream the start codon of *tssM* in 17-2Δ*tssL*	This study
17-2 Δ*tssJ gfp-tssM*	*gfp-mut2* inserted downstream the start codon of *tssM* in 17-2Δ*tssJ*	This study

Plasmids

Vectors	Description	Source
Expression vectors		
pUC-Hcp$_{FL}$	*sci1 hcp* gene cloned into pUC12, P*lac*, C-terminal FLAG epitope	Aschtgen *et al.*, 2008
pIBA-TssM	*sci1 tssM* gene cloned into pASK-IBA37(+), P*tet*, N-terminal FLAG epitope	This study
Vectors for TssJLM and protein purification		
pRSF-Duet1	Expression vector, *lacI*, P*T7*, Kan^{R}	Addgene
pRSF-TssJ^{S}-^{F}L-^{H}M	*tssJ*-StrepII, FLAG-*tssLL* and 6×His-*tssM* cloned into pRSF-Duet1	This study
pETG20A	Gateway destination vector, TRX-6×His followed by a TEV cleavage site	Arie Gerlof
pHEN6-nb25	pHEN6 vector encoding the nb25 nanobody	NGuyen *et al.*, 2015
pETG20A-TssJ	*sci1 tssJ* mature form cloned into pETG20A, N-terminal TRX-His-TEV epitope	Felisberto-Rodrigues *et al.*, 2011
pETG20A-TssMp	*sci1 tssM* periplasmic domain (aa 386-1129) cloned into pETG20A, N-terminal TRX-His-TEV epitope	Felisberto-Rodrigues *et al.*, 2011

pETG20A-TssM$_{26Ct}$	*sci1 tssM* C-terminal fragment (aa 869-1107) cloned into pETG20A, N-terminal TRX-His-TEV epitope	This study
Vectors for chromosomal insertions		
pKD4	Kan^R cassette flanked by FRT recombination sites, used for chromosomal deletion	Datsenko and Wanner, 2000
pKD4$_{Nter\text{-}gfp}$	*gfp-mut2* (*sf-gfp*) gene cloned upstream the Kan^R cassette in pKD4, used for chromosomal insertion of *gfp-mut2* (N-terminal GFP)	This study
pKD4$_{Cter\text{-}mCherry}$	*mCherry* gene cloned downstream the Kan^R cassette in pKD4, used for chromosomal insertion of *mCherry* (C-terminal mCherry)	This study
pCP20	Amp^R, Cm^R, FRT recombinase gene	Datsenko and Wanner, 2000

Oligonucleotides

Name	Destination	Sequence (5' → 3')
For strain construction [a]		
5-*tssB-mCherry*	insertion of *mCherry* at the 3' end of *tssB*	CCGGCACTGAGTCAGACGCTGCGTGATGAACTGCGTGCACTGGTG CCGGAAAAGGCGGCAGCGGCCGGCGGAGGG
3-*tssB-mCherry*	insertion of *mCherry* at the 3' end of *tssB*	GCAACGTTCTTTTCTTTCTGTACAGACATCAGCATTTTCTCTCGTAA TCCGTTAAACATATGAATATCCTCCTTAGTTCCTATTCCGAAGTTCC
5-*gfp-tssL*	insertion of *gfp-mut2* (or *mCherry*) at the 5' of *tssL*	CTACACCCCGGCATCGCTGGGAGATGTGAAACTGGAACTTTTTGC GGTGCTGCGGACATGACGATTGTGTAGGCTGGAGCTGCTTCGAAGTTCCTATAC

3-*gfp-tssL*	insertion of *gfp-mut2* (or *mCherry*) at the 5' of *tssL*	TGACCATCAGCCAGCCGGGATAAAAAATCTGTTCAGCCCGGGAGA TAACAGGTTTATTCCCTCCGCCGGCCGCTGC
5-*gfp-tssM*	insertion of *gfp-mut2* at the 5' of *tssM*	TTCTCATCCGGAGAAGAACATTTTATCAGTACTGTTACATCAGGAA ACCAGAATGAATAACGATTGTGTAGGCTGGAGCTGCTTCGAAGTTCCTATAC
3-*gfp-tssM*	insertion of *gfp-mut2* at the 5' of *tssM*	CACACCAATAAATACAATCCCCGGTCGCCCAAAGCGACCAGACAG ACAGGCCAGTTTATTCCCTCCGCCGGCCGCTGC
5-*tssJ-gfp*	insertion of *gfp-mut2* at the 3' of *tssJ*	CACGCCCCGTCTTATTGAAGTATCCGGTAACACCCTGACCCTGTTA CCGGTGAAGGATAAAGCAGCGGCCGGCGGAGGG
3-*tssJ-gfp*	insertion of *gfp-mut2* at the 3' of *tssJ*	GTTTAACTCCAGCCCGCCAGTGAAATTGCCATAGAGAATTTCATAA AGGGAAGGACGCGGCATCACATATGAATATCCTCCTTAGTTCCTATTCCGAAGTTCC

For plasmid construction [b,c,d]		
IBA37-TssM-FLAG-5	insertion of *tssM* with N-terminal FLAG epitope into pASK-IBA37	GACAAAAATCTAGAAATAATTTTGTTTAACTTTAAGAAGGAGATAT ACAAATG*GATTATAAAGACGACGATGACAAA*AATAAACTGGCCTGTCTGTCTGGTCGCTTTGGG
IBA37-TssM-3	insertion of *tssM* with N-terminal FLAG epitope into pASK-IBA37	GATGGTGATGGTGATGCGATCCTCTGCTAGCTCAGTCAGTCTCCTC CACGGTATCCCCGG
KD4-Nt-sfGFP-5	insertion of *gfp-mut2* into pKD4	CGGAATAGGAACTAAGGAGGATATTCATATGTCTAAAGGTGAAGAAC TGTTCACCG
KD4-Nt-sfGFP-3	insertion of *gfp-mut2* into pKD4	CTGACATGGGAATTAGCCATGGTCCCCTCCGCCGGCCGCTGCTTTGTAGA GCTCATCCATGCCG
KD4-Ct-mCherry-5	insertion of *mCherry* into pKD4	GCAGCATTACACGTCTTGAGCGATTGCAGCGGCCGGCGGAGG
KD4-Ct- mCherry-3	insertion of *mCherry* into pKD4	CTTCGAAGCAGCTCCAGCCTACACTTACTTGTACAGCTCGTCCATGCC GCC
5-pETG20-TssM$_{26Ct}$	insertion of *tssM* (aa 868-1107) into pETG20A	GACAAGTTTGTACAAAAAAGCAGGCTTAGAAAACCTGTACT TCCAGGGTACGCCCGCGGCAGAAAGTCTG
3-pETG20-TssM$_{26Ct}$	insertion of *tssM* (aa 868-1107) into pETG20A	CCACTTTGTACAAGAAAGCTGGGTTTATTCGAAAACCGTTT CCGGCAGAAC
RSF-Js-Fwd	insertion of StrepII-tagged *tssJ* into pRSF-Duet	ATGGTA**CATATG**ATGGCGATTATCGCTGGTAAGGCTGGTGG

		AATTCCATATGGCGATTATCGCTGGTAAGGCTGGTTACGGTC
RSF-Js-Rev	insertion of StrepII-tagged *tssJ* into pRSF-Duet	AATCCG**CTCGAG**TCA*TTTTTCGAACTGCGGGTGGCTCCA*TTT ATCCTTCACCGGTAACAGGGTCAGGGTG
RSF-flL-Fwd	insertion of FLAG-tagged *tssL* into pRSF-Duet	GCAGTTCGAAAAATGACTCGAGAAGGAGATATACCATG*GA TTATAAAGATGACGATGACAAG*AATAAACCTGTTATCTCCCGGGC
RSF-flL-Rev	insertion of FLAG-tagged *tssL* into pRSF-Duet	ATGTATATCTCCTTTTATCCCTGCCCGGTAAGCCGTGCCACC TGGTCTG
RSF-hM-Fwd	insertion of 6×His-tagged *tssM* into pRSF-Duet	GGATAAAAGGAGATATACATATG*CATCACCATCATCACCACC ATCAC*AATAAACTGGCCTGTCTGTCTGGTC
RSF-hM-Rev	insertion of 6×His-tagged *tssM* into pRSF-Duet	GCGGTTTCTTTACCAGACTCGAGTCAGTCAGTCTCCTCCACG GTATCC

For site-directed mutagenesis [e]

A-TssJ C1S	Cys1-to-Ser substitution in *tssJ*	TTATCAGGATCCGGTCTGACGCAAAGAGTGGCAGACGGTACGGTATCTGC
B-TssJ C1S	Cys1-to-Ser substitution in *tssJ*	GTCAGACCGGATCCTGATAACGACAGGGAAAACAACGCAATAAT
A-TssM-C727S	Cys727-to-Ser substitution in *tssM*	GAATACGCTGGCGGTTCAGGGATCCACTGGCCAGCCCCGGGAAG
B-TssM-C727S	Cys727-to-Ser substitution in *tssM*	CTTCCCGGGGCTGGCCAGTGGATCCCTGAACCGCCAGCGTATTC
A-TssM-T972C	Thr972-to-Cys substitution in *tssM*	ATAGCGGATGTGGCGTTCACCTGTGGTAACGCGGGGCTGCATTTTG
B-TssM-T972C	Thr972-to-Cys substitution in *tssM*	CAAAATGCAGCCCCGCGTTACCACAGGTGAACGCCACATCCGCTAT
A-TssM-V989C	Val989-to-Cys substitution in *tssM*	CGCCCGGGAACTGCTGCCGGTTGTATGCAGACGACGCTGATAAC
B- TssM-V989C	Val989-to-Cys substitution in *tssM*	GTTATCAGCGTCGTCTGCATACAACCGGCAGCAGTTCCCGGGCG
A-TssM-N1005C	Asn1005-to-Cys substitution in *tssM*	GATAATCAGAAACTGATTTATGTTTGTCAGATGCCGGTATGGAAGCG
B- TssM-N1005C	Asn1005-to-Cys substitution in *tssM*	CGCTTCCATACCGGCATCTGACAAACATAAATCAGTTTCTGATTATC
A-TssM-T1019C	Thr1019-to-Cys substitution in *tssM*	GATTTACCTGGCCGGCTGATTGTGAAGCACCTGGCGCCAGTTTAAG
B- TssM-T1019C	Thr1019-to-Cys substitution in *tssM*	CTTAAACTGGCGCCAGGTGCTTCACAATCAGCCGGCCAGGTAAATC
A-TssM-T1035C	Thr1035-to-Cys substitution in *tssM*	GGGTAAGCACTCAGGCCGTGTCCCGTCAGTATGCAGACCTGCCGGG
B- TssM-T1035C	Thr1035-to-Cys substitution in *tssM*	CCCGGCAGGTCTGCATACTGACGGGACACGGCCTGAGTGCTTTACCC
A-TssM-V1062C	Val1062-to-Cys substitution in *tssM*	GACGGAAAGCCGCACCGGTGTTTGCCAGTGGCTGGAGCCTGAG
B- TssM-V1062C	Val1062-to-Cys substitution in *tssM*	CTCAGGCTCCAGCCACTGGCAAACACCGGTGCGGCTTTCCGTC
A-TssM-G1075C	Gly1075-to-Cys substitution in *tssM*	CTGAGCTGGCAGGCGCAGGACTGTCGTATGCTGAATTACACACTGC
B- TssM-G1075C	Gly1075-to-Cys substitution in *tssM*	GCAGTGTGTAATTCAGCATACGACAGTCCTGCGCCTGCCAGCTCAG

A-TssM-V1092C	Val1092-to-Cys substitution in *tssM*	GGGGAAGGGCCGCTTTGTTTGCTGAAACTCCGCAATTTTG
B- TssM-V1092C	Val1092-to-Cys substitution in *tssM*	CAAAATTGCGGAGTTTCAGCAAACAAAGCGGCCCTTCCCC
A-TssM-S1109C	Ser1109-to-Cys substitution in *tssM*	GAAACGGTTTTCGAACTCTGCGGCACGTCAGCGTTTAC
B-TssM-S1109C	Ser1009-to-Cys substitution in *tssM*	GTAAACGCTGACGTGCCGCAGAGTTCGAAAACCGTTTC

[a] Sequences corresponding to the downstream and upstream regions of the gene to be deleted underlined.
[b] Sequence annealing on the target plasmid underlined.
[c] Restriction sites in **Bold**.
[d] FLAG, StrepII or 6× His tag coding sequence *italicized*.
[e] mutagenized codon underlined.

General discussion and additional results

4.1 The assembly of the T6SS membrane complex

Our study revealed the *in vivo* localization of the T6SS membrane complex and its assembly pathway. In average, 1-3 complexes can be visualized per cell using fluorescent-labeled TssM and TssL proteins. These complexes are not dynamic and can be used for several rounds of sheath elongation/contraction. TssJ is the first protein that positions at the site of assembly, and is followed by TssM and TssL. Nevertheless, we do not know yet whether TssJ finds the site of assembly by itself or whether an additional component is required to control its positioning. None of the GFP or mCherry fusions to TssJ were functional, and therefore these data will be difficult to obtain. It is also worthy to note that the fact that TssJLM foci are static suggest that there is not a target cell contact-dependent positioning.

The assembly pathway of the T6SS membrane complex proceeds inward, *i.e.*, from the outermost part of the cell to the interior. Inward biogenesis of cell envelope complexes is the rule. For secretion systems, outer membrane components are usually nucleation factors. In the *V. cholerae* T2SS, the outer membrane secretin EpsD is critical to the localization of T2SS subunits (Lybarger et al., 2009). Assembly of the *Yersinia* T3SS starts with the YscC outer membrane secretin (Diepold et al., 2010). Assembly of the T4SS is also initiated by the outer membrane-associated VirB7-VirB9 complex (Kumar and Das, 2002)(Judd et al., 2005)

4.2 Architecture of the system

The structure of the T6SS confirms that each double-membrane-spanning system possesses a unique structure and export mechanism, but individual protein components exhibit similarities in structure, shape and/or function (Costa et al., 2015).

We have reported the structure of the T6SS membrane complex from EAEC. However, we do not know whether this TssJLM complex represents a prototypical structure and whether variability exists between T6SS membrane complexes. Variability is likely to exist as the T6SS membrane components from different species have differences. For examples, the vast majority of T6SS gene clusters does not encode a TagL component, but rather have a peptidoglycan-binding domain fused at the C-terminus of TssL (Aschtgen et al., 2010a). So these TssJLM complexes should have an

extra-density in the periplasm. It has also been shown that the tssM genes of *Citrobacter rodentium* and *Yersinia pseudotuberculosis* encode two different length variants due to RNA polymerase frameshifting (Gueguen et al., 2014). Hence, the TssJLM complexes should also exhibit significant differences. Finally, the TssM protein of the *P. aeruginosa* H1-T6SS is predicted to have a single trans-membrane segment (compared to the 3-transmembrane segment of classical TssM proteins). Thus, one immediate perspective to this work will be to purify and image TssJLM complexes from different species, including those cited above. Similarly, the TssJLM complexes of *Francisella tularensis* and of *Bacteroidetes* species, that belong to distinct T6SS families could be interesting targets.

It is also important to note that the structure of the EAEC TssJLM membrane complex was solved from a purified complex produced in a heterologous host, in absence of other T6SS subunits. It would therefore be interesting to purify and image the TssJLM complex from native, chromosomal expression, and to compare this structure with the one we have reported. This approach may provide supplemental information such as conformational changes of the membrane complex that may undergo upon baseplate docking or sheath contraction, or information regarding the *in vivo* symmetry. The purified TssJLM complex exhibits 5-fold symmetry, which is different from the 6-fold symmetry of TssA or the predicted 6-fold symmetry of the baseplate (Zoued et al., 2017), and it remains possible that the 5-fold symmetry corresponds to a more stable conformation, but that TssA may act as a chaperone to impose a 6-fold symmetry *in vivo* (Zoued et al., 2017). This situation is possible as TssA interacts with the TssJM complex, prior to the recruitment of TssL and the polymerization of the membrane complex (Zoued et al., 2016b). Imaging the T6SS membrane complex *in vivo* is therefore a very exciting perspective to define the *in vivo* symmetry of the TssJLM complex and to define its structure once bound to the baseplate or after firing. To answer this question, we have to develop an *in vivo* approach that aims to visualize the membrane complex and the full T6SS in the bacterial cell.

4.3 Additional results

Visualizing membrane complexes directly inside bacterial cells is a challenge. However, recent progresses in electron cryo-tomography (ECT) have revealed the structure of several large complexes, including flagellum, chemotaxis machineries, T3SS, T4SS, T6SS and Type IV pili (Oikonomou and Jensen, 2017)(Beeby et al., 2016)(Briegel et al., 2016)(Ghosal et al., 2017)(Chang et al., 2016)(Chang et al., 2017)(Hu et al., 2017). ECT produces three-dimensional images of cells in a near native state at a macromolecular resolution. This *in situ* technique requires no purification and is label-free. To achieve this project, our laboratory had initiated collaboration with the group of Martin Pilhofer (ETH Zürich, Switzerland), a recognized expert in ECT. However, one limitation of ECT is the thickness of the sample, as thin samples will provide better images. Thin samples could be obtained by milling the surface of the bacterial cell or by genetically decreasing the size of the bacterial cell (Farley et al., 2016)(Rigort et al., 2012). As T6SS sheath contraction is usually responsive to cell envelope perturbations, it will be easier to achieve our goal by genetically manipulating EAEC.

4.3.1 *E. coli* mutants that form skinny and minicells.

As mentioned above, bacterial cells are too thick to allow high-resolution as they reduce the quality of the tomographic images. It has been previously shown that mutations can induce significant reduction of the length and width of bacterial cells (Figure 4.25) (Liu et al., 2011). A specific mutation on the bacterial actin homolog, MreB, A125V has been shown to affect the thickness of rod-shaped cells, and hence causes the formation of thinner bacterial cells called "skinny cells". (Liu et al., 2011). Size decrease could be obtained by deletion of the *minCDE* genes, which are responsible for proper positioning of the cell divisome at the septum. Deletion of the *minCDE* genes thus induces asymmetric cell division, and the production of spherical "minicells" (Carleton et al., 2013). By inactivating the Min system in skinny $mreB^{A125V}$ cells, we can obtain "skinny minicells" that may provide good imagining conditions.

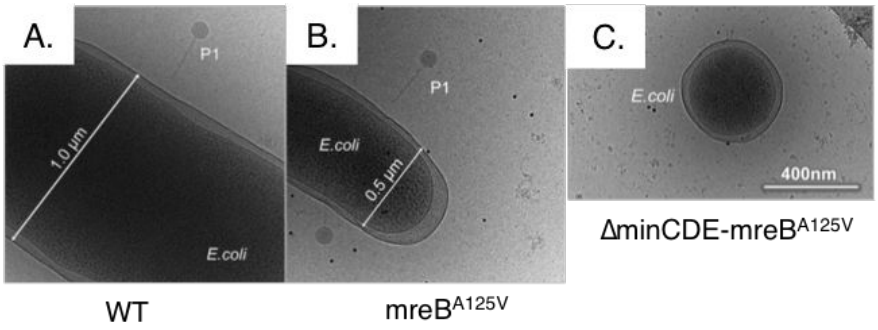

Figure 4.25: **Size comparison of standard versus engineered tiny *E. coli*.** Cryo-EM of a typical wild-type *E. coli* cell with an average diameter of 1μm **(A)**, a skinny WM3433 *E. coli* cell with a diameter of 0.5 μm **(B)** and a minicell from WM3433 with a diameter of less than 0.4 μm . All three cultures were in exponential phase prior to dilution for the growth curve measurements (Liu et al., 2011).

The aims of our project are triple: (i) visualize the membrane complex with a heterologous expression in BL21(DE3) and compare with the purified complex extracted from BL21(DE3) cells; (ii) visualize the membrane complex in strain 17.2; and (iii) visualize the entire T6SS under different conformations, using deletion backgrounds (*i.e.*, without the baseplate (*tssK* mutant), without the sheath (*tssBC* mutant), with accumulated contracted sheaths (*clpV* mutant)). To do so, I introduced the *minCDE* deletion and the $mreB^{A125V}$ mutation in *E. coli* BL21(DE3) and EAEC 17-2. In addition, these mutations were also introduced in 17-2 cells bearing the chromosomal GFP-TssM (to test whether TssJLM complex are observable in minicells) or the chromosomal TssB-GFP fusion (to test whether sheath dynamics are observable in minicells). To genetically engineer E. coli and EAEC skinny minicells, mutations were introduced directly into the chromosome. Deletion of the *minCDE* operon was achieved by the Datsenko and Wanner one-step inactivation method using PCR products and short-length recombination by the λ red recombinase (Datsenko and Wanner, 2000). The $mreB^{A125V}$ mutation was introduced by double homologous recombination using the pKO3 suicide vector (Link et al., 1997)(List of strains, plasmids and primers in *Table S1* presented in *Annexe*).

4.3.2 Morphological characterization of skinny, mini and skinny mini-cells

In collaboration with Leon Espinosa (Plateforme de Biophotonique, LCB, CNRS-Marseille), I analyzed these strains by using the MicrobeJ software (Ducret et al., 2016), allowing an automatic characterization of the different strains. First, we quantified the percentage of minicells in the different populations.

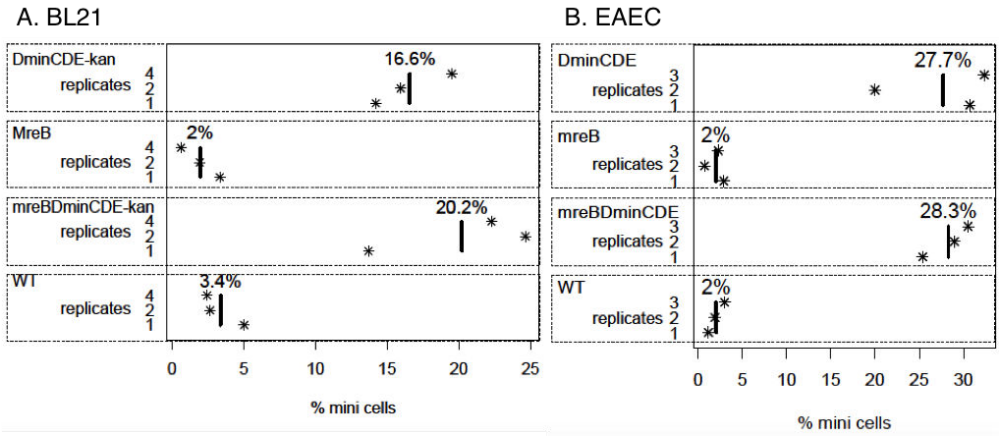

Figure 4.26: **Percentage of minicells produced in the engineered strains** The percentage of minicells were calculated for each engineered strain as indicated. Three independent experiments were analyzed and noted as an asterisk.

Figure 4.26 shows that a wild-type and a $mreB^{A125V}$ mutant produce ≈ 2 % of minicells in both BL21(DE3) (A) and EAEC (B). As expected, deletion of the *min* genes increases the production of minicells to 16.6 % and 27.7 % in BL21(DE3) and EAEC, respectively. Combination of the two mutations does not significantly change the percentage of minicells compared to *minCDE* mutants with minicells representations of 20.2 % and 28.3 % in BL21(DE3) and EAEC. In addition to the percentage, we can visualize the entire population by representing cells on a diagram with the X and Y-axis Figure 4.27, upper panel. It allows us to better appreciate the morphology of minicells compared to normal sized cells. We can see that the length and the width are reduced. It is worth to note that the double mutation homogenizes minicells size. The populations of minicells are shown separately on a different diagram Figure 4.27, lower panel. As conclusion, deletion of the *minCDE* and introduction of the $mreB^{A125V}$ mutation induced the expected phenotypes, observed in *E. coli* K-12.

4.3.3 Impact of *minCDE* and *mreB* mutations on T6SS function

Minicells are not simply small cells that lack a chromosome. They have different sizes, as the positioning of the Z-ring is impaired. They remain metabolically active even if we can observe variation in minicell sizes from a single bacterial culture. We do not know if mutations impairing the cell division have an impact on the function of the T6SS. To test T6SS function, I performed an antibacterial assay on the entire population of each strain. Figure 4.28 shows that all engineered strains have a killing activity comparable to a WT strain, demonstrating that the *minCDE* and *mreB* mutations do not affect T6SS function.

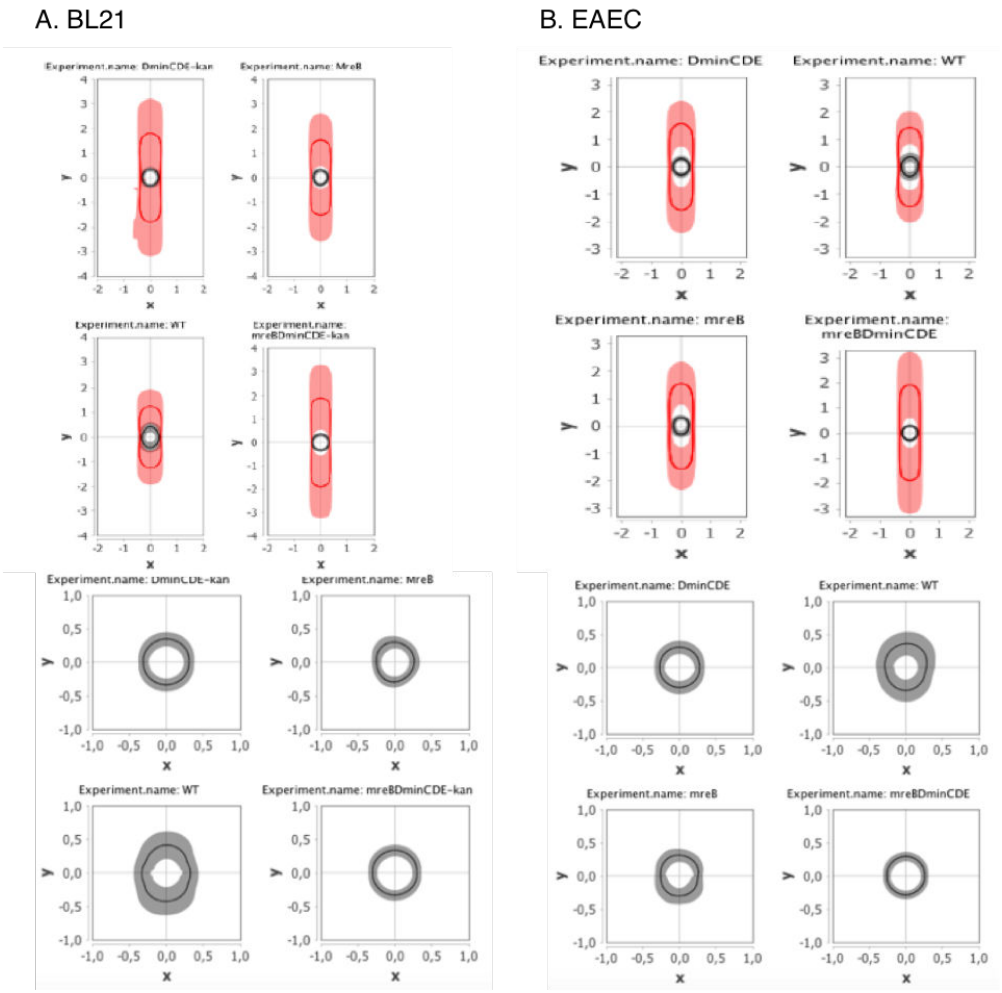

Figure 4.27: **Morphological characterization of the engineered strains.** Diagrams showing the morphology of the entire population (upper panels) and the minicell population (lower panels) of each engineered strains according the X- and Y- axis. The scale is in μm.

4.3.4 Isolation of minicells

As for electron microscopy, the resolution of the final model relies on the initial number of particles observed. However, because bacterial strain produces a mixture of filaments and minicells, pilot experiments showed that we were limited by the low amount of minicells on each ECT grids. To obtain more usable objects, I decided to isolate minicells from the population. Several methods have been developed for the purification of minicells such as differential centrifugation, multiple density gradient centrifugation and multistep filtration (Farley et al., 2016). For the first attempt, we decided to use differential centrifugation in order to minimize damages to the cells, and to limit the use of additional compound. This isolation protocol was improved to obtain satisfying results (Figure 4.29).

Using this protocol, we can obtain 99.9% of minicells. The improved protocol is at follows: A volume of 10 mL of bacterial culture was grown in SIM at 37°C. Once the culture reached an OD_{600nm} of 0.8, cells were harvested and collected by three successive centrifugations at 2000 x g for 15 min to remove the majority of larger cells and cellular debris. Supernatant fractions were collected each time. Minicells were then subject to a high-speed centrifugation at 15000 x g for

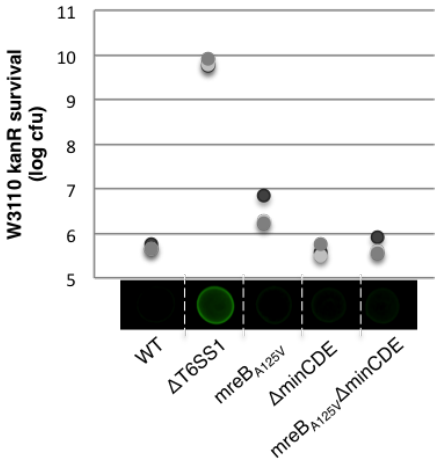

Figure 4.28: **Antibacterial assay.** *E. coli* K-12 prey cells (W3110 kan^R) were mixed with the indicated attacker cells, spotted onto SIM agar plates, and incubated for 4h at 37° C. The number of recovered *E. coli* prey cells is indicated in the graph (in log10 of colony-forming unit). The circles indicate values from three independent assays, and the average is indicated by the bar.

30 min. Supernatants were discarded and a volume of 150 μL was left for pellet resuspension. All fractions were then pooled into an eppendorf tube to a last centrifugation step at 15000 x g for 15 min. The totality of the supernatant was removed and enriched minicells fractions were finally resuspended with 40 μL of PBS.

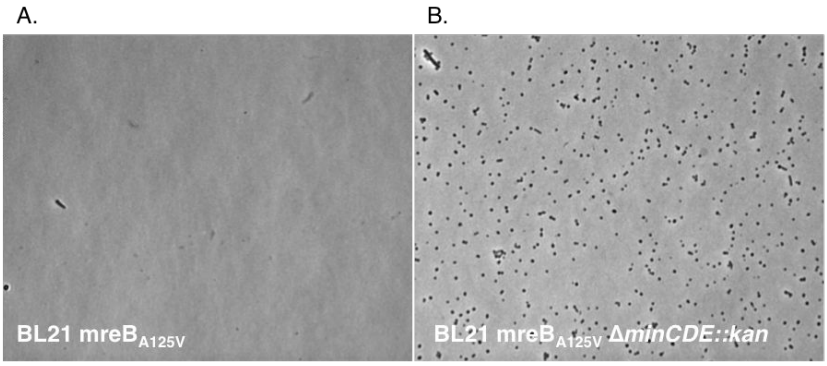

Figure 4.29: **Minicells enrichment.** Phase contrast micrographs of cells of BL21*mreB*^{A125V} **(A)** and BL21*mreB*^{A125V}Δ*minCDE*:kan **(B)** after isolation.

4.3.5 Imaging the T6SS in skinny minicells

In BL21(DE3). Using the pRSF-TssJLM plasmid, utilized in the *Article 2* to purify the TssJLM complex, we are able to produce a high number of TssJLM complexes in BL21(DE3) cells.

In EAEC. In EAEC, the TssJLM complex is produced at native levels, which correspond to 1-3 complexes per cell (up to 8). The number of complexes is therefore limiting, and as a consequence, it is difficult to observe TssJLM complexes. To increase the detection of these complexes, we can develop a correlative approach, in which both fluorescence microscopy and ECT are performed on

the same sample. The fluorescent signal is then used to identify and locate the items of interest for later imaging by ECT. For this, we will use the skinny minicells producing GFP-TssM. Figure 4.30 shows that fluorescent foci are observed in minicells and hence that the correlative approach could be an interesting perspective.

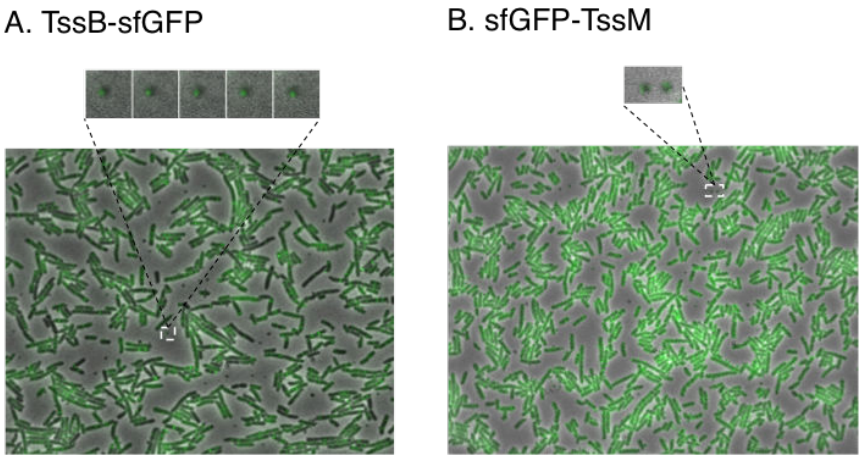

Figure 4.30: **Skinny minicells producing GFP fusion proteins.** Fluorescence microscopy images of skinny minicells producing TssB-sfGFP **(A)** and sfGFP-TssM **(B)**. Differential interference contrast and GFP channels are merged. The magnifications show fluorescent foci in minicells.

The different strains were subjected to ECT observations in a frozen-hydrated state. A 3-D reconstruction at low resolution was then carried out from a series of images at different tilted angles and collected at very low electron dose. The first tomograms allowed to observe contracted and elongated sheaths, as well as TssJLM complexes (Figure 4.31). A 3-D model of the membrane complex was constructed. Figure 4.32 shows that the TssJLM complex adopts a C5 symmetry and has an architecture similar to that obtained *in vitro* (Figure 4.32).

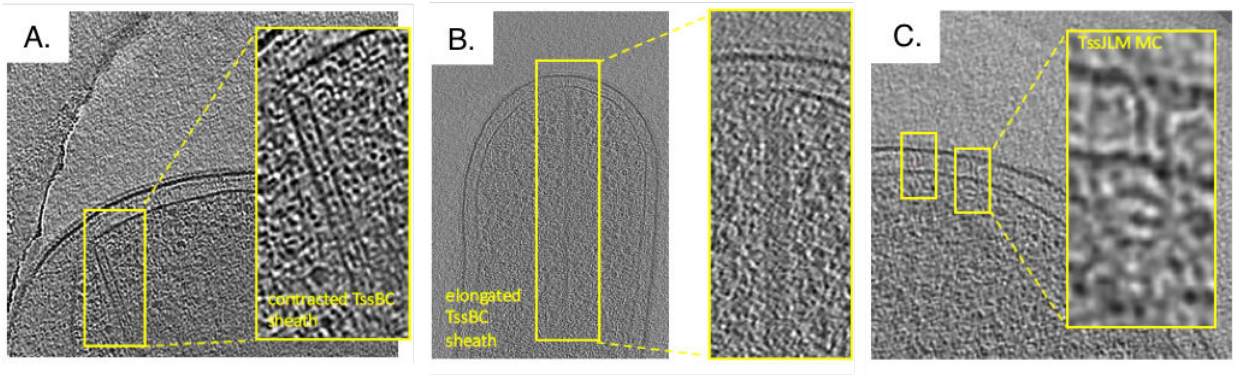

Figure 4.31: **T6SS tomographs.** 2D images from a tomograph recorded on EAEC overproducing TssJLM. The TssBC sheath contracted **(A)**, elongated **(B)** and the TssJLM membrane complex **(C)** are shown. OM, outer membrane; IM, inner membrane.

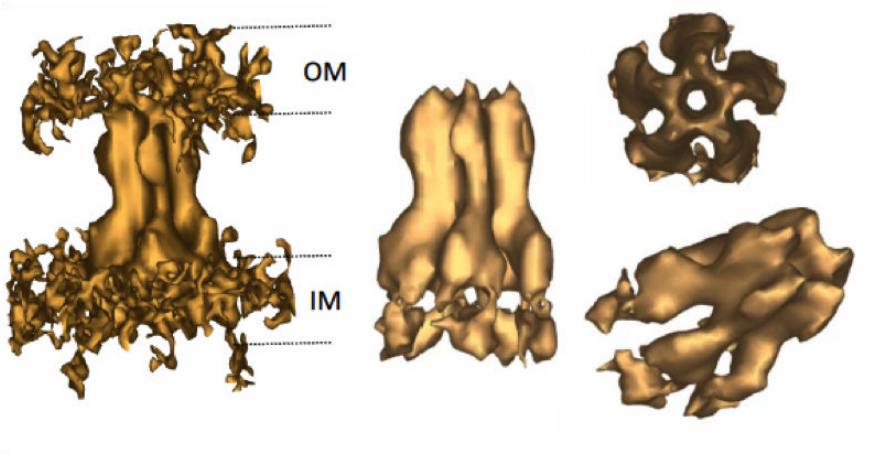

Figure 4.32: **TssJLM reconstruction.** 3D reconstruction of TssJLM membrane complex by averaging 420 sub-tomograms.

Our collaborators at ETH Zürich currently put efforts to obtain better images with the goal to reconstruct a high resolution structure of the membrane complex and of the entire apparatus. For this, more images will be collected and a sub-tomogram averaging approach will be used to analyze several thousand of sub-tomograms containing all or part of the T6SS. During the process, a 3D classification will allow us to visualize and to model different conformations and to identify conformational changes, which might be of biological importance.

It is worth to note that two articles have been recently published on the structure of the T6SS complex from *Myxococcus xanthus* (Chang et al., 2017) and a T6S-like tail structure in *Amoebophilus asiaticus* (Böck et al., 2017) using ECT.

4.4 The T6SS membrane complex undergoes conformational changes to form the pore

The crystal structure of C-terminal region of TssM shows that it is composed of two domains. The N-terminal domain is constituted of four α-helices, a β-hairpin and an elongated stretch. The C-terminal domain comprises nine β-strands followed by α-helix 5 and a stretch of residues with no secondary structure. Based on this structure, we could not detect any obvious transmembrane region that may form the outer membrane channel. To gain information on the location of this domain relative to the membrane, we introduced cysteine residues between each β-strands and tested their accessibility in WT, $\Delta tssJ$ and $\Delta tssBC$ cells. In the wild-type situation, cysteine side-chains located at the tip of the TssM C-terminal region were labeled in a WT strain but not labeled in $\Delta tssBC$ cells. This suggests that the tip is transiently exposed to the exterior during sheath polymerization and/or contraction. This experiment also sheds light on the fact that the TssM α-5 helix permanently crosses the outer membrane, except when TssJ is absent.

We conclude that the membrane complex is assembled in a closed conformation named “resting state”, in which only helix α-5 is inserted into the outer membrane. This closed conformation would prevent entry of toxic compounds into the periplasm. Once the baseplate and the sheath

are assembled, we propose that the tip of TssM must undergo large conformational changes to cross the OM and form the pore to allow the passage of the tube. One hypothesis will be that the internal pillars would move outward to open a large channel compatible with the passage of the Hcp needle. Interestingly, limited proteolysis experiments have shown that TssM undergoes conformational changes that permit to interact with Hcp in *Agrobacterium tumefaciens* (Ma et al., 2012).

4.5 Sensing the prey cell

Whole-cell accessibility studies revealed that the C-terminal extension of TssM is exposed to the outside. It is thus the only region of the entire T6SS that is exposed to the cell exterior, and this makes the TssM C-terminal extension a good candidate for sensing the prey. In addition, *Article 3* will show that the cytoplasmic domain of TssM mediates contacts with baseplate components – TssG and TssK, and one may imagine that the information regarding the presence of the prey might be transduced to the sheath through TssM and the baseplate. As described in the introduction section, sheath contraction is initiated at the baseplate. Similarly, in contractile bacteriophages, long tail fibers transduce the information (*i.e.*, reception on the host cell) to the baseplate. We then hypothesize that TssM might play the role of phage fibers by connecting the sensing of the contact with the contraction of the sheath. If this hypothesis is true, understanding the contribution of the TssM C-terminal extension in T6SS function is important. In the following *Additional results* section, I will describe the results I obtained on this extension.

4.6 Additional results

4.6.1 The C-terminal extension is well conserved among *Escherichia coli* strains.

To better understand the role of the C-terminal extension, I first performed a bioinformatics approach. Because the TssM proteins are very diverse (*e.g.*, the TssM protein associated with the *P. aeruginosa* H1-T6SS is predicted to have a single transmembrane segment compared to the prototypical TssM proteins; the TssM proteins of *Citrobacter rodentium* and *Yersinia pseudotuberculosis* are produced as two different length variants (Gueguen et al., 2014), I focused my studies on *Escherichia coli* strains. Using T-coffee, I generated a sequence alignment for the TssM C-terminal extremity (starting from the beginning of the last long α-helix) from 70 *Escherichia coli* strains. Sequences were found using the web-based resource for T6SS SecReT6 (Li et al., 2015)(http://db-mml.sjtu.edu.cn/SecReT6/). Figure 4.33 shows that the C-terminal extremities can be categorized into three groups. Interestingly, these groups correspond to the T6SS groups already identified: T6SS-1 (or i2), T6SS-2 (or i1), and T6SS-3 (or i4b) (Journet and Cascales, 2016)(Li et al., 2015). Within each group the sequences are highly conserved. The TssM protein associated with the EAEC Sci-1 T6SS belongs to group i2, a group of TssM proteins that bear an additional C-terminal region compared to the T6SS-2 family; which corresponds to the cell surface exposed region defined by the cysteine accessibility approach in *Article 2*. This additional region is negatively charged, with the presence of a large number of aspartate and glutamate residues. For

example, the EAEC Sci-1 TssM C-terminal extremity possesses 8 negatively charged residues for a 23-aminoacid long sequence (35%). It is worthy to note that the T6SS-2 family (*i.e.*, without this additional extracellular region) groups T6SS gene clusters that encode FHA, a protein involved in the post-translational activation pathway. Thus, we have two categories: T6SS-2 with FHA and likely a simplified form of post-translational pathway for activation of the T6SS, and T6SS-1 with no FHA but for which TssM proteins bear a cell surface exposed additional region.

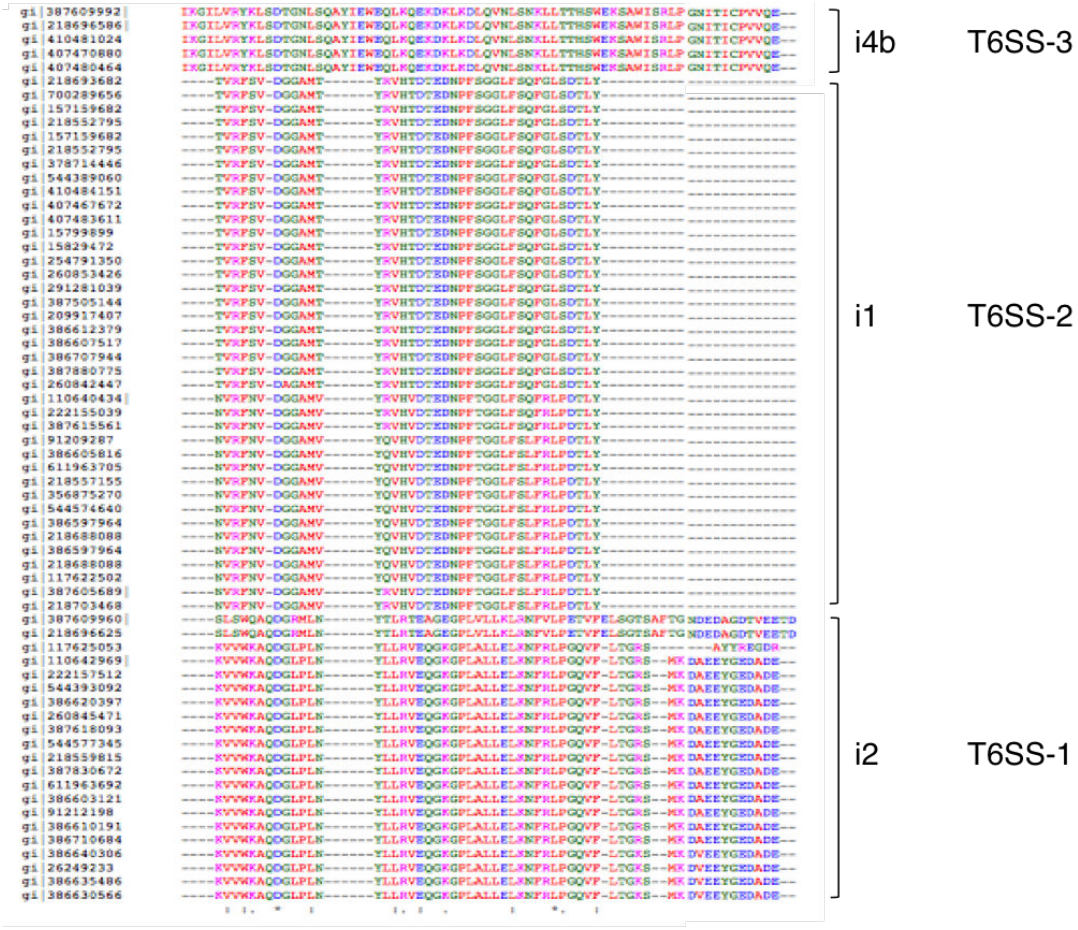

Figure 4.33: **Sequence alignment of the C-terminal extension from TssM homologues.** T-coffee sequence alignment of the C-terminal extension from *E. coli* strains is shown. Sequences were found on the web-based resource for T6SS SecReT6 (Li et al., 2015). This figure has been prepared with T-COFFEE (Di Tommaso et al., 2011).

To define whether this dichotomy observed in *E. coli* strains could be extended to other T6SS, I performed a sequence alignment between randomly selected TssM proteins belonging to T6SS gene clusters encoding - or not - the post-translation pathway (*P. aeruginosa* H1, *Agrobacterium tumefaciens*, etc). Figure 4.34 shows that similarly to EAEC, *E. tarda* has a long C-terminal region whereas *P. aeruginosa*, *A. tumefaciens*, *S. enterica*, *A. hydrophila* or *V. cholera* contain a short version. Interestingly, this length difference is more correlated with the presence on the Walker A / B and GTP specific motif than a post-translational activation pathway. Moreover, the NTPase domain of *E. tarda* has been shown to be inactive which could explain this example. Further analysis needs to be carried out to decipher the link between NTPase domain and the length of the

C-terminal region.

Figure 4.34: **Sequence alignment between randomly selected TssM proteins.** T-COFFEE sequence alignment of the C-terminal region of TssM of (from top to bottom) enteroaggregative *Escherichia coli* (EAEC) Sci-1 (EAEC 17-2), *Y. pseudotuberculosis* (IP31758)T6SS-3, *Yersinia pseudotuberculosis* (IP31758) T6SS-5, *Vibrio cholerae* (O395), *Salmonella enterica* Typhimurium (LT2), *Agrobacterium tumefaciens* (C58), *Pseudomonas aeruginosa* H1-T6SS (PA01), *Aeromonas hydrophila* (ATCC7966), and *Edwardsiella tarda*. Local homologies are indicated by a colour code (bad to good from blue to red). The figure has been prepared with T-COFFEE.

4.6.2 The C-terminal extension is essential for T6SS antibacterial activity.

To better understand the contribution of this additional C-terminal extremity for T6SS activity, I decided to target this region. To avoid problems due to TssM overproduction, mutations were introduced on the chromosome. Based on the bioinformatics analysis, I constructed three TssM variants (Figure 4.36): (i) deletion the entire C-terminal extremity (*i.e.*, the 30 amino-acids located after the last α-helix); (ii) substitution of all the E and D residues to alanines (Figure 4.36 sequence (1)); and (iii) modification of the order of residues without changing the net charge by creating a "scrambled" C-terminal extension (Figure 4.36 sequence (2)-.

Cter-WT VLPETVFELSGTSAFTGNDEDAGDTVEETD
Cter-Ala VLPATVFALSGTSAFTGNAAAAGATVAATA (1)
Cter-Scr VGDLTAPSGEADTFTVTVFGEENELDTSED (2)

Figure 4.35: **Sequences of the C-terminal variants.** Sequences of the wild-type C-terminal extension (C-ter WT) and the two variants are shown **(1-2)**. The position of the serine residue (in orange) was labeled with the BSA-maleimide. The negative amino-acids Aspartate (D) and Glutamate (E) are in blue. Residues that were substituted by an Alanine residue (A) are in red.

Hence, I engineered pKD4 vectors encoding the C-terminal fragment of TssM in order to use the one-step inactivation procedure (Datsenko and Wanner, 2000) for chromosomal insertion. These vectors were constructed as follow: DNA fragments corresponding to the sequences described above were synthesized by IDT (see *Table S2* presented in *Annexe*). They were cloned by megapriming into the pKD4 plasmid. Oligonuclotides and plasmids used in this study are listed in the *Table S2*. The pKD4 vectors constructed were then used as template for DNA amplification and recombination on the chromosome after electroporation.

Once obtained, the strains with TssM C-terminal extension variants at the native chromosomal locus were used as attackers for an antibacterial assay. As seen in Figure 4.36, the three engineered strains are unable to kill target cells, as their antibacterial activities are comparable to Δ*tssM*. From these data, I concluded that the TssM C-terminal extension, and more specifically the charged residues and the order of the sequence, are required for T6SS antibacterial activity.

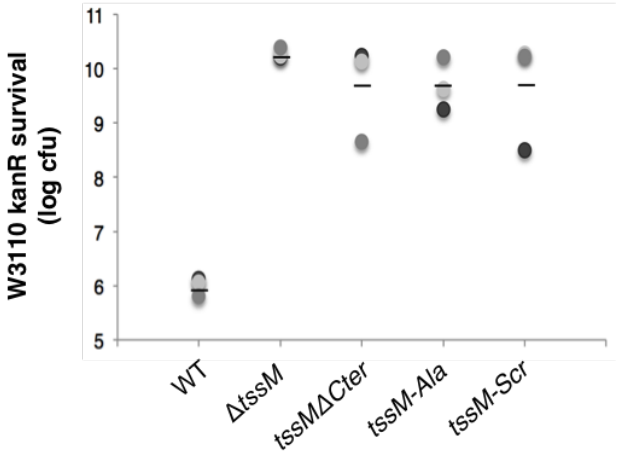

Figure 4.36: **The TssM C-terminal extension is essential for T6SS antibacterial activity.** *E. coli* K-12 prey cells (W3110 kan^R) were mixed with the indicated attacker cells, spotted onto SIM agar plates, and incubated for 4h at 37°C. The number of recovered *E. coli* prey cells is indicated in the graph (in log10 of colony-forming unit). The circles indicate values from three independent assays, and the average is indicated by the bar.

4.6.3 The EAEC Sci-1 T6SS is able to kill an *E. coli* rough target cell.

If the cell surface-exposed region of TssM has a role in sensing the target cell, identifying the "receptor" of the TssM extension will be of high interest. Previous unpublished studies in the laboratory have shown that the EAEC Sci-1 T6SS is able to provide a competitive advantage to diverse bacterial species, including different *E. coli* pathotypes, *Salmonella enterica* and *Citrobacter rodentium* but has no effect on Gram positive bacteria such as *Bacillus subtilis*. Thus, if TssM recognizes a "receptor", we hypothesize that such "receptor" should be surface exposed, and conserved within these species. Although these bacterial species are all enteric strains, they are sufficiently different to hypothesize that the lipopolysaccharide (LPS) might be a good candidate.

To test this hypothesis, I used an *E. coli* rough strain. Strain CA8000 (kindly provided by R. Lloubès)(Raina and Georgopoulos, 1990) has a transposon insertion in the *htrM* gene (Raina and Costa, 1991)(Karow et al., 1991). HtrM (also called RfaD or HldD) is an epimerase implicated in the final step of the ADP-L-glycero-D-manno-heptose pathway (Figure 4.37, A) (Kneidinger et al., 2002). The final product of this pathway forms the precursor inner core LPS (Figure 4.37, B). Thus, the *htrM* mutation results in a truncated LPS lacking the O-antigen and outer core. The antibacterial assay shown in Figure 4.38 demonstrates that the wild-type EAEC attacker strain is capable of killing rough target cells to levels comparable to a smooth strain. Therefore, it seems

that the O-antigen and outer core of the LPS is not the signal sensed for the activation of the EAEC Sci-1 T6SS.

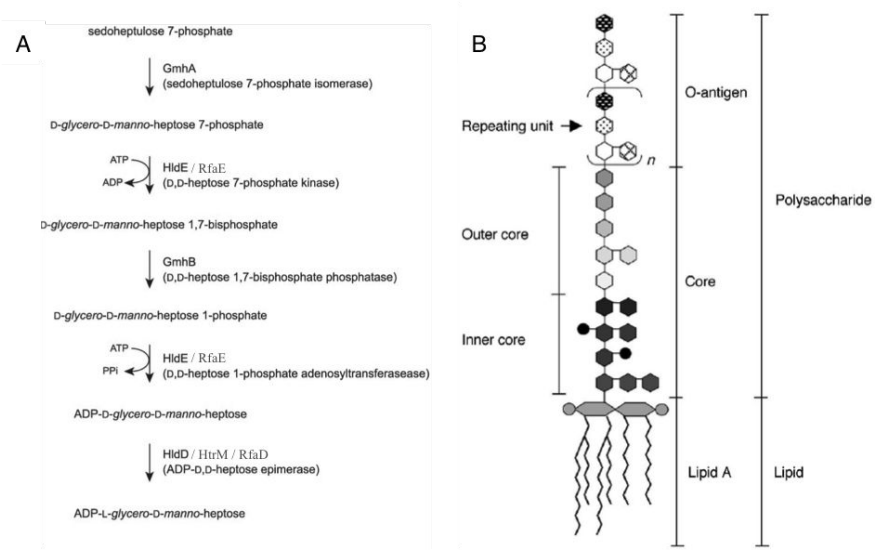

Figure 4.37: ***E. coli* lipopolysaccharids.** **(A)** Biosynthesis pathway for ADP-L-glycero-D-manno-heptose. The HtrM (also called RfaD or HldD) enzyme is implicated in the final step of the ADP-L-glycero-D-manno-heptose synthesis (Raetz and Whitfield, 2002). **(B)** Schematic representation of the LPS, highlighting the different structures: O-antigen, core and lipid A.

The results obtained with the TssM C-terminal extension variants demonstrated that this region is critical for T6SS activity. However, these results might be indirect and could be the consequence of a non-proper insertion of TssM, of an instability of TssM or of a weaken interaction with TssJ. I therefore performed a BACTH experiment to test whether the TssM variants interact with TssJ.

4.6.4 TssM periplasmic variants interact with TssJ.

To test whether the TssM C-terminal variants interact with TssJ, I constructed BACTH plasmids encoding the periplasmic domains of the TssM variants upstream and downstream T18 and T25. These constructs were tested against TssJ fused to the complementary Cya domains. As expected from the co-crystal $TssM_{26Ct}$-TssJ structure, the deletion or modification of the C-terminal region do not impact TssM-TssJ complex formation (Figure 4.39). Hence, the TssM C-terminal variants properly interact with TssJ.

These experiments showed that the TssM C-terminal extension is necessary for T6SS function, but the variants we have engineered do not affect the ability of TssM to interact with TssJ. We have now to understand which stage of the T6SS biogenesis is impacted by the modification of the TssM C-terminal extension: TssM recruitment, baseplate docking, sheath extension, sheath contraction,.... I project to gain information by performing fluorescence microscopy experiments to follow the localization and dynamics of (i) the TssM variants fused to the GFP, and (ii) the GFP-TssA, TssK-GFP and TssB-GFP fusions when the TssM variants are produced.

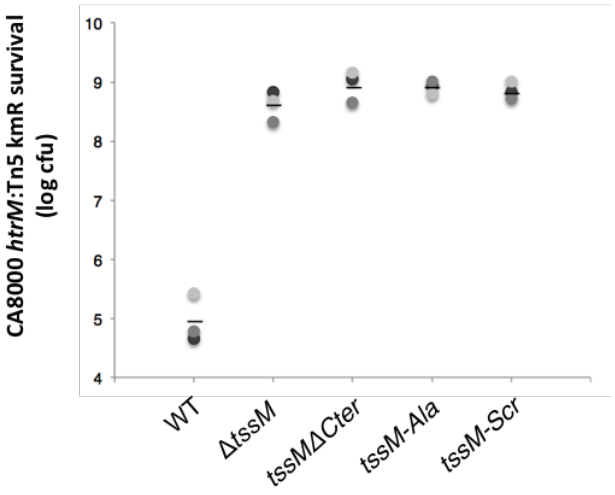

Figure 4.38: **A rough prey cell has no impact on the T6SS antibacterial activity.** *E. coli* K-12 prey cells (CA8000 htrM:Tn5 kanR) were mixed with the indicated attacker cells, spotted onto SIM agar plates, and incubates for 4h at 37 degree C. The number of recovered *E. coli* prey cells is indicated in the graph (in log10 of colony-forming unit). The circles indicate values from three independent assays, and the average is indicated by the bar.

Many questions remain to understand how the presence of the target cell is sensed and to define the signal that triggers the assembly of the apparatus and/or the contraction of the sheath. Based on the observation that the TssM C-terminal extension, present in TssM proteins belonging to T6SS lacking the post-translational pathway is necessary for T6SS activity, we hypothesized that this region might be involved in signal sensing. Our results cannot refute this hypothesis and there is still a lot of experiments to perform. In addition to the fluorescence microscopy experiments described above, it would be interesting to (i) identify the receptor, *i.e.*, what is recognized at the cell surface of the target cell, and (ii) to define the signaling pathway. Regarding the putative receptor, we have also to keep in mind that it could be not genetically encoded, as we can imagine that a "surface tension" is sensed, *i.e.*, a difference of pressure exerted at the outer membrane. This hypothesis could be tested by following T6SS sheath extension/contraction events under agar pads made with different concentrations of agar. Regarding how the signal is sensed, one other possibility is that the TssJ outer membrane lipoprotein is involved in sensing. It has been shown that RscF, a regulator of capsule synthesis, is a surface-exposed outer membrane lipoprotein and senses defects at the outer membrane (Cho et al., 2014)(Konovalova et al., 2014).

Once the signal found, we have to decipher how the signal is transmitted to the baseplate to regulate sheath extension or contraction. The topology of the T6SS membrane proteins and the structure of the TssJLM complex demonstrated that there is a large cytoplasmic base (Durand et al., 2015) and further fluorescence microscopy experiments showed that the baseplate is recruited to the assembled membrane complex (Brunet et al., 2015b). It is therefore likely that the cytoplasmic base of the TssJLM complex, which comprises the TssL and TssM cytoplasmic domains, could be involved in the transmission of the information. We therefore decided to gain information on the structure of the TssM cytoplasmic domain and to better understand its contribution for baseplate docking.

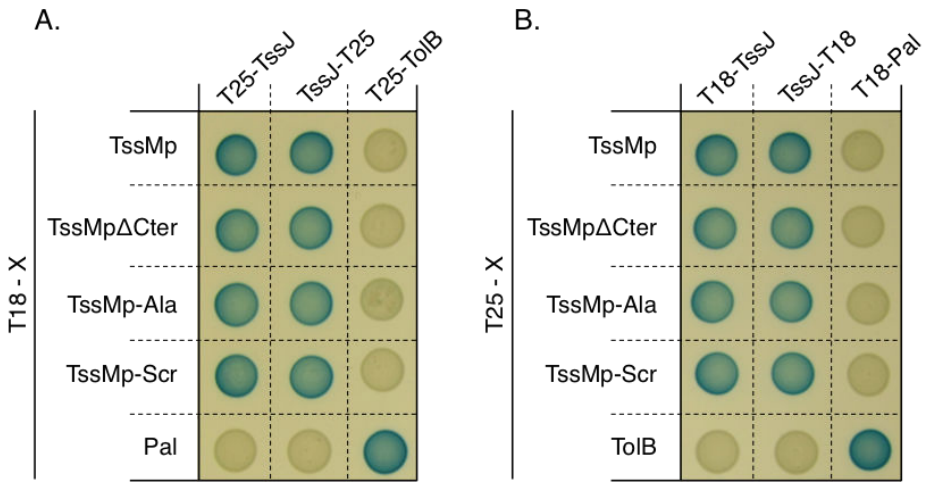

Figure 4.39: **TssM periplasmic variants interact with TssJ.** BTH101 reporter cells carrying pairs of plasmids producing the indicated T6SS proteins fused to the T18 or T25 domain of the Bordetella adelynate cyclase were spotted on X-Gal-IPTG indicator LB agar plates as described. Only periplasmic (p) soluble domains were used. Controls include T18 and T25 fusions to TolB and Pal, two proteins that interact but are unrelated to the T6SS.

Previous studies reported that the cytoplasmic part of TssM interacts with two components of the baseplate, TssG and TssK (Brunet et al., 2015b)(Zoued et al., 2013). The cytoplasmic domain of TssL also mediates contact with baseplate components: TssE and TssK (Zoued et al., 2013)(Zoued et al., 2016a). Thus, docking of the baseplate onto the membrane complex involves multiple contacts. Nevertheless, the cytoplasmic face of TssM appears to play an important role in the assembly of the T6SS, but we lack information on its architecture, structure and details on the interaction with the baseplate. Interestingly, the TssM cytoplasmic domains come into different flavours. Most TssM cytoplasmic domains harbour a Walker A motif, which is a typical motif associated with binding and hydrolysis of nucleotide triphosphate such as GTP and ATP. However, controversial data on the role of this TssM Walker A motif have been reported in the literature. In *Agrobacterium tumefaciens*, TssM-mediated ATP binding and hydrolysis has been shown to be essential for T6SS function and regulates conformational changes within the TssM periplasmic domain (Ma et al., 2009b)(Ma et al., 2012). By contrast, TssM variants bearing mutations within the Walker A motif are fully functional in *Edwarsiella tarda* (Zheng and Leung, 2007). We therefore decided to provide a detailed analysis of the EAEC TssM cytoplasmic domain and of the molecular interface between this domain and the baseplate components.

Article 3: Molecular dissection of the interface between the type VI secretion TssM cytoplasmic domain and the TssG baseplate component

Article 3: Molecular dissection of the interface between the type VI secretion TssM cytoplasmic domain and the TssG baseplate component

In this study, we conducted a topological study of TssM to define the boundaries of the different domains and trans-membrane segments. We then defined the interaction network of the cytoplasmic domain of TssM. Beside numerous attempts we did not succeed to purify the TssM cytoplasmic domain for *in vitro* protein interaction assays, biophysical characterization and X-ray crystallography. To gain information on the putative structure of this domain, we performed structural modelling based on homologous domain. Finally, we performed a structure-function analysis by targeting conserved residues and motifs and tested their contribution for TssM interactions.

Our results showed that the EAEC TssM protein is a polytopic IM protein bearing three transmembrane helices (TMH). The TssM N-terminus locates in the cytoplasm whereas the C-terminus locates in the periplasm. The TMH boundaries were defined by a cysteine accessibility assay using maleimide-propionyl biocytin, a thiol-reactive compound that crosses the outer membrane but unable to reach the cytoplasm. We found that the three TMH, at positions 13-29 (TMH1), 44-62 (TMH2) and 360-382 (TMH3) are oriented in-to-out, out-to-in and in-to-out, respectively. TMH2 and TMH3 delimitate a 35-kDa cytoplasmic domain ($TssM_{Cyto}$) that is conserved among TssM homologues. The bioinformatic analyses revealed that the TssM cytoplasmic domain comprises a subdomain with a nucleotide triphosphatase (NTPase)-like fold (residues 62-248), followed by a 110-amino-acid region (residues 249-360). This region comprises a dumpy-30 (DPY-30)-like motif, a dimerization motif initially found in the histone methyltransferase complex in eukaryotic cells. Interestingly, we found that although the EAEC TssM cytoplasmic domain comprises a NTPase-like subdomain, the Walkers A and B and NTP specific motifs are degenerated or are lacking. Therefore, the T6SS TssM proteins can be categorized in three families: (i) TssM with an active NTPase-domain such as in *A. tumefaciens*, (ii) TssM with an inactive NTPase-domain such as in *E. tarda*, and (iii) TssM with the classical NTPase fold but lacking the functional motifs such as in EAEC.

Then, I investigated the contribution of the two subdomains to the $TssM_{Cyto}$ interactions. The TssM NTPase-like subdomain mediates interaction with TssK, while the TssM DPY-30 motif is

involved in dimerization of $TssM_{Cyto}$ and interaction with TssG. Finally, I identified specific conserved motifs that mediate $TssM_{Cyto}$ dimerization (F278-E284) and interaction with TssG (L309-S315), and showed that these motifs are essential for T6SS function, sheath assembly and baseplate stability.

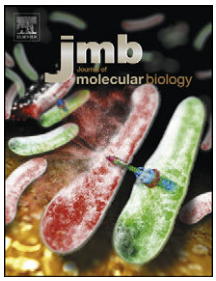

Molecular Dissection of the Interface between the Type VI Secretion TssM Cytoplasmic Domain and the TssG Baseplate Component

Laureen Logger, Marie-Stéphanie Aschtgen, Marie Guérin, Eric Cascales and Eric Durand

Laboratoire d'Ingénierie des Systèmes Macromoléculaires, *Institut de Microbiologie de la Méditerranée, Aix-Marseille Université, CNRS – UMR 7255, 31 Chemin Joseph Aiguier, 13402 Marseille Cedex 20, France*

Correspondence to Eric Cascales and Eric Durand: *cascales@imm.cnrs.fr; edurand@imm.cnrs.fr*
http://dx.doi.org/10.1016/j.jmb.2016.08.032
Edited by Bert Poolman

Abstract

The type VI secretion system (T6SS) is a multiprotein complex that catalyses toxin secretion through the bacterial cell envelope of various Gram-negative bacteria including important human pathogens. This machine uses a bacteriophage-like contractile tail to puncture the prey cell and inject harmful toxins. The T6SS tail comprises an inner tube capped by the cell-puncturing spike and wrapped by the contractile sheath. This structure is built on an assembly platform, the baseplate, which is anchored to the bacterial cell envelope by the TssJLM membrane complex (MC). This MC serves as both a tail docking station and a channel for the passage of the inner tube. The TssM transmembrane protein is a key component of the MC as it connects the inner and outer membranes. In this study, we define the TssM topology, highlighting a large but poorly studied 35-kDa cytoplasmic domain, $TssM_{Cyto}$, located between two transmembrane segments. Protein–protein interaction assays further show that $TssM_{Cyto}$ oligomerises and makes contacts with several baseplate components. Using computer predictions, we delineate two subdomains in $TssM_{Cyto}$, including a nucleotide triphosphatase (NTPase) domain, followed by a 110-aa extension. Finally, site-directed mutagenesis coupled to functional assays reveals the contribution of these subdomains and conserved motifs to the interaction with T6SS partners and to the function of the secretion apparatus.

Introduction

The type VI secretion system (T6SS) is a versatile multiprotein secretory machine that is implicated in both interbacterial competition and anti-eukaryotic host activities. The T6SS delivers a broad arsenal of toxins with peptidoglycan, phospholipid, or DNA hydrolysis activities or induces cytoskeleton rearrangements directly into the target cell [1–4].

For toxin delivery, the T6SS uses a contractile mechanism that is comparable to that of *Myoviridae* phages or R-pyocins [5–10]. This machine is composed of 13 core subunits, categorised in three subcomplexes [8,10–12]: a cytoplasmic tubular structure built on an assembly platform—or baseplate (BP)—that is evolutionarily, structurally, and functionally related to bacteriophage contractile tails [5,13–15] and is anchored to the cell envelope by a membrane complex (MC) [16].

The T6SS tail is composed of an inner tube made of stacked Hcp hexameric rings and is wrapped into a sheath-like structure, formed by the polymerisation of TssB–TssC heterodimeric complexes and that is assembled in an extended conformation [14,17–19]. Indeed, the assembly of the tail can be followed by time-lapse microscopy: fluorescent-labelled sheath components assemble a ~600-nm-long tubular structure in tens of seconds, which then contracts in a few milliseconds [14,20]. The contraction of the sheath coincides with bacterial prey lysis, suggesting that similar to phages, sheath contraction propels the inner tube towards the target cell, allowing the delivery of toxin effectors [8,11,20,21]. The assembly of the tube and the sheath is coordinated by TssA, a protein that controls the elongation of the tail at the distal end and that maintains the sheath under the extended conformation [22]. The inner tube is tipped by a spike constituted of a trimer of the VgrG

protein, which is proposed to puncture the target cell membrane [13,23]. The VgrG trimer is also part of the BP that is used as an assembly platform for the tail. Recently, the T6SS BP composition has been revealed. In addition to VgrG, it is composed of the TssE, -F, and -G subunits, the homologues of the phage T4 gp25, gp6, and gp7 proteins, respectively, and of TssK, a protein of unknown function with limited homologies to phage T4 gp8 or gp10 proteins that has been proposed to be a connector to the MC [15,24–27]. This MC is composed of the two TssL and TssM inner membrane (IM) proteins and of the TssJ outer membrane (OM) lipoprotein [28–32]. TssL and TssM interact in the IM, whereas the C-terminal periplasmic domain of TssM contacts the TssJ lipoprotein close to the OM [16,29,30,33–35]. The MC serves as a docking station for the BP and the tail but has also been proposed to serve as a channel for the passage of the inner tube during sheath contraction [16]. In the recent years, the assembly pathway of the T6SS has been well defined. T6SS biogenesis progresses from the OM to the cytoplasm. It starts with the positioning of the TssJ lipoprotein and the successive recruitments of TssM and TssL [16]. Recruitment of TssA then positions the BP complex onto the MC and primes the polymerisation of the tail tube/sheath [15,22,36]. This ordered assembly pathway requires tight contacts between the different subunits. Indeed, docking of the BP onto the MC requires multiple contacts including the interactions of TssE and TssK with TssL and of TssG and TssK with TssM [15,24]. TssM is therefore a key component as it mediates contact with the OM TssJ lipoprotein and with cytoplasmic BC subunits.

Here, we show that the enteroaggregative *Escherichia coli* (EAEC) TssM protein is a polytopic membrane protein, inserted into the IM by three transmembrane helices (TMH). The C-terminal portion of TssM is in the periplasm and interacts with TssJ [34]. TMH2 and TMH3 delimitates a ~35-kDa cytoplasmic domain, $TssM_{Cyto}$, which is conserved among TssM homologues. Computer analyses show that $TssM_{Cyto}$ is constituted of two subdomains: a subdomain with a nucleotide triphosphatase (NTPase)-like domain, followed by an extension. Indeed, TssM has been previously shown to bind and hydrolyse nucleotide triphosphates (NTPs) [37]. However, the role of the NTP-binding motif and its functional implication during T6SS activity are still a matter of debate [29,33]. The extension comprises a eukaryotic Dumpy-30 (DPY-30)-like dimerisation motif. We show that the NTPase-like domain mediates the interaction with TssK, whereas the extension is necessary and sufficient for $TssM_{Cyto}$ oligomerisation and interaction with TssG. Site-directed mutagenesis of conserved motifs within the extension revealed their contribution for $TssM_{Cyto}$ oligomerisation and $TssM_{Cyto}$–TssG interaction and for proper assembly of the T6SS. Our results thus provide details on the molecular interface between the T6SS membrane and the BP complexes.

Results

TssM is a polytopic IM protein

The TssM protein encoded within the EAEC *sci-1* gene cluster [EC042_4539; Genbank accession (GI): 284924260] is a large protein of 1129 aa. Based on hydrophobicity plots, the most widely used computer tools predict TssM as an IM protein with three TMH (Fig. 1a). Indeed, fractionation experiments showed that TssM co-fractionates with membrane proteins (data not shown). To experimentally define the TssM topology and determine the TMH boundaries, we performed a cysteine accessibility assay using the substituted cysteine accessibility method [38]. This assay relies on the ability of 3-(*N*-maleimidylpropionyl) biocytin (MPB), a sulfhydryl reagent, to cross the OM but not the IM of Gram-negative bacteria including EAEC [30,31]. TssM possesses nine native cysteine residues, with one (C727) predicted to locate in the periplasm. Hence, the wild-type (WT) TssM protein is labelled by MPB *in vivo* (Fig. 1b). In agreement with the computer predictions, a TssM protein, in which the cysteine at position 727 is substituted to serine (C727S), was not labelled with MPB (Fig. 1b). These data suggest that C727 is located in the periplasm, whereas all other eight cysteine residues are located in the cytoplasm or buried into the structure of the protein and are then inaccessible to MPB. We then introduced cysteine substitutions in the C727S TssM variant at various positions along the protein (at positions 37, 67, 352, and 386; Fig. 1a). All these mutated proteins were produced at similar levels (Fig. 1b) and were able to complement the effect of the *tssM* mutant in an Hcp secretion assay (data not shown). The A37C and S386C variants were biotinylated with MPB, suggesting that the A37 and S386 residues are located in the periplasm (Fig. 1b). By contrast, the V67C and S352C variants were not labelled, indicating that the V67 and S352 residues are located in the cytoplasm (Fig. 1b). Altogether, the data of the cysteine accessibility defined the topology of TssM; TssM is constituted of three TMH, with the N terminus in the cytoplasm and the C terminus in the periplasm. TssM spans the IM through two TMH-oriented in-to-out (TMH1, residues 13–29; TMH3, residues 360–382) and one TMH-oriented out-to-in (TMH2, residues 44–62; Fig. 1c). TMH2 and TMH3 thus delimitate a ~35-kDa domain located in the cytoplasm, called $TssM_{Cyto}$ hereafter.

The cytoplasmic domain of TssM oligomerises and interacts with the components of the T6SS membrane and BP complexes

The topology of TssM indicates the existence of two soluble domains, one in the periplasm ($TssM_{Peri}$,

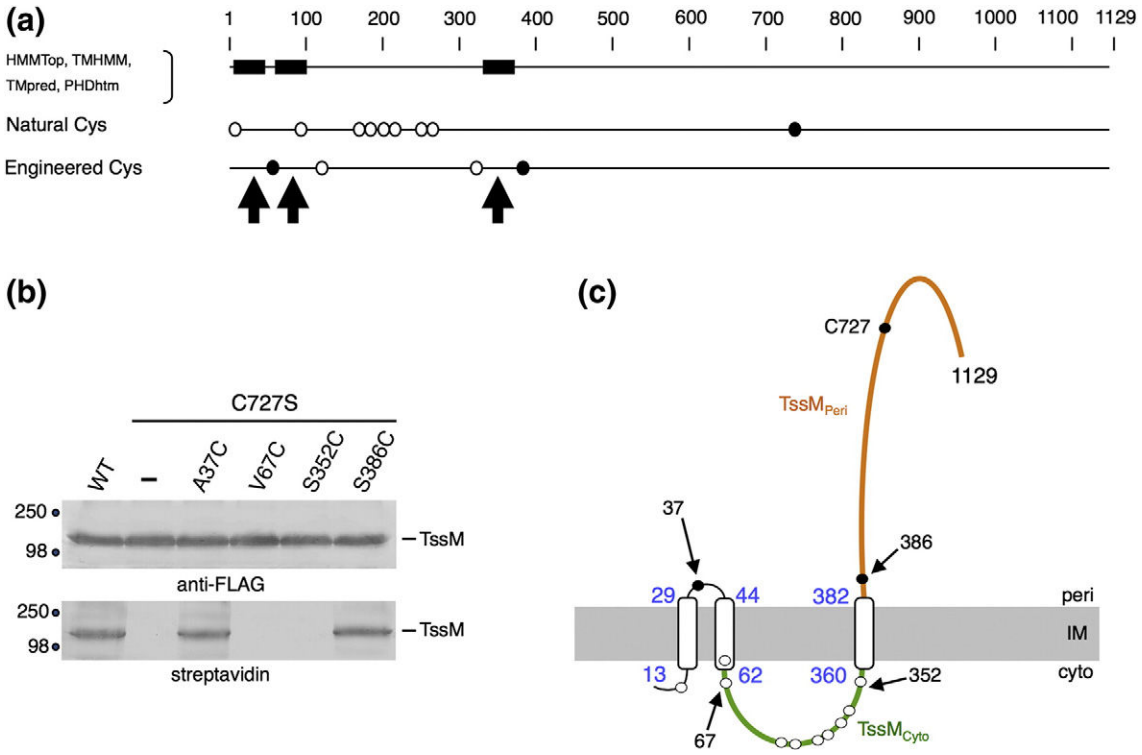

Fig. 1. TssM is a polytopic IM protein. (a) The transmembrane helices (TMH) predicted using the algorithms listed on the left are represented by black rectangles. The EAEC Sci-1 TssM natural cysteine residues and the cysteine substitutions engineered in this study are indicated. Filled circles indicate cysteine residues labelled with the 3-(*N*-maleimidylpropionyl) biocytin (MPB) probe, whereas open circles indicate unlabelled cysteine residues. Arrowheads indicate transmembrane segments determined experimentally. (b) Accessibility of cysteine residues. Whole EAEC Δ*tssM* cells producing WT TssM (WT) or the indicated mutant proteins were labelled with the MPB probe, lysed, and solubilised, and TssM and mutant proteins were immunoprecipitated with anti-FLAG-coupled beads. The precipitated material was subjected to SDS-PAGE and Western blot analysis using anti-FLAG antibody (TssM detection, upper panel) and streptavidin coupled to alkaline phosphatase (MPB-labelled TssM detection, lower panel). Molecular weight markers are indicated on the left. (c) Topology model for the EAEC TssM protein at the IM. The localisations of the labelled and unlabelled cysteine residues are indicated by filled and open circles, respectively. The cytoplasmic ($TssM_{Cyto}$) and periplasmic ($TssM_{Peri}$) domains are highlighted in green and orange, respectively. The three transmembrane segments identified by the accessibility studies are shown, with their membrane boundaries (in blue).

amino acids 383–1129) and one residing into the cytoplasm ($TssM_{Cyto}$, amino acids 63–359). The T6SS is a multiprotein complex in that the large protein domains might be necessary for interacting with other T6SS components. Indeed, we and others have previously demonstrated that $TssM_{Peri}$ interacts with the TssJ OM lipoprotein in *Edwardsiella tarda* and EAEC [33,34]. By contrast, little is known regarding the cytoplasmic domain of TssM. To gain further insights into $TssM_{Cyto}$ partners, we used $TssM_{Cyto}$ as a bait for an *in vivo* systematic, bacterial two-hybrid assay. $TssM_{Cyto}$ was fused to the T18 domain of the *Bordetella* adenylate cyclase, and all the other T6SS proteins—or soluble domains—were fused at their N or C terminus of the T25 domain. The results presented in Fig. 2 show that $TssM_{Cyto}$ interacts with itself and TssK whatever the constructions used. In addition, $TssM_{Cyto}$ interacts with TssG and the cytoplasmic domain of TssL ($TssL_{Cyto}$) when fused at the N terminus of T25. In conclusion, $TssM_{Cyto}$ is capable of oligomerisation and interacts with the components of the T6SS membrane ($TssL_{Cyto}$) and BP (TssK and TssG) complexes. These results are in agreement with the previously published bacterial two-hybrid screens and co-immunoprecipitations that identified TssM–TssK, TssM–TssL, and TssM–TssG interactions [15,24,29,30].

Subdomain architecture of $TssM_{Cyto}$

Pfam, Blast, and HHPred analyses suggest that EAEC $TssM_{Cyto}$ is organised as an NTPase domain ($TssM_{Cyto/NTP}$; amino acids 62–248; Pfam accession: PF06858), followed by a C-terminal extension ($TssM_{Cyto/Ct}$; amino acids 254–360; Fig. 3 and Supplementary Figs. S1 and S2). However, despite

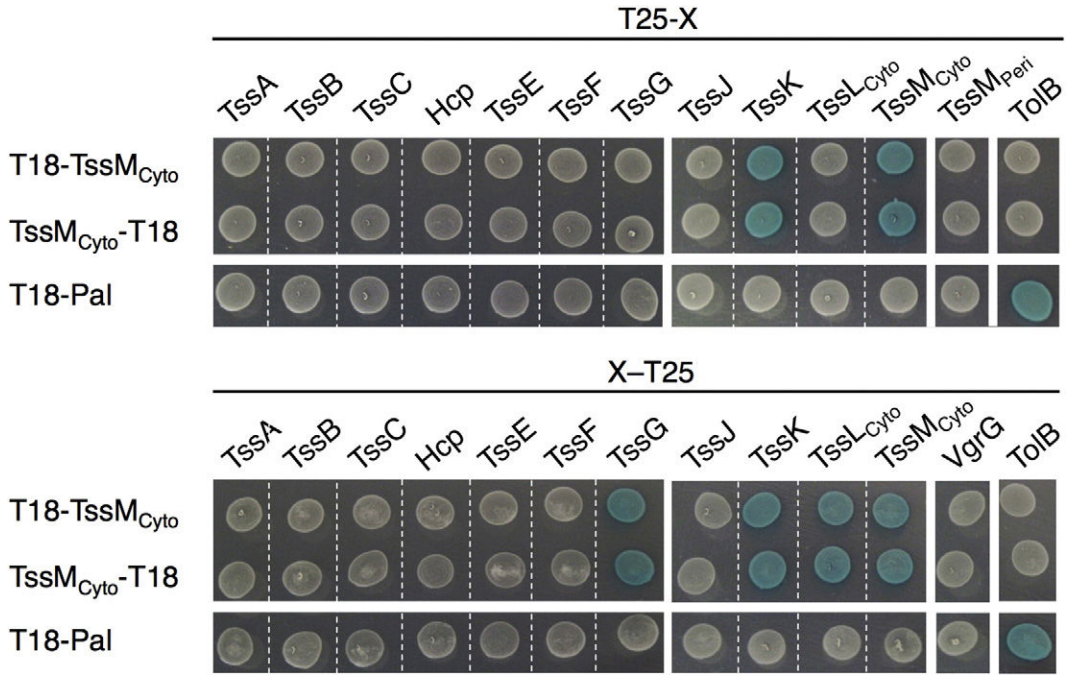

Fig. 2. TssM$_{Cyto}$ interaction network identified by bacterial two-hybrid analysis. BTH101 reporter cells carrying pairs of plasmids producing the indicated T6SS proteins fused to the T18 or T25 domain of the *Bordetella* adenylate cyclase were spotted on X-Gal-IPTG indicator LB agar plates. Only the cytoplasmic (Cyto) or periplasmic (Peri) domains were used for membrane-anchored proteins. Controls include T18 and T25 fusions to TolB and Pal, two proteins that interact but are unrelated to the T6SS.

the fact that the overall NTPase domain is conserved among the TssM$_{Cyto}$ homologues, the sequence alignment shows that the NTP-binding and hydrolysis motifs (Walkers A & B and NTP specific motif) are not well conserved (Supplementary Fig. S1). In agreement with this observation, an evolutionary analysis of TssM$_{Cyto}$ NTPase domains shows that they categorise into two subgroups: while the TssM proteins encoded within the *Pseudomonas aeruginosa* H1, *Agrobacterium tumefaciens*, and *E. tarda* T6SS gene clusters carry a complete NTPase domain, a number of TssM, including that of EAEC, *Serratia*, and *Citrobacter*, possess an NTPase domain amputated of hydrolysis motifs (Supplementary Figs. S1 and S2).

Our attempts to produce and purify the EAEC TssM$_{Cyto}$ domain or the TssM$_{C}$ NTPase subdomain in order to gain structural information were unsuccessful, as the different constructs used were all insoluble. Consequently, we sought to construct homology-based models of both TssM$_{Cyto}$ subdomains using a bioinformatic approach. The TssM$_{Cyto/NTP}$ structure was predicted using HHpred [39]. The program confirmed that the EAEC TssM$_{Cyto/NTP}$ protein resembles the solved structure of various Guanosine triphosphate (GTP)-hydrolysing proteins (Supplementary Fig. S3). The X-ray structure of the *Burkholderia thailandensis* EngB GTP-binding protein (PDB ID: 4DHE) [40] was subsequently used as template to build a homology model of the EAEC TssM$_{Cyto/NTP}$ domain. Figure 3 shows that TssM$_{Cyto/NTP}$ adopts a compact fold consisting of a four-stranded parallel β-sheet with one side being in contact with three α-helices. The TssM$_{Cyto/NTP}$ domain belongs to the α/β class, harbouring an incomplete Rossmann fold, a motif associated with nucleotide-binding proteins [41]. The EAEC TssM$_{Cyto/NTP}$ architecture is typical of P-loop NTP hydrolases. The predicted structure of EAEC TssM$_{Cyto/NTP}$ diverges, however, from the classical αβα sandwich architecture, as the second α-helix is not strictly sandwiching the β-strand. As expected, the large loops that bear the binding and hydrolysis motifs are absent in the EAEC TssM$_{Cyto/NTP}$, by contrast to EngB or the homology model of the *A. tumefaciens* TssM$_{Cyto/NTP}$ domain (Supplementary Fig. S4). The TssM$_{Cyto/Ct}$ homology model was constructed using the Swiss-Model server based on the X-ray structure of the C-terminal domain of human DPY-30-like protein, a component of the eukaryotic histone methyltransferase complex (PDB ID: 3G36) [42], as template (Supplementary Fig. S3). The TssM$_{Cyto/Ct}$ structure was confidently modelled from residue Q254 to N289 (Fig. 3). This fragment encompasses the two-helix 40-aa DPY-30 motif (Pfam accession: PF05186) found in DPY-30 proteins and is involved in DPY-30 dimerisation [42].

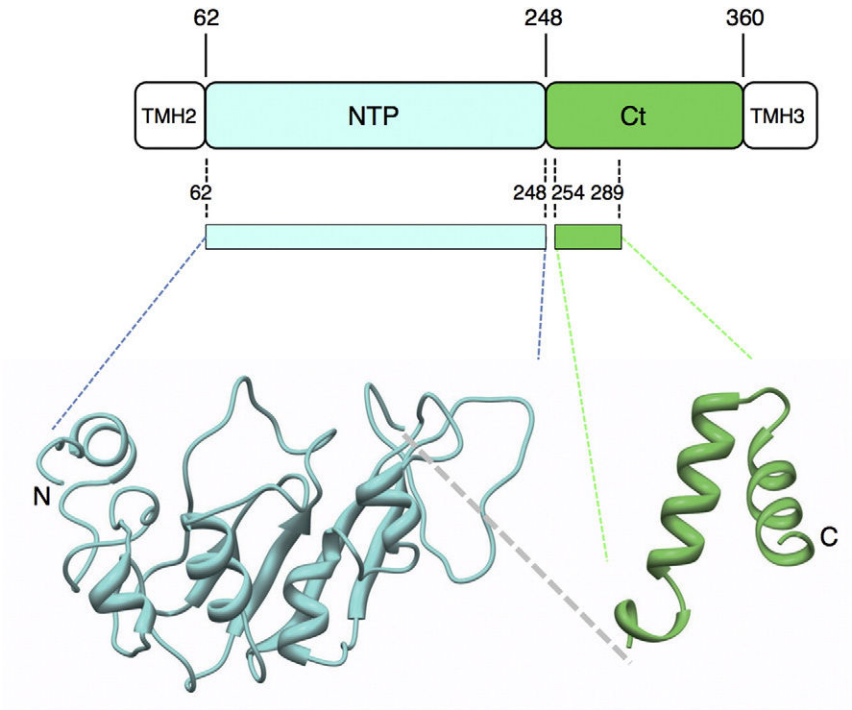

Fig. 3. Structural architecture of $TssM_{Cyto}$. (a) The cytoplasmic domain of TssM and $TssM_{Cyto}$, delimitated by the TMH2 and TMH3 could be partitioned into an NTPase-like domain (NTP, blue) and a C-terminal extension (Ct, green). $TssM_{Cyto/NTP}$ was modelled using HHpred based on the X-ray structure of the *Burkholderia thailandensis* EngB GTP-binding protein (PDB ID: 4DHE). $TssM_{Cyto/Ct}$ was modelled using SwissModel based on the X-ray structure of the C-terminal domain of the human DPY-30-like protein, a component of the histone methyltransferase complex (PDB ID: 3G36). All images were made with Chimera [66].

Specific motifs are involved in $TssM_{Cyto}$ oligomerisation and interaction with TssG

The structural organisation of $TssM_{Cyto}$ prompted us to investigate the contribution of the two subdomains to the $TssM_{Cyto}$ interactions. The interaction network of $TssM_{Cyto/NTP}$ and $TssM_{Cyto/Ct}$ was assessed by bacterial two-hybrid. As shown in Fig. 4a, $TssM_{Cyto/NTP}$ interacts with TssK, whereas $TssM_{Cyto/Ct}$ mediates oligomerisation and interactions with TssG and $TssL_{Cyto}$. Interestingly, the interaction network of the isolated subdomains, $TssM_{Cyto/NTP}$ and $TssM_{Cyto/Ct}$, recapitulates the interaction network of $TssM_{Cyto}$ (Fig. 4a), supporting the hypothesis of two independently folded domains. The $TssM_{Cyto/Ct}$–TssG and $TssM_{Cyto/NTP}$–TssK interactions were further confirmed by co-immunoprecipitation experiments; TssG was co-precipitated with $TssM_{Cyto}$ and $TssM_{Cyto/Ct}$ (Fig. 4b, upper panel). As previously shown [24], TssK did not interact with $TssM_{Cyto}$ by co-immunoprecipitation. However, our results suggest that it is prevented by the extension, as the $TssM_{Cyto/NTP}$ domain alone interacts with TssK (Fig. 4B, lower panel).

Interestingly, the $TssM_{Cyto/Ct}$ subdomain interacts with several partners from the membrane and BP subcomplexes. We therefore questioned whether these different interactions involve the same recognition motif or different binding epitopes on $TssM_{Cyto}$. The sequence alignment of $TssM_{Cyto}$ homologues emphasised two well-conserved regions, F278-E284 and L309-S315 (Supplementary Fig. S1). Region F278-E294 is specifically conserved in $TssM_{Cyto}$ lacking functional NTPase domain, whereas the L309-S315 motif is conserved among all $TssM_{Cyto}$ (Supplementary Fig. S1). Using site-directed mutagenesis, we engineered $TssM_{Cyto}$ variants in which these motifs were targeted. Although these two motifs do not appear to be involved in $TssM_{Cyto}$–$TssL_{Cyto}$ interactions, substitutions within the L309-S315 motif specifically abolished the $TssM_{Cyto}$–TssG interaction (Fig. 5a and B). We also noted that the substitutions within the F278-E284 motif impacted $TssM_{Cyto}$ oligomerisation. However, although the L279W and L282W/A283W mutations prevented the interaction with $TssM_{Cyto}$ in the bacterial two-hybrid assay (Fig. 5a), only the L279W mutations had a strong effect on multimerisation in the co-immunoprecipitation assay (Fig. 5b). It is worthy to note that the $TssM_{Cyto/Ct}$ F278-E284 residues correspond to the dimerisation motif in DPY-30 proteins (Supplementary Fig. S4B).

$TssM_{Cyto}$ oligomerisation and interaction with the TssG BP subunit are critical for T6SS function

The mutations that specifically affect $TssM_{Cyto}$ oligomerisation and $TssM_{Cyto}$–TssG complex formation were tested for their repercussion on T6SS function. EAEC Sci-1 T6SS function could be monitored by measuring its antibacterial activity [43]. The four TssM substitutions were introduced within the native, chromosomal *tssM* gene. Figure 6a shows that all four mutated strains were defective in T6SS-dependent killing of prey bacterial cells. We therefore conclude that $TssM_{Cyto}$ oligomerisation and interaction with TssG are required for the proper function of the type VI secretion apparatus.

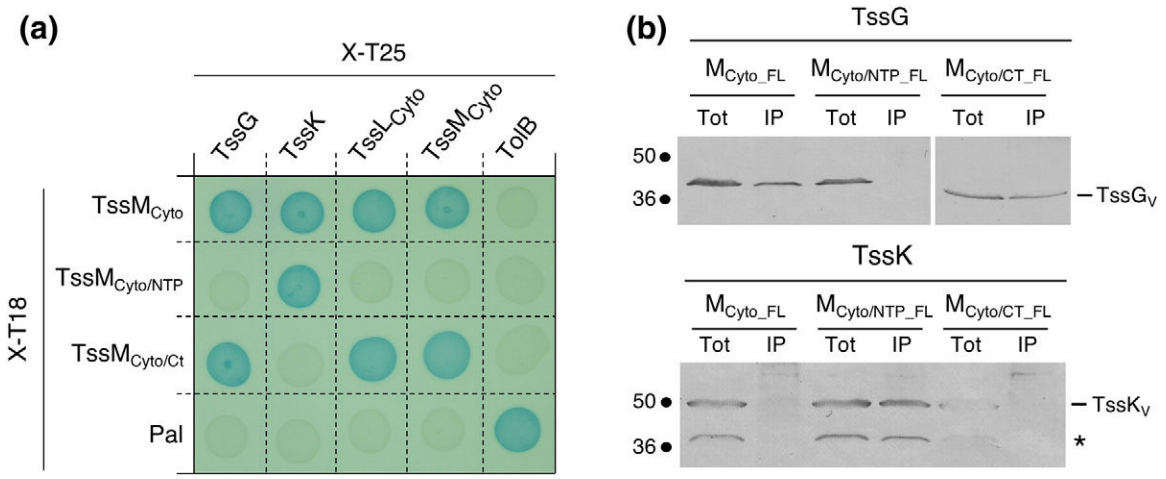

Fig. 4. The two TssM$_{Cyto}$ subdomains mediate the interaction with two BP components. (a) Bacterial two-hybrid assay. BTH101 reporter cells carrying pairs of plasmids producing the indicated T6SS proteins fused to the T18 or T25 domain of the *Bordetella* adenylate cyclase were spotted on X-Gal-IPTG indicator LB agar plates. Only the cytoplasmic ($_C$) or periplasmic ($_P$) domains were used for membrane-anchored proteins. Controls include T18 and T25 fusions to TolB and Pal, two proteins that interact but are unrelated to the T6SS. (b) Co-immunoprecipitation assay. Soluble lysates from 5×10^{10} *E. coli* K12 W3110 cells producing FLAG-tagged TssM$_{Cyto}$ (M$_{Cyto_FL}$), FLAG-tagged TssM$_{Cyto/NTP}$ (NTP$_{FL}$) or FLAG-tagged TssM$_{Cyto/Ct}$ (Ct$_{FL}$), and VSV-G-tagged TssG (TssG$_V$) or TssK (TssK$_V$) proteins were subjected to immunoprecipitation with anti-FLAG-coupled beads. The total soluble (Tot) and the immunoprecipitated (IP) material were separated by 12.5% acrylamide SDS-PAGE and immunodetected with anti-VSVG (TssG$_V$ or TssK$_V$) monoclonal antibodies. Molecular weight markers (in kDa) are indicated on the left. The asterisk on the lower panel indicates a degradation product from the TssK protein.

T6SS biogenesis starts with the assembly of the MC and is followed by (i) the recruitment of the BP and (ii) tail polymerisation. We therefore sought to define which stage of T6SS biogenesis is impacted by these mutations. We first tested the effects of these mutations on T6SS sheath assembly by following the

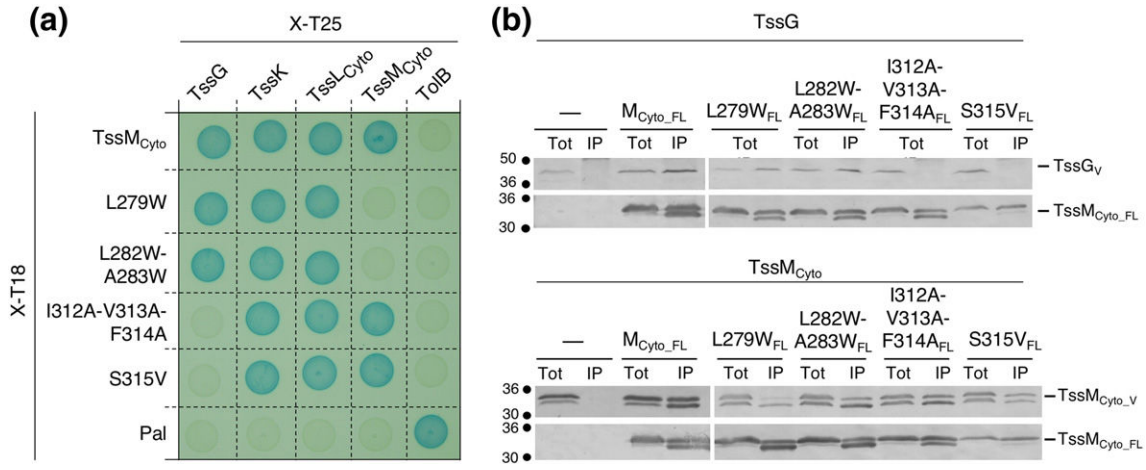

Fig. 5. Specific conserved motifs mediate TssM$_{Cyto}$ dimerisation and interaction with TssG. (a) Bacterial two-hybrid assay. BTH101 reporter cells carrying pairs of plasmids producing the indicated T6SS proteins fused to the T18 or T25 domain of the *Bordetella* adenylate cyclase were spotted on X-Gal-IPTG indicator LB agar plates. Only the cytoplasmic ($_C$) or periplasmic ($_P$) domains were used for membrane-anchored proteins. Controls include T18 and T25 fusions to TolB and Pal, two proteins that interact but are unrelated to the T6SS. (b) Co-immunoprecipitation assay. Soluble lysates from 5×10^{10} *E. coli* K12 W3110 cells producing FLAG-tagged TssM$_C$ WT (M$_{Cyto_FL}$) or mutants and VSV-G-tagged TssG (TssG$_V$) or TssM$_{Cyto}$ (TssM$_{Cyto_V}$) proteins were subjected to immunoprecipitation with anti-FLAG-coupled beads. The total soluble (Tot) and the immunoprecipitated (IP) material were separated by 12.5% acrylamide SDS-PAGE and immunodetected with anti-FLAG (lower panels) and anti-VSV-G (upper panels) monoclonal antibodies. Molecular weight markers (in kDa) are indicated on the left.

dynamics of a chromosomally encoded TssB-sfGFP fusion using fluorescence microscopy (Fig. 6b). All the substitutions severely affected T6SS sheath assembly as indicated by the decrease in the number of sheath per bacterial cell (Fig. 6b). While ~25% of the WT cells assembled sheath structures, the TssBC sheath assembled on rare occasions in cells carrying mutations affecting $TssM_{Cyto}$ oligomerisation (3–4% of cells with sheath structures). The effect of the $TssM_{Cyto}$–TssG disruption was even more drastic, as sheath assembly was observed in ~1% of the cells.

Second, we tested the effect of these mutations on the recruitment of the BP. By following the dynamics of a sfGFP–TssF fusion, a recent study concluded that the MC recruits and stabilises the T6SS BP [15]. We therefore investigated whether the mutations affecting the oligomerisation of the cytoplasmic loop of TssM and the contacts between this loop and the TssG BP component impact BP assembly, stability, and recruitment. As TssG-to-sfGFP fusions were previously shown to be nonfunctional [15], we introduced the TssM point mutations in a strain producing the chromosomal and functional sfGFP–TssF fusion, which is a TssG protein partner, and we monitored the formation and stability of BP foci by fluorescence microscopy (Fig. 6c). All four mutations significantly decreased the number of cells with sfGFP–TssF foci

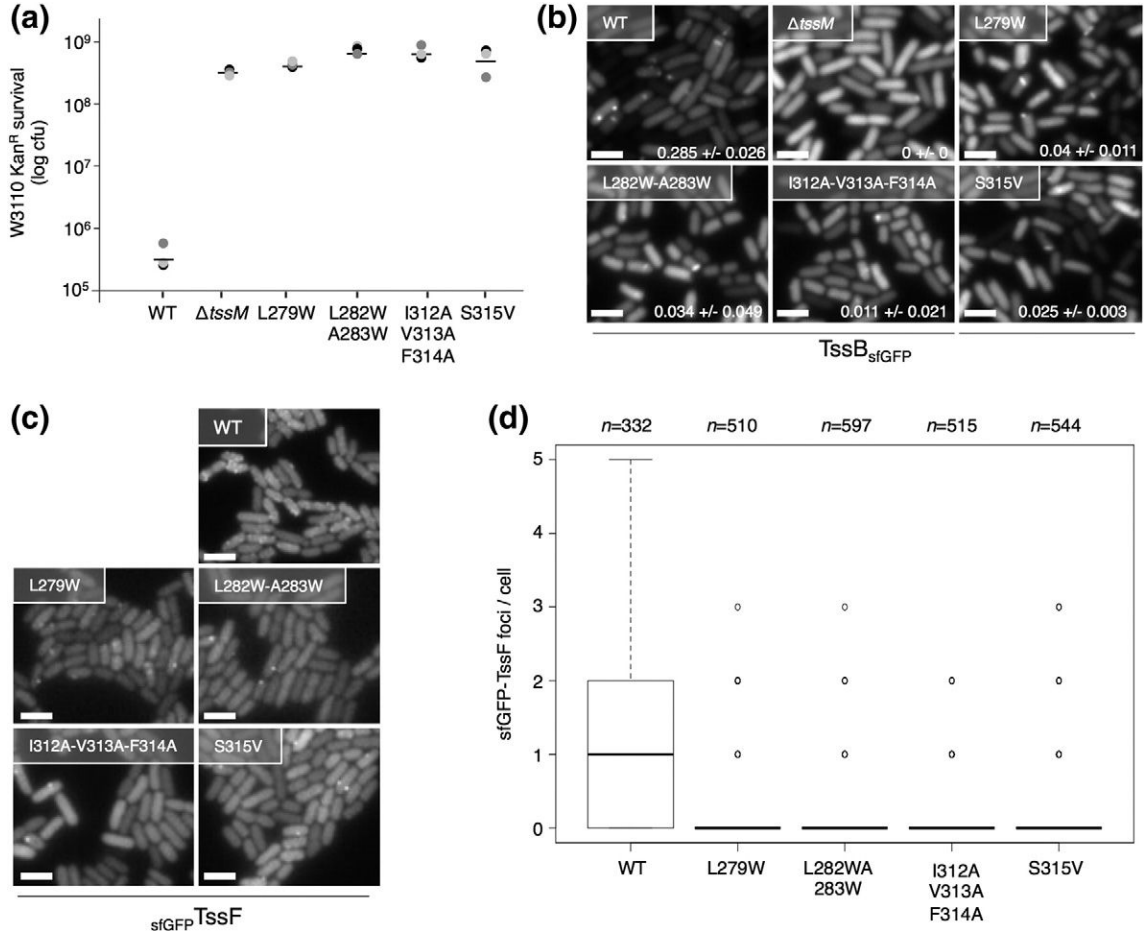

Fig. 6. $TssM_{Cyto}$ oligomerisation and interaction with the TssG BP are essential for T6SS function, sheath assembly, and BP stability. (a) Antibacterial assay. *E. coli* K-12 prey cells (W3110 *gfp*$^+$, kan^R) were mixed with the indicated attacker cells, spotted onto SIM agar plates, and incubated for 4 h at 37 °C. The number of recovered *E. coli* prey cells is indicated in the graph (in log10 of colony-forming unit). The circles indicate values from three independent assays, and the average is indicated by the bar. (b) Image recordings of the TssB-sfGFP fusion protein in the indicated cells. Statistical analyses (*n* = number of sheath/cell) are indicated under each strain. The number of cells studied per strain (*n*) is 150. The scale bar represents 2 μm. (c) Image recordings of the super folder Green Fluorescent Protein (sfGFP)–TssF fusion protein in the indicated cells. The scale bar represents 2 μm. (d) Statistical analyses of sfGFP–TssF in the indicated strains. Shown are box-and-whisker plots of the measured number of sfGFP–TssF foci per cell for each strain with the lower and upper boundaries of the boxes corresponding the 25% and 75% percentiles, respectively. The black bold horizontal bar represents the median values for each strain, and the whiskers represent the 10% and 90% percentiles. Outliers are shown as an open circle. *n* indicates the number of cells analysed per strain.

and the average number of foci per cell (1 cluster in 15–25% of the mutated cells compared to 1–3 foci in ~65% for WT cells; Fig. 6c and d). Taken together, these data demonstrate that the mutations that affect $TssM_{Cyto}$ oligomerisation and $TssM_{Cyto}$–TssG complex formation abolish T6SS sheath formation and function by impacting T6SS BP assembly and stability.

Discussion

In this manuscript, we report the characterisation of the cytoplasmic domain of the T6SS membrane core complex protein TssM from EAEC. We showed that $TssM_{Cyto}$ comprises two subdomains, a domain resembling NTPases but lacking nucleotide-binding and hydrolysis motifs, followed by a ~110-aa extension. Protein–protein interaction studies revealed that this extension mediates $TssM_{Cyto}$ oligomerisation and interaction with the TssG BP subunit. We finally defined the specific motifs involved in these interactions and reported that these interactions are critical for the assembly of a functional T6SS. Models summarizing the findings reported in this study are depicted in Fig. 7.

We first defined the boundaries of the TssM transmembrane segments using cysteine accessibility experiments. We determined that TssM is constituted of three TMH. The TssM N terminus locates in the cytoplasm and is followed by a transmembrane hairpin, a cytoplasmic domain, and the third TMH, TMH3. Finally, the ~750-aa C-terminal domain locates in the periplasm (Fig. 1c). This topology is similar to the topology of the *A. tumefaciens* TssM protein previously defined using translational reporter fusions [29]. Computer analyses of TssM proteins encoded within well-studied T6SS gene cluster showed that this topology is likely shared among all the homologues with the notable exception of the *P. aeruginosa* H1-T6SS TssM protein that is predicted to have a single TMH corresponding to TMH3 (Supplementary Fig. S5).

The topology experiments also defined that TssM TMH2 and TMH3 delimit a 35-kDa cytoplasmic domain, $TssM_{Cyto}$. Our data showed that $TssM_{Cyto}$ oligomerises and interacts with $TssL_{Cyto}$. The $TssM_{Cyto}$–$TssM_{Cyto}$ and $TssM_{Cyto}$–$TssL_{Cyto}$ interactions have been reported in the *A. tumefaciens* T6SS [29]. The conservation of $TssM_{Cyto}$ oligomerisation and the interaction with $TssL_{Cyto}$ between *A. tumefaciens* and EAEC suggest that these contacts are important for T6SS function. Indeed, mutation of L279, a residue that participates to $TssM_{Cyto}$ oligomerisation, severely impacts T6SS function in EAEC. The low resolution of the recently

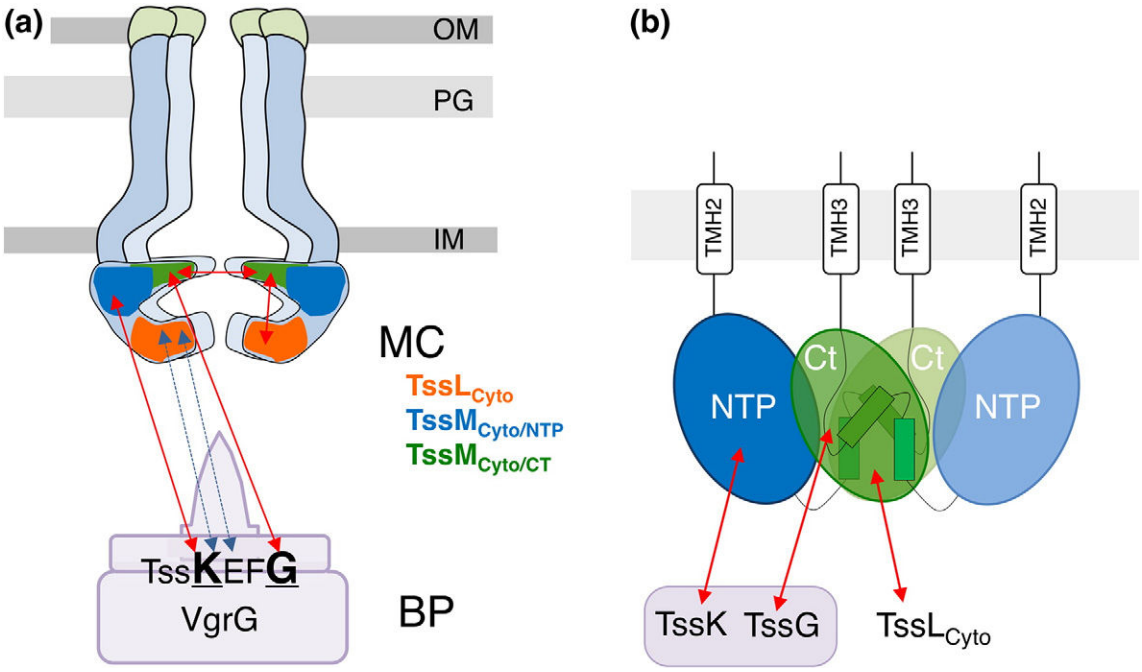

Fig. 7. Schematic representation of the $TssM_{Cyto}$ interaction network. (a) Schematic representation of the TssJLM MC and its interactions with the TssKEFG–VgrG BP complex. The $TssM_{Cyto/NTP}$ and $TssM_{Cyto/Ct}$ and the TssL cytoplasmic domain ($TssL_{Cyto}$) are shown in blue, green, and orange, respectively. The interactions defined in this study are indicated by red arrows. Interactions determined previously [24] or in the accompanying article [69] are shown in blue dashed arrows. (b) Schematic representation of a $TssM_{Cyto}$ dimer ($TssM_{Cyto/NTP}$ are shown in blue; $TssM_{Cyto/Ct}$ are shown in green). The cartoon highlights the $TssM_{Cyto/Ct}$–$TssM_{Cyto/Ct}$ interface and the interaction with TssK, TssG, and the cytoplasmic domain of TssL.

published electron microscopy map of the 5-fold symmetry TssJLM MC does not allow the of use docking simulations to precisely locate the TssM cytoplasmic domain and therefore provide insight onto its oligomeric state in the complex. However, stoichiometry analyses and reconstruction of the MC suggested that it is constituted of five dimers of the TssJLM heterotrimers [16]. These information suggest that, similar to the TssL cytoplasmic domain [32], $TssM_{Cyto}$ dimerises. The biogenesis of the MC may therefore start with the formation of dimers of the heterotrimers that will then symmetrise. Based on the $TssM_{Cyto}$ interaction with the TssL cytoplasmic domain, it has been proposed that these two domains form the large base of the T6SS MC [16]. This cytoplasmic base corresponds to the docking site for the TssEFGK–VgrG BP complex [15,16,22]. Indeed, our bacterial two-hybrid and co-immunoprecipitation experiments confirmed that $TssM_{Cyto}$ interacts with two BP components, TssK and TssG (Fig. 7).

Bioinformatic analyses predict that $TssM_{Cyto}$ comprises an N-terminal NTPase domain and a C-terminal DPY-30-like domain named $TssM_{Cyto/NTP}$ and $TssM_{Cyto/Ct}$, respectively. However, although the EAEC $TssM_{Cyto/NTP}$ domain belongs to the NTPase fold, it misses the specific binding and hydrolysis motifs found in functional NTPases, such as the Walker A and B motifs. Sequence alignment of $TssM_{Cyto/NTP}$ domains from various bacterial species revealed that they categorise in two subfamilies. While a number of $TssM_{Cyto/NTP}$ domains do not carry these motifs, other TssM possess Walker A and B signatures, including that of *A. tumefaciens*, *E. tarda*, or *P. aeruginosa* H1-T6SS (Supplementary Fig. S2). Indeed, the detergent-solubilised *A. tumefaciens* TssM protein exhibits ATPase activity [37]. However, mutations of these motifs in *A. tumefaciens* and *E. tarda* did not have the same impact on the function of the T6SS. Production of the K124A TssM variant in *Edwardsiella* was fully functional as shown by T6SS-dependent Hcp, VgrG, and EvpP release [33]. By contrast, ATP binding and hydrolysis regulate conformational changes within the periplasmic domain of the *A. tumefaciens* TssM protein, and the *Agrobacterium* TssM K145A variant is unable to restore Hcp release [29,37]. Therefore, $TssM_{Cyto/NTP}$ domains come in different flavours: active NTPase domains (e.g., *A. tumefaciens*), inactive NTPase domains (e.g., *E. tarda*), and NTPase fold lacking the functional motifs (e.g., EAEC). Interestingly, our protein–protein interaction studies showed that $TssM_{Cyto/NTP}$ contacts TssK. In the case of TssM with functional NTP domains, it would be interesting to test whether the presence of TssK influences NTP binding and hydrolysis.

The $TssM_{Cyto}$ C-terminal extension shares structural homologies with the dimerisation motif of DPY-30, a subunit of the histone methyltransferase complex in eukaryotic cells. This two-α-helix motif forms an antiparallel bundle at the dimer interface, which is mediated by extensive hydrophobic and van der Waals interactions (Supplementary Fig. S4) [42]. Indeed, this DPY-30-like hairpin and, notably, the conserved L279 residues are involved in $TssM_{Cyto}$ oligomerisation. In addition to its role in $TssM_{Cyto}$ oligomerisation, this subdomain is also required for proper interaction with the cytoplasmic domain of TssL and $TssL_{Cyto}$ and with TssG, one of the components of the T6SS BP (Fig. 7). Whereas we have not identified in this study the residues of $TssM_{Cyto/Ct}$ mediating the interaction with $TssL_{Cyto}$, a conserved hydrophobic sequence (L-A-G-I-V-F-S in EAEC) is required for $TssM_{Cyto}$–TssG complex formation. Taken together, our results show that this relatively small subdomain is responsible for several interactions. Interestingly, a similar case has been reported for DPY-30, which is a partner of several complexes involved in the regulation of chromatin and nucleosome organisation [44]. One may hypothesise that $TssM_{Cyto/Ct}$ uses its DPY-30-like domain to interact sequentially with its different protein partners. Purification of the $TssM_{Cyto}$–$TssL_{Cyto}$–TssG complex or the high-resolution structure of the different binary complexes involving $TssM_{Cyto/Ct}$ will shed light on the dynamic nature of these interactions.

The interactions between $TssM_{Cyto}$ and TssK and TssG, the two components of the BP complex, might be important to recruit or stabilise the BC at the cytoplasmic base of the TssJLM MC. In addition to this structural role, it is likely that these interactions are required for proper function of the BP. As shown for other contractile structures such as bacteriophages, the BP serves as an assembly platform for the tail but is also responsible for initiating sheath contraction [26,45–47]. The $TssM_{Cyto}$–TssG interaction might therefore be important to regulate BP assembly, recruitment or sheath assembly, and/or contraction. Indeed, point mutations disrupting the $TssM_{Cyto}$–TssG interaction destabilise the BP complex and prevent the elongation of the tail sheath. It is interesting to note that TssM undergoes structural transitions [37], and one may suggest that TssM conformational changes might be transduced to the BP *via* the $TssM_{Cyto/NTP}$–TssK and/or $TssM_{Cyto/Ct}$–TssG interactions leading to sheath assembly. As TssM has a large periplasmic domain and a short extension that lies outside of the cell [16], it is a strong candidate to sense the modifications of the cell envelope, such as an attack by neighbouring cells or a contact with a prey, and to transmit the information to the BP complex. Further experiments will provide insights on how sheath assembly and/or contraction are regulated.

Our results also pointed that mutations disrupting $TssM_{Cyto}$ oligomerisation and $TssM_{Cyto}$–TssG complex formation affect T6SS-dependent activities, as they abolish TssBC sheath assembly and inhibit

bacterial prey killing. The drastic effect of these mutations makes these interactions attractive targets for the rationale design of drugs that, by binding to $TssM_{Cyto}$, would hamper the T6SS activity and the delivery of harmful toxins. This approach has been successfully achieved in the case of the *Brucella* type IV secretion VirB8 IM subunit for which specific inhibitors of its dimerisation were identified by a high-throughput bacterial two-hybrid screen and were further shown to inhibit *Brucella* infection of macrophages [48,49]. This example emphasises the importance of understanding protein–protein interactions in bacterial secretion systems with the ultimate goal of targeting specific interactions with small-molecule inhibitors.

Materials and Methods

Bacterial strains, media, growth conditions, and chemicals

Strains used in this study are listed in Supplementary Table S1. *E. coli* K-12 DH5α, BTH101, and W3110 were used for cloning procedures, bacterial two-hybrid, and co-immunoprecipitation, respectively. The *E. coli* K-12 W3110 strain carrying the pUA66-*rrnB* plasmid (*gfp* under the control of the constitutive *rrnB* ribosomal promoter specifying strong and constitutive fluorescence and kanamycin resistance) [50] was used as prey in antibacterial competition experiments. EAEC strain 17-2 and its Δ*tssM*, *tssB-GFP*, and *GFP-tssF* derivatives [15,24,30] were used in this study. Chromosomal fluorescent reporter insertions were obtained using the modified one-step inactivation procedure [51] using the red recombinase expressed from pKOBEG [52], as previously described [28], using p*gfp*-KD4 as a template for PCR amplification. Briefly, the sfGFP-coding sequence and the kanamycin cassette were amplified from the p*gfp*-KD4 vector [15] with oligonucleotides carrying 50-nt extensions homologous to regions that are adjacent to the site of insertion. The PCR product was column purified (PCR and Gel Clean up kit, Promega) and electroporated. Kanamycin-resistant clones were recovered, and the insertion of the kanamycin cassette at the targeted site was verified by PCR. Kanamycin cassettes were then excised using pCP20 [51]. *tssM* point mutations were engineered at the native locus on the chromosome by allelic replacement using the pKO3 suicide vector [53,54]. Briefly, 17-2 *tssB-GFP* or *GFP-tssF* cells were transformed with a pKO3 plasmid in which a fragment of the *tssM* gene carrying the point mutations has been cloned (see below). Insertion of the plasmid into the chromosome was selected on chloramphenicol plates at 42 °C. Plasmid sequence removal was then selected on 5% sucrose plates without antibiotic, and *tssM* point mutation recombinant strains were screened by PCR and confirmed by DNA sequencing (Eurofins, MWG). Unless specified, cells were grown in LB or in *sci-1*-inducing medium (SIM; M9 minimal medium, 0.2% glycerol, 1 μg/mL vitamin B1, 100 μg/mL casaminoacids, and 10% LB, supplemented with or without 1.5% bactoagar) [55] at 37 °C with shaking. Plasmids were maintained by the addition of ampicillin (100 μg/mL), kanamycin (50 μg/mL), or chloramphenicol (30 μg/mL). Gene expression from pASK-IBA37+ and pBAD vectors was induced by the addition 0.1 μg/mL of anhydrotetracyclin (AHT; IBA Technology) and 0.02% of L-arabinose (Sigma-Aldrich), respectively.

Plasmid construction

Plasmids used in this study are listed in Supplementary Table S1. PCRs were performed using a Biometra thermocycler using the Q5 high-fidelity DNA polymerase (New England Biolabs). Restriction enzymes were purchased from New England Biolabs and used according to the manufacturer's instructions. Custom oligonucleotides, listed in Supplementary Table S1, were synthesised by Sigma-Aldrich. EAEC 17-2 chromosomal DNA was used as a template for all PCRs. *E. coli* strain DH5α was used for cloning procedures. With the exception of the pKO3-′*tssM*′ vector, plasmids have been constructed by restriction-free cloning [56] as previously described [30]. Briefly, genes of interest were amplified with oligonucleotides introducing the extensions annealing to the target vector. The double-stranded product of the first PCR has then been used as oligonucleotides for a second PCR using the target vector as a template. pKO3-′*tssM*′ has been constructed by the restriction–ligation procedure. A *Bam*HI-*Sal*I PCR product corresponding to a fragment of the *tssM* gene (nucleotides 216–1569) was ligated into pKO3 digested by the same enzymes using T4 DNA ligase (New England Biolabs). Substitutions into pIBA37-$_{FLAG}$TssM, pTssM$_{Cyto}$-T18, pT18-TssM$_{Cyto}$, and pKO3-′*tssM*′ have been introduced by site-directed mutagenesis using complementary pairs of oligonucleotides and the Pfu Turbo high-fidelity polymerase (Agilent Techologies). All constructs have been verified by restriction analysis and DNA sequencing (Eurofins, MWG).

Antibacterial assay

The antibacterial competition growth assay was performed as described [43]. The WT *E. coli* strain W3110 bearing the green fluorescent kanamycin-resistant pUA66-*rrnB* plasmid [50] was used as prey in the competition assay. The kanamycin-resistant pUA66-*rrnB* plasmid provides a strong constitutive green fluorescent phenotype. Attacker and prey cells were grown for 16 h in SIM and then diluted 100-fold in SIM. Once the culture reached an OD_{600} of 0.8, cells were harvested and resuspended to an OD_{600nm} of 10 in SIM. Attacker and prey cells were mixed to a 4:1 ratio, and 20-μL drops of the mixture were spotted in triplicate onto a prewarmed dry SIM agar plate. After incubation for 4 h at 37 °C, the bacterial spots were resuspended in LB, and bacterial suspensions were normalised to an OD_{600} of 0.5. For the enumeration of viable prey cells, bacterial suspensions were serially diluted and spotted onto selective LB agar plates supplemented with kanamycin (for the *E. coli* prey cells). The experiments were done in triplicate, with identical results, and we report here the results of a representative experiment.

Substituted cysteine accessibility method

Cysteine accessibility experiments were carried out as described [57,58] with modifications [30,31]. A 40-mL

culture of strain Δ*tssM* producing the TssM or cysteine-substituted TssM derivatives was induced for *tssM* gene expression with 0.02% AHT for 2 h. Cells were harvested and then resuspended in buffer A [100 mM Hepes (pH 7.5), 250 mM sucrose, 25 mM $MgCl_2$, and 0.1 mM KCl] to a final OD_{600} of 12 in 500 μL of buffer A. MPB (Molecular Probes) was added to a final concentration of 100 μM (from a 20-mM stock freshly dissolved in Diméthylsulfoxyde (DMSO)), and the cells were incubated for 30 min at 25 °C. β-Mercaptoethanol (20 mM final concentration) was added to quench the biotinylation reaction, and cells were washed twice in buffer A and resuspended in buffer A containing *N*-ethylmaleimide (5 mM final concentration) to block all free sulfhydryl residues. After incubation for 20 min at 25 °C, cells were disrupted by four passages at the French press at 800 psi. Membranes recovered by ultracentrifugation for 40 min at 100,000*g* were resuspended in 1 mL of buffer B [10 mM Tris (pH 8.0), 100 mM NaCl, 1% (wt/vol) Triton X-100, and protease inhibitor cocktail (Complete, Roche)]. After incubation on a wheel for 2 h, unsolubilised material was removed by centrifugation for 15 min at 20,000*g*, and solubilised proteins were subjected to immunoprecipitations using anti-FLAG M2 affinity gel (Sigma-Aldrich). After 3 h of incubation on a wheel, the beads were washed twice with 1 mL buffer B and once with buffer C [10 mM Tris (pH 8.0), 100 mM NaCl, and 0.1% (wt/vol) Triton X-100]. Beads were air-dried, resuspended in Laemmli buffer, and subjected to SDS-PAGE and immunodetection with anti-FLAG antibodies and streptavidin coupled to alkaline phosphatase.

Bacterial two-hybrid assay

The adenylate cyclase-based bacterial two-hybrid technique [59] was used as previously published [24,60]. Briefly, pairs of proteins to be tested were fused to the isolated T18 and T25 catalytic domains of the *Bordetella* adelynate cyclase. After the transformation of the two plasmids producing the fusion proteins into the reporter BTH101 strain, plates were incubated at 30 °C for 48 h. Three independent colonies for each transformation were inoculated into 600 μL of LB medium supplemented with ampicillin, kanamycin, and IPTG (0.5 mM). After overnight growth at 30 °C, 10 μL of each culture was dropped onto LB supplemented with 40 μg/mL bromo-chloro-indolyl-β-D-galactopyrannoside (X-Gal) and was incubated for 16 h at 30 °C. The experiments were done at least in triplicate, and a representative result is shown.

Co-immunoprecipitation

100 mL of W3110 cells producing proteins of interest were grown to an OD600 of 0.4 and the expression of the cloned genes were induced with AHT or L-arabinose for 45 min. The cells were harvested, and the pellets were resuspended in 20 mM Tris–HCl (pH 8.0), 100 mM NaCl, 30% sucrose, 1 mM EDTA, 100 μg/mL lysozyme, 100 μg/mL DNase, and 100 μg/mL RNase supplemented with protease inhibitors (Complete, Roche) to an OD_{600} of 80 and were incubated on ice for 20 min. Cells were lysed by three passages at the French Press (800 psi), and lysates were clarified by centrifugation at 20,000*g* for 20 min. Supernatants were used for co-immunoprecipitation using anti-FLAG M2 affinity gel (Sigma-Aldrich). After 3 h of incubation, the beads were washed three times with 1 mL of 20 mM Tris–HCl (pH 8.0), 100 mM NaCl, and 15% sucrose, were resuspended in 25 μL of Laemmli loading buffer, boiled for 10 min, and subjected to SDS-PAGE and immunodetection analyses.

Fluorescence microscopy and statistical analyses

Overnight cultures of EAEC 17-2 derivative strains were diluted 1:100 in SIM medium and grown for 6 h to an OD_{600} of ~1.0 to maximise the expression of the *sci-1* T6SS gene cluster [55]. Cells were washed in phosphate-buffered saline (PBS), resuspended in PBS to an OD_{600} of ~50, and spotted on a thin pad of 1.5% agarose in PBS and covered with a cover slip. Microscopy recording and digital image processing have been performed as previously described [15,16,18,20,24]. The Z project (average intensity) plugin has been used to merge and flatten all Z-planes. Microscopy analyses were performed at least six times, each with technical triplicate, and a representative experiment is shown. The number of sheath per number of cells and sfGFP–TssF foci was measured manually.

Computer analyses

TMH predictions were made using HMMTop [61], TMHMM [62], TMpred [63], and PHDhtm [64]. Secondary structure predictions were made using the Psipred server†. Structural predictions and homology modelling of the tri-dimensional structure of $TssM_{Cyto/NTP}$ and $TssM_{Cyto/Ct}$ were performed using HHpred [39] or Swiss-Model [65], respectively. Figures were made using Chimera [66]. Amino acid sequences were aligned with T-COFFEE [67], and phylogenetic analyses were performed with phylogeny.fr [68].

Miscellaneous

SDS-PAGE was performed using standard protocols. For immunostaining, proteins were transferred onto nitrocellulose membranes, and immunoblots were probed with primary antibodies and goat secondary antibodies coupled to alkaline phosphatase and were developed in alkaline buffer in the presence of 5-bromo-4-chloro-3-indolylphosphate and nitro-blue tetrazolium. The anti-FLAG (M2 clone, Sigma-Aldrich), anti-VSV-G (clone P5D4, Sigma-Aldrich) monoclonal antibodies, the alkaline phosphatase-conjugated streptavidin (Pierce), and alkaline phosphatase-conjugated goat anti-mouse secondary antibodies (Beckman Coulter) have been purchased as indicated and used as recommended by the manufacturer.

Supplementary data to this article can be found online at http://dx.doi.org/10.1016/j.jmb.2016.08.032.

Acknowledgements

We thank the members of the Cascales, Lloubès, Cambillau, Sturgis, and Bouveret research groups for helpful discussions; Laure Journet for critical reading of the manuscript; Emmanuelle Bouveret and Julie Viala for advices and protocols for pKO3-dependent

chromosomal engineering; Abdlerahim Zoued for statistical analyses; Olivier Uderso, Isabelle Bringer, and Annick Brun for technical assistance; and Jimmy Switrumpey for encouragements. This work was supported by the Centre National de la Recherche Scientifique, the Aix-Marseille Université and the grants from the Agence Nationale de la Recherche to E.C. (ANR-10-JCJC-1303-03 and ANR-14-CE14-0006-02) and from the European Society of Clinical Microbiology and Infectious Diseases (ESCMID) to E.D. L.L. is supported by a doctoral fellowship from the French Ministry of Research and an end-of-thesis fellowship from the Fondation pour la Recherche Médicale (FDT20160435498). E.D. was supported by an EMBO short-term fellowship (ASTF-417-2015).

Received 1 August 2016;
Received in revised form 29 August 2016;
Accepted 30 August 2016
Available online 4 September 2016

Keywords:
protein transport;
protein secretion;
type VI secretion;
bacterial competition;
membrane complex

Present address: M.-S. Aschtgen, Laboratoire des Sciences de l'Environnement Marin (LEMAR), Institut Universitaire Européen de la Mer (IUEM), Université de Bretagne Occidentale, CNRS, IRD, Ifremer – UMR 6539, Technopôle Brest Iroise, 29280 Plouzané, France; M. Guérin, Maquet Intervascular, 13600 La Ciotat, France.

†http://bioinf.cs.ucl.ac.uk/psipred/

Abbreviations used:
T6SS, type VI secretion system; BP, baseplate; MC, membrane complex; IM, inner membrane; OM, outer membrane; EAEC, enteroaggregative *Escherichia coli*; TMH, transmembrane helices; NTPase, nucleotide triphosphatase; NTP, nucleotide triphosphate; DPY-30, Dumpy-30; MPB, 3-(*N*-maleimidylpropionyl) biocytin; WT, wild-type; SIM, *sci-1*-inducing medium; AHT, anhydrotetracyclin; PBS, phosphate-buffered saline; spGFP, super folder Green Fluorescent Protein; DMSO, Diméthylsulfoxyde; GTP, Guanosine triphosphate.

References

[1] A.B. Russell, S.B. Peterson, J.D. Mougous, Type VI secretion system effectors: poisons with a purpose, Nat. Rev. Microbiol. 12 (2014) 137–148.
[2] E. Durand, C. Cambillau, E. Cascales, L. Journet, VgrG, Tae, Tle, and beyond: the versatile arsenal of type VI secretion effectors, Trends Microbiol. 22 (2014) 498–507.
[3] J. Alcoforado Diniz, Y.C. Liu, S.J. Coulthurst, Molecular weaponry: diverse effectors delivered by the type VI secretion system, Cell. Microbiol. 17 (2015) 1742–1751.
[4] A. Hachani, T.E. Wood, A. Filloux, Type VI secretion and anti-host effectors, Curr. Opin. Microbiol. 29 (2015) 81–93.
[5] G. Bönemann, A. Pietrosiuk, A. Mogk, Tubules and donuts: a type VI secretion story, Mol. Microbiol. 76 (2010) 815–821.
[6] E. Cascales, C. Cambillau, Structural biology of type VI secretion systems, Philos. Trans. R. Soc. Lond. Ser. B Biol. Sci. 367 (2012) 1102–1111.
[7] S.J. Coulthurst, The type VI secretion system—a widespread and versatile cell targeting system, Res. Microbiol. 164 (2013) 640–654.
[8] A. Zoued, Y.R. Brunet, E. Durand, M.S. Aschtgen, L. Logger, B. Douzi, L. Journet, C. Cambillau, E. Cascales, Architecture and assembly of the type VI secretion system, Biochim. Biophys. Acta 1843 (2014) 1664–1673.
[9] S. Kube, P. Wendler, Structural comparison of contractile nanomachines, AIMS Biophys. 2 (2015) 88–115.
[10] M. Basler, Type VI secretion system: secretion by a contractile nanomachine, Philos. Trans. R. Soc. Lond. Ser. B Biol. Sci. 370 (2015) 1679.
[11] B.T. Ho, T.G. Dong, J.J. Mekalanos, A view to a kill: the bacterial type VI secretion system, Cell Host Microbe 15 (2014) 9–21.
[12] F.R. Cianfanelli, L. Monlezun, S.J. Coulthurst, Aim, load, fire: the type VI secretion system, a bacterial nanoweapon, Trends Microbiol. 24 (2016) 51–62.
[13] P.G. Leiman, M. Basler, U.A. Ramagopal, J.B. Bonanno, J.M. Sauder, S. Pukatzki, S.K. Burley, S.C. Almo, J.J. Mekalanos, Type VI secretion apparatus and phage tail-associated protein complexes share a common evolutionary origin, Proc. Natl. Acad. Sci. U. S. A. 106 (2009) 4154–4159.
[14] M. Basler, M. Pilhofer, G.P. Henderson, G.J. Jensen, J.J. Mekalanos, Type VI secretion requires a dynamic contractile phage tail-like structure, Nature 483 (2012) 182–186.
[15] Y.R. Brunet, A. Zoued, F. Boyer, B. Douzi, E. Cascales, The type VI secretion TssEFGK-VgrG phage-like baseplate is recruited to the TssJLM membrane complex via multiple contacts and serves as assembly platform for tail tube/sheath polymerization, PLoS Genet. 15 (3) (2015) e1005545, 315–321.
[16] E. Durand, V.S. Nguyen, A. Zoued, L. Logger, G. Péhau-Arnaudet, M.S. Aschtgen, S. Spinelli, A. Desmyter, B. Bardiaux, A. Dujeancourt, A. Roussel, C. Cambillau, E. Cascales, R. Fronzes, Biogenesis and structure of a type VI secretion membrane core complex, Nature 523 (2015) 555–560.
[17] E.R. Ballister, A.H. Lai, R.N. Zuckermann, Y. Cheng, J.D. Mougous, *In vitro* self-assembly of tailorable nanotubes from a simple protein building block, Proc. Natl. Acad. Sci. U. S. A. 105 (2008) 3733–3738.
[18] Y.R. Brunet, J. Hénin, H. Celia, E. Cascales, Type VI secretion and bacteriophage tail tubes share a common assembly pathway, EMBO Rep. 15 (2014) 315–321.
[19] M. Kudryashev, R.Y. Wang, M. Brackmann, S. Scherer, T. Maier, D. Baker, F. DiMaio, H. Stahlberg, E.H. Egelman, M. Basler, Structure of the type VI secretion system contractile sheath, Cell 160 (2015) 952–962.
[20] Y.R. Brunet, L. Espinosa, S. Harchouni, T. Mignot, E. Cascales, Imaging type VI secretion-mediated bacterial killing, Cell Rep. 3 (2013) 36–41.
[21] M. Basler, B.T. Ho, J.J. Mekalanos, Tit-for-tat: type VI secretion system counterattack during bacterial cell–cell interactions, Cell 152 (2013) 884–894.

[22] A. Zoued, E. Durand, Y.R. Brunet, S. Spinelli, B. Douzi, M. Guzzo, N. Flaugnatti, P. Legrand, L. Journet, R. Fronzes, T. Mignot, C. Cambillau, E. Cascales, Priming and polymerization of a bacterial contractile tail structure, Nature 531 (2016) 59–63.
[23] S. Pukatzki, A.T. Ma, A.T. Revel, D. Sturtevant, J.J. Mekalanos, Type VI secretion system translocates a phage tail spike-like protein into target cells where it cross-links actin, Proc. Natl. Acad. Sci. U. S. A. 104 (2007) 15,508–15,513.
[24] A. Zoued, E. Durand, C. Bebeacua, Y.R. Brunet, B. Douzi, C. Cambillau, E. Cascales, L. Journet, TssK is a trimeric cytoplasmic protein interacting with components of both phage-like and membrane anchoring complexes of the type VI secretion system, J. Biol. Chem. 288 (2013) 27,031–27,041.
[25] G. English, O. Byron, F.R. Cianfanelli, A.R. Prescott, S.J. Coulthurst, Biochemical analysis of TssK, a core component of the bacterial type VI secretion system, reveals distinct oligomeric states of TssK and identifies a TssK–TssFG subcomplex, Biochem. J. 461 (2014) 291–304.
[26] N.M. Taylor, N.S. Prokhorov, R.C. Guerrero-Ferreira, M.M. Shneider, C. Browning, K.N. Goldie, H. Stahlberg, P.G. Leiman, Structure of the T4 baseplate and its function in triggering sheath contraction, Nature 533 (2016) 346–352.
[27] S. Planamente, O. Salih, E. Manoli, D. Albesa-Jové, P.S. Freemont, A. Filloux, TssA forms a gp6-like ring attached to the type VI secretion sheath, EMBO J. 35 (15) (Aug 1 2016) 1613–1627, http://dx.doi.org/10.15252/embj.201694024 (Epub 2016 Jun 10).
[28] M.S. Aschtgen, C.S. Bernard, S. De Bentzmann, R. Lloubès, E. Cascales, SciN is an outer membrane lipoprotein required for type VI secretion in enteroaggregative *Escherichia coli*, J. Bacteriol. 190 (2008) 7523–7531.
[29] L.S. Ma, J.S. Lin, E.M. Lai, An IcmF family protein, ImpLM, is an integral inner membrane protein interacting with ImpKL, and its walker a motif is required for type VI secretion system-mediated hcp secretion in *Agrobacterium tumefaciens*, J. Bacteriol. 191 (2009) 4316–4129.
[30] M.S. Aschtgen, M. Gavioli, A. Dessen, R. Lloubès, E. Cascales, The SciZ protein anchors the enteroaggregative *Escherichia coli* type VI secretion system to the cell wall, Mol. Microbiol. 75 (2010) 886–899.
[31] M.S. Aschtgen, A. Zoued, R. Lloubès, L. Journet, E. Cascales, The C-tail anchored TssL subunit, an essential protein of the enteroaggregative *Escherichia coli* Sci-1 type VI secretion system, is inserted by YidC, Microbiologyopen 1 (2012) 71–82.
[32] E. Durand, A. Zoued, S. Spinelli, P.J. Watson, M.S. Aschtgen, L. Journet, C. Cambillau, E. Cascales, Structural characterization and oligomerization of the TssL protein, a component shared by bacterial type VI and type IVb secretion systems, J. Biol. Chem. 287 (2012) 14,157–14,168.
[33] J. Zheng, K.Y. Leung, Dissection of a type VI secretion system in *Edwardsiella tarda*, Mol. Microbiol. 66 (2007) 1192–1206.
[34] C. Felisberto-Rodrigues, E. Durand, M.S. Aschtgen, S. Blangy, M. Ortiz-Lombardia, B. Douzi, C. Cambillau, E. Cascales, Towards a structural comprehension of bacterial type VI secretion systems: characterization of the TssJ–TssM complex of an *Escherichia coli* pathovar, PLoS One. 10 (3) (Mar 26 2015) e0122187.
[35] V.S. Nguyen, L. Logger, S. Spinelli, A. Desmyter, T.T. Le, C. Kellenberger, B. Douzi, E. Durand, A. Roussel, E. Cascales, C. Cambillau, Inhibition of type VI secretion by an anti-TssM llama nanobody, PLoS One 10 (3) (Mar 26 2015) e0122187.
[36] A.J. Gerc, A. Diepold, K. Trunk, M. Porter, C. Rickman, J.P. Armitage, N.R. Stanley-Wall, S.J. Coulthurst, Visualization of the Serratia type VI secretion system reveals unprovoked attacks and dynamic assembly, Cell Rep. 12 (2015) 2131–2142.
[37] L.S. Ma, F. Narberhaus, E.M. Lai, IcmF family protein TssM exhibits ATPase activity and energizes type VI secretion, J. Biol. Chem. 287 (2012) 15,610–15,621.
[38] M. Bogdanov, W. Zhang, J. Xie, W. Dowhan, Transmembrane protein topology mapping by the substituted cysteine accessibility method (SCAM(TM)): application to lipid-specific membrane protein topogenesis, Methods 36 (2005) 148–171.
[39] J. Söding, A. Biegert, A.N. Lupas, The HHpred interactive server for protein homology detection and structure prediction, Nucleic Acids Res. 33 (2005) W244–W248.
[40] L. Baugh, L.A. Gallagher, R. Patrapuvich, M.C. Clifton, A.S. Gardberg, T.E. Edwards, B. Armour, D.W. Begley, S.H. Dieterich, D.M. Dranow, J. Abendroth, J.W. Fairman, D. Fox III, B.L. Staker, I. Phan, A. Gillespie, R. Choi, S. Nakazawa-Hewitt, M.T. Nguyen, A. Napuli, L. Barrett, G.W. Buchko, R. Stacy, P.J. Myler, L.J. Stewart, C. Manoil, W.C. Van Voorhis, Combining functional and structural genomics to sample the essential *Burkholderia* structome, PLoS One 8 (1) (2013) e53851, http://dx.doi.org/10.1371/journal.pone.0053851 (Epub 2013 Jan 31).
[41] I. Hanukoglu, Rossmann fold: a beta-alpha-beta fold at dinucleotide binding sites, Biochem. Mol. Biol. Educ. 43 (2015) 206–209.
[42] X. Wang, Z. Lou, X. Dong, W. Yang, Y. Peng, B. Yin, Y. Gong, J. Yuan, W. Zhou, M. Bartlam, X. Peng, Z. Rao, Crystal structure of the C-terminal domain of human DPY-30-like protein: a component of the histone methyltransferase complex, J. Mol. Biol. 390 (2009) 530–537.
[43] N. Flaugnatti, T.T. Le, S. Canaan, M.S. Aschtgen, V.S. Nguyen, S. Blangy, C. Kellenberger, A. Roussel, C. Cambillau, E. Cascales, L. Journet, A phospholipase A1 anti-bacterial T6SS effector interacts directly with the C-terminal domain of the VgrG spike protein for delivery, Mol. Microbiol. 99 (2016) 1099–1118.
[44] V. Tremblay, P. Zhang, C.P. Chaturvedi, J. Thornton, J.S. Brunzelle, G. Skiniotis, A. Shilatifard, M. Brand, J.F. Couture, Molecular basis for DPY-30 association to COMPASS-like and NURF complexes, Structure 22 (2014) 1821–1830.
[45] V.A. Kostyuchenko, P.G. Leiman, P.R. Chipman, S. Kanamaru, M.J. van Raaij, F. Arisaka, V.V. Mesyanzhinov, M.G. Rossmann, Three-dimensional structure of bacteriophage T4 baseplate, Nat. Struct. Biol. 10 (2003) 688–693.
[46] V.A. Kostyuchenko, P.R. Chipman, P.G. Leiman, F. Arisaka, V.V. Mesyanzhinov, M.G. Rossmann, The tail structure of bacteriophage T4 and its mechanism of contraction, Nat. Struct. Mol. Biol. 12 (2005) 810–813.
[47] P.G. Leiman, F. Arisaka, M.J. van Raaij, V.A. Kostyuchenko, A.A. Aksyuk, S. Kanamaru, M.G. Rossmann, Morphogenesis of the T4 tail and tail fibers, Virol. J. 7 (2010) 355.
[48] A. Paschos, A. den Hartigh, M.A. Smith, V.L. Atluri, D. Sivanesan, R.M. Tsolis, C. Baron, An *in vivo* high-throughput screening approach targeting the type IV secretion system component VirB8 identified inhibitors of *Brucella* abortus 2308 proliferation, Infect. Immun. 79 (2011) 1033–1043.
[49] M.A. Smith, M. Coinçon, A. Paschos, B. Jolicoeur, P. Lavallée, J. Sygusch, C. Baron, Identification of the binding site of *Brucella* VirB8 interaction inhibitors, Chem. Biol. 19 (2012) 1041–1048.
[50] A. Zaslaver, A. Bren, M. Ronen, S. Itzkovitz, I. Kikoin, S. Shavit, W. Liebermeister, M.G. Surette, U. Alon, A comprehensive library of fluorescent transcriptional reporters for *Escherichia coli*, Nat. Methods 3 (2006) 623–628.

[51] K.A. Datsenko, B.L. Wanner, One-step inactivation of chromosomal genes in *Escherichia coli* K-12 using PCR products, Proc. Natl. Acad. Sci. U. S. A. 97 (2000) 6640–6645.
[52] M.K. Chaveroche, J.M. Ghigo, C. d'Enfert, A rapid method for efficient gene replacement in the filamentous fungus *Aspergillus nidulans*, Nucleic Acids Res. 28 (2000) E97.
[53] A.J. Link, D. Phillips, G.M. Church, Methods for generating precise deletions and insertions in the genome of wild-type *Escherichia coli*: application to open reading frame characterization, J. Bacteriol. 179 (1997) 6228–6237.
[54] A. Battesti, E. Bouveret, Acyl carrier protein/SpoT interaction, the switch linking SpoT-dependent stress response to fatty acid metabolism, Mol. Microbiol. 62 (2006) 1048–1063.
[55] Y.R. Brunet, C.S. Bernard, M. Gavioli, R. Lloubès, E. Cascales, An epigenetic switch involving overlapping fur and DNA methylation optimizes expression of a type VI secretion gene cluster, PLoS Genet. 7 (7) (Jul 2011) e1002205, http://dx.doi.org/10.1371/journal.pgen.1002205 (Epub 2011 Jul 28).
[56] F. van den Ent, J. Löwe, RF cloning: a restriction-free method for inserting target genes into plasmids, J. Biochem. Biophys. Methods 67 (2006) 67–74.
[57] S.J. Jakubowski, V. Krishnamoorthy, E. Cascales, P.J. Christie, *Agrobacterium tumefaciens* VirB6 domains direct the ordered export of a DNA substrate through a type IV secretion system, J. Mol. Biol. 341 (2004) 961–977.
[58] E.L. Goemaere, A. Devert, R. Lloubès, E. Cascales, Movements of the TolR C-terminal domain depend on TolQR ionizable key residues and regulate activity of the Tol complex, J. Biol. Chem. 282 (2007) 17,749–17,757.
[59] G. Karimova, J. Pidoux, A. Ullmann, D. Ladant, A bacterial two-hybrid system based on a reconstituted signal transduction pathway, Proc. Natl. Acad. Sci. U. S. A. 95 (1998) 5752–5756.
[60] A. Battesti, E. Bouveret, The bacterial two-hybrid system based on adenylate cyclase reconstitution in *Escherichia coli*, Methods 58 (2012) 325–334.
[61] G.E. Tusnády, I. Simon, Principles governing amino acid composition of integral membrane proteins: application to topology prediction, J. Mol. Biol. 283 (1998) 489–506.
[62] A. Krogh, B. Larsson, G. von Heijne, E.L. Sonnhammer, Predicting transmembrane protein topology with a hidden Markov model: application to complete genomes, J. Mol. Biol. 305 (2001) 567–580.
[63] K. Hofmann, W. Stoffel, A database of membrane spanning protein segments, Biol. Chem. 374 (1993) 166.
[64] B. Rost, P. Fariselli, R. Casadio, Topology prediction for helical transmembrane proteins at 86% accuracy, Protein Sci. 5 (1996) 1704–1718.
[65] M. Biasini, S. Bienert, A. Waterhouse, K. Arnold, G. Studer, T. Schmidt, F. Kiefer, T. Gallo Cassarino, M. Bertoni, L. Bordoli, T. Schwede, SWISS-MODEL: modelling protein tertiary and quaternary structure using evolutionary information, Nucleic Acids Res. 42 (2014) W252–W258.
[66] E.F. Pettersen, T.D. Goddard, C.C. Huang, G.S. Couch, D.M. Greenblatt, E.C. Meng, T.E. Ferrin, UCSF chimera–a visualization system for exploratory research and analysis, J. Comput. Chem. 25 (2004) 1605–1612.
[67] P. Di Tommaso, S. Moretti, I. Xenarios, M. Orobitg, A. Montanyola, J.M. Chang, J.F. Taly, C. Notredame, T-coffee: a web server for the multiple sequence alignment of protein and RNA sequences using structural information and homology extension, Nucleic Acids Res. 39 (2011) W13–W17.
[68] A. Dereeper, V. Guignon, G. Blanc, S. Audic, S. Buffet, F. Chevenet, J.F. Dufayard, S. Guindon, V. Lefort, M. Lescot, J.M. Claverie, O. Gascuel, Phylogeny.fr: robust phylogenetic analysis for the non-specialist, Nucleic Acids Res. 36 (2008) W465–W469.
[69] A. Zoued, C.J. Cassaro, E. Durand, B. Douzi, A.P. España, C. Cambillau, L. Journet, E. Cascales, Structure–function analysis of the TssL cytoplasmic domain reveals a new interaction between the type VI secretion baseplate and membrane complexes, J. Mol. Biol. 428 (2016) 4413–4423.

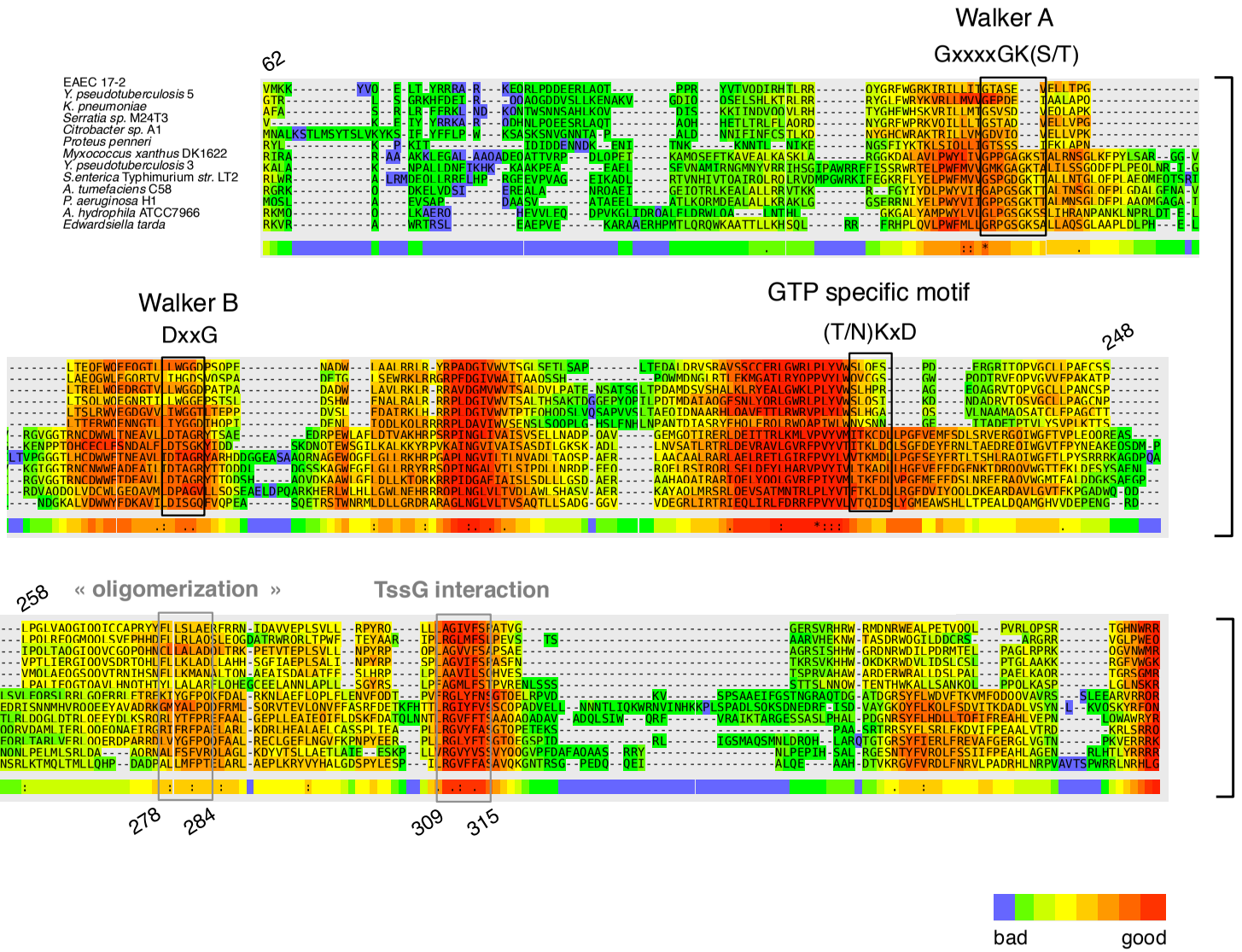

Logger *et al.* Figure S1

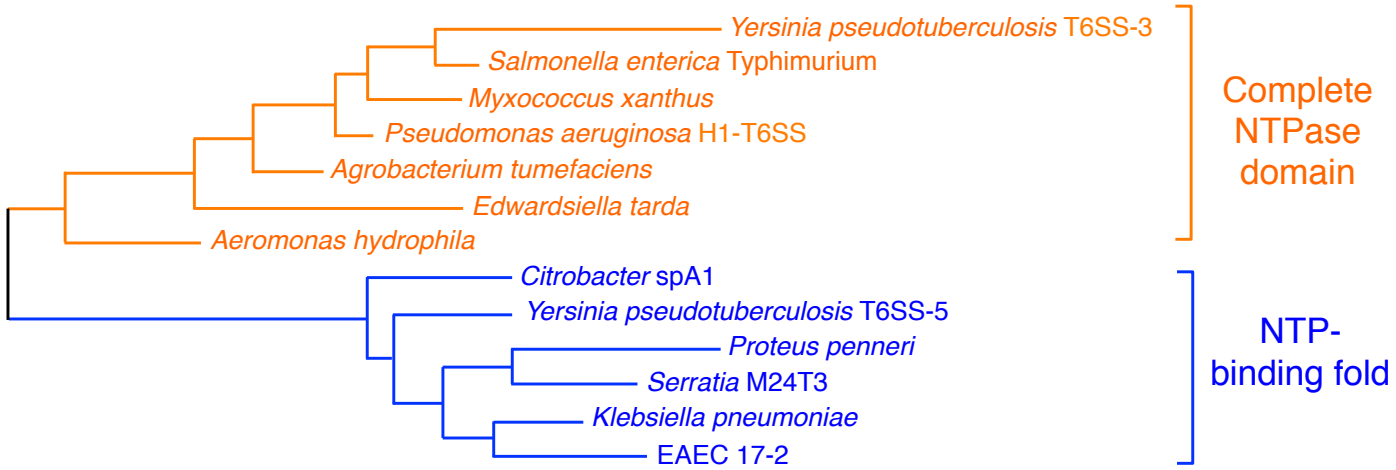

Logger *et al.* Figure S2

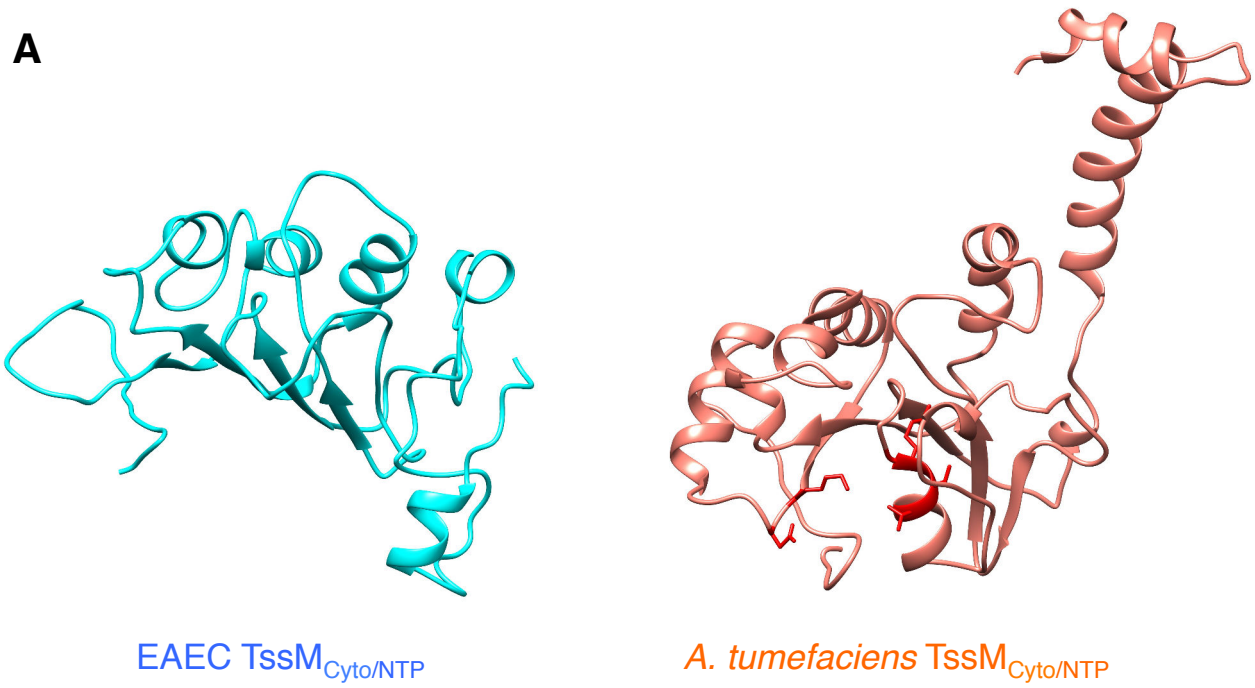

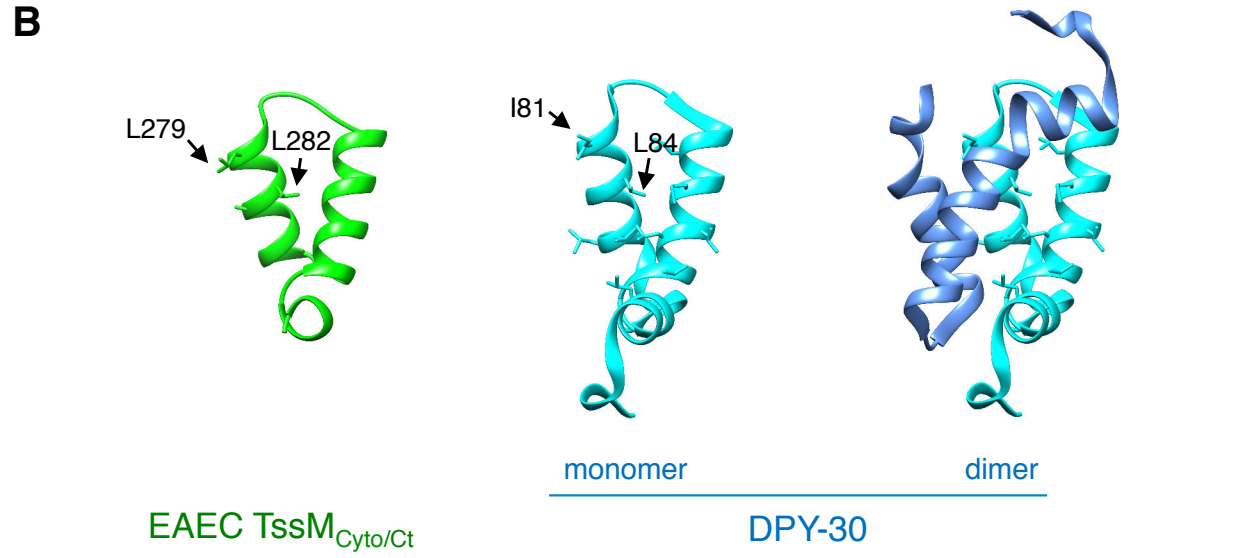

Logger *et al.* Figure S3

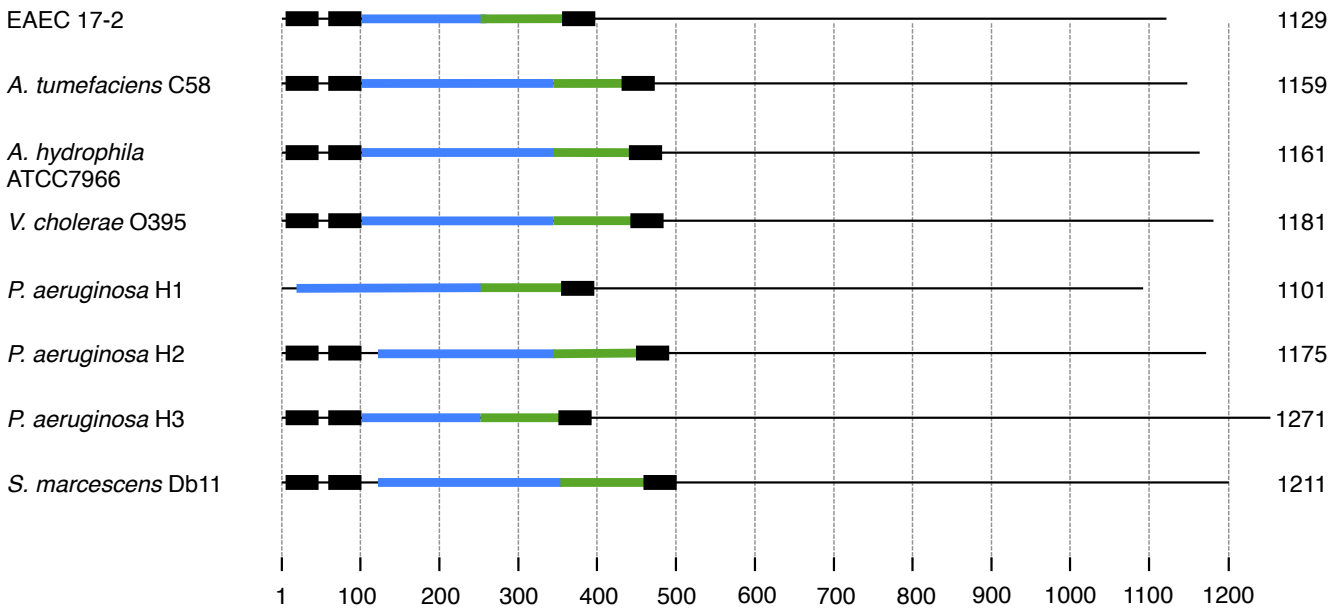

Logger *et al.* Figure S4

SUPPLEMENTAL DATA

Molecular dissection of the interface between the Type VI secretion TssM cytoplasmic domain and the TssG baseplate component.

L. Logger, M.S. Aschtgen, M. Guérin, E. Cascales & E. Durand

Supplemental Table S1. Strains, plasmids and oligonucleotides used in this study.

Strains

Strains	Description and genotype	Source
E. coli K-12		
DH5α	F-, Δ(*argF-lac*)U169, *phoA*, *supE44*, Δ(lacZ)M15, *relA*, *endA*, *thi*, *hsdR*	New England Biolabs
W3110	F-, lambda- IN(*rrnD-rrnE*)1 *rph*-1	Laboratory collection
BTH101	F-, *cya-99, araD139, galE15, galK16, rpsL1 (Str r), hsdR2, mcrA1, mcrB1.*	Karimova *et al.*, 1998
Enteroaggregative *E. coli*		
17-2	WT enteroaggregative *Escherichia coli*	A. Darfeuille-Michaud
17-2Δ*tssM*	17-2 deleted of the *tssM* gene of the *sci1* T6SS gene cluster	Aschtgen *et al.*, 2010
17-2 *tssB-gfp*	*gfp* inserted upstream the stop codon of *tssB* in 17-2	This study
17-2Δ*tssM tssB-gfp Ω Kan*	*gfp* inserted upstream the stop codon of *tssB* in 17-2 Δ*tssM*	This study
17-2 *tssB-gfp tssM*-L279W	Chromosomal point mutation Leu279-to-Trp substitution of *tssM* in 17-2 *tssB-gfp*	This study
17-2 *tssB-gfp tssM*-L282W-A283W	Chromosomal point mutation Leu282 and Ala283-to-Trp substitutions of *tssM* in 17-2 *tssB-gfp*	This study
17-2 *tssB-gfp tssM*-I312A-V313A-F314A	Chromosomal point mutation Ile312 and Val313 and Phe314-to-Ala substitutions of *tssM* in 17-2 *tssB-gfp*	This study
17-2 *tssB-gfp tssM*-S315W	Chromosomal point mutation Ser315-to-Val substitution of *tssM* in 17-2 *tssB-gfp*	This study
17-2 *gfp-tssF*	*gfp* inserted downstream the start codon of *tssF* in 17-2	Brunet, Zoued *et al.*, 2015
17-2Δ*tssM gfp-tssF Ω Kan*	*gfp* inserted downstream the start codon of *tssF* in 17-2 Δ*tssM*	This study
17-2 *gfp-tssF tssM*-L279W	Chromosomal point mutation Leu279-to-Trp substitution of *tssM* in 17-2 *gfp-tssF*	This study
17- *gfp-tssF tssM*-L282W-A283W	Chromosomal point mutation Leu282 and Ala283-to-Trp substitutions of *tssM* in 17-2 *gfp-tssF*	This study
17-2 *gfp-tssF tssM*-I312A-V313A-F314A	Chromosomal point mutation Ile312 and Val313 and Phe314-to-Ala substitutions of *tssM* in 17-2 *gfp-tssF*	This study
17-2 *gfp-tssF tssM*-S315W	Chromosomal point mutation Ser315 to Val substitution of *tssM* in 17-2 *gfp-tssF*	This study

Plasmids

Vectors	Description	Source
Vectors for chromosomal insertions		
pKD4	One-step gene inactivation vector, Kan^R	Datsenko & Wanner, 2000
p*gfp*-KD4	superfolder-*gfp* cloned upstream the 3' –FRT site of pKD4. Used for chromosomal C-terminal GFP fusion	Brunet, Zoued *et al.*, 2015
pKOBEG	Recombination vector, phage *λ recγβα* operon under the control of the pBAD promoter, Cm^R	Chaveroche *et al.*, 2000
Expression vectors		
pUA66-*rrnb*	P_{rrnB} *::gfpmut2* transcriptional fusion in pUA66	Zaslaver *et al.*, 2006
pASK-IBA37(+)	cloning vector, P*tet*, f1 origin, Amp^R	IBA Technology
pASK-IBA37-$_{FLAG}$TssM	*sci-1 tssM* carrying N-terminal FLAG tag cloned into pASK-IBA37	Aschtgen *et al.*, 2010
pIBA37-$_{FLAG}$TssM-C727S	Introduction of the TssM Cys727-to-Ser substitution into pIBA37-$_{FLAG}$TssM	This study
pIBA37-$_{FLAG}$TssM-C727S-A37C	Introduction of the TssM Ala37-to-Cys substitution into pIBA37-$_{FLAG}$TssM-C727S	This study
pIBA37-$_{FLAG}$TssM-C727S-V67C	Introduction of the TssM Val67-to-Cys substitution into pIBA37-$_{FLAG}$TssM-C727S	This study
pIBA37-$_{FLAG}$TssM-C727S-S352C	Introduction of the TssM Ser352-to-Cys substitution into pIBA37-$_{FLAG}$TssM-C727S	This study
pIBA37-$_{FLAG}$TssM-C727S-S386C	Introduction of the TssM Ser386-to-Cys substitution into pIBA37-$_{FLAG}$TssM-C727S	This study
pIBA37-TssM$_{Cyto_FLAG}$	*sci-1 tssM* residues 62-360 cloned into pASK-IBA37, C-terminal FLAG epitope	Zoued *et al.*, 2013
pIBA37-TssM$_{Cyto}$-NTP$_{FLAG}$	*sci-1 tssM* residues 62-273 cloned into pASK-IBA37, C-terminal FLAG epitope	This study
pIBA37-TssM$_{Cyto}$-Cter$_{FLAG}$	*sci-1 tssM* residues 274-360 cloned into pASK-IBA37, C-terminal FLAG epitope	This study
pIBA37-TssM$_{Cyto}$-L279W$_{FLAG}$	Introduction of the TssM Leu279-to-Trp substitution into pIBA37-TssM$_{Cyto\ FLAG}$	This study
pIBA37-TssM$_{Cyto}$-L282W -A283W$_{FLAG}$	Introduction of the TssM Leu282 and Ala283-to-Trp substitutions into pIBA37-TssM$_{Cyto_FLAG}$	This study
pIBA37-TssM$_{Cyto}$-I312A -V313A-F314A$_{FLAG}$	Introduction of the TssM Ile312 and Val313 and Phe314-to-Ala substitutions into pIBA37-TssM$_{Cyto\ FLAG}$	This study
pIBA37-TssM$_{Cyto}$-S315V$_{FLAG}$	Introduction of the TssM Ser 315-to-Val substitution into pIBA37-TssM$_{Cyto_FLAG}$	This study
pBAD33	cloning vector, P15A origin, *Para*, *araC,* Cm^R	Guzman *et al.*, 1995
pBAD33-TssM$_{Cyto_VSV-G}$	*sci1 tssM$_{Cyto}$* cloned into pBAD33, C-terminal VSV-G epitope	This study
pBAD33-TssG$_{VSV-G}$	*sci1 tssG* cloned into pBAD33, C-terminal VSV-G epitope	Brunet, Zoued *et al.*, 2015
pBAD33-TssK$_{VSV-G}$	*sci1 tssK* cloned into pBAD33, C-terminal VSV-G epitope	Brunet, Zoued *et al.*, 2015

Bacterial Two-Hybrid vectors

pT18-FLAG	Bacterial two-hybrid vector, ColE1 origin, P*lac*, T18 fragment of *Bordetella pertussis* CyaA, Amp^R	Battesti & Bouveret, 2008
$pTssM_{Cyto}$-T18	Cytoplasmic region of *tssM* ($TssM_{62-360}$ fragment) cloned upstream T18 in pT18-FLAG	Zoued *et al.*, 2013
pT18-$TssM_{Cyto}$	Cytoplasmic region of *tssM* ($TssM_{62-360}$ fragment) cloned downstream T18 in pT18-FLAG	Zoued *et al.*, 2013
$pTssM_{Cyto}$-NTP-T18	*sci-1 tssM* residues 62-273 cloned upstream T18 into pT18-FLAG	This study
$pTssM_{Cyto}$-Cter-T18	*sci-1 tssM* residues 274-360 cloned upstream T18 into pT18-FLAG	This study
$pTssM_{Cyto}$-L279W-T18	Introduction of the $TssM_{Cyto}$ Leu279-to-Trp substitution into $pTssM_{Cyto}$-T18	This study
$pTssM_{Cyto}$-L282W-A283W-T18	Introduction of the $TssM_{Cyto}$ Leu282 and Ala283-to-Trp substitutions into $pTssM_{Cyto}$-T18	This study
$pTssM_{Cyto}$-I312A-V313A-F314A-T18	Introduction of the $TssM_{Cyto}$ Ile312 and Val313 and Phe314-to-Ala substitutions into $pTssM_{Cyto}$-T18	This study
$pTssM_{Cyto}$-S315V-T18	Introduction of the $TssM_{Cyto}$ Ser315-to-Val substitution into $pTssM_{Cyto}$-T18	This study
pT18-Pal	*pal* cloned downstream the T18 coding sequence in pT18-FLAG	Battesti & Bouveret, 2008
pT25-FLAG	Bacterial two-hybrid vector, P15A origin, P*lac*, T25 fragment of *Bordetella pertussis* CyaA, Kan^R	Battesti & Bouveret, 2008
pT25-TssA	*tssA* cloned downstream the T25 coding sequence in pT25-FLAG	Zoued *et al.*, 2013
pTssA-T25	*tssA* cloned upstream the T25 coding sequence in pT25-FLAG	Zoued *et al.*, 2013
pT25-TssB	*tssB* cloned downstream the T25 coding sequence in pT25-FLAG	Zoued *et al.*, 2013
pTssB-T25	*tssB* cloned upstream the T25 coding sequence in pT25-FLAG	Zoued *et al.*, 2013
pT25-TssC	*tssC* cloned downstream the T25 coding sequence in pT25-FLAG	Zoued *et al.*, 2013
pTssC-T25	*tssC* cloned upstream the T25 coding sequence in pT25-FLAG	Zoued *et al.*, 2013
pT25-Hcp	*hcp* cloned downstream the T25 coding sequence in pT25-FLAG	Zoued *et al.*, 2013
pHcp-T25	*hcp* cloned upstream the T25 coding sequence in pT25-FLAG	Zoued *et al.*, 2013
pT25-TssE	*tssE* cloned downstream the T25 coding sequence in pT25-FLAG	Zoued *et al.*, 2013
pTssE-T25	*tssE* cloned upstream the T25 coding sequence in pT25-FLAG	Zoued *et al.*, 2013
pT25-TssF	*tssF* cloned downstream the T25 coding sequence in pT25-FLAG	Zoued *et al.*, 2013
pTssF-T25	*tssF* cloned upstream the T25 coding sequence in pT25-FLAG	Zoued *et al.*, 2013
pT25-TssG	*tssG* cloned downstream the T25 coding sequence in pT25-FLAG	Zoued *et al.*, 2013
pTssG-T25	*tssG* cloned upstream the T25 coding sequence in pT25-FLAG	Zoued *et al.*, 2013
pT25-VgrG	*vgrG* cloned downstream the T25 coding sequence in pT25-FLAG	Zoued *et al.*, 2013
pVgrG-T25	*vgrG* cloned upstream the T25 coding sequence in pT25-FLAG	Zoued *et al.*, 2013
pT25-$TssJ_{sol}$	$tssJ_{sol}$ ($TssJ_{2-152}$ fragment of the processed form) cloned downstream the T25 coding sequence in pT25-FLAG	Zoued *et al.*, 2013
p$TssJ_{sol}$-T25	$tssJ_{sol}$ ($TssJ_{2-152}$ fragment of the processed form) cloned upstream the T25 coding sequence in pT25-FLAG	Zoued *et al.*, 2013
pT25-TssK	*tssK* cloned downstream the T25 coding sequence in pT25-FLAG	Zoued *et al.*, 2013
pTssK-T25	*tssK* cloned upstream the T25 coding sequence in pT25-FLAG	Zoued *et al.*, 2013
pT25-$TssL_{Cyto}$	Cytoplasmic fragment of *tssL* ($TssL_{1-184}$ fragment) cloned downstream the T25 coding sequence in pT25-FLAG	Durand *et al.*, 2012
p$TssL_{Cyto}$-T25	Cytoplasmic fragment of *tssL* ($TssL_{1-184}$ fragment) cloned upstream the T25 coding sequence in pT25-FLAG	Durand *et al.*, 2012
pT25-$TssM_{Cyto}$	Cytoplasmic fragment of *tssM* ($TssM_{62-360}$ fragment) cloned downstream T25 in pT25-FLAG	Zoued *et al.*, 2013
$pTssM_{Cyto}$-T25	Cytoplasmic fragment of *tssM* ($TssM_{62-360}$ fragment) cloned upstream T25 in pT25-FLAG	Zoued *et al.*, 2013

pT25-TssM$_{Peri}$	Periplasmic région of *tssM* (TssM$_{386-1129}$ fragment) cloned downstream T25 in pT25-FLAG	Zoued *et al.,* 2013
pTssM$_{Peri}$-T25	Periplasmic région of *tssM* (TssM$_{386-1129}$ fragment) cloned upstream T25 in pT25-FLAG	Zoued *et al.*, 2013
pTolB-T25	*tolB* cloned upstream the T25 coding sequence in pT25-FLAG	Battesti & Bouveret, 2008

Chromosomal mutagenesis vectors

pKO3	*sacB*, *repA*(pSC101^{ts}), M13 origin, Cm^{R}	Link *et al.*, 1997
pKO3-*tssM*	Region of *tssM* cloned into the pKO3 vector	This study
pKO3-*tssM*- L279W	Introduction of the TssM Leu279-to-Trp substitution into pKO3-*tssM*	This study
pKO3-*tssM*-L282W-A283W	Introduction of the TssM Leu282 and Ala283-to-Trp substitutions into pKO3-*tssM*	This study
pKO3-*tssM*-I312A-V313A-F314A	Introduction of the TssM Ile312 and Val313 and Phe314-to-Ala substitutions into pKO3-*tssM*	This study
pKO3-*tssM*-S315W	Introduction of the TssM Ser315-to-Val substitution into pKO3-*tssM*	This study

Oligonucleotides

Name	Destination	Sequence (5' ➔ 3')
For site-directed mutagenesis [a]		
M-C727S-5	pASK-IBA37-$_{FLAG}$TssM	GAATACGCTGGCGGTTCAG**GGATCC**ACTGGCCAGCCCCGGGAAG
M-C727S-3	pASK-IBA37-$_{FLAG}$TssM	CTTCCCGGGGCTGGCCAGT**GGATCC**CTGAACCGCCAGCGTATTC
M-A36C-5	pIBA37-$_{FLAG}$TssM-C727S	GATAACCCGATATGGAGCATA**CCTAGG**GTGTGAAACACGCCGGGATCAAATAC
M-A36C-3	pIBA37-$_{FLAG}$TssM-C727S	GTATTTGATCCCGGCGTGTTTCACAC**CCTAGG**TATGCTCCATATCGGGTTATC
M-V67C-5	pIBA37-$_{FLAG}$TssM-C727S	CTGCCTGTGATGAAAAA**ATATT**GTCAGGAACTGACATATCGAC
M-V67C-3	pIBA37-$_{FLAG}$TssM-C727S	GTCGATATGTCAGTTCCTGAC**AATATT**TTTTCATCACAGGVAG
M-S352C-5	pIBA37-$_{FLAG}$TssM-C727S	AATTACCTGTCCGGCTACAGCC**CTGCAGG**ACAGGTCATAACTGGCGCAG
M-S352C-3	pIBA37-$_{FLAG}$TssM-C727S	CTGCGCCAGTTATGACCTGTCC**CTGCAG**GGCTGTAGCCGGACAGGTAATTG
M-S386C-5	pIBA37-$_{FLAG}$TssM-C727S	GGTGGTTTCCTTTCTGGCAA**ATCGAT**GTCTGGTTGCTGAAGTCAG
M-S386C-3	pIBA37-$_{FLAG}$TssM-C727S	CTGTACTTCAGCAACCAGAC**ATCGAT**TTGCCAGAAAGGAAACCACC
A-L279W	pTssM$_{Cyto}$-T18, pIBA37-TssM$_{Cyto_FL}$ or pKO3-*tssM*	CCCTCGGTATTATTTT**TGG**TTGTCGCTGGCAGAGC
B-L279W	pTssM$_{Cyto}$-T18, pIBA37-TssM$_{Cyto_FL}$ or pKO3-*tssM*	ATAATACCGAGGGGCACAGCATATCTGCTG
A-L282W-A283W	pTssM$_{Cyto}$-T18, pIBA37-TssM$_{Cyto_FL}$ or pKO3-*tssM*	CCCTCGGTATTATTTTTTGTTGTCG**TGGTGG**GAGCGATTCAGACGAA
B- L282W-A283W	pTssM$_{Cyto}$-T18, pIBA37-TssM$_{Cyto_FL}$ or pKO3-*tssM*	ATAATACCGAGGGGCACAGCATATCTGCTG
A-I312A-V313A-F314A	pTssM$_{Cyto}$-T18, pIBA37-TssM$_{Cyto_FL}$ or pKO3-*tssM*	GTTGTTGCTGGCGGGT**GCGGCGGCG**AGTCCGGCAACTGTCG
B- I312A-V313A-F314A	pTssM$_{Cyto}$-T18, pIBA37-TssM$_{Cyto_FL}$or pKO3-*tssM*	CGCCAGCAACAACTGACGGTATGGACGGAG
A- S315V	pTssM$_{Cyto}$-T18, pIBA37-TssM$_{Cyto_FL}$ or pKO3-*tssM*	GTTGTTGCTGGCGGGTATTGTTTTC**GTG**CCGGCAACTGTCGGCG
B- S315V	pTssM$_{Cyto}$-T18, pIBA37-TssM$_{Cyto_FL}$ or pKO3-*tssM*	CGCCAGCAACAACTGACGGTATGGACGGAG
For plasmid construction [b,c,d]		
5-pIBA37-TssM$_{Cyto}$-NTP$_{FLAG}$	insertion of *tssM*$_{62-273}$ fragment into pASK-IBA37	GACAAAAATCTAGAAATAATTTTGTTTAACTTTAAGAAGGAGATATACA AATGGTGATGAAAAAATATGTTCAGGAACTGACATATC
3-pIBA37-TssM$_{Cyto}$-NTP$_{FLAG}$	insertion of *tssM*$_{62-273}$ fragment into pASK-IBA37	GATGGTGATGGTGATGCGATCCTCTGCTAGCTTA*ATTTATCATCGTCGTCTT* *TATAATC*GGCACAGCATATCTGCTGTATCCC
5- pIBA37-TssM$_{Cyto}$-CT$_{FLAG}$	insertion of *tssM*$_{274-360}$ fragment into pASK-IBA37	GACAAAAATCTAGAAATAATTTTGTTTAACTTTAAGAAGGAGATATACA AATGCCTCGGTATTATTTTTTGTTGTCGCTGGC
3- pIBA37-TssM$_{Cyto}$-CT$_{FLAG}$	insertion of *tssM*$_{274-360}$ fragment into pASK-IBA37	GATGGTGATGGTGATGCGATCCTCTGCTAGCTTA*CTTGTCATCGTCGTCCT* *TATAATC*TCTGCGCCAGTTATGACCTGTGCGGGA

T25T18C-5-TssM$_{Cyto}$-NTP	insertion of *tssM*$_{62\text{-}273}$ fragment downstream the T18 domain	CGGATAACAATTTCACACAGGAAACAGCTATGACCATGGTGAT GAAAAAATATGTTCAGGAACTGACATATCG
T18C-3- TssM$_{Cyto}$-NTP	insertion of *tssM*$_{62\text{-}273}$ fragment downstream the T18 domain	CCTCGCTGGCGGCTAAGCTTGGCGTAATGGCACAGCATATCTG CTGTATCCC
T25T18C-5-TssM$_{Cyto}$-CT	insertion of *tssM*$_{274\text{-}360}$ fragment downstream the T18 domain	CGGATAACAATTTCACACAGGAAACAGCTATGACCATGCCTCG GTATTATTTTTTGTTGTCGCTGGC
T18C-3- TssM$_{Cyto}$-CT	insertion of *tssM*$_{274\text{-}360}$ fragment downstream the T18 domain	CCTCGCTGGCGGCTAAGCTTGGCGTAATTCTGCGCCAGTTATGA CCTGTGCG
5-pBAD-TssM$_{Cyto}$	insertion of *tssM*$_{274\text{-}360}$ fragment into pBAD33	CTCTCTACTGTTTCTCCATACCCGTTTTTTTGGGCTAGCAGGAGGTATTAC ACCATGGTGATGAAAAAATATGTTCAGGAACTGACATATCGAC
3-pBAD-TssM$_{Cyto}$-VSVG	insertion of *tssM*$_{62\text{-}360}$ fragment into pBAD33	GGTCGACTCTAGAGGATCCCCGGGTACCTTA*TTTTCCTAATCTATTCATTTCA ATATCTGTATA*TCTGCGCCAGTTATGACCTGTGCGGGA
5-pKO3-BamHI-TssM$_{Cyto}$	insertion of *tssM* fragment into pKO3	GACC**GGATCC**CGACGCAGGGCCCGTAAG
3-pKO3-SalI-TssM$_{Cyto}$	insertion of *tssM* fragment into pKO3	CCCG**GTCGAC**CTGTGGCCATTCCCGCATGAG
For strain construction [e]		
5-*tssB-gfp*	insertion of *gfp-mut2* at the 3' end of *tssB*	CCGGCACTGAGTCAGACGCTGCGTGATGAACTGCGTGCACTGGTGCCGGA AAAGGCGGCAGCGGCCGGCGGAGGG
3-*tssB-gfp*	insertion of *gfp-mut2* at the 3' end of *tssB*	GCAACGTTCTTTTCTTTCTGTACAGACATCAGCATTTTCTCTCGTAATCCG TTAAACATATGAATATCCTCCTTAGTTCCTATTCCGAAGTTCC

[a] Mutagenesized codon in **Bold.**
[b] Sequence annealing on the target plasmid underlined.
[c] FLAG or VSV-G epitope coding sequence *italicized*.
[d] Restriction sites in **Bold.**
[e] Sequences corresponding to the downstream and upstream regions of the gene to be inserted underlined

Article 4: Type VI secretion TssK baseplate protein exhibits structural similarities with phage receptor binding protein and evolved to bind the membrane complex

Article 4: Type VI secretion TssK baseplate protein exhibits structural similarities with phage receptor binding protein and evolved to bind the membrane complex

During T6SS biogenesis, the baseplate docks to the membrane complex. A number of interactions involving baseplate and membrane components have been identified: TssM interacts with TssG and TssK (Zoued et al., 2013)(Brunet et al., 2015b)(*Article 3)*, and TssL interacts with TssE and TssK (Zoued et al., 2013)(Zoued et al., 2016a). TssK is particularly important as it is involved in binding both TssL and TssM cytoplasmic domain, and bioinformatic analyses revealed that the *tssK* gene co-occurs with the *tssL* gene in 3/4 of the T6SS gene clusters (Boyer et al., 2009)(Zoued et al., 2013). Previous studies have demonstrated that TssK is a cytoplasmic protein that forms trimers (Zoued et al., 2013)(English et al., 2014) and by interacting with the TssFG complex, is also part of the baseplate (English et al., 2014)(Brunet et al., 2015b). The fact that TssK is a baseplate component was hypothesized based on the stability of the TssFGK complex (English et al., 2014) and on the involvement of TssK in Hcp tube formation (Brunet et al., 2014). However, contrarily to other T6SS baseplate components that share homologies with bacteriophage baseplate subunits (TssE/gp25, VgrG/gp27, TssF/gp6, TssG/gp53), TssK does not share obvious similarity to phage proteins. Based on secondary structure prediction, Planamente et al. proposed that TssK presents similarity with gp8 (Planamente et al., 2016). Based on the TssK interaction network, Taylor et al. proposed that TssK has functional similarity to gp10 (Taylor et al., 2016).

Due to the TssK central role in the baseplate and in baseplate docking to the membrane complex, it was critical to gain structural and functional information on this T6SS subunit. In this study, the crystal structure of the full-length TssK was solved at 2.6-Å resolution in complex with a camelid nanobody (nbK18). The TssK structure reveals a three-domain protein organized as a tightly packed trimer. Due to its general architecture, the three domains were named "shoulder" (N-terminal domain,), "neck" (central domain) and "head" (C-terminal domain). The trimer is 110-Å long, and 85-Å wide at the base (shoulder) and 40-Å wide at the neck.

The N-terminal shoulder (residues 19-174) is a β-sandwich and is followed by a linker (residues

174-193), the four-helix-bundle neck domain (residues 194-313) and the C-terminal head domain (residues 315-447). The structure of the C-terminal domain was improved to 1.6 Å by using a new construct comprising this isolated domain. It is a very compact domain of three α-helices and seven β-strands. Initially, the structure of the bottom of the shoulder domain was missing: residues 1-19 and loop 130-144. Using another nanobody, nbK27, this problem was overcome. Nbk27 binds the base of the shoulder domain and hence structurally orders this region by preventing flexibility. However, the most important information of the structural characterization of TssK is that TssK does not share any similarity with gp8 and gp10, but rather that it has the global architecture of siphophage RBPs and that its N-terminal domain is superimposable to the shoulder domains of RBPs.

I tested the contribution of each domain to the interaction with TssK partners. Using bacterial-two hybrid and co-immunoprecipation, I showed that the C-terminal head domain ($TssK_H$) interacts with $TssL_{Cyto}$ and $TssM_{Cyto}$ whereas the N-terminal shoulder domain ($TssK_S$) interacts with TssFG. In addition, as expected from the structure, the neck is necessary for TssK oligomerization. These results were confirmed by co-purification as TssKFG and $TssK_S$-FG complexes were purified. Finally, a nanobody binding experiment showed that nbK18 binds to the $TssK_S$-FG complex whereas nbK27 does not. Because nbK27 binds the bottom of the TssK trimer and that formation of the TssKFG complex prevents nbK27 binding, it was concluded that TssFG binds the bottom of $TssK_S$.

Based on these data, we concluded that TssK has the general architecture of a classical RBP protein. The TssK shoulder domain is structurally homologous to shoulder domains of RBPs, and such as these domains, it mediates insertion into the baseplate. By contrast, the C-terminal head domain is very distinct structurally and binds the membrane complex. Because RBP head domains are responsible for receptor recognition and binding, these results suggest that TssK has evolved a different head domain to use the membrane complex as a receptor in order to allow baseplate docking and to properly orient the T6SS tail towards the cell exterior.

nature microbiology

ARTICLES

PUBLISHED: 26 JUNE 2017 | VOLUME: 2 | ARTICLE NUMBER: 17103

Type VI secretion TssK baseplate protein exhibits structural similarity with phage receptor-binding proteins and evolved to bind the membrane complex

Van Son Nguyen[1,2], Laureen Logger[3], Silvia Spinelli[1,2], Pierre Legrand[4], Thi Thanh Huyen Pham[1,2,5], Thi Trang Nhung Trinh[1,2,5], Yassine Cherrak[3], Abdelrahim Zoued[3], Aline Desmyter[1,2], Eric Durand[3], Alain Roussel[1,2], Christine Kellenberger[1,2], Eric Cascales[3]* and Christian Cambillau[1,2]*

The type VI secretion system (T6SS) is a multiprotein machine widespread in Gram-negative bacteria that delivers toxins into both eukaryotic and prokaryotic cells. The mechanism of action of the T6SS is comparable to that of contractile myophages. The T6SS builds a tail-like structure made of an inner tube wrapped by a sheath, assembled under an extended conformation. Contraction of the sheath propels the inner tube towards the target cell. The T6SS tail is assembled on a platform—the baseplate—which is functionally similar to bacteriophage baseplates. In addition, the baseplate docks the tail to a trans-envelope membrane complex that orients the tail towards the target. Here, we report the crystal structure of TssK, a central component of the T6SS baseplate. We show that TssK is composed of three domains, and establish the contribution of each domain to the interaction with TssK partners. Importantly, this study reveals that the N-terminal domain of TssK is structurally homologous to the shoulder domain of phage receptor-binding proteins, and the C-terminal domain binds the membrane complex. We propose that TssK has conserved the domain of attachment to the virion particle but has evolved the reception domain to use the T6SS membrane complex as receptor.

Delivery of bacterial effector proteins and toxins into target cells relies on trans-envelope nanomachines called secretion systems. These machines select and transport effectors in the milieu or directly into the target cell[1]. Most of these secretion systems evolved from efflux pumps or from machineries involved in conjugation or flagellar, twitching or gliding motility[1]. The type VI secretion system (T6SS) is a fascinating machine that uses a contractile mechanism similar to that of the bacteriophage or R-pyocin contractile tail[2–7]. The T6SS delivers toxins and effectors in both eukaryotic and prokaryotic cells, and participates in bacterial pathogenesis and interbacterial competition[8,9]. By eliminating competing bacteria, the T6SS confers an increased ability to colonize a niche[10–16].

The T6SS, in essence, can be viewed as a contractile tail oriented towards the target cell, and anchored to the cell envelope by a membrane complex (MC)[3,17]. The MC is evolutionarily related to a subcomplex associated with the type IVb secretion system[18,19], and is a 1.7 MDa trans-envelope structure composed of three conserved subunits: the TssJ outer membrane lipoprotein and the TssL and TssM inner membrane proteins[20–26]. In several cases, the MC is properly inserted and anchored to the cell wall by additional proteins with peptidoglycan hydrolysis and peptidoglycan binding properties[21,27–29]. The contractile tail is composed of an inner tube made of hexamers of the Hcp protein, stacked on each other[30,31], tipped by VgrG, and surrounded by a contractile sheath made of the TssBC proteins[30–32]. Polymerization of the tail tube/sheath tubular structure is initiated on an assembly platform—the baseplate (BP), the less characterized T6SS subcomplex—and is coordinated by the TssA protein[33–35]. The T6SS contractile tail shares functional and structural homologies with the tails of several bacteriophages[5,6,30,36–38]. Once the T6SS tail is assembled, the sheath contracts and propels the inner tube/spike needle complex towards the target cell[39–42], and it has been proposed that this needle complex traverses the cell envelope through the MC (ref. 26). A recent *in vivo* study identified five components of the BP: TssE, TssF, TssG, TssK and VgrG (ref. 34). Although TssA was also identified in this screen, later observations demonstrated that TssA is not a structural component of the BP *per se*[35]. TssE is a homologue of gp25, a bacteriophage T4 BP wedge protein[18,19,43]. By contrast, no tridimensional structure is available for TssF, TssG or TssK. *In silico* analyses recently predicted that TssF and TssG share limited homologies with gp6 and gp7, respectively[34] and controversies exist regarding TssK (refs 44, 45). Interestingly, T6SS BP subcomplexes could be isolated in *Serratia marcescens* and uropathogenic *Escherichia coli* (UPEC), including the TssKFG or TssKFGE complexes[33,45]. These complexes probably represent the equivalent of wedge complexes of phage BPs, which assemble around the central gp27–gp5 hub/spike[46,47]. In addition to appearing central for the assembly of the T6SS wedges, TssK is a key BP subunit mediating contacts with the cytoplasmic domains of MC components[35,48,49]. Hence, TssK is an essential BP component connecting the MC, BP and tail components. However, we still lack structural information on TssK. Although we have shown that TssK assembles trimeric complexes in enteroaggregative *E. coli* (EAEC)[48], a study has reported that it assembles

[1]Architecture et Fonction des Macromolécules Biologiques, Aix-Marseille Université, Campus de Luminy, Case 932, 13288 Marseille Cedex 09, France. [2]Architecture et Fonction des Macromolécules Biologiques, Centre National de la Recherche Scientifique (CNRS), Campus de Luminy, Case 932, 13288 Marseille Cedex 09, France. [3]Laboratoire d'Ingénierie des Systèmes Macromoléculaires, Institut de Microbiologie de la Méditerranée, Aix-Marseille Univ. Centre National de la Recherche Scientifique (UMR7255), 31 Chemin Joseph Aiguier, 13402 Marseille Cedex 20, France. [4]Synchrotron Soleil, L'Orme des Merisiers, Saint-Aubin – BP 48, 91192 Gif-sur-Yvette Cedex, France. [5]University of Science and Technology of Hanoi, Training and Services Building, Vietnam Academy of Science and Technology, 18 Hoang Quoc Viet, Cau Giay District, Hanoi, VietNam. *e-mail: cascales@imm.cnrs.fr; cambillau@afmb.univ-mrs.fr

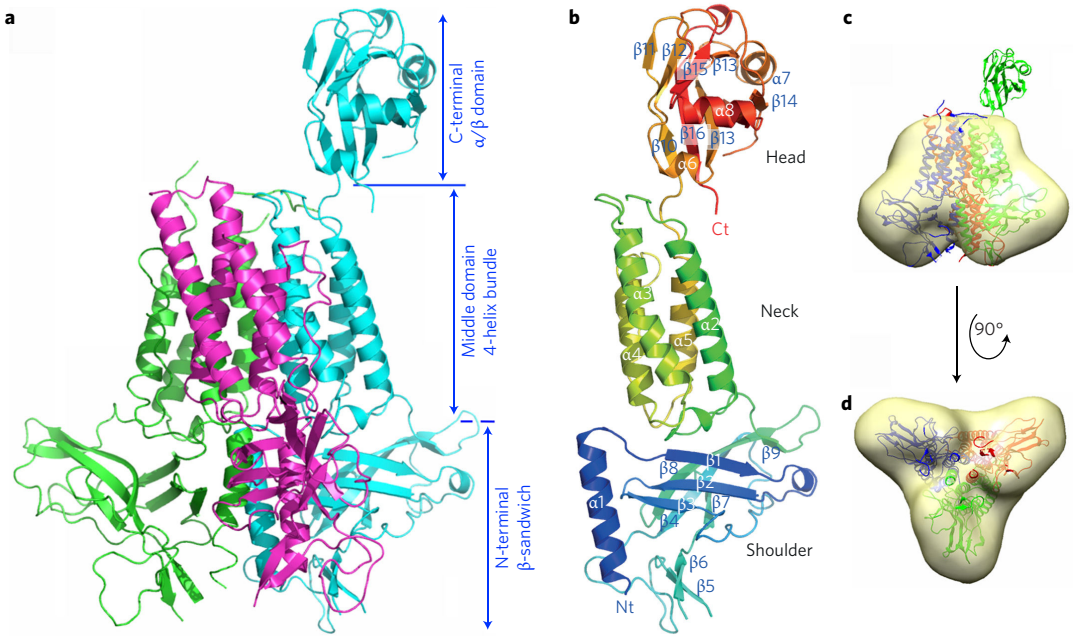

Figure 1 | Structure of TssK. a, Ribbon view of the TssK trimer. Monomers A, B and C are in pink, blue and green, respectively. The locations of the N-terminal (shoulder), central (neck) and C-terminal (head) domains are indicated. **b**, Ribbon view of TssK monomer B (full-length TssK). The monomer is rainbow-coloured (blue to red from N to C terminal). The α-helices and β-strands are numbered. **c**,**d**, Side (**c**) and bottom (**d**) views of the TssK X-ray structure fitted into the TssK negative-stain EM map (EMD-5739), highlighting that the TssK C-terminal head domain is disordered.

trimers and hexamers in *S. marcescens*[33]. The available structural information on the EAEC TssK protein (accession no. EC042_4526) consists of a low-resolution (~26 Å) negative-stained electron microscopy (EM) structure of the TssK trimer, as well as its small-angle X-ray scattering envelope[48]. Despite intensive efforts, neither full-length nor cleaved forms of TssK could be crystallized. Here, we report the crystal structure of the full-length EAEC TssK protein, obtained as a complex with a camelid nanobody that facilitated the crystallization process. The structure of trimeric TssK reveals an unexpected homology of its N-terminal domain with siphophage receptor-binding protein (RBP) shoulders, hence expanding the number of homologous proteins between T6SS and bacteriophages. The TssK N-terminal domain attaches to the rest of the T6SS BP, and the C-terminal domain binds the MC and has evolved to use the T6SS MC as a receptor for docking the BP. In addition, the flexibility of the TssK C-terminal domain suggests that TssK may establish a flexible link to maintain the anchorage of the BP to the T6SS MC before, during and after tail contraction.

Results

TssK crystallization is facilitated when complexed to the TssK-specific nb18 nanobody. Despite extensive efforts, previous attempts to crystallize TssK were unsuccessful. Crystallization of proteins has been shown previously to be facilitated once the protein of interest is complexed to camelid single-chain antibodies (called nanobodies)[50]. We used this approach for crystallization of the periplasmic domain of the T6SS TssM subunit[26,51,52]. We immunized a llama with purified TssK and isolated nanobodies that bind TssK: nbK18, nbK25 and nbK27. The crystal structure of nbK18 was determined (Supplementary Fig. 1a) and its complexation with TssK was then monitored by biolayer interferometry (BLI). Kinetic and steady-state analyses provided dissociation constant (K_d) values of 2.4 and 3.1 nM, respectively.

The TssK structure reveals a three-domain protein organized as a tightly packed trimer. The structure of the nbK18–TssK co-crystallized complex was determined at 2.6 Å resolution. The complex contains three TssK molecules to which three nbK18 units are bound (Supplementary Fig. 1b). TssK trimerization is in agreement with previous gel filtration data suggesting that TssK forms a trimer[48]. Each nanobody interacts with two monomers of TssK and covers ~700 Å^2 of the accessible surface area of a TssK monomer and 80 Å^2 of a second monomer. Interaction of nbK18 with TssK is mainly mediated by nbK18 complementarity-determining region 3 (CDR3), but also by the two other CDRs and the conserved skeleton (Supplementary Fig. 1b and Supplementary Table 2), a feature already observed in other cases[53,54]. NbK18 binds the TssK N-terminal β-sandwich and more specifically the L4–5 and L6–7 loops (Supplementary Fig. 1b inset and Supplementary Table 2).

The TssK trimer has the overall structure of an apple core, or an hourglass, with two globular domains—the N-terminal shoulder (hereafter named $TssK_S$) and the C-terminal head ($TssK_H$)—separated by a helical stalk, the neck ($TssK_N$). The TssK trimer is tightly packed, as 1,400–1,570 Å^2 of the accessible surface area of each monomer is covered by the two other monomers (Fig. 1a). The structure exhibits high B-factors (~100 Å^2), and the side chains of solvent-exposed residues are often disordered when not involved in crystal packing contacts. A large segment is missing at the bottom of the shoulder domain between residues 130 and 144, and a short loop is incomplete at the top of the neck domain, between residues 221 and 224. These segments have not been incorporated into the model (Fig. 1a). Two of the three monomers are not complete: their amino-acid chains start at residue 19 and end at residues 320 and 315 for monomers A and C, respectively, suggesting that their C-terminal domains might be totally disordered. In contrast, the main chain of monomer B could be traced up to residue 334, and the side-chain identity can be assigned (Fig. 1a). However, despite its stabilization by crystal contacts, the C-terminal domain of chain B exhibits an average B-factor double that of the rest of the structure, impeding its complete assignment (Fig. 1a).

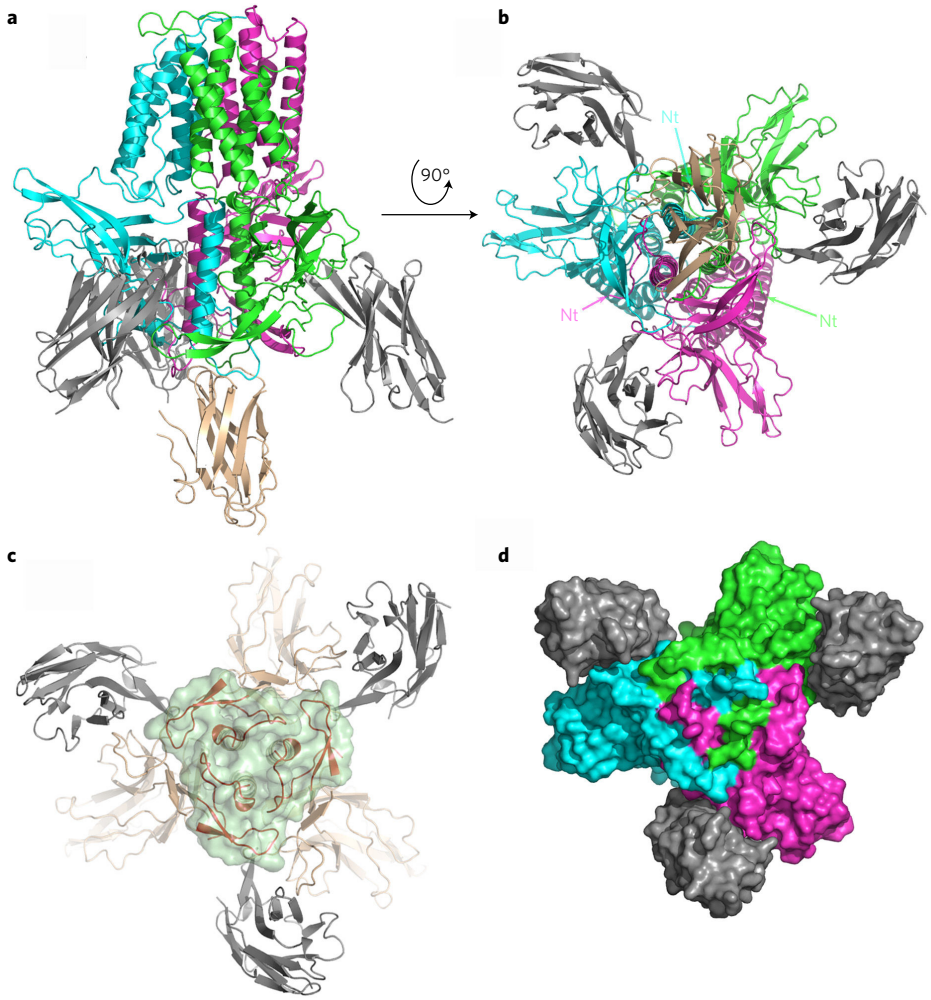

Figure 2 | Structure of the $TssK_{SN}$–nbK18–nbK27 complex. a, Ribbon view of the $TssK_{SN}$–nbK18–nbK27 complex. Monomers A, B and C are in pink, blue and green, respectively. The three nbK18 are in grey and the unique nbK27 is in beige. **b**, Same view as in **a**, rotated by 90°, presenting the bottom of the $TssK_{SN}$ domain. **c**, Same orientation and colours as in **b**, but with a molecular surface representation. The $TssK_{SN}$ domain trimer (beige) and the nbK18 nanobody (grey) are represented as ribbons. The $TssK_{SN}$ N-terminal segments ordered upon surface binding are identified by their darker coloured ribbon (brown) and their green semi-transparent surface. **d**, Same orientation as in **b**.

The TssK monomer structure comprises three domains: an N-terminal β-sandwich domain (shoulder, $TssK_S$, residues 19–174), a linker (residues 175–193) and a four-helix-bundle middle domain (neck, $TssK_N$, residues 194–313) and, in chain B only, a partially traced C-terminal domain (head, $TssK_H$, residues 315–447) (Fig. 1b). The N-terminal domain starts with a long α-helix followed by three anti-parallel β-strands forming a β-sheet (β1–β3). After β-strand 4, a short β-hairpin (β4, β5) is followed by β-strands 6 and 7. Together, β-strands 4, 6 and 7 form the second β-sheet of the β-sandwich. After a long linker, α-helices 2, 3 and 4 form an antiparallel bundle. Helix 4 is then followed by a long unstructured stretch of residues returning in the direction of the N terminus and positioning α-helix 5 parallel to α-helix 3, allowing the chain to continue in a direction opposite to the N terminus. The C-terminal domain, starting at residue 317, is predicted by JPRED[55] as assembling three α-helices and seven β-strands. We assigned 106 amino acids for a total of 125 for the complete C-terminal domain. At this stage it comprised two complete α-helices and an incomplete one, as well as two β-sheets forming a β-sandwich of putatively seven β-strands, but most connections were not visible in the electron density map.

To obtain a better model of TssK, the C-terminal domain (amino acids 316–445) was produced, crystallized and its structure solved at 1.6 Å resolution. This domain is very compact and comprises three α-helices (α6–8) and seven β-strands (β10–16) (Fig. 1b). The structure of the isolated C-terminal domain was reintroduced in the structure of full-length TssK and refinement was performed. Apart from loop 372–382, which has a different conformation, the domain conformations are very close in the isolated and full-length structures (r.m.s.d. = 1.2 Å on 115 residues) (Supplementary Fig. 2). Notably, the C-terminal domain of chain B establishes stabilizing packing contacts, involving mainly loop 372–382. As such, the complete TssK trimer is ~110 Å long and ~85 Å wide at the level of the shoulder domains and ~40 Å wide at the level of the central domain (Fig. 1a).

We previously reported the negative-stain EM structure of TssK (ref. 48). The crystal structure of TssK was fitted into the EM map using Chimera[56] (Fig. 1c,d). With the exception of the C-terminal domain of monomer B, TssK fits exquisitely well into the EM structure with a correlation of 0.89 and 93% of atoms included in the map.

Nanobody epitope analysis performed by BLI revealed that nbK27 and nbK25 bind TssK using an epitope different to that for nbK18. We therefore co-crystallized the cloned $TssK_{SN}$ domain (shoulders and neck domain, residues 1–315) with nbK18 and nbK27. Crystals of $TssK_{SN}$–nbK18–nbK27 were obtained and

the structure was solved (Supplementary Table 1). The structure of $TssK_{SN}$–nbK18–nbK27 superimposes well with that of the TssK–nbK18 complex, with a small rotation of the three nbK18. In contrast to nbK18, which binds each TssK monomer, a unique nbK27 binds the trimeric assembly along the three-fold axis at the bottom of the shoulder domains (Fig. 2a,b), resulting in a $TssK_3/nbK18_3/nbK27_1$ stoichiometry. The most striking result of nbK27 binding to TssK is ordering of the bottom of the shoulder domains segments, which were disordered in the TssK–nbK18 complex: N-terminal segment 1–19 and β-hairpin 130–144 (Fig. 2c,d). This ordering results in strong domain-swapped-like interactions of the 1–19 segment with the $i-1$ monomer, and of the 130–144 β-hairpin with the $i+1$ monomer (Fig. 2c). Notably, the stabilized structures comprise all the bottom part of TssK, a surface with a diameter of ~50 Å (Fig. 2d). The list of domains or segments present in the different crystal structures is summarized as a linear sequence representation with secondary structures in Supplementary Fig. 3.

The TssK N-terminal domain shares structure similarities with phage RBP shoulder domains. The three domains of TssK were subjected to DALI server (http://ekhidna2.biocenter.helsinki.fi/dali/) analyses to detect structural similarities. Interestingly, DALI retrieved strong similarities between the TssK N-terminal β-sandwich domain and the shoulder domains from lactococcal siphophage RBPs (Fig. 3), including phages 1358 (PDB: 4L9B, $Z=9.0$, r.m.s.d. = 3.0 Å; ref. 57) and p2 (PDB: 1ZRU, $Z=6.0$ r.m.s.d.= 3.0 Å; ref. 58). In addition, although helix bundles represent a common structural fold, DALI analyses detected similarities between the TssK neck domain and a domain of the human adenylosuccinate lyase (PDB: 4FFX, $Z=9.4$, r.m.s.d. = 3.1 Å; ref. 59) (Supplementary Fig. 4).

Interaction analyses of TssK domains. Previous studies have shown that TssK is a central subunit of the T6SS, as it interacts with components of the MC (the cytoplasmic domains of TssL ($TssL_C$) and TssM ($TssM_C$)), of the BP (the TssFG complex) and of the tail (TssA, TssC and Hcp)[33,34,39,48,60]. We therefore sought to define the domains mediating TssK interactions with MC and BP. First, the N-terminal shoulder and neck ($TssK_{SN}$), shoulder ($TssK_S$), neck ($TssK_N$) and C-terminal head ($TssK_H$) domains of TssK were cloned in two-hybrid vectors and tested for their ability to promote oligomerization and to interact with TssFG, $TssL_C$ and $TssM_C$ (Fig. 4a). In agreement with the crystal structure of the TssK trimer (Fig. 1a), both shoulder and neck domains oligomerize, whereas the TssK head domain does not interact with TssK (Fig. 4a, first column). More interestingly, the two-hybrid analyses revealed that the N-terminal shoulder domain mediates contacts with the TssFG complex, whereas the C-terminal head domain interacts with $TssL_C$, $TssM_C$ and to a lesser extent to TssFG. We then monitored co-immunoprecipitation experiments. Soluble lysates of cells producing the VSV-G-tagged TssK domains were combined with lysates containing FLAG-tagged TssF and TssG, or the cytoplasmic domains of TssL ($TssL_C$) or TssM ($TssM_C$). FLAG-tagged proteins were immobilized on agarose beads coupled to the monoclonal anti-FLAG antibody and the eluted material was analysed by sodium dodecyl sulfate polyacrylamide gel electrophoresis (SDS–PAGE) and immunostaining. Figure 4b shows that the $TssK_S$ domain is co-precipitated with the TssFG complex, whereas the the $TssK_H$ domain co-precipitates with $TssL_C$ and $TssM_C$, and—and to a lower extent—with TssFG. The results of bacterial two-hybrid (BACTH) and co-immunoprecipitation analyses are summarized in Supplementary Fig. 5.

To confirm these results, we engineered vectors producing TssFG as well as either 6×His-tagged $TssK_{SN}$ or $TssK_H$. High-performance liquid chromatography (HPLC) indicated that TssKFG and $TssK_{SN}$FG complexes form (Supplementary Fig. 6a). However, although we succeeded in purifying the $TssK_{SN}$FG complex (Fig. 4c and Supplementary Fig. 6a), $TssK_H$ was purified alone and did not co-purify with TssFG (isolated TssFG is not observed on the chromatogram as it is insoluble) (Supplementary Fig. 7a). These results confirm the $TssK_{SN}$/TssFG complex interaction and indicate that the low $TssK_H$/TssFG interaction, observed by BACTH and co-immunoprecipitation, should be weaker and in fast exchange. To gain further insights into the contribution of the $TssK_{SN}$ domain for binding to the TssFG complex, we then tested binding of the TssK-specific nbK18 and nbK27 nanobodies to the $TssK_{SN}$FG complex. The purified $TssK_{SN}$FG complex was mixed with an excess of nanobody and analysed by gel filtration and HPLC. First, we confirmed that nbK18 and nbK27 bind alone and simultaneously to $TssK_{SN}$. We then performed an analysis of $TssK_{SN}$FG in the presence of nbK18, nbK27 and nbK18 + nbK27 (Supplementary Fig. 6b). We found that nbK18 binds to the $TssK_{SN}$FG complex (Fig. 4c,d and Supplementary Fig. 6c) whereas nbK27 does not (Fig. 4c,e). From these results, we concluded that nbK27 and TssFG share the same binding site as TssK and, hence, that TssFG should bind to the bottom of the $TssK_S$ domain comprising the residues 1–19 segment and the 130–144 β-hairpin. Taken together, the results of the co-purification and nanobody binding experiments confirmed the interaction of $TssK_S$ with the TssFG complex and suggested that TssFG binds the bottom of $TssK_S$.

We could not assay the $TssK_H$ interaction with the TssMc domain, as it is insoluble. However, we performed a gel filtration of a mixture of TssLc and $TssK_H$, and found that they do not co-purify. As an interaction is observed by double-hybrid and co-immunoprecipitation, this latter result suggests that this interaction is rather weak (~1–10 mM) and in fast exchange. Indeed, this does not reflect the biological situation in which the interaction of several TssK trimers and several Lc dimers occurs, leading certainly to a tremendous avidity increase.

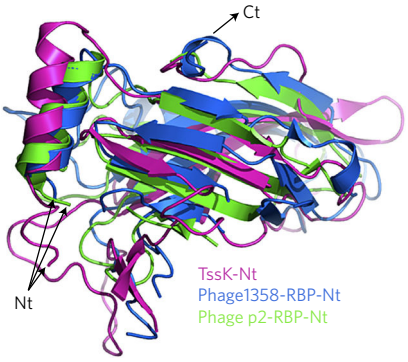

Figure 3 | Structural comparison of the TssK N-terminal shoulder domain with shoulder domains of siphophage RBPs. Superimposed ribbon views of the TssK N-terminal shoulder domain (pink) with the shoulder domains of phages p2 (green) and 1358 (blue) RBPs (PDB 1ZRU and 4L9B, respectively).

Discussion

In this Article, we present the crystal structure and a domain analysis of a T6SS core component, TssK. Previous studies have demonstrated that TssK is a trimer and is an essential subunit of the type VI secretion apparatus by connecting the trans-envelope MC to the phage-like contractile tail[48]. In addition, TssK has been shown to be part of the T6SS assembly platform or BP[33,34,39,45,48]. It has been reported recently that phage T4 is a very complex phage and that phage Mu is simpler, widespread, and better paradigm for phages with contractile tails[61]. Notably, TssK has no counterpart in phage Mu, whereas other T6SS baseplate components have counterparts in both phages T4 (ref. 45) and Mu (ref. 61): TssE

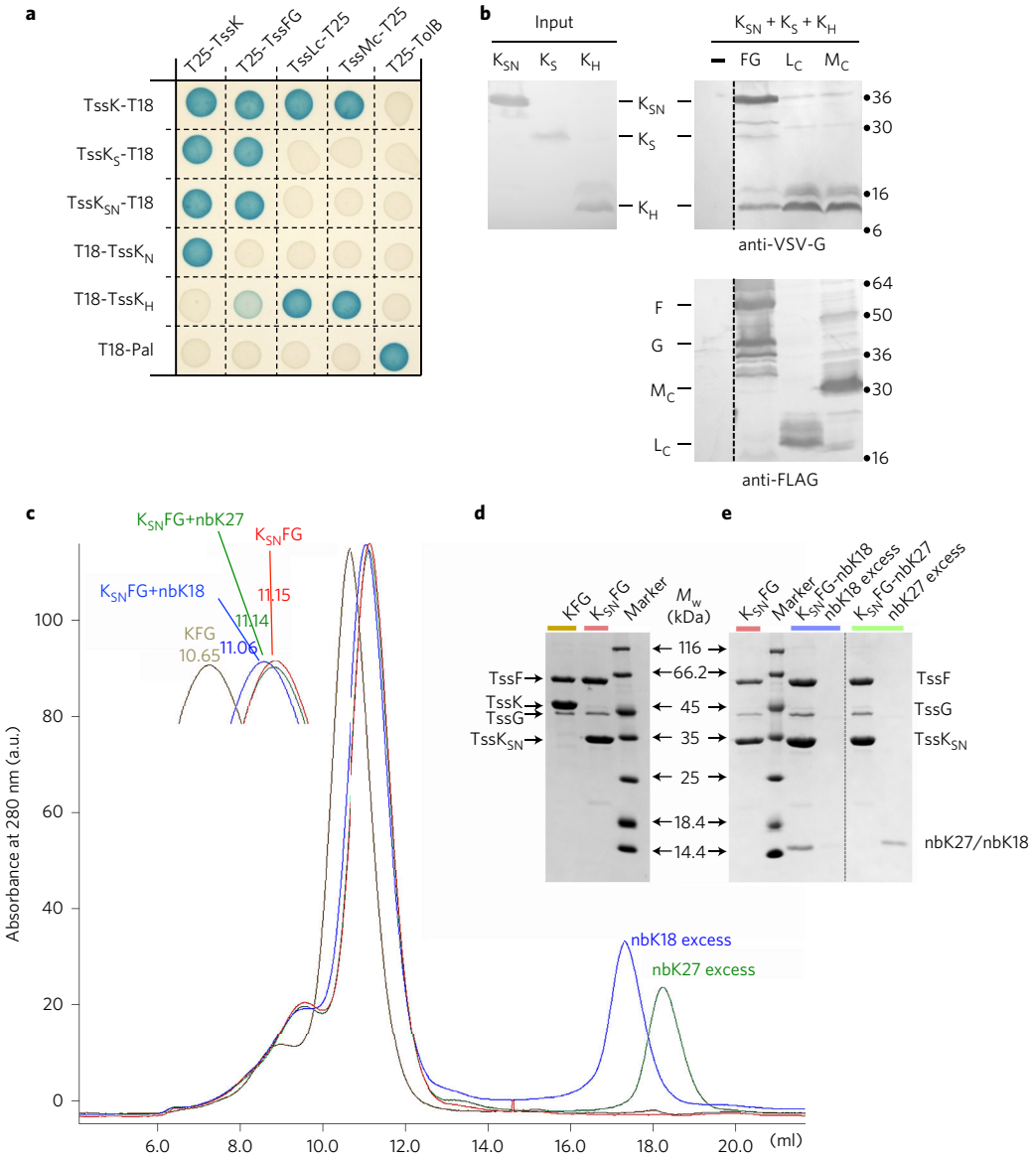

Figure 4 | Protein–protein interaction study of TssK domains. a, Bacterial two-hybrid assay. BTH101 reporter cells producing the indicated proteins or domains (K, TssK; K_{SN}, TssK shoulder and neck domains; K_S, TssK shoulder domain; K_N, TssK neck domain; K_H, TssK head domain) fused to the T18 or T25 domain of the *Bordetella* adenylate cyclase were spotted on X-gal indicator plates. The blue colour of the colony reflects the interaction between the two proteins. TolB and Pal are two proteins known to interact but unrelated to the T6SS. The BACTH experiments were performed in triplicate with identical results. **b**, Co-immunoprecipitation assay. A mixture of soluble lysates from 2×10^{10} *E. coli* K-12 W3110 cells producing VSV-G-tagged TssK shoulder + neck (K_{SN}), TssK shoulder (K_S) and TssK head (K_H) domains (individually shown on the left panel) was mixed with FLAG-tagged TssF+TssG, $TssL_C$ or $TssM_C$. FLAG-tagged proteins were subjected to immunoprecipitation with anti-FLAG-coupled beads and the immunoprecipitated material was separated by 12.5% acrylamide SDS–PAGE and immunodetected anti-VSV-G monoclonal antibodies. The position of each protein and domain is indicated, molecular weight markers (in kDa) are indicated on the right. The co-immunoprecipitation experiments were performed in duplicate with identical results. **c**, Gel filtration chromatograms of TssKFG (brown), $TssK_{SN}FG$ (red), $TssK_{SN}FG$+nbK18 (blue) and $TssK_{SN}FG$+nbK27 (green). Inset: enlargement of the top of the peaks, with the elution time indicated above each peak. a.u., arbitrary units. **d**, SDS gels of the main peak of TssKFG (brown) and $TssK_{SN}FG$ (red) showing the presence of TssK, TssF and TssG, and $TssK_{SN}$, TssF and TssG, respectively. The stoichiometry of complexes TssK/TssF/TssG and TssKsn/TssF/TssG were found to be 4.04/1.86/1 and 4.6/1.97/1, respectively (values reported: 4.1/1.8/1 (ref. 33) and 3.36/2.18/1 (ref. 45); expected ratio: 3–6/2/1). **e**, SDS gels of the main peak of $TssK_{SN}FG$ (red), $TssK_{SN}FG$+nbK18 (blue) and $TssK_{SN}FG$+nbK27 (green) showing the presence of nbK18 attached to $TssK_{SN}FG$, but not nbK27. M_w, molecular weight. In **a** and **b**, experiments were performed at least in triplicate, and a representative result is shown. In **c**–**e**, experiments were performed in triplicate, and a representative result is shown.

corresponds to gp25 (T4) and Mup46 (Mu), TssF to gp6 and Mup47, and TssG to Mup48 (no homologue in T4).

The X-ray structure of TssK confirms that TssK exists as a trimer. The TssK trimer has an overall architecture resembling that of an apple core: a shoulder base and a distal head separated by the central neck. The structure of TssK is modular. It comprises three domains: an N-terminal domain, essentially β-stranded and comparable to the N-terminal shoulder domains of phages p2 and 1358 RBPs, followed by an α-helical central domain and a mixed α–β C-terminal globular domain. *In vivo* interaction studies with

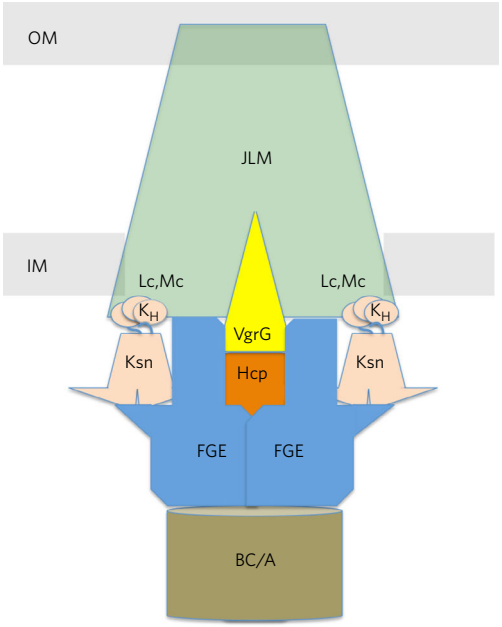

Figure 5 | Schematic model of the baseplate docked to the membrane complex, highlighting the connector role of TssK. The TssJLM membrane complex (MC) is represented in green, TssK is in beige and the other BP components are in blue (TssFGE), yellow (VgrG) and orange (Hcp). The tail complex is shown in dark green. The three domains of TssK are represented in beige, with the N-terminal shoulder domain anchored to the BP and the C-terminal head domain bound to the MC. OM, outer membrane; IM, inner membrane.

known partners of TssK support the idea that TssK acts as a connector between two T6SS complexes that are evolutionarily unrelated: the phage-like BP/tail and the T4bSS IcmF/DotU-like MC (Fig. 5). From the protein–protein interaction assays we concluded that the TssK N-terminal shoulder domain binds to TssFG and that the C-terminal head domain mediates interactions with the TssL and TssM inner membrane proteins.

The fascinating observation of this study is that TssK shares an overall architecture similar to that of lactococcal siphophage RBPs. These RBPs are trimers and comprise shoulder and head domains separated by a neck[57,58,62]. They recognize the host cell surface and are responsible for properly orienting the phage onto the host cell[63,64]. RBPs are anchored to the virion and bind to receptors at the cell surface of the target cell. Anchorage to the virion particle is mediated by the shoulder domain, whereas the ability to recognize the cell envelope receptor is conferred by the head domain. It has been reported that in each lactococcal phage family, the shoulder domain structure is strictly conserved whereas the head domain is relatively diverse and confers specificity for binding to the proper target cell[57,58,62,63,65]. Another striking similarity between the TssK and RBP shoulder domains is the ordering of their bottom segments upon binding to partners. When the phage p2 RBP is expressed alone, the 20 N-terminal residues are disordered and not visible in the electron map density. In contrast, they are ordered when the RBP is complexed with the other BP components, forming the main contributors to the interaction. It is worth noticing that the 'arm and hand' domain of the Dit protein inserts between the three N termini, thus holding the RBP trimer[58,62,65]. A similar situation may exist with TssK. Although we do not have the structure of TssK within the TssKFG complex, nanobody binding experiments on the TssKFG complex have shown that the TssFG binding site on TssK involves the bottom of the trimer, including the N termini (Supplementary Fig. 8). The ordering of this site upon nbK27 binding suggests that this nanobody acts as a surrogate of the TssFG complex.

In myophages, such as phages T4 or Mu, both the BP and tail sheath change conformation upon contraction[45,61]. The tail sheath conformational change is also documented for the T6SS (ref. 32). It is therefore expected that a conformational reorganization also occurs for the T6SS BP (refs 35, 38). The flexibility of the TssK head domain relative to the rest of the trimer suggests that TssK may constitute a flexible link between the T6SS BP and its membrane domain to accommodate the different conformations and radii before and after tail contraction. The TssK flexible hinge would therefore prevent disruption of the contact between the membrane and the BP complexes during sheath contraction.

By sharing the overall architecture and the N-terminal shoulder domain with RBPs, we propose that TssK represents a RBP-like component of T6SS. As in RBPs, the TssK has a modular architecture with an N-terminal shoulder domain and a C-terminal head domain. The TssK shoulder domain interacts with the other T6SS BP components (TssFG). By contrast, the head domain of TssK mediates interaction with the cytoplasmic domains of TssL and TssM and hence docks the BP to the MC (Fig. 5). These data are consistent with previous fluorescence microscopy imaging demonstrating that green fluorescent protein-labelled TssK is recruited to the MC and is necessary for recruiting the gp6/Mup47-like TssF BP subunit[34]. Based on these data and on the observation of TssE and TssG interactions with the cytoplasmic domains of TssL and TssM, respectively[34,49,66], we propose that TssK first interacts with the MC and that TssF–TssL and TssG–TssL additional contacts stabilize the MC–BP complex. TssK therefore has a function similar to that of RBPs: it is anchored to the phage-like structure by a conserved shoulder domain but, instead of allowing the phage particle to bind to the target cell surface, it has evolved a distinct head domain to recognize and bind to the T6SS MC. It should be stressed that although TssFG have sequence similarity with Myoviridae phage BP components, the TssK shoulder domain has structural similarity with Siphoviridae phage RBPs and has no counterpart in Myoviridae. Therefore, even if the origin of the T6SS tail and BP is from Myoviridae phages, the TssK N-terminal domain may derive from horizontal transfer from a Siphoviridae component to provide the ability to bind the TssJLM complex of T6SS. These results point to a more complicated evolutionary process leading to the T6SS, in which elements of different phage types were combined.

Methods

Bacterial strains, growth conditions and chemicals. The strains used in this study are listed in Supplementary Table 3. *E. coli* K-12 strains DH5α, W3110, BTH101 and T7 Iq pLys were used for cloning procedures, co-immunoprecipitation, bacterial two-hybrid and protein purification, respectively. EAEC wild-type O3:H2 17-2 strain genomic DNA was used as template for cloning. *E. coli* K-12 and EAEC cells were routinely grown in Luria-Bertani (LB) broth at 37 °C, with aeration. For protein production, cells were grown in terrific broth. Plasmids and mutations were maintained by the addition of ampicillin (100 μg ml^{-1}), kanamycin (50 μg ml^{-1}) or chloramphenicol (40 μg ml^{-1}). Gene expression was induced by the addition of iso-propyl-β-D-thio-galactopyranoside (IPTG, Sigma-Aldrich, 1 mM for nanobodies, 0.5 mM for TssK and TssK domain production and BACTH analyses), L-arabinose (Sigma-Aldrich, 0.2%) or anhydrotetracyclin (AHT, IBA Technologies, 0.2 μg ml^{-1}).

Plasmid construction. PCR analyses were performed with a Biometra thermocycler, using Pfu Turbo DNA polymerase (Stratagene). Plasmids and oligonucleotides are listed in Supplementary Table 3. Plasmids producing EAEC TssK domains fused to a VSV-G tag or to the T18 or T25 domains of the *Bordetella pertussis* adenylate cyclase were engineered by restriction-free cloning[67]. Briefly, DNA fragments corresponding to TssK domains were amplified from EAEC 17-2 genomic DNA using oligonucleotides bearing 5′ extensions annealed on the target plasmid. The PCR products were then used as primers for amplification of the target plasmid. Constructs were screened by colony PCR and verified by DNA sequencing. The $TssK_H$ domain (residues S316–T445) was cloned into the pETG20A expression vector using the same procedure.

tssK, *tssF* and *tssG* were initially cloned in a pCDF-Duet1 vector with Cter His_6tag, Nter TREP tag and Cter FLAG tag, respectively (Supplementary Fig. 8). The TREP and FLAG tags were removed by overlapping PCR (Supplementary Fig. 8). The $tssK_{SN}FG$ and $tssK_{H}FG$ vectors were obtained by Gibson assembly (Gibson Assembly Cloning Kit, New England BioLabs) (Supplementary Fig. 9).

Bacterial two-hybrid assay. The adenylate cyclase-based bacterial two-hybrid technique[68] was used as previously described[69]. Briefly, the proteins to be tested were fused to the isolated T18 and T25 catalytic domains of the *Bordetella* adenylate cyclase. After introduction of the two plasmids producing the fusion proteins in the reporter BTH101 strain, plates were incubated at 30 °C for 24 h. Three independent colonies for each transformation were inoculated into 600 µl of LB medium supplemented with ampicillin, kanamycin and IPTG (0.5 mM). After overnight growth at 30 °C, 10 µl volumes of each culture were dropped onto LB plates supplemented with ampicillin, kanamycin, IPTG and 5-bromo-4-chloro-3-indolyl-β-D-galactopyranoside (X-gal) and incubated for 12 h at 30 °C. Controls include interaction assays with TolB and Pal, two protein partners unrelated to the T6SS. The experiments were conducted at least in triplicate, and a representative result is shown.

Co-immunoprecipitation. Co-immunoprecipitation experiments were performed as previously described[35]. A total of 1 × 1011 exponentially growing cells producing the proteins of interest were collected and resuspended in CellLytic B Cell Lysis reagent (Sigma-Aldrich) supplemented with protease inhibitors (Complete, Roche), lysozyme (100 µg ml^{-1}) and DNase (100 µg ml^{-1}), then incubated for 1 h with strong shaking. The insoluble material was discarded by centrifugation for 45 min at 60,000*g* and the supernatant from 2×10^{10} cells was incubated overnight at 4 °C with anti-FLAG M2 affinity beads (Sigma-Aldrich). Beads were then washed twice with CellLytic and once with Tris-HCl 20 mM pH 8.0, NaCl 100 mM. The total extract and immunoprecipitated material were resuspended and boiled in Laemmli loading buffer before analyses by SDS–PAGE and immunoblotting.

High-performance liquid size-exclusion chromatography. Size exclusion chromatography was performed on an Ultimate 3000 HPLC system (Dionex) using a Superdex 200 increase 10/30 GL column equilibrated in Tris 10 mM pH 8, NaCl 150 mM, at a flow rate of 0.6 ml min^{-1}. Accurate injections of 30 µl samples were done using the autosampler and detection was monitored at 280 nm.

Gel filtration analyses. The effect of domains deletions on TssKFG as well as the binding of nanobodies nbK18 and nbK27 to $TssK_{SN}FG$ were analysed using nickel affinity chromatography and gel filtration chromatography. The three constructs possess a unique module bearing a His_6 tag (Supplementary Fig. 9): on TssK for the TssKFG construct, on $TssK_H$ for the $TssK_HFG$ construct and on $TssK_{SN}$ for the $TssK_{NS}FG$ construct. The purification procedures were similar to those used for the TssK–nbK18 complex (see section 'Protein purification'). A 1.2 molar excess of nanobody, nbK18 or nbK25, was added to the $TssK_{SN}FG$ complex and submitted to nickel affinity purification followed by gel filtration. The mixtures were immobilized on a 5 ml Ni^{2+} HisTrap prepacked column (GE Healthcare) using an AKTA FPLC system. After extensive washing steps in the absence or presence of 50 mM imidazole, they were eluted with 250 mM imidazole. The fractions containing the His_6-tagged proteins were pooled and loaded onto a preparative 10/300 Superdex 200 gel filtration column (GE Healthcare) equilibrated in 20 mM Tris-HCl, pH 8.0, 150 mM NaCl. The peaks were analysed by SDS gels. The same conditions were applied to the $TssK_HFG$ construct. Fractions containing the His_6-tagged proteins were pooled and loaded onto a HiLoad 16/600 Superdex 200 column equilibrated in 20 mM Tris-HCl pH 8.0, 150 mM NaCl buffer.

Protein purification. 6×His-tagged TssK was purified as previously described[48]. *E. coli* T7 Iq pLys cells carrying pRSF–TssK ($TssK_{6His}$) or pETG20A–$TssK_{Ct}$ (TssK C-terminal domain fused to a thioredoxin-6×His-TEV N-terminal extension, TRX–6His-TEV–$TssK_{Ct}$) were grown at 37 °C in terrific broth to an optimal optical density (OD_{600}) of ~0.6–1.0 and *tssK* expression was induced with 0.5 mM IPTG for 16 h at 17 °C. Cells were collected, resuspended in 50 mM Tris-HCl pH 8.0, 300 mM NaCl supplemented with 1 mM phenylmethylsulfonyl fluoride, 0.25 mg ml^{-1} lysozyme, 100 µg ml^{-1} DNase I and 20 mM $MgCl_2$. After sonication, soluble proteins were separated from inclusion bodies and cell debris by centrifugation at 20,000*g* for 30 min. $TssK_{6His}$ and TRX–6His-TEV–$TssK_{Ct}$ were immobilized on a 5 ml Ni^{2+} HisTrap prepacked column (GE Healthcare) using an AKTA FPLC system. After extensive washing steps in the absence or presence of 50 mM imidazole, $TssK_{6His}$ and TRX–6His-TEV–$TssK_{Ct}$ were eluted with 250 mM imidazole. The fractions containing the $TssK_{6His}$ protein were pooled and loaded onto a preparative Superdex 200 gel filtration column (GE Healthcare) equilibrated in 20 mM Tris-HCl, pH 8.0, 150 mM NaCl. $TssK_{6His}$ was concentrated to 25 mg ml^{-1} and stored at 4 °C for crystallization trials. The fractions containing TRX–6His-TEV–$TssK_{Ct}$ were pooled and incubated with TEV protease (protein:TEV in a 20:1 molecular ratio) coupled to dialysis against 50 mM Tris-HCl pH 8.0, 300 mM NaCl supplemented with 10 mM imidazole overnight at 4 °C. The proteins were then subjected to a second Ni^{2+} HisTrap prepacked column. The untagged $TssK_H$ protein was collected in the flowthrough and concentrated on a preparative Superdex 200 gel filtration column equilibrated in 20 mM Tris-HCl, pH 8.0, 150 mM NaCl. $TssK_H$ was concentrated to 26 mg ml^{-1} and stored at 4 °C for crystallization trials. pETG20A–$TssK_{SN}$ (TssK N-terminal domain fused to a thioredoxin-6×His-TEV N-terminal extension, TRX–6His-TEV–$TssK_{SN}$) was prepared and purified in the same conditions as $TssK_{6His}$.

Generation and purification of TssK-specific llama nanobodies. To obtain nanobodies against TssK, a llama (*Lama glama*) was immunized with purified $TssK_{6His}$ (Ardèche-lamas France). Approximately 400 µg of $TssK_{6His}$ in 10 mM HEPES, 150 mM NaCl, pH 7.5, was injected subcutaneously four times at one-week intervals using incomplete Freund's adjuvant, followed by a fifth injection two weeks later. Blood samples were collected aseptically 5 days after the last boost. Lymphocytes were isolated from blood samples and cDNA was synthesized from the acquired RNA using a reverse PCR protocol. A nanobody phage display library of $\sim 1 \times 10^9$ independent transformants was generated using the phagemid vector pHEN4 (refs 70, 71). Phage display selection and screening of specific nanobodies were performed as previously described[72]. Enrichment of antigen-specific clones was observed after two consecutive rounds of selection on solid-phase coated antigen. After the second round, TssK-specific nanobodies were identified and the inserts of the corresponding pHEN4-derived plasmids were sequenced and cloned into the pHEN6 vector. *E. coli* WK6 cells carrying the pHEN6 derivatives were grown at 37 °C in terrific broth supplemented with 0.1% glucose and 100 µg ml^{-1} ampicillin to an optical density of ~0.6–1.0 and the expression of the nanobodies was induced by the addition of 1 mM IPTG for 16 h at 28 °C. The periplasmic fraction containing the nanobodies was prepared using mild osmotic shock and the His-tagged nanobodies were immobilized on a 5 ml Ni-NTA column equilibrated in 50 mM Tris-HCl, pH 8.0, 300 mM NaCl and 10 mM imidazole. Nanobodies were eluted in 250 mM imidazole and concentrated using the Amicon technology (10 kDa cutoff) before loading on a HiLoad 16/60 Superdex 75 gel filtration column equilibrated in 20 mM Tris-HCl, pH 8.0, 150 mM NaCl. The final concentrations for NbK18 and NbK27 were 13 mg ml^{-1} and 10 mg ml^{-1}, respectively.

Crystallization and structure determination of nbK18, TssK–nbK18 complex, $TssK_H$ and $TssK_{SN}$–nbK18–nbK27. Crystallization screening experiments were performed with several commercial kits, including STURA, WIZARD and MDL. The nanodrop crystallization experiments were performed in SWISSCI three-well plates. The reservoirs of the SWISSCI plates were filled up using a TECAN pipetting robot, and the nanodrops were dispensed with a Mosquito robot. All crystallization experiments were performed at 293 K. For nbK18, a single crystal was obtained by mixing 100 nl of the nbK18 protein solution with 100 nl of 0.2 M Li_2SO_4, 0.1 M NaAc, pH 4.75 and 30% *m*/*v* PEG8000. The crystal was cryo-cooled in reservoir liquid supplemented with 5% ethylene glycol. For the TssK–nbK18 complex, purified TssK was mixed with nbK18 (TssK:nbK18 at 1:1.2 molecular ratio) and then adjusted to a concentration of 10 mg ml^{-1} for 1 h before crystallization experiments. Small crystals were obtained in 100 mM Tris-HCl, pH 8.5, 200 mM $MgCl_2$, 15% PEG-6000. Optimization was achieved by varying the concentration of PEG-6000 from 8 to 20% *m*/*v* and the pH from 8 to 9. Quality crystals were obtained in 100 mM Tris-HCl, pH 8.3, 200 mM $MgCl_2$, 10% PEG-6000. All crystals, including CsI/NaI derivatives, were cryo-cooled in a well solution supplemented with 20% ethylene glycol. For the CsI/NaI derivatives, the TssK–nb18 crystals were soaked for a few seconds in a well solution supplemented with 20% ethylene glycol and 0.5 M CsI/NaI. For $TssK_H$, the best crystals appeared in 400 mM NaH_2PO_4, 1.6 M K_2HPO_4, 100 mM imidazole, pH 8.0. Crystals were flash-cooled in 5 M sodium formate. Crystals of the $TssK_{SN}$–nbK18–nbK27 complex were obtained in the STURA Footprint Screening plate. $TssK_{SN}$ (35 mg ml^{-1}) was mixed with the purified nanobodies nbK18 and nbK27 at concentrations of 10 mg ml^{-1}, with a molar excess of 1.2 versus $TssK_{SN}$. A volume of 100 nl of the protein mixtures was mixed with 45% PEG-600, 0.1 M HEPES pH 7.5 and dispersed over the reservoir. Crystals appeared in a few days. Crystals were cryo-cooled in the mother liquor.

Data collection was performed at ID23-2 of the ESRF synchrotron (Grenoble, France) for nbK18 and $TssK_H$ and at Proxima 1 of the Soleil synchrotron (Saint-Aubin, France) for the TssK–nbK18 complex, and the data for the crystal of the $TssK_{SN}$–nbK18–nbK27 complex were collected at ESRF beamline ID30A-3 (Supplementary Table 1). The data were integrated and scaled with the XDS/XSCALE package and converted to a ccp4 input format file by XDSCONV (ref. 73). For nbK18, the crystal diffracted up to 1.5 Å (Supplementary Table 1) and belonged to space group $P4_3$, with cell dimensions $a = b = 53.4$ Å, $c = 88.0$ Å, $\alpha = \beta = \gamma = 90°$. Two molecules in the symmetric unit yielded a Vm value of 2.29 $Å^3$ Da^{-1} and 46.35% solvent. Molecular replacement was performed using MOLREP (ref. 74) and with a truncated nanobody structure as a starting model. Refinement was performed using autoBUSTER (ref. 75) alternating with rebuilding with COOT (ref. 76). Two nbK18 molecules are contained in an asymmetric unit and possess a shorter CDR3 compared to those usually found in camelid single-chain domains. For TssK–nbK18, the crystal belonged to the orthorhombic space group $P2_12_12_1$ with cell dimensions $a = 93.3$, $b = 153.7$, $c = 154.8$ Å, $\alpha = \beta = \gamma = 90°$. Diffraction images were processed and scaled with the XDS/XSCALE package[73]. The high-resolution data cutoffs were defined based on the CC1/2 statistical indicator[77]. Molecular replacement on the native data set using the structure of nbK18 provided the positions of three nbK18, but this did not yield a good enough initial electron

density map. Therefore, three 360° rotation data sets were collected at different positions of the large single CsI/NaI crystal derivative at 1.7712 Å X-ray wavelength to 3.5 Å resolution. The heavy atom substructure, comprising 20 sites, was obtained with the SHELXC/D/E software suite[78] using the HKL2MAP graphical interface[79]. This substructure was subsequently refined and used for phase calculation with PHASER (ref. 80). Phase improvement and extension by density modification using three-fold non-crystallographic symmetry averaging performed with PARROT (ref. 81) produced readily interpretable maps that allowed positioning of the three nbK18 and a first rough TssK model to be built. Inspection of electron density maps and model adjustment and rebuilding were performed using COOT (ref. 76) and BUSTER was used for model refinements[75]. The initial refined model was then positioned by molecular replacement with MOLREP (ref. 74) in a 2.7 Å resolution native data set collected at 0.9786 Å wavelength with cell dimensions $a = 93.3$, $b = 153.7$, $c = 154.8$ Å. Then, several iterations of model improvement were conducted by cycling through refinement with autoBUSTER (ref. 75), phase improvement by density modification with PARROT (ref. 81), autotracing with BUCCANEER (ref. 82) and manual pruning and rebuilding using COOT (ref. 76). The structure of $TssK_H$ was obtained by molecular replacement using MOLREP (ref. 74) using the partial structure in the refined full-length TssK and a 1.6 Å resolution data set. Refinement and manual building were performed as for TssK-nbK18. The $TssK_{SN}$–nbK18–nbK27 data were processed and scaled with the XDS/XSCALE package[73]. The crystals belong to the same space group as TssK–nbK18 ($P2_12_12_1$) with comparable packing and cell dimensions of $a = 90.9$, $b = 143.3$, $c = 150.3$ Å. The structure was determined by molecular replacement with MOLREP (ref. 74) using the $TssK_{SN}$ and nbK18 structures as separate models. The resulting map made it possible to complete the missing segments of $TssK_{SN}$ (1–19 and 130–144) as well to construct the nbK27 model using alternative manual fitting with COOT (ref. 76) and autoBUSTER (ref. 75) for model refinements at 2.2 Å resolution (Supplementary Table 1).

BLI. NbK18 was biotinylated using the EZ-Link NHS-PEG4-Biotin kit (Perbio Science). The reaction was stopped by removing excess biotin reagent using a Zeba Spin Desalting column (Perbio Science). BLI assays were performed in black 96-well plates using an OctetRed96 (ForteBio) apparatus. The total working volume for samples or buffer was 0.2 ml and the r.p.m. setting was 1,000 r.p.m. for baseline, loading and association and dissociation steps. The experiments were performed at 25 °C. Before each assay, streptavidin (SA) biosensor tips (ForteBio) were hydrated in 0.2 ml kinetic buffer (KB, ForteBio) for 20 min. SA biosensor tips were then loaded with biotinylated nbK18 at 5 mg ml^{-1} in KB, followed by a quenching step using biocytin. A baseline was recorded and nbK18 binding to $TssK_{6His}$ was performed at concentrations of 0.08–50 nM. Association and dissociation were carried out for 300 and 600 s, respectively. Complete dissociation of the complex was achieved by threefold regeneration (5 s in glycine 10 mM, pH 1.7) and neutralization (5 s in KB).

Data availability. The structures of nbK18, TssK–nbK18 complex, $TssK_{SN}$–nbK18–nbK27 complex and $TssK_H$ have been deposited in the Protein Data Bank (PDB) under accession codes 5M2W, 5M30, 5MWN and 5M2Y, respectively.

Received 22 January 2017; accepted 24 May 2017; published 26 June 2017

References

1. Costa, T. R. *et al.* Secretion systems in Gram-negative bacteria: structural and mechanistic insights. *Nat. Rev. Microbiol.* **13,** 343–359 (2015).
2. Bonemann, G., Pietrosiuk, A. & Mogk, A. Tubules and donuts: a type VI secretion story. *Mol. Microbiol.* **76,** 815–821 (2010).
3. Cascales, E. & Cambillau, C. Structural biology of type VI secretion systems. *Phil. Trans. R. Soc. Lond. B* **367,** 1102–1111 (2012).
4. Kapitein, N. & Mogk, A. Deadly syringes: type VI secretion system activities in pathogenicity and interbacterial competition. *Curr. Opin. Microbiol.* **16,** 52–58 (2013).
5. Zoued, A. *et al.* Architecture and assembly of the type VI secretion system. *Biochim. Biophys. Acta* **1843,** 1664–1673 (2014).
6. Ho, B. T., Dong, T. G. & Mekalanos, J. J. A view to a kill: the bacterial type VI secretion system. *Cell Host Microbe* **15,** 9–21 (2014).
7. Basler, M. Type VI secretion system: secretion by a contractile nanomachine. *Phil. Trans. R. Soc. Lond. B* **370,** 20150021 (2015).
8. Durand, E., Cambillau, C., Cascales, E. & Journet, L. Vgrg, Tae, Tle, and beyond: the versatile arsenal of type VI secretion effectors. *Trends Microbiol.* **22,** 498–507 (2014).
9. Russell, A. B., Peterson, S. B. & Mougous, J. D. Type VI secretion system effectors: poisons with a purpose. *Nat. Rev. Microbiol.* **12,** 137–148 (2014).
10. Kapitein, N. & Mogk, A. Type VI secretion system helps find a niche. *Cell Host Microbe* **16,** 5–6 (2014).
11. Wexler, A. G. *et al.* Human symbionts inject and neutralize antibacterial toxins to persist in the gut. *Proc. Natl Acad. Sci. USA* **113,** 3639–3644 (2016).
12. Chatzidaki-Livanis, M., Geva-Zatorsky, N. & Comstock, L. E. *Bacteroides fragilis* type VI secretion systems use novel effector and immunity proteins to antagonize human gut Bacteroidales species. *Proc. Natl Acad. Sci. USA* **113,** 3627–3632 (2016).
13. Sana, T. G. *et al. Salmonella typhimurium* utilizes a T6SS-mediated antibacterial weapon to establish in the host gut. *Proc. Natl Acad. Sci. USA* **113,** E5044–E5051 (2016).
14. Hecht, A. L. *et al.* Strain competition restricts colonization of an enteric pathogen and prevents colitis. *EMBO Rep.* **17,** 1281–1291 (2016).
15. Fu, Y., Waldor, M. K. & Mekalanos, J. J. Tn-Seq analysis of *Vibrio cholerae* intestinal colonization reveals a role for T6SS-mediated antibacterial activity in the host. *Cell Host Microbe* **14,** 652–663 (2013).
16. Ma, L. S., Hachani, A., Lin, J. S., Filloux, A. & Lai, E. M. *Agrobacterium tumefaciens* deploys a superfamily of type VI secretion DNase effectors as weapons for interbacterial competition in planta. *Cell Host Microbe* **16,** 94–104 (2014).
17. Coulthurst, S. J. The type VI secretion system—a widespread and versatile cell targeting system. *Res. Microbiol.* **164,** 640–654 (2013).
18. Bingle, L. E., Bailey, C. M. & Pallen, M. J. Type VI secretion: a beginner's guide. *Curr. Opin. Microbiol.* **11,** 3–8 (2008).
19. Cascales, E. The type VI secretion toolkit. *EMBO Rep.* **9,** 735–741 (2008).
20. Aschtgen, M. S., Bernard, C. S., De Bentzmann, S., Lloubes, R. & Cascales, E. Scin is an outer membrane lipoprotein required for type VI secretion in enteroaggregative *Escherichia coli*. *J. Bacteriol.* **190,** 7523–7531 (2008).
21. Aschtgen, M. S., Gavioli, M., Dessen, A., Lloubes, R. & Cascales, E. The SciZ protein anchors the enteroaggregative *Escherichia coli* type VI secretion system to the cell wall. *Mol. Microbiol.* **75,** 886–899 (2010).
22. Ma, L. S., Lin, J. S. & Lai, E. M. An IcmF family protein, ImpLM, is an integral inner membrane protein interacting with ImpKL, and its walker a motif is required for type VI secretion system-mediated Hcp secretion in *Agrobacterium tumefaciens*. *J. Bacteriol.* **191,** 4316–4329 (2009).
23. Felisberto-Rodrigues, C. *et al.* Towards a structural comprehension of bacterial type VI secretion systems: characterization of the TssJ–TssM complex of an *Escherichia coli* pathovar. *PLoS Pathog.* **7,** e1002386 (2011).
24. Aschtgen, M. S., Zoued, A., Lloubes, R., Journet, L. & Cascales, E. The C-tail anchored TssL subunit, an essential protein of the enteroaggregative *Escherichia coli* Sci-1 type VI secretion system, is inserted by YidC. *Microbiology Open* **1,** 71–82 (2012).
25. Durand, E. *et al.* Structural characterization and oligomerization of the TssL protein, a component shared by bacterial type VI and type IVb secretion systems. *J. Biol. Chem.* **287,** 14157–14168 (2012).
26. Durand, E. *et al.* Biogenesis and structure of a type VI secretion membrane core complex. *Nature* **523,** 555–560 (2015).
27. Aschtgen, M. S., Thomas, M. S. & Cascales, E. Anchoring the type VI secretion system to the peptidoglycan: TssL, TagL, TagP… what else? *Virulence* **1,** 535–540 (2010).
28. Weber, B. S. *et al.* Genetic dissection of the type VI secretion system in *Acinetobacter* and identification of a novel peptidoglycan hydrolase, TagX, required for its biogenesis. *mBio* **7,** e01253-16 (2016).
29. Santin, Y. G. & Cascales, E. Domestication of a housekeeping transglycosylase for assembly of a type VI secretion system. *EMBO Rep.* **18,** 138–149 (2017).
30. Leiman, P. G. *et al.* Type VI secretion apparatus and phage tail-associated protein complexes share a common evolutionary origin. *Proc. Natl Acad. Sci. USA* **106,** 4154–4159 (2009).
31. Brunet, Y. R., Henin, J., Celia, H. & Cascales, E. Type VI secretion and bacteriophage tail tubes share a common assembly pathway. *EMBO Rep.* **15,** 315–321 (2014).
32. Kudryashev, M. *et al.* Structure of the type VI secretion system contractile sheath. *Cell* **160,** 952–962 (2015).
33. English, G., Byron, O., Cianfanelli, F. R., Prescott, A. R. & Coulthurst, S. J. Biochemical analysis of TssK, a core component of the bacterial type VI secretion system, reveals distinct oligomeric states of TssK and identifies a TssK–TssFG sub-complex. *Biochem. J.* **461,** 291–304 (2014).
34. Brunet, Y. R., Zoued, A., Boyer, F., Douzi, B. & Cascales, E. The type VI secretion TssEFGK–VgrG phage-like baseplate is recruited to the TssJLM membrane complex via multiple contacts and serves as assembly platform for tail tube/sheath polymerization. *PLoS Genet.* **11,** e1005545 (2015).
35. Zoued, A. *et al.* Priming and polymerization of a bacterial contractile tail structure. *Nature* **531,** 59–63 (2016).
36. Boyer, F., Fichant, G., Berthod, J., Vandenbrouck, Y. & Attree, I. Dissecting the bacterial type VI secretion system by a genome wide *in silico* analysis: what can be learned from available microbial genomic resources? *BMC Genomics* **10,** 104 (2009).
37. Pell, L. G., Kanelis, V., Donaldson, L. W., Howell, P. L. & Davidson, A. R. The phage λ major tail protein structure reveals a common evolution for long-tailed phages and the type VI bacterial secretion system. *Proc. Natl Acad. Sci. USA* **106,** 4160–4165 (2009).
38. Kube, S. *et al.* Structure of the VipA/B type VI secretion complex suggests a contraction-state-specific recycling mechanism. *Cell Rep.* **8,** 20–30 (2014).
39. Basler, M., Pilhofer, M., Henderson, G. P., Jensen, G. J. & Mekalanos, J. J. Type VI secretion requires a dynamic contractile phage tail-like structure. *Nature* **483,** 182–186 (2012).

40. LeRoux, M. *et al.* Quantitative single-cell characterization of bacterial interactions reveals type VI secretion is a double-edged sword. *Proc. Natl Acad. Sci. USA* **109,** 19804–19809 (2012).
41. Basler, M., Ho, B. T. & Mekalanos, J. J. Tit-for-tat: type VI secretion system counterattack during bacterial cell–cell interactions. *Cell* **152,** 884–894 (2013).
42. Brunet, Y. R., Espinosa, L., Harchouni, S., Mignot, T. & Cascales, E. Imaging type VI secretion-mediated bacterial killing. *Cell Rep.* **3,** 36–41 (2013).
43. Lossi, N. S., Dajani, R., Freemont, P. & Filloux, A. Structure–function analysis of HsiF, a gp25-like component of the type VI secretion system, in *Pseudomonas aeruginosa*. *Microbiology* **157,** 3292–3305 (2011).
44. Planamente, S. *et al.* TssA forms a gp6-like ring attached to the type VI secretion sheath. *EMBO J.* **35,** 1613–1627 (2016).
45. Taylor, N. M. *et al.* Structure of the T4 baseplate and its function in triggering sheath contraction. *Nature* **533,** 346–352 (2016).
46. Leiman, P. G. *et al.* Morphogenesis of the T4 tail and tail fibers. *Virol. J.* **7,** 355 (2010).
47. Leiman, P. G. & Shneider, M. M. Contractile tail machines of bacteriophages. *Adv. Exp. Med. Biol.* **726,** 93–114 (2012).
48. Zoued, A. *et al.* Tssk is a trimeric cytoplasmic protein interacting with components of both phage-like and membrane anchoring complexes of the type VI secretion system. *J. Biol. Chem.* **288,** 27031–27041 (2013).
49. Logger, L., Aschtgen, M. S., Guerin, M., Cascales, E. & Durand, E. Molecular dissection of the interface between the type VI secretion TssM cytoplasmic domain and the TssG baseplate component. *J. Mol. Biol.* **428,** 4424–4437 (2016).
50. Desmyter, A., Spinelli, S., Roussel, A. & Cambillau, C. Camelid nanobodies: killing two birds with one stone. *Curr. Opin. Struct. Biol.* **32,** 1–8 (2015).
51. Nguyen, V. S. *et al.* Inhibition of type VI secretion by an anti-TssM llama nanobody. *PLoS ONE* **10,** e0122187 (2015).
52. Nguyen, V. S. *et al.* Production, crystallization and X-ray diffraction analysis of a complex between a fragment of the TssM T6SS protein and a camelid nanobody. *Acta Crystallogr. F* **71,** 266–271 (2015).
53. Desmyter, A. *et al.* Three camelid VHH domains in complex with porcine pancreatic alpha-amylase—inhibition and versatility of binding topology. *J. Biol. Chem.* **277,** 23645–23650 (2002).
54. Spinelli, S., Tegoni, M., Frenken, L., van Vliet, C. & Cambillau, C. Lateral recognition of a dye hapten by a llama VHH domain. *J. Mol. Biol.* **311,** 123–129 (2001).
55. Drozdetskiy, A., Cole, C., Procter, J. & Barton, G. J. JPred4: a Protein secondary structure prediction server. *Nucleic Acids Res.* **43,** W389–W394 (2015).
56. Pettersen, E. F. *et al.* UCSF Chimera—a visualization system for exploratory research and analysis. *J. Comput. Chem.* **25,** 1605–1612 (2004).
57. Farenc, C. *et al.* Molecular insights on the recognition of a *Lactococcus lactis* cell wall pellicle by phage 1358 receptor binding protein. *J. Virol.* **88,** 7005–7015 (2014).
58. Spinelli, S. *et al.* Lactococcal bacteriophage p2 receptor-binding protein structure suggests a common ancestor gene with bacterial and mammalian viruses. *Nat. Struct. Mol. Biol.* **13,** 85–89 (2006).
59. Ray, S. P. *et al.* Structural and biochemical characterization of human adenylosuccinate lyase (ADSL) and the R303C ADSL deficiency-associated mutation. *Biochemistry* **51,** 6701–6713 (2012).
60. Casabona, M. G., Vandenbrouck, Y., Attree, I. & Coute, Y. Proteomic characterization of *Pseudomonas aeruginosa* PAO1 inner membrane. *Proteomics* **13,** 2419–2423 (2013).
61. Buttner, C. R., Wu, Y., Maxwell, K. L. & Davidson, A. R. Baseplate assembly of phage Mu: defining the conserved core components of contractile-tailed phages and related bacterial systems. *Proc. Natl Acad. Sci. USA* **113,** 10174–10179 (2016).
62. Spinelli, S. *et al.* Modular structure of the receptor binding proteins of *Lactococcus lactis* phages. The RBP structure of the temperate phage TP901-1. *J. Biol. Chem.* **281,** 14256–14262 (2006).
63. Casjens, S. R. & Molineux, I. J. Short noncontractile tail machines: adsorption and DNA delivery by podoviruses. *Adv. Exp. Med. Biol.* **726,** 143–179 (2012).
64. Spinelli, S., Veesler, D., Bebeacua, C. & Cambillau, C. Structures and host-adhesion mechanisms of lactococcal siphophages. *Front. Microbiol.* **5,** 3 (2014).
65. Sciara, G. *et al.* Structure of lactococcal phage p2 baseplate and its mechanism of activation. *Proc. Natl Acad. Sci. USA* **107,** 6852–6857 (2010).
66. Zoued, A. *et al.* Structure–function analysis of the TssL cytoplasmic domain reveals a new interaction between the type VI secretion baseplate and membrane complexes. *J. Mol. Biol.* **428,** 4413–4423 (2016).
67. van den Ent, F. & Löwe, J. RF cloning: a restriction-free method for inserting target genes into plasmids. *J. Biochem. Biophys. Methods* **67,** 67–74 (2006).
68. Karimova, G., Pidoux, J., Ullmann, A. & Ladant, D. A bacterial two-hybrid system based on a reconstituted signal transduction pathway. *Proc. Natl Acad. Sci. USA* **95,** 5752–5756 (1998).
69. Battesti, A. & Bouveret, E. The bacterial two-hybrid system based on adenylate cyclase reconstitution in *Escherichia coli*. *Methods* **58,** 325–334 (2012).
70. Pardon, E. *et al.* A general protocol for the generation of nanobodies for structural biology. *Nat. Protoc.* **9,** 674–693 (2014).
71. Arbabi Ghahroudi, M., Desmyter, A., Wyns, L., Hamers, R. & Muyldermans, S. Selection and identification of single domain antibody fragments from camel heavy-chain antibodies. *FEBS Lett.* **414,** 521–526 (1997).
72. Desmyter, A. *et al.* Viral infection modulation and neutralization by camelid nanobodies. *Proc. Natl Acad. Sci. USA* **110,** E1371–E1379 (2013).
73. Kabsch, W. XDS. *Acta Crystallogr. D* **66,** 125–132 (2010).
74. Vagin, A. & Teplyakov, A. Molecular replacement with MOLREP. *Acta Crystallogr. D* **66,** 22–25 (2010).
75. Blanc, E. *et al.* Refinement of severely incomplete structures with maximum likelihood in BUSTER-TNT. *Acta Crystallogr. D* **60,** 2210–2221 (2004).
76. Emsley, P., Lohkamp, B., Scott, W. G. & Cowtan, K. Features and development of Coot. *Acta Crystallogr. D* **66,** 486–501 (2010).
77. Karplus, P. A. & Diederichs, K. Linking crystallographic model and data quality. *Science* **336,** 1030–1033 (2012).
78. Sheldrick, G. M. A short history of SHELX. *Acta Crystallogr. A* **64,** 112–122 (2008).
79. Pape, T. & Schneider, T. R. HKL2MAP: a graphical user interface for macromolecular phasing with SHELX programs. *J. Appl. Crystallogr.* **37,** 843–844 (2004).
80. McCoy, A. J. *et al.* Phaser crystallographic software. *J. Appl. Crystallogr.* **40,** 658–674 (2007).
81. Cowtan, K. Recent developments in classical density modification. *Acta Crystallogr. D* **66,** 470–478 (2010).
82. Cowtan, K. The Buccaneer software for automated model building. 1. Tracing protein chains. *Acta Crystallogr. D* **62,** 1002–1011 (2006).

Acknowledgements

The authors thank the members of the Cambillau/Roussel and Cascales laboratories for discussions, A. Kassa for initial work on TssK, L. Journet for critical reading of the manuscript, the Soleil (Saint Aubin, France) and ESRF (Grenoble, France) synchrotrons for beam time allocation and A. Brun, I. Bringer and O. Uderso for technical assistance. This work was supported by the Centre National de la Recherche Scientifique and the Aix-Marseille Université and grants from the Agence Nationale de la Recherche (ANR-14-CE14-0006-02) and the French Infrastructure for Integrated Structural Biology (FRISBI). V.S.N. was supported by a fellowship from the French Embassy in Vietnam. L.L. and A.Z. were supported by doctoral fellowships of the Ministère Français de l'Enseignement Supérieur et de la Recherche and end-of-thesis fellowships from the Fondation pour la Recherche Médicale (FRM) (FDT20160435498 and FDT20140931060, respectively). T.T.N.T. was supported by a grant from the Ministère des Affaires Etrangères, France (no. 861733C). Y.C. is supported by a doctoral school PhD fellowship from the FRM (ECO20160736014).

Author contributions

V.S.N., E.C. and C.C. designed the study. V.S.N., L.L., S.S., P.L., T.T.H.P., T.T.N.T., Y.C., A.Z., A.D., E.D., A.R., C.K., E.C. and C.C. contributed to analysis of the data and preparation of this manuscript. V.S.N., S.S., P.L. and C.C. perform the protein production, crystallization and crystallographic experiments. T.T.H.P. and T.T.N.T. contributed to protein production and crystallization. A.D. performed nanobodies selection and characterization. E.D. provided the TssKFG clone. C.K. performed the BLI and HPLC experiments. L.L., Y.C., A.Z. and E.C performed the double hybrid and co-immunoprecipitation experiments.

Additional information

Supplementary information is available for this paper.

Reprints and permissions information is available at www.nature.com/reprints.

Correspondence and requests for materials should be addressed to E.C. and C.C.

How to cite this article: Nguyen, V. S. *et al.* Type VI secretion TssK baseplate protein exhibits structural similarity with phage receptor-binding proteins and evolved to bind the membrane complex. *Nat. Microbiol.* **2,** 17103 (2017).

Competing interests

The authors declare no competing financial interests.

nature microbiology

SUPPLEMENTARY INFORMATION

VOLUME: 2 | ARTICLE NUMBER: 17103

In the format provided by the authors and unedited.

Type VI secretion TssK baseplate protein exhibits structural similarity with phage receptor-binding proteins and evolved to bind the membrane complex

Van Son Nguyen, Laureen Logger, Silvia Spinelli, Pierre Legrand, Thi Thanh Huyen Pham, Thi Trang Nhung Trinh, Yassine Cherrak, Abdelrahim Zoued, Aline Desmyter, Eric Durand, Alain Roussel, Christine Kellenberger, Eric Cascales* and Christian Cambillau*

- corresponding authors: Eric Cascales (cascales@imm.cnrs.fr) and Christian Cambillau (cambillau@afmb.univ-mrs.fr).

This PDF file includes:

Supplementary Figures 1-10

Supplementary Tables 1-3

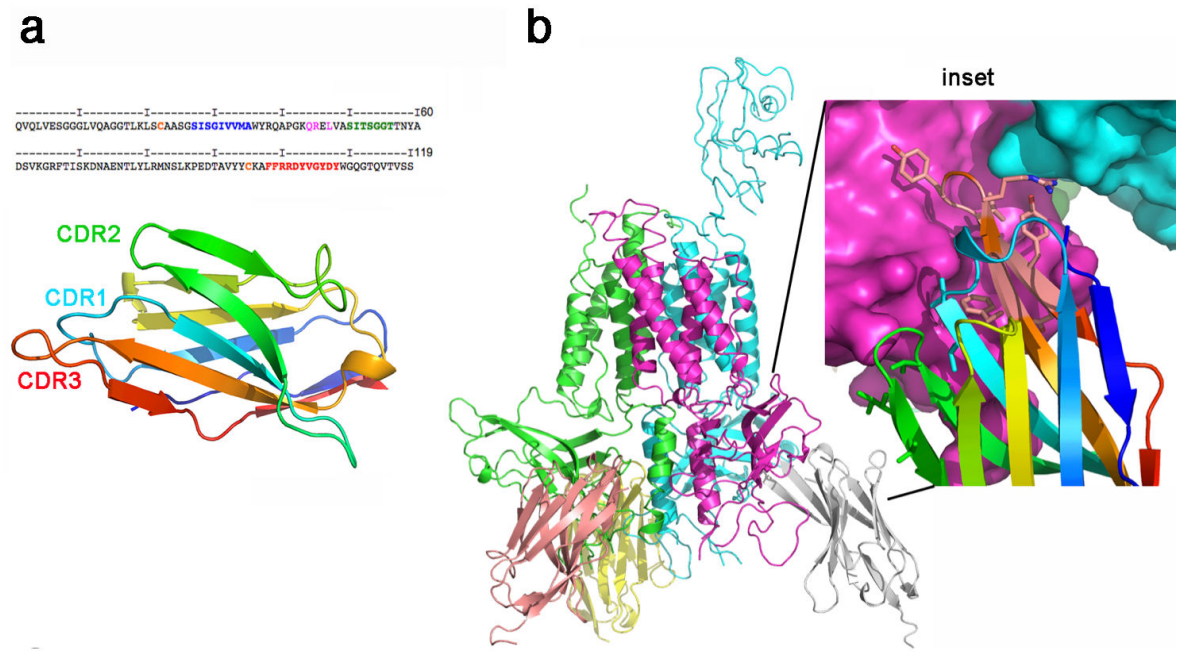

Supplementary Figure 1. Characterization of the nbK18 nanobody and its interaction with TssK. a, sequence and structure of TssK-specific nbK18 llama single-chain antibody. The nbK18 sequence is presented on top of its rainbow-colored ribbon structure. The three complementary-determining regions (CDR) are colored blue, green and red, respectively in the sequence and indicated with the same color code in the ribbon structure. **b,** structure of the trimeric TssK-nbK18 complex. Each TssK is colored as in Fig. 1A (monomers A, B and C in pink, blue and green, respectively) and the three nbK18 nanobodies, bound to TssK shoulder domain, are shown in grey, yellow and salmon, respectively. In the inset is shown a close-up of the TssK-nbK18 interaction at monomer A. TssK is shown in surface representation whereas nbK18 is shown in ribbon. The magnification highlights the side-chains of nbK18 that contact TssK.

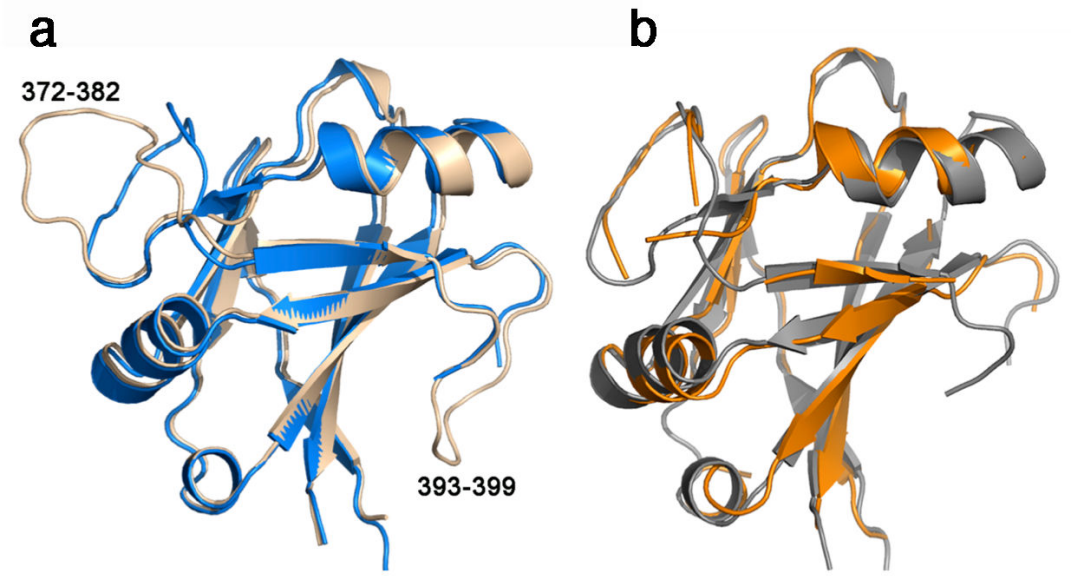

Supplementary Figure 2. Structural analysis of the TssK C-terminal domain. a, overlay between the TssK C-terminal head domain crystallized alone (beige) and in the refined full-length structure after insertion of the TssK C-terminal shoulder domain structure (blue). **b,** overlay between the TssK C-terminal head domain crystallized alone (grey) and in the full-length structure before the TssK C-terminal head structure insertion (orange).

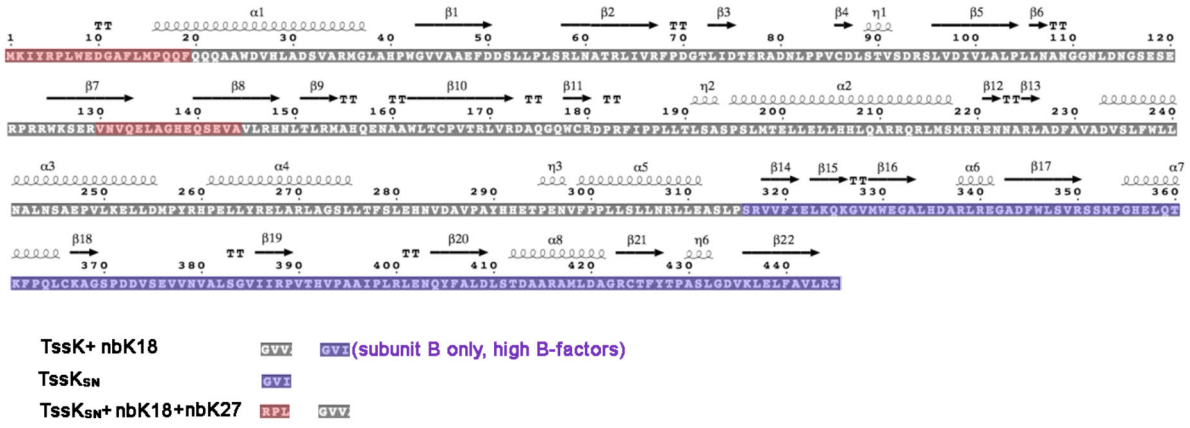

Supplementary Figure 3. Linear sequence representation of TssK with secondary structures. The domains or segments present in the different crystal structures are identified with different colors.

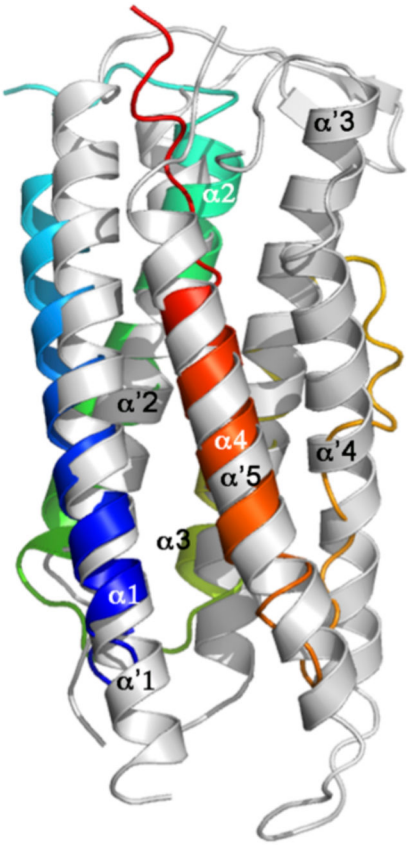

Supplementary Figure 4. Structural homologies of the TssK central domain (neck). Ribbon view of the overlay of t $TssK_N$ helical bundle (rainbow colored) with the Human adenylosuccinate lyase (grey, PDB: 4FFX).

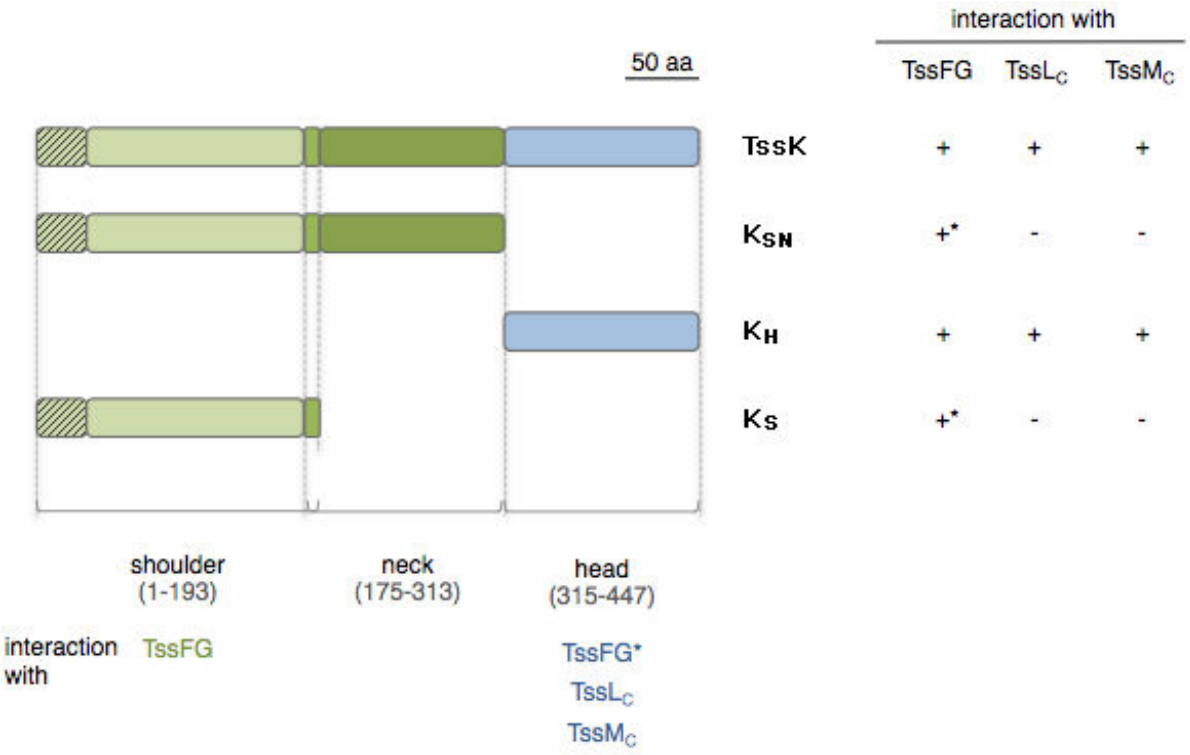

Supplementary Figure 5. Summary of the TssK domains interaction study. The different constructs used for the co-immunoprecipitation analyses are shown on left, with their boundaries (light green, N-terminal shoulder domain (K_S), amino-acids 1-193; dark green, central neck domain (K_N), amino-acids 175-313; blue, C-terminal head domain (K_H), amino-acids 315-447). The interactions identified by co-immunoprecipitations are indicated with '+' on the right (*, interaction observed by co-immunoprecipitation but not confirmed by co-purification and nanobody binding assays).

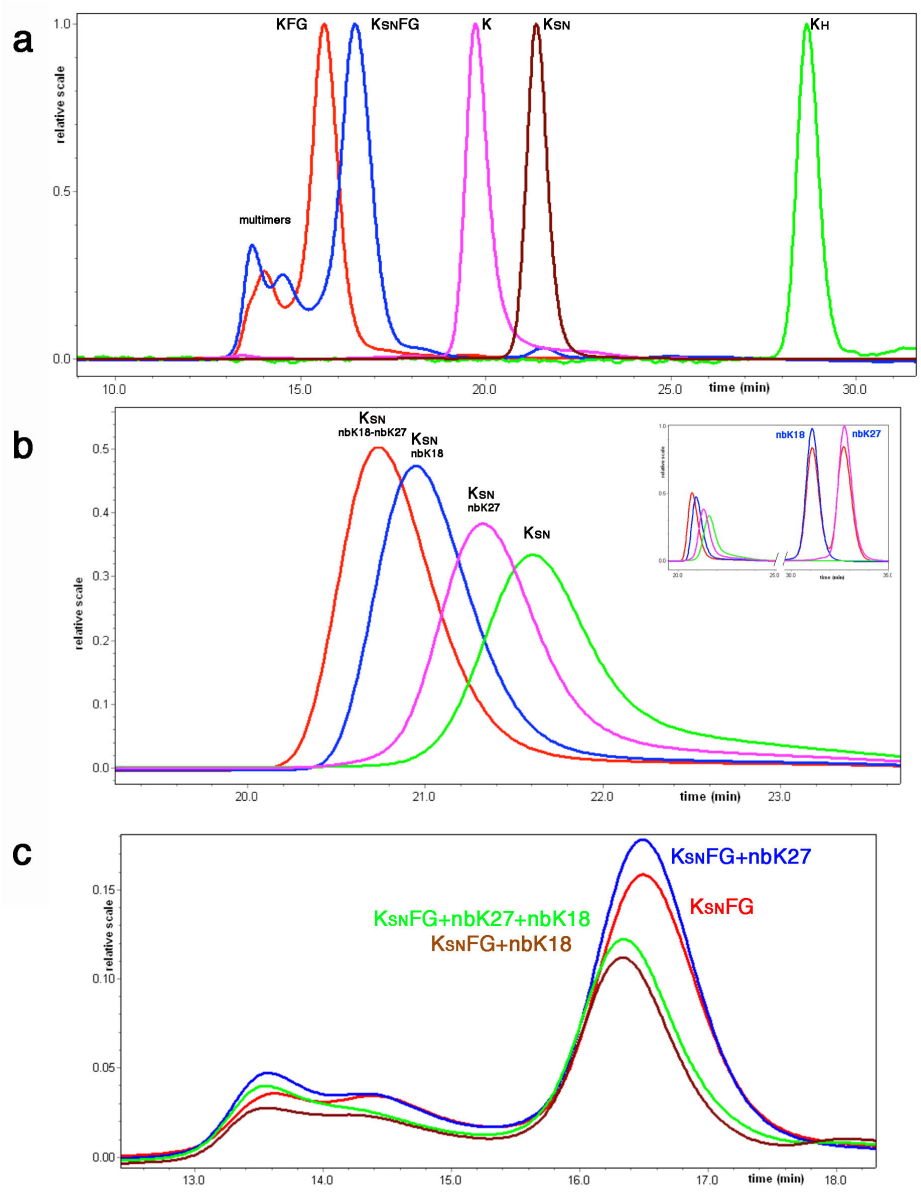

Supplementary Figure 6. **a,** HPLC gel Filtration chromatograms of TssKH, TssKSN, TssK, TssKSNFG and TssKFG. The peaks appearing before TssKFG are assigned to multimers. The peak amplitude has been scaled to 1.0. **b,** HPLC gel Filtration chromatograms of TssKSN in the presence of an excess of nbK18, nbK27 and nbK18, nbK27. **Inset**: the full chromatogram with the nanobodies. **c,** HPLC gel Filtration chromatograms of TssKSNFG alone or in the presence of an excess nbK27 of nbK18, and nbK18 + nbK27. **a,c**: the experiments were done in triplicate and a representative result is shown.

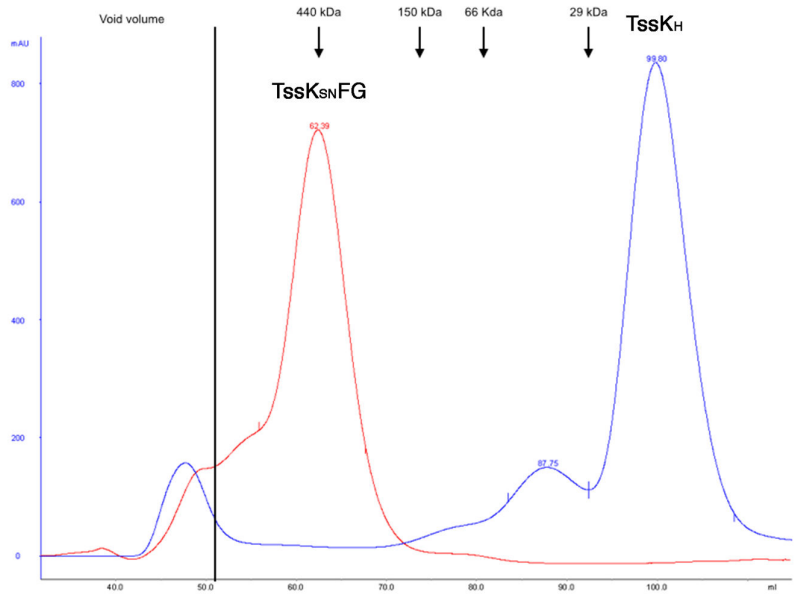

Supplementary Figure 7. Gel Filtration chromatograms of the product resulting from the *tssK$_H$FG* expression (blue) compared to the *tssKSNFG* expression (blue). The main peak of the blue chromatogram corresponds to TssKH alone, indicating that a stable TssKHFG complex is not formed. The experiments was done in duplicate and a representative result is shown.

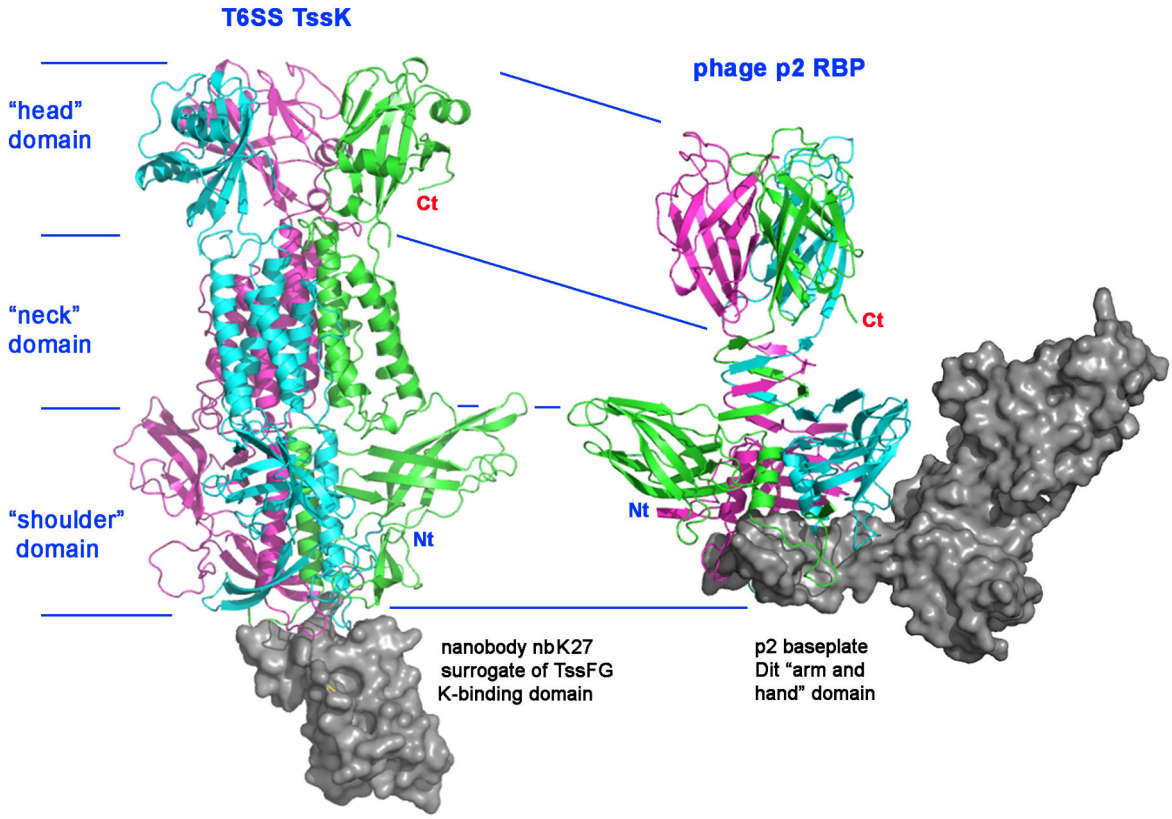

Supplementary Figure 8. Comparison of the TssK and phage p2 RBP structures evidencing the common topology of these trimers formed of shoulder, neck and head domains. The binding of TssK to nbK27 (that occupies the binding site of TssFG) is reminiscent of the binding of the Dit arm and hand extension of the phage p2 Dit molecule.

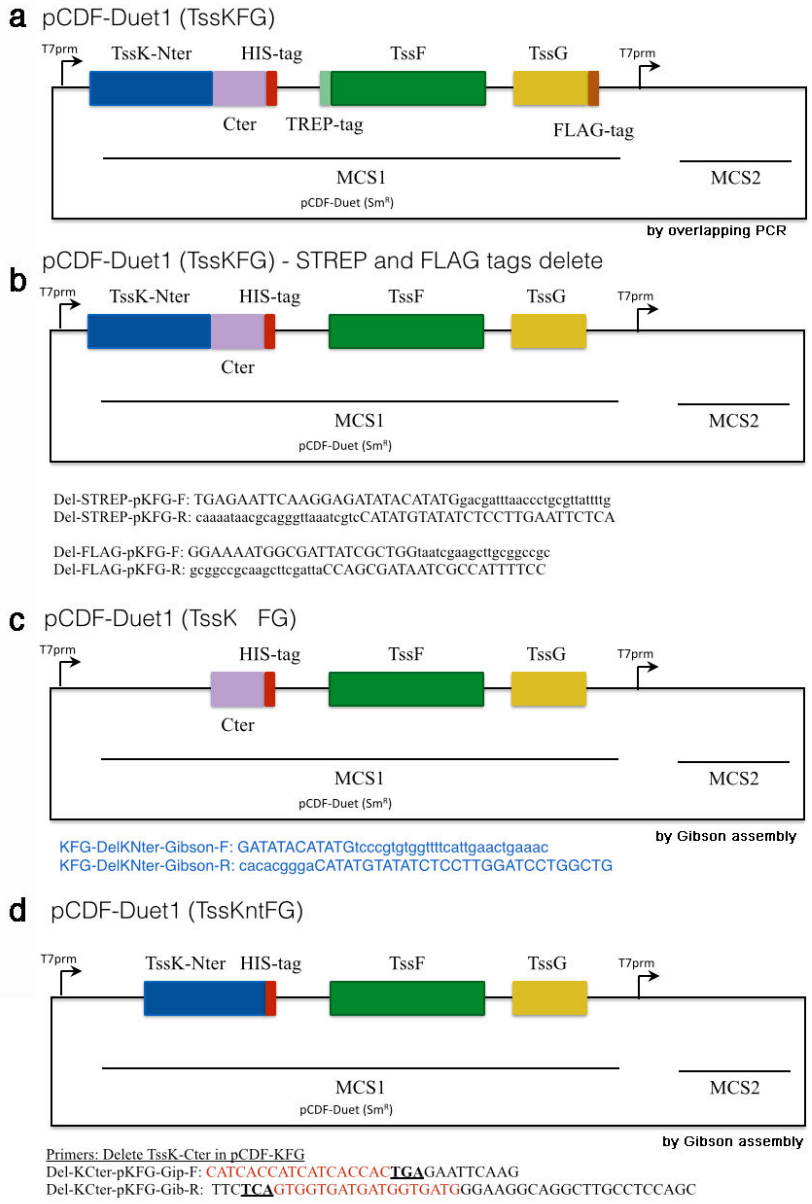

Supplementary Figure 9. Schematic representation of the *tssKFG His, strep and flag* **(a),** *tssKFG His* **(b),** *tss*K_{SN}*FG* **(c)** and *tss*K_{H}*FG* **(d)** constructs used in this study.

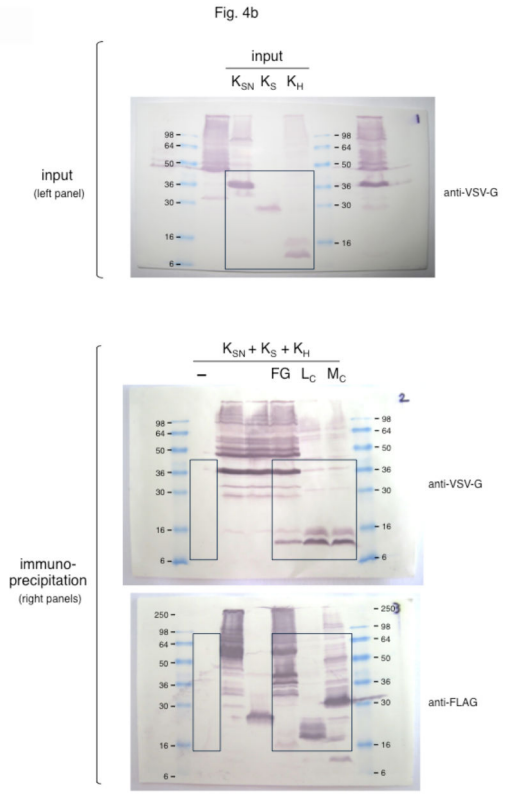

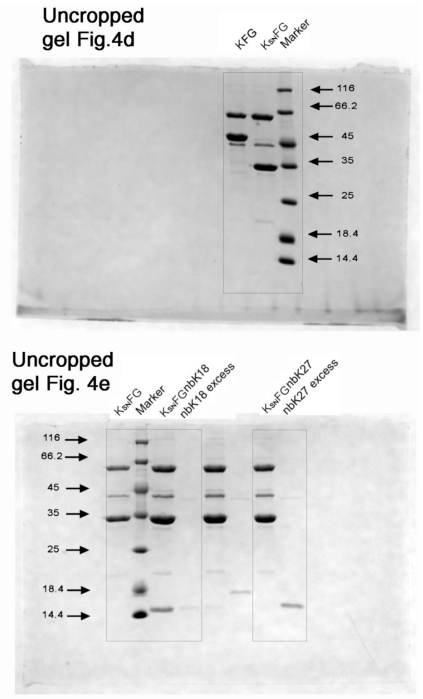

Supplementary Figure 10. Uncropped blots and gels.

Supplementary Table 1. Data collection and refinement statistics of nbK18, nbK18-TssK and $TssK_{SN}$-nbK18-nbK27 complexes, and $TssK_H$ domain. (numbers in brackets refer to the highest resolution bin)

DATA COLLECTION	nbK18	TssK-nbK18 CsI/NaI	TssK-nbK18 native	$TssK_{SN}$-nbK18-nbK27	$TssK_H$
PDB	5M2W		5M30	5MWN	5M2Y
Source	ESRF ID23-2	Soleil PX 1	Soleil PX 1	ESRF ID30A-3	ESRF ID23-1
Wavelength (Å)	0.9786	1.7712	0.9786	0.9677	0.9789
Space group	$P4_3$	$P2_12_12_1$	$P2_12_12_1$	$P2_12_12_1$	$P3_2$
Cell (Å)	a=b=53.4 Å, c = 88.0 Å	a=93.4,b=153.7 c=154.2	a=93.2, b=153.7, c=154.8	a=90.9, b=143.3, c=150.3	a=b=63.8, c=63.1
Angles (°)	α=β=γ=90	α=β=γ=90	α=β=γ=90	α=β=γ=90	α=β=90;
Nr. of monomers	2	3/3	3/3	3/3/1	2
Resolution limits (Å)	20-1.50 (1.59-1.5)	50-3.49 (3.6-3.49)	50.0-2.6 (2.66-2.6)	50.0-2.20 (2.33-2.20)	41.6-1.61 (1.71-1.61)
Rmerge (Rpim[a])	0.088 (0.785)	0.016 (1.8)	0.018 (1.40) [a]	0.077 (0.84)	0.06 (0.65)
CC1/2	0.994 (0.61)	0.999 (0.32)	1.0 (0.30)	0.993 (0.5)	0.99 (0.90)
Unique reflections	38858 (6348)	54138	69265 (4986)	100494 (16357)	36972 (5934)
Mean((I)/sd(I))	7.8 (1.6)	14.6 (1.0)	19.6 (0.5)	6.5 (1.0)	22.79 (3.36)
Completeness (%)	98.7 (98.2)	100 (99.5)	99.8 (99.2)	95.5 (92.4)	99.9 (99.5)
Multiplicity	3.5 (3.3)	18 (8)	11.0 (10.7)	4.8 (4.4)	10.6 (10.5)
SigAno (4.18 Å)		7.9 (0.94)			
CCano (4.18 Å)		0.98 (0.14)			
REFINEMENT					
Resolution (Å)	12.1-1.5 (1.54-1.5)		48.9-2.6 (2.67-2.6)	45.0-2.20 (2.26-2.20)	12.7-1.61 (1.65 1.61)
Number of reflections	38782 (2908)		59771 (4503)	98369 (6904)	36903 (2686)
Number of protein / water / ions atoms	1712/296/15		10297/120	10822/694	1966/223
Test set reflections	1940 (146)		2988	5032	1845
R_{work}/R_{free}	0.195/0.212 (0.3/0.28)		0.198/0.218 (0.249/0.295)	0.199/0.220 (0.232/0.249)	0.198/0.199 (0.216/0.246)
r.m.s.d.bonds (Å)/angles (°)	0.011 / 1.13		0.009 / 1.09	0.008 / 1.07	0.012 / 1.12
B-Wilson / B-mean Å	22.7 / 28.6		108.5/107.1	57.1/66.4	25.7/32.2
Ramachandran: preferred / allowed / outliers (%)	96.3 / 3.7 / 0		97.1/2.6/0.3	79.9/2.1/0	98.0/2.0/0

Supplementary Table 2. Interaction contacts between TssK and the nbK18 nanobody (obtained with the PISA server (Krissinel & Henrick, 2007)). ASA: accessible surface area (Å^2). BSA: buried surface area (Å^2). **a)** surface of nbK18; blue: CDR1; green: CDR2; pink: CDR3. **b)** surface of TssK. (The bars indicate the percentage of the ASA covered; 1 bar = 10%).

a)

	H-bonds	ASA	BSA
VAL 32		56.25	42.21 ||||||||
VAL 33		37.25	32.81 ||||||||
ALA 35		8.52	8.37 |||||||||
TYR 37	H	41.54	25.97 |||||||
total			125
LEU 47		79.47	60.17 ||||||||
SER 50		18.33	10.61 ||||||
THR 52	H	49.89	18.84 ||||
GLY 54		75.43	13.20 ||
THR 56	H	86.79	9.83 ||
ALA 60		21.75	13.55 |||||||
total			132
LYS 96	H	33.05	22.99 |||||||
PHE 98		73.41	72.20 |||||||||
ARG 100	H	133.07	69.68 ||||||
TYR 103		188.69	110.41 ||||||
VAL 104		79.31	32.53 |||||
GLY 105	H	38.52	38.52 |||||||||
TYR 106		89.32	33.59 ||||
ASP 107	H	79.14	65.47 ||||||||
total			452
Grand total			709

b)

	H-bonds	ASA	BSA
PRO 69		47.50	37.02 ||||||||
ASP 70		44.65	21.34 |||||
LEU 105		78.77	78.45 |||||||||
LEU 106	H	70.66	33.60 |||||
ASN 107	H	42.33	36.39 ||||||||
ALA 108	H	106.15	35.88 ||||
ASN 109	H	149.19	58.67 ||||
GLY 110		39.76	11.02 |||
GLU 118		170.72	61.86 ||||
SER 119		48.16	17.95 ||||
GLU 120	H	165.08	139.61 ||||||||
ARG 121		54.64	43.11 |||||||
GLU 158	H	160.85	84.97 ||||||
ALA 160	H	97.20	48.41 |||||
ALA 161		35.99	24.80 ||||||
TRP 162	H	48.61	8.76 ||
LEU 163		22.45	21.13 ||||||||

Supplementary Table 3. Strains, plasmids and oligonucleotides used in this study.

Strains

Strains	Description and genotype	Source
E. coli K-12		
DH5α	F-, Δ(*argF-lac*)U169, *phoA*, *supE44*, Δ(lacZ)M15, *relA*, *endA*, *thi*, *hsdR*	New England Biolabs
W3110	F-, lambda- IN(*rrnD-rrnE*)1 *rph*-1	Laboratory collection
BTH101	F-, *cya-99, araD139, galE15, galK16, rpsL1 (Str r), hsdR2, mcrA1, mcrB1.*	Karimova *et al.*, 2005
T7 Iq pLys	MiniF, *lysY, lacI*^{q} (Cam^{R}), *fhuA2*, *lacZ::T7 gene1*, *ompT*, *gal*, *sulA11*, *R(mcr-73::miniTn10*--Tet^{S}*)2*, *dcm*, *R(zgb-210::Tn10*--Tet^{S}*) endA1 Δ(mcrC-mrr)*	New England Biolabs
Enteroaggregative *E. coli*		
17-2	WT enteroaggregative *Escherichia coli*	Arlette Darfeuille-Michaud

Plasmids

Vectors	Description	Source
Protein production vectors		
pRSF-1	cloning vector, P*T7*, Kan^R	Novagen
pRSF-$TssK_{6His}$	*sci-1 tssK* cloned into pRSF-1, C-terminal 6×His sequence	This study
pETG20A	Gateway® destination vector, 6×His-TRX followed by a TEV cleavage site	Arie Geerlof
pETG-$TssK_{Ct}$	*sci-1 tssK* residues 316-445 cloned into pETG20A	This study
Expression vectors		
pASK-IBA37	cloning vector, P*tet*, Amp^R	IBA Technology
pASK-IBA37-$TssA_{FLAG}$	*sci-1 tssA* cloned into pASK-IBA37, C-terminal FLAG epitope	Zoued *et al*., 2016
pASK-IBA37-$TssF_{FLAG}$	*sci-1 tssF* cloned into pASK-IBA37, C-terminal FLAG epitope	Brunet *et al*., 2015
pASK-IBA37-$TssG_{FLAG}$	*sci-1 tssG* cloned into pASK-IBA37, C-terminal FLAG epitope	Brunet *et al*., 2015
pASK-IBA37-$_{FLAG}$TssLc	*sci-1 tssL* residues 1-184 cloned into pASK-IBA37, N-terminal FLAG epitope	Aschtgen *et al*., 2012
pASK-IBA37-$TssM_C$-NTP_{FLAG}	*sci-1 tssM* residues 62-273 cloned into pASK-IBA37, C-terminal FLAG epitope	Logger *et al*., 2016
pBAD33	cloning vector, pACYC184 origin, *Para*, *araC,* Cm^R	Guzman *et al*., 1995
pBAD33-$TssK_{VSV-G}$	*sci-1 tssK* cloned into pBAD33, C-terminal VSV-G epitope	Brunet *et al*., 2015
pBAD33-TssK-SN_{VSV-G}	*sci-1 tssK* residues 1-315 cloned into pBAD33, C-terminal VSV-G epitope	This study
pBAD33-TssK-H_{VSV-G}	*sci-1 tssK* residues 315-445 cloned into pBAD33, C-terminal VSV-G epitope	This study
pBAD33-TssK-S_{VSV-G}	*sci-1 tssK* residues 1-193 cloned into pBAD33, C-terminal VSV-G epitope	This study
pBAD33-TssK-N_{VSV-G}	*sci-1 tssK* residues 175-315 cloned into pBAD33, C-terminal VSV-G epitope	This study
pUC-Hcp_{FLAG}	*sci-1 hcp* cloned into pUC12, P*lac*, C-terminal FLAG epitope	Aschtgen *et al.*, 2008

Bacterial Two-Hybrid vectors		
pT18-FLAG	Bacterial Two Hybrid vector, ColE1 origin, P*lac*, T18 fragment of *Bordetella pertussis* CyaA, Amp^R	Battesti & Bouveret, 2008
pTssK-T18	*tssK* cloned upstream T18 in pT18-FLAG	Zoued *et al.*, 2013
pTssK$_S$-T18	*tssK* residues 1-193 cloned upstream T18 in pT18-FLAG	This study
pT18-TssK$_N$	*tssK* residues 175-315 cloned downstream T18 into pT18-FLAG	This study
pTssK$_{SN}$-T18	*tssK* residues 1-315 cloned upstream T18 into pT18-FLAG	This study
pT18-TssK$_H$	*tssK* residues 315-445 cloned downstream T18 into pT18-FLAG	This study
pT18-Pal	*pal* cloned downstream the T18 coding sequence in pT18-FLAG	Battesti & Bouveret, 2008
pT25-FLAG	Bacterial Two Hybrid vector, p15A origin, P*lac*, T25 fragment of *Bordetella pertussis* CyaA, Kan^R	Battesti & Bouveret, 2008
pT25-TssFG	*tssFG* cloned downstream the T25 coding sequence in pT25-FLAG	Brunet *et al.*, 2015
pT25-TssK	*tssK* cloned downstream the T25 coding sequence in pT25-FLAG	Zoued *et al.*, 2013
pTssL$_C$-T25	*tssL* residues 1-184 cloned downstream the T25 coding sequence in pT25-FLAG	Durand *et al.*, 2012
pTssM$_C$-T25	*tssM* residues 62-360 cloned upstream the T25 coding sequence in pT25-FLAG	Zoued *et al.*, 2013
pT25-TolB	*tolB* cloned upstream the T25 coding sequence in pT25-FLAG	Battesti & Bouveret, 2008

Oligonucleotides

Name	Destination	Sequence (5' → 3')
For plasmid construction [b,c,d]		
5- pBAD33-TssK-SN$_{VSV-G}$	insertion of *tssK*$_{1-315}$ fragment into pBAD33	CTCTCTACTGTTTCTCCATACCCGTTTTTTTGGGCT AGCAGGAGGTATTACACCATGAAGATTTATCGCCCA TTATGGGAAGACG
3- pBAD33-TssK-SN$_{VSV-G}$	insertion of *tssK*$_{1-315}$ fragment into pBAD33	GGTCGACTCTAGAGGATCCCCGGGTACCTTA*TTT TCCTAATCTATTCATTTCAATATCTGTATA*GGAAGG CAGGCTTGCCTCCAGC
5- pBAD33-TssK-H$_{VSV-G}$	insertion of *tssK*$_{315-445}$ fragment into pBAD33	CTCTCTACTGTTTCTCCATACCCGTTTTTTTGGGCT AGCAGGAGGTATTACACCATGCGTGTGG TTTTCATTGAACTGAAACAAAAGGC
3- pBAD33-TssK-H$_{VSV-G}$	insertion of *tssK*$_{315-445}$ fragment into pBAD33	GGTCGACTCTAGAGGATCCCCGGGTACCTTA*TTT TCCTAATCTATTCATTTCAATATCTGTATA*TGT CCGCAGCACCGCAAAAAGTTC
3-pBAD33-TssK-S$_{VSV-G}$	insertion of *tssK*$_{1-193}$ fragment into pBAD33	GGTCGACTCTAGAGGATCCCCGGGTACCTTA *TTTTCCTAATCTATTCATTTCAATATCTGTATA* GGCAGACAGCGTCAGCAGAGGG
5-pBAD33-TssK-N$_{VSV-G}$	insertion of *tssK*$_{175-315}$ fragment into pBAD33	CTCTCTACTGTTTCTCCATACCCGTTTTTTTGGGCT AGCAGGAGGTATTACACCATGGGACAGTGG TGCAGGGACCCGCG
5-pTssK$_S$-T18	insertion of *tssK*$_{1-193}$ fragment into pT18-Flag	CGGATAACAATTTCACACAGGAAACAGCTATGACC ATGAAGATTTATCGCCCATTATGGGAAGACG
3-pTssK$_S$-T18	insertion of *tssK*$_{1-193}$ fragment into pT18-Flag	CCTCGCTGGCGGCTAAGCTTGGCGTAAT GGCAGACAGCGTCAGCAGAGGG
5-pT18-TssK$_N$	insertion of *tssK*$_{175-315}$ fragment into pT18-Flag	GCCACTGCAGGGATTATAAAGATGACGATGA CAAGGGACAGTGGTGCAGGGACCCGC
3-pT18-TssK$_N$	insertion of *tssK*$_{175-315}$ fragment into pT18-Flag	AGGTCGACGGTATCGATAAGCTTGATATCGAATTC

		TAGTTAGGAAGGCAGGCTTGCCTCCAGC
5-pTssK$_{SN}$-T18	insertion of *tssK*$_{1-315}$ fragment into pT18-Flag	CGGATAACAATTTCACACAGGAAACAGCTATGACC ATGAAGATTTATCGCCCATTATGGGAAGACG
3-TssK$_{SN}$-T18	insertion of *tssK*$_{1-315}$ fragment into pT18-Flag	CCTCGCTGGCGGCTAAGCTTGGCGTAATGGAAG GCAGGCTTGCCTCCAGC
5-pT18-TssK$_{H}$	insertion of *tssK*$_{315-445}$ fragment into pT18-Flag	CGCCACTGCAGGGATTATAAAGATGACGATGACA AGCGTGTGGTTTTCATTGAACTGAAACAAAAGGG
3-pT18-TssK$_{H}$	insertion of *tssK*$_{315-445}$ fragment into pT18-Flag	CGAGGTCGACGGTATCGATAAGCTTGATATCGAA TTCTAGTTATGTCCGCAGCACCGCAAAAAGTTC
T6_K316-445_p17_F	insertion of *tssK*$_{316-445}$ fragment into pETG20A	GGCTTAGAAAACCTGTACTTCCAGGGTTCCCGT GTGGTTTTCATTGAACTGAAAC
T6_K316-445_p17_R	insertion of *tssK*$_{316-445}$ fragment into pETG20A	ACCACTTTGTACAAGAAAGCTGGGTTTATTATGTCC GCAGCACCGCAAAAAGTTCC

[a] Sequence annealing on the target plasmid underlined.
[b] VSV-G epitope coding sequence *italicized*.

General discussion and additional results

5.1 General discussion

Articles 3 and *4* provide details on how the membrane complex and the baseplate are connected. In *Article 3*, I have characterized the TssM cytoplasmic loop and have determined domains and motifs that mediate interaction with TssG and TssK. In *Article 4*, I have participated to the structure-function analysis of TssK, showing that the shoulder and head domains of this RBP-like protein are involved in the interaction with the baseplate and the membrane complex, respectively.

The TssM cytoplasmic domain is composed of two subdomains: a domain with a NTPase fold followed by a DPY-30-like 110-aminoacid region. The DPY-30-like region is responsible for $TssM_{Cyto}$ oligomerization and interaction with TssG. The NTPase-like domain interacts with TssK. TssK is composed of three domains, and assembles trimers. The N-terminal domain is structurally homologous to the shoulder of RBPs that interacts with baseplate components whereas the C-terminal domain interacts with the membrane complex. Therefore, TssK connects the TssJLM membrane complex to the baseplate.

The motifs of TssM and TssK involved in TssM-TssK interaction have not been addressed in this work. It would be interesting to better understand how these two proteins interact. The head domain is an α/β globular domain with several loops. A mutagenesis study of these loops could be performed in order to understand how they contribute to interactions to TssL and TssM.

Structural servers predict that part of the TssM cytoplasmic domain present a fold associated with NTPases. However, no structure of TssM cytoplasmic domains is available. Proteins with NTPase proteins are known to regulate cellular processes by switching between different conformations, depending on the NTP binding and/or hydrolysis and on associated GEF and/or GAP proteins (Bos et al., 2007a)(Cherfils and Zeghouf, 2013)(Wittinghofer and Vetter, 2011). Indeed, the TssM protein from *A. tumefaciens* has been shown to be responsive to ATP binding and hydrolysis, and to change conformation. However, in the EAEC Sci-1 TssM protein, the Walker A and B motifs involved in NTP binding and hydrolysis are lacking. One interesting immediate perspective to this work will be to define whether TssM changes conformation depending on the conditions (presence of the target cell, baseplate docking, sheath contraction,...). We have shown that TssK interacts with the TssM NTPase-like domain, and it will be thus interesting to determine whether TssK modulates TssM conformation.

To validate that the cytoplasmic domain of TssM presents an NTPase-like fold, we wished to purify TssM for structural studies.

5.2 Additional results

This study revealed that the predicted TssM NTP-like fold region binds to TssK. TssK was previously shown to connect the membrane complex and the phage-like complex (Zoued et al., 2013). Moreover, NTPase proteins (more specifically GTPase) constitute switches that quickly activate or inhibit various cellular processes (Wittinghofer and Vetter, 2011). To gain further information in the cytoplasmic domain of TssM and how it is connected to the baseplate, we wished: (i) to produce the TssM$_{Cyto}$ domain, alone or with TssK; (ii) to test the TssM$_{Cyto}$ domains from EAEC, and *Salmonella* for their ability to bind and/or hydrolyse nucleotides; (iii) to define whether TssK contribute to these activities; (iv) to purify TssM$_{Cyto}$ and/or the TssM$_{Cyto}$-TssK complex for crystallization trials; and (v) to determine precisely how TssM$_{Cyto}$ and TssK interact.

The sequence encoding the cytoplasmic domain of the EAEC TssM protein was cloned into the pETG20A vector. This vector is dedicated to T7-driven protein production and purification by affinity chromatography. In this construct, TssM$_{Cyto}$ is fused to the thioredoxin (TRX) followed by 6-His tag and a cleavage site for the TEV protease (Strains, plasmids and primers are listed in *Table S3* presented in *Annexe*). The 6-His epitope allows immobilization of the protein on nickel/cobalt affinity column and its elution using an imidazole gradient. The TRX improves protein solubility whereas the cleavage site could be used to obtain the native protein. In addition to EAEC TssM$_{Cyto}$, the sequence encoding the cytoplasmic domain of the *S. enterica* Typhimurium TssM was also cloned (*Table S3*). The *S. enterica* Typhimurium TssM cytoplasmic domain bears the catalytic residues required for NTP binding and hydrolysis. The expression of the cloned fragments was induced in BL21(DE3) cells with 1 mM of IPTG. The two proteins were produced but after cell lysis and ultracentrifugation, SDS-PAGE analyses of soluble and insoluble fractions showed that both proteins are insoluble. Both proteins aggregated (data not shown).

However, the analysis of the TssM$_{Cyto}$ sequence showed that it harbours a hydrophobic region at its C-terminus. We then constructed new versions encoding only the NTPase-like domain of the EAEC and the S. Typhimurium TssM$_{Cyto}$ domains (*Table S3*). A small fraction of the S. Typhimurium TssM$_{Cyto}$ remained soluble. After purification by affinity chromatography, SDS-PAGE analyses showed that several bands are observable, likely corresponding to TssM$_{Cyto}$ degradation products and multimers (Figure 5.40).

Previous analyses have demonstrated that the TssM cytoplasmic domain interacts with TssK. We then co-produced TssM$_{Cyto}$ and TssK with the hypothesis that TssK will help TssM$_{Cyto}$ solubilization. Proteins were still located in inclusion bodies (data not shown). We decided to stop this project, but many experiments could be done to purify TssM$_{Cyto}$: solubilization by urea or guanidine and refolding in specific buffers, solubilization in presence of detergents,... Another perspective to continue this project will be the co-purification of the TssJLM complex with TssK.

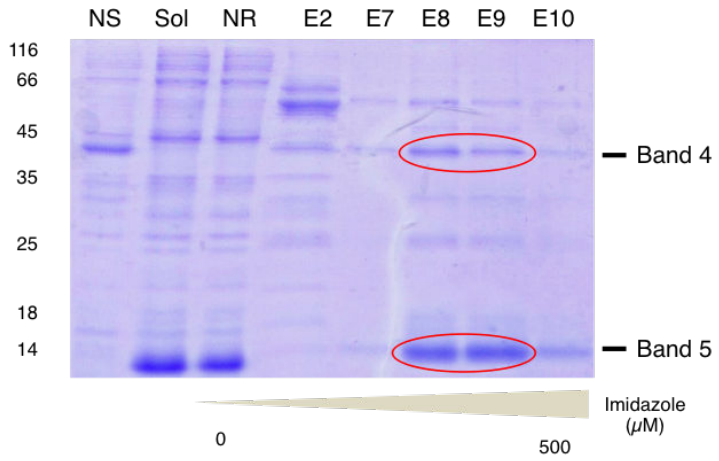

Figure 5.40: **Protein profile of fractions after purification by affinity chromatography of TssM$_{Cyto}$-NTP-Stm.** NS, non soluble; Sol, soluble; NR, flow-through; E, eluted fractions. Fractions were eluted with an imidazole gradient). Band 4 corresponds to the protein TRX-6His-TssMc-NTP-Stm. Band 5 corresponds to TRX cleaved at TEV site.

This will provide significant information on how TssK interacts with the cytoplasmic face of the membrane complex. In addition, a mutagenesis study could be performed to define the residues implicated in TssM$_{Cyto}$-TssK complex formation.

5.3 Anchoring the baseplate to the membrane complex

The T6SS baseplate and the membrane complex are evolutionarily distinct. The T6SS tail and baseplate are structurally, evolutionarily and functionally similar to the contractile tailed bacteriophages whereas the TssM and TssL membrane complex subunits have homologies with the IcmF and IcmH/DotU proteins, two accessory subunits of the Type IVb secretion system (T4bSS) (Sexton et al., 2004)(vanRheenen 2004). This evolutionary difference is highlighted by the mismatch symmetry between the two complexes. As shown in *Article 2*, the membrane complex has a 5-fold symmetry whereas the T6SS baseplate has likely a 6-fold symmetry such as TssA, the inner Hcp tube or the sheath, and similarly to baseplate bacteriophages.

Several hypotheses have been raised. First, it might be a real symmetry mismatch that could be of functional importance, *e.g.*, the symmetry mismatch allows a strong flexibility necessary for rotation of one complex compared to the other. Such a symmetry mismatch exists between the 6-fold symmetry tail portal and the pentagonal vertex of several bacteriophages, allowing the packaging of the DNA into the capsid (Hendrix, 1978). Second, no symmetry mismatch exists, and the TssJLM complex purified from BL21(DE3), *i.e.*, in absence of the other T6SS components, has a more-stable 5-fold symmetry, but is forced to a 6-fold symmetry *in vivo*, in presence of the remaining of the T6SS machine. This hypothesis is also possible as TssA has been shown to interact with the TssJM complex, before the recruitment of TssL and the polymerization of the TssJLM complex (Zoued et al., 2016b). Therefore, TssA might act as a chaperone to guide the 6-fold symmetrization of the TssJLM complex (Zoued et al., 2017). Testing this hypothesis is quite simple, by purifying the TssJLM-A complex. Third, the symmetry mismatch could be

accommodated by an adaptor. The role of symmetry adaptor could be done by TssK, which has been shown to interact with both baseplate and membrane complex components. Prior to the publication of *Article 4*, it was proposed in the literature that TssK may have homologies with bacteriophage T4 gp8 (Planamente et al., 2016). This hypothesis, based on limited conserved secondary elements predicted using algorithms, was extravagant. The crystal structure of TssK solved this issue and revealed that the N-terminal domain of TssK harbors structural homology with shoulder domains of siphophage RBPs. In phages, shoulder domains anchor the RBP in the phage baseplate. Similarly, the N-terminal shoulder domain of TssK interacts with the TssFG complex. In phages, the head domains of RBPs contain the receptor-binding motif that specifically recognizes receptors at the host cell surface. In the case of TssK, the C-terminal "head" domain interacts with the membrane complex. TssK then uses the membrane complex as a receptor, which permits proper anchoring to the cell envelope and proper orientation towards the cell exterior. Therefore, bacteria have acquired (probably by horizontal transfer) a RBP and evolved its C-terminal domain to recognize and bind the base of the T6SS membrane complex, which comprises the cytoplasmic domains of both TssM and TssL. The TssM and TssL proteins have homologies with the T4bSS-associated IcmF and IcmH/DotU proteins (Bingle et al., 2008)(Cascales, 2008). One may predict that the TssK head domain would have the same origin. It would be therefore interesting to determine whether one of the IcmF or DotU partners has a domain structurally homologous to the TssK head-like domain.

Interestingly, the crystal structure of TssK showed that the structure of several loops within the head domain could not be solved easily, due to intrinsic flexibility. This means that the membrane complex-TssK interface is likely very flexible, and this may prevent disruption of the contact between the membrane and baseplate complexes during the large conformation changes that is induced during sheath contraction.

Based on these findings, I propose a multi-step model for the anchoring the baseplate to the membrane complex: (1) TssA binds the membrane complex and acts as a chaperon protein by reconciling the symmetry mismatch; (2) TssK, in complex with baseplate components, interacts with TssM and TssL; (3) Then, additional contacts involving TssG and TssE stabilize the membrane complex-baseplate interface. A first step toward testing this model will be to obtain affinity data between the different complexes involved in baseplate docking to the membrane complex: TssK-TssM, TssK-TssL, TssG-TssM, TssE-TssL.

In addition to the experiments proposed above, it would be interesting to purify and image by negative-strain or cryo-electron microscopy the TssJLM complex with and without TssK to understand how TssK plays its connector role. Finally, the strains engineered for electron cryo-tomography (see *Additional results* of *Article 2*) will be of particular interest to determine how the baseplate is docked to the membrane complex *in vivo*. Very recently, the structure of the T6SS from *Myxococcus xanthus* was visualized by ECT (Chang et al., 2017). The sub-tomogram averaging revealed a density of 300 Å between the membrane complex and the sheath/Hcp tube. The baseplate suggests a layer organization from the tail to the membrane complex with a thin and a thinker layer followed by a cage-like structure. The exact composition of these layers needs to be determined.

Additional studies

During my PhD, in addition to my main work on the TssM protein, I had the opportunity to participate to several studies, and more specifically on studies related to the T6SS tail sheath.

During my first internship in the lab, Basler et al showed by fluorescence microscopy that T6SS assembles sheath structures that oscillated between extended and contracted conformations (Basler and Mekalanos, 2012). I first participated to a study showing that the histone-like H-NS protein represses the expression of the Type VI secretion gene cluster in *Salmonella enterica* ser. Typhimurium. In this study, I engineered a TssB-GFP fusion on the chromosome of *S.* Typhimurium and imaged the dynamics of T6SS sheath by fluorescence microscopy. This work has been published in Infection and Immunity and is presented in *Annexe 1.*

I then participated to a work on the complex between the TssB and TssC subunits, and more specifically on the domains of TssB involved in TssBC complex formation. In this study, we have shown that the N-terminal region of TssC and a long α-helix close to the TssB C-terminus are implicated in TssB-C interaction. This work, published in PLOS One, is presented in *Annexe 2.* Similar data were obtained by a Swedish group on the *Francisella* TssBC proteins (Bröms et al., 2013).

More recently, the group of M. Basler has provided the cryo-EM structure of the T6SS sheath in its contracted conformation (Kudryashev et al., 2015). However, the C-terminal fragment of TssB, comprising the long α-helix was missing in this structure. We thus tried to obtain structural information on this missing piece. We obtained crystals of a short C-terminal fragment of TssB and solved the structure. The TssB C-terminal domain comprises the long α-helix followed by a hairpin. The structure showed that this hairpin bears an important number of positively and negatively charged residues that are exposed at the surface of the protein. I then carried out a structure-function analysis by substituting these residues by opposite charges and testing the impact of these mutations on T6SS activity and sheath dynamics. A manuscript describing these data, currently submitted to J Mol Biol, is presented in *Annexe 3.*

Finally, I have also been involved in the redaction of a review describing the architecture and the assembly of the T6SS (*Annexe 4*) and in the redaction of a method chapter describing two fusion reporter approaches to study interactions between transmembrane helices in bacterial membranes (*Annexe 5*).

Part III

General Conclusion and Perspectives

General Conclusion and Perspectives

In the environment, bacteria live in complex multispecies communities. In these communities, bacteria communicate and compete with one another for colonization and survival. They have developed several strategies as diverse as the competitors they encounter. During my PhD, I have been working on the Type VI secretion system, a key actor of bacterial competition in the soil and in the human body.

Each secretion system has a specific overall structure, biogenesis, and function. The T6SS fits to this rule. It is a unique secretory apparatus, combining two evolutionarily distinct sub-assemblies. The contractile tail-like complex resembles contractile injection systems such as bacteriophages T4 and Mu, or R-type pyocins. By contrast, the inner membrane part of the membrane complex is similar to the accessory complex of the Type IVb secretion system.

We recently shed light on the overall architecture of the T6SS membrane complex. This great advance in the field paves the way to further *in situ* experiments such as ECT. This "in-cell "approach will for sure fill gaps and help to answer many questions regarding the structure of the membrane complex or that of the baseplate.

During my PhD, I have been interested on the TssM protein and how this protein is connected to the baseplate: How a protein that spans the entire periplasm is involved in the assembly of the system? How TssM is organized at the outer membrane? What are the molecular determinants of the connection between TssM and the baseplate? Does TssM participate in the sensing of the prey? I have presented in this manuscript the data I have obtained during my Ph.D.

The EAEC TssM protein is a large protein of 1129 amino acids. Topological experiments have shown that TssM is constituted of three TMH, with the N-terminus in the cytoplasm and the C-terminus in the periplasm (*Article 3*).

6.1 TssM cell surface exposition: a role in sensing the target cell?

I have participated to the structural characterization of the periplasmic domain of TssM in complex with TssJ. By using specific nanobodies that compete with TssM-TssJ complex formation and hence inhibits T6SS activity (*Article 1*), our collaborators succeeded to crystallize a fragment of the TssM periplasmic domain, alone and in complex with TssJ. Based on this structure and by using a cysteine-labelling approach, I revealed that a C-terminal extension of TssM, located after the last α-helix, is exposed at the cell surface (*Article 2*). Based on the secondary structures

and on the fact that a few cases of α-helix insertion into the OM (Chandran et al., 2009)(Low et al., 2014)(Ford et al., 2009)(Dong et al., 2006) have been reported, we propose that this long α-helix crosses the outer membrane. Cell surface exposition of the TssM C-terminal extension is dependent on the TssJ lipoprotein, and this is reminiscent of most trans-envelope apparati in which outer membrane lipoproteins chaperone outer membrane components and/or facilitate their insertion. Because the TssM C-terminal extension represents the only extracellular portion of the T6SS (as far as we know), an exciting hypothesis is that this extension participates in the sensing of the target cell. Although this is not a proof, an argument for this hypothesis is that TssM proteins associated with T6SS that do not encode the post-translational TagQRST-PpkA-PppA-FHA activation pathway have a C-terminal extension. Fluorescence microscopy recordings have shown that the T6SS responds rapidly to a contact with a target cell. Pre-assembled membrane complexes and a fragment permanently exposed outside of the cell is the perfect combination to sense a stimulus and fire efficiently. Thus, how the target is sensed and how the signal is transmitted to induce machine assembly or sheath contraction are two questions that need to be answered. I have presented here additional results to better characterize the TssM C-terminal extension but much more experiments need to be conducted. In addition, the sensing is likely not an easy task, as T6SS are versatile machines that could inject effectors into both prokaryotic and eukaryotic cells. In this case, is the signal different according to the target cell? The hypothesis of sensing a "surface tension" will reconcile these questions.

6.2 TssM: a transient pore at the OM ?

The cysteine accessibility approach also revealed that the β-strands of the TssM β-domain, located upstream the α-helix, are transiently exposed to the cell exterior (*Article 2*). One hypothesis is that this region inserts into the membrane allowing formation of the outer membrane pore when the sheath contracts. This hypothesis is interesting as it would explain (i) how the bacteria is protected from the formation of a deleterious permanent large pore at the outer membrane, and (ii) how the needle can cross the outer membrane without perturbing the cell envelope. Of course, it is a challenging project to monitor the insertion of TssM in the outer membrane. Does the baseplate recruitment induce a rearrangement of the β-strands? Does the sheath contraction that expulses the cell-puncturing device and the tube loaded with the effectors indeed modify this domain to form the channel? A reconstitution approach in the heterologous host *E. coli* might be used to understand this process: following TssM β-strands insertion in the TssJLM complex on which additional subunits (TssK? all baseplate components?) are added. The opposite experiments, *i.e.*, deletion of specific genes, might be used to define the determinants of TssM β-strands exposition.

If TssM is used to sense the target cell and to transmit the information, it will play a role comparable to the *Myoviridae* long tail fibers.

During infection, binding of the LTFs on the target cell induces a structural transition that propagates from the extremity of the LTF to the sheath through the baseplate. Upon contact with the target, components at the interface between LTFs and the baseplate are reorganized: a rotation of the gp10-gp11-gp12 module and gp9 transfers information to gp7 that induces a reorganization

of the inner baseplate (gp6)2-gp7 heterotrimers. As the diameter of the (gp6)2-gp7 ring increases, the gp25 and gp53 proteins dissociate from the hub an cause sheath contraction (Taylor et al., 2016).

If TssM is functionally similar to the LTF, this hypothesis suggests that (i) the information is transmitted through the inner membrane, and (ii) that $TssM_{Cyto}$ is connected to the baseplate, which is the complex that controls tail extension and contraction.

6.3 Transmitting information through the inner membrane

Usually, information are transduced through the inner membrane by structural modification of the trans-membrane helices. A number of bacterial transporters, permeases and molecular motors such as the flagellar stator, the ExbBD and TolQR complexes, transmit the information (coupling between proton-motive force and conformational changes) by cis-trans isomerization of proline residues located at the TMH boundaries (Jing et al., 1998)(Braun et al., 1999)(Goemaere et al., 2007). Interestingly, TMH1 and TMH2 contain proline residues at the interface with the cytoplasm. Hence, it would be interesting to test whether the TssM TMH proline residues are required to control TssM conformational changes (observed in *A. tumefaciens*) (Ma et al., 2009b)(Ma et al., 2012) and whether these residues are required for T6SS assembly and function.

6.4 Transmitting the information to the baseplate

The topological experiments showed that TMH2 and TMH3 delimitate a 35-kDa domain located in the cytoplasm that has been the focus in the *Article 3*. I have defined that this cytoplasmic domain comprises two domain: a 25-kDa domain that likely folds as an NTPase, although the Walker A and B motifs are missing, and a C-terminal dimerization hairpin. In addition, I have shown that the NTPase domain interacts with the TssK baseplate component, whereas a conserved motif within the C-terminal region mediates interaction with TssG (*Article 3*). On the other hand, the structure of TssK revealed that it folds as a *Siphoviridae* receptor binding protein with a classical shoulder-neck-head architecture. Protein-protein interaction studies have then demonstrated that the head domain binds and recognizes the cytoplasmic base of the membrane complex (*Article 4*). Additional data are required to better understand the interface between the membrane complex and the baseplate: a structure-function analysis of the TssK head loops, and *in vivo* imaging of the T6SS. The development of electron cryo-tomography imaging of the T6SS requires the engineering of smaller cells. I have deleted the *minCDE* genes and inserted a point mutation on the *mreB* gene within the EAEC chromosome, and have characterized the resulting skinny mini-cells, which will be an important tool for our collaborators at the ETH Zürich.

6.5 A working model for a sensor role for TssM

Baseplate subunits are universally conserved in contractile injection systems. Based on the structural transition undergone by the bacteriophage T4 baseplate, I can propose a working model for

T6SS activation. the C-terminal extension of TssM "senses" the target cells, hence modifying its intrinsic structure. Through movements of the transmembrane domains, the NTPase subdomain of the cytoplasmic domain switches, allowing (i) interaction with TssK or (ii) a modification of the $TssM_{Cyto}$/TssK or $TssM_{Cyto}$/TssG interface. The transduction of the information to TssK and/or TssG then triggers reorganization of the central baseplate by transferring the signal to the TssEFG complex to initiate sheath contraction. If we take account that several contacts between the membrane complex and the baseplate components have been identified, a slight modification in the TssM structure may have a huge impact on the baseplate allowing large conformational changes.

According to our model, each domain of TssM may participate to signal transmission. Determining their role is an exciting future project to shed light on how the T6SS is activated.

Part IV

Bibliography

Bibliography

Ackermann, H. W. (2001). Frequency of morphological phage descriptions in the year 2000. Brief review. *Archives of virology*, 146(5):843–57.

Ackermann, H.-W. (2009). Phage classification and characterization. *Methods in molecular biology (Clifton, N.J.)*, 501:127–40.

Aksyuk, A. A., Kurochkina, L. P., Fokine, A., Forouhar, F., Mesyanzhinov, V. V., Tong, L., and Rossmann, M. G. (2011). Structural conservation of the myoviridae phage tail sheath protein fold. *Structure*, 19(12):1885–1894.

Aksyuk, A. A., Leiman, P. G., Kurochkina, L. P., Shneider, M. M., Kostyuchenko, V. A., Mesyanzhinov, V. V., and Rossmann, M. G. (2009). The tail sheath structure of bacteriophage T4: a molecular machine for infecting bacteria. *The EMBO Journal*, 28(7):821–829.

Alcoforado Diniz, J., Liu, Y. C., and Coulthurst, S. J. (2015). Molecular weaponry: Diverse effectors delivered by the Type VI secretion system. *Cellular Microbiology*, 17(12):1742–1751.

Allan, N. D., Kooi, C., Sokol, P. a., and Beveridge, T. J. (2003). Putative virulence factors are released in association with membrane vesicles from Burkholderia cepacia. *Canadian Journal of Microbiology*, 49(10):613–624.

Alteri, C. J., Himpsl, S. D., Pickens, S. R., Lindner, J. R., Zora, J. S., Miller, J. E., Arno, P. D., Straight, S. W., and Mobley, H. L. T. (2013). Multicellular Bacteria Deploy the Type VI Secretion System to Preemptively Strike Neighboring Cells. *PLoS Pathogens*, 9(9):e1003608.

Alteri, C. J. and Mobley, H. L. (2016). The Versatile Type VI Secretion System. *Microbiology Spectrum*, 4(2):37–54.

Alves, N. J., Turner, K. B., Medintz, I. L., and Walper, S. A. (2016). Protecting enzymatic function through directed packaging into bacterial outer membrane vesicles. *Scientific Reports*, 6(1):24866.

Anderson, M. C., Vonaesch, P., Saffarian, A., Marteyn, B. S., and Sansonetti, P. J. (2017). Shigella sonnei Encodes a Functional T6SS Used for Interbacterial Competition and Niche Occupancy. *Cell Host and Microbe*, 21(6):769–776.

Anderson, M. S., Garcia, E. C., and Cotter, P. A. (2012). The Burkholderia bcpAIOB Genes Define Unique Classes of Two-Partner Secretion and Contact Dependent Growth Inhibition Systems. *PLoS Genetics*, 8(8):e1002877.

Anderson, M. S., Garcia, E. C., and Cotter, P. A. (2014). Kind Discrimination and Competitive Exclusion Mediated by Contact-Dependent Growth Inhibition Systems Shape Biofilm Community Structure. *PLoS Pathogens*, 10(4):e1004076.

Aoki, S. K., Diner, E. J., de Roodenbeke, C. t., Burgess, B. R., Poole, S. J., Braaten, B. A., Jones, A. M., Webb, J. S., Hayes, C. S., Cotter, P. A., and Low, D. A. (2010). A widespread family of polymorphic contact-dependent toxin delivery systems in bacteria. *Nature*, 468(7322):439–442.

Aoki, S. K., Malinverni, J. C., Jacoby, K., Thomas, B., Pamma, R., Trinh, B. N., Remers, S., Webb, J., Braaten, B. A., Silhavy, T. J., and Low, D. A. (2008). Contact-dependent growth inhibition requires the essential outer membrane protein BamA (YaeT) as the receptor and the inner membrane transport protein AcrB. *Molecular Microbiology*, 70(2):323–340.

Aoki, S. K., Pamma, R., and Hernday, A. D. (2005). Contact-Dependent Inhibition of Growth in Escherichia coli. 309(August):1245–1249.

Aoki, S. K., Poole, S. J., Hayes, C. S., and Low, D. A. (2011). Toxin on a stick. *Virulence*, 2(4):356–359.

Armitano, J., Méjean, V., and Jourlin-Castelli, C. (2014). Gram-negative bacteria can also form pellicles. *Environmental Microbiology Reports*, 6(6):534–544.

Aschtgen, M. S., Bernard, C. S., De Bentzmann, S., Lloubès, R., and Cascales, E. (2008). SciN is an outer membrane lipoprotein required for type VI secretion in enteroaggregative Escherichia coli. *Journal of Bacteriology*, 190(22):7523–7531.

Aschtgen, M. S., Gavioli, M., Dessen, A., Lloubès, R., and Cascales, E. (2010a). The SciZ protein anchors the enteroaggregative Escherichia coli Type VI secretion system to the cell wall. *Molecular Microbiology*, 75(4):886–899.

Aschtgen, M.-S., Thomas, M. S., and Cascales, E. (2010b). Anchoring the type VI secretion system to the peptidoglycan: TssL, TagL, TagP... what else? *Virulence*, 1(6):535–540.

Aschtgen, M. S., Zoued, A., Lloubès, R., Journet, L., and Cascales, E. (2012). The C-tail anchored TssL subunit, an essential protein of the enteroaggregative Escherichia coli Sci-1 Type VI secretion system, is inserted by YidC. *MicrobiologyOpen*, 1(1):71–82.

Ballister, E. R., Lai, A. H., Zuckermann, R. N., Cheng, Y., and Mougous, J. D. (2008). In vitro self-assembly of tailorable nanotubes from a simple protein building block. *Proceedings of the National Academy of Sciences, USA*, 105(10):3733–3738.

Banin, E., Khare, S. K., Naider, F., and Rosenberg, E. (2001). Proline-Rich Peptide from the Coral Pathogen Vibrio shiloi That Inhibits Photosynthesis of Zooxanthellae. *Applied and Environmental Microbiology*, 67(4):1536–1541.

Bartual, S. G., Otero, J. M., Garcia-Doval, C., Llamas-Saiz, A. L., Kahn, R., Fox, G. C., and van Raaij, M. J. (2010). Structure of the bacteriophage T4 long tail fiber receptor-binding tip. *Proceedings of the National Academy of Sciences, USA*, 107(47):20287–20292.

Basler, M., Ho, B. T., and Mekalanos, J. J. (2013). Tit-for-tat: Type VI secretion system counter-attack during bacterial cell-cell interactions. *Cell*, 152(4):884–894.

Basler, M. and Mekalanos, J. J. (2012). Type 6 secretion dynamics within and between bacterial cells. *Science*, 337(6096):815.

Basler, M., Pilhofer, M., Henderson, G. P., Jensen, G. J., and Mekalanos, J. J. (2012). Type VI secretion requires a dynamic contractile phage tail-like structure. *Nature*, 483(7388):182–186.

Bassler, B. L. and Losick, R. (2006). Bacterially Speaking. *Cell*, 125(2):237–246.

Bayliss, R., Harris, R., Coutte, L., Monier, A., Fronzes, R., Christie, P. J., Driscoll, P. C., and Waksman, G. (2007). NMR structure of a complex between the VirB9/VirB7 interaction domains of the pKM101 type IV secretion system. *Proceedings of the National Academy of Sciences, USA*, 104(5):1673–8.

Beck, C. M., Diner, E. J., Kim, J. J., Low, D. A., and Hayes, C. S. (2014). The F pilus mediates a novel pathway of CDI toxin import. *Molecular Microbiology*, 93(2):276–290.

Beck, C. M., Willett, J. L. E., Cunningham, D. A., Kim, J. J., Low, D. A., and Hayes, C. S. (2016). CdiA Effectors from Uropathogenic Escherichia coli Use Heterotrimeric Osmoporins as Receptors to Recognize Target Bacteria. *PLOS Pathogens*, 12(10):e1005925.

Beeby, M., Ribardo, D. A., Brennan, C. A., Ruby, E. G., Jensen, G. J., and Hendrixson, D. R. (2016). Diverse high-torque bacterial flagellar motors assemble wider stator rings using a conserved protein scaffold. *Proceedings of the National Academy of Sciences, USA*, 113(13):E1917–E1926.

Behrens, H. M., Six, A., Walker, D., and Kleanthous, C. (2017). The therapeutic potential of bacteriocins as protein antibiotics. *Emerging Topics in Life Sciences*, 1(1):65–74.

Beloin, C., Roux, A., and Ghigo, J. M. (2008). Escherichia coli biofilms. *Current topics in microbiology and immunology*, 322:249–89.

Benomar, S., Ranava, D., Cárdenas, M. L., Trably, E., Rafrafi, Y., Ducret, A., Hamelin, J., Lojou, E., Steyer, J.-P., and Giudici-Orticoni, M.-T. (2015). Nutritional stress induces exchange of cell material and energetic coupling between bacterial species. *Nature Communications*, 6:6283.

Berleman, J. and Auer, M. (2013). The role of bacterial outer membrane vesicles for intra- and interspecies delivery. *Environmental Microbiology*, 15(2):347–354.

Berleman, J. E. and Kirby, J. R. (2009). Deciphering the hunting strategy of a bacterial wolfpack. *FEMS Microbiology Reviews*, 33(5):942–957.

Bernadac, A., Gavioli, M., Lazzaroni, J. C., Raina, S., and Lloubès, R. (1998). Escherichia coli tol-pal mutants form outer membrane vesicles. *Journal of bacteriology*, 180(18):4872–8.

Bernal, P., Allsopp, L. P., Filloux, A., and Llamas, M. A. (2017). The Pseudomonas putida T6SS is a plant warden against phytopathogens. *The ISME Journal*, 11(4):972–987.

Bernard, C. S., Brunet, Y. R., Gueguen, E., and Cascales, E. (2010). Nooks and crannies in type VI secretion regulation. *Journal of Bacteriology*, 192(15):3850–3860.

Berry, J., Rajaure, M., Pang, T., and Young, R. (2012). The spanin complex is essential for lambda lysis. *Journal of Bacteriology*, 194(20):5667–5674.

Bielaszewska, M., Rüter, C., Bauwens, A., Greune, L., Jarosch, K.-A., Steil, D., Zhang, W., He, X., Lloubes, R., Fruth, A., Kim, K. S., Schmidt, M. A., Dobrindt, U., Mellmann, A., and Karch, H. (2017). Host cell interactions of outer membrane vesicle-associated virulence factors of enterohemorrhagic Escherichia coli O157: Intracellular delivery, trafficking and mechanisms of cell injury. *PLoS pathogens*, 13(2):e1006159.

Bingle, L. E., Bailey, C. M., and Pallen, M. J. (2008). Type VI secretion: a beginner's guide. *Current Opinion in Microbiology*, 11(1):3–8.

Bitto, N. J., Chapman, R., Pidot, S., Costin, A., Lo, C., Choi, J., D'Cruze, T., Reynolds, E. C., Dashper, S. G., Turnbull, L., Whitchurch, C. B., Stinear, T. P., Stacey, K. J., and Ferrero, R. L. (2017). Bacterial membrane vesicles transport their DNA cargo into host cells. *Scientific Reports*, 7(1):7072.

Bleves, S. (2016). Game of Trans-Kingdom Effectors. *Trends in Microbiology*, 24(10):773–774.

Böck, D., Medeiros, J. M., Tsao, H.-f., Penz, T., Weiss, G. L., Aistleitner, K., Horn, M., and Pilhofer, M. (2017). Injection System. 717(August):713–717.

Bondage, D. D., Lin, J.-S., Ma, L.-S., Kuo, C.-H., and Lai, E.-M. (2016). VgrG C terminus confers the type VI effector transport specificity and is required for binding with PAAR and adaptor–effector complex. *Proceedings of the National Academy of Sciences*, 113(27):E3931–E3940.

Bönemann, G., Pietrosiuk, A., Diemand, A., Zentgraf, H., and Mogk, A. (2009). Remodelling of VipA/VipB tubules by ClpV-mediated threading is crucial for type VI protein secretion. *The EMBO Journal*, 28(4):315–325.

Borenstein, D. B., Ringel, P., Basler, M., and Wingreen, N. S. (2015). Established Microbial Colonies Can Survive Type VI Secretion Assault. *PLOS Computational Biology*, 11(10):e1004520.

Bos, J. L., Rehmann, H., and Wittinghofer, A. (2007a). GEFs and GAPs: critical elements in the control of small G proteins. *Cell*, 129(5):865–77.

Bos, M. P., Robert, V., and Tommassen, J. (2007b). Biogenesis of the Gram-Negative Bacterial Outer Membrane. *Annual Review of Microbiology*, 61(1):191–214.

Bowman, J. P. (2007). Bioactive compound synthetic capacity and ecological significance of marine bacterial genus Pseudoalteromonas. *Marine Drugs*, 5(4):220–241.

Boyer, F., Fichant, G., Berthod, J., Vandenbrouck, Y., and Attree, I. (2009). Dissecting the bacterial type VI secretion system by a genome wide in silico analysis: what can be learned from available microbial genomic resources? *BMC Genomics*, 10(1):104.

Braun, T. F., Poulson, S., Gully, J. B., Empey, J. C., Van Way, S., Putnam, A., and Blair, D. F. (1999). Function of proline residues of MotA in torque generation by the flagellar motor of Escherichia coli. *Journal of Bacteriology*, 181(11):3542–3551.

Braun, V., Patzer, S. I., and Hantke, K. (2002). Ton-dependent colicins and microcins: Modular design and evolution. *Biochimie*, 84(5-6):365–380.

Braun, V., Pilsl, H., and Gross, P. (1994). Colicins: structures, modes of action, transfer through membranes, and evolution. *Archives of microbiology*, 161(3):199–206.

Brenner, K., Karig, D. K., Weiss, R., and Arnold, F. H. (2007). Engineered bidirectional communication mediates a consensus in a microbial biofilm consortium. *Proceedings of the National Academy of Sciences of the United States of America*, 104(44):17300–17304.

Briegel, A., Ortega, D. R., Mann, P., Kjær, A., Ringgaard, S., and Jensen, G. J. (2016). Chemotaxis cluster 1 proteins form cytoplasmic arrays in ¡i¿Vibrio cholerae¡/i¿ and are stabilized by a double signaling domain receptor DosM. *Proceedings of the National Academy of Sciences*, 113(37):10412–10417.

Brinkhoff, T., Bach, G., Heidorn, T., Liang, L., Schlingloff, A., and Simon, M. (2004). Antibiotic Production by a Roseobacter Clade-Affiliated Species from the German Wadden Sea and Its Antagonistic Effects on Indigenous Isolates. *Applied and Environmental Microbiology*, 70(4):2560–2565.

Bröms, J. E., Ishikawa, T., Wai, S. N., and Sjöstedt, A. (2013). A functional VipA-VipB interaction is required for the type VI secretion system activity of Vibrio cholerae O1 strain A1552. *BMC microbiology*, 13:96.

Broms, J. E., Lavander, M., and Sjöstedt, A. (2009). A conserved α-helix essential for a type VI secretion-like system of francisella tularensis. *Journal of Bacteriology*, 191(8):2431–2446.

Brooks, T. M., Unterweger, D., Bachmann, V., Kostiuk, B., and Pukatzki, S. (2013). Lytic activity of the Vibrio cholerae type VI secretion toxin VgrG-3 is inhibited by the antitoxin TsaB. *Journal of Biological Chemistry*, 288(11):7618–7625.

Brown, L., Wolf, J. M., Prados-Rosales, R., and Casadevall, A. (2015). Through the wall: extracellular vesicles in Gram-positive bacteria, mycobacteria and fungi. *Nature Reviews Microbiology*, 13(10):620–630.

Brunet, Y. R., Bernard, C. S., Gavioli, M., Lloubès, R., and Cascales, E. (2011). An epigenetic switch involving overlapping fur and DNA methylation optimizes expression of a type VI secretion gene cluster. *PLoS Genetics*, 7(7).

Brunet, Y. R., Espinosa, L., Harchouni, S., Mignot, T., and Cascales, E. (2013). Imaging Type VI Secretion-Mediated Bacterial Killing. *Cell Reports*, 3(1):36–41.

Brunet, Y. R., Hénin, J., Celia, H., and Cascales, E. (2014). Type VI secretion and bacteriophage tail tubes share a common assembly pathway. *EMBO Reports*, 15(3):315–321.

Brunet, Y. R., Khodr, A., Logger, L., Aussel, L., Mignot, T., Rimsky, S., and Cascales, E. (2015a). H-NS Silencing of the Salmonella Pathogenicity Island 6-Encoded Type VI Secretion System Limits Salmonella enterica Serovar Typhimurium Interbacterial Killing. *Infection and immunity*, 83(7):2738–50.

Brunet, Y. R., Zoued, A., Boyer, F., Douzi, B., and Cascales, E. (2015b). The Type VI Secretion TssEFGK-VgrG Phage-Like Baseplate Is Recruited to the TssJLM Membrane Complex via Multiple Contacts and Serves As Assembly Platform for Tail Tube/Sheath Polymerization. *PLoS Genetics*, 11(10):1–21.

Buchanan, S. K., Lukacik, P., Grizot, S., Ghirlando, R., Ali, M. M. U., Barnard, T. J., Jakes, K. S., Kienker, P. K., and Esser, L. (2007). Structure of colicin I receptor bound to the R-domain of colicin Ia: implications for protein import. *The EMBO journal*, 26(10):2594–604.

Bullock, J. O., Cohen, F. S., Dankert, J. R., and Cramer, W. A. (1983). Comparison of the macroscopic and single channel conductance properties of colicin E1 and its COOH-terminal tryptic peptide. *The Journal of biological chemistry*, 258(16):9908–12.

Busby, J. N., Panjikar, S., Landsberg, M. J., Hurst, M. R. H., and Lott, J. S. (2013). The BC component of ABC toxins is an RHS-repeat-containing protein encapsulation device. *Nature*, 501(7468):547–550.

Büttner, C. R., Wu, Y., Maxwell, K. L., and Davidson, A. R. (2016). Baseplate assembly of phage Mu: Defining the conserved core components of contractile-tailed phages and related bacterial systems. *Proceedings of the National Academy of Sciences of the United States of America*, 113(36):10174–9.

Campbell, A. and Delcampillo-Campbell, A. (1963). Mutant of Lambda Bacteriophage Producing a Thermolabile Endolysin. *Journal of bacteriology*, 85:1202–1207.

Cao, Z. and Klebba, P. E. (2002). Mechanisms of colicin binding and transport through outer membrane porins. *Biochimie*, 84(5-6):399–412.

Carleton, H. A., Lara-Tejero, M., Liu, X., and Galán, J. E. (2013). Engineering the type III secretion system in non-replicating bacterial minicells for antigen delivery. *Nat Commun*, 4:1590.

Caron, D. (2000). Symbiosis and mixotrophy among pelagic microorganisms. *Microbial ecology of the oceans*, Wiley-Liss:495–523.

Carruthers, M. D., Nicholson, P. A., Tracy, E. N., and Munson, R. S. (2013). Acinetobacter baumannii Utilizes a Type VI Secretion System for Bacterial Competition. *PLoS ONE*, 8(3):e59388.

Casabona, M. G., Silverman, J. M., Sall, K. M., Boyer, F., Couté, Y., Poirel, J., Grunwald, D., Mougous, J. D., Elsen, S., and Attree, I. (2013). An ABC transporter and an outer membrane lipoprotein participate in posttranslational activation of type VI secretion in Pseudomonas aeruginosa. *Environmental Microbiology*, 15(2):471–486.

Cascales, E. (2008). The type VI secretion toolkit. *EMBO reports*, 9(8):735–741.

Cascales, E. (2017). Microbiology: and Amoebophilus invented the machine gun! *Current Biology*, 27(21):3521–23.

Cascales, E., Buchanan, S. K., Duche, D., Kleanthous, C., Lloubes, R., Postle, K., Riley, M., Slatin, S., and Cavard, D. (2007). Colicin Biology. *Microbiology and Molecular Biology Reviews*, 71(1):158–229.

Cavard, D., Baty, D., Howard, S. P., Verheij, H. M., and Lazdunski, C. (1987). Lipoprotein nature of the colicin A lysis protein: Effect of amino acid substitutions at the site of modification and processing. *Journal of Bacteriology*, 169(5):2187–2194.

Chai, T. J. and Foulds, J. (1977). Escherichia coli K-12 tolF mutants: alterations in protein composition of the outer membrane. *Journal of Bacteriology*, 130(2):781–786.

Chai, T. J. and Foulds, J. (1979). Isolation and partial characterization of protein E, a major protein found in certain Escherichia coli K-12 mutant strains: relationship to other outer membrane proteins. *J Bacteriol*, 139(2):418–423.

Chak, K. F., Kuo, W. S., Lu, F. M., and James, R. (1991). Cloning and characterization of the ColE7 plasmid. *Journal of general microbiology*, 137:91–100.

Chandran, V., Fronzes, R., Duquerroy, S., Cronin, N., Navaza, J., and Waksman, G. (2009). Structure of the outer membrane complex of a type IV secretion system. *Nature*, 462(7276):1011–1015.

Chang, J. H. and Kim, Y.-G. (2015). Crystal structure of the bacterial type VI secretion system component TssL from Vibrio cholerae. *Journal of microbiology*, 53(1):32–7.

Chang, Y., Rettberg, L. A., Ortega, D. R., and Jensen, G. J. (2017). ¡i¿In vivo¡/i¿ structures of an intact type VI secretion system revealed by electron cryotomography. *EMBO reports*, 18(7):1090–1099.

Chang, Y.-W., Rettberg, L. A., Treuner-Lange, A., Iwasa, J., Søgaard-Andersen, L., and Jensen, G. J. (2016). Architecture of the type IVa pilus machine. *Science*, 351(6278):aad2001.

Chao, L. and Levin, B. R. (1981). Structured habitats and the evolution of anticompetitor toxins in bacteria. *Proceedings of the National Academy of Sciences*, 78(10):6324–6328.

Chatzidaki-Livanis, M., Geva-Zatorsky, N., and Comstock, L. E. (2016). ¡i¿Bacteroides fragilis¡/i¿ type VI secretion systems use novel effector and immunity proteins to antagonize human gut Bacteroidales species. *Proceedings of the National Academy of Sciences*, 113(13):3627–3632.

Cherfils, J. and Zeghouf, M. (2013). Regulation of Small GTPases by GEFs, GAPs, and GDIs. *Physiological Reviews*, 93(1):269–309.

Cho, S. H., Szewczyk, J., Pesavento, C., Zietek, M., Banzhaf, M., Roszczenko, P., Asmar, A., Laloux, G., Hov, A. K., Leverrier, P., Van Der Henst, C., Vertommen, D., Typas, A., and Collet, J. F. (2014). Detecting envelope stress by monitoring β-barrel assembly. *Cell*, 159(7):1652–1664.

Chou, S., Bui, N. K., Russell, A. B., Lexa, K. W., Gardiner, T. E., LeRoux, M., Vollmer, W., and Mougous, J. D. (2012). Structure of a Peptidoglycan Amidase Effector Targeted to Gram-Negative Bacteria by the Type VI Secretion System. *Cell Reports*, 1(6):656–664.

Cianfanelli, F. R., Monlezun, L., and Coulthurst, S. J. (2016). Aim, Load, Fire: The Type VI Secretion System, a Bacterial Nanoweapon. *Trends in Microbiology*, 24(1):51–62.

Clemens, D. L., Ge, P., Lee, B. Y., Horwitz, M. A., and Zhou, Z. H. (2015). Atomic structure of T6SS reveals interlaced array essential to function. *Cell*, 160(5):940–951.

Costa, T. R. D., Felisberto-rodrigues, C., Meir, A., Prevost, M. S., Redzej, A., Trokter, M., and Waksman, G. (2015). Secretion systems in Gram-negative insights. *Nature Publishing Group*, 13(6):343–359.

Cotter, P. A., Yuk, M. H., Mattoo, S., Akerley, B. J., Boschwitz, J., Relman, D. A., and Miller, J. F. (1998). Filamentous hemagglutinin of Bordetella bronchiseptica is required for efficient establishment of tracheal colonization. *Infection and Immunity*, 66(12):5921–5929.

Danka, E. S., Garcia, E. C., and Cotter, P. A. (2017). Are CDI Systems Multicolored, Facultative, Helping Greenbeards? *Trends in Microbiology*, 25(5):391–401.

Das, S. and Chaudhuri, K. (2003). Identification of a unique IAHP (IcmF associated homologous proteins) cluster in Vibrio cholerae and other proteobacteria through in silico analysis. *In silico biology*, 3(3):287–300.

Datsenko, K. A. and Wanner, B. L. (2000). One-step inactivation of chromosomal genes in Escherichia coli K-12 using PCR products. *Proceedings of the National Academy of Sciences of the United States of America*, 97(12):6640–5.

Davies, J. (2013). Specialized microbial metabolites: functions and origins. *The Journal of Antibiotics*, 66(7):361–364.

Davies, J. and Ryan, K. S. (2012). Introducing the parvome: Bioactive compounds in the microbial world. *ACS Chemical Biology*, 7(2):252–259.

Davies, J. K. and Reeves, P. (1975). Genetics of resistance to colicins in Escherichia coli Genetics of Resistance to Colicins in Escherichia coli K-12 : Cross-Resistance Among Colicins of Group B. 123(1):102–117.

Day, P. J., Pinheiro, T. J. T., Roberts, L. M., and Lord, J. M. (2002). Binding of ricin A-chain to negatively charged phospholipid vesicles leads to protein structural changes and destabilizes the lipid bilayer. *Biochemistry*, 41(8):2836–2843.

de Graaf, F. K., Stukart, M. J., Boogerd, F. C., and Metselaar, K. (1978). Limited proteolysis of cloacin DF13 and characterization of the cleavage products. *Biochemistry*, 17(6):1137–42.

de Vos, W. M. (2015). Microbial biofilms and the human intestinal microbiome. *npj Biofilms and Microbiomes*, 1(1):15005.

Delattre, A. S., Saint, N., Clantin, B., Willery, E., Lippens, G., Locht, C., Villeret, V., and Jacob-Dubuisson, F. (2011). Substrate recognition by the POTRA domains of TpsB transporter FhaC. *Molecular Microbiology*, 81(1):99–112.

Desvaux, M., Cooper, L. M., Filenko, N. A., Scott-Tucker, A., Turner, S. M., Cole, J. A., and Henderson, I. R. (2006). The unusual extended signal peptide region of the type V secretion system is phylogenetically restricted. *FEMS Microbiology Letters*, 264(1):22–30.

Di Masi, D. R., White, J. C., Schnaitman, C. A., and Bradbeer, C. (1973). Transport of vitamin B12 in Escherichia coli: common receptor sites for vitamin B12 and the E colicins on the outer membrane of the cell envelope. *Journal of bacteriology*, 115(2):506–13.

Di Tommaso, P., Moretti, S., Xenarios, I., Orobitg, M., Montanyola, A., Chang, J. M., Taly, J. F., and Notredame, C. (2011). T-Coffee: A web server for the multiple sequence alignment of protein and RNA sequences using structural information and homology extension. *Nucleic Acids Research*, 39:13–17.

Diepold, A., Amstutz, M., Abel, S., Sorg, I., Jenal, U., and Cornelis, G. R. (2010). Deciphering the assembly of the Yersinia type III secretion injectisome. *The EMBO Journal*, 29(11):1928–1940.

Dobson, A., Cotter, P. D., Paul Ross, R., and Hill, C. (2012). Bacteriocin production: A probiotic trait? *Applied and Environmental Microbiology*, 78(1):1–6.

Donaldson, G. P., Lee, S. M., and Mazmanian, S. K. (2015). Gut biogeography of the bacterial microbiota. *Nature Reviews Microbiology*, 14(1):20–32.

Dong, C., Beis, K., Nesper, J., Brunkan-LaMontagne, A. L., Clarke, B. R., Whitfield, C., and Naismith, J. H. (2006). Wza the translocon for E. coli capsular polysaccharides defines a new class of membrane protein. *Nature*, 444(7116):226–229.

Dong, T. G., Ho, B. T., Yoder-Himes, D. R., and Mekalanos, J. J. (2013). Identification of T6SS-dependent effector and immunity proteins by Tn-seq in Vibrio cholerae. *Proceedings of the National Academy of Sciences*, 110(7):2623–2628.

Dorosky, R. J., Yu, J. M., Pierson, L. S., and Pierson, E. A. (2014). Pseudomonas chlororaphis produces two distinct R-tailocins that contribute to bacterial competition in biofilms and on roots. *Applied and Environmental Microbiology*, 83(15):1–16.

Douzi, B., Brunet, Y. R., Spinelli, S., Lensi, V., Legrand, P., Blangy, S., Kumar, A., Journet, L., Cascales, E., and Cambillau, C. (2016). Structure and specificity of the Type VI secretion system ClpV-TssC interaction in enteroaggregative Escherichia coli. *Scientific Reports*, 6(1):34405.

Douzi, B., Spinelli, S., Blangy, S., Roussel, A., Durand, E., Brunet, Y. R., Cascales, E., and Cambillau, C. (2014). Crystal structure and self-interaction of the type VI secretion tail-tube protein from enteroaggregative Escherichia coli. *PLoS ONE*, 9(2):1–9.

Duché, D., Frenkian, A., Prima, V., and Lloubès, R. (2006). Release of immunity protein requires functional endonuclease colicin import machinery. *Journal of Bacteriology*, 188(24):8593–8600.

Ducret, A., Quardokus, E. M., and Brun, Y. V. (2016). MicrobeJ, a tool for high throughput bacterial cell detection and quantitative analysis. *Nature Microbiology*, 1(7):16077.

Ducret, A., Valignat, M.-P., Mouhamar, F., Mignot, T., and Theodoly, O. (2012). Wet-surface-enhanced ellipsometric contrast microscopy identifies slime as a major adhesion factor during bacterial surface motility. *Proceedings of the National Academy of Sciences*, 109(25):10036–10041.

Dudley, E. G., Thomson, N. R., Parkhill, J., Morin, N. P., and Nataro, J. P. (2006). Proteomic and microarray characterization of the AggR regulon identifies a pheU pathogenicity island in enteroaggregative Escherichia coli. *Molecular Microbiology*, 61(5):1267–1282.

Dupraz, C. and Visscher, P. T. (2005). Microbial lithification in marine stromatolites and hypersaline mats. *Trends in Microbiology*, 13(9):429–438.

Durand, E., Cambillau, C., Cascales, E., and Journet, L. (2014). VgrG, Tae, Tle, and beyond: The versatile arsenal of Type VI secretion effectors. *Trends in Microbiology*, 22(9):498–507.

Durand, E., Derrez, E., Audoly, G., Spinelli, S., Ortiz-Lombardia, M., Raoult, D., Cascales, E., and Cambillau, C. (2012a). Crystal structure of the VgrG1 actin cross-linking domain of the Vibrio cholerae type VI secretion system. *Journal of Biological Chemistry*, 287(45):38190–38199.

Durand, E., Nguyen, V. S., Zoued, A., Logger, L., Pehau-Arnaudet, G., Aschtgen, M. S., Spinelli, S., Desmyter, A., Bardiaux, B., Dujeancourt, A., Roussel, A., Cambillau, C., Cascales, E., and Fronzes, R. (2015). Biogenesis and structure of a type VI secretion membrane core complex. *Nature*, 523(7562):555–560.

Durand, E., Zoued, A., Spinelli, S., Watson, P. J. H., Aschtgen, M. S., Journet, L., Cambillau, C., and Cascales, E. (2012b). Structural characterization and oligomerization of the TssL protein, a component shared by bacterial type VI and type IVb secretion systems. *Journal of Biological Chemistry*, 287(17):14157–14168.

Dworkin, M. (1996). Recent advances in the social and developmental biology of the myxobacteria. *Microbiological reviews*, 60(1):70–102.

Elvers, K. T. and Lappin-Scott, H. M. (2004). Biofilms and biofoulding. *The desk encyclopedia of microbiology*, Elsevier A:161–167.

English, G., Byron, O., Cianfanelli, F., Prescott, A., and Coulthurst, S. (2014). Biochemical analysis of TssK, a core component of the bacterial Type VI secretion system, reveals distinct oligomeric states of TssK and identifies a TssK–TssFG subcomplex. *Biochemical Journal*, 461(2):291–304.

English, G., Trunk, K., Rao, V. A., Srikannathasan, V., Hunter, W. N., and Coulthurst, S. J. (2012). New secreted toxins and immunity proteins encoded within the type VI secretion system gene cluster of Serratia marcescens. *Molecular Microbiology*, 86(4):921–936.

Evans, K. J., Lambert, C., and Sockett, R. E. (2007). Predation by Bdellovibrio bacteriovorus HD100 requires type IV pili. *Journal of Bacteriology*, 189(13):4850–4859.

Farenc, C., Spinelli, S., Vinogradov, E., Tremblay, D., Blangy, S., Sadovskaya, I., Moineau, S., and Cambillau, C. (2014). Molecular Insights on the Recognition of a Lactococcus lactis Cell Wall Pellicle by the Phage 1358 Receptor Binding Protein. *Journal of Virology*, 88(12):7005–7015.

Farley, M. M., Hu, B., and Margolin, W. (2016). Minicells , Back in Fashion. 198(8):1186–1195.

Faust, K. and Raes, J. (2012). Microbial interactions: from networks to models. *Nature Reviews Microbiology*, 10(8):538–550.

Felisberto-Rodrigues, C., Durand, E., Aschtgen, M. S., Blangy, S., Ortiz-Lombardia, M., Douzi, B., Cambillau, C., and Cascales, E. (2011). Towards a structural comprehension of bacterial type vi secretion systems: Characterization of the TssJ-TssM complex of an escherichia coli pathovar. *PLoS Pathogens*, 7(11):1–11.

Fenchel, T. (2002). Microbial behavior in a heterogeneous world. *Science (New York, N.Y.)*, 296(5570):1068–1071.

Ferguson, P. L. and Coombs, D. H. (2000). Pulse-chase analysis of the in vivo assembly of the bacteriophage T4 tail. *Journal of molecular biology*, 297(1):99–117.

Flaugnatti, N., Le, T. T. H., Canaan, S., Aschtgen, M. S., Nguyen, V. S., Blangy, S., Kellenberger, C., Roussel, A., Cambillau, C., Cascales, E., and Journet, L. (2016). A phospholipase A1 antibacterial Type VI secretion effector interacts directly with the C-terminal domain of the VgrG spike protein for delivery. *Molecular Microbiology*, 99(6):1099–1118.

Flemming, H.-C., Wingender, J., Szewzyk, U., Steinberg, P., Rice, S. A., and Kjelleberg, S. (2016). Biofilms: an emergent form of bacterial life. *Nature reviews. Microbiology*, 14(9):563–75.

Fokine, A., Zhang, Z., Kanamaru, S., Bowman, V. D., Aksyuk, A. A., Arisaka, F., Rao, V. B., and Rossmann, M. G. (2013). The molecular architecture of the bacteriophage T4 neck. *Journal of Molecular Biology*, 425(10):1731–1744.

Ford, R. C., Brunkan-LaMontagne, A. L., Collins, R. F., Clarke, B. R., Harris, R., Naismith, J. H., and Whitfield, C. (2009). Structure-function relationships of the outer membrane translocon Wza investigated by cryo-electron microscopy and mutagenesis. *Journal of Structural Biology*, 166(2):172–182.

Fredericq, P. (1946). Sur la pluralité des récepteurs d'antibiose de E. coli. *C. R. Soc. Biol*, 140:1189–1194.

Fröstl, J. M. and Overmann, J. (1998). Physiology and tactic response of the phototrophic consortium 'Chlorochromatium aggregatum'. *Archives of Microbiology*, 169(2):129–135.

Fröstl, J. M. and Overmann, J. (2000). Phylogenetic affiliation of the bacteria that constitute phototrophic consortia. *Archives of Microbiology*, 174(1-2):50–58.

Fu, Y., Waldor, M. K., and Mekalanos, J. J. (2013). Tn-seq analysis of vibrio cholerae intestinal colonization reveals a role for T6SS-mediated antibacterial activity in the host. *Cell Host and Microbe*, 14(6):652–663.

García, C., Rendueles, M., and Díaz, M. (2017). Microbial amensalism in Lactobacillus casei and Pseudomonas taetrolens mixed culture. *Bioprocess and Biosystems Engineering*, 40(7):1111–1122.

Garcia, E. C., Anderson, M. S., Hagar, J. A., and Cotter, P. A. (2013). BurkholderiaBcpA mediates biofilm formation independently of interbacterial contact-dependent growth inhibition. *Molecular Microbiology*, 89(6):1213–1225.

Ge, P., Scholl, D., Leiman, P. G., Yu, X., Miller, J. F., and Zhou, Z. H. (2015). Atomic structures of a bactericidal contractile nanotube in its pre- and postcontraction states. *Nature Structural & Molecular Biology*, 22(5):377–382.

Gensollen, T., Iyer, S. S., Kasper, D. L., and Blumberg, R. S. (2016). How colonization by microbiota in early life shapes the immune system. *Science*, 352(6285):539–544.

Gerding, M. A., Ogata, Y., Pecora, N. D., Niki, H., and De Boer, P. A. J. (2007). The trans-envelope Tol-Pal complex is part of the cell division machinery and required for proper outer-membrane invagination during cell constriction in E. coli. *Molecular Microbiology*, 63(4):1008–1025.

Ghosal, D., Chang, Y., Jeong, K. C., Vogel, J. P., and Jensen, G. J. (2017). ¡i¿In situ¡/i¿ structure of the ¡i¿Legionella¡/i¿ Dot/Icm type IV secretion system by electron cryotomography. *EMBO reports*, 18(5):726–732.

Gibbs, K. A., Urbanowski, M. L., and Greenberg, E. P. (2008). Genetic Determinants of Self Identity and Social Recognition in Bacteria. *Science*, 321(5886):256–259.

Gibbs, K. A., Wenren, L. M., and Greenberg, E. P. (2011). Identity gene expression in Proteus mirabilis. *Journal of Bacteriology*, 193(13):3286–3292.

Gillespie, J. P., Kanost, M. R., and Trenczek, T. (1997). Biological mediators of insect immunity. *Annual review of entomology*, 42(2):611–43.

Gillor, O., Giladi, I., and Riley, M. A. (2009). Persistence of colicinogenic Escherichia coli in the mouse gastrointestinal tract. *BMC Microbiology*, 9(1):165.

Glaeser, J. and Overmann, J. (2003). Characterization and in situ carbon metabolism of phototrophic consortia. *Applied and Environmental Microbiology*, 69(7):3739–3750.

Goemaere, E. L., Cascales, E., and Lloubès, R. (2007). Mutational Analyses Define Helix Organization and Key Residues of a Bacterial Membrane Energy-transducing Complex. *Journal of Molecular Biology*, 366(5):1424–1436.

Gominet, M., Compain, F., Beloin, C., and Lebeaux, D. (2017). Central venous catheters and biofilms: where do we stand in 2017? *Apmis*, 125(4):365–375.

Goodrich, J. K., Davenport, E. R., Waters, J. L., Clark, A. G., and Ley, R. E. (2016). Cross-species comparisons of host genetic associations with the microbiome. *Science*, 352(6285):532–535.

Gottig, N., Garavaglia, B. S., Garofalo, C. G., Orellano, E. G., and Ottado, J. (2009). A filamentous hemagglutinin-like protein of Xanthomonas axonopodis pv. citri, the phytopathogen responsible for citrus canker, is involved in bacterial virulence. *PLoS ONE*, 4(2):e4358.

Govan, J. R. W. (1974). Studies on the Pyocins of Pseudomonas aeruginosa: Morphology and Mode of Action of Contractile Pyocins. *Journal of General Microbiology*, 80(1):1–15.

Gueguen, E. and Cascales, E. (2013). Promoter Swapping Unveils the Role of the Citrobacter rodentium CTS1 Type VI Secretion System in Interbacterial Competition. *Applied and Environmental Microbiology*, 79(1):32–38.

Gueguen, E., Wills, N. M., Atkins, J. F., and Cascales, E. (2014). Transcriptional Frameshifting Rescues Citrobacter rodentium Type VI Secretion by the Production of Two Length Variants from the Prematurely Interrupted tssM Gene. *PLoS Genetics*, 10(12):e1004869.

Guilhabert, M. R. and Kirkpatrick, B. C. (2005). Identification of Xylella fastidiosa antivirulence genes: hemagglutinin adhesins contribute a biofilm maturation to X. fastidios and colonization and attenuate virulence. *Molecular plant-microbe interactions*, 18(8):856–868.

Hachani, A., Allsopp, L. P., Oduko, Y., and Filloux, A. (2014). The VgrG proteins are "à la carte" delivery systems for bacterial type VI effectors. *Journal of Biological Chemistry*, 289(25):17872–17884.

Hachani, A., Wood, T. E., and Filloux, A. (2016). Type VI secretion and anti-host effectors. *Current Opinion in Microbiology*, 29:81–93.

Haggard-Ljungquist, E., Jacobsen, E., Rishovd, S., Six, E. W., Nilssen, O., Sunshine, M. G., Lindqvist, B. H., Kim, K. J., Barreiro, V., Koonin, E. V., and Et Al. (1995). Bacteriophage P2: genes involved in baseplate assembly. *Virology*, 213(1):109–121.

Hall, A. B., Tolonen, A. C., and Xavier, R. J. (2017). Human genetic variation and the gut microbiome in disease. *Nat Rev Genet*, Advanced o.

Hall-Stoodley, L., Costerton, J. W., and Stoodley, P. (2004). Bacterial biofilms: from the Natural environment to infectious diseases. *Nature Reviews Microbiology*, 2(2):95–108.

Hardy, K. G., Meynell, G. G., Dowman, J. E., and Spratt, B. G. (1973). Two major groups of colicin factors: Their evolutionary significance. *MGG Molecular & General Genetics*, 125(3):217–230.

Harrington, S. M., Dudley, E. G., and Nataro, J. P. (2006). Pathogenesis of enteroaggregative Escherichia coli infection. *FEMS Microbiology Letters*, 254(1):12–18.

Harrison, F., Paul, J., Massey, R. C., and Buckling, A. (2008). Interspecific competition and siderophore-mediated cooperation in Pseudomonas aeruginosa. *The ISME Journal*, 2(1):49–55.

Hecht, A. L., Casterline, B. W., Earley, Z. M., Goo, Y. A., Goodlett, D. R., and Bubeck Wardenburg, J. (2016). Strain competition restricts colonization of an enteric pathogen and prevents colitis. *EMBO reports*, 17(9):1281–1291.

Hendrix, R. W. (1978). Symmetry mismatch and DNA packaging in large bacteriophages. *Proceedings of the National Academy of Sciences of the United States of America*, 75(10):4779–83.

Henry, T., Pommier, S., Journet, L., Bernadac, A., Gorvel, J. P., and Lloubès, R. (2004). Improved methods for producing outer membrane vesicles in Gram-negative bacteria. *Research in Microbiology*, 155(6):437–446.

Heymann, J. B., Bartho, J. D., Rybakova, D., Venugopal, H. P., Winkler, D. C., Sen, A., Hurst, M. R., and Mitra, A. K. (2013). Three-dimensional structure of the toxin-delivery particle antifeeding prophage of serratia entomophila. *Journal of Biological Chemistry*, 288(35):25276–25284.

Hibbing, M. E., Fuqua, C., Parsek, M. R., and Peterson, S. B. (2010). Bacterial competition: surviving and thriving in the microbial jungle. *Nature Reviews Microbiology*, 8(1):15–25.

Hood, R. D., Singh, P., Hsu, F., Güvener, T., Carl, M. A., Trinidad, R. R. S., Silverman, J. M., Ohlson, B. B., Hicks, K. G., Plemel, R. L., Li, M., Schwarz, S., Wang, W. Y., Merz, A. J., Goodlett, D. R., and Mougous, J. D. (2010). A Type VI Secretion System of Pseudomonas aeruginosa Targets a Toxin to Bacteria. *Cell Host and Microbe*, 7(1):25–37.

Housden, N. G., Hopper, J. T. S., Lukoyanova, N., Rodriguez-Larrea, D., Wojdyla, J. A., Klein, A., Kaminska, R., Bayley, H., Saibil, H. R., Robinson, C. V., and Kleanthous, C. (2013). Intrinsically Disordered Protein Threads Through the Bacterial Outer-Membrane Porin OmpF. *Science*, 340(6140):1570–1574.

Hu, B., Lara-Tejero, M., Kong, Q., Galán, J. E., and Liu, J. (2017). In Situ Molecular Architecture of the Salmonella Type III Secretion Machine. *Cell*, 168(6):1065–1074.

Hu, B., Margolin, W., Molineux, I. J., and Liu, J. (2015). Structural remodeling of bacteriophage T4 and host membranes during infection initiation. *Proceedings of the National Academy of Sciences*, 112(35):E4919–E4928.

Huang, Y., Callahan, S., and Hadfield, M. G. (2012). Recruitment in the sea: bacterial genes required for inducing larval settlement in a polychaete worm. *Scientific Reports*, 2(1):228.

Hurst, M. R. H., Beard, S. S., Jackson, T. A., and Jones, S. M. (2007). Isolation and characterization of the Serratia entomophila antifeeding prophage. *FEMS Microbiology Letters*, 270(1):42–48.

Ishii, S. I., Nishi, Y., and Egami, F. (1965). The fine structure of a pyocin. *Journal of molecular biology*, 13(2):428–31.

Jacob, F. (1954). Induced biosynthesis and mode of action of a pyocine, antibiotic produced by Pseudomonas aeruginosa. *Annales de l'Institut Pasteur*, 86(2):149–60.

Jacob-Dubuisson, F., Guérin, J., Baelen, S., and Clantin, B. (2013). Two-partner secretion: As simple as it sounds? *Research in Microbiology*, 164(6):583–595.

Jiang, F., Wang, X., Wang, B., Chen, L., Zhao, Z., Waterfield, N. R., Yang, G., and Jin, Q. (2016). The Pseudomonas aeruginosa Type VI Secretion PGAP1-like Effector Induces Host Autophagy by Activating Endoplasmic Reticulum Stress. *Cell Reports*, 16(6):1502–1509.

Jiang, F., Waterfield, N. R., Yang, J., Yang, G., and Jin, Q. (2014). A Pseudomonas aeruginosa type VI secretion phospholipase D effector targets both prokaryotic and eukaryotic cells. *Cell Host and Microbe*, 15(5):600–610.

Jing, P. I., Dogovski, C., and Pittard, A. J. (1998). Functional consequences of changing proline residues in the phenylalanine-specific permease of Escherichia coli. *Journal of Bacteriology*, 180(21):5515–5519.

Jobichen, C., Chakraborty, S., Li, M., Zheng, J., Joseph, L., Mok, Y. K., Leung, Y. K., and Sivaraman, J. (2010). Structural basis for the secretion of evpc: A key type vi secretion system protein from edwardsiella tarda. *PLoS ONE*, 5(9):1–10.

Jones, A. M., Garza-Sánchez, F., So, J., Hayes, C. S., and Low, D. A. (2017). Activation of contact-dependent antibacterial tRNase toxins by translation elongation factors. *Proceedings of the National Academy of Sciences*, 114(10):E1951–E1957.

Journet, L. and Cascales, E. (2016). The Type VI Secretion System in Escherichia coli and Related Species. *EcoSal Plus*, 9:1–20.

Judd, P. K., Kumar, R. B., and Das, A. (2005). Spatial location and requirements for the assembly of the Agrobacterium tumefaciens type IV secretion apparatus. *Proceedings of the National Academy of Sciences of the United States of America*, 102(32):11498–503.

Kadouri, D. E. and O'Toole, G. A. (2005). Susceptibility of biofilms to ¡i¿Bdellovibrio bacteriovorus¡/i¿ attack. *Applied and Environmental Microbiology*, 71(7):4044–4051.

Kadurugamuwa, J. L. and Beveridge, T. J. (1996). Bacteriolytic effect of membrane vesicles from Pseudomonas aeruginosa on other bacteria including pathogens: conceptually new antibiotics. *Journal of Bacteriology*, 178(10):2767–2774.

Kadurugamuwa, J. L. and Beveridge, T. J. (1999). Membrane vesicles derived f rom Pseudornonas aeruginosa and Shigella flexneri can be integrated into the surfaces of other Gram-negative bacteria. (1999):2051–2060.

Kanamaru, S., Ishiwata, Y., Suzuki, T., Rossmann, M. G., and Arisaka, F. (2005). Control of bacteriophage T4 tail lysozyme activity during the infection process. *Journal of Molecular Biology*, 346(4):1013–1020.

Kanamaru, S., Leiman, P. G., Kostyuchenko, V. A., Chipman, P. R., Mesyanzhinov, V. V., Arisaka, F., and Rossmann, M. G. (2002). Structure of the cell-puncturing device of bacteriophage T4. *Nature*, 415(6871):553–557.

Kaper, J. B., Nataro, J. P., and Mobley, H. L. T. (2004). Pathogenic Escherichia coli. *Nature Reviews Microbiology*, 2(2):123–140.

Kapitein, N., Bönemann, G., Pietrosiuk, A., Seyffer, F., Hausser, I., Locker, J. K., and Mogk, A. (2013). ClpV recycles VipA/VipB tubules and prevents non-productive tubule formation to ensure efficient type VI protein secretion. *Molecular Microbiology*, 87(5):1013–1028.

Karow, M., Raina, S., Georgopoulos, C., and Fayet, O. (1991). Complex phenotypes of null mutations in the htr genes, whose products are essential for Escherichia coli growth at elevated temperatures. *Research in Microbiology*, 142(2-3):289–294.

Keane, R. and Berleman, J. (2016). The predatory life cycle of Myxococcus xanthus. *Microbiology (United Kingdom)*, 162(1):1–11.

Kerr, B., Riley, M. A., Feldman, M. W., and Bohannan, B. J. M. (2002). Local dispersal promotes biodiversity in a real-life game of rock–paper–scissors. *Nature*, 418(6894):171–174.

King, J. (1968). Assembly of the tail of bacteriophage T4. *Journal of molecular biology*, 32(2):231–62.

King, J. (1971). Bacteriophage T4 tail assembly: four steps in core formation. *Journal of molecular biology*, 58(3):693–709.

Kirkup, B. C. (2006). Bacteriocins as oral and gastrointestinal antibiotics: theoretical considerations, applied research, and practical applications. *Current medicinal chemistry*, 13(27):3335–50.

Kirkup, B. C. and Riley, M. A. (2004). Antibiotic-mediated antagonism leads to a bacterial game of rock–paper–scissors in vivo. *Nature*, 428(6981):412–414.

Kneidinger, B., Marolda, C., Graninger, M., Zamyatina, A., McArthur, F., Kosma, P., Valvano, M. A., and Messner, P. (2002). Biosynthesis pathway of ADP-L-glycero-beta-D-manno-heptose in Escherichia coli. *Journal of bacteriology*, 184(2):363–9.

Kommineni, S., Bretl, D. J., Lam, V., Chakraborty, R., Hayward, M., Simpson, P., Cao, Y., Bousounis, P., Kristich, C. J., and Salzman, N. H. (2015). Bacteriocin production augments niche competition by enterococci in the mammalian gastrointestinal tract. *Nature*, 526(7575):719–722.

Konovalova, A., Perlman, D. H., Cowles, C. E., and Silhavy, T. J. (2014). Transmembrane domain of surface-exposed outer membrane lipoprotein RcsF is threaded through the lumen of -barrel proteins. *Proceedings of the National Academy of Sciences*, 111(41):E4350–E4358.

Koskiniemi, S., Garza-Sánchez, F., Sandegren, L., Webb, J. S., Braaten, B. A., Poole, S. J., Andersson, D. I., Hayes, C. S., and Low, D. A. (2014). Selection of Orphan Rhs Toxin Expression in Evolved Salmonella enterica Serovar Typhimurium. *PLoS Genetics*, 10(3):e1004255.

Koskiniemi, S., Lamoureux, J. G., Nikolakakis, K. C., t'Kint de Roodenbeke, C., Kaplan, M. D., Low, D. A., and Hayes, C. S. (2013). Rhs proteins from diverse bacteria mediate intercellular competition. *Proceedings of the National Academy of Sciences*, 110(17):7032–7037.

Kostyuchenko, V. A., Chipman, P. R., Leiman, P. G., Arisaka, F., Mesyanzhinov, V. V., and Rossmann, M. G. (2005). The tail structure of bacteriophage T4 and its mechanism of contraction. *Nature Structural & Molecular Biology*, 12(9):810–813.

Kostyuchenko, V. A., Leiman, P. G., Chipman, P. R., Kanamaru, S., van Raaij, M. J., Arisaka, F., Mesyanzhinov, V. V., and Rossmann, M. G. (2003). Three-dimensional structure of bacteriophage T4 baseplate. *Nature Structural Biology*, 10(9):688–693.

Kostyuchenko, V. A., Navruzbekov, G. A., Kurochkina, L. P., Strelkov, S. V., Mesyanzhinov, V. V., and Rossmann, M. G. (1999). The structure of bacteriophage T4 gene product 9: The trigger for tail contraction. *Structure*, 7(10):1213–1222.

Koval, S. F. and Bayer, M. E. (1997). Bacterial capsules: No barrier against Bdellovibrio. *Microbiology*, 143(3):749–753.

Kube, S., Kapitein, N., Zimniak, T., Herzog, F., Mogk, A., and Wendler, P. (2014). Structure of the VipA/B type VI secretion complex suggests a contraction-state-specific recycling mechanism. *Cell Reports*, 8(1):20–30.

Kudryashev, M., Wang, R.-R., Brackmann, M., Scherer, S., Maier, T., Baker, D., DiMaio, F., Stahlberg, H., Egelman, E., and Basler, M. (2015). Structure of the Type VI Secretion System Contractile Sheath. *Cell*, 160(5):952–962.

Kull, K. (2010). Ecosystems are Made of Semiosic Bonds: Consortia, Umwelten, Biophony and Ecological Codes. *Biosemiotics*, 3(3):347–357.

Kumar, R. B. and Das, A. (2002). Polar location and functional domains of the Agrobacterium tumefaciens DNA transfer protein VirD4. *Molecular Microbiology*, 43(6):1523–1532.

Kurisu, G., Zakharov, S. D., Zhalnina, M. V., Bano, S., Eroukova, V. Y., Rokitskaya, T. I., Antonenko, Y. N., Wiener, M. C., and Cramer, W. A. (2003). The structure of BtuB with bound colicin E3 R-domain implies a translocon. *Nature Structural Biology*, 10(11):948–954.

Kwan, J. C., Meickle, T., Ladwa, D., Teplitski, M., Paul, V., and Luesch, H. (2011). Lyngbyoic acid, a "tagged" fatty acid from a marine cyanobacterium, disrupts quorum sensing in Pseudomonas aeruginosa. *Molecular BioSystems*, 7(4):1205.

Lambert, C., Evans, K. J., Till, R., Hobley, L., Capeness, M., Rendulic, S., Schuster, S. C., Aizawa, S. I., and Sockett, R. E. (2006a). Characterizing the flagellar filament and the role of motility in bacterial prey-penetration by Bdellovibrio bacteriovorus. *Molecular Microbiology*, 60(2):274–286.

Lambert, C., Morehouse, K. A., Chang, C. Y., and Sockett, R. E. (2006b). Bdellovibrio: growth and development during the predatory cycle. *Current Opinion in Microbiology*, 9(6):639–644.

Lauterborn, R. (1906). Zur Kenntnis der sapropelischen Flora. *Allg Bot Z*, 14:196–197.

Lazdunski, C. J., Bouveret, E., Rigal, A., Journet, L., Lloubès, R., Bénédetti, H., and Lloube, R. (1998). Colicin Import into Escherichia coli Cells. *Journal of Bacteriology*, 180(19):4993–5002.

Lazzaroni, J. C., Dubuisson, J. F., and Vianney, A. (2002). The Tol proteins of Escherichia coli and their involvement in the translocation of group A colicins. *Biochimie*, 84(5-6):391–397.

Le Roux, M., Kirkpatrick, R. L., Montauti, E. I., Tran, B. Q., Brook Peterson, S., Harding, B. N., Whitney, J. C., Russell, A. B., Traxler, B., Goo, Y. A., Goodlett, D. R., Wiggins, P. A., and Mougous, J. D. (2015). Kin cell lysis is a danger signal that activates antibacterial pathways of pseudomonas aeruginosa. *eLife*, 2015(4):1–65.

Leadbetter, J. R. and Greenberg, E. P. (2000). Metabolism of Acyl-Homoserine Lactone Quorum-Sensing Signals by Variovorax paradoxus. *Journal of bacteriology*, 182(24):6921–6926.

Leiman, P. G., Basler, M., Ramagopal, U. A., Bonanno, J. B., Sauder, J. M., Pukatzki, S., Burley, S. K., Almo, S. C., and Mekalanos, J. J. (2009). Type VI secretion apparatus and phage tail-associated protein complexes share a common evolutionary origin. *Proceedings of the National Academy of Sciences*, 106(11):4154–4159.

Leiman, P. G., Chipman, P. R., Kostyuchenko, V. A., Mesyanzhinov, V. V., and Rossmann, M. G. (2004). Three-dimensional rearrangement of proteins in the tail of bacteriophage T4 on infection of its host. *Cell*, 118(4):419–429.

Leiman, P. G. and Shneider, M. M. (2012). Contractile Tail Machines of Bacteriophages. *Advances in experimental medicine and biology*, 726:93–114.

Leo, J. C., Grin, I., and Linke, D. (2012). Type V secretion: mechanism(s) of autotransport through the bacterial outer membrane. *Philosophical Transactions of the Royal Society B: Biological Sciences*, 367(1592):1088–1101.

LeRoux, M., De Leon, J. A., Kuwanda, N. J., Russell, A. B., Pinto-Santini, D., Hood, R. D., Agnello, D., Robertson, S. M., Wiggins, P. A., and Mougous, J. D. (2012). Quantitative single-cell characterization of bacterial interactions. *Proceedings of the National Academy of Sciences of the United States of America*, 109(48):19804–19809.

Lery, L. M., Frangeul, L., Tomas, A., Passet, V., Almeida, A. S., Bialek-Davenet, S., Barbe, V., Bengoechea, J. A., Sansonetti, P., Brisse, S., and Tournebize, R. (2014). Comparative analysis of Klebsiella pneumoniae genomes identifies a phospholipase D family protein as a novel virulence factor. *BMC Biology*, 12(1):41.

Leschine, S. B. (1995). Cellulose Degradation in Anaerobic Environments. *Annual Review of Microbiology*, 49(1):399–426.

Li, J., Yao, Y., Xu, H. H., Hao, L., Deng, Z., Rajakumar, K., and Ou, H. Y. (2015). SecReT6: A web-based resource for type VI secretion systems found in bacteria. *Environmental Microbiology*, 17(7):2196–2202.

Li, L., Zhang, W., Liu, Q., Gao, Y., Gao, Y., Wang, Y., Wang, D. Z., Li, Z., and Wang, T. (2013). Structural insights on the bacteriolytic and self-protection mechanism of muramidase effector Tse3 in pseudomonas aeruginosa. *Journal of Biological Chemistry*, 288(42):30607–30613.

Li, M., Le Trong, I., Carl, M. A., Larson, E. T., Chou, S., de Leon, J. A., Dove, S. L., Stenkamp, R. E., and Mougous, J. D. (2012). Structural basis for type VI secretion effector recognition by a cognate immunity protein. *PLoS Pathogens*, 8(4):e1002613.

Liang, X., Moore, R., Wilton, M., Wong, M. J. Q., Lam, L., and Dong, T. G. (2015). Identification of divergent type VI secretion effectors using a conserved chaperone domain. *Proceedings of the National Academy of Sciences*, 112(29):9106–9111.

Lien, Y.-W. and Lai, E.-M. (2017). Type VI Secretion Effectors: Methodologies and Biology. *Frontiers in cellular and infection microbiology*, 7(7):254.

Lin, J.-S., Wu, H.-H., Hsu, P.-H., Ma, L.-S., Pang, Y.-Y., Tsai, M.-D., and Lai, E.-M. (2014). Fha interaction with phosphothreonine of TssL activates type VI secretion in Agrobacterium tumefaciens. *PLoS pathogens*, 10(3):e1003991.

Link, A. J., Phillips, D., and Church, G. M. (1997). Methods for generating precise deletions and insertions in the genome of wild-type Escherichia coli: application to open reading frame characterization. *Journal of bacteriology*, 179(20):6228–37.

Little, J. W. and Mount, D. W. (1982). The SOS Regulatory Escherichia coli System of Review. *Cell*, 29:11–22.

Liu, J., Chen, C. Y., Shiomi, D., Niki, H., and Margolin, W. (2011). Visualization of bacteriophage P1 infection by cryo-electron tomography of tiny Escherichia coli. *Virology*, 417(2):304–311.

Lloubes, R., Baty, D., and Lazdunski, C. (1986). effects of convergent transcription and Lex A protein Nucleic Acids Research. *Nucleic Acids Research*, 14(6):2621–36.

Logger, L., Aschtgen, M. S., Gu??rin, M., Cascales, E., and Durand, E. (2016). Molecular Dissection of the Interface between the Type VI Secretion TssM Cytoplasmic Domain and the TssG Baseplate Component. *Journal of Molecular Biology*, 428(22):4424–4437.

Lossi, N. S., Dajani, R., Freemont, P., and Filloux, A. (2011). Structure-function analysis of HsiF, a gp25-like component of the type VI secretion system, in Pseudomonas aeruginosa. *Microbiology*, 157(12):3292–3305.

Lossi, N. S., Manoli, E., Förster, A., Dajani, R., Pape, T., Freemont, P., and Filloux, A. (2013). The HsiB1C1 (TssB-TssC) complex of the Pseudomonas aeruginosa type VI secretion system forms a bacteriophage tail sheathlike structure. *Journal of Biological Chemistry*, 288(11):7536–7548.

Low, H. H., Gubellini, F., Rivera-Calzada, A., Braun, N., Connery, S., Dujeancourt, A., Lu, F., Redzej, A., Fronzes, R., Orlova, E. V., and Waksman, G. (2014). Structure of a type IV secretion system. *Nature*, 508(7497):550–553.

Lybarger, S. R., Johnson, T. L., Gray, M. D., Sikora, A. E., and Sandkvist, M. (2009). Docking and assembly of the type II secretion complex of Vibrio cholerae. *Journal of Bacteriology*, 191(9):3149–3161.

Ma, A. T., McAuley, S., Pukatzki, S., and Mekalanos, J. J. (2009a). Translocation of a Vibrio cholerae Type VI Secretion Effector Requires Bacterial Endocytosis by Host Cells. *Cell Host and Microbe*, 5(3):234–243.

Ma, A. T. and Mekalanos, J. J. (2010). In vivo actin cross-linking induced by Vibrio cholerae type VI secretion system is associated with intestinal inflammation. *Proceedings of the National Academy of Sciences*, 107(9):4365–4370.

Ma, J., Sun, M., Dong, W., Pan, Z., Lu, C., and Yao, H. (2017). PAAR-Rhs proteins harbor various C-terminal toxins to diversify the antibacterial pathways of type VI secretion systems. *Environmental Microbiology*, 19(1):345–360.

Ma, L. S., Hachani, A., Lin, J. S., Filloux, A., and Lai, E. M. (2014). Agrobacterium tumefaciens deploys a superfamily of type VI secretion DNase effectors as weapons for interbacterial competition in planta. *Cell Host and Microbe*, 16(1):94–104.

Ma, L. S., Lin, J. S., and Lai, E. M. (2009b). An IcmF family protein, ImpLM, is an integral inner membrane protein interacting with ImpKL, and its Walker a motif is required for type VI secretion system-mediated Hcp secretion in Agrobacterium tumefaciens. *Journal of Bacteriology*, 191(13):4316–4329.

Ma, L. S., Narberhaus, F., and Lai, E. M. (2012). IcmF family protein TssM exhibits ATPase activity and energizes type VI secretion. *Journal of Biological Chemistry*, 287(19):15610–15621.

MacIntyre, D. L., Miyata, S. T., Kitaoka, M., and Pukatzki, S. (2010). The Vibrio cholerae type VI secretion system displays antimicrobial properties. *Proceedings of the National Academy of Sciences*, 107(45):19520–19524.

Majeed, H., Gillor, O., Kerr, B., and Riley, M. A. (2011). Competitive interactions in Escherichia coli populations: the role of bacteriocins. *The ISME Journal*, 5(1):71–81.

Marques, F. Z., Mackay, C. R., and Kaye, D. M. (2017). Beyond gut feelings: how the gut microbiota regulates blood pressure. *Nat Rev Cardiol*, advance on.

Martinez, M. C., Lazdunski, C., and Pattus, F. (1983). Isolation, molecular and functional properties of the C-terminal domain of colicin A. *The EMBO journal*, 2(9):1501–7.

Mashburn, L. M. and Whiteley, M. (2005). Membrane vesicles traffic signals and facilitate group activities in a prokaryote. *Nature*, 437(7057):422–425.

Matin, A. and Rittenberg, S. C. (1972). Kinetics of Deoxyribonucleic Acid Destruction and Synthesis During Growth of Bdellovibrio bacteriovorus Strain 109D on Pseudomonas putida and Escherichia coli. *Journal of Bacteriology*, 111(3):664–673.

McNally, L., Bernardy, E., Thomas, J., Kalziqi, A., Pentz, J., Brown, S. P., Hammer, B. K., Yunker, P. J., and Ratcliff, W. C. (2017). Killing by Type VI secretion drives genetic phase separation and correlates with increased cooperation. *Nature Communications*, 8:14371.

Meezan, E. and Wood, W. B. (1971). The sequence of gene product interaction in bacteriophage T4 tail core assembly. *Journal of molecular biology*, 58(3):685–92.

Michel-Briand, Y. and Baysse, C. (2002). The pyocins of Pseudomonas aeruginosa. *Biochimie*, 84(5-6):499–510.

Miller, M. B. and Bassler, B. L. (2001). Ensing in. *Annual Review of Microbiology*, 55:165–99.

Miyata, S. T., Bachmann, V., and Pukatzki, S. (2013). Type VI secretion system regulation as a consequence of evolutionary pressure. *Journal of medical microbiology*, 62(Pt 5):663–76.

Miyata, S. T., Kitaoka, M., Brooks, T. M., McAuley, S. B., and Pukatzki, S. (2011). Vibrio cholerae requires the type VI secretion system virulence factor vasx to kill dictyostelium discoideum. *Infection and Immunity*, 79(7):2941–2949.

Morin, N., Santiago, A. E., Ernst, R. K., Guillot, S. J., and Nataro, J. P. (2013). Characterization of the AggR regulon in enteroaggregative Escherichia coli. *Infection and Immunity*, 81(1):122–132.

Mougi, A. (2016). The roles of amensalistic and commensalistic interactions in large ecological network stability. *Scientific Reports*, 6(1):29929.

Mougous, J. D. (2006). A Virulence Locus of Pseudomonas aeruginosa Encodes a Protein Secretion Apparatus. *Science*, 312(5779):1526–1530.

Mougous, J. D., Gifford, C. A., Ramsdell, T. L., and Mekalanos, J. J. (2007). Threonine phosphorylation post-translationally regulates protein secretion in Pseudomonas aeruginosa. *Nature Cell Biology*, 9(7):797–803.

Muñoz-Dorado, J., Marcos-Torres, F. J., García-Bravo, E., Moraleda-Muñoz, A., and Pérez, J. (2016). Myxobacteria: Moving, killing, feeding, and surviving together. *Frontiers in Microbiology*, 7:1–18.

Murdoch, S. L., Trunk, K., English, G., Fritsch, M. J., Pourkarimi, E., and Coulthurst, S. J. (2011). The opportunistic pathogen Serratia marcescens utilizes type VI secretion to target bacterial competitors. *Journal of Bacteriology*, 193(21):6057–6069.

Nakayama, K., Takashima, K., Ishihara, H., Shinomiya, T., Kageyama, M., Kanaya, S., Ohnishi, M., Murata, T., Mori, H., and Hayashi, T. (2000). The R-type pyocin of Pseudomonas aeruginosa is related to P2 phage, and the F-type is related to lambda phage. *Molecular Microbiology*, 38(2):213–231.

Narisawa, N., Haruta, S., Arai, H., Ishii, M., and Igarashi, Y. (2008). Coexistence of antibiotic-producing and antibiotic-sensitive bacteria in biofilms is mediated by resistant bacteria. *Applied and Environmental Microbiology*, 74(12):3887–3894.

Nataro, J. P., Deng, Y., Maneval, D. R., German, A. L., Martin, W. C., and Levine, M. M. (1992). Aggregative adherence fimbriae I of enteroaggregative Escherichia coli mediate adherence to HEp-2 cells and hemagglutination Aggregative Adherence Fimbriae I of Enteroaggregative Escherichia coli Mediate Adherence to HEp-2 Cells and Hemagglutination of Hu. *Infection and immunity*, 60(6):2297–04.

Nataro, J. P., Kaper, J. B., Robins-Browne, R., Prado, V., Vial, P., and Levine, M. M. (1987). Patterns of adherence of diarrheagenic Escherichia coli to HEp-2 cells. *The Pediatric infectious disease journal*, 6(9):829–31.

Nataro, J. P., Yikang, D., Cookson, S., Cravioto, A., Savarino, S. J., Guers, L. D., Levine, M. M., and Tacket, C. O. (1995). Heterogeneity of enteroaggregative escherichia coli virulence demonstrated. *Journal of Infectious Diseases*, 171(2):465–468.

Nataro, J. P., Yikang, D., Yingkang, D., and Walker, K. (1994). AggR, a transcriptional activator of aggregative adherence fimbria I expression in enteroaggregative Escherichia coli. *Journal of Bacteriology*, 176(15):4691–4699.

Neil, R. B. and Apicella, M. A. (2009). Role of HrpA in biofilm formation of Neisseria meningitidis and regulation of the hrpBAS transcripts. *Infection and Immunity*, 77(6):2285–2293.

Nguyen, V., Logger, L., Spinelli, S., Legrand, P., Huyen Pham, T., Nhung Trinh, T., Cherrak, Y., Zoued, A., Desmyter, A., Durand, E., Roussel, A., Kellenberger, C., Cascales, E., and Cambillau, C. (2017). Type VI secretion TssK baseplate protein exhibits structural similarity with phage receptor-binding proteins and evolved to bind the membrane complex. *Nature Microbiology*, 2:17103.

Nicholson, A. (1954). An outline of the dynamics of animal populations. *Australian Journal of Zoology*, 2(1):9.

Nikolakakis, K., Amber, S., Wilbur, J. S., Diner, E. J., Aoki, S. K., Poole, S. J., Tuanyok, A., Keim, P. S., Peacock, S., Hayes, C. S., and Low, D. A. (2012). The toxin/immunity network of Burkholderia pseudomallei contact-dependent growth inhibition (CDI) systems. *Molecular Microbiology*, 84(3):516–529.

Nissimov, J., Rosenberg, E., and Munn, C. B. (2009). Antimicrobial properties of resident coral mucus bacteria of Oculina patagonica. *FEMS Microbiology Letters*, 292(2):210–215.

Noel, G. J., Love, D. C., and Mosser, D. M. (1994). High-molecular-weight proteins of nontypeable Haemophilus influenzae mediate bacterial adhesion to cellular proteoglycans. *Infection and Immunity*, 62(9):4028–4033.

Noinaj, N., Kuszak, A. J., Gumbart, J. C., Lukacik, P., Chang, H., Easley, N. C., Lithgow, T., and Buchanan, S. K. (2013). Structural insight into the biogenesis of β-barrel membrane proteins. *Nature*, 501(7467):385–390.

O'Hara, A. M. and Shanahan, F. (2006). The gut flora as a forgotten organ. *EMBO reports*, 7(7):688–693.

Oikonomou, C. M. and Jensen, G. J. (2017). Cellular Electron Cryotomography: Toward Structural Biology In Situ TEM: transmission electron microscopy. *Annual Review of Biochemistry*, 86:873–896.

Overmann, J., Tuschak, C., Fröstl, J. M., and Sass, H. (1998). The ecological niche of the consortium 'Pelochromatium roseum'. *Archives of Microbiology*, 169(2):120–128.

Overmann, J. and Van Gemerden, H. (2000). Microbial interactions involving sulfur bacteria: implications for the ecology and evolution of bacterial communities. *FEMS Microbiol Ecol*, 24:591–599.

Palmer, C., Bik, E. M., DiGiulio, D. B., Relman, D. A., and Brown, P. O. (2007). Development of the human infant intestinal microbiota. *PLoS Biology*, 5(7):1556–1573.

Palsdottir, H., Remis, J. P., Schaudinn, C., O'Toole, E., Lux, R., Shi, W., McDonald, K. L., Costerton, J. W., and Auer, M. (2009). Three-dimensional macromolecular organization of cryofixed myxococcus xanthus biofilms as revealed by electron microscopic tomography. *Journal of Bacteriology*, 191(7):2077–2082.

Pande, S., Shitut, S., Freund, L., Westermann, M., Bertels, F., Colesie, C., Bischofs, I. B., and Kost, C. (2015). Metabolic cross-feeding via intercellular nanotubes among bacteria. *Nature Communications*, 6:6238.

Pell, L. G., Kanelis, V., Donaldson, L. W., Lynne Howell, P., and Davidson, A. R. (2009). The phage major tail protein structure reveals a common evolution for long-tailed phages and the type VI bacterial secretion system. *Proceedings of the National Academy of Sciences*, 106(11):4160–4165.

Pérez, J., Moraleda-Muñoz, A., Marcos-Torres, F. J., and Muñoz-Dorado, J. (2016). Bacterial predation: 75 years and counting! *Environmental Microbiology*, 18(3):766–779.

Pham, V. D., Shebelut, C. W., Diodati, M. E., Bull, C. T., and Singer, M. (2005). Mutations affecting predation ability of the soil bacterium Myxococcus xanthus. *Microbiology*, 151(6):1865–1874.

Pietrosiuk, A., Lenherr, E. D., Falk, S., Bönemann, G., Kopp, J., Zentgraf, H., Sinning, I., and Mogk, A. (2011). Molecular basis for the unique role of the AAA + chaperone ClpV in type VI protein secretion. *Journal of Biological Chemistry*, 286(34):30010–30021.

Planamente, S., Salih, O., Manoli, E., Albesa-Jové, D., Freemont, P. S., and Filloux, A. (2016). TssA forms a gp6-like ring attached to the type VI secretion sheath. *The EMBO journal*, 35(15):e201694024.

Plishker, M. F., Rangwala, S. H., and Bergett, P. B. (1988). Isolation of Bacteriophage T4 Baseplate Proteins P7 and P8 and In Vitro Formation of the P10 / P7 / P8 Assembly Intermediate. 62(2):400–406.

Poole, S. J., Diner, E. J., Aoki, S. K., Braaten, B. A., t'Kint de Roodenbeke, C., Low, D. A., and Hayes, C. S. (2011). Identification of functional toxin/immunity genes linked to contact-dependent growth inhibition (cdi) and rearrangement hotspot (rhs) systems. *PLoS Genetics*, 7(8):e1002217.

Popa, R. (2004). Between necessity and probability: Searching for the definition and origin of life. *Springer*.

Postle, K. and Kadner, R. J. (2003). Touch and go: Tying TonB to transport. *Molecular Microbiology*, 49(4):869–882.

Powers, M. J., Sanabria-Valentin, E., Bowers, A. A., and Shank, E. A. (2015). Inhibition of cell differentiation in Bacillus subtilis by Pseudomonas protegens. *Journal of Bacteriology*, 197(13):2129–2138.

Pross, E., Soussoula, L., Seitl, I., Lupo, D., and Kuhn, A. (2016). Membrane Targeting and Insertion of the C-Tail Protein SciP. *Journal of Molecular Biology*, 428(20):4218–4227.

Pugsley, A. P. (1984). Genetic analysis of ColN plasmid determinants for colicin production, release, and immunity. *Journal of Bacteriology*, 158(2):523–529.

Pukatzki, S., Ma, A. T., Revel, A. T., Sturtevant, D., and Mekalanos, J. J. (2007). Type VI secretion system translocates a phage tail spike-like protein into target cells where it cross-links actin. *Proceedings of the National Academy of Sciences*, 104(39):15508–15513.

Pukatzki, S., Ma, A. T., Sturtevant, D., Krastins, B., Sarracino, D., Nelson, W. C., Heidelberg, J. F., and Mekalanos, J. J. (2006). Identification of a conserved bacterial protein secretion system in Vibrio cholerae using the Dictyostelium host model system. *Proceedings of the National Academy of Sciences*, 103(5):1528–1533.

Raetz, C. R. H. and Whitfield, C. (2002). Lipopolysaccharide Endotoxins. *Annual Review of Biochemistry*, 71(1):635–700.

Raina, S. and Costa, G. (1991). The htrM gene, whose product is essential for Escherichia coli viability only at elevated temperatures, is identical to the rfaD gene. *Nucleic Acids Research*, 19(14):3811–3819.

Raina, S. and Georgopoulos, C. (1990). A new Escherichia coli heat shock gene, htrC, whose product is essential for viability only at high temperature. *Journal of Bacteriology*, 172(6):3417–3426.

Rao, J., Damron, F. H., Basler, M., DiGiandomenico, A., Sherman, N. E., Fox, J. W., Mekalanos, J. J., and Goldberg, J. B. (2011). Comparisons of two proteomic analyses of non-mucoid and mucoid Pseudomonas aeruginosa clinical isolates from a cystic fibrosis patient. *Frontiers in Microbiology*, 2(AUG):1–12.

Relman, D. (2001). The meaning and impact of the human genome sequence for microbiology. *Trends in Microbiology*, 9(5):206–208.

Relman, D., Tuomanen, E., Falkow, S., Golenbock, D. T., Saukkonen, K., Wrighp, S. D., and Wright, S. D. (1990). Recognition of a bacterial adhesin by an integrin: Macrophage CR3 (αMβ2, CD11bCD18) binds filamentous hemagglutinin of Bordetella pertussis. *Cell*, 61(7):1375–1382.

Renelli, M., Matias, V., Lo, R. Y., and Beveridge, T. J. (2004). DNA-containing membrane vesicles of Pseudomonas aeruginosa PAO1 and their genetic transformation potential. *Microbiology*, 150(7):2161–2169.

Ricci, D. P. and Silhavy, T. J. (2012). The Bam machine: A molecular cooper. *Biochimica et Biophysica Acta - Biomembranes*, 1818(4):1067–1084.

Rigort, A., Bauerlein, F. J. B., Villa, E., Eibauer, M., Laugks, T., Baumeister, W., and Plitzko, J. M. (2012). Focused ion beam micromachining of eukaryotic cells for cryoelectron tomography. *Proceedings of the National Academy of Sciences*, 109(12):4449–4454.

Riley, M. A., Goldstone, C. M., Wertz, J. E., and Gordon, D. (2003). A phylogenetic approach to assessing the targets of microbial warfare. *Journal of Evolutionary Biology*, 16(4):690–697.

Riley, M. a. and Gordon, D. M. (1992). A survey of Col plasmids in natural isolates of Escherichia coli and an investigation into the stability of Col-plasmid lineages. *Journal of general microbiology*, 138(7):1345–52.

Riley, M. A. and Wertz, J. E. (2002). Bacteriocins: Evolution, Ecology, and Application. *Annual Review of Microbiology*, 56(1):117–137.

Riley, M. A., Wertz, J. E., Goldstone, C., Editor, S., and Riley, M. (2004). The Ecology and Evolution of Microbial Defense Systems in Escherichia coli. (4):1–13.

Robb, C. S., Assmus, M., Nano, F. E., and Boraston, A. B. (2013). Structure of the T6SS lipoprotein TssJ1 from Pseudomonas aeruginosa. *Acta Crystallographica Section F: Structural Biology and Crystallization Communications*, 69(6):607–610.

Roier, S., Zingl, F. G., Cakar, F., Durakovic, S., Kohl, P., Eichmann, T. O., Klug, L., Gadermaier, B., Weinzerl, K., Prassl, R., Lass, A., Daum, G., Reidl, J., Feldman, M. F., and Schild, S. (2016). A novel mechanism for the biogenesis of outer membrane vesicles in Gram-negative bacteria. *Nature Communications*, 7:10515.

Rojas, C. M., Ham, J. H., Schechter, L. M., Kim, J. F., Beer, S. V., and Collmer, A. (2004). The Erwinia chrysanthemi EC16 hrp/hrc gene cluster encodes an active Hrp type III secretion system that is flanked by virulence genes functionally unrelated to the Hrp system. *Mol Plant Microbe Interact*, 17(6):644–653.

Rosenberg, E., Koren, O., Reshef, L., Efrony, R., and Zilber-Rosenberg, I. (2007). The role of microorganisms in coral health, disease and evolution. *Nature Reviews Microbiology*, 5(5):355–362.

Rosson, R. A. and Rittenberg, S. C. (1979). Regulated breakdown of Escherichia coli deoxyribonucleic acid during intraperiplasmic growth of Bdellovibrio bacteriovorus 109J. *Journal of Bacteriology*, 140(2):620–33.

Ruhe, Z. C., Low, D. A., and Hayes, C. S. (2013a). Bacterial contact-dependent growth inhibition. *Trends in Microbiology*, 21(5):230–237.

Ruhe, Z. C., Nguyen, J. Y., Beck, C. M., Low, D. A., and Hayes, C. S. (2014). The proton-motive force is required for translocation of CDI toxins across the inner membrane of target bacteria. *Molecular Microbiology*, 94(2):466–481.

Ruhe, Z. C., Nguyen, J. Y., Xiong, J., Koskiniemi, S., Beck, C. M., Perkins, B. R., Low, D. A., and Hayes, C. S. (2017). CdiA Effectors Use Modular Receptor-Binding Domains To Recognize Target Bacteria. *mBio*, 8(2):00290–17.

Ruhe, Z. C., Townsley, L., Wallace, A. B., King, A., Van der Woude, M. W., Low, D. A., Yildiz, F. H., and Hayes, C. S. (2015). CdiA promotes receptor-independent intercellular adhesion. *Molecular Microbiology*, 98(1):175–192.

Ruhe, Z. C., Wallace, A. B., Low, D. A., and Hayes, C. S. (2013b). Receptor polymorphism restricts contact-dependent growth inhibition to members of the same species. *mBio*, 4(4):1–9.

Russell, A. B., Hood, R. D., Bui, N. K., LeRoux, M., Vollmer, W., and Mougous, J. D. (2011). Type VI secretion delivers bacteriolytic effectors to target cells. *Nature*, 475(7356):343–347.

Russell, A. B., LeRoux, M., Hathazi, K., Agnello, D. M., Ishikawa, T., Wiggins, P. A., Wai, S. N., and Mougous, J. D. (2013). Diverse type VI secretion phospholipases are functionally plastic antibacterial effectors. *Nature*, 496(7446):508–512.

Russell, A. B., Peterson, S. B., and Mougous, J. D. (2014). Type VI secretion system effectors: poisons with a purpose. *Nature Reviews Microbiology*, 12(2):137–148.

Russell, A. B., Singh, P., Brittnacher, M., Bui, N. K., Hood, R. D., Carl, M. A., Agnello, D. M., Schwarz, S., Goodlett, D. R., Vollmer, W., and Mougous, J. D. (2012). A Widespread Bacterial Type VI Secretion Effector Superfamily Identified Using a Heuristic Approach. *Cell Host & Microbe*, 11(5):538–549.

Rybakova, D., Schramm, P., Mitra, A. K., and Hurst, M. R. H. (2015). Afp14 is involved in regulating the length of Anti-feeding prophage (Afp). *Molecular Microbiology*, 96(4):815–826.

Salomon, D., Gonzalez, H., Updegraff, B. L., and Orth, K. (2013). Vibrio parahaemolyticus Type VI Secretion System 1 Is Activated in Marine Conditions to Target Bacteria, and Is Differentially Regulated from System 2. *PLoS ONE*, 8(4):e61086.

Salomon, D., Kinch, L. N., Trudgian, D. C., Guo, X., Klimko, J. A., Grishin, N. V., Mirzaei, H., and Orth, K. (2014). Marker for type VI secretion system effectors. *Proceedings of the National Academy of Sciences*, 111(25):9271–9276.

Salvucci, E. (2014). Microbiome, holobiont and the net of life. *Critical Reviews in Microbiology*, 7828(May):1–10.

Sana, T. G., Baumann, C., Merdes, A., Soscia, C., Rattei, T., Hachani, A., Jones, C., Bennett, K. L., Filloux, A., Superti-Furga, G., Voulhoux, R., and Bleves, S. (2015). Internalization of Pseudomonas aeruginosa Strain PAO1 into Epithelial Cells Is Promoted by Interaction of a T6SS Effector with the Microtubule Network. *mBio*, 6(3):00712–15.

Sana, T. G., Flaugnatti, N., Lugo, K. A., Lam, L. H., Jacobson, A., Baylot, V., Durand, E., Journet, L., Cascales, E., and Monack, D. M. (2016). ¡i¿Salmonella¡/i¿ Typhimurium utilizes a T6SS-mediated antibacterial weapon to establish in the host gut. *Proceedings of the National Academy of Sciences*, 113(34):E5044–E5051.

Sana, T. G., Hachani, A., Bucior, I., Soscia, C., Garvis, S., Termine, E., Engel, J., Filloux, A., and Bleves, S. (2012). The second type VI secretion system of Pseudomonas aeruginosa strain PAO1 is regulated by quorum sensing and fur and modulates internalization in epithelial cells. *Journal of Biological Chemistry*, 287(32):27095–27105.

Santin, Y. G. and Cascales, E. (2016). Domestication of a housekeeping transglycosylase for assembly of a Type VI secretion system. *EMBO reports*, 18(1):138–149.

Sarris, P. F., Ladoukakis, E. D., Panopoulos, N. J., and Scoulica, E. V. (2014). A phage tail-derived element withwide distribution among both prokaryotic domains: A comparative genomic and phylogenetic study. *Genome Biology and Evolution*, 6(7):1739–1747.

Sassone-Corsi, M., Nuccio, S.-P., Liu, H., Hernandez, D., Vu, C. T., Takahashi, A. A., Edwards, R. A., and Raffatellu, M. (2016). Microcins mediate competition among Enterobacteriaceae in the inflamed gut. *Nature*, 540(7632):280–283.

Sauer, K., Camper, A. K., Ehrlich, G. D., Costerton, J. W., and Davies, D. G. (2002). Pseudomonas aeruginosa. *Journal of Bacteriology*, 184(4):1140–1154.

Schrempf, H. and Merling, P. (2015). Extracellular Streptomyces lividans vesicles: Composition, biogenesis and antimicrobial activity. *Microbial Biotechnology*, 8(4):644–658.

Schwarz, S., Singh, P., Robertson, J. D., LeRoux, M., Skerrett, S. J., Goodlett, D. R., Eoin West, T., and Mougous, J. D. (2014). VgrG-5 is a Burkholderia type VI secretion system-exported protein required for multinucleated giant cell formation and virulence. *Infection and Immunity*, 82(4):1445–1452.

Schwarz, S., West, T. E., Boyer, F., Chiang, W. C., Carl, M. A., Hood, R. D., Rohmer, L., Tolker-Nielsen, T., Skerrett, S. J., and Mougous, J. D. (2010). Burkholderia type vi secretion systems have distinct roles in eukaryotic and bacterial cell interactions. *PLoS Pathogens*, 6(8):77–78.

Sciara, G., Bebeacua, C., Bron, P., Tremblay, D., Ortiz-Lombardia, M., Lichiere, J., van Heel, M., Campanacci, V., Moineau, S., and Cambillau, C. (2010). Structure of lactococcal phage p2 baseplate and its mechanism of activation. *Proceedings of the National Academy of Sciences*, 107(15):6852–6857.

Sender, R., Fuchs, S., and Milo, R. (2016). Revised Estimates for the Number of Human and Bacteria Cells in the Body. *PLoS Biology*, 14(8):1–14.

Senior, B. W. (1977). The Dienes phenomenon: identification of the determinants of compatibility. *Journal of general microbiology*, 102(2):235–44.

Sexton, J. a., Miller, J. L., Yoneda, A., Kehl-fie, T. E., and Vogel, J. P. (2004). Legionella pneumophila. *Society*, 72(10):5983–5992.

Shalom, G., Shaw, J. G., and Thomas, M. S. (2007). In vivo expression technology identifies a type VI secretion system locus in Burkholderia pseudomallei that is induced upon invasion of macrophages. *Microbiology*, 153(8):2689–2699.

Shi, W. and Zusman, D. R. (1993). The two motility systems of Myxococcus xanthus show different selective advantages on various surfaces. *Proceedings of the National Academy of Sciences of the United States of America*, 90(8):3378–3382.

Shikuma, N. J., Pilhofer, M., Weiss, G. L., Hadfield, M. G., Jensen, G. J., and Newman, D. K. (2014). Marine Tubeworm Metamorphosis Induced by Arrays of Bacterial Phage Tail-Like Structures. *Science*, 343(6170):529–533.

Shilo, M. (1970). Lysis of blue-green algae by myxobacter. *Journal of Bacteriology*, 104(1):453–461.

Shneider, M. M., Buth, S. A., Ho, B. T., Basler, M., Mekalanos, J. J., and Leiman, P. G. (2013). PAAR-repeat proteins sharpen and diversify the type VI secretion system spike. *Nature*, 500(7462):350–353.

Si, M., Wang, Y., Zhang, B., Zhao, C., Kang, Y., Bai, H., Wei, D., Zhu, L., Zhang, L., Dong, T. G., and Shen, X. (2017a). The Type VI Secretion System Engages a Redox-Regulated Dual-Functional Heme Transporter for Zinc Acquisition. *Cell Reports*, 20(4):949–959.

Si, M., Zhao, C., Burkinshaw, B., Zhang, B., Wei, D., Wang, Y., Dong, T. G., and Shen, X. (2017b). Manganese scavenging and oxidative stress response mediated by type VI secretion system in Burkholderia thailandensis. *Proceedings of the National Academy of Sciences*, 114(11):E2233–E2242.

Silverman, J., Agnello, D., Zheng, H., Andrews, B., Li, M., Catalano, C., Gonen, T., and Mougous, J. (2013). Haemolysin Coregulated Protein Is an Exported Receptor and Chaperone of Type VI Secretion Substrates. *Molecular Cell*, 51(5):584–593.

Silverman, J. M., Brunet, Y. R., Cascales, E., and Mougous, J. D. (2012). Structure and Regulation of the Type VI Secretion System. *Annual Review of Microbiology*, 66(1):453–472.

Simpson, D. J., Sacher, J. C., and Szymanski, C. M. (2016). Development of an assay for the identification of receptor binding proteins from bacteriophages. *Viruses*, 8(1):17.

Singh, Y., Ahmad, J., Musarrat, J., Ehtesham, N. Z., and Hasnain, S. E. (2013). Emerging importance of holobionts in evolution and in probiotics. *Gut Pathogens*, 5(1):12.

Sockett, R. E. (2009). Predatory Lifestyle of Bdellovibrio bacteriovorus. *Annual Review of Microbiology*, 63(1):523–539.

Spinelli, S., Campanacci, V., Blangy, S., Moineau, S., Tegoni, M., and Cambillau, C. (2006a). Modular structure of the receptor binding proteins of Lactococcus lactis phages: The RBP structure of the temperate phage TP901-1. *Journal of Biological Chemistry*, 281(20):14256–14262.

Spinelli, S., Desmyter, A., Verrips, C. T., de Haard, H. J. W., Moineau, S., and Cambillau, C. (2006b). Lactococcal bacteriophage p2 receptor-binding protein structure suggests a common ancestor gene with bacterial and mammalian viruses. *Nature Structural & Molecular Biology*, 13(1):85–89.

Spinelli, S., Veesler, D., Bebeacua, C., and Cambillau, C. (2014). Structures and host-adhesion mechanisms of lactococcal siphophages. *Frontiers in Microbiology*, 5:1–13.

Spínola-Amilibia, M., Davó-Siguero, I., Ruiz, F. M., Santillana, E., Medrano, F. J., and Romero, A. (2016). The structure of VgrG1 from Pseudomonas aeruginosa, the needle tip of the bacterial type VI secretion system. *Acta crystallographica. Section D, Structural biology*, 72:22–33.

Srikannathasan, V., English, G., Bui, N. K., Trunk, K., O'Rourke, P. E. F., Rao, V. A., Vollmer, W., Coulthurst, S. J., and Hunter, W. N. (2013). Structural basis for type VI secreted peptidoglycan dl-endopeptidase function, specificity and neutralization in Serratia marcescens. *Acta Crystallographica Section D: Biological Crystallography*, 69(12):2468–2482.

Stewart, P. S. (2012). Mini-review: Convection around biofilms. *Biofouling*, 28(2):187–198.

Stoodley, P., Sauer, K., Davies, D. G., and Costerton, J. W. (2002). Biofilms as Complex Differentiated Communities. *Annual Review of Microbiology*, 56(1):187–209.

Stubbendieck, R. M. and Straight, P. D. (2016). Multifaceted interfaces of bacterial competition. *Journal of Bacteriology*, 198(16):2145–2155.

Suarez, G., Sierra, J. C., Erova, T. E., Sha, J., Horneman, A. J., and Chopra, A. K. (2010). A type VI secretion system effector protein, VgrG1, from Aeromonas hydrophila that induces host cell toxicity by ADP ribosylation of actin. *Journal of Bacteriology*, 192(1):155–168.

Sutherland, I. W. (2001). The biofilm matrix - An immobilized but dynamic microbial environment. *Trends in Microbiology*, 9(5):222–227.

Takeda, Y. and Kageyama, M. (1975). Subunit arrangement in the extended sheath of pyocin R. *Journal of biochemistry*, 77(3):679–84.

Talà, A., Progida, C., De Stefano, M., Cogli, L., Spinosa, M. R., Bucci, C., and Alifano, P. (2008). The HrpB-HrpA two-partner secretion system is essential for intracellular survival of Neisseria meningitidis. *Cellular Microbiology*, 10(12):2461–2482.

Taylor, N. M. I., Prokhorov, N. S., Guerrero-Ferreira, R. C., Shneider, M. M., Browning, C., Goldie, K. N., Stahlberg, H., and Leiman, P. G. (2016). Structure of the T4 baseplate and its function in triggering sheath contraction. *Nature*, 533(7603):346–352.

Teasdale, M. E., Liu, J., Wallace, J., Akhlaghi, F., and Rowley, D. C. (2009). Secondary metabolites produced by the marine bacterium halobacillus salinus that Inhibit quorum sensing-controlled phenotypes in gram-negative bacteria. *Applied and Environmental Microbiology*, 75(3):567–572.

The Human Microbiome Project Consortium (2012). Structure, function and diversity of the healthy human microbiome. *Nature*, 486(7402):207–214.

Tian, Y., Zhao, Y., Shi, L., Cui, Z., Hu, B., and Zhao, Y. (2017). Type VI Secretion Systems of Erwinia amylovora Contribute to Bacterial Competition, Virulence, and Exopolysaccharide Production. *Phytopathology*, 107(6):654–661.

Toesca, I. J., French, C. T., and Miller, J. F. (2014). The type VI secretion system spike protein VgrG5 mediates membrane fusion during intercellular spread by pseudomallei group Burkholderia species. *Infection and Immunity*, 82(4):1436–1444.

Uchida, K., Leiman, P. G., Arisaka, F., and Kanamaru, S. (2014). Structure and properties of the c-terminal β-helical domain of vgrg protein from escherichia coli O157. *Journal of Biochemistry*, 155(3):173–182.

Unterweger, D., Kostiuk, B., Otjengerdes, R., Wilton, A., Diaz-Satizabal, L., and Pukatzki, S. (2015). Chimeric adaptor proteins translocate diverse type VI secretion system effectors in Vibrio cholerae. *The EMBO Journal*, 34(16):2198–2210.

Vaccari, L., Molaei, M., Niepa, T. H., Lee, D., Leheny, R. L., and Stebe, K. J. (2017). Films of bacteria at interfaces. *Advances in Colloid and Interface Science*, 247(30):561–572.

Vegge, C. S., Brøndsted, L., Neve, H., McGrath, S., Van Sinderen, D., and Vogensen, F. K. (2005). Structural characterization and assembly of the distal tail structure of the temperate lactococcal bacteriophage TP901-1. *Journal of Bacteriology*, 187(12):4187–4197.

Vettiger, A. and Basler, M. (2016). Type VI Secretion System Substrates Are Transferred and Reused among Sister Cells. *Cell*, 167(1):99–110.

Vettiger, A., Winter, J., Lin, L., and Basler, M. (2017). The type VI secretion system sheath assembles at the end distal from the membrane anchor. *Nature Communications*, 8:16088.

Vial, P. A., Robins-Browne, R., Lior, H., Prado, V., Kaper, J. B., Nataro, J. P., Maneval, D., Elsayed, A.-e.-d., and Levine, M. M. (1988). Characterization of enteroadherent-aggregative Escherichia coli, a putative agent of diarrheal disease. *The Journal of infectious diseases*, 158(1):70–9.

Voegel, T. M., Warren, J. G., Matsumoto, A., Igo, M. M., and Kirkpatrick, B. C. (2010). Localization and characterization of Xylella fastidiosa haemagglutinin adhesins. *Microbiology*, 156(7):2172–2179.

Wan, B., Zhang, Q., Ni, J., Li, S., Wen, D., Li, J., Xiao, H., He, P., Ou, H. Y., Tao, J., Teng, Q., Lu, J., Wu, W., and Yao, Y. F. (2017). Type VI secretion system contributes to Enterohemorrhagic Escherichia coli virulence by secreting catalase against host reactive oxygen species (ROS). *PLoS Pathogens*, 13(3):1–28.

Wandersman, C. and Delepelaire, P. (2004). Bacterial Iron Sources: From Siderophores to Hemophores. *Annual Review of Microbiology*, 58(1):611–647.

Wang, I.-N., Smith, D. L., and Young, R. (2000). Holins: The Protein Clocks of Bacteriophage Infections. *Annual Review of Microbiology*, 54(1):799–825.

Wang, J., Brackmann, M., Castaño-Díez, D., Kudryashev, M., Goldie, K. N., Maier, T., Stahlberg, H., and Basler, M. (2017). Cryo-EM structure of the extended type VI secretion system sheath–tube complex. *Nature Microbiology*.

Wang, T., Si, M., Song, Y., Zhu, W., Gao, F., Wang, Y., Zhang, L., Zhang, W., Wei, G., Luo, Z.-Q., and Shen, X. (2015). Type VI Secretion System Transports Zn2+ to Combat Multiple Stresses and Host Immunity. *PLOS Pathogens*, 11(7):e1005020.

Wang, Y. J. and Leadbetter, J. R. (2005). Rapid acyl-homoserine lactone quorum signal biodegradation in diverse soils. *Applied and Environmental Microbiology*, 71(3):1291–1299.

Wanner, G., Vogl, K., and Overmann, J. (2008). Ultrastructural characterization of the prokaryotic symbiosis in "Chlorochromatium aggregation ". *Journal of Bacteriology*, 190(10):3721–3730.

Weaver, C. A., Redborg, A. H., and Konisky, J. (1981). Plasmid-determined immunity of Escherichia coli K-12 to colicin Ia is mediated by a plasmid-encoded membrane protein. *Journal of Bacteriology*, 148(3):817–828.

Weaver, V. B. and Kolter, R. (2004). Burkholderia spp. Alter Pseudomonas aeruginosa Physiology through Iron Sequestration. *Journal of Bacteriology*, 186(8):2376–2384.

Weber, B. S., Hennon, S. W., Wright, M. S., Scott, N. E., de Berardinis, V., Foster, L. J., Ayala, J. A., Adams, M. D., and Feldman, M. F. (2016). Genetic dissection of the type VI secretion system in Acinetobacter and identification of a novel peptidoglycan hydrolase, TagX, required for its biogenesis. *mBio*, 7(5):1–17.

Wenren, L. M., Sullivan, N. L., and Cardarelli, L. (2013). Are Linked by Type VI-Dependent Export. *mBio*, 4(4):1–10.

West, S. A. and Buckling, A. (2003). Cooperation, virulence and siderophore production in bacterial parasites. *Proceedings of the Royal Society B: Biological Sciences*, 270(1510):37–44.

Wexler, A. G., Bao, Y., Whitney, J. C., Bobay, L.-M., Xavier, J. B., Schofield, W. B., Barry, N. A., Russell, A. B., Tran, B. Q., Goo, Y. A., Goodlett, D. R., Ochman, H., Mougous, J. D., and Goodman, A. L. (2016). Human symbionts inject and neutralize antibacterial toxins to persist in the gut. *Proceedings of the National Academy of Sciences*, 113(13):3639–3644.

Whiteley, L., Meffert, T., Haug, M., Weidenmaier, C., Hopf, V., Bitschar, K., Schittek, B., Kohler, C., Steinmetz, I., West, T. E., and Schwarz, S. (2017). Entry, intracellular survival and multinucleated giant cell-forming activity of Burkholderia pseudomallei in human primary phagocytic and non-phagocytic cells. *Infection and Immunity*, pages 00468–17.

Whitney, J. C., Beck, C. M., Goo, Y. A., Russell, A. B., Harding, B. N., De Leon, J. A., Cunningham, D. A., Tran, B. Q., Low, D. A., Goodlett, D. R., Hayes, C. S., and Mougous, J. D. (2014). Genetically distinct pathways guide effector export through the type VI secretion system. *Molecular Microbiology*, 92(3):529–542.

Whitney, J. C., Chou, S., Russell, A. B., Biboy, J., Gardiner, T. E., Ferrin, M. A., Brittnacher, M., Vollmer, W., and Mougous, J. D. (2013). Identification, structure, and function of a novel type VI secretion peptidoglycan glycoside hydrolase effector-immunity pair. *Journal of Biological Chemistry*, 288(37):26616–26624.

Whitney, J. C., Quentin, D., Sawai, S., LeRoux, M., Harding, B. N., Ledvina, H. E., Tran, B. Q., Robinson, H., Goo, Y. A., Goodlett, D. R., Raunser, S., and Mougous, J. D. (2015). An Interbacterial NAD(P)+ Glycohydrolase Toxin Requires Elongation Factor Tu for Delivery to Target Cells. *Cell*, 163(3):607–619.

Willett, J. L., Ruhe, Z. C., Goulding, C. W., Low, D. A., and Hayes, C. S. (2015). Contact-Dependent Growth Inhibition (CDI) and CdiB/CdiA Two-Partner Secretion Proteins. *Journal of Molecular Biology*, 427(23):3754–3765.

Williams, S. R., Gebhart, D., Martin, D. W., and Scholl, D. (2008). Retargeting R-type pyocins to generate novel bactericidal protein complexes. *Applied and Environmental Microbiology*, 74(12):3868–3876.

Wilson, D. S. and Sober, E. (1989). Reviving the superorganism. *Journal of Theoretical Biology*, 136(3):337–356.

Wittinghofer, A. and Vetter, I. R. (2011). Structure-Function Relationships of the G Domain, a Canonical Switch Motif. *Annual Review of Biochemistry*, 80(1):943–971.

Wolgemuth, C., Hoiczyk, E., Kaiser, D., and Oster, G. (2002). How myxobacteria glide. *Current Biology*, 12(5):369–377.

Wommack, K. E. and Colwell, R. R. (2000). Virioplankton: Viruses in Aquatic Ecosystems. *Microbiology and Molecular Biology Reviews*, 64(1):69–114.

Wu, Y., Xia, L., Yu, Z., Shabbir, S., and Kerr, P. G. (2014). In situ bioremediation of surface waters by periphytons. *Bioresource Technology*, 151:367–372.

Xu, Y., Larsen, L. H., Lorenzen, J., Hall-Stoodley, L., Kikhney, J., Moter, A., and Thomsen, T. R. (2017). Microbiological diagnosis of device-related biofilm infections. *Apmis*, 125(4):289–303.

Yang, G., Dowling, A. J., Gerike, U., Ffrench-Constant, R. H., and Waterfield, N. R. (2006). Photorhabdus virulence cassettes confer injectable insecticidal activity against the wax moth. *Journal of Bacteriology*, 188(6):2254–2261.

Yap, M. L., Mio, K., Leiman, P. G., Kanamaru, S., and Arisaka, F. (2010). The Baseplate Wedges of Bacteriophage T4 Spontaneously Assemble into Hubless Baseplate-Like Structure In Vitro. *Journal of Molecular Biology*, 395(2):349–360.

Yap, M. L. and Rossmann, M. G. (2014). Structure and function of bacteriophage T4. *Future Microbiology*, 9(12):1319–1327.

Yatsunenko, T., Rey, F. E., Manary, M. J., Trehan, I., Dominguez-Bello, M. G., Contreras, M., Magris, M., Hidalgo, G., Baldassano, R. N., Anokhin, A. P., Heath, A. C., Warner, B., Reeder, J., Kuczynski, J., Caporaso, J. G., Lozupone, C. A., Lauber, C., Clemente, J. C., Knights, D., Knight, R., and Gordon, J. I. (2012). Human gut microbiome viewed across age and geography. *Nature*, 486(7402):222–7.

Yim, G., Huimi Wang, H., and Davies FRS, J. (2007). Antibiotics as signalling molecules. *Philosophical Transactions of the Royal Society B: Biological Sciences*, 362(1483):1195–1200.

Young, R. (2013). Phage lysis: Do we have the hole story yet? *Current Opinion in Microbiology*, 16(6):790–797.

Zhang, D., de Souza, R. F., Anantharaman, V., Iyer, L. M., and Aravind, L. (2012a). Polymorphic toxin systems: Comprehensive characterization of trafficking modes, processing, mechanisms of action, immunity and ecology using comparative genomics. *Biology Direct*, 7(1):18.

Zhang, D., Iyer, L. M., and Aravind, L. (2011). A novel immunity system for bacterial nucleic acid degrading toxins and its recruitment in various eukaryotic and DNA viral systems. *Nucleic Acids Research*, 39(11):4532–4552.

Zhang, X. Y., Brunet, Y. R., Logger, L., Douzi, B., Cambillau, C., Journet, L., and Cascales, E. (2013). Dissection of the TssB-TssC interface during type VI secretion sheath complex formation. *PLoS ONE*, 8(11):e81074.

Zhang, Y., Ducret, A., Shaevitz, J., and Mignot, T. (2012b). From individual cell motility to collective behaviors: Insights from a prokaryote, Myxococcus xanthus. *FEMS Microbiology Reviews*, 36(1):149–164.

Zheng, J. and Leung, K. Y. (2007). Dissection of a type VI secretion system in Edwardsiella tarda. *Molecular Microbiology*, 66(5):1192–1206.

Zheng, W., Wang, F., Taylor, N. M. I., Guerrero-Ferreira, R. C., Leiman, P. G., and Egelman, E. H. (2017). Refined Cryo-EM Structure of the T4 Tail Tube: Exploring the Lowest Dose Limit. *Structure*, 25(9):1436–1441.

Zilber-Rosenberg, I. and Rosenberg, E. (2008). Role of microorganisms in the evolution of animals and plants: The hologenome theory of evolution. *FEMS Microbiology Reviews*, 32(5):723–735.

Zoued, A., Brunet, Y. R., Durand, E., Aschtgen, M.-S., Logger, L., Douzi, B., Journet, L., Cambillau, C., and Cascales, E. (2014). Architecture and assembly of the Type VI secretion system. *Biochimica et biophysica acta*, 1843(8):1664–73.

Zoued, A., Cassaro, C. J., Durand, E., Douzi, B., España, A. P., Cambillau, C., Journet, L., and Cascales, E. (2016a). Structure–Function Analysis of the TssL Cytoplasmic Domain Reveals a New Interaction between the Type VI Secretion Baseplate and Membrane Complexes. *Journal of Molecular Biology*, 428(22):4413–4423.

Zoued, A., Durand, E., Bebeacua, C., Brunet, Y. R., Douzi, B., Cambillau, C., Cascales, E., and Journet, L. (2013). TssK is a trimeric cytoplasmic protein interacting with components of both phage-like and membrane anchoring complexes of the type VI secretion system. *Journal of Biological Chemistry*, 288(38):27031–27041.

Zoued, A., Durand, E., Brunet, Y. R., Spinelli, S., Douzi, B., Guzzo, M., Flaugnatti, N., Legrand, P., Journet, L., Fronzes, R., Mignot, T., Cambillau, C., and Cascales, E. (2016b). Priming and polymerization of a bacterial contractile tail structure. *Nature*, 531(7592):59–63.

Zoued, A., Durand, E., Santin, Y. G., Journet, L., Roussel, A., Cambillau, C., and Cascales, E. (2017). TssA: The cap protein of the Type VI secretion system tail. *BioEssays*, 1600262:1600262.

Zusman, T., Feldman, M., Halperin, E., and Segal, G. (2004). Characterization of the icmH and icmF genes required for Legionella pneumophila intracellular growth, genes that are present in many bacteria associated with eukaryotic cells. *Society*, 72(6):3398–3409.

Part V

Annexes

Annexe 1: H-NS silencing of the SPI-6-encoded type VI secretion system limits *Salmonella enterica* serovar Typhimurium interbacterial killing

IAI Journals.ASM.org

H-NS Silencing of the *Salmonella* Pathogenicity Island 6-Encoded Type VI Secretion System Limits *Salmonella enterica* Serovar Typhimurium Interbacterial Killing

Yannick R. Brunet,[a]* Ahmad Khodr,[b]* Laureen Logger,[a] Laurent Aussel,[c] Tâm Mignot,[c] Sylvie Rimsky,[b] Eric Cascales[a]

Laboratoire d'Ingénierie des Systèmes Macromoléculaires, Institut de Microbiologie de la Méditerranée, Aix-Marseille Université, CNRS UMR7255, Marseille, France[a]; Laboratoire de Biologie et de Pharmacologie Appliqué, ENS Cachan, CNRS, Cachan, France[b]; Laboratoire de Chimie Bactérienne, Institut de Microbiologie de la Méditerranée, Aix-Marseille Université, CNRS UMR7283, Marseille, France[c]

The secretion of bacterial toxin proteins is achieved by dedicated machineries called secretion systems. The type VI secretion system (T6SS) is a widespread versatile machine used for the delivery of protein toxins to both prokaryotic and eukaryotic cells. In *Salmonella enterica* serovar Typhimurium, the expression of the T6SS genes is activated during macrophage or mouse infection. Here, we show that the T6SS gene cluster is silenced by the histone-like nucleoid structuring H-NS protein using a combination of reporter fusions, electrophoretic mobility shift assays, DNase footprinting, and fluorescence microscopy. We further demonstrate that derepression of the *S.* Typhimurium T6SS genes induces T6SS-dependent intoxication of competing bacteria. Our results suggest that relieving T6SS H-NS silencing may be used as a sense-and-kill mechanism that will help *S.* Typhimurium to homogenize and synchronize the microbial population to gain efficiency during infection.

During the course of infection, bacteria produce and secrete bacterial toxins. Secretion of these toxin proteins is achieved by dedicated, specialized machineries called secretion systems. The type VI secretion system (T6SS) is required for the virulence of several Gram-negative pathogens. In *Vibrio cholerae*, the T6SS translocates VgrG1, a toxin that carries a domain responsible for actin cross-linking in eukaryotic cells (1–4). However, the role of the T6SS is not limited to virulence toward eukaryotes; an increasing number of reports demonstrate that the T6SS is also involved in interbacterial intoxication (5–10). With bacteriocins and contact-dependent inhibition (CDI), the T6SS is therefore involved in shaping bacterial communities (11–14) by delivering antibacterial toxins, including murein hydrolases, DNases, and phospholipases, directly into the target recipient bacterial cell (5, 6, 15; for recent reviews see references 14, 16 and 17). The attacker cell is protected from these toxins by the coproduction of cognate proteins that confer immunity (15, 18). The T6SS therefore confers a growth advantage to bacteria in mixed cultures and has been suggested to be important in environmental niches where bacterial competition for nutrients is critical for survival or for the uptake of DNA for transformation and acquisition of new traits (14, 19). However, while the role of the T6SS in interbacterial competition has been evidenced and characterized under laboratory conditions, its role in shaping bacterial communities of the microbiota is not yet clearly elucidated.

At the molecular level, the T6SS is assembled from 13 proteins, called core components, that form a transenvelope apparatus anchoring a cytoplasmic tubular structure to the membrane (20–24). Based on structural homologies with bacteriophage tail components, this tubular structure has been proposed to be constituted of an inner tube assembled by stacked hexameric rings of the Hcp protein, resembling the tail tube of bacteriophages, tipped by the VgrG protein (21, 25–27). The current model describes the internal tube as a conduit for the secretion of the effector toxins (13, 28–30). This model has been recently supported by data demonstrating direct contacts between the Hcp protein and effectors (31). However, additional mechanisms have recently been reported, such as the tip protein, VgrG, or an adaptor protein, PAAR (proline, alanine, alanine, arginine), serving as a carrier for effectors (17, 32, 33). The Hcp internal tube is wrapped into a coating cylinder resembling the sheath of contractile phages (21, 26, 34). Cryo-electron and fluorescence microscopies showed that this sheath-like structure is dynamic and undergoes cycles of elongation and contraction (21). Similarly to the bacteriophage infection mechanism, it has been proposed that upon contact with a bacterial neighbor, contraction of the T6SS sheath propels the Hcp tube toward the target cell (2, 9, 35, 36). Because of the T6SS function in bacterial virulence and interbacterial competition, the expression of T6SS genes needs to be tightly controlled. A broad variety of transcriptional, translational, and posttranslational regulatory mechanisms have been identified and characterized (13, 37, 38).

In *Salmonella enterica* serotypes, T6SS gene clusters are encoded within different pathogenicity islands (SPIs), the most

Received 14 February 2015 **Returned for modification** 10 March 2015
Accepted 16 April 2015

Accepted manuscript posted online 27 April 2015

Citation Brunet YR, Khodr A, Logger L, Aussel L, Mignot T, Rimsky S, Cascales E. 2015. H-NS silencing of the *Salmonella* pathogenicity island 6-encoded type VI secretion system limits *Salmonella enterica* serovar Typhimurium interbacterial killing. Infect Immun 83:2738–2750. doi:10.1128/IAI.00198-15.

Editor: A. J. Bäumler

Address correspondence to Eric Cascales, cascales@imm.cnrs.fr.

* Present address: Yannick R. Brunet, Department of Microbiology and Immunobiology, Harvard Medical School, Boston, Massachusetts, USA; Ahmad Khodr, Biology of Intracellular Bacteria Unit, Institut Pasteur, Paris, France.

Supplemental material for this article may be found at http://dx.doi.org/10.1128/IAI.00198-15.

doi:10.1128/IAI.00198-15

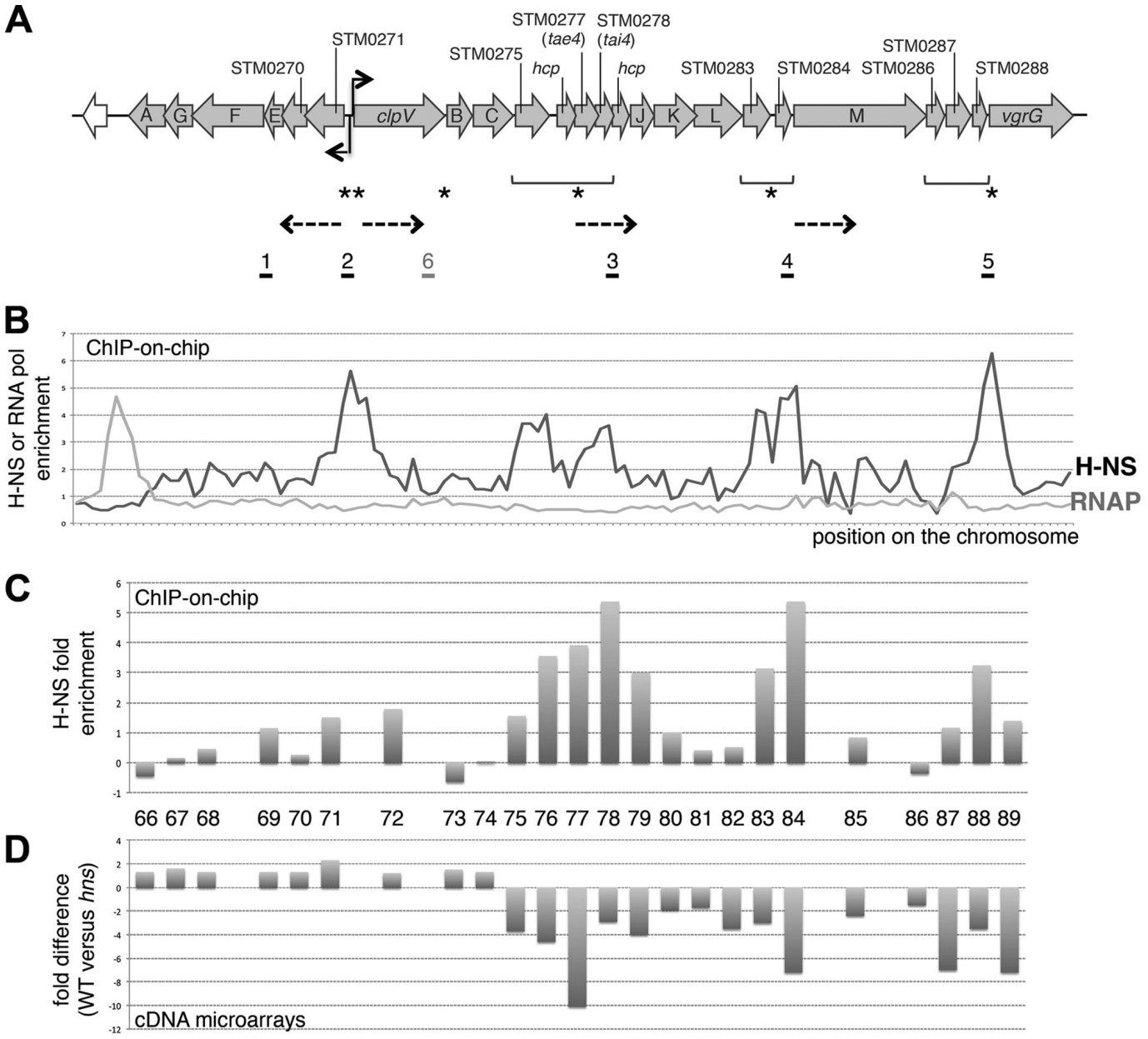

FIG 1 Summary of genome-wide studies on H-NS in *Salmonella* Typhimurium focusing on the T6SS gene cluster. (A) Schematic representation of the *Salmonella* Typhimurium SPI-6-encoded T6SS gene cluster. The names of the different genes are indicated (the *tss* nomenclature has been used for the T6SS core components except for the generic names for *hcp*, *vgrG*, and *clpV*). The two promoters identified in this study are indicated by arrows. The noncore clusters and the potential promoters identified by Mulder et al. (41) are indicated by horizontal brackets and asterisks, respectively. The positions and orientations of the *lacZ* transcriptional reporter fusions used in this study are indicated by the dashed arrows (beginning of the arrow represents the fusion joint). (B and C) Summary of the ChIP-on-chip experiments showing the enrichment of H-NS and of the RNA polymerase (RNAP) (56) (B) or the enrichment on H-NS for each gene (57) (C). In panel B, the locations of the six DNA fragments used for the electrophoretic mobility shift assays (Fig. 4) are indicated above the graph (black underlining, fragment with H-NS binding sites predicted with high scores; gray underlining, fragment with no predicted H-NS binding site, used as a negative control). (D) Summary of the microarray data (from reference 57). Bars represent the fold change for each T6SS gene in WT cells compared to the level in *hns* mutant cells (−10 means that the transcript is 10-fold more abundant in *hns* cells than in wild-type cells [57]). The STM gene numbers are indicated between the bars of the corresponding genes in panels C and D (e.g., *STM02xx*).

commonly distributed being the T6SS associated with SPI-6 (39). In *S. enterica* serovar Typhimurium (*S.* Typhimurium), the causative agent of gastroenteritis, only a single T6SS gene cluster is found on the genome, within SPI-6. This T6SS gene cluster is composed of two operons organized in divergent orientations (Fig. 1A) (39, 40). A recent bioinformatics study demonstrated that the genes encoding the core components are separated by noncore clusters of genes, probably acquired more recently (Fig. 1A) (41). The gene cluster encodes all the genes required to assemble a functional secretion apparatus, as well as three effectors (STM0277, *tae4*; STM0291 and STM0292, *rhs*) and their cognate immunity proteins (STM0278, *tai4*; STM0291b and STM0293, *rhsI*) (42–45). *tae4* encodes a toxin with peptidoglycan hydrolase activity, whereas the Rhs C-terminal domains carry putative nu-

clease activities (42–45). The upstream operon (*STM0266-STM0271*) consists of a number of genes encoding machine subunits and two genes of unknown function. The downstream operon (*STM0272-STM0289*) consists of the remaining machine core component genes and the toxin/antitoxin pairs. The expression of T6SS genes encoded within the SPI-6 pathogenicity island is not detected under laboratory *in vitro* conditions (41, 46, 47); however, promoter-reporter and transcriptional profiling studies showed that the expression of these genes is activated in the late stages of macrophage and epithelial cell infection (41, 48). Indeed, the SPI-6 T6SS was first identified as a modulator of intracellular proliferation in macrophages (46, 49). Recent studies further revealed that the SPI-6 T6SS is an important actor for virulence toward mice and for chicken gastrointestinal colonization (50–52). The undetectable level of T6SS expression under *in vitro* conditions suggests that these genes are silenced and that this silencing might be counteracted *in vivo*. The major bacterial silencing protein is the histone-like nucleoid structuring protein (H-NS). H-NS usually binds to and represses the expression of A/T-rich genes, such as those acquired by horizontal gene transfer, and therefore acts as a general xenogeneic silencer (53–55). Upon examination of published *S.* Typhimurium genome-wide H-NS transcriptional profiling reports and of data from combined chromatin immunoprecipitation and microarray (ChIP-on-chip) analysis (56–57) (Fig. 1B to D), we noted a significant enrichment in H-NS binding to the SPI-6 T6SS gene cluster (Fig. 1B and C) and upregulated expression of these genes in *hns* mutant cells (Fig. 1D). In this study, we confirm that H-NS acts as a silencer for SPI-6 T6SS genes in *S.* Typhimurium using chromosomal reporter fusions. Electrophoretic mobility shift assays further demonstrate that H-NS binds to different regions of the gene cluster. DNase I footprinting of the noncoding region between the two divergent operons revealed that H-NS binds to discrete sites and then spreads from them to upstream and downstream regions. Finally, we show that derepression of the T6SS leads to the assembly of dynamic sheath-like structures and provides a growth advantage to *S.* Typhimurium in bacterial competition experiments.

MATERIALS AND METHODS

Bacterial strains, growth conditions, and chemicals. *Escherichia coli* K-12 DH5α and W3110 strains were used for cloning procedures and competition assays, respectively. The *S. enterica* serovar Typhimurium strain LT2 (kindly provided by Josep Casadesus, University of Sevilla, Spain) was used for this study. The *S.* Typhimurium LT2 strain is leaky for *rpoS*, a mutation that counteracts the lethality of the *hns* null mutation (57). Strains were routinely grown in LB broth at 37°C with aeration. Plasmids were maintained by the addition of ampicillin (100 $\mu g \cdot ml^{-1}$), kanamycin (50 $\mu g \cdot ml^{-1}$), or chloramphenicol (40 $\mu g \cdot ml^{-1}$).

Strain construction. Strains and oligonucleotides used for strain constructions are listed in Table S1 in the supplemental material.

(i) Construction of *E. coli* mutant strains. The *E. coli* W3110 *hns* mutant strain was constructed by P1 transduction of the BW25112 *hns*::*kan* cassette obtained from the Keio collection (58) into W3110. Deletion of the kanamycin cassette was obtained by using the Flp recognition target (FRT)-specific flippase-encoded pCP20 plasmid (59).

(ii) Construction of *S.* Typhimurium mutant strains. Isogenic mutant strains were constructed by λ-Red recombination engineering using the one-step inactivation procedure developed by Datsenko and Wanner (59) using pKD4-amplified PCR products. λ-Red functions were expressed from plasmid pKD46 (59). Strains were verified by colony PCR before transfer of the mutations into new LT2 cells by P22 transduction. Cassettes were excised with the pCP20 plasmid as described previously (59).

(iii) Construction of chromosomal transcriptional fusions to *lacZ*. Chromosomal transcriptional fusions were inserted at the original locus as described previously (60). Briefly a kanamycin resistance cassette (from pKD4) (59) flanked by two FRT sites was inserted downstream of both *STM0271* and *STM0272* promoter regions or in place of the *STM0277* (*tae4*) or *STM0285* (*tssM*) gene in *S.* Typhimurium LT2 using λ-Red recombination and then excised using pCP20, generating strains carrying a single FRT site. Chromosomal *lacZ* fusions were constructed by integrating the plasmid pCE36 (60) and selected on LB agar plates supplemented with kanamycin at 37°C. Strains were verified by PCR before P22 transduction of the chromosomal fusions into new LT2 cells.

(iv) Construction of the chromosomal *tssB-sfgfp* fusion. To insert the gene encoding the superfolder green fluorescent protein (sfGFP) on the chromosome of *S.* Typhimurium, we first engineered a pKD4 derivative plasmid carrying the *sfgfp* gene upstream of the FRT site. This plasmid was constructed by restriction-free cloning (61). Then the sfGFP-FRT-Kan-FRT fragment was PCR amplified and inserted in frame at the 3′ end of *tssB* using λ-Red recombination. The strain was verified by colony PCR before transfer of the mutations into new LT2 cells by P22 transduction and cassette excision using pCP20.

(v) Construction of *S.* Typhimurium *hns* mutant strains. The *hns* mutation was transferred by P22 transduction from a P22 lysate of *Salmonella* ATCC 14028 Δ*hns* (62) kindly provided by Françoise Norel (Institut Pasteur, Paris, France).

β-Galactosidase activity assay. β-Galactosidase activities were measured as described previously (63) from mid-exponential-growth-phase cells (optical density at 600 nm [OD_{600}] of 0.8) as *S.* Typhimurium *hns* cells present a growth defect. The values reported are the averages of β-galactosidase activities of 27 measurements, representing experimental triplicates of three independent clones for each transduction (three independent *hns* P22 transductions).

Flow cytometry. *Salmonella* cells were grown overnight in LB broth, diluted 100-fold in LB broth, and grown to an OD_{600} of ~1. Cells were harvested, diluted in LB broth to ~10^6 cells $\cdot$ ml^{-1}, and fixed by addition of paraformaldehyde (3.2% final concentration) for 10 min. Fixed cells were sorted at a debit rate of 7.5 $\mu l \cdot min^{-1}$ and a sheath pressure of 2×10^4 Pa using an A50 Micro flow cytometer instrument (Apogee) equipped with a 50-mW argon ion laser (488 nm) for excitation. Prior to sorting, flow cytometer settings were calibrated with Apogee Flow Systems 1-μm beads. Acquisition was triggered with small (224/65,535) and large (980/65,535) scatters to discriminate bacterial populations from the noise. Data were acquired with the PC Control, version 3.40, and Histogram, version 110.0, software programs (Apogee) and analyzed using FlowJo, version 10 (TreeStar, Inc.). Experiments were carried out in duplicate with a technical duplication. Each experiment gave similar results. The data are presented as the number of total cells (from the four replicates) as a function of the fluorescence level (in arbitrary units).

5′ RACE assay. Total RNA was isolated from 8×10^9 LT2 or LT2 *hns* exponentially growing (OD_{600} of ~0.8) cells using a PureYield RNA Midiprep system (Promega). RNAs were eluted with 1 ml of water, cleaned with DNase (Ambion), and precipitated overnight at −80°C by ammonium sulfate-ethanol procedures. After a washing step, pellet RNA was resuspended into 45 μl of nuclease-free water. RNA quality and integrity were tested on agarose gel and by the absorbance ratio at 260/280 nm. Total RNAs (80 $\mu g \cdot ml^{-1}$) were then subjected to transcriptional +1 mapping using a 5′ rapid amplification of cDNA ends (RACE) system (Invitrogen). The oligonucleotides designed for amplification and cloning of cDNA are listed in Table S1 in the supplemental material.

H-NS purification. *E. coli* K-12 H-NS was purified according to published protocols (64). The *S. enterica* Typhimurium LT2 and *E. coli* H-NS proteins share 95% identity and 98% similarity at the protein level.

Electrophoretic mobility shift assays (EMSAs). PCR products were generated with Phusion *Taq* polymerase (New England BioLabs) using *S.*

Typhimurium genomic DNA (purified using a DNeasy blood and tissue kit; Qiagen), a mix of deoxynucleoside triphosphates (dNTPs) supplemented with [α-^{32}P]dGTP (2.5 μCi per PCR in a total volume of 50 μl; Perkin-Elmer), and oligonucleotide pairs (see Tables S1 and S2 in the supplemental material) and then column purified (Wizard Gel and PCR Cleanup kit; Promega). PCR products were incubated for 30 min at 20°C with the indicated concentration of H-NS (see Fig. 4) in a final volume of 10 μl in H-NS binding buffer (20 mM HEPES, pH 8.0, 8 mM magnesium aspartate, 60 mM potassium glutamate, 5 mM dithiothreitol [DTT], 0.05% [vol/vol] Nonidet P-40 [Sigma], and 0.3 mg · ml^{-1} bovine serum albumin [BSA; New England BioLabs]). After incubation, the mixture was loaded on a prerun 8% nondenaturing polyacrylamide (Tris-borate) gel, and DNA and DNA complexes were separated at 100 V in Tris-borate buffer (45 mM Tris base, 45 mM boric acid, 100 mM $MnCl_2$ buffer). Gels were fixed in 10% trichloroacetic acid for 10 min and exposed to Kodak BioMax MR films.

DNase I footprints. A fragment was obtained by PCR using Phusion *Taq* polymerase and a couple of primers in which one was labeled prior to the PCR. The primer was end labeled with [γ-^{32}P]ATP (3,000 Ci · mmol^{-1}) using phage T4 polynucleotide kinase (New England BioLabs) and purified on a Sephadex G-25 column (Amersham Biotech). The 5′-end-radiolabeled fragment (2.5 nM) was incubated for 30 min at 20°C with the indicated concentration of H-NS (see Fig. 5A) in H-NS binding buffer (see the paragraph above on EMSAs). The DNA was then incubated for 30 s with 0.25 μg · ml^{-1} of DNase I (Worthington Biochemicals), and the reaction was quenched by the addition of 180 μl of phenol-chloroform (5:1; pH 8.0) and 180 μl of DNase Stop buffer (0.2 M sodium acetate, pH 5.0, 100 μg · ml^{-1} calf thymus DNA, 200 mM EDTA, 100 μg · ml^{-1} glycogen) successively. After centrifugation (15,000 × *g* for 3 min), the aqueous phase was submitted to ethanol precipitation. Samples were washed, dried, and resuspended in 5 μl of formamide blue buffer (Tris-borate–EDTA [TBE] buffer supplemented with 90% [wt/vol] formamide, 0.01% [wt/vol] xylene cyanol, 0.025% [wt/vol] bromophenol blue). Samples were heated at 90°C for 4 min and loaded on 7% (wt/vol) polyacrylamide–8 M urea denaturing gels. Gels were fixed in 20% ethanol–10% acetic acid for 10 min, dried, and exposed to a phosphor storage screen (GE Healthcare).

H-NS binding quantification/quantitative gel analysis. Quantitative analyses of the DNase footprint were performed as previously described (65). Briefly, the intensity of each band in digital images of the gels was quantified using ImageQuant, version 5.0, software (GE Healthcare) and normalized with the intensity of the corresponding band in the absence of protein (66). Nonlinear least-square curve fitting of the data was carried out using the Origin software (OriginLab) and the following binding equation: $Y = L + (U - L) \times k^n x^n/(1 + k^n x^n)$, where L is the lower y value, U is the upper y value, K is the affinity constant, and n is the Hill coefficient. The values obtained for U and L were used to normalize the data from 1 to 0 to obtain the value for the normalized band intensity. We determined the fractional saturation of sites and fitted these data by the nonlinear least-squares method. Apparent dissociation equilibrium constants (K_ds) for H-NS binding were calculated from the curves.

Fluorescence microscopy. Overnight cultures of *S.* Typhimurium cells bearing the chromosomal *tssB-sfgfp* fusion were diluted 1:100 into LB medium and cultivated at 37°C to an OD_{600} of ~1.0. Cells were washed in phosphate-buffered saline (PBS), resuspended to an OD_{600} of 50 in PBS, and spotted on a thin pad of 1.5% agarose in PBS covered with a coverslip. Fluorescence and phase-contrast micrographs were recorded using an automated and inverted epifluorescence microscope (TE2000-E-PFS; Nikon, France), equipped with a CoolSNAP HQ 2 camera (Roper Scientific SARL, France) and a 100×/1.4 DLL objective and the Perfect Focus System (PFS), as previously described (9, 67). Images were collected every 15 s, using an exposure time of 100 ms for sfGFP fluorescence and 5 ms for phase contrast using MetaMorph software (Molecular Devices). sfGFP and phase-contrast channels were adjusted and merged using ImageJ.

Bacterial growth competition assay. Growth competition assays were performed using *S.* Typhimurium and its *hns* derivative as an attacker and *E. coli* K-12 W3110 and *S.* Typhimurium strains bearing the pUA66-*rrnB* plasmid (68) as prey, as described previously (9, 10). Briefly, cells were grown in LB medium at 37°C to an OD_{600} of 1, adjusted to an OD_{600} of 0.5, and mixed at a 4:1 ratio (attacker/prey). Then, 25 μl of the mixture was spotted in triplicate onto prewarmed dry agar plates and incubated overnight at 30°C. Bacterial spots were cut out, and cells were resuspended in 1 ml of LB medium. Triplicates (150 μl each) were transferred into wells of a black 96-well plate (Greiner), and the optical density at 600 nm and fluorescence (excitation, 485 nm; emission, 530 nm) were measured with a Tecan Infinite M200 microplate reader (nine measurements per mixture per tested combination). The relative fluorescence was expressed as the intensity of fluorescence divided by the absorbance at 600 nm after the value of a blank, nonfluorescent sample (the attacker alone) was subtracted. The experiments were done in triplicate with identical results, and the results of a representative experiment are reported. For enumeration of viable prey cells, the bacterial suspensions recovered from the spots were serially diluted and spotted on selective kanamycin plates.

Protein separation, transfer, and immunodetection. SDS-polyacrylamide gel electrophoresis (SDS-PAGE), Western blotting, and immunodetection were performed using Bio-Rad material and standard procedures. Proteins were immunodetected using anti-GFP monoclonal antibody (Roche) and anti-Pal antibodies from our laboratory collection (69) and secondary antibodies coupled to alkaline phosphatase and revealed using 5-bromo-4-chloro-3-indolylphosphate and nitroblue tetrazolium chloride.

RESULTS

H-NS silences the expression of the two divergent T6SS gene operons. cDNA microarray comparisons of *S. enterica* Typhimurium wild-type (WT) and *hns* strains identified regions of the genome silenced by H-NS (57). Among these regions, the expression of the T6SS genes encoded within *Salmonella* pathogenicity island 6 (SPI-6) increased 1.9- to 10.1-fold in *hns* mutant cells (Fig. 1D). Silencing by H-NS is generally caused by direct binding of this protein on target A/T-rich sequences. Using genome-wide ChIP-on-chip analysis for systematically testing H-NS binding on the *S.* Typhimurium genome, Lucchini et al. (56) and Navarre et al. (57) reported a 1.5- to 6-fold increase of H-NS binding to the T6SS locus (Fig. 1B and C).

To confirm these data, we first tested whether an *hns* mutation impacted the expression of the two divergent operons encoding the T6SS in strain *S.* Typhimurium LT2. Strain LT2 was used in this study as it carries an *rpoS* gene starting with a rare UUG start codon that results in decreased RpoS activity and avirulence (70, 71) and counteracts the lethal effect of the *hns* mutation (57). Hence, LT2 tolerates *hns* mutations, but such mutants exhibit a reduced growth rate (57). Expression of the two operons was tested using chromosomal transcriptional fusions in which the β-galactosidase gene was inserted on the chromosome at the T6SS locus in place of the *STM0271* or *STM0272* (*clpV*) gene. Additional *lacZ* fusions were created within the downstream gene operon (*STM0272-STM0289*) in place of the *STM0277* (*tae4*) and *STM0285* (*tssM*) genes. β-Galactosidase activity measurements showed that the expression of the two operons, as well as that of the two internal reporter fusions, was detected at very low levels (4 to 7 Miller units) in Luria broth (Fig. 2, open bars) independently of the growth phase (data not shown). Similar measurements in minimal Eagle's or M63 medium also demonstrated that the *S.* Typhimurium SPI-6 T6SS loci are expressed at similar levels (data

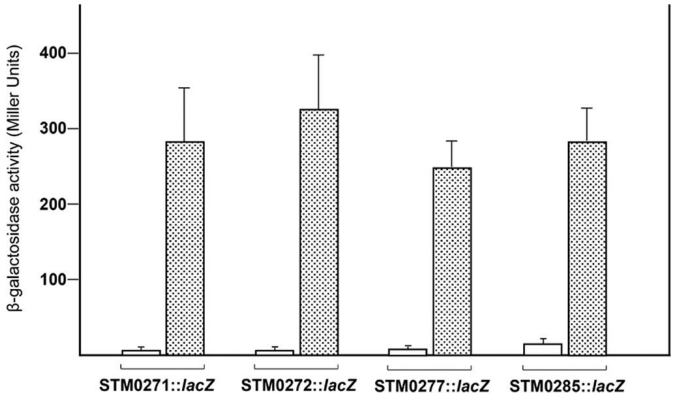

FIG 2 H-NS represses the expression of the type VI secretion gene operons. The activities of chromosomal reporter fusions of *STM0271*, *STM0272* (*clpV*), *STM0277* (*tae4*), and *STM0285* (*tssM*) to the *lacZ* reporter gene were measured in the WT *Salmonella enterica* Typhimurium LT2 (open bars) and its *hns* isogenic mutant (dotted bars). The β-galactosidase activities are the average of 27 measurements.

not shown). When the *hns* mutation was transduced into these reporter strains, the activity of the four reporter fusions increased to reach 200 to 300 Miller units (Fig. 2, dotted bars). These results demonstrate that H-NS silences the expression of both T6SS gene operons in *S.* Typhimurium.

Identification of transcriptional +1 sites. In a recent study, Kröger and colleagues used a genome-wide approach to systematically sequence mRNAs with the goal of identifying +1 transcriptional sites on the *S.* Typhimurium chromosome (47). The observation that no +1 transcriptional sites were identified in the SPI-6 T6SS locus suggested that T6SS mRNAs are not produced *in vitro* (47). We used 5′ RACE assays to define the +1 transcriptional sites of *STM0271* and *clpV*, the first genes of the two divergent T6SS operons, using mRNAs purified from *S.* Typhimurium WT and *hns* cells. In agreement with the results published by Kröger et al. (47) and with the reporter fusions, we did not obtain PCR products from WT total mRNA extracts, but PCR products were amplified from *hns* mutant mRNA extracts. Sequencing of these PCR products indicated +1 sites (Fig. 3). Potential −10 and −35 boxes can be readily identified at appropriate positions with respect to these +1 sites (Fig. 3A and B).

Binding of H-NS on the T6SS locus. *In silico* analyses using Virtual Footprint software (72) predict the existence of a large number of putative H-NS binding sites within the *S.* Typhimurium T6SS locus, distributed in the promoter region or within coding sequences. To test whether H-NS binds to the T6SS locus *in vitro*, we selected five DNA fragments that bear putative H-NS binding sites (Fig. 1B, fragments 1 to 5), including a fragment encompassing the divergent promoter (fragment 2) and a control fragment within the *clpV* gene for which no H-NS binding site is predicted (Fig. 1B, fragment 6). The six fragments were radiolabeled and subjected to electrophoretic mobility shift assays using purified *E. coli* H-NS (which shares 98% similarity and identical DNA-binding sites with the *S.* Typhimurium H-NS protein). Figure 4 shows that fragments 1 to 5 were retarded in the presence of increasing amounts of H-NS. Fragment 6 was not retarded in the presence of up to 300 nM H-NS. Image analyses of the shifts estimated that H-NS binds to fragments 1 to 5 with apparent K_ds of 50 to 75 nM. We conclude that H-NS specifically binds on different regions of the *S.* Typhimurium SPI-6 T6SS locus.

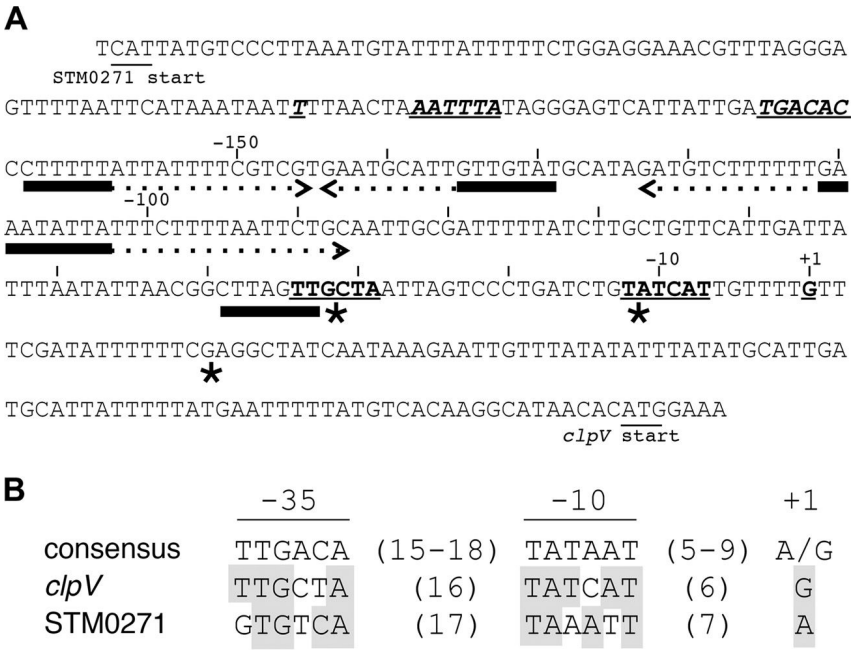

FIG 3 Identification of the promoters of the two divergent operons. (A) Sequence of the *STM0271-STM0272* (*clpV*) intergenic region. The +1 transcriptional start sites identified by 5′ RACE and the corresponding −10 and −35 boxes are indicated in bold letters (roman letters, promoter for *STM0272* [*clpV*]; italics, promoter for *STM0271*). The translational start sites are indicated for the two genes. The regions protected by H-NS in the DNase footprint (Fig. 5) are indicated by solid lines while extensions of these protected regions are indicated by dotted lines. DNase hyperactivity sites are indicated by asterisks. The sequence is numbered identically to the DNase footprint (relative to the *clpV* +1 transcriptional start site). (B) Sequence alignment of the *clpV* and *STM0271* promoters with the *E. coli* σ^{70}-RNA polymerase binding consensus. Bases identical to the consensus are shaded in gray.

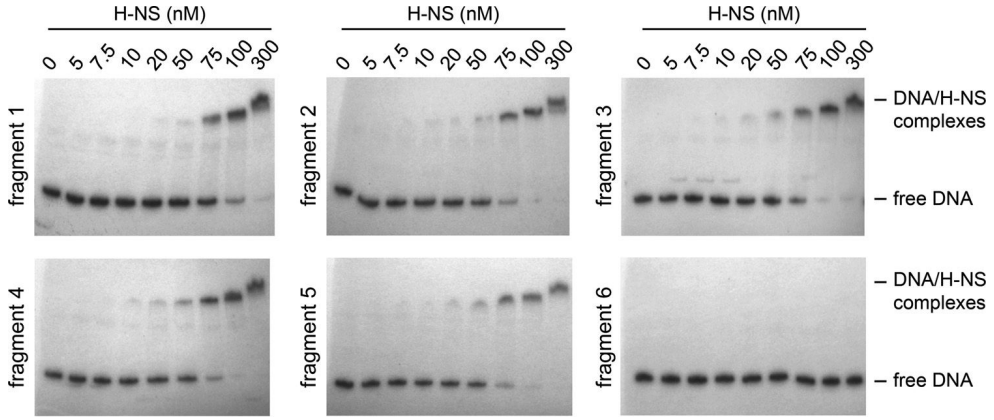

FIG 4 H-NS binds to several regions on the type VI secretion gene cluster. Electrophoretic mobility shift assays using radiolabeled DNA fragments corresponding to regions of the T6SS gene cluster (numbered 1 to 6) (Fig. 1B; see also Table S2 in the supplemental material). Fragment 6 corresponds to a negative control (no H-NS binding site predicted). Radiolabeled fragments were mixed with increasing concentrations of purified *Escherichia coli* H-NS (0, 5, 7.5, 10, 20, 50, 75, 100, and 300 nM).

H-NS binds to and spreads on the T6SS divergent promoter. To gain further insights into H-NS binding on the divergent promoter region, we performed DNase I protection assays. The analysis of the DNase I footprint shown in Fig. 5A demonstrates that H-NS binds to four regions within the fragment: −32 to −50, −100 to −110, −126 to −136, and −156 to −164 (positions relative to the *clpV* +1 transcriptional site) (Fig. 3A and 5A, solid lines). We also noticed a number of DNase hyperactive sites (Fig. 3A and 5A, asterisks). DNase hyperactive sites reflect local distortion of the DNA structure, induced by H-NS binding in adjacent regions, that might affect binding of transcriptional regulators or of the RNA polymerase (Pol) (54). Interestingly, these sites are gathered within the −32 to +18 region, suggesting that distortion of the extended RNA polymerase binding site might contribute to H-NS silencing of the SPI-6 T6SS promoter. H-NS binding is also clearly observable when the densities of the bands from the DNase I footprint are plotted as a function of H-NS concentration (Fig. 5B). DNase footprints also suggest H-NS cooperativity as higher H-NS concentrations led to the extension of the protected region to adjacent zones downstream and upstream (Fig. 3A and 5A, dotted lines). The degree of protection by H-NS at positions −107 (high affinity) and −147 (low affinity) was quantified (Fig. 5C). H-NS binds with an estimated apparent dissociation constant (K_d) of 30 nM at position −107 while the K_d at position −147 is estimated at 350 nM. This observation suggests that H-NS spreads from an initial, high-affinity binding site used as a nucleation center to occupy an extensive DNA region. These characteristics of H-NS have already been studied in detail in previous work and have been proposed to be responsible for gene silencing (54, 65, 73).

Derepression of *S.* Typhimurium T6SS gene expression leads to assembly of dynamic T6SS sheath structures. Once expressed, the T6SS genes encode proteins that form a membrane complex anchoring a dynamic cytoplasmic structure (21, 24). This tubular structure is structurally and functionally related to the sheaths of contractile bacteriophages and undergoes cycles of extension and contraction (21, 26, 34). This dynamic can be followed by time-lapse fluorescence microscopy by fusing the superfolder green fluorescent protein (sfGFP) to the C terminus of one of the T6SS's sheath components, TssB (9, 21, 35, 36, 74). The *sfgfp* gene was introduced on the *S.* Typhimurium chromosome, in frame with the *tssB* coding sequence. In agreement with the results of the reporter fusion assays, the TssB-sfGFP fusion protein was not detectable by Western blot analyses (Fig. 6A), and the total cell fluorescence was very low (Fig. 6B and C). When the *hns* mutation was introduced, a significant level of TssB-sfGFP was detected by immunoblotting with anti-GFP antibody (Fig. 6A). The homogeneity of the population was assessed by flow cytometry. Figure 6B shows that although the LT2 *tssB-sfgfp* cells present fluorescence signal similar to that of WT LT2 cells, nearly 90% of the *hns tssB-sfgfp* population displays a high level of fluorescence. Expression of *tssB-sfgfp* in *hns* cells was accompanied by the observation of fluorescent intracellular tubular structures in ~60% of the cells (Fig. 6D). Time-lapse fluorescence microscopy recordings showed that these structures were dynamic, oscillating between extended and contracted conformations, with dynamic behaviors similar to those observed in *V. cholerae*, *Pseudomonas aeruginosa*, and enteroaggregative *E. coli* (Fig. 6E) (9, 21, 35, 36, 74). It is worth noting that *S.* Typhimurium cells presented a behavior similar to that observed in *P. aeruginosa* cells: an attacked sibling cell responded by triggering the assembly of a T6SS at the vicinity of the attack (Fig. 6E, blue arrowheads indicate response to contraction of the T6SS in the attacker cells indicated by red arrowheads) (35, 74, 75).

Derepression of the *S.* Typhimurium T6SS genes induces interbacterial intoxication. The T6SS has been shown to provide a fitness advantage to *P. aeruginosa*, *Burkholderia thailandensis*, *V. cholerae*, *Serratia marcescens*, *Citrobacter rodentium*, and enteroaggregative *E. coli* in mixed cultures due to its antibacterial activity (5–10, 15). The effectors delivered by these machineries target the peptidoglycan layer of the target prey cell (18, 42) or have phospholipase or DNase activity (45, 76–79). To prevent self-intoxication, these toxin proteins are produced in combination with a specific cognate immunity protein that protects the donor cell. In *S.* Typhimurium, the *STM0277* gene, named *tae4*, encodes a muramidase and is located upstream of *tai4* (*STM0278*), which encodes the cognate immunity protein (Fig. 1A) (42–44). This observation suggests that the *S.* Typhimurium T6SS might target bacteria. We therefore asked whether the T6SS provides a growth advantage to *S.* Typhimurium in mixed cultures. We first tested

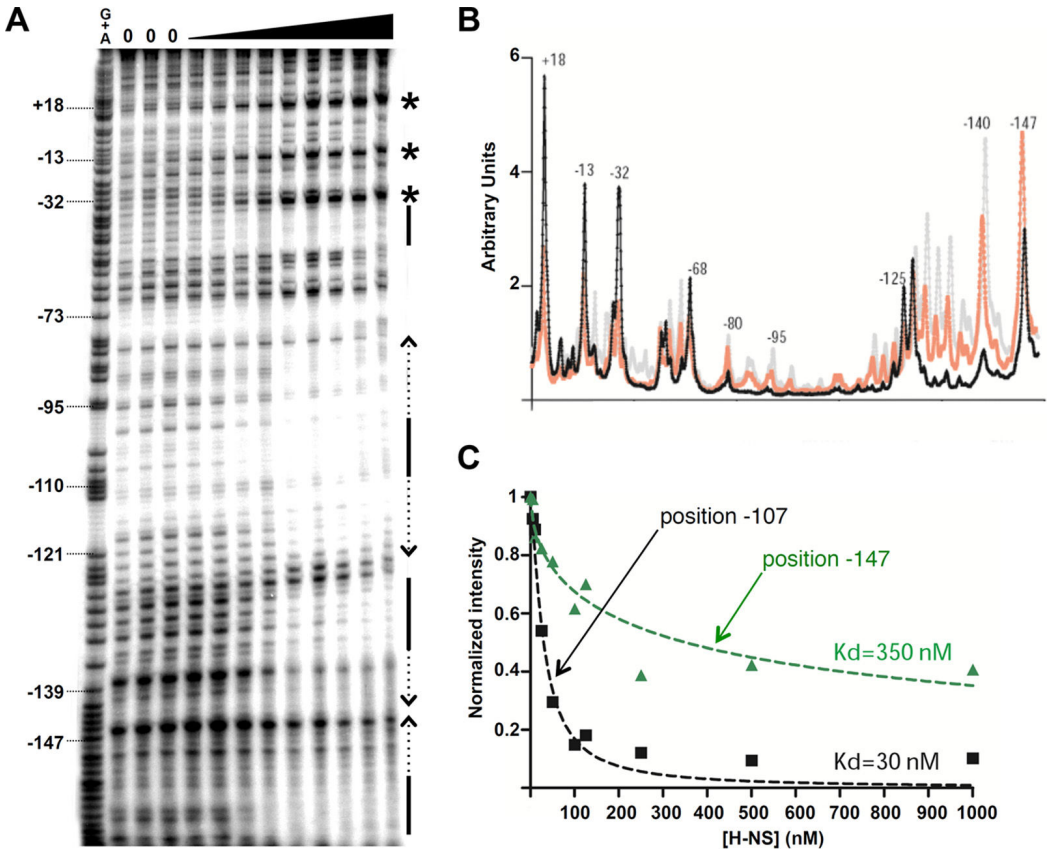

FIG 5 H-NS DNase footprint of the divergent T6SS promoter. (A) DNase footprint. DNase accessibility to a radiolabeled DNA fragment corresponding to the divergent promoter of the T6SS gene cluster (from −173 to +100 relative to the +1 transcriptional site of *STM0272*) in the presence of increasing concentrations of purified *Escherichia coli* H-NS protein (5, 10, 25, 50, 100, 125, 250, 500, and 1,000 nM). The Maxam-Gilbert (G+A) chemical degradation is shown on the left. The protected regions are indicated on the right by solid bars. Extensions of the primary protected region due to H-NS cooperativity are indicated with dotted lines (the orientation of the arrows indicates the orientation of H-NS polymerization). Regions of DNase I hyperactivity are indicated by asterisks. (B) Line representation of the protection pattern of H-NS (gray, free DNA; orange, H-NS at 25 nM; black, H-NS at 125 nM). The densities of the DNase footprint bands (indicated in arbitrary units) are plotted as a migration (from the top to bottom of the DNase footprint). (C) Quantification of H-NS binding at positions −107 and −147. The intensities (band intensity at the indicated H-NS concentration relative to the band intensity in the free DNA fragment) are plotted as a function of the H-NS concentration (in nM). The dissociation constants (K_ds) were calculated as indicated in Materials and Methods.

the interspecies competition using an *E. coli* K-12 strain (W3110, a strain devoid of T6SS genes) as prey. Since WT *E. coli* and *S.* Typhimurium *hns* cells have different growth behaviors, an *E. coli hns* mutant strain was used in these experiments in order to have comparable generation times. As shown in Fig. 7A, the *S.* Typhimurium WT strain had no impact on *E. coli* growth. However, derepression of the SPI-6 T6SS by introduction of the *hns* mutation in *S.* Typhimurium caused *E. coli* cells to die. The intoxication of *E. coli* by *S.* Typhimurium *hns* cells is due to the SPI-6 T6SS as *S.* Typhimurium *hns* cells carrying a deletion of the upstream (Δ*STM0271-STM0266*) or downstream (Δ*STM0272-STM0289*) T6SS gene operon had no impact on *E. coli* growth (Fig. 7A). We further tested intraspecies activity. Here, again, although the WT *S.* Typhimurium strain had no impact on its own growth, the *S.* Typhimurium *hns* strain presented antibacterial activity against its parental, wild-type strain (Fig. 7B). This activity was dependent on the SPI-6 T6SS as an *hns* strain with a deletion of the downstream or upstream operon had no intoxication activity. It is worth noting that the WT prey cells are not protected, suggesting that the T6SS gene operon in these cells is not expressed at all, even during the attack. Interestingly, T6SS-disabled *S.* Typhimurium *hns* prey cells have different behaviors: while cells deleted of the upstream operon were resistant to *hns* attacker cells, cells deleted of the downstream operon were intoxicated (Fig. 7B). The latter result suggests that immunity genes to T6SS-delivered effectors are encoded within the downstream operon and is consistent with the presence of *tai4* and *rhsI* (the genes encoding the immunities to Tae4 and Rhs, respectively) in this operon.

DISCUSSION

In this study, we provide evidence that expression of the *S.* Typhimurium SPI-6 T6SS gene cluster is silenced by the nucleoid-structuring protein H-NS. H-NS binds to different regions of the cluster on high-affinity sites and then spreads onto adjacent regions to silence the expression of these genes. Once derepressed, the T6SS genes are produced and assemble a functionally active machine that is used to intoxicate competing bacteria.

ChIP-on-chip genome-wide studies on the *S.* Typhimurium chromosome showed that H-NS binds to several regions, including the horizontally acquired SPI-6 pathogenicity island (56, 57). This island comprises a gene cluster encoding a type VI secretion system consisting of two divergent operons (39, 40). Using elec-

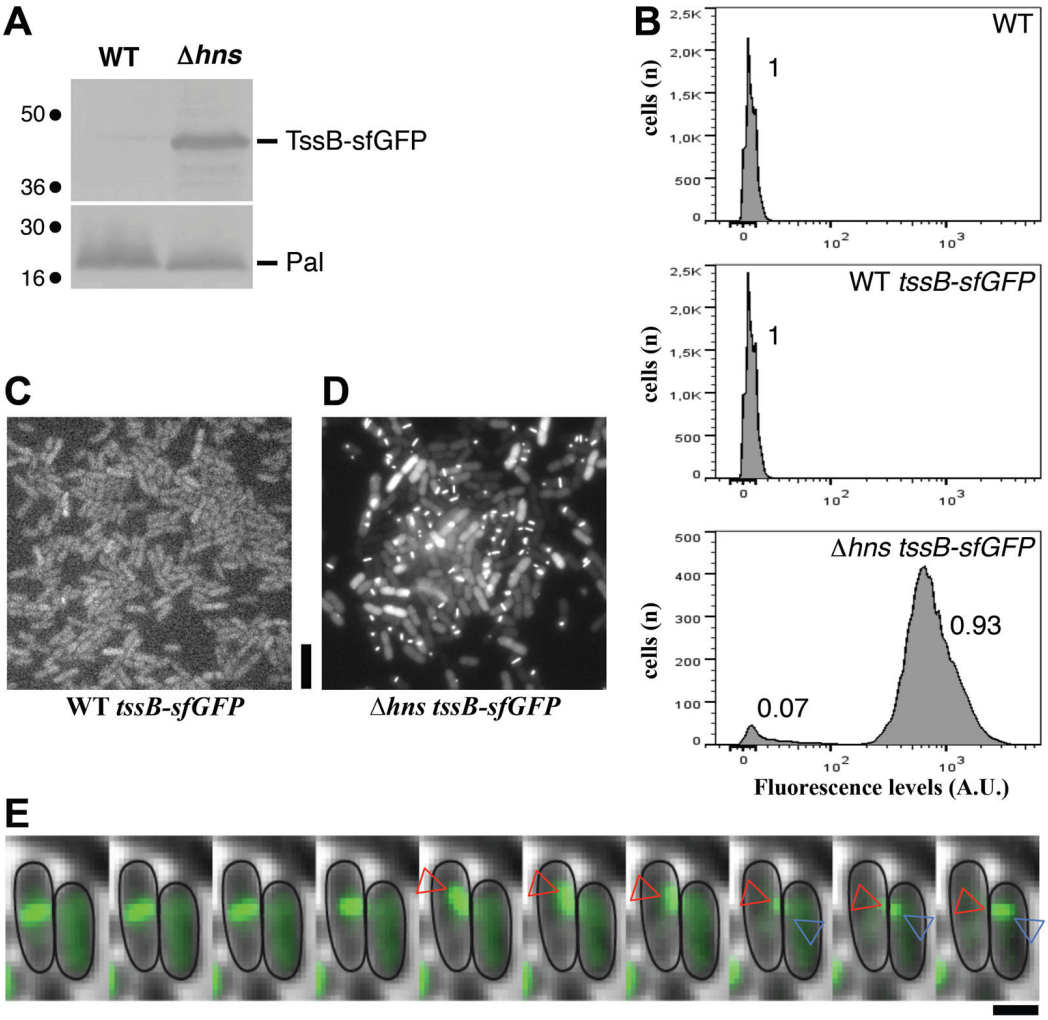

FIG 6 Derepression of the *S.* Typhimurium SPI-6 T6SS leads to assembly of the secretion apparatus. (A) Western blot analyses of *S.* Typhimurium WT and *hns* cells engineered to produce the TssB-sfGFP from the original locus. Total cell extracts from 2×10^8 cells were analyzed by SDS-PAGE. The TssB-sfGFP and the control Pal protein were immunodetected using anti-GFP (upper panel) and anti-Pal (lower panel) antibodies. The two proteins are indicated, as well as the molecular mass markers (at left; kDa). (B) Flow cytometry analyses of WT cells, WT cells carrying the chromosomal *tssB-sfgfp* fusion, and *hns* cells carrying the chromosomal *tssB-sfgfp* fusion. The number of cells (*n*) is plotted against the fluorescence level (AU, arbitrary units). Peaks reflect populations with different fluorescence levels. The number of individual cells in each population is proportional to the surface area of the corresponding peak and is indicated on the right of the peak (ratio to the total population). (C and D) Fluorescence microscopy analyses of *S.* Typhimurium WT and *hns* cells producing the TssB-sfGFP fusion protein (GFP channel). Scale bar, 10 μm. (E) Fluorescence microscopy time-lapse recordings of *S.* Typhimurium *hns* cells producing TssB-sfGFP (one image taken every 15 s, merged differential interference contrast and GFP channels). The arrowheads point the extension (blue) and contraction (red) of the T6SS sheath-like structures. For better visualization, the bacterial limits are outlined in black. Scale bar, 2 μm.

trophoretic mobility shift assays, we confirmed that the purified H-NS protein directly binds to the T6SS genes, including the interoperon region carrying the two divergent promoters. H-NS binding is accompanied by silencing of T6SS gene expression, as shown with chromosomal reporter fusions positioned on different locations within the gene cluster. H-NS-dependent silencing of the T6SS genes was suggested from the microarrays data (56) and more recently by the observation that no +1 transcriptional site was identified in the SPI-6 T6SS region using sequencing of total mRNA of the wild-type strain (47). Indeed, using 5′ RACE on total RNA isolated from the WT strain, we were unable to amplify a PCR product corresponding to the SPI-6 T6SS region; however, when 5′ RACE was performed on total RNA isolated from LT2 *hns* cells, we identified two transcriptional sites, upstream of the *clpV* and *STM0271* genes, the two first genes of the divergent operons. The corresponding −10 and −35 boxes can be readily identified. DNase footprinting on the *clpV* promoter further showed that H-NS binds to different regions, including the −35 box, and then spreads on downstream and upstream fragments. This observation is consistent with the two-step mechanism of H-NS silencing in which H-NS first binds to high-affinity sites that nucleate cooperative binding, leading to H-NS polymerization onto adjacent DNA regions (54, 55, 65, 73). H-NS-dependent silencing of the *S.* Typhimurium T6SS gene cluster is not an isolated case as previous studies showed that the *Acinetobacter baumannii*, *Pseudomonas aeruginosa* HSI-2 and HSI-3, *Pseudomonas Putida*, and *Vibrio parahaemolyticus* T6SS gene clusters as well as the *Edwardsiella tarda* T6SS *evpP-evpO* genes are repressed by H-NS-like proteins (80–84).

Recently, Mulder et al. noted that the SPI-6 T6SS gene region

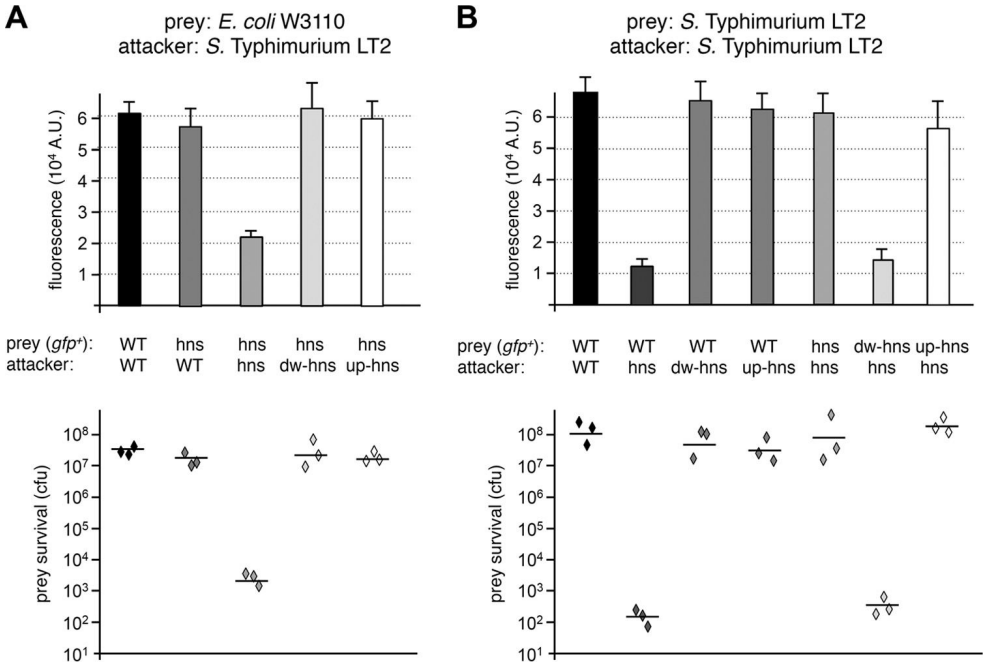

FIG 7 Derepression of the *S.* Typhimurium T6SS confers a growth advantage in inter- and intraspecific competitions. Data are from interspecific (A) and intraspecific (B) growth competition assays. The indicated attacker and *gfp*$^+$ prey strains were mixed, spotted onto LB agar plates, and incubated for 14 h. Recovered mixtures were analyzed for total relative fluorescence (expressed in arbitrary units [A.U.]). The recovered prey cells were numbered on selective plates, and values are reported in the lower graphs (each symbol represents values from three independent assays, and the average is indicated by a horizontal bar). WT, wild type; hns, Δ*hns* strains; dw, deletion of the SPI-6 T6SS downstream operon, Δ*STM0272-STM0289*; up, deletion of the SPI-6 T6SS upstream operon, Δ*STM0271-STM0266*).

comprises genes encoding the T6SS core components that share synteny with the genes of the *Burkholderia mallei* T6SS-3 gene cluster (41); however, in *S.* Typhimurium, these core genes are separated by genes acquired more recently, named noncore clusters 1 to 4 (cluster 1, *STM0275-STM0278*; cluster 2, *STM0283-STM0284*; cluster 3, *STM0286-STM0288*; cluster 4, *STM0290-STM0298*) (Fig. 1A) (41). These regions correspond to DNA fragments that do not encode T6SS core components but, rather, accessory components and/or effector/immunity pairs. Indeed, the ChIP-on-chip data (Fig. 1B) showed that H-NS preferentially binds to these regions, and our EMSAs (Fig. 4) demonstrated that H-NS binds to these regions with high affinity.

Interestingly, although the SPI-6 T6SS gene cluster is silenced *in vitro*, transcriptional profiling, reporter fusion, real-time PCR, and Western blot studies showed that its expression increased in the late stages of macrophage infection (41, 46, 48). Indeed, SPI-6 T6SS mutant strains present defects in intracellular replication and systemic dissemination in mice (41, 46). All of these studies point out that a functional SPI-6 T6SS is expressed during *in vivo* infection and further suggest that H-NS silencing should be counteracted under these conditions. Derepression of H-NS-silenced genes, known as countersilencing, can occur by competition with sequence-specific DNA binding regulators or by disruption of H-NS nucleoprotein filaments by DNA bending (53, 85). A number of transcriptional activators, including PhoP, SlyA, and LeuO, have been shown to antagonize H-NS silencing in *E. coli* and *S.* Typhimurium (86–91). However, deletion of *phoP* or *slyA* had only a minor effect on the expression of the SPI-6 T6SS genes (41, 92). The roles of LeuO and SinR, a transcriptional regulator encoded within the SPI-6 pathogenicity island, in countersilencing the expression of the SPI-6 T6SS gene cluster need to be tested.

We observed that derepression of the SPI-6 T6SS gene cluster in *hns* mutant cells induces assembly and function of the secretion machine and causes intoxication of *E. coli* prey cells. As previously shown for *P. aeruginosa*, *V. cholerae*, and enteroaggregative *E. coli* (9, 35, 74, 75), T6SS activity in *S.* Typhimurium cells induces higher T6SS activities in neighboring cells, a phenomenon referred to as dueling (Fig. 6E). This dueling appears only if the attacked cell is a sibling with the *hns* mutation as intraspecies competition showed that WT prey cells are efficiently killed. This further suggests that the attack is not sufficient to induce T6SS assembly but, rather, that a functional T6SS requires both proper transcriptional expression and sensing of the attack coupled to posttranslational activation. A mechanism of posttranslational activation, named the threonine phosphorylation pathway (TPP), has been described in *P. aeruginosa* and *Agrobacterium tumefaciens*. It requires sensing and signaling of the attack by the TagQRST proteins, leading to the PpkA-dependent phosphorylation of a forkhead-associated protein (FHA) or of the TssL T6SS core component and, ultimately, to the activation of the late stages of T6SS assembly (93–97). However, no homologue subunits to the TagQRST-PpkA-PppA-FHA threonine phosphorylation pathway are encoded within the *S.* Typhimurium SPI-6 T6SS gene cluster, suggesting that the mechanism of sensing and posttranslational activation is different from that described in *P. aeruginosa* or *A. tumefaciens*. As shown in Fig. 7, we observed that *S.* Typhimurium *hns* cells have antibacterial activity on *S.* Typhimurium WT prey cells but had no effect on the isogenic *hns* mutant cells. These data are consistent with the H-NS-mediated silencing of *tai4* (*STM0278*), a gene encoding an immunity protein to the peptidoglycan hydrolase *tae4* (*STM0277*) in the WT background. In the absence of activation of the T6SS in prey cells, the action of

Tae4 delivered by attackers cannot be counteracted. The activation of the gene cluster (and particularly of Tae4) during the late stages of infection might also explain the previous observation that *tai4* mutant cells display significant replication defects (41). Here, again, the absence of the immunity protein upon activation of the T6SS gene cluster may cause self-intoxication and decreased replication behavior. Although we cannot rule out that the *S.* Typhimurium SPI-6 T6SS has a role in pathogenesis, these data clearly show that this gene cluster confers antibacterial properties to *S.* Typhimurium. However, our antibacterial competition experiments also showed that the expression of the *S.* Typhimurium T6SS genes is not activated when WT cells are in contact with competing bacteria (Fig. 7). This and the data demonstrating activation of these genes during infection (41, 46, 48) strongly suggest that the antibacterial activity of the *S.* Typhimurium T6SS is important when *Salmonella* is in contact with eukaryotic cells. A similar situation may exist for the *P. aeruginosa* HSI-1, *V. cholerae*, and *A. tumefaciens* T6SSs, which are activated during infection and have antibacterial activity (78, 98, 99). Indeed, a very recent study suggested that the *V. cholerae* T6SS-dependent antibacterial activity influences the indigenous microbiota in the host (99). What can be the role of specifically activating the SPI-6 T6SS-dependent antibacterial activity during infection? One may hypothesize that it may help *S.* Typhimurium to clear its niche, either in the early stage of infection by competing with the gut flora or after phagocytosis by clearing the *Salmonella*-containing vacuole (SCV); however, the SCV usually contains a clonal population of bacteria, issued from a single bacterium (100). Additionally, activating the T6SS might help to synchronize or homogenize the *S.* Typhimurium kin population at a specific stage of infection as cells for which the SPI-6 T6SS has not been activated would be eliminated. H-NS derepression of the T6SS genes might therefore fine-tune the infection process by discarding disabled cells of the progeny. It would be interesting to perform *in vivo* experiments in mice or macrophages in which WT *S.* Typhimurium cells are challenged with T6SS- or Tai4-deficient bacteria. This will help us better understand the role of the T6SS in shaping bacterial communities during infection.

ACKNOWLEDGMENTS

We thank Manon Vinay, Nathalie Franche, and Mireille Ansaldi (LCB, Marseille, France) for help with the flow cytometry analyses, Javier López-Garrido and Josep Casadesùs (Seville, Spain) for sharing ideas, protocols, and strains and for fruitful discussions, Françoise Norel (Institut Pasteur, Paris, France) for P22 phage *hns* lysates and for sharing protocols, Laure Journet and Laetitia Houot for critical reading of the manuscript, Julie Viala for discussions regarding *Salmonella*, as well as the members of the Cascales, Lloubès, Mignot, Cambillau, Bouveret, and Sturgis research groups for discussions. We are indebted to Annick Brun, Isabelle Bringer, and Olivier Uderso for technical assistance and to Adhémar Patakess for encouragement.

Work in E.C.'s laboratory is supported by the Centre National de la Recherche Scientifique, the Aix-Marseille Université, and grants from the Agence National de la Recherche (ANR-10-JCJC-1303-03 and ANR-14-CE14-0006-02). Work in S.R.'s laboratory was supported by an ANR grant (ANR-09-BLAN-0367-02). Y.R.B., A.K. and L.L. were supported by fellowships from the French Ministry of Research.

REFERENCES

1. **Pukatzki S, Ma AT, Sturtevant D, Krastins B, Sarracino D, Nelson WC, Heidelberg JF, Mekalanos JJ.** 2006. Identification of a conserved bacterial protein secretion system in *Vibrio cholerae* using the *Dictyostelium* host model system. Proc Natl Acad Sci U S A **103:**1528–1533. http://dx.doi.org/10.1073/pnas.0510322103.
2. **Pukatzki S, Ma AT, Revel AT, Sturtevant D, Mekalanos JJ.** 2007. Type VI secretion system translocates a phage tail spike-like protein into target cells where it cross-links actin. Proc Natl Acad Sci U S A **104:**15508–15513. http://dx.doi.org/10.1073/pnas.0706532104.
3. **Ma AT, McAuley S, Pukatzki S, Mekalanos JJ.** 2009. Translocation of a *Vibrio cholerae* type VI secretion effector requires bacterial endocytosis by host cells. Cell Host Microbe **5:**234–243. http://dx.doi.org/10.1016/j.chom.2009.02.005.
4. **Durand E, Derrez E, Audoly G, Spinelli S, Ortiz-Lombardia M, Raoult D, Cascales E, Cambillau C.** 2012. Crystal structure of the VgrG1 actin cross-linking domain of the *Vibrio cholerae* type VI secretion system. J Biol Chem **287:**38190–38199. http://dx.doi.org/10.1074/jbc.M112.390153.
5. **Schwarz S, Hood RD, Mougous JD.** 2010. What is type VI secretion doing in all those bugs? Trends Microbiol **18:**531–537. http://dx.doi.org/10.1016/j.tim.2010.09.001.
6. **Schwarz S, West TE, Boyer F, Chiang WC, Carl MA, Hood RD, Rohmer L, Tolker-Nielsen T, Skerrett SJ, Mougous JD.** 2010. *Burkholderia* type VI secretion systems have distinct roles in eukaryotic and bacterial cell interactions. PLoS Pathog **6:**e1001068. http://dx.doi.org/10.1371/journal.ppat.1001068.
7. **MacIntyre DL, Miyata ST, Kitaoka M, Pukatzki S.** 2010. The *Vibrio cholerae* type VI secretion system displays antimicrobial properties. Proc Natl Acad Sci U S A **107:**19520–19524. http://dx.doi.org/10.1073/pnas.1012931107.
8. **Murdoch SL, Trunk K, English G, Fritsch MJ, Pourkarimi E, Coulthurst SJ.** 2011. The opportunistic pathogen *Serratia marcescens* utilizes type VI secretion to target bacterial competitors. J Bacteriol **193:**6057–6069. http://dx.doi.org/10.1128/JB.05671-11.
9. **Brunet YR, Espinosa L, Harchouni S, Mignot T, Cascales E.** 2013. Imaging type VI secretion mediated bacterial killing. Cell Rep **3:**36–41. http://dx.doi.org/10.1016/j.celrep.2012.11.027.
10. **Gueguen E, Cascales E.** 2013. Promoter swapping unveils the role of the *Citrobacter rodentium* CTS1 type VI secretion system in interbacterial competition. Appl Environ Microbiol **79:**32–38. http://dx.doi.org/10.1128/AEM.02504-12.
11. **Cascales E, Buchanan SK, Duché D, Kleanthous C, Lloubès R, Postle K, Riley M, Slatin S, Cavard D.** 2007. Colicin biology. Microbiol Mol Biol Rev **71:**158–229. http://dx.doi.org/10.1128/MMBR.00036-06.
12. **Ruhe ZC, Low DA, Hayes CS.** 2013. Bacterial contact-dependent growth inhibition. Trends Microbiol **21:**230–237. http://dx.doi.org/10.1016/j.tim.2013.02.003.
13. **Silverman JM, Brunet YR, Cascales E, Mougous JD.** 2012. Structure and regulation of the type VI secretion system. Annu Rev Microbiol **66:**453–472. http://dx.doi.org/10.1146/annurev-micro-121809-151619.
14. **Russell AB, Peterson SB, Mougous JD.** 2014. Type VI secretion effectors: poisons with a purpose. Nat Rev Microbiol **12:**137–148. http://dx.doi.org/10.1038/nrmicro3185.
15. **Hood RD, Singh P, Hsu F, Güvener T, Carl MA, Trinidad RR, Silverman JM, Ohlson BB, Hicks KG, Plemel RL, Li M, Schwarz S, Wang WY, Merz AJ, Goodlett DR, Mougous JD.** 2010. A type VI secretion system of *Pseudomonas aeruginosa* targets a toxin to bacteria. Cell Host Microbe **7:**25–37. http://dx.doi.org/10.1016/j.chom.2009.12.007.
16. **Benz J, Meinhart A.** 2014. Antibacterial effector/immunity systems: it's just the tip of the iceberg. Curr Opin Microbiol **17:**1–10. http://dx.doi.org/10.1016/j.mib.2013.11.002.
17. **Durand E, Cambillau C, Cascales E, Journet L.** 2014. VgrG, Tae, Tle, and beyond: the versatile arsenal of type VI secretion effectors. Trends Microbiol **22:**498–507. http://dx.doi.org/10.1016/j.tim.2014.06.004.
18. **Russell AB, Hood RD, Bui NK, Leroux M, Vollmer W, Mougous JD.** 2011. Type VI secretion delivers bacteriolytic effectors to target cells. Nature **475:**343–347. http://dx.doi.org/10.1038/nature10244.
19. **Borgeaud S, Metzger LC, Scrignari T, Blokesch M.** 2015. The type VI secretion system of *Vibrio cholerae* fosters horizontal gene transfer. Science **347:**63–67. http://dx.doi.org/10.1126/science.1260064.
20. **Aschtgen MS, Gavioli M, Dessen A, Lloubes R, Cascales E.** 2010. The SciZ protein anchors the enteroaggregative *Escherichia coli* type VI secretion system to the cell wall. Mol Microbiol **75:**886–899. http://dx.doi.org/10.1111/j.1365-2958.2009.07028.x.
21. **Basler M, Pilhofer M, Henderson GP, Jensen GJ, Mekalanos JJ.** 2012.

Type VI secretion requires a dynamic contractile phage tail-like structure. Nature **483:**182–186. http://dx.doi.org/10.1038/nature10846.
22. **Cascales E, Cambillau C.** 2012. Structural biology of type VI secretion systems. Philos Trans R Soc Lond B Biol Sci **367:**1102–1111. http://dx.doi.org/10.1098/rstb.2011.0209.
23. **Ho BT, Dong TG, Mekalanos JJ.** 2014. A view to a kill: the bacterial type VI secretion system. Cell Host Microbe **15:**9–21. http://dx.doi.org/10.1016/j.chom.2013.11.008.
24. **Zoued A, Brunet YR, Durand E, Aschtgen MS, Logger L, Douzi B, Journet L, Cambillau C, Cascales E.** 2014. Architecture and assembly of the type VI secretion system. Biochim Biophys Acta **1843:**1664–1673. http://dx.doi.org/10.1016/j.bbamcr.2014.03.018.
25. **Pell LG, Kanelis V, Donaldson LW, Howell PL, Davidson AR.** 2009. The phage lambda major tail protein structure reveals a common evolution for long-tailed phages and the type VI bacterial secretion system. Proc Natl Acad Sci U S A **106:**4160–4165. http://dx.doi.org/10.1073/pnas.0900044106.
26. **Leiman PG, Basler M, Ramagopal UA, Bonanno JB, Sauder JM, Pukatzki S, Burley SK, Almo SC, Mekalanos JJ.** 2009. Type VI secretion apparatus and phage tail-associated protein complexes share a common evolutionary origin. Proc Natl Acad Sci U S A **106:**4154–4159. http://dx.doi.org/10.1073/pnas.0813360106.
27. **Brunet YR, Hénin J, Celia H, Cascales E.** 2014. The type VI secretion and bacteriophage tail tubes share a common assembly pathway. EMBO Rep **15:**315–321. http://dx.doi.org/10.1002/embr.201337936.
28. **Bönemann G, Pietrosiuk A, Mogk A.** 2010. Tubules and donuts: a type VI secretion story. Mol Microbiol **76:**815–821. http://dx.doi.org/10.1111/j.1365-2958.2010.07171.x.
29. **Coulthurst SJ.** 2013. The type VI secretion system—a widespread and versatile cell targeting system. Res Microbiol **164:**640–654. http://dx.doi.org/10.1016/j.resmic.2013.03.017.
30. **Kapitein N, Mogk A.** 2013. Deadly syringes: type VI secretion system activities in pathogenicity and interbacterial competition. Curr Opin Microbiol **16:**52–58. http://dx.doi.org/10.1016/j.mib.2012.11.009.
31. **Silverman JM, Agnello DM, Zheng H, Andrews BT, Li M, Catalano CE, Gonen T, Mougous JD.** 2013. Haemolysin coregulated protein is an exported receptor and chaperone of type VI secretion substrates. Mol Cell **51:**584–593. http://dx.doi.org/10.1016/j.molcel.2013.07.025.
32. **Shneider MM, Buth SA, Ho BT, Basler M, Mekalanos JJ, Leiman PG.** 2013. PAAR-repeat proteins sharpen and diversify the type VI secretion system spike. Nature **500:**350–353. http://dx.doi.org/10.1038/nature12453.
33. **Whitney JC, Beck CM, Goo YA, Russell AB, Harding BN, De Leon JA, Cunningham DA, Tran BQ, Low DA, Goodlett DR, Hayes CS, Mougous JD.** 2014. Genetically distinct pathways guide effector export through the type VI secretion system. Mol Microbiol **92:**529–542. http://dx.doi.org/10.1111/mmi.12571.
34. **Bönemann G, Pietrosiuk A, Diemand A, Zentgraf H, Mogk A.** 2009. Remodelling of VipA/VipB tubules by ClpV-mediated threading is crucial for type VI protein secretion. EMBO J **28:**315–325. http://dx.doi.org/10.1038/emboj.2008.269.
35. **LeRoux M, De Leon JA, Kuwada NJ, Russell AB, Pinto-Santini D, Hood RD, Agnello DM, Robertson SM, Wiggins PA, Mougous JD.** 2012. Quantitative single-cell characterization of bacterial interactions reveals type VI secretion is a double-edged sword. Proc Natl Acad Sci U S A **109:**19804–19809. http://dx.doi.org/10.1073/pnas.1213963109.
36. **Kapitein N, Bonemann G, Pietrosiuk A, Seyffer F, Hausser I, Locker JK, Mogk A.** 2013. ClpV recycles VipA/VipB tubules and prevents non-productive tubule formation to ensure efficient type VI protein secretion. Mol Microbiol **87:**1013–1028. http://dx.doi.org/10.1111/mmi.12147.
37. **Bernard CS, Brunet YR, Gueguen E, Cascales E.** 2010. Nooks and crannies in type VI secretion regulation. J Bacteriol **192:**3850–3860. http://dx.doi.org/10.1128/JB.00370-10.
38. **Leung KY, Siame BA, Snowball H, Mok YK.** 2011. Type VI secretion regulation: crosstalk and intracellular communication. Curr Opin Microbiol **14:**9–15. http://dx.doi.org/10.1016/j.mib.2010.09.017.
39. **Blondel CJ, Jiménez JC, Contreras I, Santiviago CA.** 2009. Comparative genomic analysis uncovers 3 novel loci encoding type six secretion systems differentially distributed in *Salmonella* serotypes. BMC Genomics **10:**354. http://dx.doi.org/10.1186/1471-2164-10-354.
40. **Folkesson A, Löfdahl S, Normark S.** 2002. The *Salmonella enterica* subspecies I specific centisome 7 genomic island encodes novel protein families present in bacteria living in close contact with eukaryotic cells. Res Microbiol **153:**537–545. http://dx.doi.org/10.1016/S0923-2508(02)01348-7.
41. **Mulder DT, Cooper CA, Coombes BK.** 2012. Type VI secretion system-associated gene clusters contribute to pathogenesis of *Salmonella enterica* serovar Typhimurium. Infect Immun **80:**1996–2007. http://dx.doi.org/10.1128/IAI.06205-11.
42. **Russell AB, Singh P, Brittnacher M, Bui NK, Hood RD, Carl MA, Agnello DM, Schwarz S, Goodlett DR, Vollmer W, Mougous JD.** 2012. A widespread bacterial type VI secretion effector superfamily identified using a heuristic approach. Cell Host Microbe **11:**538–549. http://dx.doi.org/10.1016/j.chom.2012.04.007.
43. **Zhang H, Zhang H, Gao ZQ, Wang WJ, Liu GF, Xu JH, Su XD, Dong YH.** 2013. Structure of the type VI effector-immunity complex (Tae4-Tai4) provides novel insights into the inhibition mechanism of the effector by its immunity protein. J Biol Chem **288:**5928–5939. http://dx.doi.org/10.1074/jbc.M112.434357.
44. **Benz J, Reinstein J, Meinhart A.** 2013. Structural insights into the effector-immunity system Tae4/Tai4 from *Salmonella typhimurium*. PLoS One **8:**e67362. http://dx.doi.org/10.1371/journal.pone.0067362.
45. **Koskiniemi S, Garza-Sánchez F, Sandegren L, Webb JS, Braaten BA, Poole SJ, Andersson DI, Hayes CS, Low DA.** 2014. Selection of orphan Rhs toxin expression in evolved *Salmonella enterica* serovar Typhimurium. PLoS Genet **10:**e1004255. http://dx.doi.org/10.1371/journal.pgen.1004255.
46. **Parsons DA, Heffron F.** 2005. *sciS*, an *icmF* homolog in *Salmonella enterica* serovar Typhimurium, limits intracellular replication and decreases virulence. Infect Immun **73:**4338–4345. http://dx.doi.org/10.1128/IAI.73.7.4338-4345.2005.
47. **Kröger C, Dillon SC, Cameron AD, Papenfort K, Sivasankaran SK, Hokamp K, Chao Y, Sittka A, Hébrard M, Händler K, Colgan A, Leekitcharoenphon P, Langridge GC, Lohan AJ, Loftus B, Lucchini S, Ussery DW, Dorman CJ, Thomson NR, Vogel J, Hinton JC.** 2012. The transcriptional landscape and small RNAs of *Salmonella enterica* serovar Typhimurium. Proc Natl Acad Sci U S A **109:**E1277–E1286. http://dx.doi.org/10.1073/pnas.1201061109.
48. **Hautefort I, Thompson A, Eriksson-Ygberg S, Parker ML, Lucchini S, Danino V, Bongaerts RJ, Ahmad N, Rhen M, Hinton JC.** 2008. During infection of epithelial cells *Salmonella enterica* serovar Typhimurium undergoes a time-dependent transcriptional adaptation that results in simultaneous expression of three type 3 secretion systems. Cell Microbiol **10:**958–984. http://dx.doi.org/10.1111/j.1462-5822.2007.01099.x.
49. **Eriksson S, Lucchini S, Thompson A, Rhen M, Hinton JC.** 2003. Unravelling the biology of macrophage infection by gene expression profiling of intracellular *Salmonella enterica*. Mol Microbiol **47:**103–118. http://dx.doi.org/10.1046/j.1365-2958.2003.03313.x.
50. **Liu J, Guo JT, Li YG, Johnston RN, Liu GR, Liu SL.** 2013. The type VI secretion system gene cluster of *Salmonella typhimurium*: required for full virulence in mice. J Basic Microbiol **53:**600–607. http://dx.doi.org/10.1002/jobm.201200047.
51. **Pezoa D, Yang HJ, Blondel CJ, Santiviago CA, Andrews-Polymenis HL, Contreras I.** 2013. The type VI secretion system encoded in SPI-6 plays a role in gastrointestinal colonization and systemic spread of *Salmonella enterica* serovar Typhimurium in the chicken. PLoS One **8:**e63917. http://dx.doi.org/10.1371/journal.pone.0063917.
52. **Pezoa D, Blondel CJ, Silva CA, Yang HJ, Andrews-Polymenis H, Santiviago CA, Contreras I.** 2014. Only one of the two type VI secretion systems encoded in the *Salmonella enterica* serotype Dublin genome is involved in colonization of the avian and murine hosts. Vet Res **45:**2. http://dx.doi.org/10.1186/1297-9716-45-2.
53. **Navarre WW, McClelland M, Libby SJ, Fang FC.** 2007. Silencing of xenogeneic DNA by H-NS-facilitation of lateral gene transfer in bacteria by a defense system that recognizes foreign DNA. Genes Dev **21:**1456–1471. http://dx.doi.org/10.1101/gad.1543107.
54. **Fang FC, Rimsky S.** 2008. New insights into transcriptional regulation by H-NS. Curr Opin Microbiol **11:**113–120. http://dx.doi.org/10.1016/j.mib.2008.02.011.
55. **Ali SS, Xia B, Liu J, Navarre WW.** 2012. Silencing of foreign DNA in bacteria. Curr Opin Microbiol **15:**175–181. http://dx.doi.org/10.1016/j.mib.2011.12.014.
56. **Lucchini S, Rowley G, Goldberg MD, Hurd D, Harrison M, Hinton JC.** 2006. H-NS mediates the silencing of laterally acquired genes in bacteria. PLoS Pathog **2:**e81. http://dx.doi.org/10.1371/journal.ppat.0020081.

57. **Navarre WW, Porwollik S, Wang Y, McClelland M, Rosen H, Libby SJ, Fang FC.** 2006. Selective silencing of foreign DNA with low GC content by the H-NS protein in *Salmonella*. Science **313:**236–238. http://dx.doi.org/10.1126/science.1128794.
58. **Baba T, Ara T, Hasegawa M, Takai Y, Okumura Y, Baba M, Datsenko KA, Tomita M, Wanner BL, Mori H.** 2006. Construction of *Escherichia coli* K-12 in-frame, single-gene knockout mutants: the Keio collection. Mol Syst Biol **2:**2006.0008. http://dx.doi.org/10.1038/msb4100050.
59. **Datsenko KA, Wanner BL.** 2000. One-step inactivation of chromosomal genes in *Escherichia coli* K-12 using PCR products. Proc Natl Acad Sci U S A **97:**6640–6645. http://dx.doi.org/10.1073/pnas.120163297.
60. **Ellermeier CD, Janakiraman A, Slauch JM.** 2002. Construction of targeted single copy lac fusions using lambda Red and FLP-mediated site-specific recombination in bacteria. Gene **290:**153–161. http://dx.doi.org/10.1016/S0378-1119(02)00551-6.
61. **van den Ent F, Lowe J.** 2006. RF cloning: a restriction-free method for inserting target genes into plasmids. J Biochem Biophys Methods **67:**67–74. http://dx.doi.org/10.1016/j.jbbm.2005.12.008.
62. **Beraud M, Kolb A, Monteil V, D'Alayer J, Norel F.** 2010. A proteomic analysis reveals differential regulation of the σ^S-dependent *yciGFE*(*katN*) locus by YncC and H-NS in *Salmonella* and *Escherichia coli* K-12. Mol Cell Proteomics **9:**2601–2616. http://dx.doi.org/10.1074/mcp.M110.002493.
63. **Miller J.** 1972. Experiments in molecular genetics. Cold Spring Harbor Laboratory Press, Cold Spring Harbor, NY.
64. **Tanaka K, Muramatsu S, Yamada H, Mizuno T.** 1991. Systematic characterization of curved DNA segments randomly cloned from *Escherichia coli* and their functional significance. Mol Gen Genet **226:**367–376.
65. **Bouffartigues E, Buckle M, Badaut C, Travers A, Rimsky S.** 2007. H-NS cooperative binding to high-affinity sites in a regulatory element results in transcriptional silencing. Nat Struct Mol Biol **14:**441–448. http://dx.doi.org/10.1038/nsmb1233.
66. **Brenowitz M, Senear DF, Kingston RE.** 2001. DNase I footprint analysis of protein-DNA binding. Curr Protoc Mol Biol Chapter 12:Unit 12.4. http://dx.doi.org/10.1002/0471142727.mb1204s07.
67. **Zoued A, Durand E, Bebeacua C, Brunet YR, Douzi B, Cambillau C, Cascales E, Journet L.** 2013. TssK is a trimeric cytoplasmic protein interacting with components of both phage-like and membrane anchoring complexes of the type VI secretion system. J Biol Chem **288:**27031–27041. http://dx.doi.org/10.1074/jbc.M113.499772.
68. **Zaslaver A, Bren A, Ronen M, Itzkovitz S, Kikoin I, Shavit S, Liebermeister W, Surette MG, Alon U.** 2006. A comprehensive library of fluorescent transcriptional reporters for *Escherichia coli*. Nat Methods **3:**623–628. http://dx.doi.org/10.1038/nmeth895.
69. **Cascales E, Bernadac A, Gavioli M, Lazzaroni JC, Lloubes R.** 2002. Pal lipoprotein of *Escherichia coli* plays a major role in outer membrane integrity. J Bacteriol **184:**754–759. http://dx.doi.org/10.1128/JB.184.3.754-759.2002.
70. **Wilmes-Riesenberg MR, Foster JW, Curtiss R, III.** 1997. An altered *rpoS* allele contributes to the avirulence of *Salmonella typhimurium* LT2. Infect Immun **65:**203–210.
71. **Swords WE, Cannon BM, Benjamin WH, Jr.** 1997. Avirulence of LT2 strains of *Salmonella typhimurium* results from a defective *rpoS* gene. Infect Immun **65:**2451–2453.
72. **Münch R, Hiller K, Grote A, Scheer M, Klein J, Schobert M, Jahn D.** 2005. Virtual Footprint and PRODORIC: an integrative framework for regulon prediction in prokaryotes. Bioinformatics **21:**4187–4189. http://dx.doi.org/10.1093/bioinformatics/bti635.
73. **Lim CJ, Lee SY, Kenney LJ, Yan J.** 2012. Nucleoprotein filament formation is the structural basis for bacterial protein H-NS gene silencing. Sci Rep **2:**509. http://dx.doi.org/10.1038/srep00509.
74. **Basler M, Mekalanos JJ.** 2012. Type 6 secretion dynamics within and between bacterial cells. Science **337:**815. http://dx.doi.org/10.1126/science.1222901.
75. **Basler M, Ho BT, Mekalanos JJ.** 2013. Tit-for-tat: type VI secretion system counterattack during bacterial cell-cell interactions. Cell **152:**884–894. http://dx.doi.org/10.1016/j.cell.2013.01.042.
76. **Russell AB, LeRoux M, Hathazi K, Agnello DM, Ishikawa T, Wiggins PA, Wai SN, Mougous JD.** 2013. Diverse type VI secretion phospholipases are functionally plastic antibacterial effectors. Nature **496:**508–512. http://dx.doi.org/10.1038/nature12074.
77. **Koskiniemi S, Lamoureux JG, Nikolakakis KC, t'Kint de Roodenbeke C, Kaplan MD, Low DA, Hayes CS.** 2013. Rhs proteins from diverse bacteria mediate intercellular competition. Proc Natl Acad Sci U S A **110:**7032–7037. http://dx.doi.org/10.1073/pnas.1300627110.
78. **Ma LS, Hachani A, Lin JS, Filloux A, Lai EM.** 2014. *Agrobacterium tumefaciens* deploys a superfamily of type VI secretion DNase effectors as weapons for interbacterial competition *in planta*. Cell Host Microbe **16:**94–104. http://dx.doi.org/10.1016/j.chom.2014.06.002.
79. **Jiang F, Waterfield NR, Yang J, Yang G, Jin Q.** 2014. A *Pseudomonas aeruginosa* type VI secretion phospholipase D effector targets both prokaryotic and eukaryotic cells. Cell Host Microbe **15:**600–610. http://dx.doi.org/10.1016/j.chom.2014.04.010.
80. **Castang S, McManus HR, Turner KH, Dove SL.** 2008. H-NS family members function coordinately in an opportunistic pathogen. Proc Natl Acad Sci U S A **105:**18947–18952. http://dx.doi.org/10.1073/pnas.0808215105.
81. **Renzi F, Rescalli E, Galli E, Bertoni G.** 2010. Identification of genes regulated by the MvaT-like paralogues TurA and TurB of *Pseudomonas putida* KT2440. Environ Microbiol **12:**254–263. http://dx.doi.org/10.1111/j.1462-2920.2009.02064.x.
82. **Eijkelkamp BA, Stroeher UH, Hassan KA, Elbourne LD, Paulsen IT, Brown MH.** 2013. H-NS plays a role in expression of *Acinetobacter baumannii* virulence features. Infect Immun **81:**2574–2583. http://dx.doi.org/10.1128/IAI.00065-13.
83. **Salomon D, Klimko JA, Orth K.** 2014. H-NS regulates the *Vibrio parahaemolyticus* type VI secretion system 1. Microbiology **160:**1867–1873. http://dx.doi.org/10.1099/mic.0.080028-0.
84. **Zhang J, Xiao J, Zhang Y, Cui S, Liu Q, Wang Q, Wu H, Zhang Y.** 2014. A new target for the old regulator: H-NS suppress T6SS secretory protein EvpP, the major virulence factor in the fish pathogen *Edwardsiella tarda*. Lett Appl Microbiol **59:**557–564. http://dx.doi.org/10.1111/lam.12316.
85. **Will WR, Navarre WW, Fang FC.** 2015. Integrated circuits: how transcriptional silencing and counter-silencing facilitate bacterial evolution. Curr Opin Microbiol **23:**8–13. http://dx.doi.org/10.1016/j.mib.2014.10.005.
86. **Wyborn NR, Stapleton MR, Norte VA, Roberts RE, Grafton J, Green J.** 2004. Regulation of *Escherichia coli* hemolysin E expression by H-NS and *Salmonella* SlyA. J Bacteriol **186:**1620–1628. http://dx.doi.org/10.1128/JB.186.6.1620-1628.2004.
87. **Lithgow JK, Haider F, Roberts IS, Green J.** 2007. Alternate SlyA and H-NS nucleoprotein complexes control *hlyE* expression in *Escherichia coli* K-12. Mol Microbiol **66:**685–698. http://dx.doi.org/10.1111/j.1365-2958.2007.05950.x.
88. **De la Cruz MA, Fernández-Mora M, Guadarrama C, Flores-Valdez MA, Bustamante VH, Vázquez A, Calva E.** 2007. LeuO antagonizes H-NS and StpA-dependent repression in *Salmonella enterica ompS1*. Mol Microbiol **66:**727–743. http://dx.doi.org/10.1111/j.1365-2958.2007.05958.x.
89. **Perez JC, Latifi T, Groisman EA.** 2008. Overcoming H-NS-mediated transcriptional silencing of horizontally acquired genes by the PhoP and SlyA proteins in *Salmonella enterica*. J Biol Chem **283:**10773–10783. http://dx.doi.org/10.1074/jbc.M709843200.
90. **Stoebel DM, Free A, Dorman CJ.** 2008. Anti-silencing: overcoming H-NS-mediated repression of transcription in Gram-negative enteric bacteria. Microbiology **154:**2533–2545. http://dx.doi.org/10.1099/mic.0.2008/020693-0.
91. **Fass E, Groisman EA.** 2009. Control of *Salmonella* pathogenicity island-2 gene expression. Curr Opin Microbiol **12:**199–204. http://dx.doi.org/10.1016/j.mib.2009.01.004.
92. **Wang M, Luo Z, Du H, Xu S, Ni B, Zhang H, Sheng X, Xu H, Huang X.** 2011. Molecular characterization of a functional type VI secretion system in *Salmonella enterica* serovar Typhi. Curr Microbiol **63:**22–31. http://dx.doi.org/10.1007/s00284-011-9935-z.
93. **Mougous JD, Gifford CA, Ramsdell TL, Mekalanos JJ.** 2007. Threonine phosphorylation post-translationally regulates protein secretion in *Pseudomonas aeruginosa*. Nat Cell Biol **9:**797–803. http://dx.doi.org/10.1038/ncb1605.
94. **Hsu F, Schwarz S, Mougous JD.** 2009. TagR promotes PpkA-catalysed type VI secretion activation in *Pseudomonas aeruginosa*. Mol Microbiol **72:**1111–1125. http://dx.doi.org/10.1111/j.1365-2958.2009.06701.x.
95. **Silverman JM, Austin LS, Hsu F, Hicks KG, Hood RD, Mougous JD.** 2011. Separate inputs modulate phosphorylation-dependent and –independent Type VI secretion activation. Mol Microbiol **82:**1277–1290. http://dx.doi.org/10.1111/j.1365-2958.2011.07889.x.
96. **Casabona MG, Silverman JM, Sall KM, Boyer F, Couté Y, Poirel J, Grunwald D, Mougous JD, Elsen S, Attree I.** 2013. An ABC trans-

porter and an outer membrane lipoprotein participate in posttranslational activation of type VI secretion in *Pseudomonas aeruginosa*. Environ Microbiol **15:**471–486. http://dx.doi.org/10.1111/j.1462-2920.2012.02816.x.

97. **Lin JS, Wu HH, Hsu PH, Ma LS, Pang YY, Tsai MD, Lai EM.** 2014. Fha interaction with phosphothreonine of TssL activates type VI secretion in *Agrobacterium tumefaciens*. PLoS Pathog **10:**e1003991. http://dx.doi.org/10.1371/journal.ppat.1003991.
98. **Mougous JD, Cuff ME, Raunser S, Shen A, Zhou M, Gifford CA, Goodman AL, Joachimiak G, Ordoñez CL, Lory S, Walz T, Joachimiak A, Mekalanos JJ.** 2006. A virulence locus of *Pseudomonas aeruginosa* encodes a protein secretion apparatus. Science **312:**1526–1530. http://dx.doi.org/10.1126/science.1128393.
99. **Fu Y, Waldor MK, Mekalanos JJ.** 2013. Tn-Seq analysis of *Vibrio cholerae* intestinal colonization reveals a role for T6SS-mediated antibacterial activity in the host. Cell Host Microbe **14:**652–663. http://dx.doi.org/10.1016/j.chom.2013.11.001.
100. **García-del Portillo F, Núñez-Hernández C, Eisman B, Ramos-Vivas J.** 2008. Growth control in the *Salmonella*-containing vacuole. Curr Opin Microbiol **11:**46–52. http://dx.doi.org/10.1016/j.mib.2008.01.001.

Supplemental Tables

H-NS silencing of the SPI-6-encoded Type VI secretion system limits *Salmonella enterica* serovar Typhimurium interbacterial killing.

Yannick R. BRUNET, Ahmad KHODR, Laureen LOGGER, Laurent AUSSEL, Tâm MIGNOT, Sylvie RIMSKY, and Eric CASCALES

Supplemental Table S1. Strains, plasmids and oligonucleotides used in this study.

STRAINS

Strains	description and genotype	source
E. coli K12		
DH5α	F-, Δ(*argF-lac*)U169, *phoA*, *supE44*, Δ(*lacZ*)M15, *relA*, *endA*, *thi*, *hsdR*	Laboratory collection
W3110	F-, λ-, IN(*rrnD- rrnE*), *rph*-1	Laboratory collection
Salmonella enterica serovar Typhimurium		
LT2	Wild-Type, mutation in *rpoS* that confers RpoS decreased activity	Swords *et al.*, 1997
LT2 P*STM0271-lacZ*	LT2 with pCE36 plasmid fused to the promoter of *STM0271*	This study
LT2 P*clpV-lacZ*	LT2 with pCE36 plasmid fused to the promoter of *STM0272* (*clpV*)	This study
LT2 *STM0277ΩlacZ*	LT2 with pCE36 plasmid inserted in place of the *STM0277* (*tae4*) gene	This study
LT2 *STM0285ΩlacZ*	LT2 with pCE36 plasmid inserted in place of the *STM0285* (*tssM*) gene	This study
LT2 Δ*hns*	LT2 deleted of the *hns* gene	This study
LT2 Δ*hns* P*STM0271-lacZ*	Δ*hns* mutation introduced into LT2 P*STM0271-lacZ*	This study
LT2 Δ*hns* P*clpV-lacZ*	Δ*hns* mutation introduced into LT2 P*clpV-lacZ*	This study
LT2 Δ*hns STM0277ΩlacZ*	Δ*hns* mutation introduced into LT2 *STM0277ΩlacZ*	This study
LT2 Δ*hns STM0285ΩlacZ*	Δ*hns* mutation introduced into LT2 *STM0285Ω-lacZ*	This study
LT2 Δ*sci*-Up	LT2 deleted of the SPI-6 T6SS downstream operon	This study
LT2 Δ*sci*-Down	LT2 deleted of the SPI-6 T6SS upstream operon	This study
LT2 Δ*hns* Δ*sci*-Up	Δ*hns* mutation introduced into LT2 Δ*sci*-Up	This study
LT2 Δ*hns* Δ*sci*-Down	Δ*hns* mutation introduced into LT2 Δ*sci*-Down	This study
LT2 *tssB-sfGFP*	LT2 with *sfGFP* fusion to the 3' of the *tssB* gene (STM0273)	This study

LTS Δ*hns tssB-sfGFP*	Δ*hns* mutation introduced into LT2 *tssB-sfGFP*	This study

PLASMIDS

Vectors and Plasmids	main characteristics	source
pCE36	*ahp* FRT *lacZY*$^{+}$ t_{his} oriR6K	Ellermeier *et al.*, 2002
pKD46	*Bla* P_{BAD} *gam bet exo* pSC101 oriTS	Datsenko and Wanner, 2000
pKD4	*bla* FRT *ahp* FRT PS1 PS2 oriR6K	Datsenko and Wanner, 2000
pCP20	*bla cat cI857* λP_R *flp* pSC101 oriTS	Datsenko and Wanner, 2000
pKD4-sfGFP	pKD4 plasmid with sfGFP gene inserted upstream the FRT site	This study

OLIGONUCLEOTIDES

Strain construction [a, b]	
Del-sci.UP-5-DW	CTCCCTAAACGTTTCCTCCAGAAAAATAAATACATTTAAGGGACATAATG**TGTGTAGGCTGGAGCTGCTTCG**
NoDel-sci.UP-3-DW	GTTATCCGTTATACCCTGCGACTGTATTTTCCGTAATTCCCACATGTCTTGTTT**CATATGAATATCCTCCTTAG TTC**
Del-sci.DOWN-5-DW	GCATTGATGCATTATTTTTATGAATTTTTATGTCACAAGGCATAACACATG**TGTGTAGGCTGGAGCTGCTTCG**
NoDel-sci.DOWN-3-DW	GAATAGTGGGCCGGCCAGTTTTCCATACAACGCACTGCGTGAAACAGGAGTTTC**CATATGAATATCCTCCTTA GTTC**

Del-TssM-Sent-5-DW	TATCCAGGGAATTTTAAAATATTGATTATTGGGTGGCGAGTCGAAATATA**TGTGTAGGCTGGAGCTGCTTCG**
Del-TssM-Sent-3-DW	CCGAACATCGCCGGGGCTGATACCACTGCTGGCCGGCGCATTACAGCGCC**CATATGAATATCCTCCTTAGTTC**
Del-STM0277-5-DW	TACGTGTTGAGAATTAATGACCTACACAGAATTTTTAGAGGTTAAGCAAA**TGTGTAGGCTGGAGCTGCTTCG**
Del-STM0277-3-DW	CCACTTATGCTGAAAGTAACTAATATTAACCATTTCACGGCAGTATCCAT**CATATGAATATCCTCCTTAGTTC**
TssB-sfGFP-5	GCGCCGAAATCGGCCGCTACCCAGCAAGATGTGTCAGCGGATAATGAATCAGCGGAA**GCAGCGGCCGGCGGA GGG**
TssB-sfGFP-3	CGTCGGTTGCCTGCATATTACTGTTTGCCATGAAAATTCCTTAAAAATTCGACGTTA**CATATGAATATCCTCCT TAGTTCCTATTCCGAAGTTCC**

Footprint and EMSA	
5-EMSA #1	GTAGCTCAGTTCGCGGTTGTAATACTC
3-EMSA #1	TATCCGTTTCGAACCCCGGCTG
5-EMSA #2[c]	GATGACACCCTTTTTATTATTTTCGTCGTGAATGC
3-EMSA #2[c]	GTGTTATGCCTTGTGACATAAAAATTCATAAAAATAATGC
5-EMSA #3	GTAAACAATCTGTGGAGATTTACCATG
3-EMSA #3	ACAGATTAACTATTCCTGTACAGCTC
5-EMSA #4	GAAAAAGATAAGGCCAAAAATAAAGTGGC
3-EMSA #4	GCATTATATTTCGACTCGCCACC
5-EMSA #5	TGCTGTGGTTGACAATGATTACAATG
3-EMSA #5	AAGAACAGGGTATATTGCTGACAAG
5-EMSA #6	CACCACGCTATTACTCACCACC
3-EMSA #6	GCCGTGCTGTTCACTCATCC

[a] sequence complementary to chromosome underlined.
[b] sequence complementary to pKD4 or pKD4-sfGFP plasmid in bold.
[c] oligonucleotides used for the DNase I footprint experiments.

Supplemental Table S2. DNA fragments and Oligonucleotides used for *in vitro* H-NS binding and DNaseI footprint experiments.

Fragment #	STM gene # [a]	Length (in bp)	Location [b]	Oligonucleotides
1	*STM0268/269*	250	308562	5-EMSA#1 / 3-EMSA#1
2[c]	*STM0271/272*	273	310921	5-EMSA#2 / 3-EMSA#2
3	*STM0278/279*	251	318370	5-EMSA#3 / 3-EMSA#3
4	*STM0284/285*	250	323615	5-EMSA#4 / 3-EMSA#4
5	*STM0288/289*	252	329514	5-EMSA#5 / 3-EMSA#5
6	*STM0272*	250	313365	5-EMSA#6 / 3-EMSA#6

[a] When the fragment overlaps with two coding sequences, both STM numbers are indicated.
[b] Location in the *S. enterica* Typhiumurium LT2 genome (Genebank ID: AE006468.1) (bp from origin, the number is the 5' base of the fragment).
[c] This fragment was used for the DNase I footprint experiments.

Annexe 2: Dissection of the TssB-TssC interface during type VI secretion sheath complex formation

OPEN ACCESS Freely available online

PLOS ONE

Dissection of the TssB-TssC Interface during Type VI Secretion Sheath Complex Formation

Xiang Y. Zhang[1], Yannick R. Brunet[1], Laureen Logger[1], Badreddine Douzi[2], Christian Cambillau[2], Laure Journet[1], Eric Cascales[1]*

1 Laboratoire d'Ingénierie des Systèmes Macromoléculaires (LISM, UMR 7255), Institut de Microbiologie de la Méditerranée (IMM), Centre National de la Recherche Scientifique (CNRS), Aix-Marseille Université, Marseille, France, **2** Architecture et Fonction des Macromolécules Biologiques (AFMB, UMR 6098), Centre National de la Recherche Scientifique (CNRS), Aix-Marseille Université, Marseille, France

Abstract

The Type VI secretion system (T6SS) is a versatile machine that delivers toxins into either eukaryotic or bacterial cells. At a molecular level, the T6SS is composed of a membrane complex that anchors a long cytoplasmic tubular structure to the cell envelope. This structure is thought to resemble the tail of contractile bacteriophages. It is composed of the Hcp protein that assembles into hexameric rings stacked onto each other to form a tube similar to the phage tail tube. This tube is proposed to be wrapped by a structure called the sheath, composed of two proteins, TssB and TssC. It has been shown using fluorescence microscopy that the TssB and TssC proteins assemble into a tubular structure that cycles between long and short conformations suggesting that, similarly to the bacteriophage sheath, the T6SS sheath undergoes elongation and contraction events. The TssB and TssC proteins have been shown to interact and a specific α-helix of TssB is required for this interaction. Here, we confirm that the TssB and TssC proteins interact in enteroaggregative *E. coli*. We further show that this interaction requires the N-terminal region of TssC and the conserved α-helix of TssB. Using site-directed mutagenesis coupled to phenotypic analyses, we demonstrate that an hydrophobic motif located in the N-terminal region of this helix is required for interaction with TssC, sheath assembly and T6SS function.

Citation: Zhang XY, Brunet YR, Logger L, Douzi B, Cambillau C, et al. (2013) Dissection of the TssB-TssC Interface during Type VI Secretion Sheath Complex Formation. PLoS ONE 8(11): e81074. doi:10.1371/journal.pone.0081074

Editor: Janakiram Seshu, The University of Texas at San Antonio, United States of America

Received July 16, 2013; **Accepted** October 9, 2013; **Published** November 25, 2013

Funding: Work in E.C. laboratory is supported by the Centre National de la Recherche Scientifique (CNRS), the Aix-Marseille Université and a grant from the Agence Nationale de la Recherche (ANR-10-JCJC- 1303-03) to E.C. Work in C.C. laboratory is supported by the CNRS, the Aix-Marseille Université, the Plateforme Technologique de Recherche en Sciences Biologiques (IBiSA) and a grant from the Fondation pour la Recherche Médicale (FRM DEQ2011-0421282). X.Y.Z. was supported by the ANR-10-JCJC-1303-03 grant, Y.R.B by a doctoral fellowship from the French Ministère de la Recherche, and B.D. by the FRM-DEQ2011-0421282 grant. The funders had no role in study design, data collection and analysis, decision to publish, or preparation of the manuscript.

Competing Interests: Please note that Eric Cascales is a PLOS ONE Academic Editor. This does not alter the authors' adherence to all the PLOS ONE policies on sharing data and material.

* E-mail: *cascales@imm.cnrs.fr

Introduction

The Type VI secretion system (T6SS) is a widely distributed secretion system in proteobacteria [1–3]. Initially identified as a system allowing *Vibrio cholerae* to resist predation by amoeba, recent data have demonstrated that it allows virulence towards eukaryotic host cells and/or competition towards neighbouring bacteria [4–13]. Among the effector domains delivered into eukaryotic host cells, the best characterized is the C-terminal domain of the VgrG protein of *V. cholerae*, that cross-links G-actin hence abrogating cytoskeleton rearrangements and dynamics [14–16]. T6SS effectors delivered into bacterial cells have been shown to bear peptidoglycan hydrolysis or phospholipase activities [6,17–24]. At a molecular level, the T6SS is composed of a membrane complex comprising four essential components, the TssL and TssM inner membrane proteins, the TssK cytoplasmic protein and the TssJ outer membrane lipoprotein [25–33]. This membrane complex serves as anchor for a cytoplasmic tubular structure that is structurally and functionally similar to the tails of contractile bacteriophages [34–37]. This tubular structure is composed of at least 5 components that share similarities with bacteriophage subunits. The tails of contractile bacteriophages are composed of an internal tube that polymerizes onto a baseplate composed of six wedges and of the hub complex – or cell-puncturing device [38,39]. This internal tube is wrapped by a sheath structure that contracts upon attachment allowing to propel the internal tube towards the host cell [39]. The Hcp protein shares its fold with that of gpV, the tail tube protein of bacteriophage λ [40,41] whereas the VgrG protein assemble into a homotrimeric structure resembling the trimeric gp27-gp5 hub complex of bacteriophage T4 [14,35,42,43]. TssE is structurally similar to gp25, a component of the baseplate wedges [1,44]. Finally, TssB and TssC assemble into tubular structures with cogwheel patterns resembling the bacteriophage contractile sheath [45,46]. Indeed, cryo-electron tomography analyses showed that this structure exists either in an extended and thin conformation or in a short but wider conformation [47,48]. Fluorescence microscopy experiments further showed that these tubular structures are dynamic and oscillate between long and short conformations before being disassembled [13,47–49]. This mechanism is reminiscent of the bacteriophage sheath, which undergoes a contraction event when the viral particle attaches on host cell. Based on the homologies between the bacteriophage tail and several T6SS components, it is thought that the cytoplasmic tubular structure is composed of an

internal tube formed of hexamers of the Hcp protein stacked onto each other and wrapped by the TssB and TssC subunits that assemble into a sheath. Upon contact with a target cell, the sheath will contract, propelling the Hcp tube terminated by the VgrG protein towards the target cell [34–36]. It has been recently shown that contraction of the T6SS sheath coincides with the lysis of the target bacterial cell [13]. Finally, sheath disassembly is catalysed by ClpV, a specialized ATPase associated with the T6SS [45,47–50]. ClpV interacts with an α-helix of TssC after contraction and is thought to either recycle the TssB and TssC proteins for a new round of assembly or target both proteins to degradation [48,51]. The interaction between the TssB and TssC subunits has been demonstrated in several microorganisms including *Francisella tularensis*, *Vibrio cholerae*, *Burkholderia cenocepacia*, *Yersinia pseudotuberculosis*, *Salmonella enterica* Typhimurium, and *Pseudomonas aeruginosa* [45,46,52–54]. The N-terminal 212 amino-acids of TssC are required for the TssB-TssC interaction in *B. cenocepacia* and in *P. aeruginosa* [46,54] while an α-helix located between residues 100–130 of TssB are necessary in *F. tularensis*, *V. cholerae* and *P. aeruginosa* [52,55]. Here, we confirm the interaction between the TssB and TssC proteins encoded by the *sci-1* T6SS gene cluster of enteroaggregative *Escherichia coli* (EAEC) and that the N-terminal region of TssC and the α-helix of TssB are required for the interaction. Finally, we dissect the role of α-helix residues and demonstrate that an hydrophobic side of the helix located in its N-terminal region is necessary for the TssB-TssC interaction, sheath assembly and T6SS function.

Results

TssB interacts with the N-terminal domain of TssC

The TssB and TssC proteins assemble into a sheath structure that has been proposed to wrap an internal tube constituted of stacked Hcp hexamers. The interaction between these two proteins has been demonstrated in a number of bacterial strains including *V. cholerae*, *S. enterica* Typhimurium, *Y. pseudotuberculosis*, *F. tularensis*, *P. aeruginosa* and *B. cenocepacia* [44,45,51–53]. In agreement with these previous studies, we showed that TssB1 (accession numbers: EC042_4524; YP_006098801) and TssC1 (accession numbers: EC042_4525; YP_006098802), two proteins encoded within the *sci-1* T6SS gene cluster in enteroaggregative *E. coli* interact in a bacterial two-hybrid assay (Fig. 1A). We also observed that TssB1 and TssC1 oligomerize, as TssB1/TssB1 and TssC1/TssC1 combinations activated the expression of the reporter gene (Fig. 1A). Regarding TssC proteins, it has been shown in *P. aeruginosa* and *B. cenocepacia* that the N-terminal fragment comprising the first 212 amino-acids were sufficient for the interaction with TssB [46,54]. HHPred and Phyre domain analyses of TssC1 suggested that it is composed of two domains, including an N-terminal region of 384 amino-acids (residues 1–384) and a C-terminal region of 130 amino-acids (residues 385–514). We generated constructions to test the interaction between TssB1 and the N-terminal (1-384) or C-terminal (385–514) domains of TssC1. As shown in Fig. 1B, the N-terminal region of TssC1 was sufficient to interact with TssB1. Interestingly, we also noted that both the N- and C-terminal domains oligomerizes. However, no interaction between the N-terminal and C-terminal domains of TssC1 was detected (Fig. 1B).

An α-helix of TssB is required for T6SS function, TssC interaction but not for self-interaction

In *Francisella*, an α-helix of the TssB homologue IglA, located between residues 103 and 122, has been shown to be essential for the function of the FPI-encoded T6SS [52]. Yeast two-hybrid experiments further demonstrated that this region is required for efficient interaction with IglB, the *F. tularensis* homologue of TssC [52]. The mode of recognition between IglA and IglB has been shown to be conserved as the interactions between the *P. aeruginosa* HSI-3, *Y. pseudotuberculosis*, *V. cholerae* and uropathogenic *E. coli* TssB and TssC proteins require this α-helix [52,55]. Our results show that this is indeed conserved in EAEC, as deletion of the helix residues located between residues E104 and L131 of TssB1 abolishes the ability of the Sci-1 T6SS to release the Hcp1 protein (Fig. 2A) and to interact with TssC1 (Fig. 2B). However, bacterial two-hybrid experiments showed that deletion of this α-helix has no impact on TssB oligomerization (Fig. 2B).

The hydrophobic face of the α-helix is required for TssC interaction and assembly of the sheath-like structure

The sequence of the α-helix of the EAEC TssB1 protein facilitating its interaction with TssC1 is shown in Fig. 3A. Interestingly, a projection of this α-helix (Fig. 3B, 3C and 3D) showed that the N-terminal region presents an amphipathic character as it comprises both a hydrophobic side (Val-106, Ile-110, Leu-113 and Leu-117) and a polar/charged side (Glu-104, Gln-105, Arg-108, Gln-109, Arg-112, Arg-120). Finally, one face of the C-terminal region of the helix is rich in leucine residues (Leu-122, Leu-123, Leu-126, Leu-130) resembling a leucine-zipper motif (Fig. 3B, 3C and 3D). To better understand the mode of binding between the TssB and TssC proteins, we engineered TssB1 variants in which the hydrophobic, polar/charged and leucine motifs were substituted by tryptophan residues (the residues targeted in this study are highlighted in colour in Fig. 3A-D). Tryptophan-scanning mutagenesis is usually used to test interactions between α-helices as tryptophan residues do not disrupt formation of α-helices but induces a steric hindrance abolishing protein-protein contacts [56,57]. Mutations within the leucine-rich motif (L123W-L130W, called LL) had no effect on Sci-1 T6SS function and on TssB1-TssC1 interaction as shown by Hcp release (Fig. 3E) and two-hybrid (Fig. 3F) assays. Interestingly, while substitution of the polar/charged motif (R108W-R112W, called RR) had no effect on TssB1-TssC1 interaction, the function of the T6SS was abrogated, suggesting that these mutations may affect interactions with other partners or proper folding of TssB1. Finally, mutations within the hydrophobic motif (V106W-I110W-L117W) abolished both the release of Hcp and the interaction with TssC1 (Fig. 3E and 3F). We further dissected the effect of the hydrophobic motifs by generating double and single substitutions (Fig. 4). All the double substitutions within the hydrophobic faceabrogated T6SS function and TssB1-TssC1 interaction. Regarding the single substitutions, mutation of Val-106 had no effect while mutations of Ile-110 and Leu-117 abolished T6SS function (Fig. 4A) by decreasing TssB1 binding to TssC1 (Fig. 4B). It is worth noting that all the TssB1 variants used in this study accumulated at levels comparable to the wild-type TssB1 protein (data not shown).

Finally, we wondered whether disruption of the TssB-TssC interaction impacts sheath assembly. Fluorescence microscopy approaches have recently been developed to follow the assembly of TssBC sheath structures by fusing TssB to the superfolder Green Fluorescent Protein (sf-GFP) [13,33,47–50]. In Δ*tssB1* cells producing TssB1-sfGFP, the fusion protein assembles into tubular structures that undergo cycles of assembly, contraction and disassembly (Fig. 5A). These structures are not visible in Δ*tssBC1* cells (Fig. 5A), in agreement with the fact that these tubular structures are composed of both TssB and TssC proteins [45,46]. However, when the overall fluorescence levels of Δ*tssB1* or Δ*tssBC1* cells producing TssB1-sfGFP were measured, we observed

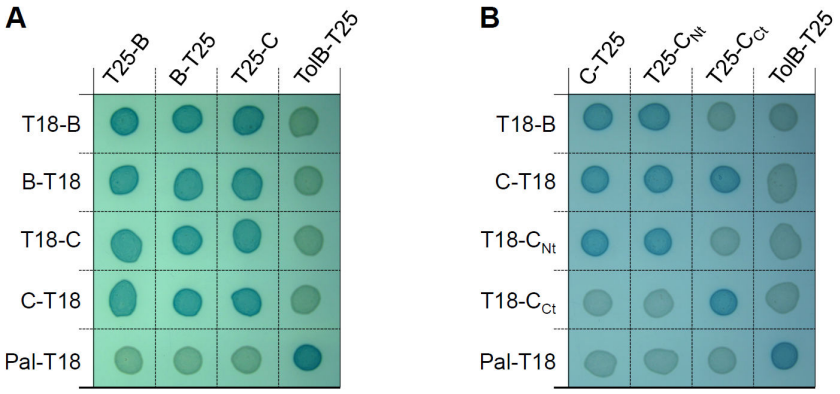

Figure 1. TssB1 interacts with the N-terminal domain of TssC1. BTH101 reporter cells carrying pairs of plasmids producing the indicated T6SS proteins or domains (B, TssB1; C, TssC1; C_{Nt}, N-terminal domain of TssC1; C_{Ct}, C-terminal domain of TssC1) fused to the T18 or T25 domain of the *Bordetella* adenylate cyclase were spotted on X-Gal indicator LB agar plates. Controls include T18 and T25 fusions to TolB and Pal, two proteins that interact but unrelated to the T6SS.
doi:10.1371/journal.pone.0081074.g001

that Δ*tssBC1* cells displayed 6–8% of fluorescence compared to Δ*tssB1* cells, suggesting that TssB1-sfGFP is less stable in absence of TssC1. When TssB1-sfGFP variants bearing single substitutions within the polar/charged or leucine-rich motif were produced in Δ*tssB1* cells, dynamic structures oscillating between extended and contracted conformations were observed, indicating a functional T6SS (Fig. 5B). By contrast, mutations of the Ile-110 or Leu-117 residue led to a diffuse fluorescence in the cell body without any identifiable tubular structures, demonstrating that disruption of the TssB-TssC interaction prevents formation of T6SS sheaths (Fig. 5B).

Discussion

The portion of the T6SS related to the bacteriophage tail is composed of an internal tube comprising hexameric rings of Hcp stacked onto each other and wrapped into a structure formed by the TssB and TssC components. The assembly of this structure oscillates between elongated and contracted conformations and is thought to be similar to the mechanism of action of bacteriophage contractile sheaths. It has been therefore proposed that conformational changes in the TssB and TssC proteins induce a large modification in this structure leading to its contraction and allowing propelling of the internal tube towards the exterior [34,35,43,45,46]. The internal tube is tipped by the VgrG protein that acts as a cell-puncturing device to perforate the host cell membrane allowing delivery of effector domains or proteins [34,36,37]. In this work, we focussed our attention on the TssB1 and TssC1 proteins encoded within the *sci-1* gene cluster of enteroaggregative *E. coli*.

Using bacterial two-hybrid experiments, we showed that (i) TssB1 interacts with itself, (ii) TssC1 interacts with itself, and (iii) TssB1 and TssC1 interact. The self-interaction of the TssB and TssC components is in agreement with the formation of long structures that should comprise hundreds of TssB and TssC molecules. We also showed that the N-terminal region of TssC1 and the C-terminal region of TssC1 self-interact. However, we did not detect interaction between the N-terminal and C-terminal regions of TssC1, suggesting that TssC1 oligomeric complex formation is driven by N-terminal/N-terminal and C-terminal/C-terminal interactions. We also showed that the N-terminal domain of TssC1 is sufficient for its interaction with TssB1. The TssB-TssC interaction was previously demonstrated in numerous studies

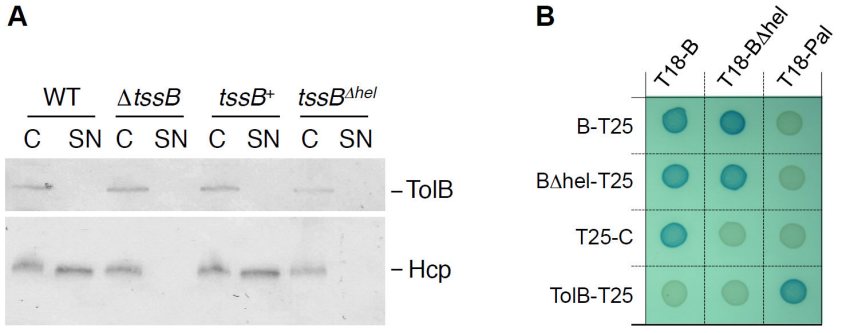

Figure 2. The α-helix located between residues 104 and 130 of TssB1 is required for T6SS function and interaction with TssC1. (A) Hcp release assay. Hcp_{FLAG} release was assessed by separating whole cells (C) and culture supernatant (SN) fractions from 2×10^9 wild-type (WT), Δ*tssB1* (Δ*tssB*) cells or Δ*tssB1* cells producing TssB1 (*tssB*$^+$) or TssB1 deleted of the α-helix 104-130 (*tssB*Δ^{hel}). Proteins were separated by 12.5%-acrylamide SDS-PAGE and Hcp was immunodetected using anti-FLAG monoclonal antibody (lower panel). The periplasmic TolB protein (immunodetected using an anti-TolB polyclonal antibodies, upper panel) was used as a marker to verify that no lysis occured. (B) Bacterial two-hybrid assay. BTH101 reporter cells carrying pairs of plasmids producing the indicated T6SS proteins (B, TssB1; BΔhel, TssB1 deleted of the α-helix; C1, TssC1) fused to the T18 or T25 domain of the *Bordetella* adenylate cyclase were spotted on X-Gal indicator LB agar plates.
doi:10.1371/journal.pone.0081074.g002

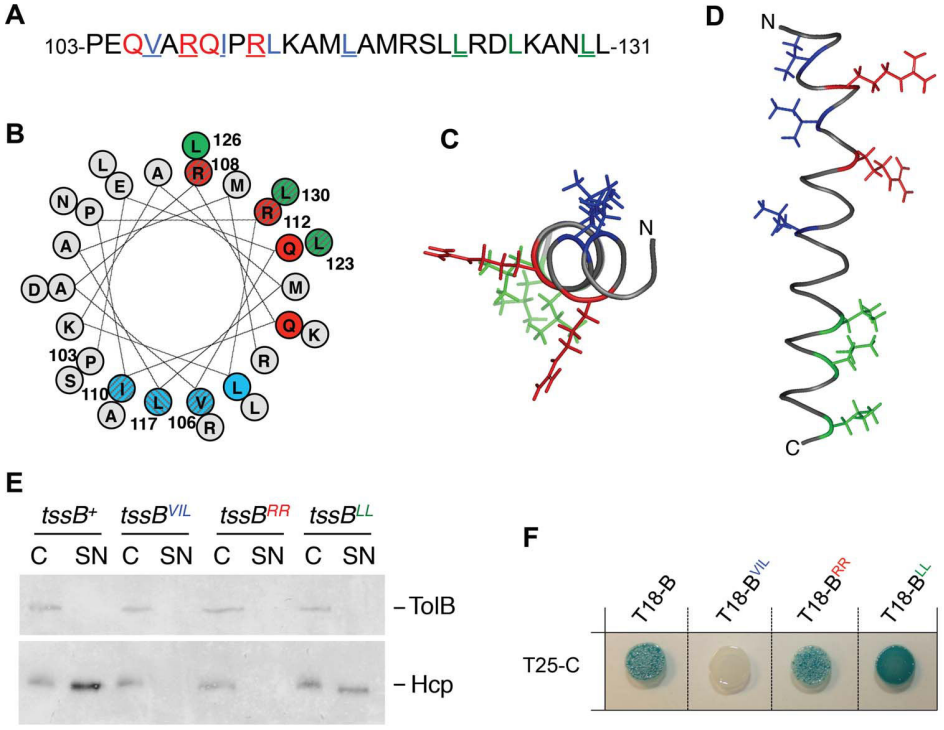

Figure 3. The hydrophobic motif of the TssB1 α-helix is required for T6SS function and interaction with TssC1. Amino-acid sequence (A) and helical wheel projection (B) of the TssB1 α-helix (from residue Pro-103 to residue Leu-131). The different motifs described in this study are highlighted in different colours: blue, N-terminal hydrophobic; red, polar/charged; green, leucine-rich. The residues of these motifs mutagenized in this study are underlined (A) or striped (B). Top-view (C) and side-view (D) projections of the TssB1 α-helix. The targeted residues are colored as in panel (A). Top- and side-views have been modelled using PyMOL v0.99. (E) Hcp release assay. Hcp_{FLAG} release was assessed by separating whole cells (C) and culture supernatant (SN) fractions from 2×10^9 Δ*tssB1* cells producing TssB1 (*tssB*$^+$) or TssB1 bearing substitutions within the hydrophobic (*tssB*^{VIL}), the polar/charged (*tssB*^{RR}) or the leucin-rich (*tssB*^{LL}) motif. Proteins were separated by 12.5%-acrylamide SDS-PAGE and Hcp and TolB were immunodetected using anti-FLAG monoclonal (lower panel) and anti-TolB polyclonal (upper panel) antibodies. (F) Bacterial two-hybrid assay. BTH101 reporter cells producing the T25 domain of the *Bordetella* adenylate cyclase fused to TssC1 (T25-C) and the T18 domain fused to TssB1 (T18-B) or TssB1 variants bearing substitutions within the hydrophobic (T18-B^{VIL}), the polar/charged (T18-B^{RR}) or the leucin-rich (T18-B^{LL}) motif were spotted on X-Gal indicator LB agar plates.
doi:10.1371/journal.pone.0081074.g003

[45,46,52–54] and the requirement of the N-terminal domain of TssC for the interaction was evidenced in *B. cenocepacia* and *P. aeruginosa* [46,54]. The interaction between TssB and TssC has been shown to stabilize both proteins [45,46,52,55]. Interestingly, our fluorescence microscopy experiments showed that the level of fluorescence of Δ*tssB1C1* cells producing TssB1-sfGFP is 6–8% of the fluorescence in Δ*tssB1* cells, confirming that TssB-sfGFP is stabilized by the presence of TssC.

The TssB1 protein of EAEC is composed of 165 amino-acids. Secondary structure predictions showed that it contains an α-helix between residues Pro-103 and Leu-131. This α-helix has been previously shown to be essential for T6SS function and TssB-TssC interaction in *F. tularensis* and *V. cholerae* [52,55]. Interestingly, the authors of this study also showed that this α-helix is essential for TssB-TssC interaction in several microorganisms including *V. cholerae*, *Y. pseudotuberculosis*, *S. enterica* Typhimurium, uropathogenic *E. coli* and *P. aeruginosa*, suggesting that the mode of binding of TssB to TssC is conserved [52]. We obtained similar results in enteroaggregative *E. coli*: deletion of this conserved α-helix causes disruption of the TssB1-TssC1 interaction and abolishes T6SS function as shown by Hcp release assay. When projected on a helical wheel, we observed that this α-helix has a strong amphipathic character in its N-terminal region. Indeed, one face of the helix is essentially constituted of hydrophobic residues (Val, Leu, Ile) while the opposite face is composed of polar or positively charged residues (Arg, Gln). The charge partition in the C-terminal region of the helix is better balanced but we observed a leucine-rich face, on the same side that the polar/charged motif. Using site-directed mutagenesis, we substituted residues within each of these motifs. Our analyses highlighted the importance of the N-terminal hydrophobic motif. Mutation of the three Val-106, Ile-110 and Leu-117 residues showed that this motif is required for TssB1-TssC1 interaction, sheath assembly and T6SS function. Single and double substitutions further showed that the Ile-110 and Leu-117 residues have a more important contribution within this motif. Our results also indicated that substitution of the arginine-rich motif within the conserved α-helix does not prevent formation of the TssB1-TssC1 complex (Fig. 3F); however, the T6SS is not functional as shown by Hcp release assay (Fig. 3E). This suggests that mutation of this motif may disrupt interaction of TssB1 with additional partners, yet to be identified, or that it prevents proper folding of TssB1. Indeed, fluorescence microscopy experiments showed that mutation of these two arginine residues abolishes sheath assembly (data not shown). However, single substitutions had no effect on sheath assembly and on T6SS function. Interestingly, while preparing this manuscript, Bröms et al. published a study where they showed that a hydrophobic motif located in the same region of the *V. cholerae* TssB α-helix is required

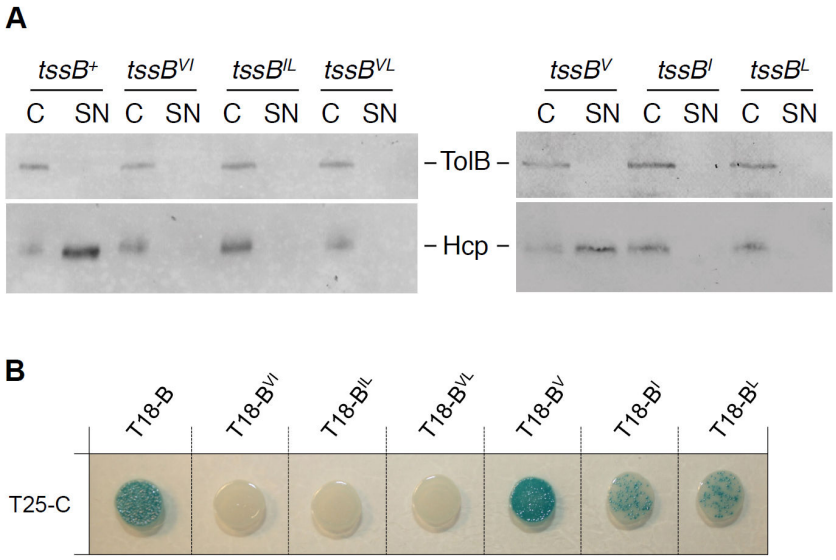

Figure 4. Mutagenesis study of the hydrophobic motif of the TssB1 α-helix. (A) Hcp release assay. Hcp_{FLAG} release was assessed by separating whole cells (C) and culture supernatant (SN) fractions from 2×10^9 Δ*tssB1* cells producing TssB1 (*tssB*$^{+}$) or TssB1 bearing double or single substitutions within the hydrophobic motif (*tssB*^{VI}, V106W-I110W; *tssB*^{IL}, I110W-L117W; *tssB*^{VL}, V106W-L117W; *tssB*^{V}, V106W; *tssB*^{I}, I110W; *tssB*^{L}, L117W). Proteins were separated by 12.5%-acrylamide SDS-PAGE and Hcp and TolB were immunodetected using anti-FLAG monoclonal (lower panel) and anti-TolB polyclonal (upper panel) antibodies. (B) Bacterial two-hybrid assay. BTH101 reporter cells producing the T25 domain of the *Bordetella* adenylate cyclase fused to TssC1 (T25-C) and the T18 domain fused to TssB1 (T18-B) or TssB1 variants bearing substitutions within the hydrophobic motif (T18-B^{VI}, V106W-I110W; T18-B^{IL}, I110W-L117W; T18-B^{VL}, V106W-L117W; T18-B^{V}, V106W; T18-B^{I}, I110W; T18-B^{L}, L117W) were spotted on X-Gal indicator LB agar plates.
doi:10.1371/journal.pone.0081074.g004

for proper interaction with TssC [55]. The results from this study and from the work described here showed that identical TssB motifs are required to functionally interact with TssC in *V. cholerae* and EAEC. We therefore hypothesize that the mode of binding of TssB to TssC is similar in T6SSs. However, Lossi et al. noted that the TssB and TssC proteins encoded by the *P. aeruginosa* HSI-1 T6SS gene cluster interact but are not able to interact with homologues encoded by a second T6SS gene cluster present on the chromosome [46]. One can hypothesize that the hydrophobic motif of the α-helix is the primary determinant for formation of the TssB-TssC complex but that additional determinants might control the proper and specific assembly of the sheath when several T6SS are produced at the same time. Further studies are required to better understand how TssB proteins identify their cognate partners.

Experimental Procedures

Bacterial strains, media and chemicals

Escherichia coli DH5α (New England Biolabs) was used for cloning procedures, BTH101 [58] for bacterial two-hybrid assays. Hcp release and fluorescence microscopy have been performed into the enteroaggregative *E. coli* strain 17-2. With the exception of the bacterial two-hybrid assay (at 30°C), cells were grown in Luria broth (LB) at 37°C. Plasmids were maintained by addition of ampicillin (100 µg/mL), chloramphenicol (40 µg/mL) or kanamycin (50 µg/mL). Gene expression was induced by 0.5 mM isopropyl-β-thio-galactoside (IPTG) or 0.01% arabinose. For the Hcp release assay, expression of the *sci-1* gene cluster was induced by addition of the iron chelator 2,2′-dipyridyl (125 µM final concentration) 30 minutes prior harvesting the cells [59]. For fluorescence microscopy experiments, cells were grown in minimal M9 medium supplemented with casaminoacids, glucose 0.4% and 10% of LB.

Strain construction

Construction of the Δ*tssB1* and Δ*tssBC1* mutant strains. The *tssB1* gene was deleted into the enteroaggregative *E. coli* 17-2 strain using a modified one-step inactivation procedure [60] as previously described [25] using plasmid pKOBEG [61]. PCR products to be elctroporated were obtained using oligonucleotides DEL-4524-5/DW (5′-*GGAGGCATCTGCGGTGATGGAACCCCT-GAGATGCAGGTTTCACAGGAGAGAGCC*TGTGTAGGCTG-GAGCTGCTTCG) and DEL-4524-3/DW (5′-*TTCTTTTCTTTCTGTACAGACATCAGCATTTTCTCTCG-TAATCCGTTAAA*CATATGAATATCCTCCTTAGTTCC) carrying 50- nucleotide extensions homologous to regions adjacent to *tssB1* (in italics). Kanamycin resistant clones were selected and verified by colony-PCR. The kanamycin cassette was then excised using plasmid pCP20 [60]. The deletion of *tssB1* was confirmed by colony-PCR. Construction of the Δ*tssBC1* strain was done identically, using oligonucleotides DEL-4524-5/DW and DEL-4525-3/DW (5′-*GCCCCGTCTTCCCATAATGGGCGA-TAAATCTTCATTTCCCGACACCTGCC*CATATGAA-TATCCTCCTTAGTTCC).

Plasmid construction

Polymerase Chain Reactions (PCR) were performed using a Biometra thermocycler using Pfu Turbo DNA polymerase (Agilent Technology). Restriction enzymes were purchased from NewEngland Biolabs and used according to the manufacturer's instructions. Custom oligonucleotides were synthesized by Sigma Aldrich. Enteroaggregative *E. coli* 17-2 chromosomal DNA was used as a template for all PCRs. *E. coli* strain DH5α was used for cloning procedures. All the plasmids have been constructed by restriction-

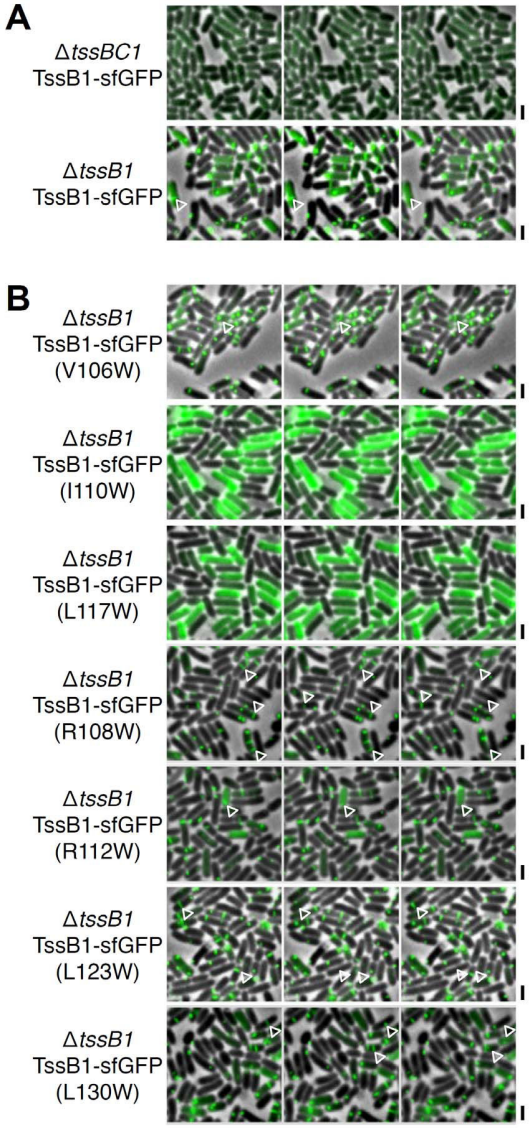

Figure 5. The hydrophobic motif of the TssB1 α-helix is required for T6SS sheath assembly. Time-lapse fluorescence microscopy recordings showing sheath dynamics in Δ*tssBC1* (Δ*tssB1*-Δ*tssC1*) or Δ*tssB1* cells producing TssB1-sfGFP (TssB1) (A) or TssB1-sfGFP bearing the indicated substitutions (B). Individual images were taken every 30 sec. Assembly and contraction events are indicated by the white open triangles. Scale bars are 2 µm.
doi:10.1371/journal.pone.0081074.g005

free cloning [62] as previously described [27]. Briefly, genes of interest were amplified with oligonucleotides introducing extensions annealing to the target vector. The double-stranded product of the first PCR has then been used as oligonucleotides for a second PCR using the target vector as template. Constructions of the bacterial two-hybrid vectors encoding TssB1 and TssC1 fusion proteins and of the pBAD33-TssB1-VSVG and pBAD-TssB1-sfGFP plasmids have been previously described [33]. Bacterial two-hybrid vectors encoding T18 and T25-TssC$_{Nt}$ fusions were constructed by insertion of a premature stop codon into T18-TssC and T25-TssC by site directed mutagenesis using oligonucleotides 5′- GAACCGGGATTATGCCTGCTTCTTCTCTTAAGC-TAACTCCGCCCAGAAACCGGCG and CGCCGGTTTCTGGGCGGAGTTAGCTTAAGAGAA-GAAGCAGGCATAATCCCGGTTC (stop codon underlined). Bacterial two-hybrid vectors encoding T18- and T25-TssC$_{Ct}$ fusions were obtained by restriction-free cloning using oligonucleotides CGCCACTGCAGGGATTATAAAGATGACGATGA-CAAGGCTAACTCCGCCCAGAAACCGGCG and CGAGGTCGACGGTATCGATAAGCTTGATATC-GAATTCTAGTTACGCTTTTGCCTTCGGCATCTGC-GAAACCAGTG (for T18) and GGCGGGCTGCAGATTA-TAAAGATGACGATGACAAGGCTAACTCCGCCCA-GAAACCGGCG and CGAGGTCGACGGTATCGATAAGCTTGATATC-GAATTCTAGTTACGCTTTTGCCTTCGGCATCTGC-GAAACCAGTG (for T25). Substitutions have been introduced by quick change site-directed mutagenesis using complementary pairs of oligonucleotides (listed in Table S1). All constructs have been verified by restriction analyses and DNA sequencing (Eurofins, MWG).

Bacterial Two-Hybrid Assay

The adenylate cyclase-based bacterial two- hybrid technique [58] was used as previously published [63]. Briefly, pairs of proteins to be tested were fused to the isolated T18 and T25 catalytic domains of the *Bordetella* adenylate cyclase. After transformation of the two plasmids producing the fusion proteins into the reporter BTH101 strain, plates were incubated at 30°C for 48 hours. Three independent colonies for each transformation were inoculated into 600 µl of LB medium supplemented with ampicillin, kanamycin and IPTG (0.5 mM). After overnight growth at 30°C. 10 µl of each culture were dropped onto MacConkey and LB supplemented with Bromo-Chloro-Indolyl-Galactopyrannoside (X-Gal) plates and incubated for 16 hours at 30 °C. The experiments were done at least in triplicate and a representative result on LB-X-Gal plate is shown.

Hcp release assay

The presence of Hcp in culture supernatants has been tested as previously described [25]. Briefly, 2×10^9 cells producing FLAG epitope-tagged Hcp were harvested and collected by centrifugation at 2,000×*g* for 5 min. The supernatant fraction was then subjected to a second low-speed centrifugation and then at 16,000×*g* for 15 min. The supernatant was then filtered on sterile polyester membranes with a pore size of 0.2 µm (membrex 25 PET, membraPure GmbH) before precipitation with trichloroacetic acid (TCA, 15% final concentration). Cells and precipitated supernatants were then resuspended in loading buffer and analyzed by SDS-PAGE and immunoblotting with the anti-FLAG antibody. As control for lysis, Western blot were immunostained with antibodies raised against the periplasmic TolB protein.

Fluorescence microscopy and image treatment

Fluorescence microscopy experiments to follow T6SS sheath assembly have been performed as previously described [13,33]. Briefly, bacterial cells carrying plasmid pBAD33-TssB1–sfGFP (encoding the TssB1 protein fused to a C-terminal superfolder Green Fluorescent Protein, [33]) or derivatives were grown overnight in LB medium and then diluted to an $OD_{600\ nm}$ ~0.05 into M9 minimal medium supplemented with glycerol, casamino acids, chloramphenicol and 10% of LB. When the $OD_{600\ nm}$ reached ~1.0, cells were harvested and washed in phosphate buffered saline (PBS), resuspended in PBS to an $OD_{600\ nm}$ ~50, and spotted on a thin pad of 1.5% agarose in PBS, covered with a cover slip and incubated for one hour at 37°C prior to microscopy acquisition. For each experiment, ten independent

fields were manually defined with a motorized stage (Prior Scientific) and stored (X, Y, Z, PFS-offset) in a custom automation system designed for time-lapse experiments. Fluorescence and phase contrast micrographs were captured every 30 sec. using an automated and inverted epifluorescence TE2000-E-PFS (Nikon, France) microscope equipped with Perfect Focus System (PFS). PFS automatically maintains focus so that the point of interest within a specimen is always kept in sharp focus at all times despite mechanical or thermal perturbations. Images were recorded with a CoolSNAP HQ 2 (Roper Scientific, Roper Scientific SARL, France) and a 100×/1.4 DLL objective. Excitation light was emitted by a 120 W metal halide light. The sfGFP images were recorded by using the ET-GFP filter set (Chroma 49002) using an exposure time of 100–200 ms. Phase contrast and fluorescence were adjusted and merged using ImageJ 1.46j (http://rsb.info.nih.gov/ij/). Fluorescence levels have been measured using a TECAN microplate reader as previously published [11,64].

Miscellaneous

Proteins resuspended in loading buffer were subjected to sodium dodecyl sulphate (SDS)-polyacrylamide gel electrophoresis (PAGE). For detection by immunostaining, proteins were transferred onto nitrocellulose membranes, and immunoblots were probed with primary antibodies, and goat secondary antibodies coupled to alkaline phosphatase, and developed in alkaline buffer in presence of 5-bromo-4-chloro-3-indolylphosphate (BCIP) and nitroblue tetrazolium (NBT). The anti-TolB polyclonal antibodies are from our laboratory collection while the anti-FLAG monoclonal antibody (clone M2, Sigma-Aldrich) and alkaline phosphatase-conjugated goat anti-rabbit and anti-mouse antibodies (Millipore) have been purchased as indicated.

Supporting Information

Table S1 Oligonucleotides used for site-directed mutagenesis.
(DOCX)

Acknowledgments

We thank Tâm Mignot for fluorescence microscopy, the members of the Cascales, Lloubès, Cambillau, Bouveret and Sturgis research groups for helpful discussions, Isabelle Bringer, Annick Brun and Olivier Uderso for technical assistance, and Sacha Touille for encouragements. We also wish to thank the reviewers for their corrections and helpful suggestions.

Author Contributions

Conceived and designed the experiments: XYZ CC LJ EC. Performed the experiments: XYZ YRB LL BD. Analyzed the data: XYZ YRB EC. Contributed reagents/materials/analysis tools: XYZ YRB LL BD CC LJ EC. Wrote the paper: EC.

References

1. Bingle LE, Bailey CM, Pallen MJ (2008) Type VI secretion: a beginner's guide. Curr Opin Microbiol 11: 3–8.
2. Cascales E (2008) The Type VI secretion toolkit. EMBO Rep 9: 735–41.
3. Boyer F, Fichant G, Berthod J, Vandenbrouck Y, Attree I (2009) Dissecting the bacterial type VI secretion system by a genome wide in silico analysis: what can be learned from available microbial genomic resources? BMC Genomics. 10: 104.
4. Pukatzki S, Ma AT, Sturtevant D, Krastins B, Sarracino D, et al. (2006) Identification of a conserved bacterial protein secretion system in Vibrio cholerae using the Dictyostelium host model system. Proc Natl Acad Sci USA. 103: 1528–33.
5. Pukatzki S, McAuley SB, Miyata ST (2009) The type VI secretion system: translocation of effectors and effector-domains. Curr Opin Microbiol. 12: 11–7.
6. Hood RD, Singh P, Hsu F, Güvener T, Carl MA, et al. (2010) A type VI secretion system of Pseudomonas aeruginosa targets a toxin to bacteria. Cell Host Microbe. 7: 25–37.
7. Schwarz S, Hood RD, Mougous JD (2010) What is Type VI secretion doing in all those bugs? Trends Microbiol 18: 531–37.
8. Schwarz S, West TE, Boyer F, Chiang WC, Carl MA, et al. (2010) Burkholderia type VI secretion systems have distinct roles in eukaryotic and bacterial cell interactions. PLoS Pathog 6: e1001068.
9. MacIntyre DL, Miyata ST, Kitaoka M, Pukatzki S (2010) The Vibrio cholerae type VI secretion system displays antimicrobial properties. Proc Natl Acad Sci U S A. 107: 19520–4.
10. Murdoch SL, Trunk K, English G, Fritsch MJ, Pourkarimi E, et al. (2011) The opportunistic pathogen Serratia marcescens utilizes type VI secretion to target bacterial competitors. J Bacteriol. 193: 6057–69.
11. Gueguen E, Cascales E (2013) Promoter swapping unveils the role of the Citrobacter rodentium CTS1 Type VI secretion system in interbacterial competition. Appl Environ Microbiol. 79: 32–8.
12. Basler M, Ho BT, Mekalanos JJ (2013) Tit-for-tat: type VI secretion system counterattack during bacterial cell-cell interactions. Cell. 152: 884–94.
13. Brunet YR, Espinosa L, Harchouni S, Mignot T, Cascales E (2013) Imaging Type VI secretion mediated bacterial killing. Cell Rep. 3: 36–41.
14. Pukatzki S, Ma AT, Revel AT, Sturtevant D, Mekalanos JJ (2007) Type VI secretion system translocates a phage tail spike-like protein into target cells where it cross-links actin. Proc Natl Acad Sci USA 104: 15508–13.
15. Ma AT, McAuley S, Pukatzki S, Mekalanos JJ (2009) Translocation of a Vibrio cholerae type VI secretion effector requires bacterial endocytosis by host cells. Cell Host Microbe. 5: 234–43.
16. Durand E, Derrez E, Audoly G, Spinelli S, Ortiz-Lombardia M, et al. (2012) Crystal structure of the VgrG1 actin cross-linking domain of the Vibrio cholerae Type VI secretion system. J Biol Chem. 287: 38190–9.
17. Russell AB, Hood RD, Bui NK, Leroux M, Vollmer W, et al. (2011) Type Vi Secretion Delivers Bacteriolytic Effectors To Target Cells. NATURE. 475: 343–7.
18. Russell AB, Singh P, Brittnacher M, Bui NK, Hood RD, et al. (2012) A widespread bacterial type VI secretion effector superfamily identified using a heuristic approach. Cell Host Microbe. 11: 538–49.
19. Chou S, Bui NK, Russell AB, Lexa KW, Gardiner TE, et al. (2012) Structure of a peptidoglycan amidase effector targeted to Gram-negative bacteria by the type VI secretion system. Cell Rep. 1: 656–64.
20. Benz J, Sendlmeier C, Barends TR, Meinhart A (2012) Structural insights into the effector-immunity system Tse1/Tsi1 from Pseudomonas aeruginosa. PLoS One. 7: e40453.
21. English G, Trunk K, Rao VA, Srikannathasan V, Hunter WN, et al. (2012) New secreted toxins and immunity proteins encoded within the Type VI secretion system gene cluster of Serratia marcescens.Mol Microbiol. 86: 921–36.
22. Dong TG, Ho BT, Yoder-Himes DR, Mekalanos JJ (2013) Identification of T6SS-dependent effector and immunity proteins by Tn-seq in Vibrio cholerae. Proc Natl Acad Sci U S A. 110: 2623–8.
23. Brooks TM, Unterweger D, Bachmann V, Kostiuk B, Pukatzki S (2013) Lytic activity of the Vibrio cholerae type VI secretion toxin VgrG-3 is inhibited by the antitoxin TsaB. J Biol Chem. 288: 7618–25.
24. Russell AB, LeRoux M, Hathazi K, Agnello DM, Ishikawa T, et al. (2013) Diverse type VI secretion phospholipases are functionally plastic antibacterial effectors. Nature. 496: 508–12.
25. Aschtgen MS, Bernard CS, de Bentzmann S, Lloubes R, Cascales E (2008) SciN is an outer membrane lipoprotein required for type VI secretion in enteroaggregative Escherichia coli. J Bacteriol 190: 7523–31.
26. Ma LS, Lin JS, Lai EM (2009) An IcmF family protein, $ImpL_M$, is an integral inner membrane protein interacting with $ImpK_L$, and its walker a motif is required for type VI secretion system-mediated Hcp secretion in Agrobacterium tumefaciens. J Bacteriol 191: 4316–29.
27. Aschtgen MS, Gavioli M, Dessen A, Lloubes R, Cascales E (2010) The SciZ protein anchors the enteroaggregative Escherichia coli Type VI secretion system to the cell wall. Mol Microbiol 75: 886–99.
28. Aschtgen MS, Thomas MS, Cascales E (2010) Anchoring the type VI secretion system to the peptidoglycan: TssL, TagL, TagP… what else? Virulence 1: 535–40.
29. Felisberto-Rodrigues C, Durand E, Aschtgen MS, Blangy S, Ortiz-Lombardia M, et al. (2011) Towards a structural comprehension of bacterial type VI secretion systems: characterization of the TssJ-TssM complex of an Escherichia coli pathovar. PLoS Pathog. 7: e1002386.
30. Aschtgen MS, Zoued A, Lloubès R, Journet L, Cascales E (2012) The C-tail anchored TssL subunit, an essential protein of the enteroaggregative Escherichia coli Sci-1 Type VI secretion system, is inserted by YidC. Microbiologyopen. 1: 71–82.
31. Durand E, Zoued A, Spinelli S, Watson PJ, Aschtgen MS, et al. (2012) Structural characterization and oligomerization of the TssL protein, a component shared by bacterial type VI and type IVb secretion systems. J Biol Chem. 287: 14157–68.

32. Rao VA, Shepherd SM, English G, Coulthurst SJ, Hunter WN (2011) The structure of Serratia marcescens Lip, a membrane-bound component of the type VI secretion system. Acta Crystallogr D Biol Crystallogr. 67: 1065–72.
33. Zoued A, Durand E, Bebeacua C, Brunet YR, Douzi B, Cambillau C, Cascales E, Journet L (2013) TssK is a trimeric cytoplasmic protein interacting with components of both phage-like and membrane anchoring complexes of the Type VI secretion system. J Biol Chem 288: 27031–41.
34. Bonemann G., Pietrosiuk A., and Mogk A (2010) Tubules and donuts: a type VI secretion story. *Mol. Microbiol.* 76: 815–21
35. Cascales E, Cambillau C (2012) Structural biology of type VI secretion systems. Philos Trans R Soc Lond B Biol Sci. 367: 1102–11.
36. Silverman JM, Brunet YR, Cascales E, Mougous JD (2012) Structure and regulation of the type VI secretion system. Annu Rev Microbiol. 66: 453–72.
37. Coulthurst SJ (2013) The Type VI secretion system - a widespread and versatile cell targeting system. Res Microbiol. 164: 640–54.
38. Leiman PG, Arisaka F, van Raaij MJ, Kostyuchenko VA, Aksyuk AA, et al. (2010) Morphogenesis of the T4 tail and tail fibers. Virol J. 7: 355.
39. Leiman PG, Shneider MM (2012) Contractile tail machines of bacteriophages. Adv Exp Med Biol. 726: 93–114.
40. Mougous JD, Cuff ME, Raunser S, Shen A, Zhou M, et al. (2006) A virulence locus of Pseudomonas aeruginosa encodes a protein secretion apparatus. Science 312: 1526–30.
41. Pell LG, Kanelis V, Donaldson LW, Howell PL, Davidson AR (2009) The phage lambda major tail protein structure reveals a common evolution for long-tailed phages and the type VI bacterial secretion system. Proc Natl Acad Sci USA 106: 4160–65.
42. Kanamaru S, Leiman PG, Kostyuchenko VA, Chipman PR, Mesyanzhinov VV, et al. (2002) Structure of the cell-puncturing device of bacteriophage T4. Nature. 415: 553–7.
43. Leiman PG, Basler M, Ramagopal UA, Bonanno JB, Sauder JM, et al. (2009) Type VI secretion apparatus and phage tail-associated protein complexes share a common evolutionary origin. Proc Natl Acad Sci USA 106: 4154–59.
44. Lossi NS, Dajani R, Freemont P, Filloux A (2011) Structure-function analysis of HsiF, a gp25-like component of the type VI secretion system, in Pseudomonas aeruginosa. Microbiology. 157: 3292–305.
45. Bönemann G, Pietrosiuk A, Diemand A, Zentgraf H, Mogk A (2009) Remodelling of VipA/VipB tubules by ClpV-mediated threading is crucial for type VI protein secretion. EMBO J 28: 315–25.
46. Lossi NS, Manoli E, Forster A, Dajani R, Pape T, et al. (2013) The HsiB1C1 (TssB-TssC) complex of the Pseudomonas aeruginosa type VI secretion system forms a bacteriophage tail sheathlike structure. J. Biol. Chem. 288: 7536–48.
47. Basler M, Pilhofer M, Henderson GP, Jensen GJ, Mekalanos JJ (2012) Type VI secretion requires a dynamic contractile phage tail-like structure. Nature. 483: 182–6.
48. Kapitein N, Bonemann G, Pietrosiuk A, Seyffer F, Hausser I, et al. (2013) ClpV recycles VipA/VipB tubules and prevents non-productive tubule formation to ensure efficient type VI protein secretion. Mol. Microbiol. 87: 1013–1028.
49. Basler M, and Mekalanos JJ (2012) Type 6 secretion dynamics within and between bacterial cells. Science 337: 815.
50. LeRoux M, De Leon JA, Kuwada NJ, Russell AB, Pinto-Santini D, et al. (2012) Quantitative single-cell characterization of bacterial interactions reveals type VI secretion is a double-edged sword. Proc Natl Acad Sci U S A. 109: 19804–9.
51. Pietrosiuk A, Lenherr ED, Falk S, Bonemann G, Kopp J, et al. (2011) Molecular basis for the unique role of the AAA+ chaperone ClpV in type VI protein secretion. J. Biol. Chem. 286: 30010–21.
52. Bröms JE, Lavander M, Sjöstedt A (2009) A conserved alpha-helix essential for a type VI secretion-like system of Francisella tularensis. J Bacteriol. 191: 2431–46.
53. Karna SL, Zogaj X, Barker JR, Seshu J, Dove SL, et al. (2010) A bacterial two-hybrid system that utilizes Gateway cloning for rapid screening of protein-protein interactions. Biotechniques. 49: 831–3.
54. Aubert D, MacDonald DK, Valvano MA (2010) BcsKC is an essential protein for the type VI secretion system activity in Burkholderia cenocepacia that forms an outer membrane complex with BcsLB. J Biol Chem. 285: 35988–98.
55. Bröms JE, Ishikawa T, Wai SN, Sjöstedt A (2013) A functional VipA-VipB interaction is required for the type VI secretion system activity of Vibrio cholerae O1 strain A1552. BMC Microbiol. 13: 96.
56. Sharp LL, Zhou J, Blair DF (1995) Tryptophan-scanning mutagenesis of MotB, an integral membrane protein essential for flagellar rotation in Escherichia coli. Biochemistry. 34: 9166–71.
57. Sharp LL, Zhou J, Blair DF (1995) Features of MotA proton channel structure revealed by tryptophan-scanning mutagenesis. Proc Natl Acad Sci U S A. 92: 7946–50.
58. Karimova G, Pidoux J, Ullmann A, and Ladant D (1998) A bacterial two-hybrid system based on a reconstituted signal transduction pathway. Proc. Natl. Acad. Sci. U.S.A. 95: 5752–56.
59. Brunet YR, Bernard CS, Gavioli M, Lloubès R, Cascales E (2011) An epigenetic switch involving overlapping Fur and DNA methylation optimizes expression of a type VI secretion gene cluster. PLoS Genet. 7: e1002205.
60. Datsenko KA, and Wanner BL (2000) One-step inactivation of chromosomal genes in Escherichia coli K–12 using PCR products. Proc. Natl. Acad. Sci. U.S.A. 97: 6640–45.
61. Chaveroche MK, Ghigo JM, d'Enfert C (2000) A rapid method for efficient gene replacement in the filamentous fungus Aspergillus nidulans. Nucleic Acids Res. 28: E97.
62. van den Ent F, and Lowe J (2006) RF cloning: a restriction-free method for inserting target genes into plasmids. J. Biochem. Biophys. Methods 67: 67–74.
63. Battesti A, Bouveret E (2012) The bacterial two-hybrid system based on adenylate cyclase reconstitution in Escherichia coli. Methods 58: 325–334.
64. Gueguen E, Durand E, Zhang XY, d'Amalric Q, Journet L, et al. (2013) Expression of a *Yersinia pseudotuberculosis* Type VI secretion system is responsive to envelope stresses through the OmpR transcriptional activator. PLoS One. 8: e66615.

Dissection of the TssB-TssC interface during Type VI secretion sheath complex formation.

X. Y. Zhang, Y. R. Brunet, L. Logger, B. Douzi, C. Cambillau, L. Journet, and E. Cascales

Table S1
Oligonucleotides used for site-directed mutagenesis of EAEC TssB1

Helix deletion (amino-acids E104 to L130) [a]

CCGCAATATGAACGATTTCACGCCA*GAT*AACGTGACTTTCCGTAAAGAG
CTCTTTACGGAAAGTCACGTT*ATC*TGGCGTGAAATCGTTCATATTGCGG

Amino-acid substitutions (to tryptophan) [b]

Val-106

CGATTTCACGCCAGAGCAGTGGGCCCGACAGATTCCCCG
CGGGGAATCTGTCGGGCCCACTGCTCTGGCGTGAAATCG

Ile-110

GAGCAGGTCGCCCGACAGTGGCCCCGTCTTAAAGCCATG
CATGGCTTTAAGACGGGGCCACTGTCGGGCGACCTGCTC

Leu-117
CCCGTCTTAAAGCCATGTGGGCCATGCGTAGCCTTC
GAAGGCTACGCATGGCCCACATGGCTTTAAGACGGG

Val-106 & Ile-110

CACGCCAGAGCAGTGGGCCCGACAGTGGCCCCGTCTTAAAGCC
GGCTTTAAGACGGGGCCACTGTCGGGCCCACTGCTCTGGCGTG

Arg-108

GCCAGAGCAGGTCGCCTGGCAGATTCCCCGTCTTAAAG
CTTTAAGACGGGGAATCTGCCAGGCGACCTGCTCTGGC

Arg-112

CGCCCGACAGATTCCCTGGCTTAAAGCCATGCTGGCC
GGCCAGCATGGCTTTAAGCCAGGGAATCTGTCGGGCG

Arg-108 & Arg-112

GAGCAGGTCGCCTGGCAGATTCCCTGGCTTAAAGCCATGCTG
CAGCATGGCTTTAAGCCAGGGAATCTGCCAGGCGACCTGCTC

Leu-123

CTGGCCATGCGTAGCCTTTGGCGGGACCTGAAAGCC
GGCTTTCAGGTCCCGCCAAAGGCTACGCATGGCCAG

Leu-130

GGACCTGAAAGCCAATCTGTGGGATAACGTGACTTTCCG
CGGAAAGTCACGTTATCCCACAGATTGGCTTTCAGGTCC

a Codon upstream the deletion underlined, codon downstream the deletion italicized.
b Mutagenesized codon underlined.

Annexe 3: Structure-function analysis of the C-terminal domain of the type VI secretion TssB tail sheath subunit

Structure-function analysis of the C-terminal domain of the Type VI secretion TssB tail sheath subunit

Badreddine Douzi[1,2,¶], Laureen Logger[3], Silvia Spinelli[1,2], Stéphanie Blangy[1,2,†], Christian Cambillau[1,2*] and Eric Cascales[3*]

[1] Aix-Marseille Université, Architecture et Fonction des Macromolécules Biologiques, UMR 7257, Campus de Luminy, Case 932, 13288 Marseille Cedex 09, France

[2] Centre National de la Recherche Scientifique, Architecture et Fonction des Macromolécules Biologiques, UMR 7257, Campus de Luminy, Case 932, 13288 Marseille Cedex 09, France

[3] Laboratoire d'Ingénierie des Systèmes Macromoléculaires, Institut de Microbiologie de la Méditerranée, CNRS UMR7255, Aix-Marseille Université, 31 Chemin Joseph Aiguier, 13402 Marseille Cedex 20, France

[¶] Current address: Laboratoire d'Ingénierie des Systèmes Macromoléculaires, Institut de Microbiologie de la Méditerranée, CNRS UMR7255, Aix-Marseille Université, 31 Chemin Joseph Aiguier, 13402 Marseille Cedex 20, France

[†] Current address: Institute of Environmental Biology and Biotechnology, CEA CNRS, Aix-Marseille Université, CEA Cadarache, 13018 Saint-Paul-lès-Durance, France

[*] Corresponding authors: cascales@imm.cnrs.fr or cambillau@afmb.univ-mrs.fr

Running head: TssB structure-function analysis

ABSTRACT

The Type VI secretion system (T6SS) is a specialized macromolecular complex dedicated to the delivery of protein toxins into both eukaryotic and bacterial cells. The general mechanism of action of the T6SS is similar to the injection of DNA by contractile bacteriophages. The cytoplasmic portion of the T6SS is evolutionarily, structurally and functionally related to the phage tail complex. It is composed of an inner tube made of stacked Hcp hexameric rings and engulfed within a sheath. This sheath undergoes cycles of extension and contraction, and the current model proposes that the sheath contraction propels the inner tube towards the target cell for effector delivery. The sheath comprises two subunits: TssB and TssC that polymerize under an extended conformation. The cryo-electron microscopy atomic structure of the *Vibrio cholerae* and *Francisella novicida* T6SS contratced sheaths revealed how the TssB and TssC subunits interact. However, the C-terminal region of TssB was not observed in the map. Here, we show that TssB forms trimers and we report the crystal structure of a C-terminal fragment of TssB. This fragment comprises a long helix followed by an helical hairpin which presents charged residues at its surface. Site-directed mutagenesis coupled to functional assay further showed that these charges are required for proper assembly of the sheath.

Competing interests: The authors have declared that no competing interests exist.

INTRODUCTION

The Type VI secretion system (T6SS) is a specialized machine dedicated to the delivery of protein effectors into target cells by a contact-dependent mechanism [1-5]. T6SS gene clusters are widely distributed in Gram-negative proteobacteria with an overrepresentation in the γ phyllum [6-8]. By contrast to other specialized secretion systems, the T6SS is versatile as it can deliver protein effectors in both prokaryotic and eukaryotic cells. In agreement with these functions, T6SS protein effectors that bear broad (nucleases, phospholipases), anti-bacterial-specific (peptidoglycan hydrolases) or anti-host-specific (actin cross-linking) activities have been identified and characterized in the recent years [9-13].

At the molecular level, the T6SS is though to function such as a crossbow. It is composed of two sub-complexes: a cytoplasmic tubular structure anchored to the cell envelope by a membrane complex [3,4,14,15]. The 1.7-MDa membrane complex comprises 10 copies of the TssJ outer membrane lipoprotein in interaction with 10 copies of the TssM-TssL inner membrane heterodimer that shares homologies with the Type IVb secretion system IcmF-IcmH heterodimer [16-23]. By contrast, the cytoplasmic structure is evolutionarily, structurally and functionally homologous to the tail of contractile bacteriophages [2,24,25]. It is composed of a needle formed by the Hcp inner tube tipped by the VgrG/PAAR spike, wrapped by the TssBC contractile sheath and built onto an assembly platform, the baseplate [3,4,15,26-28]. The VgrG protein is structurally similar to the gp27-gp5 phage cell-puncturing device and is therefore considered as the spike of the T6SS [29,30]. The Hcp protein forms hexameric rings that stack on each other in a head-to-tail manner to form the inner tube [26,30,31]. However, the affinity between the Hcp hexamers is rather low, and Hcp tubular structures can only be observed when the edifice is stabilized by inter-hexamer disulphide bonds [26,32,33]. *In vivo*, the TssA protein coordinates the

assembly of the Hcp inner tube with that of a second tubular layer, the sheath, in which the Hcp tube is engulfed [34-36]. Based on the homology with the bacteriophage contractile sheath, a functional model has been proposed in which contraction of the T6SS sheath propels the inner tube tipped with the VgrG/PAAR spike towards the target cell, allowing membrane penetration and effectors delivery [3,24,37]. Indeed, by using electron cryo-tomography, Basler *et al.* showed that the T6SS sheath exists in two distinct conformations, either as long and thin tubes or as short and wide tubes [38]. Further fluorescence microscopy experiments demonstrated that the TssBC sheath is very dynamic: it assembles a ~ 600 nm-long tubular structure in tens of seconds [38-40] that then contracts in less than 5 msec [38]. Contraction of the T6SS sheath coincides with prey cell lysis, a result that supports the model that sheath contraction powers secretion of toxins [39,41,42]. The T6SS sheath is constituted of the TssB (or VipA) and TssC (or VipB) proteins [38,43]. Both TssB and TssC oligomerize, interact with a 1:1 stoichiometry and stabilize each other [43-48]. Protein-protein interaction mapping studies have demonstrated that the TssB-TssC interaction is mediated by the N-terminal 300 amino-acids of TssC and an α-helix within the central region of TssB [45,46,48,49]. Electron micrographs showed that the TssB and TssC proteins spontaneously assemble into tubular structures resembling bacteriophage polysheath, with cogwheel cross-sections comprising 12 or 13 paddles [43,46,50]. More recently, cryo-electron microscopy analyses revealed the atomic structure of the *V. cholerae* and *Francisella novicida* contracted sheaths [51,52]. As observed for the bacteriophage tail sheath, the TssBC contracted sheaths present cylindrical structures with a 250-Å external diameter and a 120-Å internal diameter. They are organized into an helical fashion with an axial C6 rotational symmetry. The cylinder is built by the packing of discs in which each disc comprises six TssBC heterodimers. The adjacent heterodimers are interconnected by the interaction between the N-terminal arm of TssB from one heterodimer with the C-terminal arm of TssC from the neighbouring heterodimer. The

packing between two stacked discs is maintained by contacts between the C-terminal parts of the TssC subunits [51,52]. Recently, the cryo-electron tomography reconstruction of the extended *Myxococcus xanthus* T6SS sheath revealed an external diameter of 220Å and an internal lumen that can accommodates the Hcp inner tube [53].

After contraction, the TssB and TssC sheath subunits are disassembled and recycled by a dedicated AAA^+ ATPase, ClpV [43,54]. The ClpV protein is recruited to the contracted sheath by recognizing an N-terminal α-helix of TssC that is though to protrude from the tubular structure in the contracted conformation only [55,56].

While recent studies have provided significant progress regarding the structure and mode of action of the T6SS sheath, the structure of the C-terminal fragment of TssB was still missing. Here, we provide structural information on the enteroaggregative *Escherichia coli* (EAEC) TssB C-terminal domain. We first validate the ability of TssB to multimerize and show that the purified TssB protein form trimers in solution. In addition, we demonstrate that the N-terminal 1-86 aminoacid region controls TssB multimerization. The analyses of purified TssB revealed that the protein undergoes proteolytic clivages to accumulate two fragments corresponding to the 105 and 78 C-terminal amino-acids respectively. We then report the crystal structure of the C-terminal shorter fragment, $TssB_{88\text{-}165}$: it comprises a long helix (H1) followed by a bundle of two smaller helices (H2 and H3). Sequence alignment of TssB C-termini showed that H1 residues that are involved in the interaction with TssC are highly conserved whereas the H2-H3 hairpin comprises a number of charged residues that are highly variable but surface exposed. Site-directed mutagenesis coupled to functional assays further showed that these charges are critical for sheath assembly and T6SS function.

RESULTS

TssB fragments expression and characterization.

The full-length enteroaggregative *Escherichia coli* (EAEC) *tssB* gene encoded within the T6SS *sci-1* gene cluster (165 amino-acids, 18 kDa, EC042_4524, GI:387609945) was cloned into the pETG20A Gateway vector, fused to a N-terminal thioredoxin followed by a TEV cleavage site. The TssB protein was produced into *E. coli* BL21(DE3) pLysS cells, and purified from cell lysates using ion metal affinity and gel filtration chromatographies. The native protein was obtained by TEV digestion and an additional affinity chromatography. Recent bacterial two-hybrid data showed that the EAEC TssB protein oligomerizes [26,48]. To gain further insights into the oligomeric state of TssB, we performed size exclusion chromatography analyses. The full-length, native TssB protein behaves as a trimer (53 kDa compared to the 54-kDa of a theoretical trimer, Fig. 1A). However, SDS-PAGE analyses showed that TssB is rapidly degraded to yield two stable, low molecular weight products of ~ 12 kDa and ~ 10 kDa (data not shown). Mass spectrometry and Edman sequencing analyses defined that these two truncated proteins were deleted of the N-terminal first 59 and 86 residues respectively. We therefore constructed new pETG20A derivatives to produce two C-terminal variants of TssB, starting at residues 60 ($TssB_{60-165}$) and 87 ($TssB_{87-165}$). These two truncated variants deletion mutants were produced and purified using a protocol identical to that of the native protein. By contrast to the full-length protein, size exclusion chromatography analyses of these truncated TssB forms revealed that $TssB_{60-165}$ is a dimer and $TssB_{87-165}$ is monomeric in solution (Fig. 1A). These data indicate that the N-terminal domain of TssB controls the oligomeric state of the protein. The importance of the N-terminal 1-86 fragment of TssB for oligomerization was confirmed by bacterial two-hybrid experiments (Fig. 1B). These data suggest that TssB assembles trimeric structures in solution

that might be used as building blocks/units during sheath polymerization. Based on the gel filtration analyses of native and truncated TssB proteins, we conclude that two independent sites for TssB multimerization are contained within the 1-59 and 60-87 sequences respectively (Fig. 1C).

Crystal structure of the $TssB_{87-165}$ fragment.

The full-length and truncated TssB proteins were subjected to crystallization trials using a robotized nanodrop protocol. Although we did not succeed to obtain TssB crystals, the $TssB_{87-165}$ fragment readily crystallized in presence of zinc acetate and PEG3350 (20%). $TssB_{87-165}$ crystals belong to space group $C222_1$ with cell dimensions a=52.6, b=69.1 and c=45.9, and contain one molecule in the asymmetric unit. A 2.0-Å resolution data set was collected and the structure was solved by single-wavelength anomalous dispersion (SAD) and refined (Table S1). The electron density map of $TssB_{87-165}$ was well defined between residues Glu-88 and Ala-165 (PDB: 4PS2)(Fig. 2A). The structure of $TssB_{87-165}$ starts with a N-terminal extended stretch between Glu-88 and Asn-97 followed by a short helical turn (residues Met-98 to Phe-101) and a three-helix bundle composed of helices H1 (Pro-103 to Lys127), H2 (Asn-133 to Leu-144; antiparallel) and H3 (Gln-151 to Arg-158) (Fig. 2A). The three α-helices are tightly maintained by an hydrophobic core formed by Met-116, Met-119, Leu-122, Leu-123 and Leu-126 from H1, Phe-136, Leu-140 and Leu-144 from H2 and Leu-153, Leu-157 and Leu-160 from H3. Superimposition of the EAEC TssB helix H1 on the *V. cholerae* VipAB structure [51] allows to position the H2-H3 hairpin and hence to complete the structure of the complex (Fig. 2B).

The TssB H1 helix is required to contact TssC.

Together, TssB and TssC assemble the T6SS sheath [43,50-52]. The TssB-TssC interaction was previously demonstrated in various species including *Francisella tularensis*, *Vibrio cholerae*, *Yersinia pseudotuberculosis*, *Salmonella enterica*, *Burkholderia cenocepacia*, EAEC and *Pseudomonas aeruginosa* [43,44-46,48]. More precisely, studies have shown the implication of helix H1 of TssB proteins in TssBC complex formation [44,48,49]. We sought to determine whether the TssB H2-H3 hairpin, which is not observed in the *V. cholerae* TssBC structure, also contributes to the interaction with TssC. Based on the crystal structure of $TssB_{87\text{-}165}$, we designed two constructs: $TssB_{\Delta 104\text{-}130}$ (deleted of helix H1) and $TssB_{\Delta 131\text{-}165}$ (deleted of the C-terminal H2/H3 hairpin) (Fig. 3A), and tested their interaction with TssC by bacterial two-hybrid. As shown in Fig. 3B, none of the deletions abolished contacts with TssB, a result in agreement with the data mentioned above showing that the TssB oligomeric state is controlled by the N-terminal 1-87 residues. However, while $TssB_{\Delta 104\text{-}130}$ lost the ability to interact with TssC, deletion of the H2 and H3 helices had no impact on the interaction with TssC (Fig. 3B). Hence, we concluded that only TssB helix H1 is necessary to contact TssC (Fig. 3C). These data are in agreement with the position of the TssB H2-H3 hairpin when superimposed with the VipAB structure (Fig. 2B).

To determine the region of TssC in contact with TssB, we purified the EAEC TssC protein. Because the full-length TssC protein was not soluble, we produced the N- (amino-acids 1-353) and C-terminal (amino-acids 354-514) domains of TssC. Whereas the N-terminal domain of TssC aggregated, its C-terminal domain was soluble, and further purified to homogeneity. Pull-down and Surface Plasmon Resonance (SPR) experiments showed that the C-terminal domain is not sufficient to interact with TssB (data not shown), a result which

is consistent with published *in vivo* data demonstrating that TssB interacts with the N-terminal region of TssC in *B. cenocepacia*, *P. aeruginosa* and EAEC [45,46,48].

The TssB H2-H3 hairpin bears surface-exposed charged residues that are essential for sheath assembly and T6SS function

A sequence alignment of selected TssB protein C-terminal domains showed that helix H1 is well conserved including the Val-106, Ile-110 and Leu-116 that are involved in TssC binding (see red stars in Fig. 4A) [48]), whereas the H2-H3 hairpin is more variable (Fig. 4A). However, the $TssB_{87-165}$ structure showed that the EAEC TssB hairpin comprises charged residues that are exposed at the surface (Fig. 4B). To gain functional information on the role of these charged residues, we targeted 7 surface-exposed residues: Arg-137, Lys-138, Glu-139, Glu-141 (helix H2), and Asp-155, Arg-158 and Glu-163 (helix H3) (see black stars in Fig. 4A). These residues were substituted by amino-acids of opposed charges (Arg and Lys residues substituted by Glu; Asp and Glu residues substituted by Lys) and the TssB variants were tested for their ability to support sheath assembly and T6SS function (Fig. 5). Fig. 5A shows that substitution of any of these residues prevented released of Hcp in the culture supernatant, suggesting that these charges are necessary for proper function of the Type VI apparatus. In agreement with this conclusion, fluorescence microscopy recordings showed that none of the TssB mutants was able to assemble dynamic sheaths (Fig. 5B and 5C). Statistical analyses of the different variants demonstrated that most of the cells producing the TssB-K138E variant did not present fluorescence, suggesting that mutation of Lys-138 destabilizes TssB. However, a few cells producing TssB-K138E, as well as the vast majority of cells producing the other TssB variant presented static foci or short tubular structures that did not exhibit any dynamics (Fig. 5C).

Position of the TssB C-terminal domain in the contracted and extended TssBC sheaths.

The recent determination of the T6SS contracted sheath structures of *Vibrio cholerae* and *Francisella novicida* [51,52] made it possible to dock the TssB C-terminal domain, and the positions of the charged residues, in the context of the complete sheath structure. Noteworthy, the sequence identities between VipA/TssB and VipB/TssC (36 and 45%, respectively) established that the three-dimensional structures of both protein pairs are very close. In the VipAB sheath molecular structure, the C-terminal part of VipA, after residue 126, is not visible in the EM map. We could however superpose the H1 helices between residues 120 and 126 of the EAEC TssB C-terminal domain onto VipA (Fig. 2B), and thus complete the sheath molecular model (Fig. 6A). When positioned in the TssBC sheath model, the two helices missing in the VipA EM map (H2 and H3 of our model) face the external lumen of the sheath, opposite to the internal sheath channel (Fig. 6A).

To date, a high-resolution molecular structure of the extended (non contracted) sheath is not available. However, a low resolution model of the extended VipAB sheath was proposed using the low resolution EM map of the extended T4 phage tail sheath [50]. By superposing the VipAB EM map to the gp18 T4 phage sheath protein, gross features of the sheath structure were obtained. We used a similar approach, but instead of the low resolution VipAB EM map, we fitted the VipAB molecular model in the extended T4 phage tail sheath. The internal channel diameter shrinks from 110 to ~95 Å diameter, and the external diameter from ~290 Å to ~190 Å. The Hcp tube external diameter is about the size of the sheath internal channel (Fig. 6B), and the internal spacing of the VipAB rings corresponds to that of the stacked Hcp hexamers. Structural superposition of our TssB C-terminal domain on VipA

in the extended sheath shows that this domain is closer to the sheath axis, but still facing the external lumen (Fig. 6B).

DISCUSSION

In this study, we report the crystal structure of the C-terminal domain of the EAEC T6SS TssB protein ($TssB_{87-165}$). The TssB protein interacts with TssC to assemble the T6SS sheath-like structure that engulfs the Hcp inner tube and functions as a contractile device, propelling this inner tube toward the target cell.

Bacterial and yeast two-hybrid studies showed that the TssB protein has the ability to oligomerize [26,47,48]. Using size exclusion chromatography, we showed that the purified EAEC native TssB protein behaves as a trimer in solution. This observation suggests that the T6SS sheath elongates by incorporating TssB trimers. However, it remains possible that the TssB-C complex behave differently. In agreement with previous studies [38,43,46], purification of the EAEC TssBC complex yielded large tubular edifices similar to polysheaths (data not shown) that were not suitable for crystallization. Although TssB behaves as a trimer in solution, its association with TssC induces polymerization. This observation is consistent with the fact that the TssB and TssC proteins stabilize each other [44,47,48]. Indeed, while the TssBC complex is very stable, the purified full-length TssB protein of EAEC yields two degradation products after several days at 4°C. Sequence analyses of these fragments demonstrated that they correspond to the 105-aminoacid ($TssB_{60-165}$) and 78-aminoacid ($TssB_{87-165}$) C-terminal fragments of the protein. Interestingly, when purified, these fragments were stable and behave as a dimer and a monomer respectively. These results suggest that

TssB trimer formation relies on two distinct regions: one located between residues 1 and 59, the second one located between residues 60 and 86 (Fig. 3C).

The TssB C-terminal fragment ($TssB_{87-165}$) is structured as a bundle of three helices: a long helix between residues 103 and 127 (H1) followed by two smaller helices that form an hairpin (H2 and H3). The H1 helix was previously shown to be essential for T6SS function [44,48,49]. Further mutagenesis studies and structural information on the TssBC complex, demonstrated that a hydrophobic face of this helix, comprising residues Val-106, Ile-110 and Leu-117, was involved in the interaction with TssC [48,49,51]. In the $TssB_{87-165}$ structure, these residues are not buried but exposed to the surface, consistent with their direct role in mediating contacts with TssC. More recently, a cryo-tomography low resolution structure of the *in vivo M. xanthus* extended T6SS tail was reported [53]. Using our available PDB structure of the TssB C-terminal domain, the authors could fit it readily electron density map, thus completing the TssB structure [53].

A sequence alignment of TssB C-terminal regions showed that surface-exposed residues include positively- and negatively-charged side-chains: Arg-137, Lys-138, Glu-139, Glu-141, Asp-155, Arg-158 and Glu-163. Substitutions of each of these residues by amino-acids of opposite charges abolished the dynamic assembly of T6SS sheaths and the release of Hcp in the culture supernatant. When replaced in the EAEC TssBC extended and contracted sheath models, these residues locate at the surface of the sheath (see red balls in Fig. 6A and 6B). In agreement with the implication of the N-terminal domain for TssB oligomerization and the implication of the H1 helix in mediating contacts with TssC, the H2-H3 charged residues unlikely contributes to sheath assembly. This observation is also in agreement with the fluorescence microscopy experiments showing that most mutations do not prevent formation of non-dynamic short tubular structures. One possible explanation regarding the

important contribution of these residues in T6SS function might be a role in the initiation of sheath polymerization by interacting with baseplate components.

MATERIAL AND METHODS

Bacterial strains, media and chemicals.

Strains used in this study are listed Table S2. *Escherichia coli* DH5α (New England Biolabs) was used for cloning procedures, BTH101 [57] for bacterial two-hybrid assays and BL21(DE3)pLys (Invitrogen) for protein purification. Enteroaggregative *E. coli* strain 17-2 was used for PCR amplification and for the Hcp release assay. The Δ*tssB* 17-2 derivative has been previously described [48]. Cells were routinely grown in Lysogeny broth (LB) at 30°C or 37°C. Sci-1 gene expression was induced in SIM (Sci-1 inducing medium; M9 minimal medium supplemented with LB 10%, glycerol 0.4%, casaminoacids 40 $\mu g.mL^{-1}$, $MgCl_2$ 2 mM, $CaCl_2$ 0.1 mM, Vitamin B1 200 $\mu g.mL^{-1}$) [58]. Plasmids were maintained by addition of ampicillin (100 $\mu g.mL^{-1}$), kanamycin (50 $\mu g.mL^{-1}$) or chloramphenicol (40 $\mu g.mL^{-1}$). Gene expression was induced with 0.5 mM isopropyl-β-thio-galactoside (IPTG) or L-arabinose (0.02%).

Plasmid construction.

Plasmids used in this study are listed Table S2. Polymerase Chain Reactions (PCR) were performed using a Biometra thermocycler using Pfu Turbo DNA polymerase (Agilent Technology). Custom oligonucleotides, listed in Table S2, were synthesized by Sigma Aldrich. Enteroaggregative *E. coli* 17-2 chromosomal DNA was used as a template for all PCRs. *E. coli* strain DH5α was used for cloning procedures.

Plasmids for *in vivo* assays. Constructions of the bacterial two-hybrid vectors encoding TssB and TssC fusion proteins have been previously described [59]. The N-terminally truncated TssB

derivatives have been constructed by restriction/ligation-free cloning [60] as previously described [16]. Briefly, fragments of interest were amplified with oligonucleotides introducing extensions annealing to the target vector. The double-stranded product of the first PCR has then been used as oligonucleotides for a second PCR using the target vector as template. Bacterial two-hybrid vectors encoding T18-TssB$_{\Delta 131-165}$ and T25-TssB$_{\Delta 131-165}$ fusions were constructed by insertion of a premature stop codon into T18-TssB and T25-TssB by site directed mutagenesis. Substitutions have been introduced by site-directed mutagenesis using complementary pairs of oligonucleotides and the Pfu Turbo high fidelity polymerase (Agilent technologies). All constructs have been verified by restriction analyses and DNA sequencing (Eurofins, MWG).

Plasmids for protein purification. The DNA sequence encoding TssB, TssB$_{60-165}$ and TssB$_{87-165}$ were cloned into the pETG-20A expression vector by the Gateway® procedure, as previously described [19]. The proteins produced are translationally fused to an N-terminal Thioredoxin followed by a 6×His tag and a TEV cleavage site.

Bacterial Two-Hybrid Assay.

The adenylate cyclase-based bacterial two-hybrid technique [57] was used as previously published [61]. Briefly, pairs of proteins to be tested were fused to the isolated T18 and T25 catalytic domains of the *Bordetella* adenylate cyclase. After transformation of the two plasmids producing the fusion proteins into the reporter BTH101 strain, plates were incubated at 30°C for 48 hours. Three independent colonies for each transformation were inoculated into 600 µl of LB medium supplemented with ampicillin, kanamycin and IPTG (0.5 mM). After overnight growth at 30°C, 10 µl of each culture were dropped onto MacConkey and LB supplemented with Bromo-Chloro-Indolyl-Galactopyrannoside (X-Gal) plates and incubated for 16 hours at 30 °C. The experiments were done at least in triplicate and a representative result on LB-X-Gal plate is shown.

Production and purification of TssB, TssB$_{60-165}$ and TssB$_{87-165}$.

E. coli BL21 (DE3) pLysS cells carrying the pETG20A derivatives were grown on Terrific Broth (TB) (1.2% peptone, 2.4% yeast extract, K_2HPO_4 72 mM, KH_2PO_4 17 mM, and glycerol 0.4%) supplemented with ampicillin, at 37°C to an OD_{600} ~ 0.6. Expression of the constructions was then induced by addition of IPTG and cultures were pursued for 18 hours at 25°C. Cells were harvested, resuspended in lysis buffer (Tris-HCl 50 mM pH 8.0, NaCl 300 mM, EDTA 1mM, lysozyme 0.5 mg/mL, phenylmethylsulfonyl fluoride (PMSF)) and submitted to 5 cycles of freeze and thaw and sonication. After addition of DNase (20 µg/mL) and $MgCl_2$ (20 mM), the soluble fraction was obtained by centrifugation for 30 min at 16,000 × *g*. Recombinant proteins were purified by ion metal affinity chromatography using a 5-ml Nickel HisTrap™ FF crude Column on an ÄKTA Express dispositive (GE healthcare) pre-equilibrated in Tris-HCl 50 mM pH8.0, NaCl 300 mM, 10 mM Imidazole (buffer A). After several washes in buffer A, 6×His tagged proteins were eluted in buffer A supplemented with 250 mM Imidazole, desalted on a HiPrep 26/10 desalting column (Sephadex™ G-25, Amersham Biosciences), cleaved with the TEV protease (1 mg/mL) for 18 hours at 4°C and loaded onto a HisTrap™ FF column pre-equilibrated in Buffer A, which selectively retains the TEV protease, the uncleaved, 6×His-tagged fusion proteins and contaminants. The native proteins were collected in the flow-through, concentrated on Centricons (Millipore; cutoff of 3 kDa), and passed through a Sephadex 200 26/60 column pre-equilibrated with Tris-HCl 25mM pH7.5, NaCl 100mM.

Biophysical characterization of native and truncated TssB proteins.

Size exclusion chromatography (SEC) was performed on an Alliance 2695 HPLC system (Waters) using a 802.5 column (Shodex) run in Tris-HCl 20 mM, pH 7.5, NaCl 100 mM at 0.5 mL/min.

Crystallization, data collection, processing and refinement of $TssB_{87-165}$.

$TssB_{87-175}$ crystallization trials were carried out by the sitting-drop vapour diffusion method in 96-well Greiner crystallization plates at 20°C using a nanodrop dispersing robot. Crystals grew in approximatively one week after mixing 200 nL of $TssB_{87-165}$ (8 mg/mL) with 100 nL of Zinc acetate

0.2 M, PEG3350 20%, pH 7.0. Crystals were cryoprotected with mother liquor supplemented with 17% Ethylene glycol. A 2.00-Å resolution dataset was collected at the SOLEIL Proxima 1 beamline (Saint-Aubin, France). After processing the data with XDS [62], the scaling was performed with SCALA [63] and the structure was solved by SAD using the Zinc atom with the program SHELX [64]. The structure was refined with AutoBUSTER [65] alternated with model rebuilding using COOT [66]. The final data collection and refinement statistics are provided in Table S1. Figures were made with PyMOL [67].

Hcp release assay.

The Hcp release assay has been performed as previously described [16] except that cells were grown in SIM [58].

Fluorescence microscopy recordings and statistical analyses.

Fluorescence microscopy recordings were performed as previously published [67]. All experiments have been done at least in triplicate and a representative result is shown. The number of dynamic sheath structures, static foci and static tubular structures were measured manually on a minimal of 130 cells followed for at least one hour.

Accession code.

The atomic coordinates and structure factors have been deposited at the Protein Data Bank under accession code 4PS2.

ACKNOWLEDGEMENTS

We thank the members of the Cascales and Cambillau laboratories for insightful discussions, Molly Ba, Isabelle Bringer, Annick Brun and Olivier Uderso for technical assistance, and

Carrie Bout for encouragements. The Soleil Synchrotron radiation facility is acknowledged for beamline allocation. This work was funded by the Centre National de la Recherche Scientifique (CNRS), the Aix-Marseille Université and a grant from the Agence Nationale de la Recherche (ANR-14-CE14-0006-02). B.D. was supported by a grant from the Fondation pour la Recherche Médicale (FRM, DEQ2011-0421282). L.L. was supported by a doctoral fellowship from the french Ministère de la Recherche et Technologie and a end-of-thesis fellowship from the FRM (FDT2016-0435498).

REFERENCES

[1] J.M. Silverman, Y.R. Brunet, E. Cascales, J.D. Mougous, Structure and regulation of the type VI secretion system, Ann. Rev. Microbiol. 66 (2012) 453–472.

[2] N, Kapitein, A. Mogk, Deadly syringes: type VI secretion system activities in pathogenicity and interbacterial competition, Curr. Opin. Microbiol. 16 (2013) 52–58.

[3] A. Zoued, Y.R. Brunet, E. Durand, M.S. Aschtgen, L. Logger, B. Douzi, L. Journet, C. Cambillau, E. Cascales, Architecture and assembly of the type VI secretion system, Biochim. Biophys. Acta 1843 (2014) 1664–1673.

[4] B.T. Ho, T.G. Dong, J.J. Mekalanos, A view to a kill: the bacterial Type VI secretion system, Cell Host Microbe 15 (2014) 9–21.

[5] F.R. Cianfanelli, L. Monlezun, S.J. Coulthurst, Aim, load, fire: the type VI secretion system, a bacterial nanoweapon, Trends Microbiol. 24 (2016) 51–62.

[6] L.E. Bingle, C.M. Bailey, M.J. Pallen, Type VI secretion: a beginner's guide, Curr. Opin. Microbiol. 11 (2008) 3–8.

[7] E. Cascales, The type VI secretion toolkit, EMBO Rep. 9 (2008) 735–741.

[8] F. Boyer, G. Fichant, J. Berthod, Y. Vandenbrouck, I. Attree, Dissecting the bacterial type VI secretion system by a genome wide in silico analysis: what can be learned from available microbial genomic resources?, BMC Genomics 10 (2009) 104.

[9] A.B. Russell, S.B. Peterson, J.D. Mougous, Type VI secretion system effectors: poisons with a purpose, Nat. Rev. microbiol. 12 (2014) 137–148.

[10] J. Benz, A. Meinhart, Antibacterial effector/immunity systems : it's just the tip of the iceberg. Curr. Opin. Microbiol. 17 (2014) 1–10.

[11] E. Durand, C. Cambillau, E. Cascales, L. Journet, VgrG, Tae, Tle, and beyond: the versatile arsenal of type VI secretion effectors, Trends Microbiol. 22 (2014) 498–507.

[12] J. Alcoforado Diniz, Y.C. Liu, S.J. Coulthurst, Molecular weaponry: diverse effectors delivered by the type VI secretion system, Cell. Microbiol. 17 (2015) 1742–1751.

[13] A. Hachani, T.E. Wood, A. Filloux, Type VI secretion and antihost effectors, Curr. Opin. Microbiol. 29 (2015) 81–93.

[14] E. Cascales, C. Cambillau, Structural biology of type VI secretion systems, Philos. Trans. R. Soc. Lond. Ser. B Biol. Sci. 367 (2012) 1102–1111.

[15] M. Basler, Type VI secretion system: secretion by a contractile nanomachine, Philos. Trans. R. Soc. Lond. Ser. B Biol. Sci. 370 (2015) 1679.

[16] M.S. Aschtgen, C.S. Bernard, S. De Bentzmann, R. Lloubès, E. Cascales, SciN is an outer membrane lipoprotein required for type VI secretion in enteroaggregative Escherichia coli, J. Bacteriol. 190 (2008) 7523–7531.

[17] M.S. Aschtgen, M. Gavioli, A. Dessen, R. Lloubès, E. Cascales, The SciZ protein anchors the enteroaggregative Escherichia coli type VI secretion system to the cell wall, Mol. Microbiol. 75 (2010) 886–899.

[18] L.S. Ma, J.S. Lin, E.M. Lai, An IcmF family protein, ImpLM, is an integral inner membrane protein interacting with ImpKL, and its walker a motif is required for type VI secretion systemmediated hcp secretion in Agrobacterium tumefaciens, J. Bacteriol. 191 (2009) 4316–4129.

[19] C. Felisberto-Rodrigues, E. Durand, M.S. Aschtgen, S. Blangy, M. Ortiz-Lombardia, B. Douzi, C. Cambillau, E. Cascales, Towards a structural comprehension of bacterial type VI

secretion systems: characterization of the TssJ–TssM complex of an Escherichia coli pathovar, PLoS Pathogens. 7 (2011) e1002386.

[20] M.S. Aschtgen, A. Zoued, R. Lloubès, L. Journet, E. Cascales, The C-tail anchored TssL subunit, an essential protein of the enteroaggregative Escherichia coli Sci-1 type VI secretion system, is inserted by YidC, Microbiologyopen 1 (2012) 71–82.

[21] E. Durand, A. Zoued, S. Spinelli, P.J. Watson, M.S. Aschtgen, L. Journet, C. Cambillau, E. Cascales, Structural characterization and oligomerization of the TssL protein, a component shared by bacterial type VI and type IVb secretion systems, J. Biol. Chem. 287 (2012) 14,157–14,168.

[22] L.S. Ma, F. Narberhaus, E.M. Lai, IcmF family protein TssM exhibits ATPase activity and energizes type VI secretion, J. Biol. Chem. 287 (2012) 15610–15621.

[23] E. Durand, V.S. Nguyen, A. Zoued, L. Logger, G. Péhau-Arnaudet, M.S. Aschtgen, S. Spinelli, A. Desmyter, B. Bardiaux, A. Dujeancourt, A. Roussel, C. Cambillau, E. Cascales, R. Fronzes, Biogenesis and structure of a type VI secretion membrane core complex, Nature 523 (2015) 555–560.

[24] G. Bönemann, A. Pietrosiuk, A. Mogk, Tubules and donuts: a type VI secretion story, Mol. Microbiol. 76 (2010) 815–821.

[25] P.G. Leiman, M.M. Shneider, Contractile tail machines of bacteriophages, Adv. Exp. Med. Biol. 726 (2012) 93–114.

[26] Y.R. Brunet, J. Hénin, H. Celia, E. Cascales, Type VI secretion and bacteriophage tail tubes share a common assembly pathway, EMBO Rep. 15 (2014) 315–321.

[27] Y.R. Brunet,A. Zoued, F.Boyer,B. Douzi, E.Cascales, The type VI secretion TssEFGK-VgrG phage-like baseplate is recruited to the TssJLM membrane complex via multiple contacts and serves as assembly platform for tail tube/sheath polymerization, PLoS Genet. 15 (3) (2015) e1005545.

[28] N.M. Taylor, N.S. Prokhorov, R.C. Guerrero-Ferreira, M.M. Shneider, C. Browning, K.N. Goldie, H. Stahlberg, P.G. Leiman, Structure of the T4 baseplate and its function in triggering sheath contraction, Nature 533 (2016) 346–352.

[29] S. Pukatzki, A.T. Ma, A.T. Revel, D. Sturtevant, J.J. Mekalanos, Type VI secretion system translocates a phage tail spike-like protein into target cells where it cross-links actin, Proc. Natl. Acad. Sci. USA. 104 (2007) 15508–15513.

[30] P.G. Leiman, M. Basler, U.A. Ramagopal, J.B. Bonanno, J.M. Sauder, S. Pukatzki, S.K. Burley, S.C. Almo, J.J. Mekalanos, Type VI secretion apparatus and phage tail associated protein complexes share a common evolutionary origin, Proc. Natl. Acad. Sci. U. S. A. 106 (2009) 4154–4159.

[31] J.D. Mougous, M.E. Cuff, S. Raunser, A. Shen, M. Zhou, C.A. Gifford, A.L. Goodman, G. Joachimiak, C.L. Ordoñez, S. Lory, T. Walz, A. Joachimiak, J.J. Mekalanos, A virulence locus of Pseudomonas aeruginosa encodes a protein secretion apparatus, Science 312 (2006) 1526–1530.

[32] E.R. Ballister, A.H. Lai, R.N. Zuckermann, Y. Cheng, J.D. Mougous, In vitro self-assembly of tailorable nanotubes from a simple protein building block, Proc. Natl. Acad. Sci. USA. 105 (2008) 3733–3738.

[33] B. Douzi, S. Spinelli, S. Blangy, A. Roussel, E. Durand, Y.R. Brunet, E. Cascales, C. Cambillau, Crystal structure and self-interaction of the Type VI Secretion tail-tube orotein from Enteroaggregative Escherichia coli, PLoS ONE 9 (2014) e86918.

[34] A. Zoued, E. Durand, Y.R. Brunet, S. Spinelli, B. Douzi, M. Guzzo, N. Flaugnatti, P. Legrand, L. Journet, R. Fronzes, T. Mignot, C. Cambillau, E. Cascales, Priming and polymerization of a bacterial contractile tail structure, Nature 531 (2016) 59–63.

[35] A. Vettiger, J. Winter, L. Lin, M. Basler, The type VI secretion system sheath assembles at the end distal from the membrane anchor, Nat Commun. 8 (2017) 16088.

[36] A. Zoued, E. Durand, Y.G. Santin, L. Journet, A. Roussel, C. Cambillau, E. Cascales, TssA: The cap protein of the Type VI secretion system tail, Bioessays. doi: 10.1002/bies.201600262 (2017).

[37] M. Brackmann, S. Nazarov, J. Wang, M. Basler, Using force to punch holes: mechanics of contractile nanomachines, Trends Cell Biol. 27 (2017) 623–632.

[38] M. Basler, M. Pilhofer, G.P. Henderson, G.J. Jensen, J.J. Mekalanos, Type VI secretion requires a dynamic contractile phage tail-like structure, Nature 483 (2012) 182–186.

[39] Y.R. Brunet, L. Espinosa, S. Harchouni, T. Mignot, E. Cascales, Imaging type VI secretion-mediated bacterial killing, Cell Rep. 3 (2013) 36–41.

[40] Y.R. Brunet, A. Khodr, L. Logger, L. Aussel, T. Mignot, S. Rimsky, E. Cascales, H-NS silencing of the Salmonella pathogenicity island 6-encoded type VI secretion system limits Salmonella enterica serovar Typhimurium interbacterial killing, Infect Immun. 83 (2015) 2738–50.

[41] M. LeRoux M, J.A. De Leon, N.J. Kuwada, A.B. Russell, D. Pinto-Santini, R.D. Hood, D.M. Agnello, S.M. Robertson, P.A. Wiggins, J.D. Mougous, Quantitative single-cell characterization of bacterial interactions reveals type VI secretion is a double-edged sword, Proc. Natl. Acad. Sci. USA. 109 (2012) 19804–19809.

[42] M. Basler, B.T. Ho, J.J. Mekalanos, Tit-for-tat: type VI secretion system counterattack during bacterial cell–cell interactions, Cell 152 (2013) 884–894.

[43] G. Bonemann, A. Pietrosiuk, A. Diemand, H. Zentgraf, A. Mogk, Remodelling of VipA/VipB tubules by ClpV-mediated threading is crucial for type VI protein secretion, EMBO J. 28 (2009) 315–325.

[44] J.E. Broms, M. Lavander, A. Sjostedt, A conserved alpha-helix essential for a type VI secretion-like system of Francisella tularensis, J. Bacteriol. 191 (2009) 2431–2446.

[45] D. Aubert, D.K. MacDonald, M.A. Valvano, BcsKC is an essential protein for the type VI secretion system activity in Burkholderia cenocepacia that forms an outer membrane complex with BcsLB, J. Biol. Chem. 285 (2010) 35988–35998.

[46] N.S. Lossi, E. Manoli, A. Forster, R. Dajani, T. Pape, P. Freemont, A. Filloux, The HsiB1C1 (TssB-TssC) complex of the Pseudomonas aeruginosa type VI secretion system forms a bacteriophage tail sheathlike structure, J. Biol. Chem. 288 (2013) 7536–7548.

[47] J.S. Lin, L.S. Ma, E.M. Lai, Systematic dissection of the agrobacterium type VI secretion system reveals machinery and secreted components for subcomplex formation, PLoS ONE. 8 (2013) e67647.

[48] X.Y. Zhang, Y.R. Brunet, L. Logger, B. Douzi, C. Cambillau, L. Journet, E. Cascales, Dissection of the TssB-TssC interface during type VI secretion sheath complex formation, PLoS ONE. 8 (2013) e81074.

[49] J.E. Broms, T. Ishikawa, S.N. Wai, A. Sjostedt, A functional VipA-VipB interaction is required for the type VI secretion system activity of Vibrio cholerae O1 strain A1552, BMC Microbiol. 13 (2013) 96.

[50] S. Kube, N. Kapitein, T. Zimniak, F. Herzog, A. Mogk, P. Wendler, Structure of the VipA/B type VI secretion complex suggests a contraction-state-specific recycling mechanism, Cell Rep. 8(2014) 20–30.

[51] M. Kudryashev, R.Y. Wang, M. Brackmann, S. Scherer, T. Maier, D. Baker, F. DiMaio, H. Stahlberg, E.H. Egelman, M. Basler, Structure of the type VI secretion system contractile sheath, Cell 160 (2015) 952–962.

[52] D.L. Clemens, P. Ge, B.Y. Lee, M.A. Horwitz, Z.H. Zhou, Atomic structure of T6SS reveals interlaced array essential to function, Cell. 160 (2015) 940–951.

[53] Y.W. Chang, L.A. Rettberg, D.R. Ortega, G.J. Jensen, In vivo structures of an intact type VI secretion system revealed by electron cryotomography, EMBO Rep. 18 (2017) 1090–1099.

[54] N. Kapitein, G. Bonemann, A. Pietrosiuk, F. Seyffer, I. Hausser I, J.K. Locker, A. Mogk, ClpV recycles VipA/VipB tubules and prevents non-productive tubule formation to ensure efficient type VI protein secretion, Mol. Microbiol. 87 (2013) 1013–1028.

[55] A. Pietrosiuk, E.D. Lenherr, S. Falk, G. Bonemann, J. Kopp, H. Zentgraf, I. Sinning, A. Mogk, Molecular basis for the unique role of the AAA+ chaperone ClpV in type VI protein secretion, J. Biol. Chem. 286 (2011) 30010–30021.

[56] B. Douzi, Y.R. Brunet, S. Spinelli, V. Lensi, P. Legrand, S. Blangy, A. Kumar, L. Journet, E. Cascales, C. Cambillau, Structure and specificity of the Type VI secretion system ClpV-TssC interaction in enteroaggregative Escherichia coli, Sci Rep. 6 (2016) 34405.

[57] G. Karimova, J. Pidoux, A. Ullmann, D. Ladant, A bacterial two-hybrid system based on a reconstituted signal transduction pathway, Proc. Natl. Acad. Sci. USA. 95 (1998) 5752–5756.

[58] Y.R. Brunet, C.S. Bernard, M. Gavioli, R. Lloubes, E. Cascales, An epigenetic switch involving overlapping fur and DNA methylation optimizes expression of a type VI secretion gene cluster, PLoS Genetics 7 (2011) e1002205.

[59] A. Zoued, E. Durand, C. Bebeacua, Y.R. Brunet, B. Douzi, C. Cambillau, E. Cascales, L. Journet, TssK is a trimeric cytoplasmic protein interacting with components of both phage-

like and membrane anchoring complexes of the Type VI secretion system, J. Biol. Chem. 288 (2013) 27031–27041.

[60] F. van den Ent, J. Lowe, RF cloning: a restriction-free method for inserting target genes into plasmids, J. Biochem. Biophys. Meth. 67 (2006) 67–74.

[61] A. Battesti, E. Bouveret, The bacterial two-hybrid system based on adenylate cyclase reconstitution in Escherichia coli, Methods 58 (2012) 325–334.

[62] W. Kabsch, Xds, Acta Crystallogr D Biol Crystallogr 66 (2010) 125–132.

[63] CCP4 CCPN, The CCP4 suite: programs for crystallography, Acta Cryst D 50 (1994) 760–766.

[64] T.R. Schneider, G.M. Sheldrick, Substructure solution with SHELXD, Acta Crystallogr D Biol Crystallogr 58 (2002) 1772–1779.

[65] E. Blanc, P. Roversi, C. Vonrhein, C. Flensburg, S.M. Lea, G. Bricogne, Refinement of severely incomplete structures with maximum likelihood in BUSTER-TNT, Acta Crystallogr D Biol Crystallogr 60 (2004) 2210–2221.

[66] P. Emsley, K. Cowtan, Coot: model-building tools for molecular graphics, Acta Crystallogr D Biol Crystallogr 60 (2004) 2126–2132.

[67] W. DeLano, The PyMOL Molecular Graphics System (http://www.pymol.org), San Carlos, CA, USA: DeLano Scientific LLC.

LEGEND TO FIGURES

Figure 1. Oligomerization of the T6SS TssB protein. (A) Size exclusion chromatography analysis of purified TssB (light grey line), $TssB_{60-165}$ (medium grey line) and $TssB_{87-165}$ (dark grey line). The column was previously calibrated using protein molecular weight standards. The molecular weights of the different TssB fragments are indicated on top (in kDa). (B) Bacterial two-hybrid analysis. BTH101 reporter cells carrying pairs of plasmids producing the indicated TssB fragments fused to the T18 or T25 domain of the *Bordetella* adenylate cyclase were spotted on X-Gal-IPTG reporter LB agar plates. Interaction between the two partners induces the blue coloring of the colony. Controls include T18 and T25 fusions to TolB and Pal, two proteins that interact but unrelated to the T6SS. (C) Schematic representation of the TssB protein. The 165-amino-acid TssB protein is shown linearly with the three domains corresponding to the proteolytic fragments. Residue positions are indicated on top. The regions required for oligomerization (TssB binding sites 1 and 2, BBS1 and BBS2), are indicated.

Figure 2. Structure of the TssB C-terminal domain. (A) Side and top ribbon views of the $TssB_{87-165}$ structure (PDB 4PS2, views prepared with Pymol [67]). The colour is in rainbow mode (blue to red), and the helices are numbered H1-H3. The structure shown on right is rotated by 90° compared to the one on left. (B) Superimposition of the EAEC $TssB_{87-165}$ structure on the *V. cholerae* VipAB complex structure (PDB 3J9G). $TssB_{87-165}$ is shown in purple whereas VipA and VipA are respectively coloured in green and cyan.

Figure 3. (A) Schematic representation of the TssB variants used in panel (B). The 165-amino-acid TssB protein is shown linearly with the three domains corresponding to the proteolytic fragments. The TssB 88-165 fragment for which the crystal structure has been solved is indicated, as well as the main secondary structures (H1, H2 and H3 corresponds to

helices 1, 2 and 3 respectively). The internal deletion of helix H1 is indicated by the Δ symbol. (A) Bacterial two-hybrid analysis. BTH101 reporter cells carrying pairs of plasmids producing the indicated T6SS proteins (or fragments) fused to the T18 or T25 domain of the *Bordetella* adenylate cyclase were spotted on X-Gal-IPTG reporter LB agar plates. Interaction between the two partners induces the blue coloring of the colony. Controls include T18 and T25 fusions to TolB and Pal, two proteins that interact but unrelated to the T6SS. (C) Schematic representation of the TssB protein and the regions involved in TssB and TssC contacts. The sites required for oligomerization (BBS1 and BBS2), and for interaction with TssC (TssC-binding site, CBS) are indicated.

Figure 4. Conservation of the TssB C-terminal region. (A) Sequence alignment of the TssB C-terminal region from EAEC and selected TssB homologues from bacteria indicated on right. The conservation is shown using a colour code (see on bottom). The secondary structures (helices 1, 2 and 3; respectively H1, H2 and H3) are indicated, as well as the conserved hydrophobic residues involved in TssC binding (red stars). The non-conserved charged residues within the H2-H3 hairpin that are targeted for the structure-function analysis are indicated by black stars. The location of this non-conserved charged residues on the $TssB_{87\text{-}165}$ structure are shown in panel (B).

Figure 5. The non-conserved charged residues at the TssB C-terminus are necessary for T6SS function. (A) Hcp release assay. FLAG-tagged Hcp (Hcp_F) release was assessed by separating cells (C) and cell-free culture supernatant (S) fractions from 10^9 cells of the indicated strain. Proteins were separated by 12.5%-acrylamide SDS-PAGE and the periplasmic TolB protein (control for cell lysis), VSV-G-tagged TssB ($TssB_V$) and Hcp_F were immunodetected using anti-TolB (upper panel), anti-VSV-G (middle panel) and anti-FLAG (lower panel) antibodies. Molecular weight markers (in kDa) are indicated on the left. (B)

Sheath dynamics. Time-lapse fluorescence microscopy recordings showing localization and dynamics of the indicated TssB-sfGFP variants. Images were taken every 30 sec (indicated on bottom). The white arrowheads indicate a sheath that exhibits elongation whereas the red arrowheads indicate a contraction event (only visible in strain producing the wild-type TssB protein, *tssB*$^{+}$). (C) Statistical analyses reporting the percentage of cells from the indicated strain that present dynamic tubes, static tubes and foci, a diffuse or no fluorescent signal. The n umber of analysed cells (*n*) is indicated on top.

Figure 6. Models of the EAEC TssBC contracted (A) and extended (B) sheaths. The TssBC proteins are indicated on grey whereas the Hcp ring (orange) has been positioned in the lumen of the extended sheath. Top and side views are shown on the left and middle panels, whereas the right panels show magnifications of the side views (black rectangles in middle panels). The crystallized TssB C-terminal fragment is shown in green, whereas the H2-H3 charged residues are highlighted in red in the magnification panels.

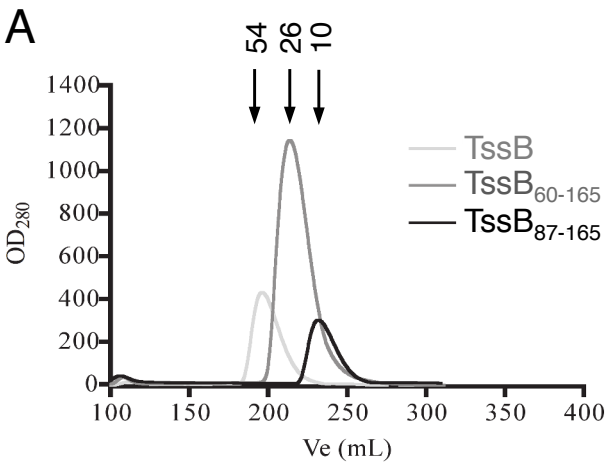

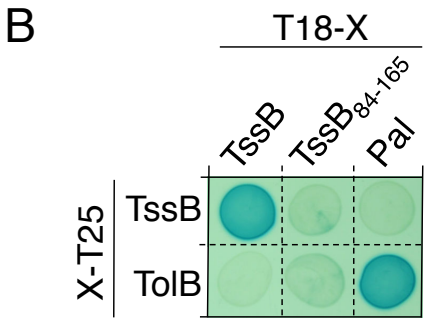

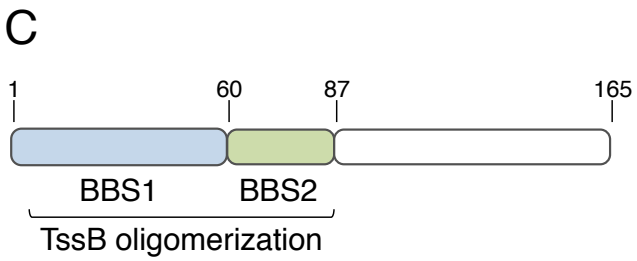

Douzi Figure 1

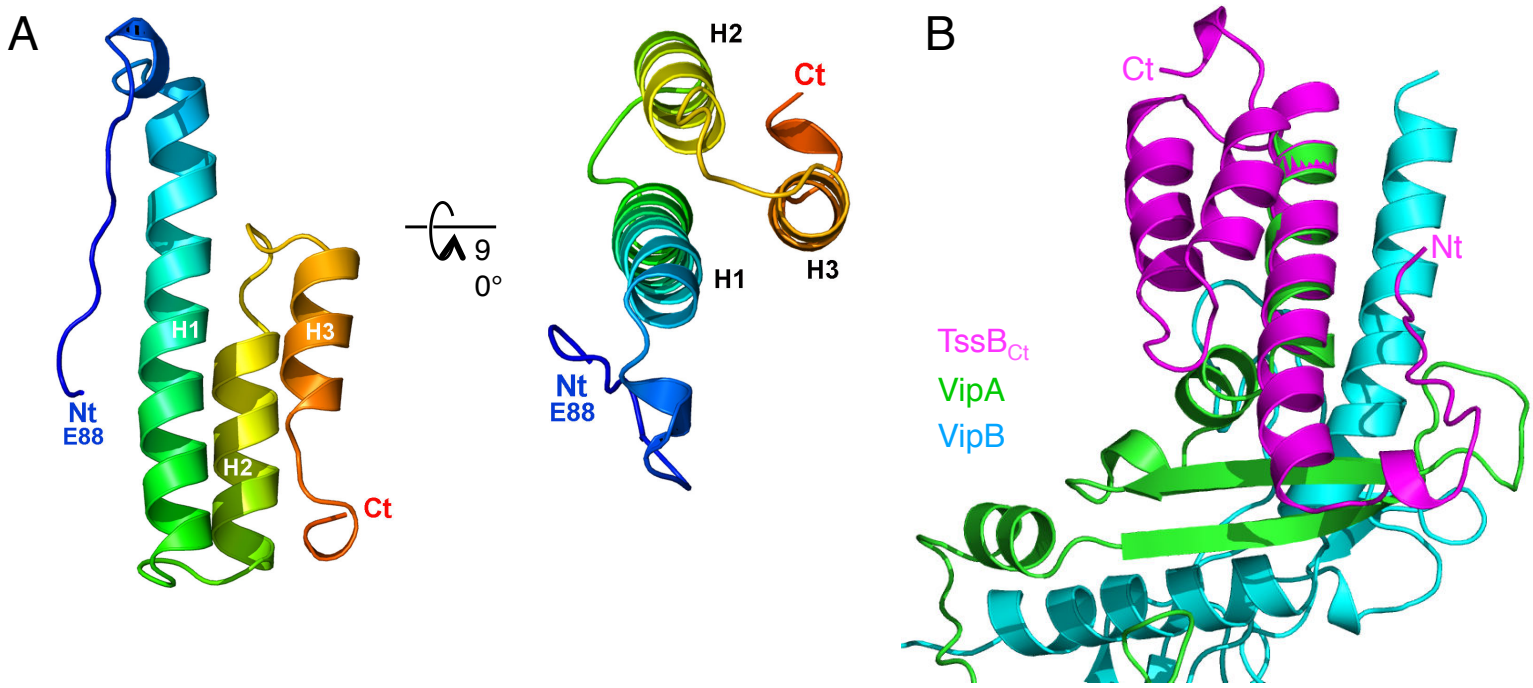

Douzi Figure 2

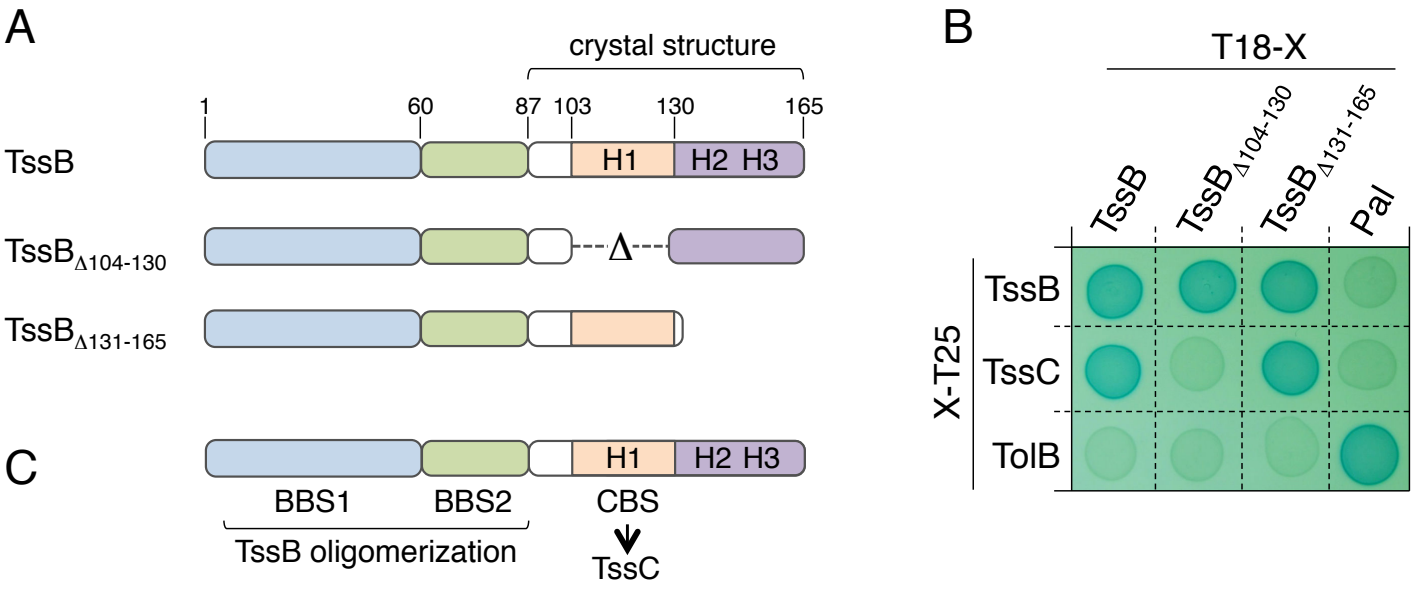

Douzi Figure 3

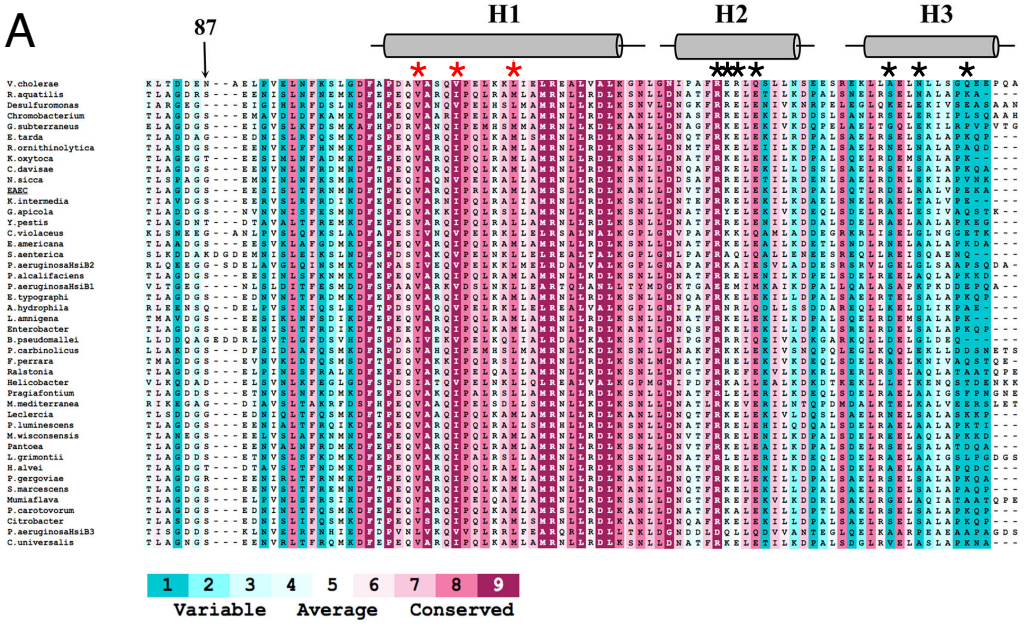

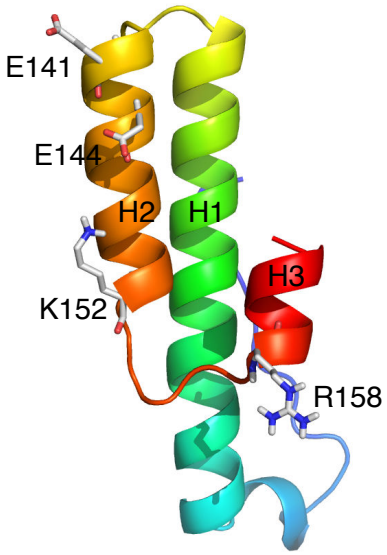

Douzi Figure 4

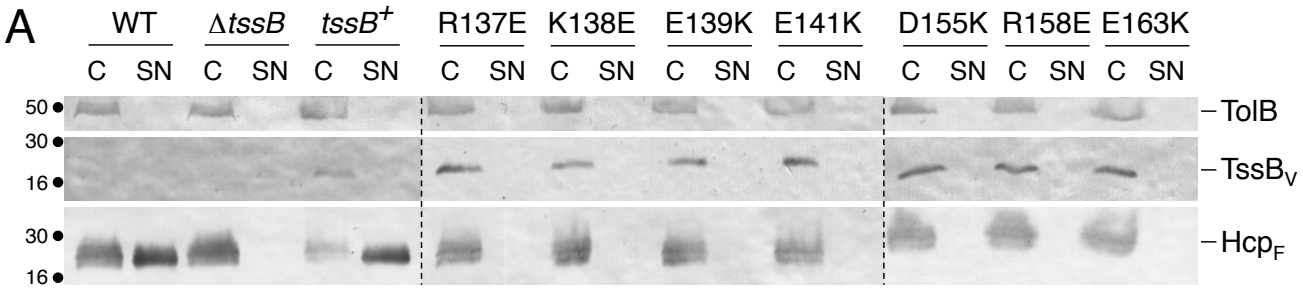

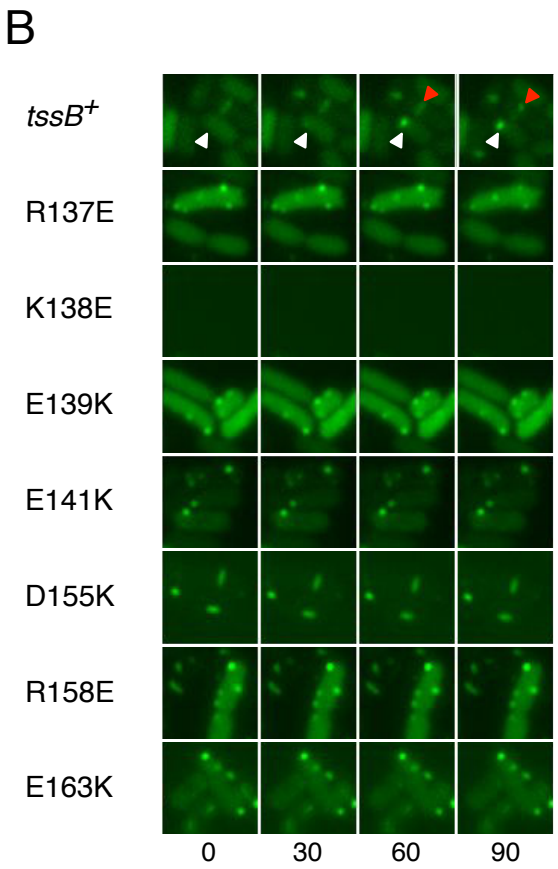

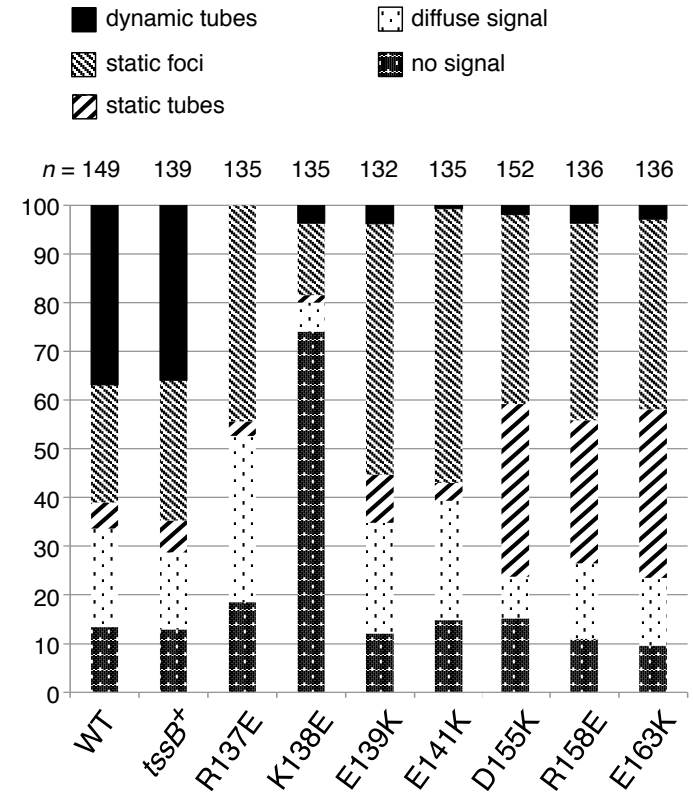

Douzi Figure 5

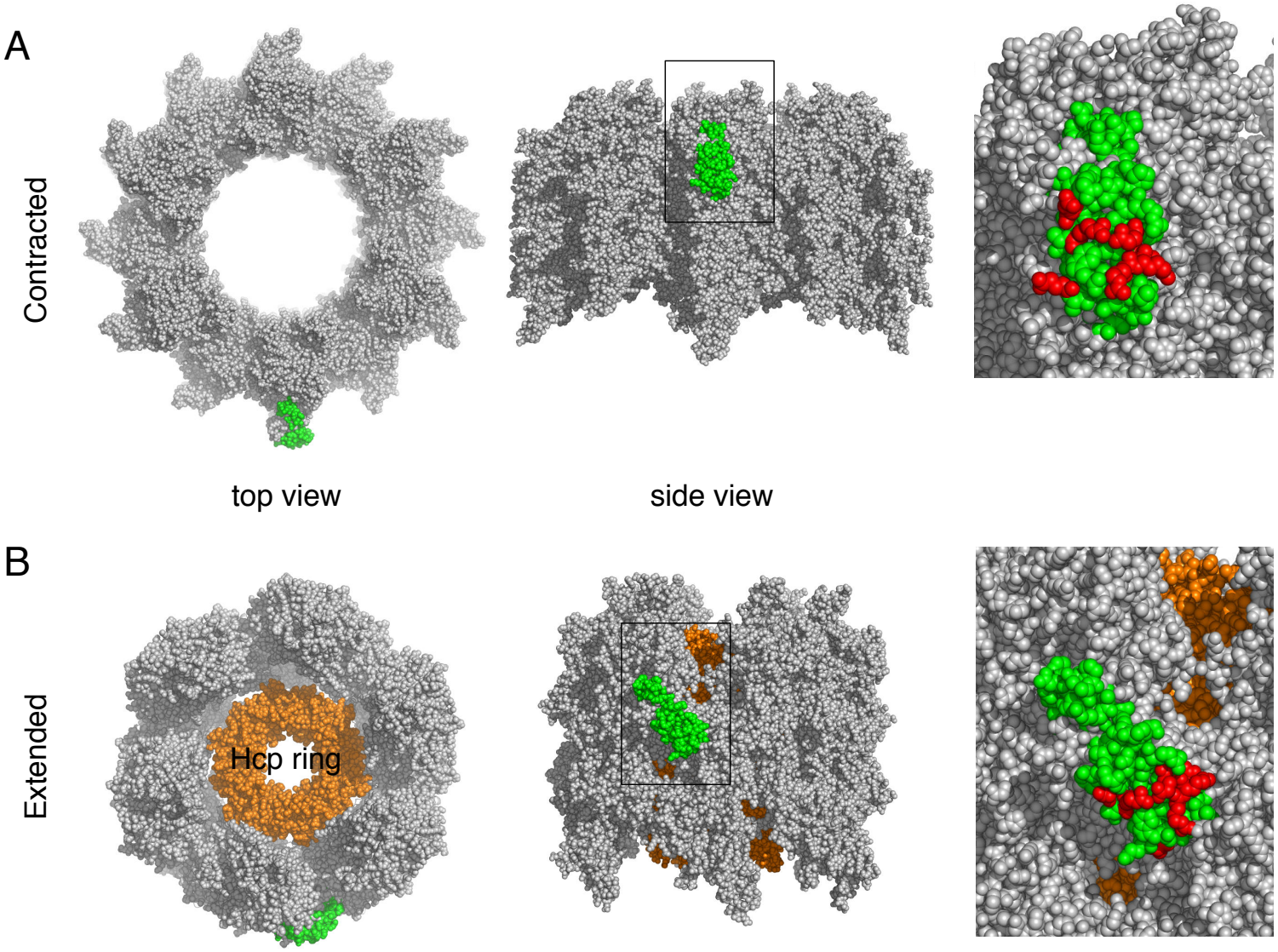

Douzi Figure 6

Table S1. **Data collection and refinement statistics**

DATA COLLECTION	
PDB	4PS2
Source	Soleil Proxima 1
Space group, cell (Å,°)	$C222_1$, 52.6 69.1 45.9
Resolution limits[a] (Å)	50.0-**2.0** (2.12-2.0)
Rmeas[a] (%)/CC(1/2)	12.3/99.8 (87/84.3)
Nr. of observations[a,b]	57501 (8628)
Nr. unique reflections[a,b]	10972 (1730)
Mean((I)/sd(I)) [a]	11.3 (2.0)
Completeness[a] (%)	99.5 (97.4)
Multiplicity[a]	5.2 (5.0)
REFINEMENT	
Resolution[a] (Å)	42-**2.0** (2.24-2.0)
Nr of reflections[a]	5913 (1505)
Atoms : protein, ions, water	631 / 2 / 95
Nr test set reflections	568
R_{work}/R_{free} [a] (%)	0.184/0.217 (0.184/0.21)
r.m.s.d.bonds (Å) / angles (°)	0.010, 0.97
B-wilson / B-average ($Å^2$)	28.1 / 33.5
Ramachandran: preferred (%)	100

[a] numbers into parenthesis refer to the highest resolution bin.

[b] Friedel pairs not merged

Table S1. **Data collection and refinement statistics**

DATA COLLECTION	
PDB	4PS2
Source	Soleil Proxima 1
Space group, cell (Å,°)	$C222_1$, 52.6 69.1 45.9
Resolution limits[a] (Å)	50.0-**2.0** (2.12-2.0)
Rmeas[a] (%)/CC(1/2)	12.3/99.8 (87/84.3)
Nr. of observations[a,b]	57501 (8628)
Nr. unique reflections[a,b]	10972 (1730)
Mean((I)/sd(I)) [a]	11.3 (2.0)
Completeness[a] (%)	99.5 (97.4)
Multiplicity[a]	5.2 (5.0)
REFINEMENT	
Resolution[a] (Å)	42-**2.0** (2.24-2.0)
Nr of reflections[a]	5913 (1505)
Atoms : protein, ions, water	631 / 2 / 95
Nr test set reflections	568
R_{work}/R_{free} [a] (%)	0.184/0.217 (0.184/0.21)
r.m.s.d.bonds (Å) / angles (°)	0.010, 0.97
B-wilson / B-average ($Å^2$)	28.1 / 33.5
Ramachandran: preferred (%)	100

[a] numbers into parenthesis refer to the highest resolution bin.

[b] Friedel pairs not merged

Annexe 4: Architecture and assembly of the Type VI secretion system

Biochimica et Biophysica Acta 1843 (2014) 1664–1673

Contents lists available at ScienceDirect

Biochimica et Biophysica Acta

journal homepage: www.elsevier.com/locate/bbamcr

Review

Architecture and assembly of the Type VI secretion system ☆

Abdelrahim Zoued [a,1], Yannick R. Brunet [a,1,2], Eric Durand [b], Marie-Stéphanie Aschtgen [a,3], Laureen Logger [a], Badreddine Douzi [b,4], Laure Journet [a], Christian Cambillau [b], Eric Cascales [a,*]

[a] Laboratoire d'Ingeniérie des Systèmes Macromoléculaires, CNRS, Aix-Marseille Université, UMR 7255, 31 Chemin Joseph Aiguier, 13402 Marseille Cedex 20, France
[b] Architecture et Fonction des Macromolécules Biologiques, CNRS, Aix-Marseille Université, UMR 7257, Campus de Luminy, Case 932, 13288 Marseille Cedex 09, France

ARTICLE INFO

Article history:
Received 12 February 2014
Received in revised form 17 March 2014
Accepted 18 March 2014
Available online 26 March 2014

Keywords:
Protein transport
Microbial communities
Secretion system
Inter-bacterial interactions
Bacteriophage
Tail
Membrane complex
Hcp
VgrG
Baseplate
Assembly platform

ABSTRACT

The Type VI secretion system (T6SS) delivers protein effectors to diverse cell types including prokaryotic and eukaryotic cells, therefore it participates in inter-bacterial competition and pathogenesis. The T6SS is constituted of an envelope-spanning complex anchoring a cytoplasmic tubular edifice. This tubular structure is evolutionarily, functionally and structurally related to the tail of contractile phages. It is composed of an inner tube tipped by a spike complex, and engulfed within a sheath-like structure. This structure assembles onto a platform called "baseplate" that is connected to the membrane subcomplex. The T6SS functions as a nano-crossbow: upon contraction of the sheath, the inner tube is propelled towards the target cell, allowing effector delivery. This review focuses on the architecture and biogenesis of this fascinating secretion machine, highlighting recent advances regarding the assembly of the membrane or tail complexes. This article is part of a Special Issue entitled: Protein trafficking and secretion in bacteria. Guest Editors: Anastassios Economou and Ross Dalbey.

1. Introduction

As emphasized in this Special Issue, a number of specialized protein targeting and secretion mechanisms are dedicated to transport proteins or other macromolecules to specific compartments of the bacterial cell or to the external milieu. These mechanisms are not only critical for bacteria to ensure the proper localization and positioning of key processes, but are essential to efficiently induce pathogenesis or colonize an ecological niche. For a bacterium, colonizing a new niche means not only adapting its fitness but also to entering into competition with other organisms participating in this niche; however, the gain and loss ratio should be strictly controlled as an ecological niche is also efficient when microorganisms coordinate their behaviors. The Type VI secretion system (T6SS) recently emerged as one of the key players in the control of these niches, as the activity of the T6SS might affect prokaryotic cells, simply or highly organized eukaryotic cells. The T6SS delivery mechanism of effector proteins requires a complex apparatus that assembles into the cytoplasm and extends through the bacterial envelope. It is broadly distributed among Gram-negative bacteria but almost exclusively confined to the α-, β- and γ-proteobacteria subgroups with an over-representation in the γ [1,2]. T6SS components are generally encoded within large clusters of genes and in most instances, the expression of these gene clusters is tightly controlled at the transcriptional, post-transcriptional and/or post-translational levels.

This review summarizes the current knowledge on the structural organization of this secretion apparatus. We refer the readers to excellent recent reviews describing the regulation of T6SS genes, the function, the biological significance and the effector proteins delivered by this apparatus [3–8].

☆ This article is part of a Special Issue entitled: Protein trafficking and secretion in bacteria. Guest Editors: Anastassios Economou and Ross Dalbey.

* Corresponding author.
E-mail address: cascales@imm.cnrs.fr (E. Cascales).

[1] These authors contributed equally to this review.

[2] Current address: Department of Microbiology and Immunobiology, Harvard Medical School, 77 Avenue Louis Pasteur, Boston, MA 02115, USA.
[3] Current address: Department of Medical Microbiology and Immunology, University of Wisconsin-Madison, 1550 Linden Drive, Madison, WI 53706, USA.
[4] Current address: Department of Biochemistry and Molecular Biology, University of British Columbia, Vancouver, Canada.

http://dx.doi.org/10.1016/j.bbamcr.2014.03.018
0167-4889/

2. Overall architecture of the Type VI secretion system

2.1. Core components and accessory subunits (Fig. 1)

The number of genes encoded within T6SS clusters varies from 16 genes in the *evp* and *hsi-2* gene clusters from *Edwarsiella tarda* and *Pseudomonas aeruginosa* to 38 genes in *Serratia marcescens* [9,10]. *In silico* analysis of the T6SS gene clusters along with a systematic mutagenesis approach coupled to phenotypic assays performed in *E. tarda*, *Vibrio cholerae* and *Agrobacterium tumefaciens* demonstrated that a minimal set of 13 genes is required to assemble a functional T6SS [2,11–13]. The 13 genes encode the minimal components to assemble a functional T6SS and are called *core components*. Fig. 1 summarizes the 13 T6SS essential genes. *In silico* phylogenetic and genomic organization studies classified these genes in two categories [2]. Four genes, *tssJ*, *tssK*, *tssL* and *tssM*, co-occur in most clusters. With the exception of TssK that locates in the cytoplasm, TssJ, TssL and TssM fractionate with the membranes. The localization of these proteins and the topology of the inner membrane components are depicted in Fig. 1. Similarly, the other nine genes co-occur, with a number of smaller blocks that bear high co-occurrence such as *tssB–tssC–hcp* and *tssE–tssF–tssG*. Although the function of a number of these genes has not been clearly defined yet, the similarities between the Hcp, VgrG and TssE proteins and three subunits associated with the bacteriophage tails (bacteriophage T4 gp19, gp27–gp5 and gp25 respectively) suggest that these nine proteins, or a subset of them, assemble a tail-like structure. These phylogenetic data have been supported by biochemical, protein–protein interaction and structural studies. These 13 core components are therefore thought to form two distinct subassemblies: a membrane complex that anchors a structure related to the tail of contractile bacteriophages to the cell envelope. The architecture, assembly and function of these two sub-assemblies are detailed below.

Aside from these core components, T6SS gene clusters usually encode *accessory* subunits. Although the function of most of these proteins remains to be determined, these accessory subunits segregate into (at least) three categories: (i) components required for the proper assembly of the secretion apparatus (see the example of the TagL protein below); (ii) regulatory subunits acting transcriptionally or post-translationally to control the expression or the activity of the T6SS; and (iii) genuine T6SS substrates and immunities [5,14,15]. In order to ease the comprehension of T6SSs among different organisms, a nomenclature has emerged recently in which the core components are called Tss (*T*ype *s*ix *s*ecretion), whereas the *accessory* subunits are refereed as Tag (*T*ype six *a*ssociated *g*ene) [16]. However, due to history of the field, a number of vernacular names are commonly used such as Hcp, VgrG, ClpV or VipA (TssB) and VipB (TssC).

2.2. General structure of the Type VI secretion system

The seminal article published by Basler and coauthors in 2012 gave an unprecedented view on the general structure of the Type VI secretion system [17]. Using cryo-tomography, the authors showed that the T6SS is composed of a cytoplasmic cylinder anchored to the cell envelope *via* two subcomplexes (Fig. 2A and B). Interestingly, the structure appears to exist in a second – shorter and larger – conformation [17]. The two conformations shown by electron microscopy are consistent with the observation that the TssB and TssC proteins assemble a tubular structure that undergoes stages of extension and contraction (see below) [17]. These results suggested that, similar to the contractile phages, the T6SS may use a contractile mechanism for effector secretion. Therefore, the T6SS is generally depicted as an inverted phage-like tail anchored to the cell envelope through its membrane-associated complex. A schematic representation of the T6SS is shown in Fig. 2C.

2.3. Caught in the act: the Type VI secretion in action

Phages of the *Myoviridae* family use a contractile mechanism, in which a sheath assembled around an inner tube contracts to propel the tube towards the bacterial target cell. In the case of the T6SS, fusion of the VipA/TssB protein to the green fluorescent protein (GFP) provided evidence that this protein polymerizes to assemble a dynamic structure that undergoes elongation and contraction events [17]. Based on these results and on the structural similarities between bacteriophage and T6SS components, the current model proposes that the mode of action of the T6SS could be divided into three main steps (Fig. 3): (i) assembly: a phage-like tail-like structure, comprising the baseplate, the tube and the sheath, is first assembled onto a membrane complex (Fig. 3a–c); (ii) substrate delivery: contraction of the sheath-like structure then propels the inner tube composed of polymerized Hcp tipped by the VgrG protein towards the target cell to deliver toxin effectors (Fig. 3d) and (iii) disassembly: the AAA + ClpV ATPase is recruited to the contracted sheath (Fig. 3e) to recycle sheath components (Fig. 3f). Similar to bacteriophages, the contraction of the T6SS sheath-like structure should lead to effector's delivery in a one-step mechanism, as sheath contraction correlates with target cell lysis [18,19]. Recently, the T6SS activity was followed by time-lapse fluorescence microscopy in a mixed bacterial population [18–21]. Taken together, these

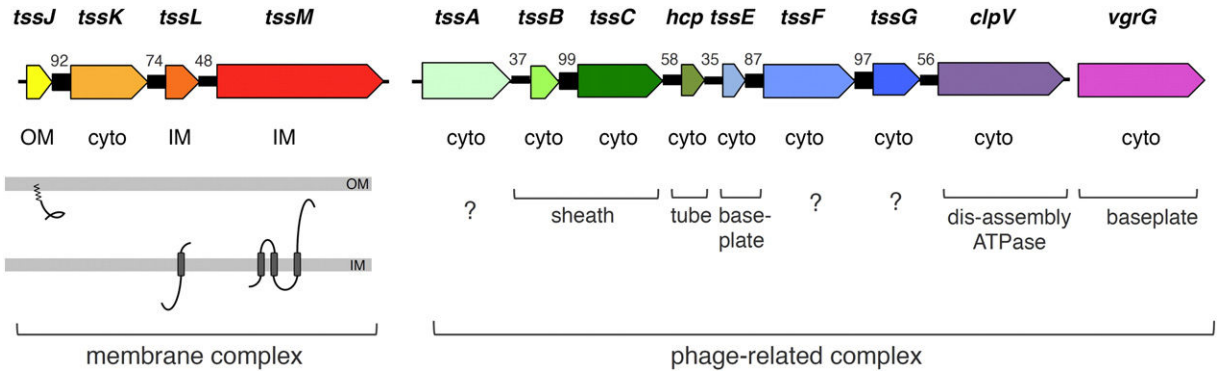

Fig. 1. Type VI secretion gene organization. The minimal set of T6SS genes required for the assembly of a functional T6SS is shown. Genes are partitioned as genes involved in the assembly of the membrane complex (*tssJ*, *tssK*, *tssL* and *tssM*) or of the tail complex (*tssA*, *tssB*, *tssC*, *hcp*, *tssE*, *tssF*, *tssG*, *clpV* and *vgrG*). Genes with conserved transcriptional orientation are connected, the percentage value indicating the conservation frequency (adapted from [2]). The localization of the products of these genes is indicated (cyto, cytoplasm; IM, inner membrane; OM, outer membrane). For membrane proteins, the location of the transmembrane segments (as defined by topology studies) is also shown. For T6SS subunits implicated in the assembly of the tail complex, the localization in the tail structure is also indicated (using the phage nomenclature: tube, sheath and baseplate). Question marks indicate genes for which no function and localization has been inferred based on experimental or phylogenetic evidence (but are thought to be part of the phage tail-related complex based on gene organization conservation). The *clpV* gene, although not related to any phage protein, is classified in the tail complex based on its interaction with the TssBC proteins and its role in the disassembly of the contracted TssBC sheath.

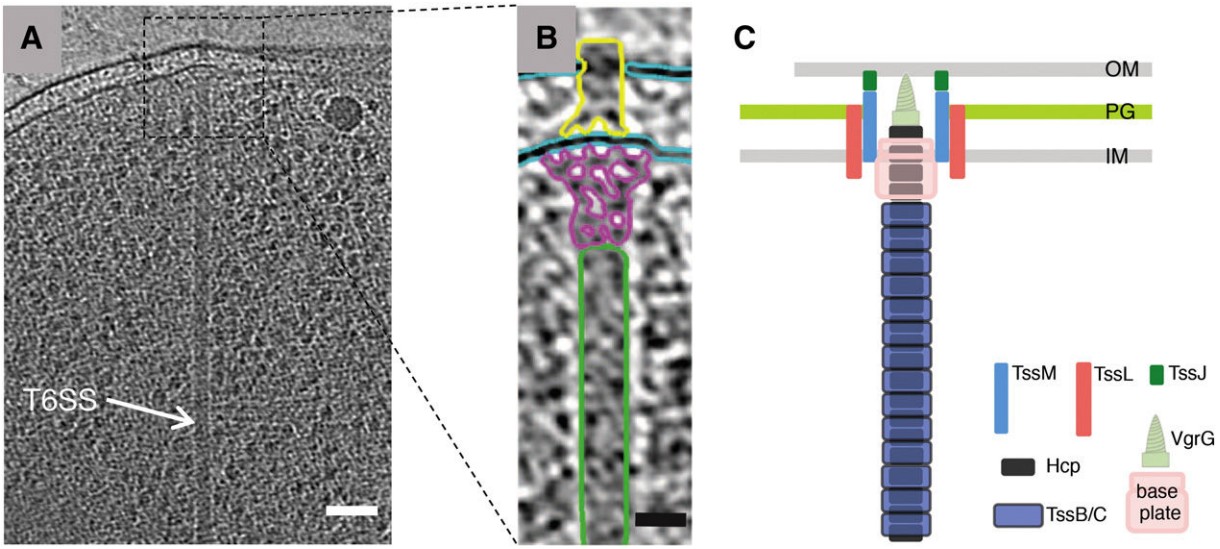

Fig. 2. Overview of the T6SS. (A) Electron cryo-tomograph of *Vibrio cholerae* cells producing the T6SS. The arrow points the long cytoplasmic tubular structure corresponding to the T6SS sheath. A magnification of the upper part of the tomograph is shown in panel B, emphasizing the presence of distinct complexes (green, tail sheath; purple, putative baseplate; yellow, putative membrane complex). Panels A and B are reprinted from [17] with permissions. (C) Schematic representation of the T6SS based on the electron cryo-tomographs and on genetic, biochemical, microscopy and structural data (IM, inner membrane; PG, peptidoglycan layer; OM, outer membrane). Scale bar is 50 nm.

approaches provide a valuable piece of evidence on how the T6SS functions during interbacterial competition. However, when and for which purpose the T6SS is assembled is different depending of the bacterium and therefore results in different comportmental behaviors. *V. cholerae* V52 assembles the T6SS constitutively, even in isolated bacteria [17]. In enteroaggregative *E. coli* (EAEC) cells assemble this sheath-like structure when in contact with different types of bacterial cells, including siblings, T6SS$^-$ or T6SS$^+$ bacteria [18]. By contrast, Leroux et al. and Basler et al. demonstrated that *P. aeruginosa* does not display anarchic T6SS activity, but rather responds, or counterattacks, to the activity of a T6SS in a neighboring cell [19–21]. The bacterial cell therefore senses the attack and hence triggers the assembly and/or the contraction of its own T6SS, a phenomenon known as "dueling" [20]. This behavior is not only important to quickly respond to an attack but also to sense the danger created by T6SS$^+$ competitors and to specifically target these cells [19]. This is consistent with the surprising observation that *P. aeruginosa* only kills efficiently T6SS$^+$ competitors, while *V. cholerae* V52 and EAEC also kill T6SS$^-$ cells [17–21]. These results also demonstrated that the T6SS is a contact-dependent mechanism, which requires sensing of neighboring bacteria and activation of a specific signaling pathway. Indeed, Basler et al. showed that both dueling between sister cells and prey selection require the TagQRST–PpkA–PppA–FHA phosphorylation-dependent regulatory pathway [19]. Briefly, the envelope-associated TagQRST regulatory system controls the activity of the PpkA kinase [22,23]. The PpkA kinase then phosphorylates the FHA protein, which, in turn, activates the T6SS. The activity of PpkA is antagonized by the PppA phosphatase that dephosphorylates FHA, therefore inactivating the T6SS [15,24]. In the absence of the T6SS post-translational regulation, *P. aeruginosa* is unable to select its prey and therefore kills them very inefficiently [19]. This observation is consistent with the idea that a T6SS apparatus must be assembled to a precise location to deliver toxins into a specific target cell. As the TagQRST–PpkA–PppA–FHA is only present in a limited number of bacterial species encoding T6SSs, it is likely that bacteria have developed different regulatory systems to fine-tune T6SS activity [6]. It is also worth to note that T6SS$^+$ cells do not only respond to T6SS-dependent attacks but trigger activity of the secretion machine in response to a broader variety of cell envelope stresses such as the action of antibiotics or conjugative plasmid transfer [25].

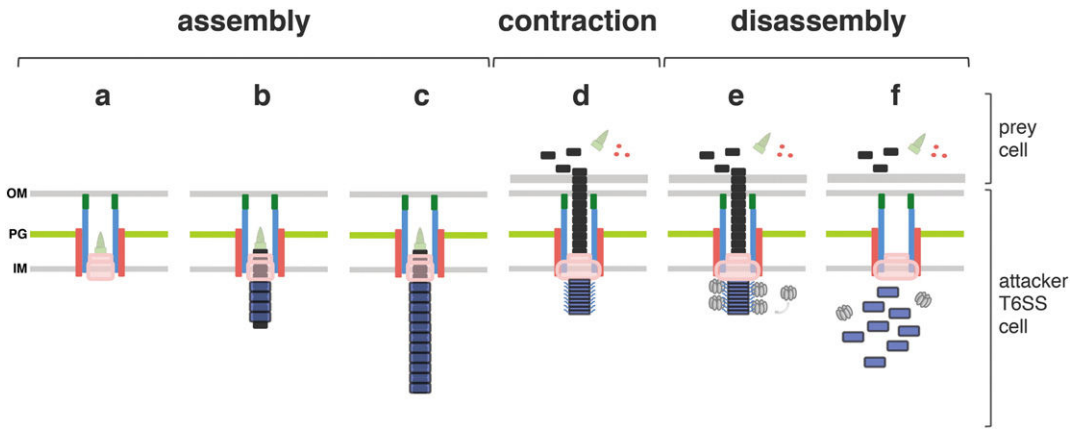

Fig. 3. Mechanism of action of the T6SS. The different stages of the assembly and mode of action of the T6SS are depicted. The biogenesis of the macromolecular complex (a, b, c) can be divided into two steps: the assembly of the membrane and baseplate complexes at the site of secretion (a) is followed by the elongation of the cytoplasmic tubular structure built by Hcp hexamers (black rectangles) stacking on each other coupled to the polymerization of the TssBC sheath (blue rectangles) (b, c). Once in contact with a prey cell, the T6SS sheath contracts hence propulsing the internal tube towards the target prey cell to deliver effector proteins (d). An α-helix from TssC protruding from the contracted sheath recruits the ClpV ATPase (e) that dis-assembles and recycles the TssBC sheath proteins (f).

3. The T6SS membrane-anchoring complex

In most T6SSs, the membrane complex is composed of three membrane-associated subunits: TssL, TssM and TssJ. The localization and topology of these proteins have been defined, and the crystal structures of TssJ and of the cytoplasmic domain of TssL have been reported (Fig. 4). In enteroaggregative *E. coli* (EAEC) and in several other bacteria, an additional component, called TagL, associates with the three above-mentioned proteins [14].

The first membrane-associated T6SS protein to be identified was TssJ. TssJ is an outer membrane protein that bears a typical lipobox sorting motif. The mature TssJ protein is tethered to the outer membrane by the acylation of the N-terminal cysteine residue and protrudes into the periplasm (Fig. 4A) [26]. TssJ multimerizes *in vivo* but its oligomeric state has not been defined [27]. *In vitro*, the purified protein behaves as a monomer [27,28]. The crystal structures of the EAEC (PDB ID: 3RX9), *S. marcescens* (PDB ID: 4A1R) and *P. aeruginosa* (PDB ID: 3ZHN) TssJ proteins have been solved [27–29]. The three structures

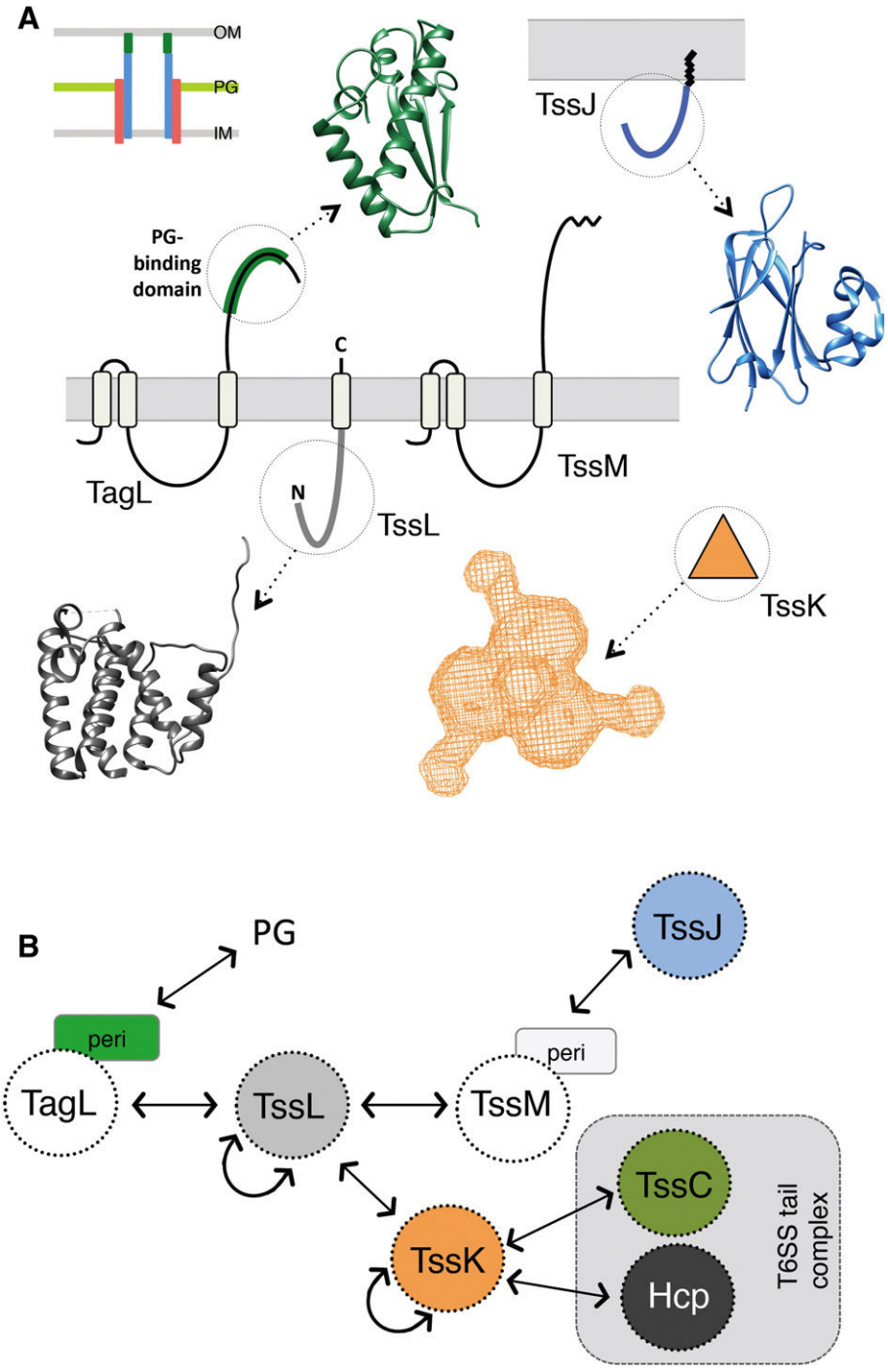

Fig. 4. The T6SS membrane complex. (A) Localization, topology and structures of T6SS membrane complex subunits. Shown are the TssJ outer membrane lipoprotein, the TssL, TssM and TagL inner membrane components and the TssK cytoplasmic protein. The high resolution structures of TssJ (from EAEC, PDB IDs: 3RX9) and of the cytoplasmic domain of TssL (from EAEC, PDB IDs: 3U66), as well as the model of the peptidoglycan-binding domain of TagL, based on the Pal structure (PDB IDs: 1OAP), are shown. The low resolution structure of the homotrimeric TssK complex obtained by SAXS is also shown. (B) Interaction network among T6SS membrane complex subunits. Proteins are schematized by dotted circles; homo and heterotypic interactions are indicated by arrows. The T6SS tail proteins in interaction with TssK are also indicated (PG, peptidoglycan; peri, periplasmic domain).

are roughly identical and share a characteristic globular transthyretin fold, composed of two 4-stranded β-sheets facing each other to form a β-sandwich (Fig. 4A). However, comparison of the three structures highlights differences in the protruding loop connecting β6 and β7 [29]. By contrast, two large loops, that connect β1 and β2 and β5 and β6, have similar sizes and conformations in the three crystal structures, suggesting that they may have important and conserved functions. Indeed, Felisberto-Rodrigues et al. showed that the β1–β2-connecting loop mediates TssJ binding to TssM (Fig. 4B) [28]. However, the β1–β2 loop is variable in terms of sequence among the TssJ orthologs. It has been therefore hypothesized that this loop could act as a specificity determinant for the interaction between cognate TssJ and TssM subunits [28]. This specificity might be essential to avoid cross-interactions between non-cognate proteins when several T6SSs are encoded within the same genome. TssM is anchored to the inner membrane by three trans-membrane helices located in the N-terminal third of the protein. The bulk of the protein, ~800 amino-acids, resides in the periplasm (Fig. 4A) [30]. This periplasmic portion is composed of a large α-helical region followed by a C-terminal all-β-sheet domain. This β-domain is responsible for contacting the TssJ lipoprotein (Fig. 4B). Biophysical studies demonstrated that the TssJ–TssM complex displays a 1:1 stoichiometry with a binding affinity in the micromolar range [28]. The inner-membrane-associated N-terminal region of TssM self-interacts, as shown by two-hybrid studies [11,30]. Although the TssM oligomeric state is not yet known, it is hypothesized that TssM multimers form a channel crossing the inner membrane and extending into the periplasm. If this is the case, one may ask how this complex manages with the cell wall and whether dedicated peptidoglycan hydrolases are required to locally degrade the peptidoglycan for the proper assembly of this large structure. Aside from its self-interaction, the N-terminal TssM region mediates contacts with TssL (see below; [30]). The TssM transmembrane helices 2 and 3 delimit a cytoplasmic loop of ~300 amino-acids. In a subset of TssM proteins, the cytoplasmic loop bears a Walker A-type ATP binding pocket. However, the relevance of this motif is not clear and might be adapted to specific requirements: while the TssM Walker motif is not necessary for the function of the T6SS in *E. tarda*, the *A. tumefaciens* TssM protein has the ability to bind and hydrolyze ATP [11,30,31]. Further studies demonstrated that the TssM ATP binding and hydrolysis activity is important for the function of the *A. tumefaciens* T6SS by modulating the structural conformation of TssM and the recruitment of Hcp to the TssM–TssL complex [31].

It is worth to note that the T6SS-associated TssM proteins share sequence, localization and topology similarities with IcmF, a component of the *Legionella pneumophila* and *Coxiella burnetii* Type IVb secretion systems (T4bSS) [1,9]. Interestingly, the T4bSS IcmF protein forms a heterodimeric complex with DotU/IcmH, a subunit that shares similarities with TssL [1,32]. In the T4bSS, the IcmF/IcmH complex and the IcmF ATP binding site are required for the stabilization of the secretion apparatus [32,33].

TssL spans the inner membrane once, with a transmembrane segment located close to the C-terminus, leaving the bulk of the protein into the cytoplasm (Fig. 4A) [30,34]. Based on this unusual topology, TssL is classified as a C-tail anchored protein, and its proper insertion into the membrane requires the YidC protein and the DnaK chaperone ([34]; see the review of Castanie-Cornet in this thematic issue [35]). Although the TssL cytoplasmic domain is monomeric in solution, two-hybrid experiments showed that it dimerizes, albeit with low efficiency. However, the dimer of the full-length TssL protein resists SDS-PAGE, suggesting that the trans-membrane domain has the ability to stabilize dimer formation [36]. The three-dimensional structures of the EAEC (PDB ID: 3U66) and *Francisella novicida* (PDB ID: 4ACL) TssL cytoplasmic domains have been reported [36,37]. TssL is constituted of two three-helix bundles, the second bundle being composed of shorter helices, yielding a global structure resembling that of a hook (Fig. 4A). The surface-exposed cavity delimitated by the two helix bundles is enriched in negatively charged residues that are conserved among TssL proteins, suggesting that this cleft might be a binding site for partners [37]. Indeed, these residues are critiques as substitutions of these amino-acids in the *Francisella tularensis* TssL protein hamper T6SS function [38]. As described above, TssL interacts with and stabilizes TssM [30,38]. Although the role of the conserved TssL residues in mediating contacts with TssM has not been addressed, substitution of these amino-acids induces TssM degradation [38].

In several T6SS, the TssL protein carries an additional C-terminal, periplasmic domain that shares similarities with the OmpA/Pal/MotB-family peptidoglycan-binding motif [30,39]. However, when this domain is missing, the T6SS gene cluster encodes a supplemental protein, usually TagL, that substitutes for peptidoglycan binding [14,39]. TagL is an inner membrane protein with three transmembrane segments, delimiting a central cytoplasmic loop and a C-terminal periplasmic domain with a functional peptidoglycan-binding motif (Fig. 4A) [14]. Mutations that abolish peptidoglycan binding affect T6SS-dependent Hcp release suggesting that anchorage to the cell wall is a requisite for the proper function of the apparatus. Using pull-down experiments, Aschtgen et al. precipitated a complex constituted of TagL, TssL, TssM and TssJ. Further pull-down experiments using detergent-solubilized cell extracts from *tssL*, *tssM* or *tssJ* cells demonstrated that TagL directly contacts TssL (Fig. 4B) [14]. Therefore, TagL acts as an anchor that ties the secretion apparatus to the cell wall.

Based on these results, the minimal T6SS membrane anchoring complex is composed of the TssL, TssM and TssJ proteins. TssM acts as a connector between the TssL inner membrane protein and the TssJ outer membrane tethered lipoprotein. The complex is stabilized through cell wall binding mediated by either the TssL or TagL component. A number of questions remain to be answered, such as (i) which is the additional component that spans the outer membrane or is the outer membrane of the attacker cell punctured by VgrG during sheath contraction? (2) Is the TssM periplasmic domain used as a conduit to guide the propelled Hcp tube through the periplasm? And (3) do peptidoglycan hydrolases locally degrade the cell wall for the proper assembly of this trans-envelope complex?

4. The T6SS tail complex

One of the most singular features of the T6SS is that it is the first example of a macromolecular complex of the bacterial envelope that shares a common evolutionary origin with the phage injection apparatus. This is supported by structural and/or bioinformatics data for four different subunits (Hcp, VgrG, TssC and TssE) and by the recent work of Basler et al. [17]. Using a combination of fluorescence microscopy and electron cryo-tomography the authors demonstrated that the TssB and TssC subunits of *V. cholerae* assemble a dynamic structure in the cytoplasm of the cell, near-perpendicular to the membrane, which is structurally and functionally related to the tail sheath of contractile bacteriophages (Fig. 2A) [17]. A wealth of data now support the conclusion that the T6SS comprises a contractile tail-like structure composed of essential elements: inner tube, sheath and baseplate.

4.1. The T6SS tail tube

The T6SS inner tube is constituted of the Hcp protein, a structural homologue of phage tail tube proteins. *In vitro*, Hcp proteins spontaneously assemble into a ~100 Å wide donut-shaped hexameric ring with an internal diameter of ~40 Å [40]. Five structures of Hcp proteins have been reported to date: Hcp1 (PDB ID: 1Y12) and Hcp3 (PDB ID: 3HE1) from *P. aeruginosa*, EvpC from *E. tarda* (PDB ID: 3EAA), Hcp1 from EAEC (PDB ID: 4HKH) and Hcp from *Yersinia pestis* (PDB ID: 3V4H) (Fig. 5A) [40–43]. The Hcp tertiary structure is very similar to that of gpV, the bacteriophage λ tail tube protein [44]. Although bacteriophage λ is not a contractile phage, this former observation strongly supports the initial postulate that polymerized Hcp proteins form the inner tube of the T6SS (Fig. 5A). Indeed, using electron microscopy, Leiman

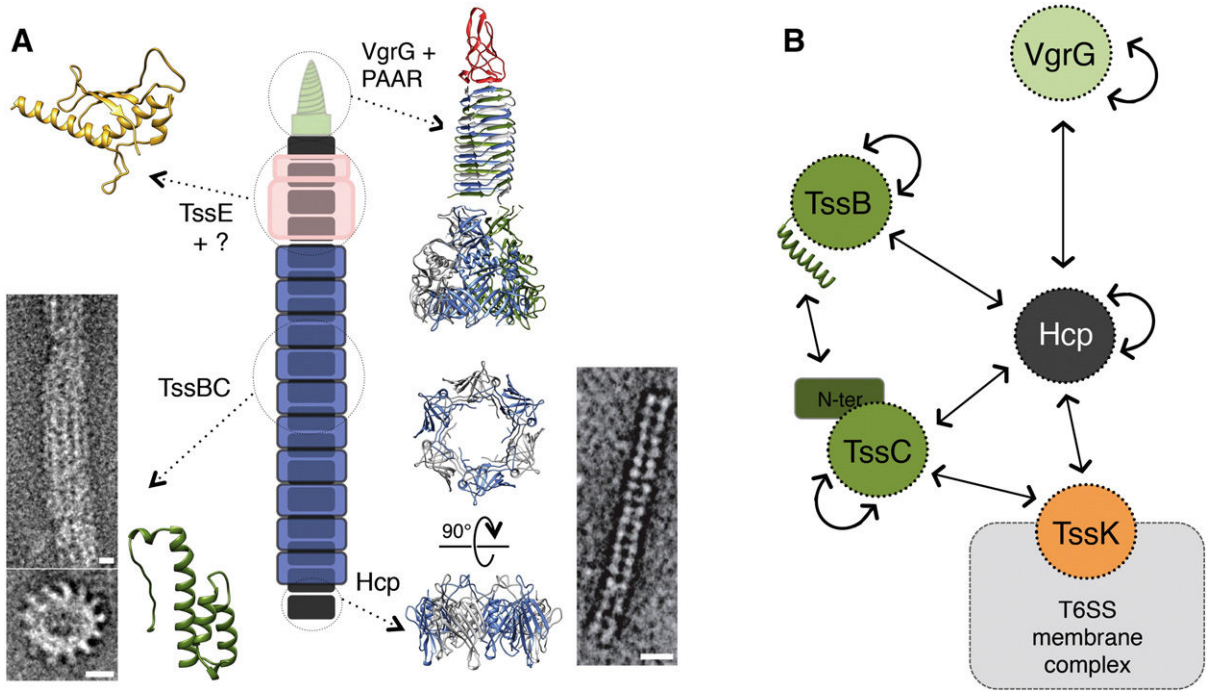

Fig. 5. The T6SS tail complex. (A) Localization, organization and structures of T6SS tail proteins. Shown are the Hcp hexamers that stack on each other to form the internal tube and the TssBC contractile sheath-like structure, assembled on the baseplated complex constituted of TssE, the VgrG–PAAR complex and probably unknown additional subunits. Electron micrographs of the artificial Hcp tube and of the TssBC sheath (cross-section in lower panel) are reprinted from [46,57], respectively, with permissions (scale bars are 10 nm). The high resolution structures of Hcp (from EAEC, PDB IDs: 4HKH), of the C-terminal domain of TssB (from EAEC, PDB IDs: 4PS2), of the VgrG–PAAR puncturing complex (from *E. coli* O6: VgrG, PDB IDs: 2P57; PAAR, PDB IDs: 4JIW) as well as the model of the TssE protein, based on the structure of the phage T4 gp25 component (PDB IDs: 4HRZ), are shown. (B) Interaction network among T6SS tail subunits. Proteins are schematized by dotted circles; homo and heterotypic interactions are indicated by arrows. Specific domain or fragments involved in the interactions are depicted (Nter, N-terminal domain). The TssK protein, that connects both membrane and tail complexes, is shown.

et al. showed that hexamers of *P. aeruginosa* Hcp3 assemble tubular structures *in vitro* [45]. Additionally, Hcp hexamers stack on each other to form tubes within the crystal lattice. This propensity to form tubules has been used to produce artificial nano-tubes of determined length, by engineering disulphide bridges at the hexamers' interfaces (Fig. 5A) [46]. *In vivo*, Hcp hexamers accumulate in the cytoplasm and the culture supernatant [40,42,47] and stack on each other in a head-to-tail manner [47]. These data suggest that Hcp assembles a channel-like structure extending in the cytoplasm. However, the Hcp tube is probably not stable by itself, as biophysical studies showed that the affinity between hexamers is rather low, approximately 7 μM [43]. This means that *in vivo*, Hcp tube formation needs to be stabilized, probably by the polymerization of the sheath. Hcp tube formation is critical for T6SS function as introduction of bulky residues at the interface of the hexamers disrupts interaction between hexamers *in vitro*, and prevents Hcp tube formation and T6SS function *in vivo* [43,47].

It is worth to note that the internal diameter of the Hcp hexamer is sufficient to accommodate a small folded protein or unfolded/partly folded protein [40]. In support to this hypothesis, two putative effectors, *E. tarda* EvpP and *A. tumefaciens* Atu4347 were shown to interact with Hcp [11,13]. More precisely, recent data demonstrated that the *P. aeruginosa* Tse2 anti-bacterial effector binds to and occludes the Hcp hexamer, providing the first evidence that the Hcp tube might be used as a cargo to deliver effectors into target cells [48].

Interestingly, while Hcp hexamers stack head-to-tail in wild-type cells, they interact in head-to-head, tail-to-tail and head-to-tail in the absence of T6SS components, suggesting that a subset of these components control the proper assembly of Hcp tubes [47]. During bacteriophage morphogenesis, tail tube/sheath assembly is dictated by a structure called the baseplate. Although the bacteriophage T4 baseplate is constituted of a large number of different subunits, Leiman and Shneider suggested that the minimal contractile bacteriophage baseplates comprise essential components, such as the gp25, gp6, gp53 (or gp7), gp27 and gp5 subunits [49]. In the T6SS, two proteins, TssE and VgrG, exhibit structural and functional similarities to gp25 and to the gp27–gp5 complex respectively [45,50,51]. Consistent with bacteriophage tail biogenesis, the VgrG protein was shown to be required for the proper polymerization of Hcp hexamers, whereas the TssB and TssC subunits were shown to be dispensable, suggesting that the T6SS sheath uses the tube as a template during assembly [47]. Although the general mechanism of tube formation seems conserved between bacteriophages and T6SSs (requirement for a baseplate-like nucleation platform, a tube serving as a template for sheath polymerization), the constituting proteins have different properties: the Hcp hexamers are extremely stable but form weak tubular edifices while phage tube proteins remain monomeric in solution but assemble stable tubular structures [44–46].

4.2. The T6SS tail sheath

In the bacteriophage T4 tail, the inner tube is engulfed within the contractile sheath made of gp18 subunits. In the T6SS, two proteins, TssB and TssC, assemble the sheath (Fig. 5A). The *tssB* and *tssC* genes co-occur in all T6SS gene clusters (Fig. 1) and the corresponding proteins interact and stabilize each other (Fig. 5B) [13,52–58]. The regions required for the TssB–TssC interaction have been mapped: the N-terminus of TssC is essential to contact TssB [56–58] while the hydrophobic face of a conserved α-helix in the central region of TssB is involved in the interaction (Fig. 5B) [54,58,59].

The purified TssB and TssC proteins spontaneously form tubular structures observable by electron microscopy that share remarkable structural similarities with the bacteriophage sheath (Fig. 5A). Image reconstruction of the particles showed that TssB and TssC assemble predominantly into 12-symmetry structures that exhibit cogwheel-like cross sections, with 12 protruding paddles (Fig. 5A) [17,53,57]. Cross-sections present external and internal diameters of ~300 Å and ~110 Å respectively [17,53,57]. Although no structural data is available yet

for TssB and TssC, bioinformatic analysis of these proteins revealed that the C-terminal 150 amino-acid region of TssC resembles the domain IV of phage sheath proteins [49]. It is worth noting that in the bacteriophage T4 tail, this domain was proposed to connect sheath subunits by an arm-exchange mechanism [49]. One may hypothesize that the C-terminus of TssC plays a role comparable to that of gp18 in maintaining T6SS sheath integrity during contraction. If this is the case, the "arm" polypeptide remains to be identified in TssC. Consistent with the role of gp18 domain IV, the deletion of the C-terminal domain of TssC has no effect on the interaction with TssB but abolishes the formation of TssBC tubules, suggesting that this domain is critical for polymerization into tubules [57]. The structure of the C-terminal region of TssB was recently obtained (PDB ID: 4PS2), providing information on the α-helix that contacts TssC (Douzi et al., unpublished) (Fig. 5A). However, this three-helix bundle has no homology with any portion of the region of gp18 for which the structure is known [60].

The TssB and TssC proteins co-fractionate with cytoplasmic proteins [53,54,56]. However, a large amount of TssB and TssC can be found associated with the membrane fraction [56,61], consistent with the observation that TssB and TssC form high molecular-weight complexes that likely co-sediment with the membrane without being really associated with it.

In 2012, using electron cryo-tomography, Basler et al. reported that a cytoplasmic tubular structure can be observed *in vivo* in T6SS-producing *V. cholerae* cells (see Fig. 2) [17]. Kapitein et al. confirmed that these structures correspond to T6SS sheaths using immunogold labeling of TssB [62]. These structures were observed in two different conformations that likely correspond to the extended and contracted states. In the contracted state, the tubular structure is hollow and its dimensions are similar to that observed in purified TssBC complexes. In the extended state, the structure is thinner and an extra-density is observed inside the tubule, suggesting that the central lumen is filled, probably by the inner Hcp tube [17]. The molecular mechanism controlling the passage from the extended to the contracted state has yet to be uncovered but, on the basis of the contractile mechanism of *Myoviridae*, it likely involves structural transitions within and between the TssBC proteins, which must therefore exist in different conformations. As noted above, the TssBC tubules in the contracted conformation have sizes and diameters that match those of the purified T6SS sheaths, suggesting that the TssBC complexes that spontaneously assemble *in vitro* represent contracted sheaths. Beside the C-terminal fragment of TssB, no structural information is available for the TssBC complex either in the extended or contracted state, probably because of the propensity of these proteins to assemble large tubular structures incompatible with crystallization or NMR studies.

As described above, time-lapse fluorescence microscopy showed that TssBC tubules exhibit a highly dynamic behavior. They first assemble an initial foci close to the membrane, which extends to form a tubular structure that spans the cell length or width in several tens of seconds. The tubes then contract to yield a foci that is disassembled [17,18,20,21,62]. A full cycle can be divided into three steps: extension/assembly, contraction and disassembly (Fig. 3). Kapitein et al. noted that after disassembly, new tubules form at the original position or at alternative sites [62]. Although the significance of this observation is not yet known, it is also interesting to note that, once contracted, the TssBC sheaths usually rotate and became obliquely oriented compared to the membrane [17].

Biochemical studies demonstrated that the TssBC proteins interact with the component of the tube, Hcp (Fig. 5B) [13,47]. It is noteworthy that the internal diameter of the TssBC complexes (~110 Å) is sufficient to accommodate the Hcp tubule (external diameter of ~100 Å) [17,53,57,63]. One may hypothesize that the zones of contact between the T6SS tail and sheath are located at the outside of the Hcp doughnut and inside the TssBC tubular structure. Interestingly, Jobichen et al. noted that a zone constituted of charged residues, located outward the Hcp hexamer is essential for Hcp release [42]. In the absence of Hcp, TssBC tubules do not form as the TssB–GFP fusion proteins present a diffuse pattern [47,62]. However, Kapitein et al. showed that, in *hcp* cells, TssBC spontaneously assemble contracted sheaths that are rapidly dissociated by ClpV [62]. Similar results were obtained in the *tssE*, *tssM* or *tssK* mutant cells, demonstrating that these three subunits are also required for polymerization of the sheath [17,47,62,64]. Regarding Hcp, it was shown that disruption of the inner tube structure by the insertion of bulky residues at the Hcp hexamer's interface also prevents sheath polymerization, suggesting that Hcp tube formation precedes sheath assembly [47]. What do these data tell us about the assembly of the tail tube/sheath? First, TssBC are not required for proper assembly of Hcp tubules in the head-to-tail conformation. Second, Hcp tube formation is required for assembly of the sheath. Based on these observations, we may hypothesize that assembly of the tube precedes sheath polymerization, or more likely that the assembly of these two structures is coordinated. In the latter case, (i) the insertion of an Hcp hexamer in the growing structure may immediately precede the incorporation of TssBC complexes or (ii) TssBC–Hcp pre-assembled complexes might be progressively incorporated. Although the coordinated assembly is more likely, cryo-tomography did not reveal assembly intermediates, *i.e.*, filled sheaths of different lengths [17].

By analogy with the mode of action of contractile phages, it has been proposed that contraction of the TssBC structure propels the Hcp tube toward the cell exterior or directly into a target cell. If this holds to be true, it means that the Hcp hexamers will be in contact with the sheath only when the sheath is in the extended state. This is consistent with (i) mass spectrometry data showing that purified T6SS sheaths (*i.e.*, in the contracted state) do not contain Hcp proteins, and (ii) that contracted TssBC sheaths are hollow compared to the extended TssBC sheaths that are filled (probably by the inner Hcp tube) as shown in electron cryo-tomographs [17]. Therefore, the TssBC–Hcp interactions observed by bacterial two-hybrid or pull-down experiments [13,47] potentially represent TssBC subunits in the extended state conformation.

4.3. Questions of length and of termination

In bacteriophages, the length of the tail is strictly controlled, usually by a tape measure protein that functions as a molecular ruler [65]. No homologue to the tape measure protein is encoded within T6SS gene clusters, suggesting that either the length of the T6SS tail is not regulated or that it involves a distinct mechanism. However, the observation that the T6SS sheaths assemble structures of different lengths support the postulate that the lengths of T6SS tails are not controlled [17,62]. More importantly, it is not yet known how the T6SS tail is terminated. Because it connects the tail tube and the sheath at the distal end, the bacteriophage tail terminator protein is a requisite for the propelling of the inner tube during sheath contraction [49,65]. In the absence of such a component, the force generated during contraction of the sheath could not be transferred to the tail tube. Nevertheless, if the requirement of a functionally similar subunit for the T6SS is not a matter of debate, the protein(s) that plays this role has not been identified yet.

4.4. The putative baseplate

During phage morphogenesis, the tail tube and sheath assemble on a platform called the baseplate [49]. Interestingly, the *V. cholerae* electron cryo-tomographs published by Basler et al. showed the existence of a flared bell-like density connecting the T6SS tail to the membrane (Fig. 2B) [17]. During tail contraction, the phage baseplate undergoes a large structural transition [66–68]. Interestingly, the bell-shape density observed in *Vibrio* cells is also subjected to a large conformational modification upon sheath contraction [17]. According to the definition given by Leiman and Shneider, the minimal baseplate (*i.e.*, the minimal set of subunits required for the proper assembly and the controlled contraction of tail-like structures) would be constituted of the central hub – the ($gp27_3$–$gp5_3$) complex – and three wedge proteins: gp6, gp25 and

probably gp53 (or gp7) [49]. As detailed below, VgrG and TssE, two T6SS core components are homologous to the central hub and gp25 respectively [1,45]. Furthermore, VgrG is required for the proper assembly of the Hcp tube [47] while TssE is required for polymerization of the TssBC sheath [17,18,62]. These results support the idea that T6SS tail biogenesis is dictated by an assembly platform functionally similar to the bacteriophage baseplate. However, the T6SS homologues of gp6 and gp53 (or gp7), if they exist, have not yet been identified.

The VgrG protein is homologous to the cell-puncturing device, or spike, of bacteriophage T4. The central hub of T4 is comprised of a double trimer ($gp27_3$–$gp5_3$) that is featured by a β-prism spike and a three-fold to six-fold symmetry adaptor domain that connects to the inner tube. The crystal structure of the N-terminal fragment of VgrG from the uropathogenic *E. coli* CFT073 strain was solved (PDB ID: 2P57) and compared to that of the ($gp27_3$–$gp5_3$) complex (Fig. 5A) [45]. The global fold of the VgrG N-terminal is very similar to that of gp27 along with the N-terminal, OB, and region of gp5, with the exception of the lysozyme domain carried by gp5. The crystal structure of the C-terminal domain of the *E. coli* O157 VgrG protein was recently reported (PDB ID: 3WIT), and as expected, displays a three-stranded β-helical fold [69]. Thus, the *vgrG* gene is a fusion of the *gp27* and *gp5* genes. By analogy with the phage tail structure and its assembly pathway, the Hcp tube is thought to assemble onto the VgrG trimer and to propel it towards the target cell as a result of TssBC contraction. The needle-shaped β-helical domain of VgrG will help to penetrate the target cell. This model is supported by the observations that (1) Hcp and VgrG exhibit a codependency for their release in culture supernatants [11,50], (2) Hcp and VgrG interact [13] and (3) VgrG is required for the proper assembly of the Hcp tube [47]. Based on these results, it is likely that VgrG acts as a baseplate subunit in T6SS. It is worth to add that a number of VgrG proteins carry C-terminal extensions located downstream the β-prism. Because these extensions may function as effector domains, these VgrGs have been named "specialized VgrGs" [50,70]. Ma et al. demonstrated that these additional domains are delivered inside target cells [71], suggesting that, similarly to its phage counterpart, VgrG acts as a spike. More recently, it was shown that an additional protein, called PAAR, usually encoded within T6SS or *vgrG* gene operons, forms a conical structure that caps the extremity of VgrG, sharpening the tip of the spike (PDB IDs: 4JIV and 4JIW) [72]. Here again, this result is consistent with the observation that a number of bacteriophage spikes are decorated with an unknown protein that also sharpens the extremity [73]. PAAR is therefore secreted in a VgrG-dependent manner and it was further proposed that PAAR may be used as a connector between VgrG and protein effectors [72]. This suggestion is supported by the observation that a number of PAAR proteins are fused to putative effector domains [72]. However, the function of PAAR is probably more complex as it is required for the release of Hcp in the culture supernatant, which reflects the assembly and function of the T6SS, and it has been therefore suggested that PAAR might be required to nucleate VgrG folding [72].

In addition to VgrG, the TssE protein is also a component of the T6SS baseplate. TssE shares a high degree of similarity with gp25, a component of the baseplate wedges of bacteriophage T4 [1,9,45,51]. The three-dimensional structure of TssE is not yet determined. However, the degree of conservation between TssE and gp25 orthologs is sufficient to build a model based on the structure of the bacteriophage T4 gp25 protein (PDB ID: 4HRZ; Browning, Shneider and Leiman, unpublished) (Fig. 5A). In the bacteriophage T4 tail, gp25 is thought to initiate the polymerization of the sheath by an arm-exchange mechanism with the first row of gp18 subunits [49]. Even though the role of TssE in T6SS biogenesis remains unknown, a similar function is in agreement with the observations that (1) TssE is a cytoplasmic protein that co-precipitates with the TssBC complex in *V. cholerae* [17,51] and (2) T6SS sheaths do not form in *tssE* cells [17,18,62].

Although no similarities were found with bacteriophage proteins in this case, the TssK has been proposed to be a component of the T6SS baseplate. TssK is a cytoplasmic subunit that oligomerizes to form a three-armed structure with an overall pyramidal shape (Fig. 4A) [64]. TssK was shown to co-precipitate with TssBC sheaths [17] through direct interaction with TssC (Figs. 4B and 5B) [64]. Fluorescence microscopy experiments further showed that TssK is required for sheath polymerization [64]. Interestingly, TssK also interacts with the cytoplasmic domain of the TssL inner membrane protein [64]. This is consistent with the conserved genomic organization between the *tssK* and genes coding for the membrane complex (Fig. 1) [2]. Although further studies are necessary to understand the exact role of TssK, it has been proposed that this subunit connects the T6SS tail to the TssJLM membrane complex (Figs. 4B and 5B).

Upon bacteriophage landing onto host cells, the attachment of the fibers induces a switch in the baseplate conformation that will ultimately trigger sheath contraction [67,74]. One may therefore hypothesize that a signal should be transmitted to the putative T6SS baseplate to initiate TssBC contraction [63]. Several T6SS have been shown to be activated by the TagQRST–PppA–PpkA–FHA phosphorylation-dependent pathway and therefore it is conceivable that this post-translational activating pathway leads to a structural modification of the T6SS baseplate or to membrane component(s) that are linked to it. However, the observation that most T6SS are devoid of this phosphorylation pathway raises the question whether additional mechanisms to sense and signal the contact with target cells exist.

4.5. Disassembly of the T6SS contracted sheath

Since the discovery of the T6SS, the energization of the system for secretion was a matter of debate. ClpV, one of the T6SS core components, belongs to the Hsp100/Clp family of AAA^+ ATPase proteins. Hsp100/Clp proteins are oligomeric ring-like machines that bind ATP *via* the conserved AAA domain and convert the energy of ATP hydrolysis into a protein-unfolding activity. The ATPase activity of ClpV has been demonstrated to be required for Type VI secretion in several organisms, including *P. aeruginosa*, *E. tarda*, and *V. cholerae* [11,40,53]. Hence, prior to the demonstration that the TssBC sub-complex functions as a phage contractile sheath, it was hypothesized that the ClpV specialized ATPase energized either the assembly of the T6SS or substrate secretion. However, Zheng and Mekalanos, and Basler et al. demonstrated that *V. cholerae clpV* mutant cells conserve ~10% of T6SS activity, demonstrating that ClpV does not power assembly or secretion but rather improve the efficiency of the apparatus [12,17]. However, in a breakthrough work, Bönemann et al. showed that ClpV interacts directly with TssB and TssC and demonstrated that ClpV disassembles TssBC tubules *in vitro* in an ATP-fuelled manner [53]. In addition, the same authors reported that the specificity of ClpV for TssBC is conferred by its N-terminal domain and can be transferred to the housekeeping ClpA ATPase by swapping their respective N-terminal domains. Using a TssB–GFP fusion, Basler et al. showed that in the absence of ClpV the TssBC complex is not dynamic anymore and that the TssB localization is similar to that observed in contracted TssBC structures [17]. Moreover Basler and Mekalanos used a combination of TssB–GFP and ClpV–mCherry fusions to demonstrate that prior to TssBC contraction, ClpV is evenly distributed in the cytosol, whereas contraction of the sheath leads to immediate co-localization of ClpV–mCherry with the contracted sheath (Figs. 3d, e, f and 6) [20]. Once the TssBC complex is disassembled, TssB and ClpV no longer co-localize to a single focus. These data were later confirmed by immunogold labeling of ClpV, demonstrating that ClpV proteins decorate contracted sheaths [62]. These results strongly support the idea that ClpV is essential for the dynamics of TssBC tubules, recycling the TssB and TssC subunits after sheath contraction. Kapitein et al. provided further evidence that in addition to recycling the pool of TssBC subunits by disassembling contracted TssBC tubules, ClpV also prevents formation of aberrant, aggregated, TssBC tubules in the cytoplasm [62]. The molecular bases by which ClpV specifically recognizes contracted sheaths came from the work of Pietrosiuk et al. [75]. The authors determined that ClpV binds with weak affinity (~40 μM) to a discrete fragment on TssC

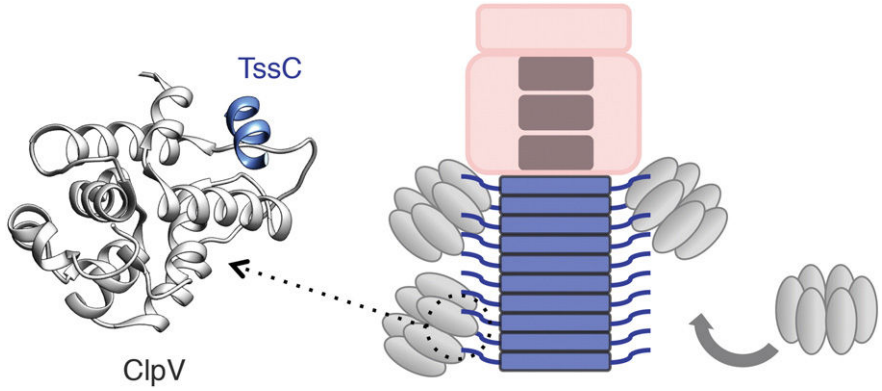

Fig. 6. Disassembly of the contracted T6SS sheath. Once contracted, the N-terminal α-helix of the TssC protein protrudes from the sheath structure and recruits the ClpV AAA$^+$ ATPase, allowing disassembly and recycling of the TssBC proteins. The high resolution structure of the ClpV N-terminal domain complexed with the TssC α-helix (from EAEC, unpublished) is shown.

corresponding to its N-terminal α-helix. The crystal structures of the *V. cholerae* and EAEC N-terminal ClpV domain alone or complexed to the TssC peptide are available (PDB IDs: 3ZRI/4HH5 for ClpV alone and PDB IDs: 3ZRJ/4HH6 for the complexes) ([75], Douzi et al., unpublished). The ClpV protein possesses an additional N-terminal α-helix, named α0, compared to other members of the Hsp100 family. The TssC α-helix binds to an hydrophobic groove located between the two first α-helices of ClpV, α0 and α1 (Fig. 6), providing the explanation why TssC is not a substrate for housekeeping Clp proteins [75]. Although this has not been formally demonstrated, the current model suggests that the TssC N-terminal α-helix is buried within the extended sheath but protrudes from the contracted sheath, allowing ClpV recruitment and activity (Fig. 6). The question whether the disassembled TssB and TssC subunits are recycled and integrated into a new cycle of assembly/contraction or are degraded remains to be clearly answered.

5. Closing remarks and prospects

Over the last few years, the T6SS became a highly exciting area of research, each week providing its batch of novelty. Breakthrough studies have shaken the field, including the discovery that T6SSs are involved in interbacterial competition or that the T6SS is structurally and functionally similar to contractile bacteriophage tails. However, while current efforts concentrate on the nature of the effectors delivered by this machine and on the secretion mechanisms, important questions regarding the overall architecture and the biogenesis of the T6SS remain to be answered. Providing structural information on the complete T6SS (or sub-complexes), such as those obtained for the Type III or Type IV apparatus will supply an unprecedented view of this machine. Identifying the T6SS baseplate components is also an exciting challenge that will pave the way to a better understanding of the molecular mechanism triggering sheath contraction. Finally, how the attacker cells sense the prey and position and activate the T6SS remains to be experimentally addressed.

Acknowledgements

We apologize for any omissions in the citations of primary reports owing to space limitations. We thank Grant Jensen, John Mekalanos, Joseph Mougous, Alain Filloux and the Nature Publishing Group for permission to reprint electron micrographs, the two anonymous reviewers for the suggestions to improve the manuscript, the members of the Lloubès, Cambillau, Sturgis and Bouveret research groups for fruitful discussions, and Léa-Rico Sonkui for encouragements. Work in the EC laboratory is supported by the Centre National de la Recherche Scientifique (CNRS), the Aix-Marseille Université, doctoral fellowships from the French Ministère de la Recherche (to A.Z., Y.R.B., M.S.A., and L.L.), a post-doctoral fellowship from the Fondation pour la Recherche Médicale (FRM-SPF20101221116; to E.D.) and a grant from the Agence Nationale de la Recherche (ANR-JCJC-2010-1303-03).

References

[1] L.E. Bingle, C.M. Bailley, M.J. Pallen, Type VI secretion: a beginner's guide, Curr. Opin. Microbiol. 11 (2008) 3–8.
[2] F. Boyer, G. Fichant, J. Berthod, Y. Vandenbrouck, I. Attree, Dissecting the bacterial Type VI secretion system by a genome wide in silico analysis: what can be learned from available microbial genomic resources, BMC Genomics 12 (2009) 10–104.
[3] C.S. Bernard, Y.R. Brunet, E. Gueguen, E. Cascales, Nooks and crannies in Type VI secretion regulation, J. Bacteriol. 192 (2010) 3850–3860.
[4] J.M. Silverman, Y.R. Brunet, E. Cascales, J.D. Mougous, Structure and regulation of the Type VI secretion system, Ann. Rev. Microbiol. 66 (2012) 453–472.
[5] S.J. Coulthurst, The Type VI secretion system — a widespread and versatile cell targeting system, Res. Microbiol. 164 (2013) 640–654.
[6] B.T. Ho, T.G. Dong, J.J. Mekalanos, A view to a kill: the bacterial Type VI secretion system, Cell Host Microbe 15 (2013) 9–21.
[7] A.B. Russel, S.B. Peterson, J.D. Mougous, Type VI secretion system effectors: poisons with a purpose, Nat. Rev. Microbiol. 12 (2014) 137–148.
[8] J. Benz, A. Meinhardt, Antibacterial effector/immunity systems: it's just the tip of the iceberg, Curr. Opin. Microbiol. 17 (2014) 1–10.
[9] E. Cascales, The Type VI secretion toolkit, EMBO Rep. 9 (2008) 735–741.
[10] S.L. Murdoch, K. Trunk, G. English, M.J. Fritsch, E. Pourkarimi, S.J. Coulthurst, The opportunistic pathogen *Serratia marcescens* utilizes Type VI secretion to target bacterial competitors, J. Bacteriol. 193 (2011) 6057–6069.
[11] J. Zheng, K.Y. Leung, Dissection of a Type VI secretion system in *Edwardsiella tarda*, Mol. Microbiol. 66 (2007) 1192–1206.
[12] J. Zheng, B. Ho, J.J. Mekalanos, Genetic analysis of anti-amoebae and anti-bacterial activities of the Type VI secretion system in *Vibrio cholerae*, PLoS One 6 (2011) e23876.
[13] J.S. Lin, L.S. Ma, E.M. Lai, Systematic dissection of the *Agrobacterium* Type VI secretion system reveals machinery and secreted components for subcomplex formation, PLoS One 8 (2013) e67647.
[14] M.S. Aschtgen, M. Gavioli, A. Dessen, R. Lloubès, E. Cascales, The SciZ protein anchors the enteroaggregative *Escherichia coli* Type VI secretion system to the cell wall, Mol. Microbiol. 75 (2010) 886–899.
[15] J.M. Silvermann, L.S. Austin, F. Hsu, K.G. Hicks, R.D. Hood, J.D. Mougous, Separate inputs modulate phosphorylation-dependent and -independent Type VI secretion activation, Mol. Microbiol. 82 (2011) 1277–1290.
[16] G. Shalom, J.G. Shaw, M.S. Thomas, In vivo expression technology identifies a Type VI secretion system locus in *Burkholderia pseudomallei* that is induced upon invasion of macrophages, Microbiology 153 (2007) 2689–2699.
[17] M. Basler, M. Pilhofer, G.P. Henderson, G.J. Jensen, J.J. Mekalanos, Type VI secretion requires a dynamic contractile phage tail-like structure, Nature 483 (2012) 182–186.
[18] Y.R. Brunet, L. Espinosa, S. Harchouni, T. Mignot, E. Cascales, Imaging Type VI secretion-mediated bacterial killing, Cell Rep. 3 (2013) 36–41.
[19] M. Basler, B.T. Ho, J.J. Mekalanos, Tit-for-tat: Type VI secretion system counterattack during bacterial cell–cell interactions, Cell 152 (2013) 884–894.
[20] M. Basler, J.J. Mekalanos, Type 6 secretion dynamics within and between bacterial cells, Science 337 (2012) 337–815.
[21] M. Leroux, J.A. De Leon, N.J. Kuwada, A.B. Russell, D. Pinto-Santini, R.D. Hood, D.M. Agnello, S.M. Robertson, P.A. Wiggins, J.D. Mougous, Quantitative single-cell characterization of bacterial interactions reveals Type VI secretion is a double-edged sword, Proc. Natl. Acad. Sci. U. S. A. 109 (2012) 19804–19809.
[22] F. Hsu, S. Schwarz, J.D. Mougous, TagR promotes PpkA-catalysed Type VI secretion activation in *Pseudomonas aeruginosa*, Mol. Microbiol. 72 (2009) 1111–1125.

[23] M.G. Casabona, J.M. Silverman, K.M. Sall, F. Boyer, Y. Couté, J. Poirel, D. Grunwald, J.D. Mougous, S. Elsen, I. Attree, An ABC transporter and an outer membrane lipoprotein participate in posttranslational activation of Type VI secretion in *Pseudomonas aeruginosa*, Environ. Microbiol. 15 (2013) 471–486.

[24] J.D. Mougous, C.A. Gifford, T.L. Ramsdell, J.J. Mekalanos, Threonine phosphorylation post-translationally regulates protein secretion in *Pseudomonas aeruginosa*, Nat. Cell Biol. 9 (2007) 797–803.

[25] B.T. Ho, M. Basler, J.J. Mekalanos, Type 6 secretion system-mediated immunity to type 4 secretion system-mediated gene transfer, Science 342 (2013) 250–253.

[26] M.S. Aschtgen, C.S. Bernard, S. Bentzmann, R. Lloubès, E. Cascales, SciN is an outer membrane lipoprotein required for Type VI secretion in enteroaggregative *Escherichia coli*, J. Bacteriol. 90 (2008) 7523–7531.

[27] V.A. Rao, S.M. Shepherd, G. English, S.J. Coulthurst, W.N. Hunter, The structure of *Serratia marcescens* Lip, a membrane-bound component of the Type VI secretion system, Acta Crystallogr. D Biol. Crystallogr. 67 (2011) 1065–1072.

[28] C. Felisberto-Rodriguez, E. Durand, M.S. Aschtgen, Y. Blangy, M. Ortis-Lombardia, B. Douzi, C. Cambillau, E. Cascales, Towards a structural comprehension of bacterial Type VI secretion systems: characterization of the TssJ–TssM complex of an *Escherichia coli* pathovar, PLoS Pathog. 7 (2011) e1002386.

[29] C.S. Robb, M. Assmus, F.E. Nano, A.B. Boraston, Structure of the T6SS lipoprotein TssJ1 from *Pseudomonas aeruginosa*, Acta Crystallogr. Sect. F: Struct. Biol. Cryst. Commun. 69 (2013) 607–610.

[30] L.S. Ma, J.S. Lin, E.M. Lai, An IcmF family protein, ImpLM, is an integral inner membrane protein interacting with ImpKL, and its walker a motif is required for Type VI secretion system-mediated Hcp secretion in *Agrobacterium tumefaciens*, J. Bacteriol. 191 (2009) 4316–4329.

[31] L.S. Ma, F. Narberhaus, E.M. Lai, IcmF family protein TssM exhibits ATPase activity and energizes Type VI secretion, J. Biol. Chem. 287 (2012) 15610–15621.

[32] J.A. Sexton, J.L. Miller, A. Yoneda, T.E. Kehl-Fie, J.P. Vogel, *Legionella pneumophila* DotU and IcmF are required for stability of the Dot/Icm complex, Infect. Immun. 72 (2004) 5983–5992.

[33] T. Zusman, M. Feldman, E. Halperin, G. Segal, Characterization of the icmH and icmF genes required for *Legionella pneumophila* intracellular growth, genes that are present in many bacteria associated with eukaryotic cells, Infect. Immun. 72 (2004) 3398–3409.

[34] M.S. Aschtgen, A. Zoued, R. Lloubès, L. Journet, E. Cascales, The C-tail anchored TssL subunit, an essential protein of the enteroaggregative *Escherichia coli* Sci-1 Type VI secretion system, is inserted by YidC, Microbiol. Open 1 (2012) 71–82.

[35] M.P. Castanie-Cornet, N. Bruel, P. Genevaux, Chaperone networking facilitates protein targeting to the bacterial cytoplasmic membrane, Biochim. Biophys. Acta. (2014), http://dx.doi.org/10.1016/j.bbamcr.2013.11.007.

[36] E. Durand, A. Zoued, S. Spinelli, P.J.H. Watson, M.S. Aschtgen, L. Journet, C. Cambillau, E. Cascales, Structural characterization and oligomerization of the TssL protein, a component shared by bacterial Type VI and Type IVb secretion systems, J. Biol. Chem. 287 (2012) 14157–14168.

[37] C.S. Robb, F.E. Nano, A.B. Boraston, The structure of the conserved type six secretion protein TssL (DotU) from *Francisella novicida*, J. Mol. Biol. 419 (2012) 277–283.

[38] J.E. Bröms, L. Meyer, M. Lavander, P. Larsson, A. Sjöstedt, DotU and VgrG, core components of Type VI secretion systems, are essential for *Francisella* LVS pathogenicity, PLoS One 7 (2012) e34639.

[39] M.S. Aschtgen, M.S. Thomas, E. Cascales, Anchoring the Type VI secretion to the peptidoglycan: TssL, TagL, TagP,… What else? Virulence 1 (2010) 535–540.

[40] J.D. Mougous, M.E. Cuff, S. Raunser, A. Shen, M. Zhou, A virulence locus of *Pseudomonas aeruginosa* encodes a protein secretion apparatus, Science 312 (2006) 1526–1530.

[41] J. Osipiuk, X. Xu, H. Cui, A. Savchenko, A. Edwards, A. Joachimiak, Crystal structure of secretory protein Hcp3 from *Pseudomonas aeruginosa*, J. Struct. Funct. Genom. 12 (2011) 21–26.

[42] C. Jobichen, S. Chakraborty, M. Li, J. Zheng, L. Joseph, Y.K. Leung, J. Sivaraman, Structural basis for the secretion of EvpC: a key Type VI secretion system protein from *Edwardsiella tarda*, PLoS One 5 (2010) e12910.

[43] B. Douzi, S. Spinelli, S. Blangy, A. Roussel, E. Durand, Y.R. Brunet, E. Cascales, C. Cambillau, Crystal structure and self-interaction of the Type VI secretion tail-tube protein from enteroaggregative *Escherichia coli*, PLoS One 9 (2014) e86918.

[44] L.G. Pell, V. Kanelis, L.W. Donaldson, P.L. Howell, A.R. Davidson, The phage lambda major tail protein structure reveals a common evolution for long-tailed phages and the Type VI bacterial secretion system, Proc. Natl. Acad. Sci. U. S. A. 106 (2009) 4160–4165.

[45] P.G. Leiman, M. Basler, U.A. Ramagopal, J.B. Bonanno, J.M. Sauder, Type VI secretion apparatus and phage tail-associated protein complexes share a common evolutionary origin, Proc. Natl. Acad. Sci. U. S. A. 106 (2009) 4154–4159.

[46] E.R. Ballister, A.H. Lai, R.N. Zuckermann, Y. Cheng, J.D. Mougous, In vitro self-assembly of tailorable nanotubes from a simple protein building block, Proc. Natl. Acad. Sci. U. S. A. 105 (2008) 3733–3738.

[47] Y.R. Brunet, J. Hénin, H. Celia, E. Cascales, Type VI secretion and bacteriophage tail tubes share a common assembly pathway, EMBO Rep. 15 (2014) 315–321.

[48] J.M. Silvermann, D.M. Agnello, H. Zheng, B.T. Andrews, M. Li, C.E. Catalano, T. Gonen, J.D. Mougous, Haemolysin coregulated protein is an exported receptor and chaperone of Type VI secretion substrates, Mol. Cell 51 (2013) 584–593.

[49] P.G. Leiman, M.M. Shneider, Contractile tail machines of bacteriophages, Adv. Exp. Med. Biol. 726 (2012) 93–114.

[50] S. Pukatzki, A.T. Ma, A.T. Revel, D. Sturtevant, J.J. Mekalanos, Type VI secretion system translocates a phage tail spike-like protein into target cells where it cross-links actin, Proc. Natl. Acad. Sci. U. S. A. 104 (2007) 15508–15513.

[51] N.S. Lossi, R. Dajani, P. Freemont, A. Filloux, Structure-function analysis of HsiF, a gp25-like component of the Type VI secretion system, in *Pseudomonas aeruginosa*, Microbiology 157 (2011) 3292–3305.

[52] O.M. de Bruin, J.S. Ludu, F.E. Nano, The *Francisella* pathogenicity island protein IglA localizes to the bacterial cytoplasm and is needed for intracellular growth, BMC Microbiol. 7 (2007) 1.

[53] G. Bönemann, A. Pietrosiuk, A. Diemand, H. Zentgraph, A. Mogk, Remodelling of VipA/VipB tubules by ClpV-mediated threading is crucial for Type VI protein secretion, EMBO J. 28 (2009) 315–325.

[54] J.E. Bröms, M. Lavander, A. Sjöstedt, A conserved alpha-helix essential for a Type VI secretion-like system of *Francisella tularensis*, J. Bacteriol. 191 (2009) 2431–2446.

[55] S.L. Karna, X. Zogaj, J.R. Barker, J. Seshu, S.L. Dove, A bacterial two-hybrid system that utilizes Gateway cloning for rapid screening of protein–protein interactions, Biotechniques 49 (2010) 831–833.

[56] D. Aubert, D.K. MacDonald, M.A. Valvano, BcsKC is an essential protein for the Type VI secretion system activity in *Burkholderia cenocepacia* that forms an outer membrane complex with BcsLB, J. Biol. Chem. 285 (2010) 35988–35998.

[57] N.S. Lossi, E. Manoli, A. Förster, R. Dajani, T. Pape, P. Freemont, A. Filloux, The HsiB1C1 (TssB–TssC) complex of the *Pseudomonas aeruginosa* Type VI secretion system forms a bacteriophage tail sheathlike structure, J. Biol. Chem. 288 (2013) 7536–7548.

[58] X.Y. Zhang, Y.R. Brunet, L. Logger, B. Douzi, C. Cambillau, L. Journet, E. Cascales, Dissection of the TssB–TssC interface during Type VI secretion sheath complex formation, PLoS One 8 (2013) e81074.

[59] J.E. Bröms, T. Ishikawa, S.N. Wai, A. Sjöstedt, A functional VipA–VipB interaction is required for the Type VI secretion system activity of *Vibrio cholerae* O1 strain A1552, 3 (2013) 13–96.

[60] A.A. Aksyuk, P.G. Leiman, L.P. Kurochkina, M.M. Shneider, V.A. Kostyuchenko, V.V. Mesyanzhinov, M.G. Rossmann, The tail sheath structure of bacteriophage T4: a molecular machine for infecting bacteria, EMBO J. 28 (2009) 821–829.

[61] M.G. Casabona, Y. Vandenbrouck, I. Attree, Y. Couté, Proteomic characterization of *Pseudomonas aeruginosa* PAO1 inner membrane, Proteomics 13 (2013) 2419–2423.

[62] N. Kapitein, G. Bonemann, A. Pietrosiuk, F. Seyffer, I. Hausser, J.K. Locker, A. Mogk, ClpV recycles VipA/VipB tubules and prevents non-productive tubule formation to ensure efficient Type VI protein secretion, Mol. Microbiol. 87 (2013) 1013–1028.

[63] E. Cascales, C. Cambillau, Structural biology of Type VI secretion systems, Philos. Trans. R. Soc. Lond. B Biol. Sci. 367 (2012) 1102–1111.

[64] A. Zoued, E. Durand, C. Bebeacua, Y.R. Brunet, B. Douzi, C. Cambillau, E. Cascales, L. Journet, TssK is a trimeric cytoplasmic protein interacting with components of both phage-like and membrane anchoring complexes of the Type VI secretion system, J. Biol. Chem. 288 (2013) 27031–27041.

[65] A.R. Davidson, L. Cardarelli, L.G. Pell, D.R. Radford, K.L. Maxwell, Long noncontractile tail machines of bacteriophages, Adv. Exp. Med. Biol. 726 (2012) 115–142.

[66] P.G. Leiman, P.R. Chipman, V.A. Kostyuchenko, V.V. Mesyanzhinov, M.G. Rossmann, Three-dimensional rearrangement of proteins in the tail of bacteriophage T4 on infection of its host, Cell 118 (2004) 419–429.

[67] M.G. Rossmann, V.V. Mesyanzhinov, F. Arisaka, P.G. Leiman, The bacteriophage T4 DNA injection machine, Curr. Opin. Struct. Biol. 14 (2004) 171–180.

[68] V.A. Kostyuchenko, P.R. Chipman, P.G. Leiman, F. Arisaka, V.V. Mesyanzhinov, M.G. Rossmann, The tail structure of bacteriophage T4 and its mechanism of contraction, Nat. Struct. Mol. Biol. 12 (2005) 810–813.

[69] K. Uchida, P.G. Leiman, F. Arisaka, S. Kanamaru, Structure and properties of the C-terminal β-helical domain of VgrG protein from *Escherichia coli* O157, J. Biochem. (2014), http://dx.doi.org/10.1093/jb/mvt109.

[70] S. Pukatzki, S.B. McAuley, S.T. Miyata, The Type VI secretion system: translocation of effectors and effector-domains, Curr. Opin. Microbiol. 12 (2009) 11–17.

[71] A.T. Ma, S. McAuley, S. Pukatzki, J.J. Mekalanos, Translocation of a *Vibrio cholerae* Type VI secretion effector requires bacterial endocytosis by host cells, Cell Host Microbe 5 (2009) 234–243.

[72] M.M. Shneider, PAAR-repeat proteins sharpen and diversify the Type VI secretion system spike, Nature 500 (2013) 350–353.

[73] V.A. Kostyuchenko, P.G. Leiman, P.R. Chipman, S. Kanamaru, M.J. Van Raaij, F. Arisaka, V.V. Mesyanzhinov, M.G. Rossmann, Three-dimensional structure of bacteriophage T4 baseplate, Nat. Struct. Biol. 10 (2003) 688–693.

[74] P.G. Leiman, F. Arisaka, M.J. Van Raaij, V.A. Kostyuchenko, A.A. Aksyuk, S. Kanamaru, M.G. Rossmann, Morphogenesis of the T4 tail and tail fibers, Virol. J. 7 (2010) 355.

[75] A. Pietrosiuk, E.D. Lenherr, S. Falk, G. Bönemann, J. Kopp, H. Zentgraf, I. Sinning, A. Mogk, Molecular basis for the unique role of the AAA + chaperone ClpV in Type VI protein secretion, J. Biol. Chem. 286 (2011) 30010–30021.

Annexe 5: Fusion reporter approaches to monitoring transmembrane helix interactions in bacterial membranes

Chapter 16

Fusion Reporter Approaches to Monitoring Transmembrane Helix Interactions in Bacterial Membranes

Laureen Logger, Abdelrahim Zoued, and Eric Cascales

Abstract

In transenvelope multiprotein machines such as bacterial secretion systems, protein–protein interactions not only occur between soluble domains but might also be mediated by helix–helix contacts in the inner membrane. Here we describe genetic assays commonly used to test interactions between transmembrane α-helices in their native membrane environment. These assays are based on the reconstitution of dimeric regulators allowing the control of expression of reporter genes. We provide detailed protocols for the TOXCAT and GALLEX assays used to monitor homotypic and heterotypic transmembrane helix–helix interactions.

Key words Membrane protein, Protein-protein interaction, Transmembrane segment, Helix–helix interaction, One-hybrid, Two-hybrid, cI repressor, TOXCAT, GALLEX

1 Introduction

The proper assembly of multiprotein complexes such as bacterial secretion systems requires specific interactions between the different subunits. While most of the interactions involve contacts between soluble domains of these subunits, the transmembrane helices (TMHs) of inner membrane proteins are also key players in membrane protein complex formation. For examples, the Type II secretion (T2SS)-associated GspC, GspL, and GspM proteins interact with each other via their TMHs [1]. A similar situation has been evidenced for the Type VI secretion system (T6SS) TssLM complex [2–4]. The TMH could be involved in homotypic interaction, i.e., participate in the formation of dimers such as the Type IV secretion (T4SS) and T6SS-associated VirB10 and TssL inner membrane proteins [4, 5] or in heterotypic interactions with other subunits [1–3]. Monitoring interactions between TMHs is not an easy task because mutations within or swapping of the TMH could interfere with the conformation of the soluble domains and therefore may indirectly affect protein–protein interactions. Thus, genetic one- or two-hybrid approaches based on fusion to transcriptional

Laure Journet and Eric Cascales (eds.), *Bacterial Protein Secretion Systems: Methods and Protocols*, Methods in Molecular Biology, vol. 1615, DOI 10.1007/978-1-4939-7033-9_16,

reporters, such as the λcI repressor, TOXCAT, GALLEX, and Bacterial Adenylate Cyclase-Based Two-Hybrid (BACTH) assays, have been developed. While cI-repressor and TOXCAT can only be used for testing homotypic interactions, the GALLEX and BACTH approaches can also be used to monitor interactions between different TMHs. This chapter provides protocols to monitor homotypic and heterotypic transmembrane helix–helix interactions using TOXCAT and GALLEX. We refer the reader to excellent reviews summarizing the forces exerted to catalyze TMH folding and insertion, as well as the different methods to analyze TMH interactions in bacteria [6, 7].

1.1 Monitoring TMH Homotypic Interactions

Methods of testing the homodimerization of TMHs, such as the λ cI repressor and TOXCAT assays, are based on the one-hybrid reporter fusion approach.

The cI transcriptional regulator represses the expression of early promoters of the bacteriophage λ genome. Repression only occurs when cI dimerizes, a behavior conferred by the C-terminal domain. The λcI repressor assay is therefore based on the reconstitution of a dimeric λcI repressor by two interacting fragments [8–10]. The construct consists of a fusion between the monomeric N-terminal DNA-binding domain of λcI (called cI') with the TMH (Fig. 1a). TMH-mediated cI' dimerization induces binding of cI to its operator sequence, allowing repression of phage λ early genes, hence conferring protection against superinfection by phage λ (Fig. 1a). The cI repressor assay has been successfully used to demonstrate that the T2SS XcpR and T4SS VirB4 and VirB11 proteins oligomerize [11–13].

The TOXCAT assay is based on the characteristics of the *Vibrio cholerae* ToxR regulator: a strict dimerization-dependent transcriptional activator consisting of an N-terminal helix-turn-helix DNA-binding domain and a C-terminal dimerization domain. The construct consists of a fusion in which the TMH is inserted between the monomeric ToxR DNA-binding domain and the MalE periplasmic protein (Fig. 1b). By supporting growth on maltose-minimal media, MalE makes it possible to verify that the TMH is properly inserted. TMH-mediated ToxR dimerization induces binding of ToxR on its operator sequence, allowing transcription of a reporter gene. In the initial ToxR system, the reporter gene is *lacZ* [14], while the TOXCAT assay uses the *cat* gene [15] (Fig. 1b). Hence, dimerization of the TMH could then be assessed by measuring the β-galactosidase and chloramphenicol acetyltransferase (resistance to chloramphenicol) activities [16]. The TOXCAT assay has been successfully used to provide evidence that the TMH of the T4SS VirB10 subunit oligomerizes [5]. Further improvements of the ToxR and TOXCAT assays have been published [17–19].

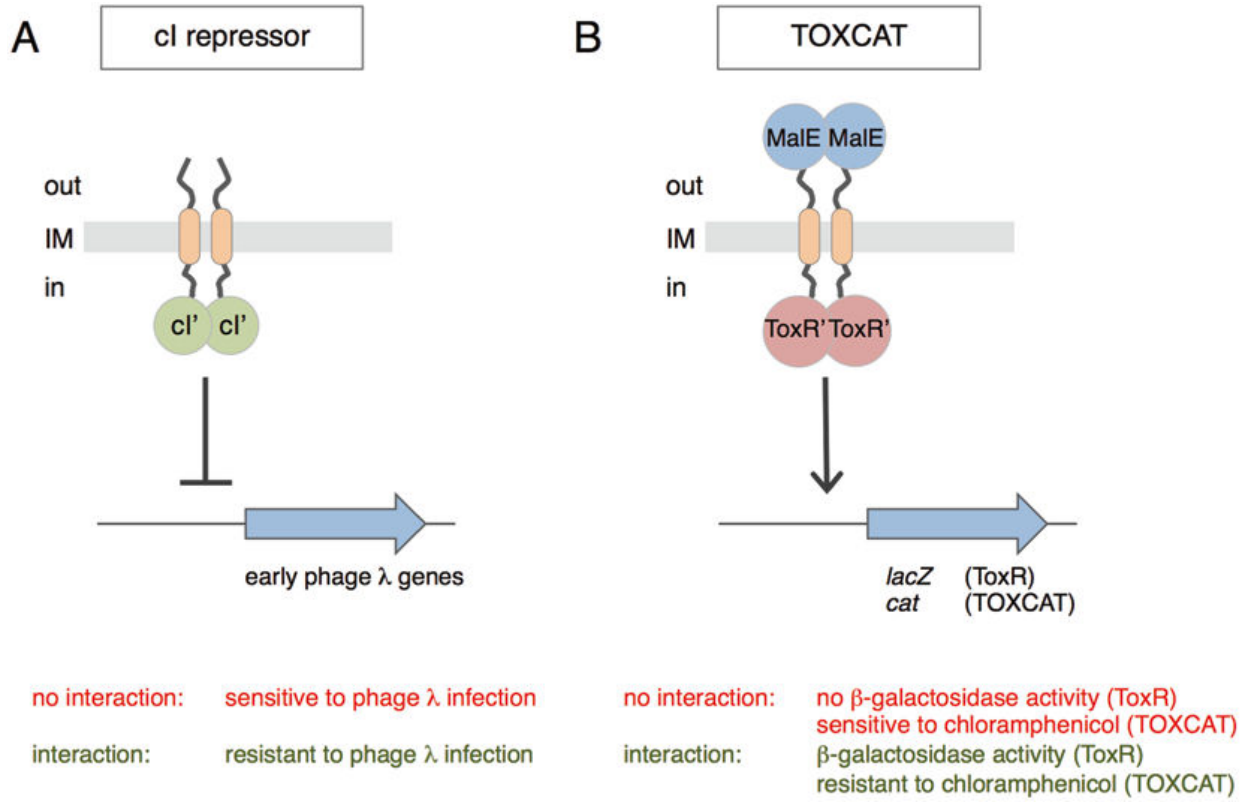

Fig. 1 Schematic representation of the assays for monitoring TMH homotypic interactions. (**a**) cI repressor assay. The TMH of interest (*orange*) is fused to the cI DNA-binding domain (*green*). Reconstitution of the cI dimer results in the repression of early phage λ genes (*blue*). Repression of phage λ genes confers protection against phage λ infection. (**b**) ToxR and TOXCAT assays. The TMH of interest (*orange*) is fused between the *Vibrio cholerae* ToxR DNA-binding domain (*red*) and the MalE protein (*blue*). Reconstitution of the ToxR dimer results in the expression of the reporter genes (*blue*, *lacZ* for the ToxR assay, *cat* for the TOXCAT assay)

1.2 Monitoring TMH Heterotypic Interactions

Methods of testing the heterodimerization of TMHs, such as the GALLEX and BACTH assays, are based on the two-hybrid reporter fusion approach.

The GALLEX assay is based on the reconstitution of a dimeric LexA transcriptional repressor by two interacting TMHs. The construct consists of a fusion in which each TMH is inserted between the monomeric LexA N-terminal DNA-binding domain and the MalE periplasmic protein. The elegant improvement is that one of the two TMHs is fused to the wild-type LexA N-terminal domain ($LexA^{WT}$), whereas the second TMH is fused to a LexA N-terminal domain variant bearing a mutation in the DNA-binding motif ($LexA^{408}$), allowing recognition of a different operator sequence (op^{408}). Formation of helix heterodimers induces binding of $LexA/LexA^{408}$ on a dual operator sequence (op^{WT}/op^{408}), allowing repression of a reporter gene [20–22] (Fig. 2a).

The BACTH assay is based on the reconstitution of the adenylate cyclase activity conferred by the T18 and T25 domains of the *Bordetella pertussis* Cya protein [23–25] (Fig. 2b). Widely

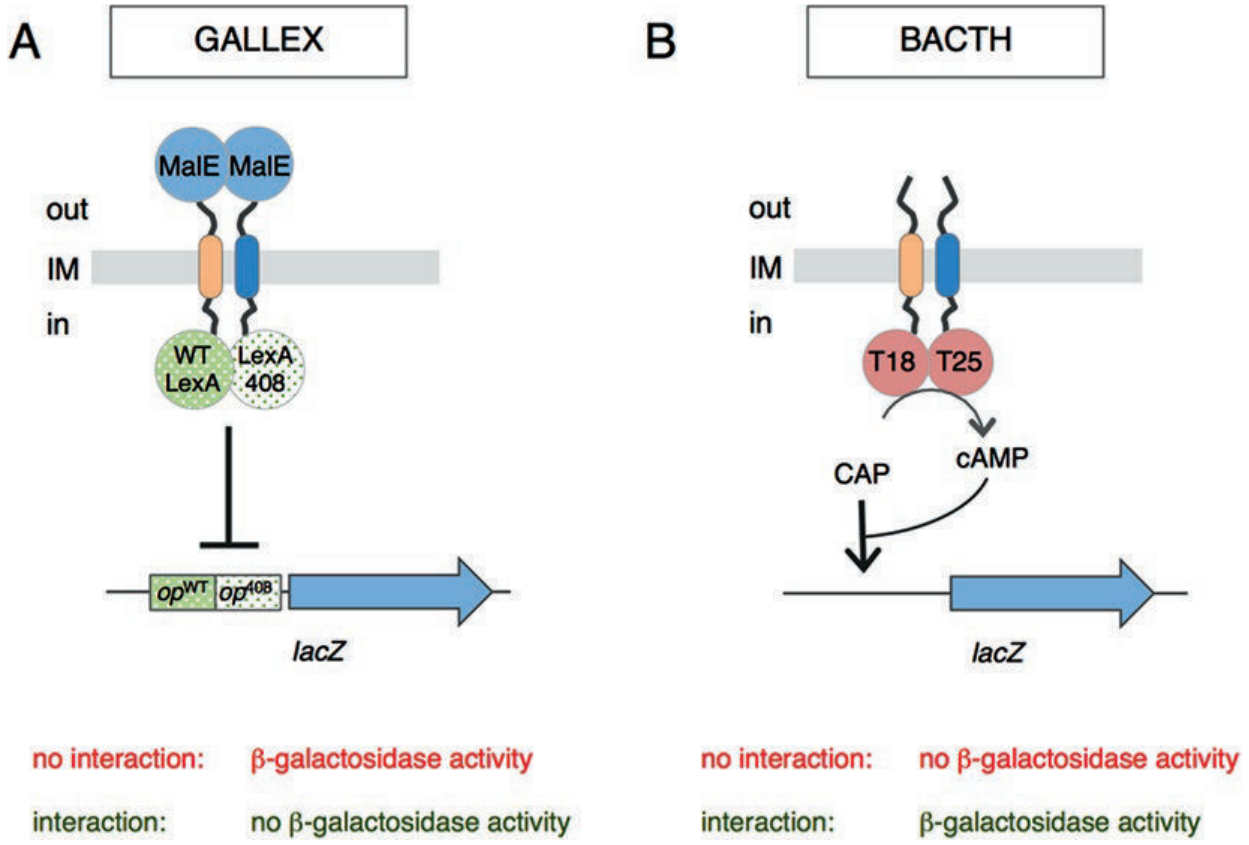

Fig. 2 Schematic representation of assays for monitoring TMH heterotypic interactions. (**a**) GALLEX assay. The first TMH of interest (*orange*) is fused between the wild-type LexA DNA-binding domain (WT LexA) and MalE, whereas the second TMH (*blue*) is fused between the $LexA^{408}$ variant (LexA 408) and MalE. Reconstitution of the $LexA^{WT}/LexA^{408}$ dimer results in the repression of the reporter gene (*blue*). (**b**) BACTH assays. The first TMH of interest (*orange*) is fused to the T18 domain of the *B. pertussis* adenylate cyclase, whereas the second TMH (*blue*) is fused to the T25 of adenylate cyclase. Reconstitution of the T18/T25 adenylate cyclase results in the production of cyclic adenosine monophosphate (cAMP). Binding of cAMP to the catabolite activator protein (CAP) induces the expression of the reporter gene (*blue*)

used for testing interactions between soluble domains or proteins in multiprotein complexes such as the divisome or secretion systems [26–34], it has only rarely been used for the study of transmembrane helix–helix interactions [35–37]. A detailed protocol for the bacterial two-hybrid assay is described in Chapter 13. In this chapter, we provide protocols for the TOXCAT and GALLEX assays.

2 Material

2.1 Monitoring TMH Homotypic Interactions: The TOXCAT Assay

1. pcckan vector [15] (*see* **Note 1**).
2. *Escherichia coli* NT326 or MM39 bacterial strains [15] (*see* **Note 2**).
3. Lysogeny broth (LB) medium: Dissolve 10 g tryptone, 5 g yeast extracts, and 10 g NaCl in 1 L distilled water. Autoclave for 15 min at 121 °C. For LB agar plates, add 15 g bacto-agar prior to autoclaving.

4. M9-maltose medium: Dissolve 0.6 g $Na_2HPO_4 \cdot 12H_2O$, 0.3 g $KH_2PO_4 \cdot H_2O$, 50 mg NaCl, 100 mg NH_4Cl, and 1.5 g bacto-agar in 90 mL distilled water. Autoclave. Add 100 mg casamino acids, 400 mg maltose, 25 mg $MgSO_4 \cdot 7H_2O$, and 1 mg $CaCl_2$.
5. Ampicillin stock solution (250×): 25 mg/mL ampicillin. Dissolve 250 mg ampicillin in 10 mL distilled water. Filter to sterilize. Store at 4 °C.
6. Chloramphenicol stock solution: Dissolve 90 mg chloramphenicol in 1 mL absolute ethanol. Store at −20 °C.
7. 2.5 mM chloramphenicol solution: Dissolve 8.1 mg chloramphenicol in 10 mL ethanol.
8. Sodium dodecyl sulfate (SDS)-polyacrylamide gel electrophoresis (PAGE) loading buffer: 60 mM Tris–HCl, pH 6.8, 2% SDS, 10% glycerol, 5% β-mercaptoethanol, 0.01% bromophenol blue.
9. Lysis buffer: 25 mM Tris–HCl, 2 mM EDTA, pH 8.0. Dissolve 303 mg Tris(hydroxymethyl) aminomethane and 58 mg ethylenediaminetetraacetic acid (EDTA, disodium salt) in 100 mL sterile distilled water. Adjust pH to 8.0.
10. Reaction buffer: 100 mM Tris–HCl, pH 7.8, 0.1 mM acetyl-CoA, 0.4 mg/mL 5,5'-dithiobis-(2 nitrobenzoic acid) (dTNB). Dissolve 121 mg Tris, 0.81 mg acetyl-CoA, and 4 mg dTNB in 10 mL sterile distilled water. Adjust pH to 7.8 with HCl.
11. 10 mm filter paper disk.
12. 96-well microplates.
13. Anti-maltose-binding protein (MBP) antibodies for MalE immunodetection.
14. Incubator.
15. Spectrophotometer.
16. Benchtop centrifuge.
17. Water bath at 96 °C.
18. Mini-gel caster system and SDS-PAGE apparatus.
19. Protein blotting apparatus.
20. Sonifier.
21. Microplate reader.

2.2 Monitoring TMH Heterotypic Interactions: The GALLEX Assay

1. pALM148 and pBML100 vectors [20].
2. *E. coli* NT326 or MM39 bacterial cells [15] (*see* **Note 2**).
3. *E. coli* SU202 bacterial strain [20, 38] (*see* **Note 3**).
4. LB medium: *see* Subheading 2.1.
5. M9-maltose medium: *see* Subheading 2.1.

6. Ampicillin stock solution (250×): *see* Subheading 2.1.
7. Tetracyclin stock solution (1000×): 12 mg/mL tetracyclin. Dissolve 120 mg tetracyclin in 10 mL ethanol. Filter to sterilize. Store at 4 °C.
8. Isopropyl-β-D-thiogalactopyranoside (IPTG) stock solution (500×). 0.1 M IPTG. Dissolve 238 mg IPTG in 10 mL sterile distilled water. Filter to sterilize. Store at 4 °C.
9. X-Gal stock solution (1000×): 40 mg/mL X-Gal. Dissolve 40 mg 5-Bromo-4-chloro-3-indolyl β-D-galactopyranoside (X-Gal) in 1 mL dimethylformamide. Prepare fresh and do not store.
10. 0.1% SDS: Dissolve 50 mg SDS in 50 mL distilled water.
11. Chloroform.
12. Ortho-nitrophenyl-β-D-galactopyranoside (ONPG) stock solution. 4 mg/mL ONPG: Dissolve 20 mg ONPG in 5 mL buffer Z.
13. SDS-PAGE loading buffer: 60 mM Tris–HCl, pH 6.8, 2% SDS, 10% glycerol, 5% β-mercaptoethanol, 0.01% bromophenol blue.
14. Buffer Z: Dissolve 2.15 g $Na_2HPO_4 \cdot 12\ H_2O$, 0.29 g $Na_2HPO_4 \cdot H_2O$, 75 mg KCl, and 25 mg $MgSO_4 \cdot 7H_2O$ in 100 mL distilled water. Adjust pH to 7.0. Add 270 µL β-mercaptoethanol. Prepare fresh and do not store.
15. Anti-MBP antibodies for MalE immunodetection.
16. 96-well microplates.
17. Incubator.
18. Spectrophotometer.
19. Benchtop centrifuge.
20. Water bath at 96 °C.
21. Mini-gel caster system and SDS-PAGE apparatus.
22. Protein blotting apparatus.
23. Microplate reader.

3 Methods

3.1 Monitoring TMH Homotypic Interactions: The TOXCAT Assay

1. Clone the DNA fragment corresponding to the TMH to be studied into the pcckan vector to yield a plasmid producing the ToxR'-TMH-MalE fusion protein. Before testing the homodimerization of the TMH, verify that your fusion protein is properly produced (**steps 3–8**) and inserted in the inner membrane (**steps 9** and **10**). The dimerization of the TMH is then assessed by the disk diffusion assay (**steps 11–16**) and quantified by measuring the chloramphenicol acetyltransferase activity (**steps 17–26**).

2. Transform the empty pcckan vector and your pcckan construct into NT326 or MM39 *E. coli* competent cells. Select on LB-ampicillin plates (*see* **Note 1**).
3. Pick a single colony of each transformation and grow cells in 20 mL LB medium supplemented with ampicillin (100 μg/mL) until an optical density at 600 nm (OD_{600}) of 0.8 is reached.
4. Harvest 2 mL of cells by centrifugation at 4000 × *g* for 5 min.
5. Discard supernatants and resuspend cell pellets into 20 μL SDS-PAGE loading buffer.
6. Boil samples for 10 min at 96 °C.
7. Separate proteins by SDS-PAGE and transfer onto nitrocellulose membrane using your favorite protocol.
8. Use western blotting to immunodetect your fusion protein using commercial anti-MalE (anti-MBP) antibodies.
9. Streak 20 μL of the bacterial culture obtained at **step 3** in Subheading 3.1 onto M9-maltose medium.
10. After incubation for 48 h at 37 °C, verify that your strain grew on M9-maltose medium.
11. Drop a 10 mm filter paper disk in center of LB-ampicillin plate (*see* **Note 4**).
12. Add 60 μL chloramphenicol stock solution (90 mg/mL) on filter paper disk.
13. Incubate LB plates with chloramphenicol disks for 6 h at 37 °C.
14. Remove disk.
15. Spread 2 mL of the culture obtained at **step 3** in Subheading 3.1 on the LB-ampicillin plate to make a lawn. Eliminate excess culture.
16. After incubation for 16 h at 37 °C, measure the halo of chloramphenicol sensitivity (*see* **Note 5**).
17. Centrifuge 3 mL of the culture obtained at **step 3** in Subheading 3.1 at 4000 × *g* for 5 min (in triplicate).
18. Discard supernatant and resuspend cell pellets in 500 μL lysis buffer. Vortex.
19. Lyse cells by sonication using a sonifier.
20. Clear lysate by centrifugation at 10,000 × *g* for 15 min.
21. In a 96-well microplate, mix 15 μL of the cleared lysate with 220 μL reaction buffer.
22. Measure absorbance at 412 nm (A_{412}) (*see* **Note 6**) and at 550 nm (A_{550}; cell debris) every 20 s for 4 min using a microplate reader.
23. Inject 15 μL 2.5 mM chloramphenicol in each well.

24. Measure absorbance at 412 nm (*see* **Note 6**) and at 550 nm (cell debris) every 20 s for 10 min using a microplate reader.
25. Divide each A_{412} value by the corresponding A_{550} value and plot these values against time.
26. Calculate the chloramphenicol acetyltransferase activity based on the slope in the linear part of the curve (initial rate).

3.2 Monitoring TMH Heterotypic Interactions: The GALLEX Assay

1. Clone the DNA fragment corresponding to the first TMH to be studied (TMH1) into the pBLM100 vector to yield a pBR322 derivative plasmid producing the $LexA_{WT}$'-TMH1-MalE fusion protein. Clone the DNA fragment corresponding to the second TMH to be studied (TMH2) into the pALM148 vector to yield a pACYC184 derivative plasmid producing the $LexA_{408}$'-TMH2-MalE fusion protein. Before testing the heterodimerization of the TMH, verify that your fusion protein is properly produced (**steps 3–8**) and inserted in the inner membrane (**steps 9** and **10**). The dimerization of the TMH is then assessed on LB-X-Gal plates (**steps 11–14**) and quantitated by measuring the β-galactosidase activity (**steps 15–22**).
2. Transform the empty pBLM100 and pALM148 vectors as well as the pBLM100-TMH1 and pALM148-TMH2 constructs into NT326 or MM39 *E. coli* competent cells. Select on LB plates supplemented with ampicillin (pBLM100 derivatives) or tetracyclin (pALM148 derivatives).
3. Pick a single colony of each transformation and grow cells in 3 mL LB medium supplemented with IPTG and ampicillin or tetracyclin until an OD_{600} of 0.8 is reached.
4. Harvest 2 mL of cells by centrifugation at 4000 × *g* for 5 min.
5. Discard supernatants and resuspend cell pellets into 20 μL of SDS-PAGE loading buffer.
6. Boil samples for 10 min at 96 °C.
7. Separate proteins by SDS-PAGE and transfer onto nitrocellulose membrane using your favorite protocol.
8. Use western blotting to immunodetect your fusion protein using commercial anti-MalE (anti-MBP) antibodies.
9. Streak 20 μL of the bacterial culture obtained at **step 3** in Subheading 3.2 onto M9-maltose medium.
10. After incubation for 48 h at 37 °C, verify that your strain grew on M9-maltose medium.
11. Cotransform pBLM100 and pBLM100-TMH1 vectors in combination with pALM148 and pALM148-TMH2 vectors into SU202 *E. coli* competent cells (*see* **Note 7**). Select on LB plates supplemented with ampicillin and tetracyclin.

12. Pick a single colony of each transformation and grow cells in 3 mL LB medium supplemented with IPTG, ampicillin, and tetracyclin until an OD_{600} of 0.8 is reached.
13. Drop 15 μL of the bacterial culture obtained at **step 12** in Subheading 3.2 onto LB plates supplemented with IPTG, ampicillin, tetracyclin, and X-Gal.
14. After 6, 14, and 24 h of incubation at 37 °C, observe the coloration of the spots. White spots correspond to strains with no β-galactosidase activity (*i.e.*, interaction between the two TMHs), whereas blue spots correspond to strains with β-galactosidase activity (*i.e.*, no interaction between the two TMHs) (*see* **Note 8**).
15. Mix 200 μL of the bacterial culture obtained at **step 12** in Subheading 3.2 with 800 μL of buffer Z into a 1.5 mL Eppendorf tube. Vortex.
16. Add one drop of 0.1% SDS and two drops of chloroform to lyse cells. Vortex for 10 s.
17. In a 96-well microplate, mix 50 μL of the cleared lysate with 150 μL buffer Z.
18. Measure the absorbance at 420 nm (absorption wavelength of ortho-nitrophenol, the product of degradation of ONPG) and at 550 nm (A_{550}; cell debris) every 30 s for 2 min using a microplate reader.
19. Inject 40 μL ONPG solution in each well.
20. Measure the absorbance at 420 nm and at 550 nm every 30 s for 20 min using a microplate reader.
21. Divide each A_{420} value by the corresponding A_{550} value and plot these values against time.
22. Calculate the β-galactosidase activity based on the slope in the linear part of the curve (initial rate).

4 Notes

1. pcckan is a vector comprising the sequence corresponding to the ToxR N-terminal domain and that corresponding to MalE separated by a multiple cloning site allowing insertion of the sequence corresponding to the TMH of interest. Positive and negative controls have been developed by Russ and Engelman corresponding to the wild-type and mutated TMH of the glycophorin A, respectively [15].
2. NT326 and MM39 strains do not produce the MBP and therefore could be used as reporters to verify the proper insertion of the ToxR'-TMH-MalE and LexA-TMH-MalE fusions.

3. Strain SU202 is a reporter for the GALLEX assay. It has a chromosomally integrated fragment corresponding to a hybrid operator sequence (op^{WT}/op^{408}) controlling the expression of the *lacZ* reporter gene. Transformed SU202 cells are not stable and therefore transformations should be made fresh and colonies should not be stored at 4°C.
4. Use three LB-ampicillin plates per strain to be tested.
5. The diameter of the halo reflects the ability of the strain to resist chloramphenicol and therefore is directly and inversely linked to the expression of the *cat* gene that is induced by TMH dimerization. If the TMH dimerizes, the expression level of *cat* will be high and, hence, the diameter of the halo small.
6. The reaction catalyzed by the chloramphenicol acetyltransferase consists in the acetylation of the chloramphenicol and the release of free coenzyme A. Coenzyme A then reacts with the 5,5'-dithiobis-(2-nitrobenzoic acid), resulting in an increase of the absorbance at 412 nm.
7. You should obtain the combinations pBLM100 + pALM148, pBLM100 + pALM148-TMH2, pBLM100-TMH1 + pALM148, and pBLM100-TMH1 + pALM148-TMH2.
8. MacConkey/maltose could be used as reporter medium instead of LB-X-Gal plates. If MacConkey/maltose plates are used, the coloration of the spots differs: yellow spots correspond to strains with no β-galactosidase activity (*i.e.*, interaction between the two TMHs), whereas red spots correspond to strains with β-galactosidase activity (*i.e.*, no interaction between the two TMHs).

Acknowledgements

Work in the EC laboratory is supported by the Centre National de la Recherche Scientifique, the Aix-Marseille Université, and grants from the Agence Nationale de la Recherche (ANR-14-CE14-0006-02 and ANR-15-CE11-0019-01). LL and AZ are recipients of doctoral fellowships from the French Ministère de l'Enseignement Supérieur et de la Recherche and end-of-thesis fellowships from the Fondation pour la Recherche Médicale (FDT20160435498 and FDT20140931060).

References

1. Lallemand M, Login FH, Guschinskaya N, Pineau C, Effantin G, Robert X, Shevchik VE (2013) Dynamic interplay between the periplasmic and transmembrane domains of GspL and GspM in the type II secretion system. PLoS One 8:e79562
2. Ma LS, Lin JS, Lai EM (2009) An IcmF family protein, ImpLM, is an integral inner membrane protein interacting with ImpKL, and its walker a motif is required for type VI secretion system-mediated Hcp secretion in Agrobacterium tumefaciens. J Bacteriol 191:4316–4329

3. Aschtgen MS, Gavioli M, Dessen A, Lloubès R, Cascales E (2010) The SciZ protein anchors the enteroaggregative Escherichia coli Type VI secretion system to the cell wall. Mol Microbiol 75:886–899
4. Durand E, Zoued A, Spinelli S, Watson PJ, Aschtgen MS, Journet L, Cambillau C, Cascales E (2012) Structural characterization and oligomerization of the TssL protein, a component shared by bacterial type VI and type IVb secretion systems. J Biol Chem 287:14157–14168
5. Garza I, Christie PJ (2013) A putative transmembrane leucine zipper of agrobacterium VirB10 is essential for T-pilus biogenesis but not type IV secretion. J Bacteriol 195:3022–3034
6. Schneider D, Finger C, Prodöhl A, Volkmer T (2007) From interactions of single transmembrane helices to folding of alpha-helical membrane proteins: analyzing transmembrane helix-helix interactions in bacteria. Curr Protein Pept Sci 8:45–61
7. Fink A, Sal-Man N, Gerber D, Shai Y (2012) Transmembrane domains interactions within the membrane milieu: principles, advances and challenges. Biochim Biophys Acta 1818:974–983
8. Hu JC (1995) Repressor fusions as a tool to study protein-protein interactions. Structure 3:431–433
9. Leeds JA, Beckwith J (1998) Lambda repressor N-terminal DNA-binding domain as an assay for protein transmembrane segment interactions in vivo. J Mol Biol 280:799–810
10. Leeds JA, Beckwith J (2000) A gene fusion method for assaying interactions of protein transmembrane segments in vivo. Methods Enzymol 2327:165–175
11. Turner LR, Olson JW, Lory S (1997) The XcpR protein of Pseudomonas aeruginosa dimerizes via its N-terminus. Mol Microbiol 26:877–887
12. Dang TA, Zhou XR, Graf B, Christie PJ (1999) Dimerization of the agrobacterium tumefaciens VirB4 ATPase and the effect of ATP-binding cassette mutations on the assembly and function of the T-DNA transporter. Mol Microbiol 32:1239–1253
13. Rashkova S, Zhou XR, Chen J, Christie PJ (2000) Self-assembly of the Agrobacterium tumefaciens VirB11 traffic ATPase. J Bacteriol 182:4137–4145
14. Langosch D, Brosig B, Kolmar H, Fritz HJ (1996) Dimerisation of the glycophorin A transmembrane segment in membranes probed with the ToxR transcription activator. J Mol Biol 263:525–530
15. Russ WP, Engelman DM (1999) TOXCAT: a measure of transmembrane helix association in a biological membrane. Proc Natl Acad Sci U S A 96:863–868
16. Joce C, Wiener A, Yin H (2011) Transmembrane domain oligomerization propensity determined by ToxR assay. J Vis Exp 51
17. Lindner E, Langosch D (2006) A ToxR-based dominant-negative system to investigate heterotypic transmembrane domain interactions. Proteins 65:803–807
18. Lindner E, Unterreitmeier S, Ridder AN, Langosch D (2007) An extended ToxR POSSYCCAT system for positive and negative selection of self-interacting transmembrane domains. J Microbiol Methods 69:298–305
19. Lis M, Blumenthal K (2006) A modified, dual reporter TOXCAT system for monitoring homodimerization of transmembrane segments of proteins. Biochem Biophys Res Commun 339:321–324
20. Schneider D, Engelman DM (2003) GALLEX, a measurement of heterologous association of transmembrane helices in a biological membrane. J Biol Chem 278:3105–3111
21. Cymer F, Sanders CR, Schneider D (2013) Analyzing oligomerization of individual transmembrane helices and of entire membrane proteins in E. coli: a hitchhiker's guide to GALLEX. Methods Mol Biol 932:259–276
22. Tome L, Steindorf D, Schneider D (2013) Genetic systems for monitoring interactions of transmembrane domains in bacterial membranes. Methods Mol Biol 1063:57–91
23. Karimova G, Pidoux J, Ullmann A, Ladant D (1998) A bacterial two-hybrid system based on a reconstituted signal transduction pathway. Proc Natl Acad Sci U S A 95:5752–5756
24. Ladant D, Karimova G (2000) Genetic systems for analyzing protein-protein interactions in bacteria. Res Microbiol 151:711–720
25. Battesti A, Bouveret E (2012) The bacterial two-hybrid system based on adenylate cyclase reconstitution in Escherichia coli. Methods 58:325–334
26. Karimova G, Dautin N, Ladant D (2005) Interaction network among Escherichia coli membrane proteins involved in cell division as revealed by bacterial two-hybrid analysis. J Bacteriol 187:2233–2243
27. Sivanesan D, Hancock MA, Villamil Giraldo AM, Baron C (2010) Quantitative analysis of VirB8-VirB9-VirB10 interactions provides a dynamic model of type IV secretion system core complex assembly. Biochemistry 49:4483–4493

28. Cisneros DA, Bond PJ, Pugsley AP, Campos M, Francetic O (2012) Minor pseudopilin self-assembly primes type II secretion pseudopilus elongation. EMBO J 31:1041–1053
29. Georgiadou M, Castagnini M, Karimova G, Ladant D, Pelicic V (2012) Large-scale study of the interactions between proteins involved in type IV pilus biology in Neisseria meningitidis: characterization of a subcomplex involved in pilus assembly. Mol Microbiol 84:857–873
30. Zoued A, Durand E, Bebeacua C, Brunet YR, Douzi B, Cambillau C, Cascales E, Journet L (2013) TssK is a trimeric cytoplasmic protein interacting with components of both phage-like and membrane anchoring complexes of the type VI secretion system. J Biol Chem 288:27031–27041
31. Pais SV, Milho C, Almeida F, Mota LJ (2013) Identification of novel type III secretion chaperone-substrate complexes of Chlamydia trachomatis. PLoS One 8:e56292
32. Pineau C, Guschinskaya N, Robert X, Gouet P, Ballut L, Shevchik VE (2014) Substrate recognition by the bacterial type II secretion system: more than a simple interaction. Mol Microbiol 94:126–140
33. Brunet YR, Zoued A, Boyer F, Douzi B, Cascales E (2015) The type VI secretion TssEFGK-VgrG phage-like baseplate is recruited to the TssJLM membrane complex via multiple contacts and serves as assembly platform for tail tube/sheath polymerization. PLoS Genet 11:e1005545
34. Zoued A, Durand E, Brunet YR, Spinelli S, Douzi B, Guzzo M, Flaugnatti N, Legrand P, Journet L, Fronzes R, Mignot T, Cambillau C, Cascales E (2016) Priming and polymerization of a bacterial contractile tail structure. Nature 531:59–63
35. Llosa M, Zunzunegui S, de la Cruz F (2003) Conjugative coupling proteins interact with cognate and heterologous VirB10-like proteins while exhibiting specificity for cognate relaxosomes. Proc Natl Acad Sci U S A 100:10465–10470
36. Segura RL, Aguila-Arcos S, Ugarte-Uribe B, Vecino AJ, de la Cruz F, Goñi FM, Alkorta I (2013) The transmembrane domain of the T4SS coupling protein TrwB and its role in protein-protein interactions. Biochim Biophys Acta 1828:2015–2025
37. Sawma P, Roth L, Blanchard C, Bagnard D, Crémel G, Bouveret E, Duneau JP, Sturgis JN, Hubert P (2014) Evidence for new homotypic and heterotypic interactions between transmembrane helices of proteins involved in receptor tyrosine kinase and neuropilin signaling. J Mol Biol 426:4099–4111
38. Dimitrova M, Younès-Cauet G, Oertel-Buchheit P, Porte D, Schnarr M, Granger-Schnarr M (1998) A new LexA-based genetic system for monitoring and analyzing protein heterodimerization in Escherichia coli. Mol Gen Genet 257:205–212

Annexe 6: Tables S1, S2 and S3

Table S1. Strains, plasmids and oligonucleotides used in this study.

Strains

Strains	Description and genotype	Source
E. coli		
DH5α	F-, Δ(*argF-lac*)U169, *phoA*, *supE44*, Δ(lacZ)M15, *relA*, *endA*, *thi*, *hsdR*	New England Biolabs
BL21(DE3)	*E.coli* B. F$^-$, *dcm ompT hsdS*(rB-mB-) *gal* λDE3	Invitrogen
BL21(DE3) Δ*minCDE*Ω*kan*	replacement of the *minCDE* operon by a kanamycin cassette into BL21(DE3), Kan^R	This study
BL21(DE3) *mreB*^{A125V}	*mreB* Ala125-to-Val substitution into BL21(DE3)	This study
BL21(DE3) *mreB*^{A125V} Δ*minCDE*Ωkan	replacement of the *minCDE* operon by a kanamycin cassette into BL21(DE3) mreB^{A125V}, Kan^R	This study
BL21(DE3) *mreB*^{A125V} Δ*minCDE*Ωcm	replacement of the *minCDE* operon by a cat cassette into BL21(DE3) *mreB*^{A125V}, Cm^R	This study
17.2	Wild-type enteroaggregative *Escherichia coli*	A. Darfeuille-Michaud
17.2 *mreB*^{A125V}	*mreB* Ala125-to-Val substitution into 17.2	This study
17.2 Δ*minCDE*	deletion of the *minCDE* operon in 17.2	This study
17.2 *mreB*^{A125V} Δ*minCDE*Ωkan	replacement of the *minCDE* operon by a kanamycin cassette into 17.2 *mreB*^{A125V}, Kan^R	This study
WM3433	*mreB*^{A125V} chromosomal mutant in *E. coli* K-12	Liu et al., 2011

Plasmids

Vectors	Description	Source
Vectors for chromosomal insertions		
pKD4	One-step gene inactivation vector, Kan^R	Datsenko&Wanner, 2000
pKOBEG	Recombination vector, phage λ *rec*γβα operon under the control of the pBAD promoter, Cm^R	Chaveroche et al. , 2000
pCP20	Amp^R, Cm^R, FRT recombinase gene	Chaveroche et al. , 2000
pKO3	*sacB, repA(*pSC101$_{ts}$), M13 origin, Cm$_R$	Link et al., 1997
pKO3-MreB^{A125V}	m*reB* fragment with *A125V* substitution cloned into pKO3	This study

Oligonucleotides

Name	Destination	Sequence (5' → 3')
For strain construction [ab]		
Del-minCDE-5-DW	deletion of the *minCDE* operon	AACATCATCGCGCGCTGGCGATGATTAATAGCTAATTGAGTAAGGCCAGG TGTGTAGGCTGGAGCTGCTTCG
Del-minCDE-3-DW	deletion of the *minCDE* operon	CAAGGCAGAGATAACTCTGCCTTGAAGATAAATGCGCTTTTACAGCGGGC CATATGAATATCCTCCTTAGTTC
5-pKO3-BamHI-MreB	insertion of *mreB* from WM3433 into pKO3	*gaccGGATCC*CTCATGGGAGTGTGCTTGTCTGCTCGCC
3-pKO3-SalI-MreB	insertion of *mreB* from WM3433 into pKO3	*cccgGTCGAC*CCGATTACTCTTCGCTGAACAGGTCGC

[a] Sequences corresponding to the downstream and upstream regions of the gene to be deleted underlined.
[c] Restriction site in *italicized* upper letters.

Table S2. Strains, plasmids and oligonucleotides used in this study.

STRAINS		
Strains	**Description**	**Source/Reference**
Enteroaggregative *E. coli*		
17-2	Wild-type enteroaggregative *Escherichia coli*	A. Darfeuille-Michaud
17-2 *ΔtssM*	17-2 deleted of the *tssM* gene of the *sci1* T6SS gene cluster	Aschtgen et al. , 2010
17-2 *tssMΔCter*	17-2 deleted of the *tssM* C-terminal region of the *sci1* T6SS gene cluster	This study
17-2 *Cter-Ala*	*tssM* C-terminal region of the *sci1* T6SS gene cluster with alanine substitution (1)	This study
17-2 *Cter-Scr*	*tssM* C-terminal region of the *sci1* T6SS gene cluster with scrambled sequence (2)	This study
E. coli K-12		
DH5a	F-, Δ*(argF-lacZ)*U169, *phoA, supE44,* Δ(lacZ)M15, *relA, endA, thi, hsdR*	New England Biolabs
CA8000 *htrM:Tn5*	HfrH *thi* Kan$_R$	Raina et al., 1990
BTH101	F-, cya-99, araD139, galE15, galK16, rpsL1 (Str r), hsdR2, mcrA1, mcrB1.	A. Karimova et al. , 1998
PLASMIDS		
pKD4	One-step gene inactivation vector, Kan^R	Datsenko&Wanner, 2000
pKOBEG	Recombination vector, phage λ recγβα operon under the control of the pBAD promoter, Cm^R	Chaveroche et al. , 2000
pDK4-CterAla	*Cter-Ala* cloned in pKD4	This study
pDK4-CterScr	*Cter-Scr* cloned in pKD4	This study
pUA66-rrnb	*PrrnB ::gfpmut2* transcriptional fusion in pUA66, Kan^R	Zaslaver et al. , 2006
pASK-IBA37-FLAG TssM	*sci-1* tssM carrying N-terminal FLAG tag cloned into pASK-IBA37	Aschtgen et al. , 2010
pASK-IBA37-FLAG TssMΔCter	insertion of a premature stop codon into pASK-IBA37-FLAG TssM after codon 1098	This study
pASK-IBA37-FLAG TssM-Ala	insertion of Ala-substituted sequence of the *tssM* C-terminal region into pASK-IBA37-FLAG TssM	This study
pASK-IBA37-FLAG TssM-Scr	insertion of scrambled sequence of the *tssM* C-terminal region into pASK-IBA37-FLAG TssM	This study
pTolB-T25	*tolB* cloned upstream the T25 coding sequence in pT25-FLAG	Battesti & Bouveret, 2008
pT18-Pal	*pal* cloned downstream the T18 coding sequence in pT18-FLAG	Battesti & Bouveret, 2008
pTssJsol -T25/T18	*tssJsol* cloned upstream the T25/T18 coding sequence in pT25/T18-FLAG	Zoued et al. , 2013
pT25/T18-TssJso	*tssJsol* cloned downstream the T25/T18 coding sequence in pT25/T18-FLAG	Zoued et al. , 2013
pT25/T18-TssM$_{Per}$	Periplasmic région of *tssM* (TssM$_{386-1129}$ fragment) cloned upstream T25/T18 in pT25-FLAG	Zoued et al. , 2013
pT25/T18-TssM$_{Per}$-ΔCter	pT25/T18-TssM$_{Per}$ carrying a premature stop codon after codon 1098	This study

pT25/T18-TssM$_{Per}$-Ala	pT25/T18-TssM$_{Per}$ carrying Ala-substituted alanine of the *tssM* C-terminal region	This study
pT25/T18-TssM$_{Per}$-Scr	pT25/T18-TssM$_{Per}$ carrying scrambled sequence of the *tssM* C-terminal region	This study

OLIGONUCLEOTIDES [a, b, c]

Insertion into pKD4 (Megapriming) [a]

5-Mp-Cter-DW	GAACTGAAGCGGGGGAAGGGCCGCTTGTATTGCTGAAACTCCGCAATTTT
3-Mp-Cter-DW	GCGAATGAATGGAAGCCATCAGTCAGTCTCCTCCACGGTATCCCCGGCATCTTCGCATATGAATATCCTCCTTAGTTC
5-TssM-1099Stop-DW	GAACTGAAGCGGGGGAAGGGCCGCTTGTATTGCTGAAACTCCGCAATTTT*TAGTAG*TGTGTAGGCTGGAGCTGCTTCG
3-TssM-1099Stop-DW	CCTGTAAACGCTGACGTGCCGGAGAGTTCGAAAACCGTTTCCGGCAGAACCATATGAATATCCTCCTTAGTTC

Site-directed mutagenesis on pASK-IBA37-FLAG TssM and BACTH plasmids [ab]

5-Mp-1099Stop	GCTGAAACTCCGCAATTTT*TAGTAG*GTTCTGCCGGAAACGGTTTTC
3-Mp-1099Stop	GAAAACCGTTTCCGGCAGAAC*CTACTA*AAAATTGCGGAGTTTCAGC
5-TssM-1099CterAla	GGCCGCTTGTATTGCTGAAACTCCGCAATTTTGTTCTGCCGGCAACGGTTTTCGC
3-TssM-1099CterAla	GAGAGTTCGAAAACCGTTTCCGGCAGAACGCGAAACGATCCTCATCCTGTCTCTTG
5-TssM-1099CterScr	GGCCGCTTGTATTGCTGAAACTCCGCAATTTTGTTGGCGATCTGACGGCCCCG

[a] sequence complementary to the pKD4, pDK4-CterAla and pDK4-CterScr vectors (underlined).
[b] insertion of a premature stop codon (italicized).

Custom DNA Synthesis (IDT)
Sequence complementary to the pKD4 vector underlined
Ala-substituted residues in bold

(1) CterAlanine
AGATTGCAGCATTACACGTCTTGAGCGATTGAACTGAAGCGGGGGAAGGGCCGCTTGTATTGCTGAAACTCCGCAATTTTGTTCTGCCG**GCA**ACGGTTTTC**G**
CACTCTCCGGCACGTCAGCGTTTACAGGCAAT**GCCGCAGCT**GCCGGG**GCT**ACCGTG**GCGGCG**ACT**GCC**TGAGTGTAGGCTGGAGCTGCTTCGAAGTTCCT
A

(2) CterScrambled
AGATTGCAGCATTACACGTCTTGAGCGATTGAACTGAAGCGGGGGAAGGGCCGCTTGTATTGCTGAAACTCCGCAATTTTGTTGGCGATCTGACGGCCCCGT
CAGGGGAAGCGGATACGTTTACCGTTACAGTGTTCGGCGAGGAAAATGAGCTCGACACTTCCGAAGACTGAGTGTAGGCTGGAGCTGCTTCGAAGTTCCTA

Table S3. Strains, plasmids and oligonucleotides used in this study.

STRAINS		
Strains	**Description**	**Source/Reference**
Enteroaggregative *E. coli*		
17-2	Wild-type enteroaggregative *Escherichia coli*	A. Darfeuille-Michaud
E. coli K-12		
DH5α	F-, Δ*(argF-lacZ)*U169, *phoA, supE44,* Δ(lacZ)M15, *relA, endA, thi, hsdR*	New England Biolabs
BL21(DE3)	*E.coli* B. F$^-$, *ompT dcm ompT hsdS*(rB-mB-) *gal* λDE3	Invitrogen
BL21(DE3)pLys	BL21(DE3) pLysS(Cm^R)	Invitrogen
PLASMIDS		
pETG20A	Gateway® vector, 6×His-TRX followed by a TEV cleavage site	Arie Gerlof
pETG20A-TssMc-NTP-Stm	$tssM_{Cyto}$*-NTP* (residues 140-375) from *S. enterica* Typhimurium cloned in pETG20A	This study
pRSF-Duet1	Expression vector, *lacI*, P*T7*, KanR	Addgene
pRSF-TssK-Ec	*tssK* from EAEC cloned in pRSF	This study
pRSF-TssK- TssMc-Ec	$tssM_{Cyto}$ from EAEC (residues 63-360) cloned in pRSF-TssK	This study
pRSF-TssK- TssMc-Stm	*tssK* and $TssM_{Cyto}$ from *S. enterica* Typhimurium cloned in pRSF	This study
OLIGONUCLEOTIDES		
Insertion into pETG20A (Gateway cloning) [a]		
Sent-TssMc_p17Tev_For	*GGGGACAAGTTTGTACAAAAAAGCAGGCTTAGAAAACCTGTACTTCCAGGGT*CGGCTGTGGCGTGCGCTGCG	
Sent-TssMc _p17_Rev	*GGGGACCACTTTGTACAAGAAAGCTGGGTTTATTA*GCGGTAACGCCAGGCCCACTG	
Sent-TssMc-NTP_p17Tev_For	*GGGGACAAGTTTGTACAAAAAAGCAGGCTTAGAAAACCTGTACTTCCAGGGT*GTACCGGTGGCAGGCGAGATC	
Sent-TssMc-NTP _p17_Rev	*GGGGACCACTTTGTACAAGAAAGCTGGGTTTATTA*CGGGTCGCCCGCTTTTCGCC	

Insertion into pRSF-TssK (restriction-ligation cloning) [a,b]	
5-NdeI-TssMc-Ec (MCS2)	*ggaattcCATATG*ATGAAAAAATATGTTCAGGAACTGACATATCGACGC
3-XhoI-TssMc-Ec-Strep	*cggCTCGAG***TTATTTTTCGAACTGCGGGTGGCTCCAAGCGCT**TCTGCGCCAGTTATGACCTGTGCGGGA
5-BamHI-TssK-Stm (MCS1)	*cgGGATCC*AGCTGGAATGACCGCGTAGTCTGGAG
3-HindIII-TssK-Stm	*ggAAGCTT*CTCCCCACAGTTCTGTCTCCAGCCCC
5-NdeI-TssMc-Stm (MCS2)	*ggaattcCATATG*ATGGTACCGGTGGCAGGCGAGATCAAAG
3-XhoI-TssMc-Stm-Strep	*cggCTCGAG***TTATTTTTCGAACTGCGGGTGGCTCCAAGCGCT**GCGGTAACGCCAGGCCCACTGGAG

[a] Restriction sites and additional bases (Restriction-ligation cloning in pRSF) or Gateway overhangs (Gateway cloning) italicized.
[b] Tag epitope sequence in bold.

The Type VI secretion membrane complex: the central role of TssM for assembly and for baseplate recruitment

In the environment, bacteria live in communities. These microbial communities harbour unique and interesting features. Inside these communities, bacteria have distinct behaviours and are able to coordinate their efforts, to develop symbiosis or antagonistic interactions. Particularly, bacteria compete with each other to acquire nutrients, to colonize or to expand their niche. Predator bacteria deploy various systems to recognize and destroy prey cells. One of the most efficient mechanisms is the type VI secretion system (T6SS). This multiprotein apparatus resembles a nano-crossbow that delivers a needle loaded with toxins directly into target cells when in contact with the prey. The needle is built on a platform that is anchored to the membrane complex. The membrane complex is inserted in the cell envelope and is composed of three proteins: TssJ, TssM and TssL.

During my thesis, I was specifically interested in the TssM subunit, which was poorly characterized. I defined its topology, participated to the structural characterization of its periplasmic domain and further showed that TssM bears a cytoplasmic GTPase-like domain that interacts with the assembly platform. Interestingly, GTPase proteins switch and regulate various cellular processes, suggesting that TssM might control the activity of the platform. In addition, I identified a fragment of the TssM protein that lies outside of the cell. Because it is the only extracellular portion of the T6SS, we hypothesized that TssM might coordinate prey sensing to T6SS assembly and more specifically that this region might be involved in sensing the prey. I further investigated the role of these two regions of TssM with the goal to provide a model for signal transmission. Finally, I have participated to the characterization of TssK, a component of the platform that directly interacts with the cytoplasmic domain of TssM and hence docks the platform to the membrane complex.